181
11-21-77

Hb.1604

GA-A14479
UC-77

HTGR FUELS AND CORE DEVELOPMENT PROGRAM

QUARTERLY PROGRESS REPORT FOR THE PERIOD ENDING AUGUST 31, 1977

Prepared under
Contract EY-76-C-03-0167
Project Agreement No. 17
for the San Francisco Operations Office
U.S. Energy Research and Development Administration

DATE PUBLISHED: SEPTEMBER 1977

GENERAL ATOMIC COMPANY

Printed in the United States of America
Available from
National Technical Information Service
U.S. Department of Commerce
5285 Port Royal Road
Springfield, Virginia 22161
Price: Printed Copy $[illegible]; Microfiche $3.00
14.00

DISCLAIMER

GA-A14479
UC-77

HTGR FUELS AND CORE DEVELOPMENT PROGRAM

QUARTERLY PROGRESS REPORT FOR THE PERIOD ENDING AUGUST 31, 1977

Prepared under
Contract EY-76-C-03-0167
Project Agreement No. 17
for the San Francisco Operations Office
U.S. Energy Research and Development Administration

GENERAL ATOMIC PROJECT 3224
DATE PUBLISHED: SEPTEMBER 1977

GENERAL ATOMIC COMPANY

QUARTERLY REPORT SERIES

GA-4072-December, 1962, through February, 1963
GA-4350-March, 1963, through May, 1963
GA-4569-June, 1963, through August, 1963
GA-4937-September, 1963, through November, 1963
GA-5104-December, 1963, through February, 1964
GA-5366-March, 1964, through May, 1964
GA-5618-June, 1964, through August, 1964
GA-5866-September, 1964, through November, 1964
GA-6113-December, 1964, through February, 1965
GA-6418-March, 1965, through May, 1965
GA-6671-June, 1965, through August, 1965
GA-6869-September, 1965, through November, 1965
GA-7010-December, 1965, through February, 1966
GA-7181-March, 1966, through May, 1966
GA-7396-June, 1966, through August, 1966
GA-7553-September, 1966, through November, 1966
GA-7801-December, 1966, through February, 1967
GA-7981-March, 1967, through May, 1967
GA-8200-June, 1967, through August, 1967
GA-8356-September, 1967, through November, 1967
GA-8530-December, 1967, through February, 1968
GA-8662-March, 1968, through May, 1968
GA-8860-June, 1968, through August, 1968
GA-9090-September, 1968, through November, 1968
GA-9227-December, 1968, through February, 1969
GA-9372-March, 1969, through May, 1969
GA-9660-June, 1969, through August, 1969
GA-9815-September, 1969, through November, 1969
GA-9944-December, 1969, through February, 1970
GA-10088-March, 1970, through May, 1970
GA-10288-June, 1970, through August, 1970
GA-10399-September, 1970, through November, 1970
GA-10501-December, 1970, through February, 1971
GA-10661-March, 1971, through May, 1971
Gulf-GA-A10784-June, 1971, through August, 1971
Gulf-GA-A10930-September, 1971, through November, 1971
Gulf-GA-A10999-December, 1971, through February, 1972
Gulf-GA-A12150-March, 1972, through May, 1972
Gulf-GA-A12222-June, 1972, through August, 1972
Gulf-GA-A12422-September, 1972, through November, 1972
Gulf-GA-A12515-December, 1972, through February, 1973
Gulf-GA-12599-March, 1973, through May, 1973
Gulf-GA-A12725-June, 1973, through August, 1973
Gulf-GA-A12818-September, 1973, through November, 1973
GA-A12916-December, 1973, through February, 1974
GA-A13030-March, 1974, through May, 1974
GA-A13126-June, 1974, through August, 1974
GA-A13253-September, 1974, through November, 1974
GA-A13353-December, 1974, through February, 1975
GA-A13444-March, 1975, through May, 1975

GA-A13592-June, 1975, through August, 1975
GA-A13737-September, 1975, through November, 1975
GA-A13804-December, 1975, through February, 1976
GA-A13941-March, 1976, through May, 1976
GA-A14046-June, 1976, through August, 1976
GA-A14180-September, 1976, through November, 1976
GA-A14298-December, 1976, through February, 1977
GA-A14418-March, 1977, through May, 1977

ABSTRACT

This publication continues the quarterly report series on the HTGR Fuels and Core Development Program. The Program covers items of the base technology of the High-Temperature Gas-Cooled Reactor (HTGR) system. The development of the HTGR system will, in part, meet the greater national objective of more effective and efficient utilization of our national resources. The work reported here includes studies of reactions between core materials and coolant impurities, basic fission product transport mechanisms, core graphite development and testing, the development and testing of recyclable fuel systems, and physics and fuel management studies. Materials studies include irradiation capsule tests of both fuel and graphite. Experimental procedures and results are discussed and, where appropriate, the data are presented in tables, graphs, and photographs. More detailed descriptions of experimental work are presented in topical reports; these are listed at the end of the report.

INTRODUCTION

This report covers the work performed by the General Atomic Company under U.S. Energy Research and Development Administration Contract EY-76-C-03-0167, Project Agreement No. 17. This Project Agreement calls for support of basic technology associated with the fuels and core of the gas-cooled, nuclear power reactor systems. The program is based on the concept of the High-Temperature Gas-Cooled Reactor (HTGR) developed by the General Atomic Company.

Characteristics of advanced large HTGR designs include:

1. A single-phase gas coolant allowing generation of high-temperature, high-pressure steam with consequent high-efficiency energy conversion and low thermal discharge.

2. A prestressed concrete reactor vessel (PCRV) offering advantages in field construction, primary system integrity, and stressed member inspectability.

3. Graphite core material assuring high-temperature structural strength, large temperature safety margins, and good neutron economy.

4. Thorium fuel cycle leading to U-233 fuel which allows good utilization of nuclear resources and minimum demands on separative work.

These basic features are incorporated into the 330-MW(e) prototype Fort St. Vrain reactor which is currently undergoing prestartup testing.

CONTENTS

FIGURES

FIGURES (Continued)

FIGURES (Continued)

FIGURES (Continued)

FIGURES (Continued)

TABLES

TABLES (Continued)

About a year ago, options were added to FIPERQ so that the code would consider:

1. The effect of different sorptivities on either side of a material interface in order to calculate the partition (ϕ) factor.

TABLES (Continued)

2. The effect of transverse purge flow in a fuel-graphite gap acting as a removal mechanism.

Both of these effects introduce nonlinearities since the ϕ factor and the purge removal rate both depend on the unknown fission metal concentrations. Two types of nonlinearity must be considered. First is the fact that the sorption relationships are nonlinear. Second is the fact that in the present FIPER formulation both ϕ and the source rate, S, are assumed to be known constants during any time step. Thus even if the sorption relationships were linear, an iteration would still be necessary to account for the functional dependence of ϕ and S on the unknown concentrations.

The FIPER method for treating any nonlinear effect is to assume the effect is constant for a given iteration and to explicitly reevaluate the effect for the next iteration. This method does not always converge. It has been concluded from recent experience that there is no convergence acceleration algorithm, short of an elaborate and costly vector-matrix approach, that will work for all problems.

The significance of this theoretical weakness was not apparent at first because early test problems worked well. However, during the past year a FIPERQ analysis of Peach Bottom driver elements disclosed two forms of numerical instability. One was caused by discontinuous jumps in the temperature history. This problem was remedied by doing a fully implicit solution to step past all temperature discontinuities, reverting to the Crank-Nicholson method for the integration over a continuous temperature domain. The second was an iteration instability in the ϕ and the purge calculations. This was temporarily fixed by employing the successive over-relaxation (SOR) method. However, continued use of the code on a multitude of cases has resulted in numerous iteration failures. These have been fixed as they occurred by a patchwork of different scalar iteration procedures of ever-increasing complexity. The present failure of these procedures is due to the fact that no scalar iteration algorithm can properly account for the coupling between components in a poorly behaved vector iteration.

Work is now under way on an interim truncated vector iteration that considers the 2 x 2 coupling at each material interface. However, it is now clear that the only valid method is to reformulate the difference equations so that linear approximations of all functional relationships are explicitly considered. A set of matrix tangent equations can then be developed for a vector analog of Newton's method.

It might be possible to adapt the present FIPER code to employ a tangent matrix formulation. However, to accomplish this, the difference equations would have to be rederived and reprogrammed, which is a significant part of the labor that would be required for development of a new code. For reasons discussed below, FIPER has other shortcomings that make a new code an attractive choice.

The present FIPER is organized so that every space point is considered to be "typical." This wastes a considerable amount of calculational effort by forcing the program to do unnecessary repetitive calculations in homogeneous regions when the only need for calculation is at material interfaces and boundaries. The following approach, recently proven in PADLOC, is much better:

1. Organize the system of equations as a network, with primary unknowns at network junctions (material interfaces) and secondary unknowns in the interior of homogeneous regions.

2. Eliminate the interior unknowns, and obtain a reduced set of global equations based on only the primary unknowns.

3. Perform all nonlinear purge, ϕ, and boundary condition iterations on the reduced system.

4. Return to the continuous regions and solve for interior unknowns.

This method has the further advantage that arbitrary geometries and boundary conditions are easier to model. For example, cylindrical and slab geometries could be mixed to verify the TRAFIC code.

Another limitation of FIPER is that the program is incapable of treating coupled multiple species interactions during diffusion; i.e., the decay-precursor effect is not considered. For some problems, e.g., krypton decaying to strontium, this could be important. A rigorous model is needed to assess such effects.

There has been considerable discussion in the past few years about non-Fickian diffusion of cesium. This has been called the two-path or two-phase effect. The simplest possible mathematical representation of this effect is to assume a zero-dimensional coupling between the paths by a rate constant mechanism. A zero-dimensional coupled path diffusion problem is mathematically identical to the coupled species problem. The equations to be solved can be written in matrix form as

$$\frac{\partial}{\partial t} \{C\} = [D] \nabla^2 \{C\} - [A] \{C\} + \{S\} \quad , \tag{4-1}$$

where [D] = a diagonal matrix of diffusion constants,
[A] = a coupling-depletion matrix.

An advanced FIPER should be organized in this general sense so that studies of these effects can be undertaken.

COPAR, an advanced particle release model, has been incorporated into TRAFIC, but it has not yet been incorporated into FIPER. It is clear that FIPER needs an advanced particle source model of this type. This interface would be more straightforward in a new code than in the present FIPER.

COPAR Code

The recently developed COPAR program is analogous to TRAFIC in many respects. It employs a parameterization and superposition technique for

eliminating interior solutions and efficiently solving a coupled boundary value problem. The similarity in approaches has led to examination of the possibility that one program could be written that would serve both functions. Some inherent limitations of TRAFIC, to be discussed below, make this one program concept a desirable choice.

TRAFIC Code

In the past year TRAFIC has suffered from numerous numerical problems. Many of these were minor underflow and overflow problems caused by the huge numerical range of the numbers involved. The two problems that have caused the most concern are:

1. The system of nonlinear equations sometimes failed to converge or converged to the wrong result.

2. The accuracy of the program was questionable with long time steps and high temperatures.

A solution to the first problem was initially attempted by modifying VECTIT, a general purpose vector iteration algorithm. Because of the lack of success with this approach, it was decided to reformulate the equations so they were intrinsically monotonic and stable. This approach ultimately proved to be successful.

No solution to the second problem is possible with the present TRAFIC formulation because the logic of the program is closely tied to the presumption that the time step sizes are known in advance. An automatic time stepping procedure with an adaptive integration is needed. However, implementing this within the present Duhamel superposition method might lead to an intolerable degradation of efficiency. Therefore, some theoretical research to discover an efficient adaptive solution method would be desirable.

Another concern with TRAFIC is that it is designed to solve problems only for one particular geometry, the 30-60-90 triangular unit cell of the LHTGR. In principle, the same parameterization and superposition method could also be used for other geometries, but the need for a general formulation was not anticipated when the TRAFIC development began.

In code validation work there is a need to employ a highly efficient TRAFIC-like code to analyze geometries such as those of the Peach Bottom or Pebble-Bed reactor. Such analyses cannot be done by the present TRAFIC code. The answer appears to be use of a general network coupling organization similar to that already suggested for FIPER. Using this technique, one could specify through input the geometry of the homogeneous regions and the nature of the interface conditions. The program could then couple the regions together and solve a reduced nonlinear system of equations for the interface conditions. It is interesting to note that adoption of this approach would provide a program capable of obtaining coupled one-dimensional analytic solutions with any heterogeneous geometry. The need for an entirely separate COPAR program would be eliminated.

Proposed Models

Based on the previous discussions, it appears that both FIPER and TRAFIC would benefit from being reorganized according to the network concept. An efficient way to develop these programs would be to employ a single-driver program for input, network analysis, and output. A FIPER-like (finite difference) or a TRAFIC-like (analytical) solution could then be obtained by calling appropriate modules from this one program. This technique has two advantages. First, duplication of programming effort is avoided. Second, such a program would be self-checking. Analytic and difference solutions for similar problems could be easily compared. The following sections present a summary description of a modular program capable of both analytic and difference solutions. The program could also use a mixture of the two methods for single species problems.

Driver Program. The driver program would control the input, the network analysis, and the output. It would call upon analytical or finite difference solution modules in various phases of the analysis. In keeping with the solution strategy already developed for TRAFIC and COPAR, two modes of solution are possible: direct solution and superposition.

In the direct mode the solution is computed in detail using all of the essential tools of the appropriate method. For the finite difference solution, this means establishing and solving a matrix equation for a fine spatial mesh of interior nodes in each branch of the network. For the analytic solution, this means evaluating some infinite series expansions.

The direct solution can be used for two purposes. It can be used in each time step of a coupled network analysis, during which the solution for the complete network is simultaneously marched forward in time. This is a costly but rigorous solution method. The other application of direct solutions is in a parameterization and superposition method (see below) similar to that now employed in TRAFIC and COPAR. Here, nondimensional direct solutions are first precomputed and tabulated for each geometry type (spherical, cylindrical, or slab). Thereafter, subsequent multiple solution evaluations are performed by linear interpolation in the tables.

Regardless of the application intended, the direct solution procedure can be accomplished using either the finite difference or the analytic solution modules. The application is controlled by the driver program.

The direct solution can be quite costly when it is done repetitively. A much faster method is to precompute some tabulated solutions (see above) and to employ a superposition principle. This parameterization and superposition technique only works when one restricts the tabulated direct solutions to the simplified case of constant (time-independent) boundary conditions. The effect of time-dependent boundary conditions is later treated by Duhamel's superposition principle. This involves a convolution (integration) of the tabulated direct solutions with the past history of the actual boundary conditions. For example, a typical expression might be

$$C(t) = \int_0^t F(t - \tau) \frac{dC_o(\tau)}{d\tau} \, d\tau \quad . \tag{4-2}$$

This integration can be quite efficient when the function F is evaluated by linear interpolation in the precomputed tables.

The superposition calculation in each time step contains a loop over time steps in the past history. For each prior time step some functions are evaluated by linear interpolation and some integrals are incremented. When complete, this process yields the coefficients of the reduced equation for the branch in question. This reduced equation takes the same algebraic form as if the equation were derived by the direct solution procedure. The driver program can then proceed with the global network solution using a typical method.

The schematic flow diagram in Fig. 4-1 shows a proposed DRIVER program that would accomplish all of the operations indicated above. This is intended to give only a broad picture of the proposed capability. If a decision is made to go ahead with this effort, the organization of this logic should be studied in more depth. It may be desirable, for example, to have more than one DRIVER calling on the same modules.

This DRIVER program is a general analytical procedure that will work for any configuration of one-dimensional network branches, including the present TRAFIC model which has mixed coordinate systems. Some care must be taken to ensure that the present calculational efficiency of TRAFIC is not compromised by this generality; however, it should be possible to accomplish this with careful planning.

Finite Difference Modules. The flow diagram shown in Fig. 4-1 calls for two finite difference modules for each geometry type:

DIFF1 - Eliminate interior unknowns to compute a reduced set of branch equations for a time step.

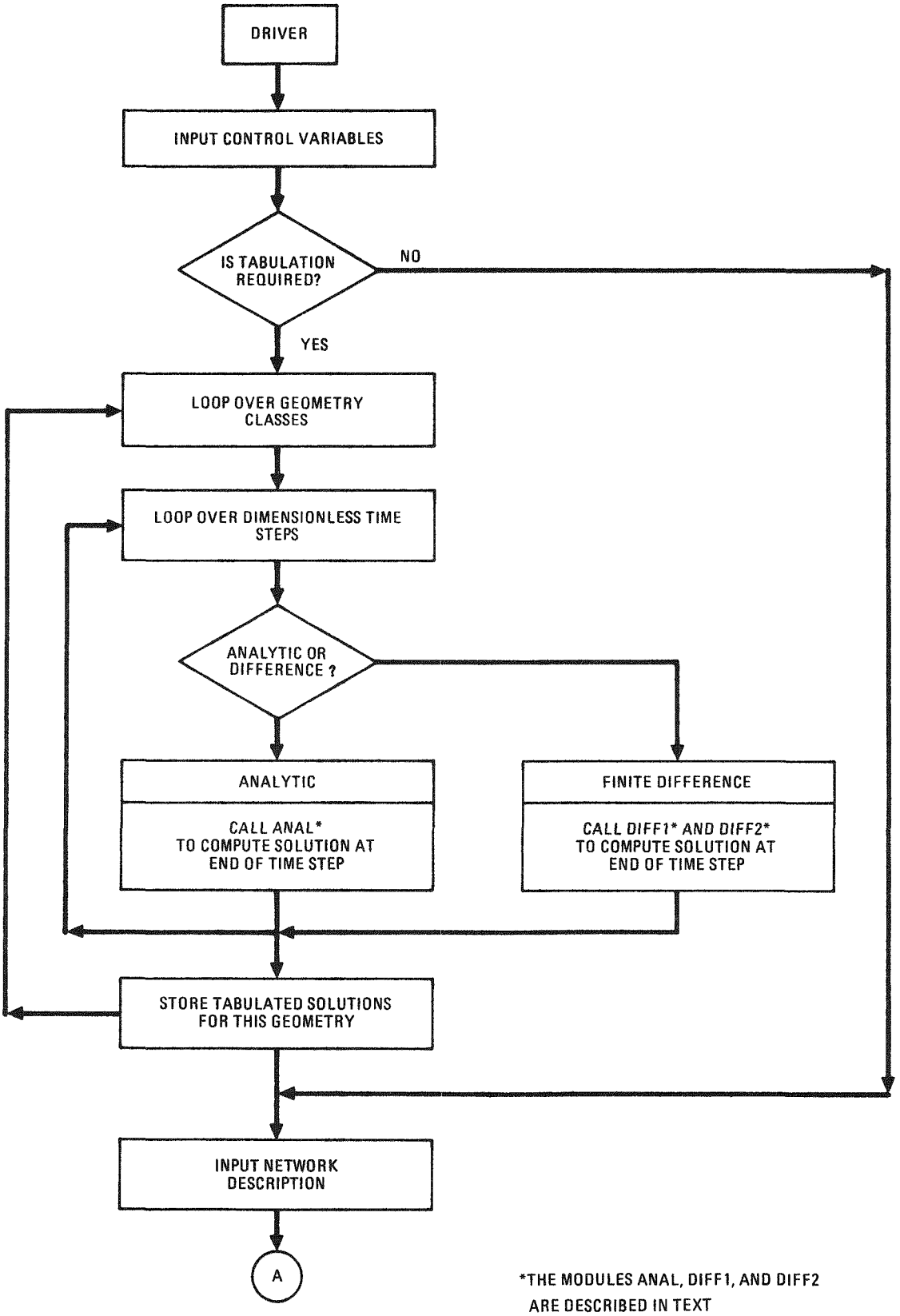

Fig. 4-1. Flow diagram for proposed DRIVER program (sheet 1 of 4)

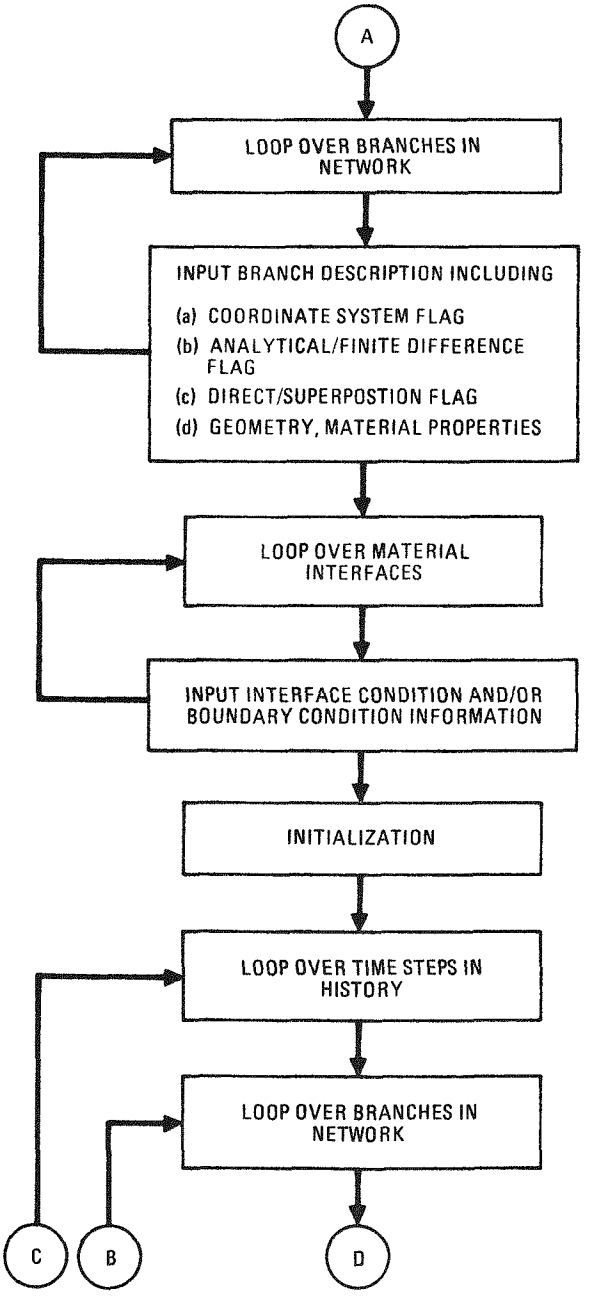

Fig. 4-1. Flow diagram for proposed DRIVER program (sheet 2 of 4)

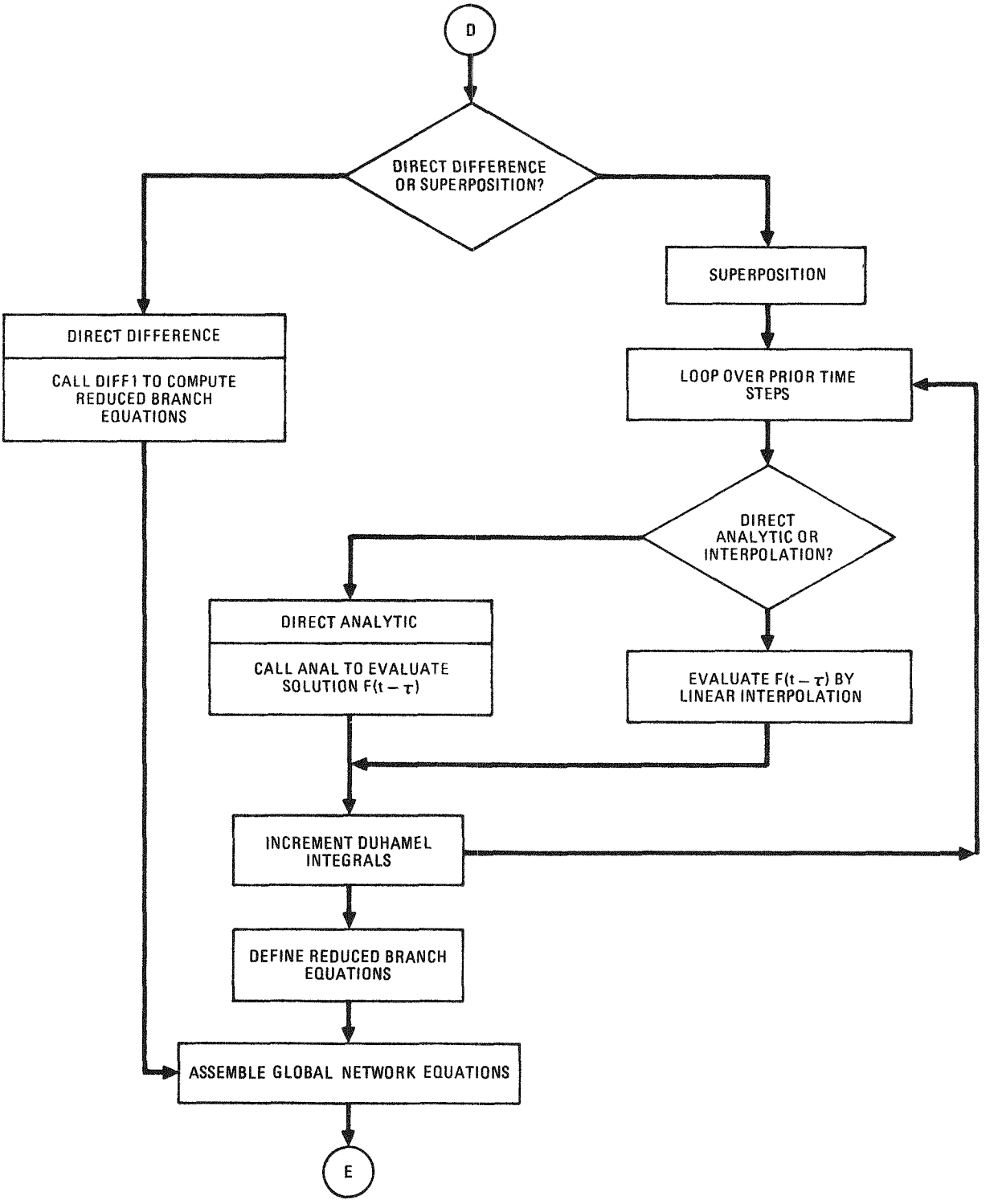

Fig. 4-1. Flow diagram for proposed DRIVER program (sheet 3 of 4)

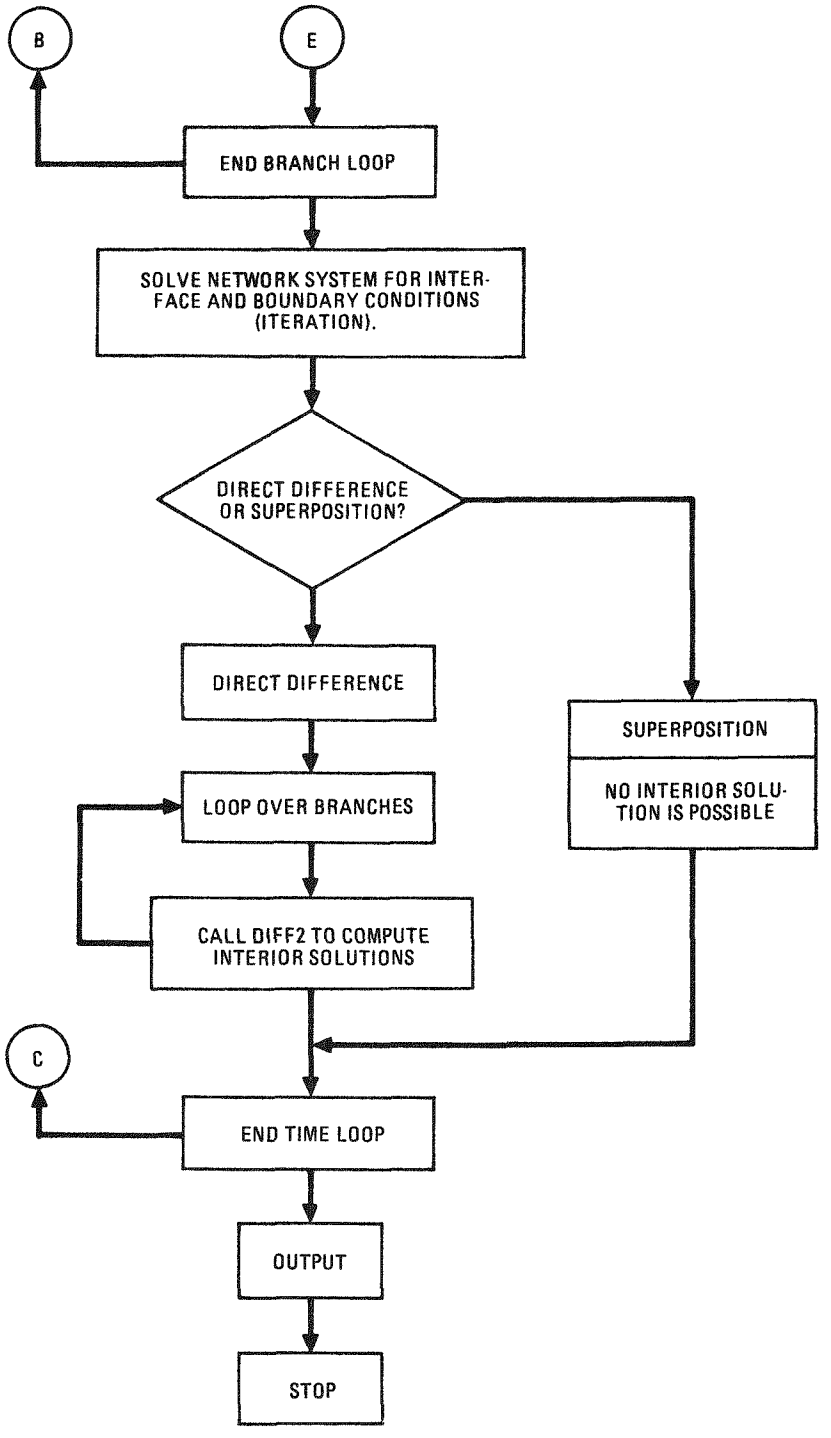

Fig. 4-1. Flow diagram for proposed DRIVER program (sheet 4 of 4)

DIFF2 - Compute the interior solution at the end of a time step when given the boundary conditions.

Separating the direct solution into two phases, commonly known as substructuring, is a useful technique when the boundary conditions are unknown or they involve nonlinear equations.

Analytical Modules. One analytical module is required for each geometry type. This module, called ANAL, is designed to compute nondimensional solution functions (e.g., F in Eq. 4-2) for the constant boundary condition case. This is done by evaluating infinite series expansions. Two applications of ANAL are shown in the DRIVER flow chart in Fig. 4-1. In the initial tabulation phase the boundary conditions are assumed to be constant; therefore, one call to ANAL in each time step serves to define the tabulated solution. In the direct analytic solution of a network (e.g., TRAFIC) it is necessary to use the Duhamel superposition principle to account for unknown time-dependent boundary conditions. Then ANAL may be called within a loop over the past history in order to evaluate Eq. 4-2. A faster approach, of course, is to interpolate in the tabulated functions.

Conclusions

A new modular program system designed to arbitrarily solve coupled one-dimensional diffusion problems has been proposed. This would embody all of the best features of FIPER, TRAFIC, and COPAR. One advantage of this scheme is that it would be more generally applicable to a variety of problem types and geometries. Another advantage is that it would ensure consistency between FIPER (reference method) and TRAFIC (fast-running design method).

The justifications for this work are the numerical problems, inadequate documentation, and difficulty of maintenance associated with the present family of programs. Although considerable work has already been done, this work must be continued to bring these programs under control.

probe. For a more detailed discussion of FSV primary coolant chemistry surveillance, see Subtask 900, FSV Chemistry Surveillance.

Peach Bottom. Analysis of Peach Bottom fission product behavior is carried out under the Peach Bottom End-of-Life (EOL) Program. Results made

TABLE 4-1
CURRENT STATUS OF FISSION PRODUCT CODE VALIDATION STUDIES

Test	Status of Validation		
	Fission Gas Release	Fission Metal Release	Fission Product Plateout
Fort St. Vrain	(Best fission gas validation test) Predicted and measured release agree within factor of 2	No data yet available; validation studies will be performed after data are made available from iodine monitor and plateout probe	
Peach Bottom	Good agreement between calculated and measured releases of Kr-85m and Xe-138	Total core release calculations in progress	Predicted Cs-137 distribution in good agreement with circuit gamma-scan data
CPL-2/1	Predicted release encompasses measured release using GA valve of $(R/B)_{failed}$ or R/B reirradiated CPL fuel rod	Initial Cs-137 release calculations show good agreement with measured release, but graphite loading overpredicted	Predicted Cs-137 plateout in good agreement with measured profiles; iodine deposition underpredicted, but temperature dependence is correct
SSL-1	R/B at 25 and 120 EFPD show good agreement with $\sqrt{t_{1/2}}$ dependence expected using design method	Cs release underpredicted, but good modeling of individual barriers noted; large uncertainties present	No applicable data
P13Q, P13R, P13S	No analysis due to large uncertainties in measured data	No measurable metal release due to good particle integrity and low irradiation temperatures	No data

Introduction and Summary

The Fission Product Code Validation Program commenced in September 1974, with the overall charter of ensuring that HTGR fission product design

TABLE 4-2
FSV RISE-TO-POWER Kr-85m R/B VALUES

Reactor Power (%)	Measured R/B	Predicted R/B
2	4.3×10^{-6}	5.8×10^{-6}
5	4.7×10^{-6}	5.7×10^{-6}
8	5.1×10^{-6}	6.0×10^{-6}
11	3.3×10^{-6}	6.2×10^{-6}
18	4.4×10^{-6}	6.9×10^{-6}
28.9	5.1×10^{-6}	1.1×10^{-5}

available for fission product code validation are included here for completeness.

Predicted Kr-85m and Xe-138 fission gas releases were found to be in excellent agreement with those measured during reactor operation. The dominant source for release was heavy metal contamination in the fuel compacts, as EOL average fuel failure fractions were found to be less than 1%. The calculated release was based on TRIGA R/B measurements carried out on several archive fuel compacts. Predicted Cs-137 distribution in the primary circuit obtained using the PAD code was found to be in good agreement with gamma scan data gathered after reactor shutdown. This provides assurance that the transport model presently employed in PAD is acceptable for characterizing plateout, provided correct wall temperatures and appropriate sorption isotherms are available. No information on predicted fission metal release from the purged fuel elements is yet available.

CPL-2. Analysis of the first CPL-2 loop test, CPL-2/1, is near completion (Refs. 4-3 through 4-6). Gaseous fission product release, cesium release, and cesium and iodine plateout have been computed using design methods and compared to measured values. Results of plateout calculations show that acceptable profiles of deposited fission products can be calculated when accurate wall temperatures and appropriate sorption isotherms are used. The equilibrium deposition model used in plateout calculations appears to be adequate for predicting condensible fission product plateout. Predicted fission metal release from CPL-2/1, specifically Cs-137 release, appears to be in good agreement with measured release. However, while the overall release was correctly modeled, cesium loading in the graphite was overpredicted. This may be an indication that the Fick's law model used in fission metal release calculations may not accurately represent the in-pile bulk diffusion of cesium in graphite. The behavior of fission gases in CPL-2/1, including the temperature dependence of release, has been adequately modeled using design methods. As expected, these results are strongly dependent on the input value of $(R/B)_{failed}$, which varies with FIMA.

SSL-1. FIPERQ was used to predict the release of Cs-137 from the SSL-1 fuel element. The observed release was found to be a factor of nine larger than that predicted using a source derived from the axial loading of cesium in the fuel element graphite. A three-fold increase in the reference value of the cesium diffusion coefficient in graphite resulted in close agreement between predicted and measured release. However, no combination of input variables could be assigned that would adequately explain all the measured results. The lack of an extensive body of PIE data prevents a more accurate assessment of the barriers controlling release. Analysis of Kr and Xe release from SSL-1 provided confirmation that in-pile fission gas release is properly modeled in the reference method by assuming a $\sqrt{\tau_{1/2}}$ dependence of fractional release at temperatures >1473 K. No assessment of the fission product plateout calculations could be carried out with the available data.

P13Q, P13R, and P13S. These capsules were designed to test the performance of reference or near-reference HTGR fuel under expected LHTGR irradiation conditions. Gamma scan results showed negligible cesium release from virtually all of the fuel bodies, a finding that confirmed the excellent performance of the fuel noted from in-pile fission gas release measurements. The lack of measureable fission metal release precluded a verification of the reference design method. Uncertainties in the in-pile fission gas data from P13R and P13S precluded analysis of the half-life dependence of Kr and Xe release. The variation in fuel irradiation temperatures and uncertainty regarding the measured in-pile fission gas release in P13Q make accurate assessment of fuel performance and fission gas release models extremely difficult. No data were available for fission product plateout calculations. No further analyses of fission product behavior in fuel performance capsules for code verification studies is planned at this time due to the very low fission product release generally noted in these tests.

Status of Cesium Release and Plateout Design Methods Verification

The following conclusions represent the tentative assessment of the validity of cesium release and plateout design methods calculations:

1. Predictions of nominal cesium release appear to be acceptable when the source strength is known. This conclusion is based on the results of the CPL-2/1 experiment where the cesium source strength in bare kernels was well-defined. The results of this test showed close agreement between predicted and observed total release. This conclusion will require additional confirmation by planned analyses of CPL-2/3, CPL-2/4, and the Idylle 03 loop, all of which had well-defined sources. (See Table 4-11 under discussion of potential future tests.)

2. The Ficks' law model used in the fission metal release design method (FIPER/TRAFIC) does not accurately describe cesium loading in graphite. This conclusion is based on the results from CPL-2/1 and SSL-1. In the former, loading in the graphite was overpredicted by approximately one order of magnitude while the overall release was correctly predicted. In the SSL-1 analyses, where the source was estimated from the cesium loading in graphite, the overall release was underpredicted by a factor of nine. Since the profile shapes in both tests were modeled correctly, it seems apparent that a more sophisticated model of cesium diffusion in graphite will be required if measured graphite loading and total release are to be reconciled.

3. The partition coefficient at the fuel rod - graphite interface is underpredicted by the reference method. This conclusion is based on results from SSL-1 and CPL-2/1. When the predicted and observed cesium loadings in graphite were equated, as was done in the SSL-1 analysis, the partition coefficient was properly modeled. However, when the source strength was derived from calculations of cesium release from kernels, as in CPL-2/1, the

partition coefficient was underpredicted. It appears that if the loading of cesium in graphite is correctly predicted by the code, the partition coefficient will likewise be correct (although total release will be simultaneously underpredicted).

4. Reliable predictions of cesium plateout on primary circuit surfaces can be derived from the PAD plateout code if proper isotherms and temperatures are used as input. This conclusion is based on the results of CPL-2/1 and Peach Bottom plateout profiles. The results of these plateout analysis confirm the validity of the PAD model, but large uncertainties remain regarding the reference isotherms used as input to the code.

5. No assessment of the model used to predict cesium release from particles can be made at this time. No reliable data on cesium release from intact and failed particles are yet available from any of the tests analyzed to date. The planned REBISE 02 capsule test has been designed to provide data on the diffusive release of cesium from intact BISO oxide kernel particles. (See Table 4-11 under discussion of potential future tests.) In addition, data from the CPL-2 and Idylle 03 tests will provide data suitable for comparison with code predictions.

These conclusions are based on analyses carried out to date and are subject to revision and change at a later date. One point should be noted, however, when reviewing the above conclusions. These assessments have been derived from short-term tests which likely overemphasize the importance of graphite as a barrier to release. When predictions are carried out over a four to six year time frame using representative operating temperatures, a large fraction of the cesium released to the graphite passes into the coolant. This finding emphasizes the need to clearly define cesium source strength from intact and failed particles.

Analysis of Cadarache Pegase Loop CPL-2 Test Data

Three-in-pile loop tests, CPL-2/1, -2/3, and -2/4, described in Ref. 4-4, have been completed in the Pegase reactor at Cadarache, France, under the auspices of the French Atomic Energy Commission (CEA). One additional loop irradiation, the CPL-2/1 Bis test, was also carried out to provide nominal operation reference data. This test was run because a water ingress incident occurred just prior to shutdown of the CPL-2/1 loop that may have altered the results of fission product transport derived from the PIE of this loop. The nominal conditions of the four loop irradiations performed were:

CPL-2/1	Nominal operation test
CPL-2/3	High coolant moisture - oxidant levels
CPL-2/4	In-situ depressurization after nominal operation
CPL-2/1 Bis	Rerun of nominal operation test

Nearly all the PIEs providing information on fission product transport in the fuel, reflector, and heat exchanger - recuperator are complete for the loops. Comparison of the CPL-2/1 PIE results with calculations performed using the GA fission product design methods is presented herein. A description of the loop and test components is also reviewed below.

Loop Description. Figure 4-2 shows a schematic of the loop used for the CPL-2 tests. Irradiations were performed by submerging the entire loop in the Pegase reactor pool and moving it up to the side of the reactor core. The test section included a graphite fuel element and reflector block, a counterflow heat exchanger - recuperator, and two fission product plateout probes. Helium was circulated upward at 5.4 MPa through the fuel element coolant channels where fission products released from the fuel rods entered the coolant. The flow then passed through the reflector block and the tube side of the heat exchanger - recuperator. Samplings of the fission product concentration in the coolant were performed continuously at the inlet and outlet of the tube side of the heat exchanger - recuperator by use of the probe tubes.

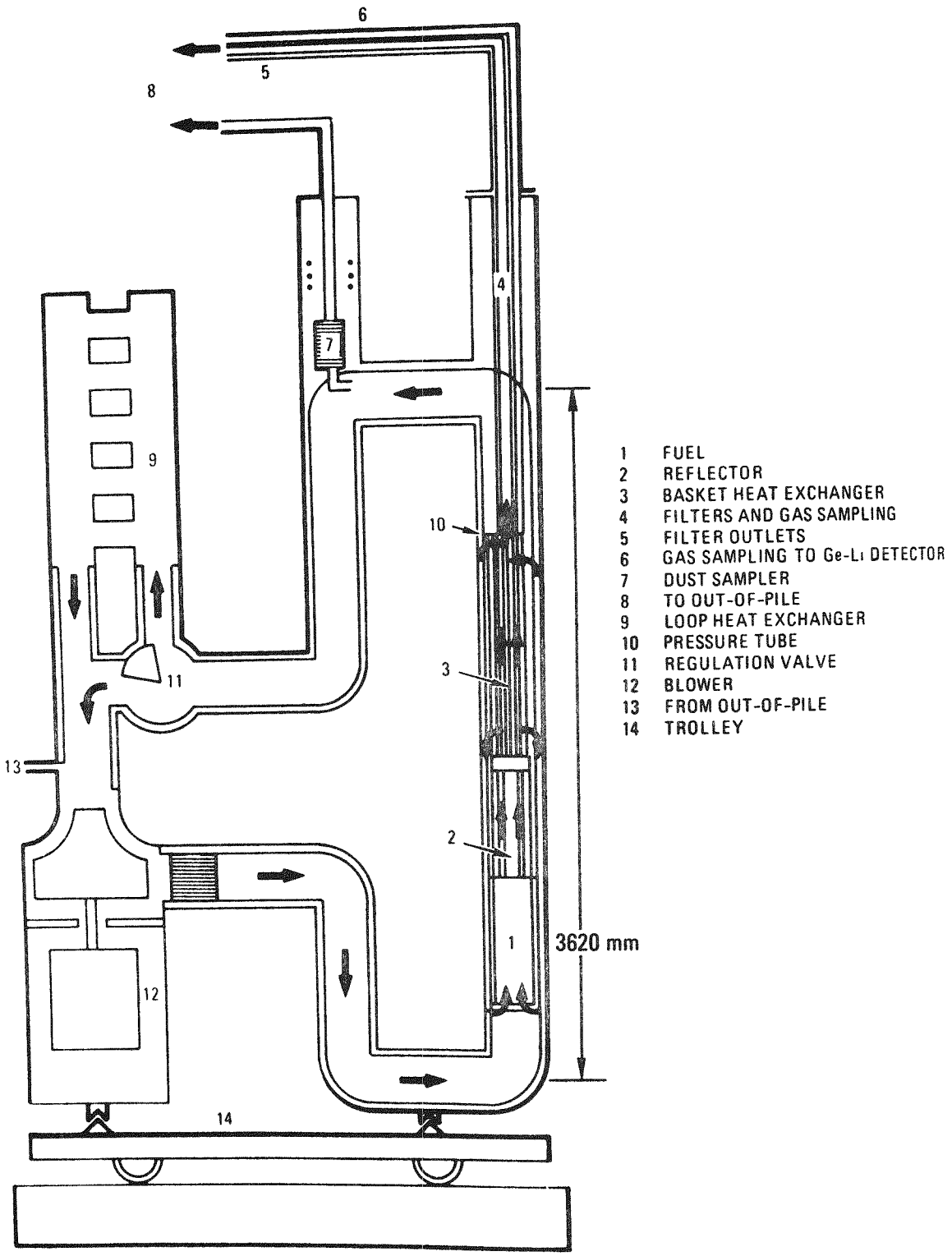

Fig. 4-2. CPL-2 loop schematic with loop flow

The cylindrical fuel element, shown in Fig. 4-3, was used in the CPL-2 tests as a representative portion of an LHTGR fuel block. The test element was 117 mm in diameter and 793 mm long and was fabricated from Pechiney P_3JHAN graphite. Seven coolant channels and 12 fuel holes were provided. Each fuel hole was loaded with 15 fuel rods, each 50 mm long. Therefore, the fuel element was identified by 15 layers, each layer containing one fuel rod in each of the 12 holes. The fuel used was Dragon-type UO_2 TRISO particles having a 12% enrichment and a porosity of approximately 20%. A known source of fission product release was provided by seeding certain fuel rods with a predetermined fraction of uncoated (bare) fuel particle kernels. As shown in the fuel element schematic in Fig. 4-3, all the fuel rods in layers 10 and 11 were seeded with 4% bare kernels, these being the layers where the peak fuel temperatures were expected to occur. Bare-kernel-seeded rods were also loaded in cooler regions of the fuel element (except in CPL-2/3) as shown in Fig. 4-3, in order to determine possible temperature effects on fission product release.

The reflector block, shown schematically in Fig. 4-4, was also made from Pechiney graphite and measured 110 mm in diameter and 793 mm in length. As shown in this figure, two H-327 graphite rods, char-loaded under vacuum, were inserted in the CPL-2/1 reflector in an attempt to study the influence of transverse flow on the transport of fission products.

The straight tube counterflow heat exchanger - recuperator (Fig. 4-5) was designed to fulfill two main purposes: (1) to permit high-temperature operation of the fuel element without imposing excessive thermal stresses on other loop components, and (2) to simulate surface and temperature conditions of the plateout surfaces in an LHTGR. The heat exchanger - recuperator consisted of 186 tubes, 4 mm I.D., 4.5 mm O.D., and 1250 mm long, hexagonally arranged inside an 86-mm-diameter cylindrical shell. Several steel types, including the French equivalents of T22 (2-1/2 Cr - 1 Mo), SS410, SS347, Hastelloy B, and Incoloy 800, were used in the fabrication of the tubes. Since the T22-like and stainless steel tubes could not withstand the helium temperatures at the tube-side inlet (bottom) region of the heat exchanger - recuperator, half tubes of these alloys were joined to

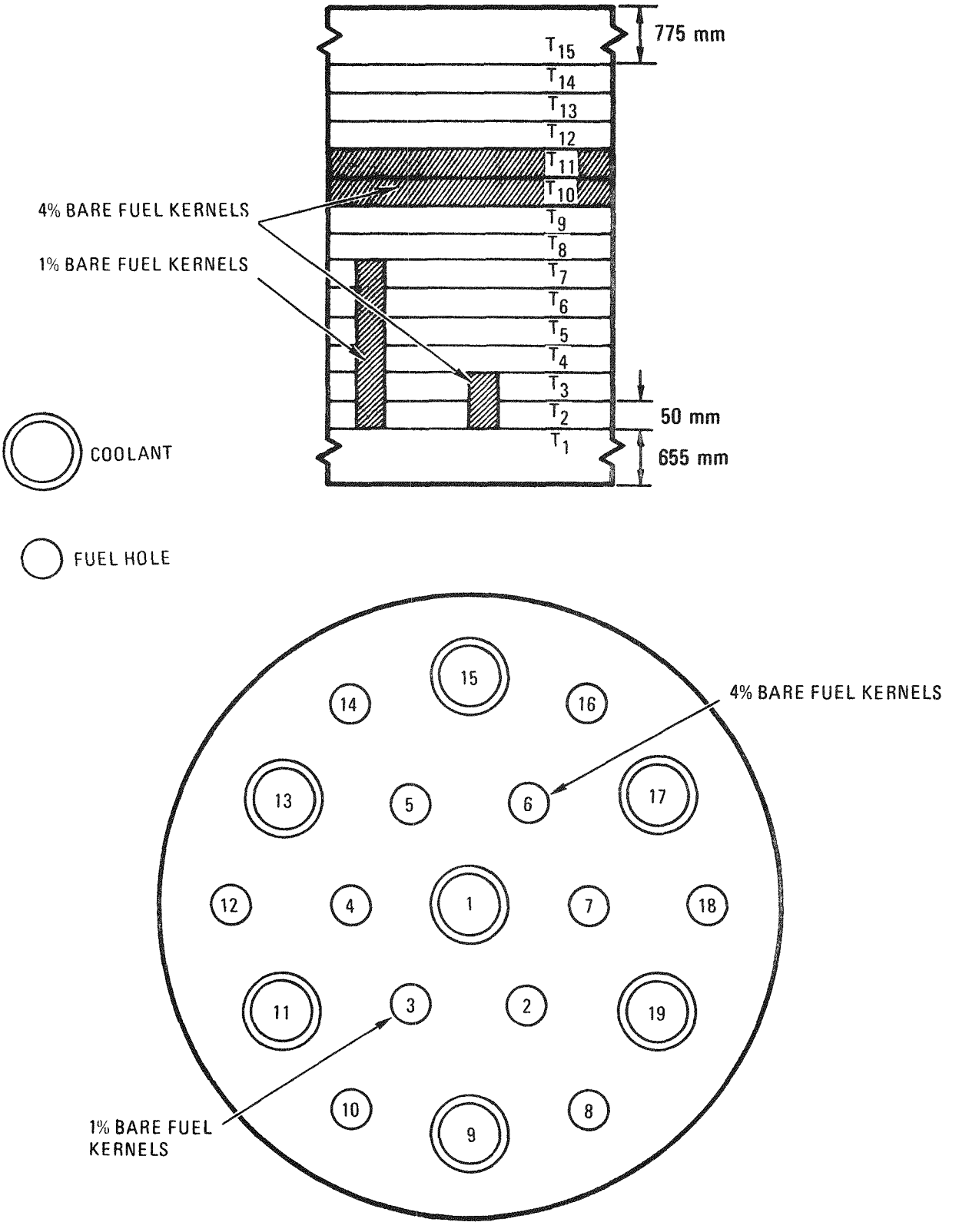

Fig. 4-3. CPL-2 fuel element

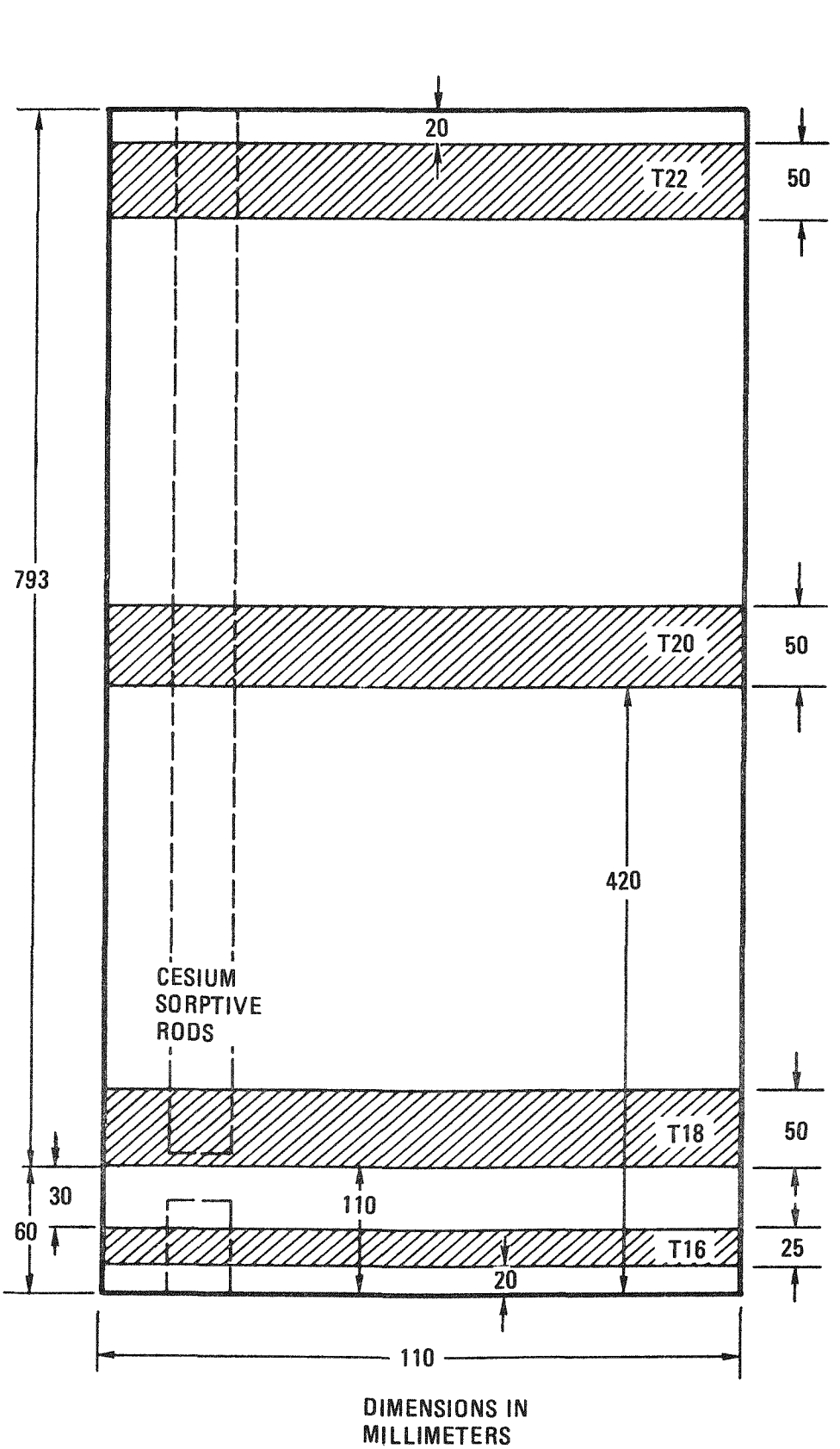

Fig. 4-4. CPL-2 reflector block

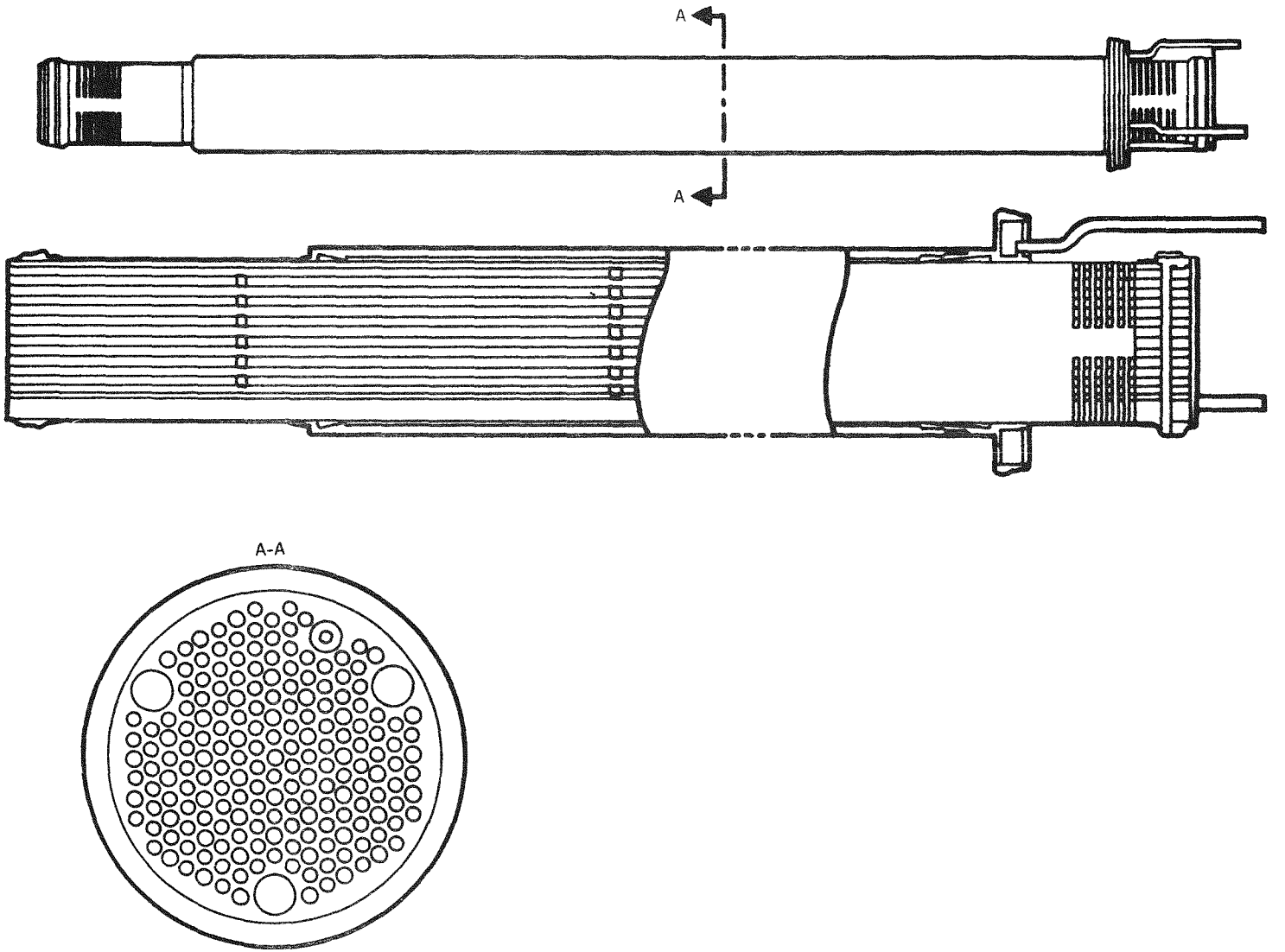

Fig. 4-5. CPL-2 heat exchanger - recuperator

half tubes of Incoloy 800 by means of a welded sleeve. Each steel type was represented by an as-received tube (i.e., no pretreatment other than degreasing was performed on the tube) and a preoxidized tube or half tube. This was done to determine the influence, if any, of the state of the metal surface on the deposition of condensible fission products. The majority of the tubes in the heat exchanger - recuperator were as-received Incoloy 800.

During loop operation, helium coolant and graphite temperatures were measured at various locations in the test section. Two plateout probes and associated filters, one opening at the inlet and the other at the outlet of the tube side of the heat exchanger - recuperator, permitted determination of fission product release from the fuel element and total deposition of condensible fission products on heat exchanger - recuperator tube surfaces. To maintain prescribed coolant moisture and oxidant levels, precise amounts of water and/or hydrogen were injected into the helium. All coolant impurities were monitored and recorded during irradiation. This information was used to study the corrosion of the fuel and reflector block graphite. In addition, a cascade impactor dust analyzer was located downstream of the test section as shown in Fig. 4-2, which provided a measure of the amount and size distribution of dust being carried around the loop by the coolant flow.

Nominal loop operating conditions for all four test loops are summarized as follows:

Mass flow rate	0.088 kg/s
Average coolant pressure	5.4 MPa
Fuel element coolant inlet temperature	813 K
Reflector block coolant outlet temperature	1017 K
Peak fuel centerline temperature	1573 K
Burnup	<1% FIMA
Fuel block average power	105 kW (th)
Total oxidant level in coolant	10 ppm

Fission Product Methods Verification Using CPL-2/1 Operational and PIE Results. GA design methods were used to calculate fission product transport in the CPL-2/1 loop. A significant part of the basic input data used in this analysis, including diffusion coefficients and sorption isotherms, was measured on materials present in the test loop. In cases where laboratory test data were not available, the GA Design Data Manual (Ref. 4-7) was employed. The results of the GA design methods calculations and comparison with measured values for fission gas release (Kr, Xe), metallic fission product release (Cs), and plateout (Cs, I) are discussed below.

Fission Gas Release

The design method given in Refs. 4-2 and 4-7 was used to calculate the fractional release, R/B (release rate divided by birth rate), of the fission gases krypton and xenon. To determine the temperature dependence of R/B, fractional releases and activation energies for the reference nuclides Kr-85m and Xe-138 were obtained from TRIGA irradiations of a CPL-2 fuel rod containing a nominal 4% bare kernels. Four different irradiation temperatures were used: 1173, 1273, 1373, and 1573 K. With these data and the assumption that all fission gas release came from bare kernels only, the R/B of Kr-85m and Xe-138 for the bare kernels in the CPL-2/1 fuel element was computed. In addition, the fractional releases of these nuclides were recalculated using the R/B (1373 K) and activation energy values for GA reference failed fuel particles given in Ref. 4-7.

Measurements of R/B for the CPL-2/1 loop were made five times during the course of irradiation. The values for Kr-85m and Xe-138 are plotted versus the effective full power days (EFPD) of operation in Figs. 4-6 and 4-7, respectively. It can be seen that the R/B for both nuclides decreased significantly during irradiation. Other nuclides not shown behave analogously. Two lines have been drawn on each plot representing (1) values of R/B calculated using the data derived from TRIGA irradiation of the CPL-2 sister fuel rod (upper line) and (2) values of R/B calculated using reference GA data. By comparing the experimental and calculated

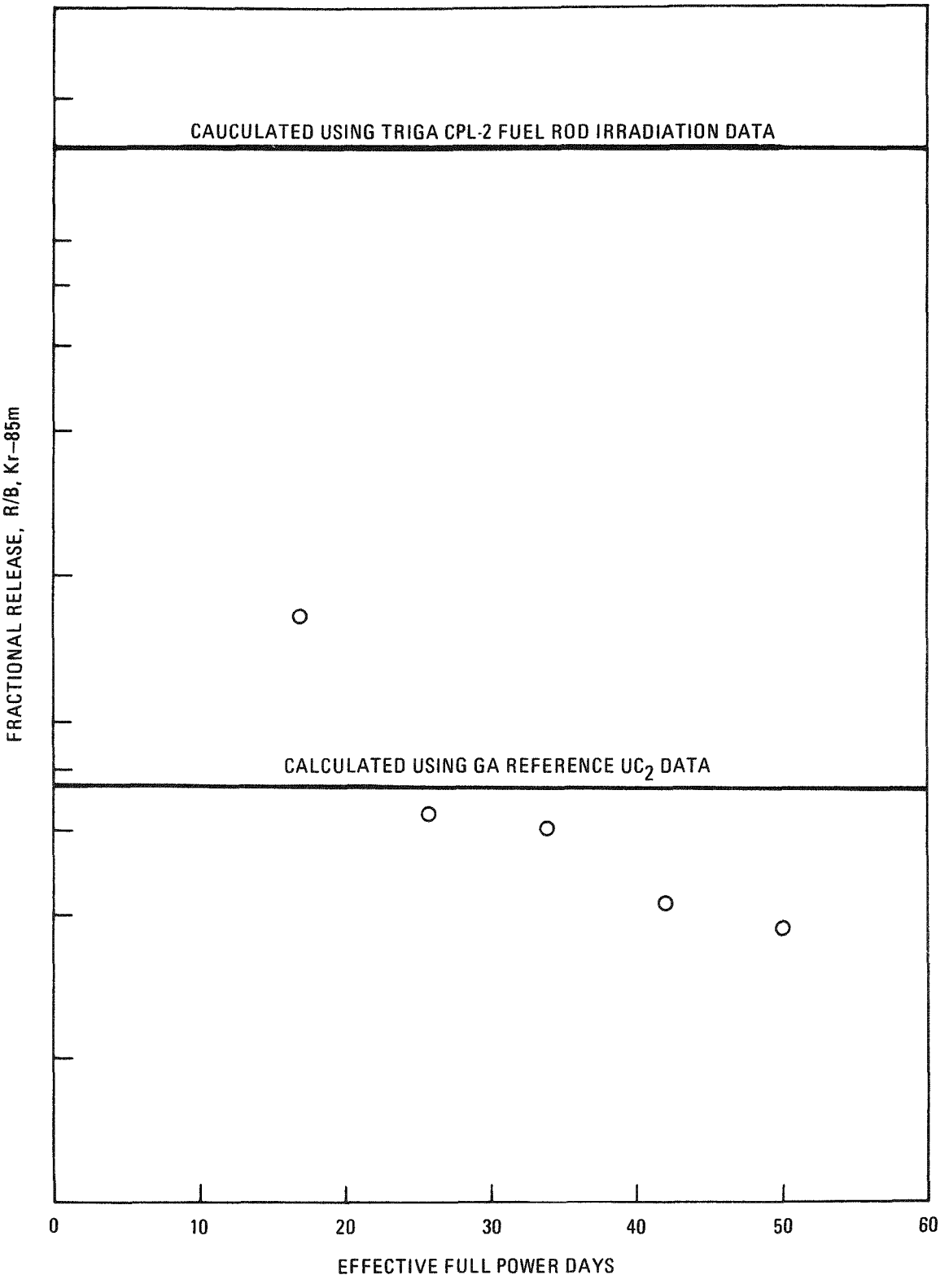

Fig. 4-6. Plot of log R/B (Kr-85m) versus effective full power days of irradiation for the CPL-2/1 test

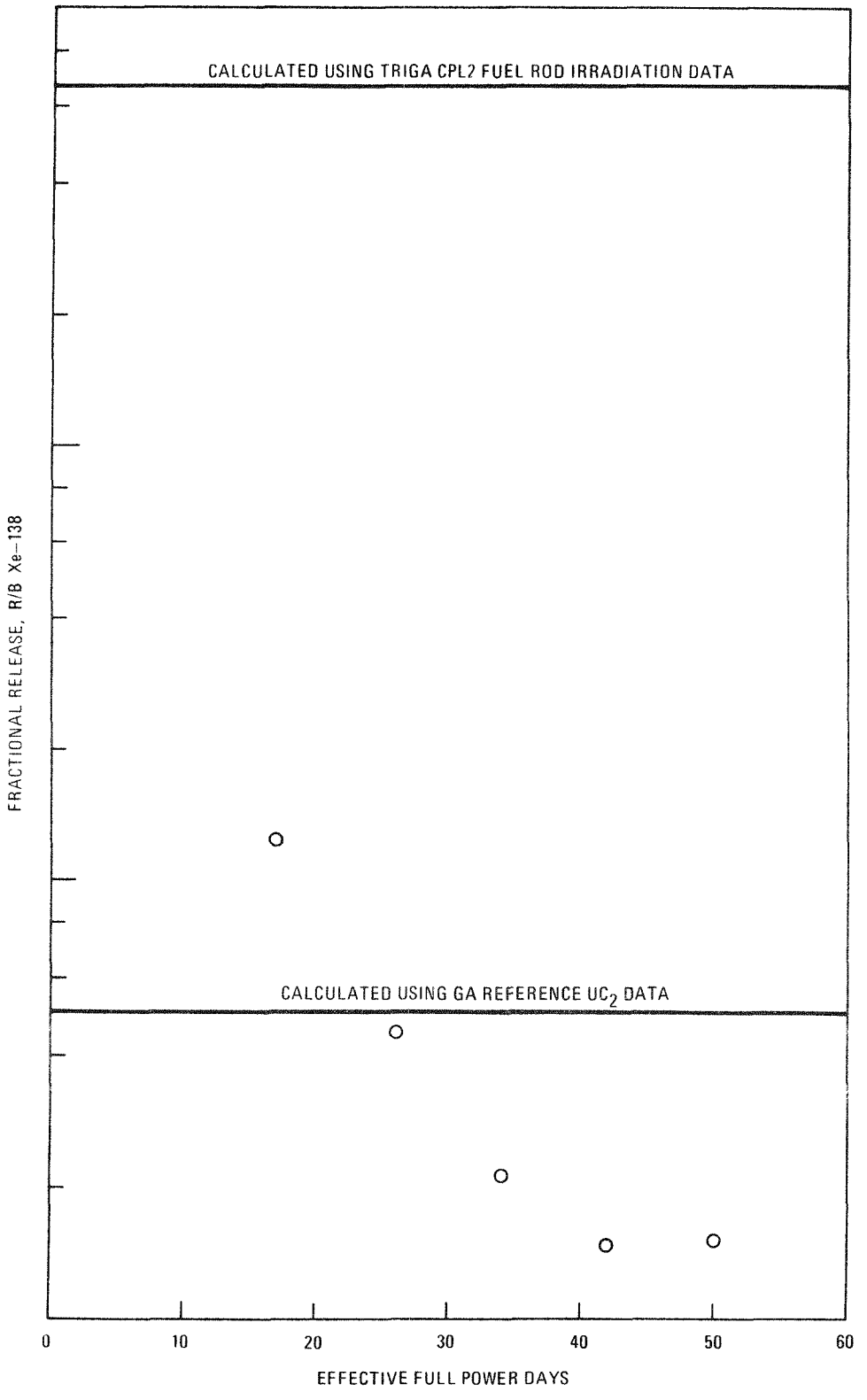

Fig. 4-7. Plot of log R/B (Xe-138) versus effective fuel power days of irradiation for the CPL-2/1 test

results, it is possible to speculate that the highly porous CPL-2 fuel kernels densified during irradiation at high temperatures. Therefore agreement of the TRIGA results and in-pile loop data measured after ∿20 minutes of irradiation would be expected since these data represent the initial high release that occurred prior to any densification of the bare kernel. On the other hand, use of the data for GA reference failed fuel particles yielded much lower values of R/B since the kernels of these particles are initially much denser than those irradiated in the CPL-2 fuel.

The fractional releases of the other krypton and xenon isotopes, specifically Kr-87, Kr-88, Kr-89, Xe-133, Xe-135, Xe-135m, and Xe-137, were calculated from the values for Kr-85m and Xe-138. Figures 4-8 and 4-9 show the plots of ln (R/B) versus ln ($\tau_{1/2}$) for the krypton and xenon isotopes, respectively, taken from the first measurement, made near the midpoint of the irradiation time, and the last measurement, made just before the irradiation was terminated. Also shown are the predicted R/B values using the CPL-2 sister fuel rod TRIGA irradiation data and the reference GA data. Least-squares fits of the two sets of data for both krypton and xenon were performed to determine the slopes of the lines which best fit the data. The results are given in Table 4-3. It can be seen that the slopes appear to decrease in going from the first measurements to the last. However, they remain greater than the theoretical value of 0.5 (for R/B $\leq$ 0.1). It can be speculated that the deviation of the predicted and observed slopes is due to the initial porosity of the fuel kernels which affords a greater void fraction to trapped gases. As the kernels densified, the measured R/Bs more closely followed a square root of half-life law.

Metallic Fission Product Release

The predicted release of Cs-137 from the CPL-2/1 fuel element was calculated using FIPERQ (Refs. 4-8, 4-9). By assuming that all release came from the bare kernels, as was done for the gaseous fission products, release calculations were performed for the seeded fuel rods only. In addition, it was also assumed that no release occurred at the outer circumference of the fuel element and that no re-deposition of released Cs-137

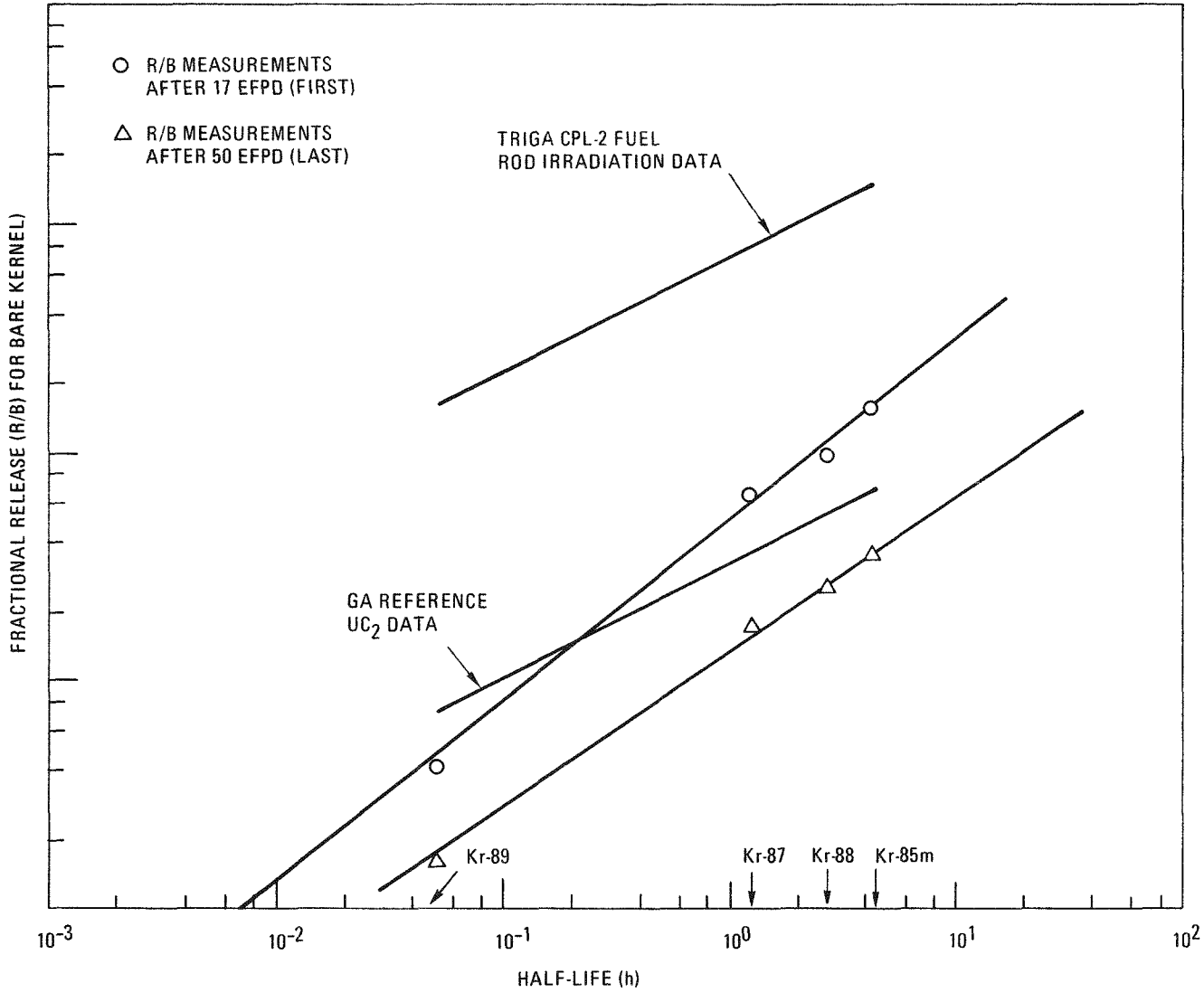

Fig. 4-8. Plot of log $(R/B)_i$ versus $\sqrt{\tau_{1/2}}$ for krypton isotopes released from the CPL-2/1 fuel element

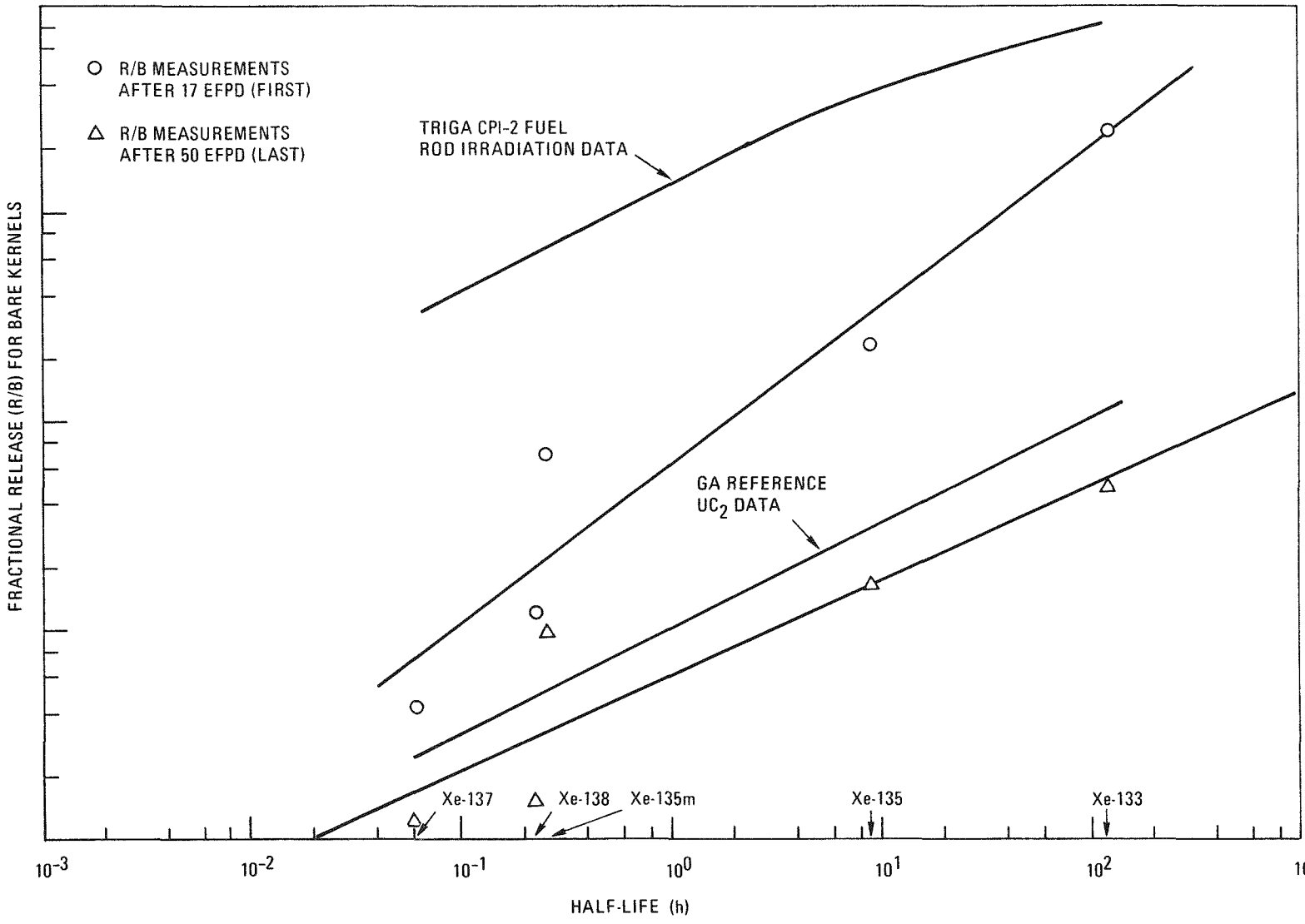

Fig. 4-9. Plot of log $(R/B)_i$ versus $\sqrt{t_{1/2}}$ for xenon isotopes released from the CPL-2/1 fuel element

TABLE 4-3
SLOPES OF LEAST-SQUARES FIT OF ln (R/B) VERSUS ln ($\tau_{1/2}$) DATA

Fission Gas	Slope of Least-Squares Fit to Data Measured After 17 EFPD	Slope of Least-Squares Fit to Data Measured After 50 EFPD
Krypton	0.79	0.67
Xenon	0.76	0.45

occurred on coolant channel walls. The input data for these calculations included sorption isotherms determined from measurements on Pechiney graphite and French fuel rod matrix material (Ref. 4-10), and the diffusion coefficient of cesium in H-451 graphite given in Ref. 4-7. Tests performed at GA showed that cesium is transported through Pechiney graphite at about the same rate as in H-451 graphite. The cesium release characteristics of the CPL-2 Dragon-type bare kernels given in Ref. 4-11 were used to define the source strength. This behavior is summarized by the curves shown in Figs. 4-10 and 4-11. Figure 4-10 is an Arrhenius plot of the "reduced diffusion coefficient" D_1 ($D_1 = D/\alpha^2$, where α is a characteristic diffusion radius) for the bare kernel versus the reciprocal fuel temperature. Having determined the reduced diffusion coefficient of cesium in the bare kernels, the fractional release, F, as a function of irradiation time was derived from the curve in Fig. 4-11. For conservatism, a single constant fractional release value, based on the total irradiation time of the CPL-2/1 fuel element, was used in the FIPERQ calculations.

Comparisons were to be made of the calculated and measured values of four essential release parameters: fractional release, partition coefficient (ratio of the matrix surface concentration to the graphite fuel hole surface concentration), radial profile in the graphite web, and the total released activity. Since measurements of the amount of activity remaining in the bare kernels and matrix are not yet available, the actual and predicted fractional releases of Cs-137 from the kernels cannot be compared at this time. In the case of the partition coefficient, measurements of the actual EOL value for two fuel rods (one in fuel element layer 3 and the other in layer 11) show the calculated value underpredicts the measured partition coefficient by more than an order of magnitude. The measured and FIPERQ-predicted Cs-137 radial profiles for three representative fuel element layers (see Fig. 4-3) are shown in Figs. 4-12 through 4-14. It can be seen that as the fractional release and graphite temperatures increased from fuel element layer 3 (Fig. 4-12) to layer 11 (Fig. 4-14), the shape of the measured profiles at the outer boundary changed, whereas the predicted profiles maintained the same form, as dictated by the Fick's-law-type diffusion model in the code. It is important to observe, however, that the

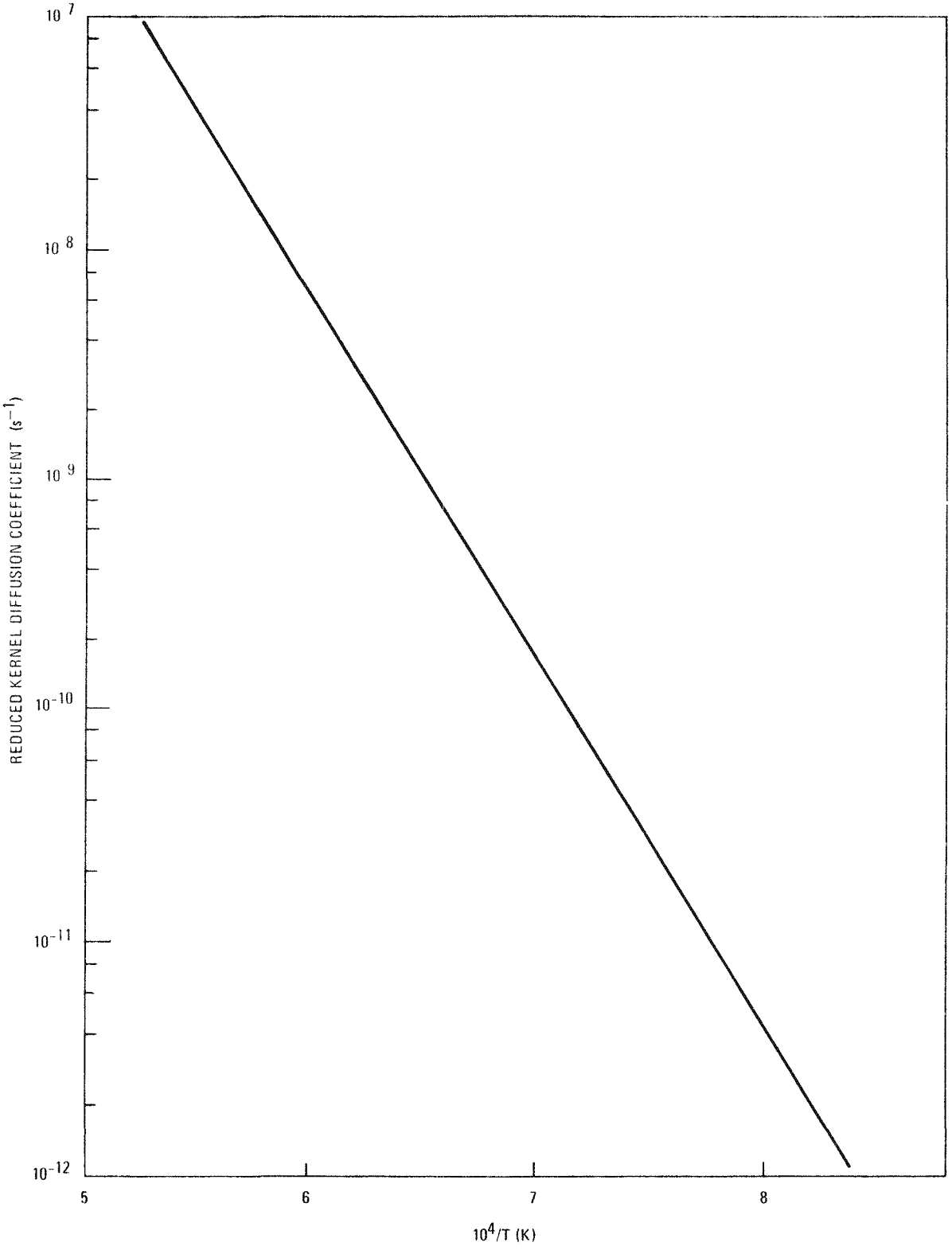

Fig. 4-10. Plot of reduced kernel diffusion coefficient for cesium versus 1/T for Dragon UO_2 fuel kernels

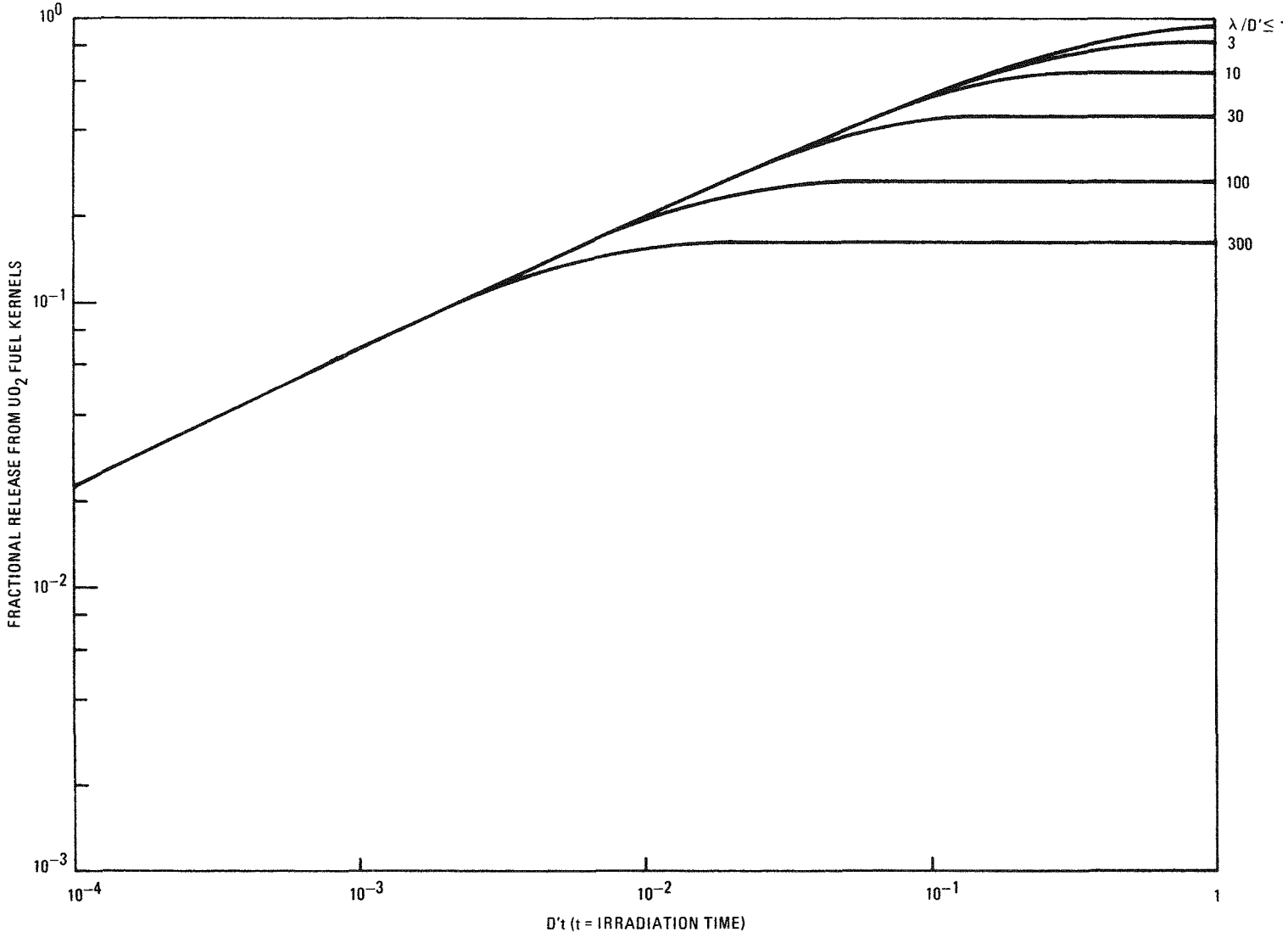

Fig. 4-11. Plot of fractional release of metal nuclide versus dimensionless time for Dragon UO_2 fuel kernels

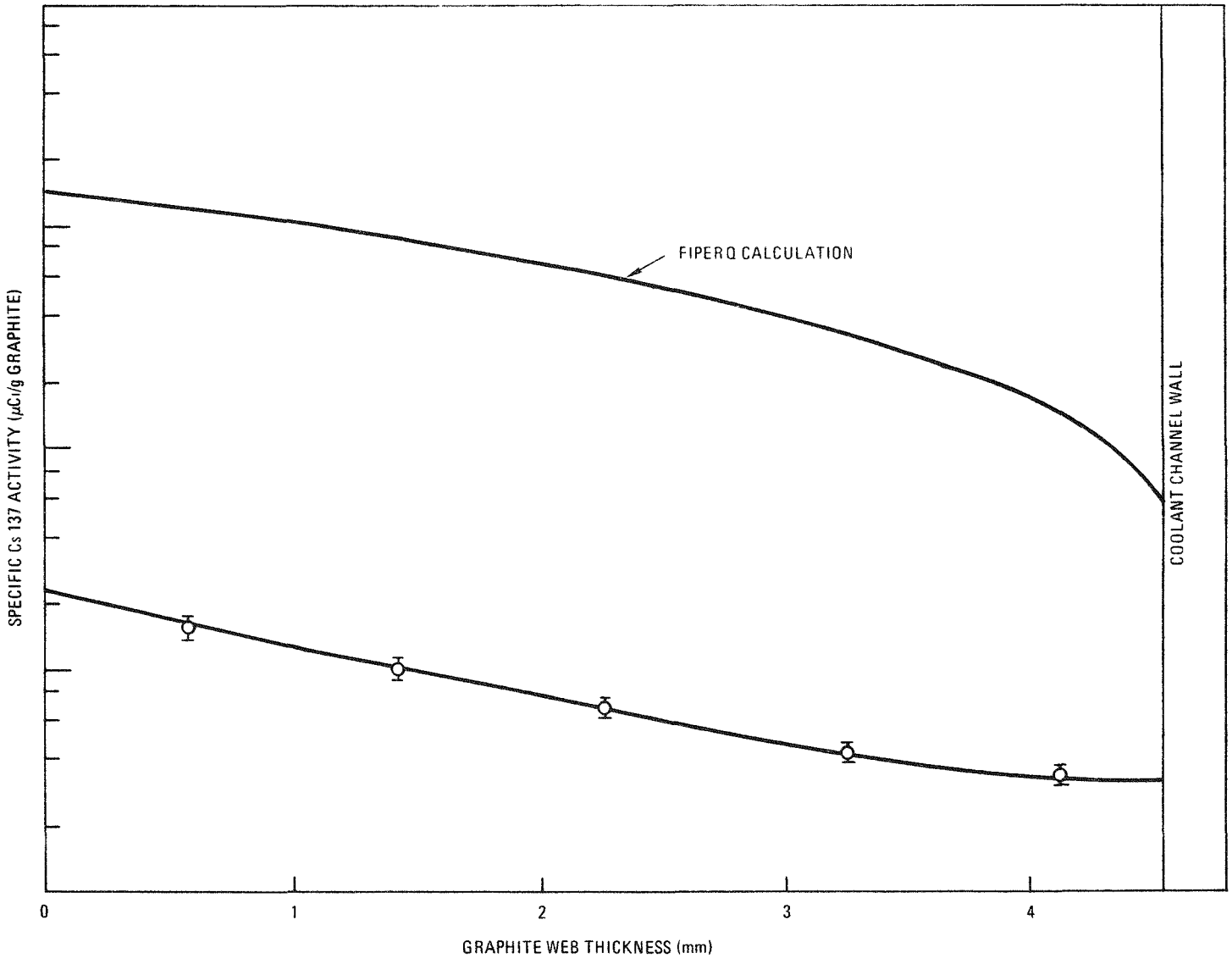

Fig. 4-12. Predicted and observed radial profiles of Cs-137 in CPL-2/1 graphite fuel body at layer 3 (fuel hole 6).

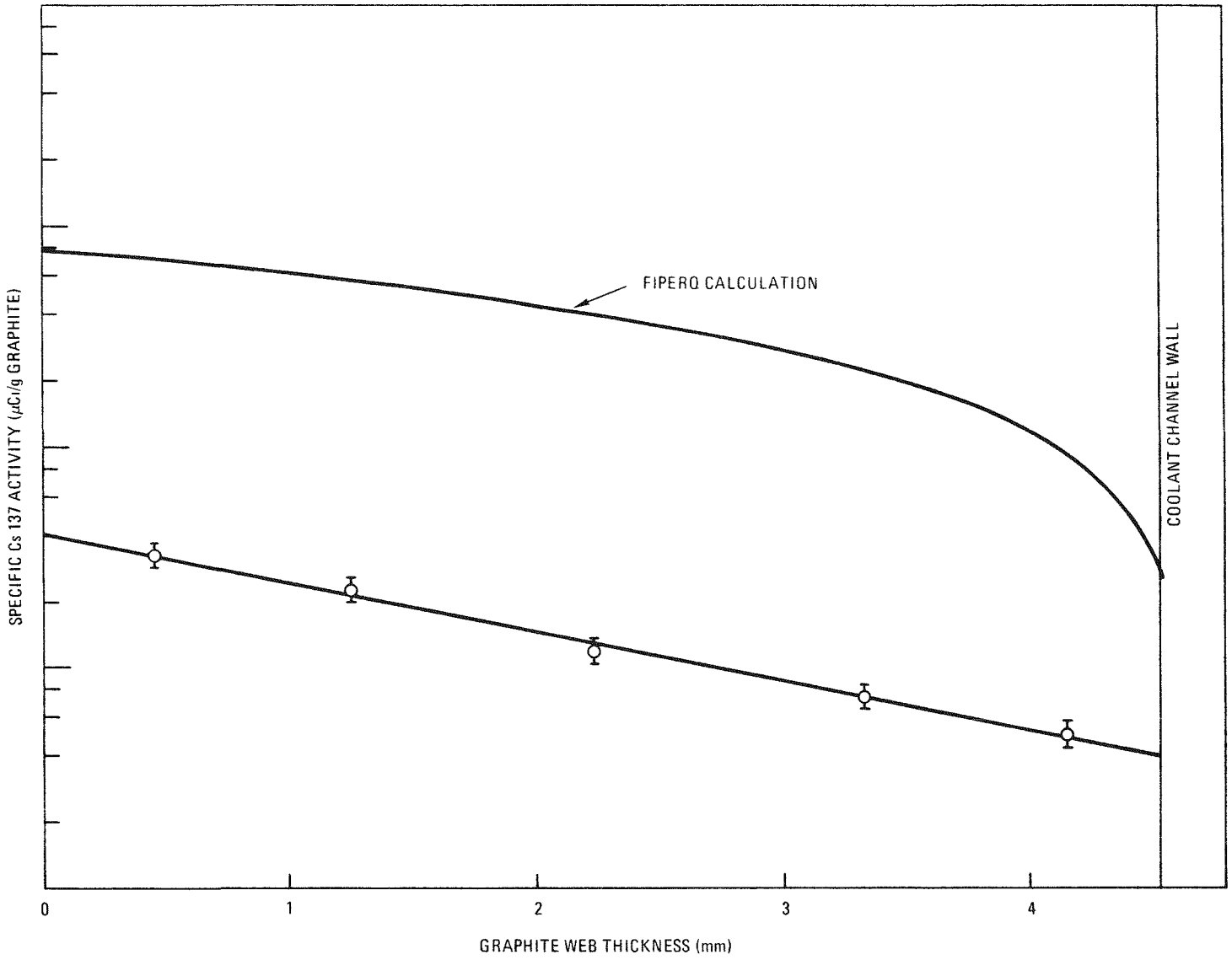

Fig. 4-13. Predicted and observed radial profiles of Cs-137 in CPL-2/1 graphite fuel body at layer 5 (fuel hole 3)

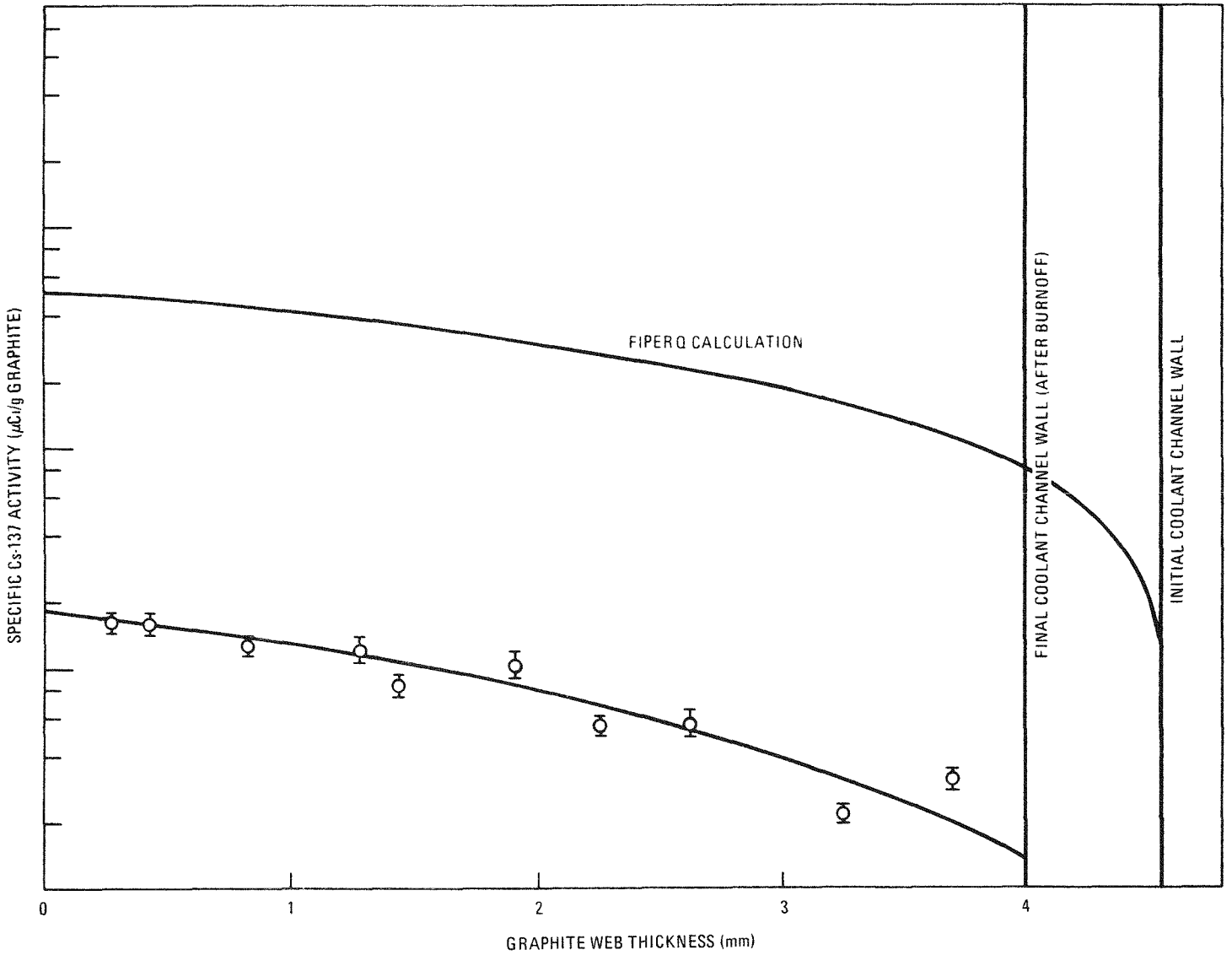

Fig. 4-14. Predicted and observed radial profiles of Cs-137 in CPL-2/1 graphite fuel body at layer 11 (fuel hole 7)

shape of the calculated and measured profiles in layer 11 do appear to agree, indicating that the relative loading of cesium in graphite in this region of the fuel element exhibited behavior that could be explained using Fick's law. A comparison of the predicted and actual total releases of Cs-137 (determined from the heat exchanger - recuperator inlet plateout probe) showed excellent agreement, although the radial profiles were overpredicted by 1 to 2 orders of magnitude. The measured profile for layer 11 showed that approximately 10% to 15% of the graphite web was removed from the coolant channel surface due to oxidation during irradiation. This corrosion was not accounted for in the calculations since graphite oxidation is not included in the metallic fission product release design method.

From these results, it appears that compensating errors in the transport model used in FIPERQ and uncertainties in the input data have yielded a total Cs-137 release which agrees with the measured value while overpredicting the loading of the graphite web and underpredicting the partition coefficient. Comparison of the calculated and predicted fractional releases from the kernels remains to be performed once the data become available. For Cs-137, it seems that with the input data and methods used in the analysis, it is necessary to overload the fuel element graphite in order to arrive at the correct total release.

Condensible Fission Product Plateout

The design method code PAD (Ref. 4-12) was used to calculate the plateout of Cs-137 and I-131 on selected tubes in the CPL-2/1 heat exchanger - recuperator. As specified in Ref. 4-5, tube wall temperature distributions were checked at CEA and a recalculation of the heat exchanger - recuperator shell-side flow and heat transfer was performed jointly by CEA and GA, using a more detailed network model. The results of this analysis differed only slightly from that reported in Ref. 4-5, the most significant difference being a flattening of the temperature profile at the tube-side outlet due to a "no-flow" condition in this region. The sorption isotherms used in the plateout analysis were estimated from sorption data measured by CEA laboratories. A Henry's law fit was arbitrarily applied to

these data, which were taken at surface temperatures covering approximately the same range as experienced by the heat exchanger - recuperator tubes, i.e., 573 to 873 K. Sorption isotherms for cesium on preoxidized and as-received Incoloy 800 and on preoxidized SS347 and Hastelloy B were estimated. In the case of iodine, sorption isotherms were derived for preoxidized and as-received Incoloy 800 and SS347, preoxidized Hastelloy B, and as-received T22 (2-1/4 Cr - 1 Mo). A cross section of the heat exchanger - recuperator is shown in Fig. 4-15. The numbered tubes were analyzed with PAD. A comparison of calculated and measured plateout profiles for various representative tubes is presented below.

In the calculation of cesium plateout, the coolant concentration of Cs-137 entering the tubes was estimated from the measurement of Cs-137 activity in the heat exchanger - recuperator inlet plateout probe and filter. Figures 4-16 and 4-17 show a comparison of the predicted and measured profiles for tube 2 (as-received Incoloy 800) and tube B41 (as-received Incoloy 800 - preoxidized SS347), respectively. In both figures two profiles were calculated for the Incoloy 800 tube, one using the sorption isotherm for preoxidized Incoloy 800 and the other using the isotherm for as-received Incoloy 800. It can be seen that in both tubes the predicted profile on the as-received Incoloy 800 using the sorption isotherm for a preoxidized surface is in closer agreement with the measured profile than the predicted results using the isotherm for an as-received surface. In Fig. 4-17, the predicted and measured plateout on the SS347 tube show good agreement both in shape and magnitude.

The design method for computing the release of iodine assumes that iodine behaves like the fission gas xenon. Thereby, the fractional release of iodine is determined from the ln (R/B) versus ln ($\tau_{1/2}$) plot for xenon. As shown in the previous section on gaseous release, the fractional release of xenon, and therefore iodine, decreased significantly during irradiation. Consequently, a constant release rate of I-131 to be used in PAD calculations could not be determined. It is the intention that once the fission gas release data from the other loop irradiations are analyzed, a reasonable estimate of the fractional release of iodine can be obtained.

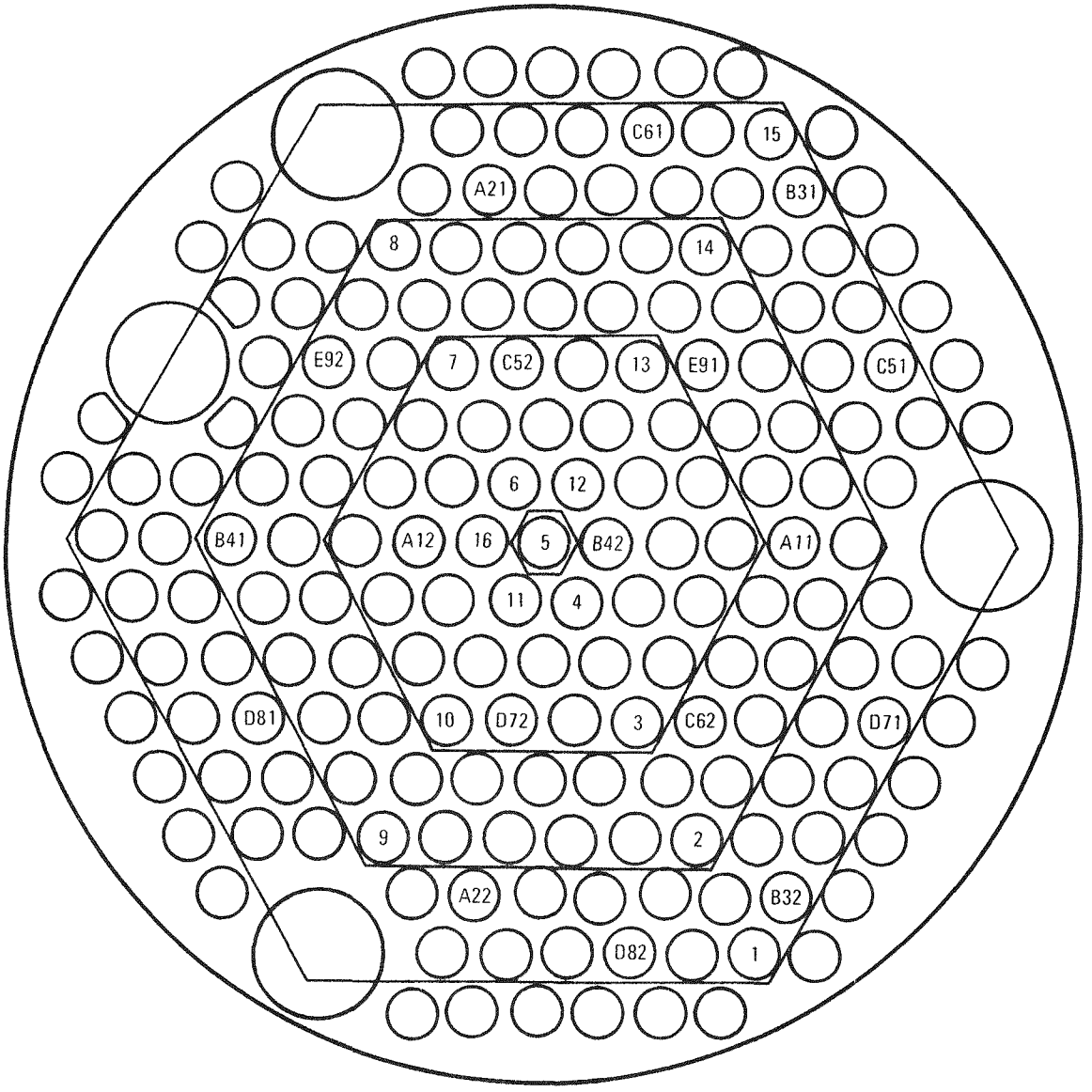

Fig. 4-15. CPL-2 heat exchanger - recuperator cross section; numbered tubes were gamma scanned

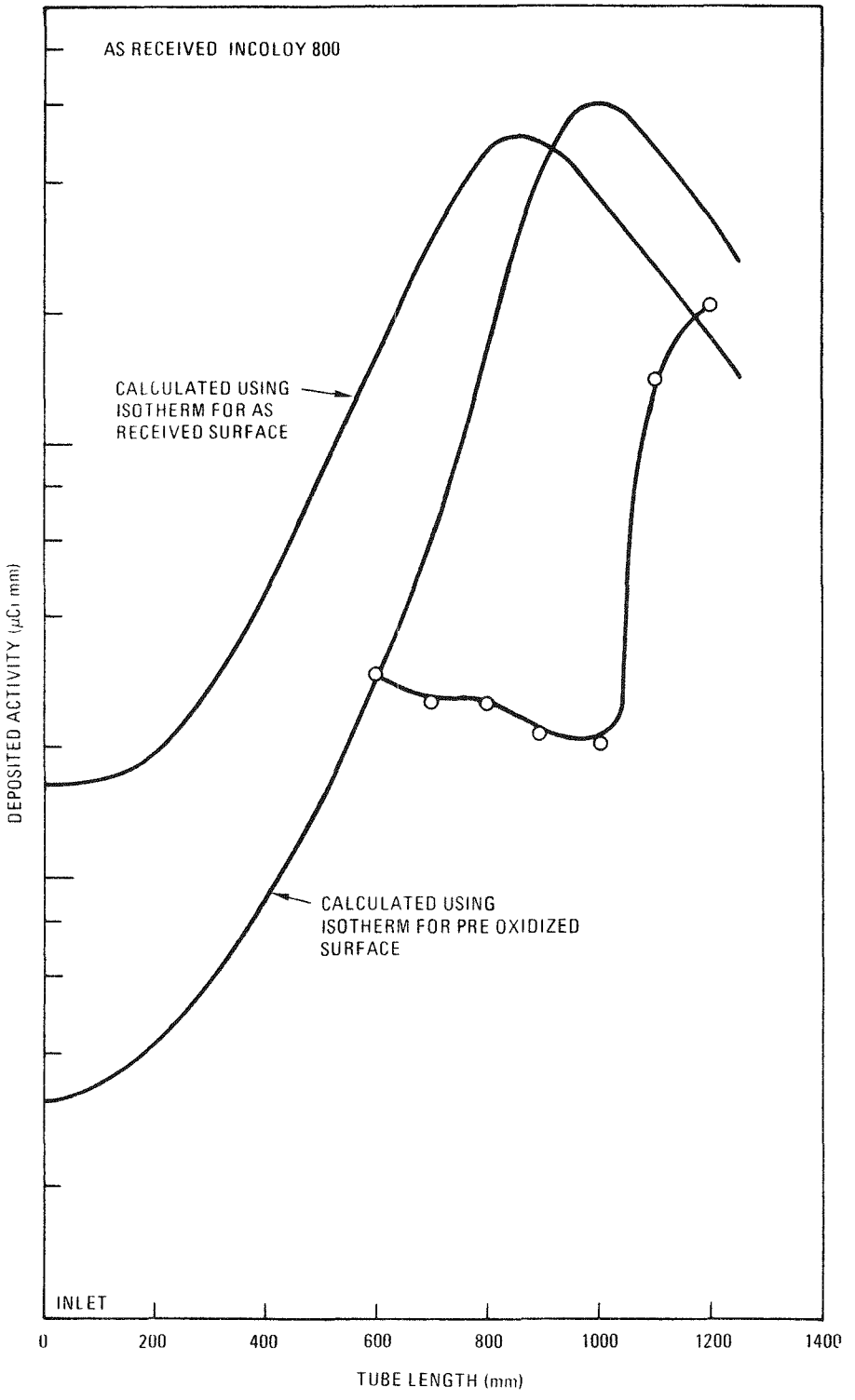

Fig. 4-16. Measured and predicted Cs-137 activity along the length of tube 2 of the CPL-2/1 heat exchanger - recuperator

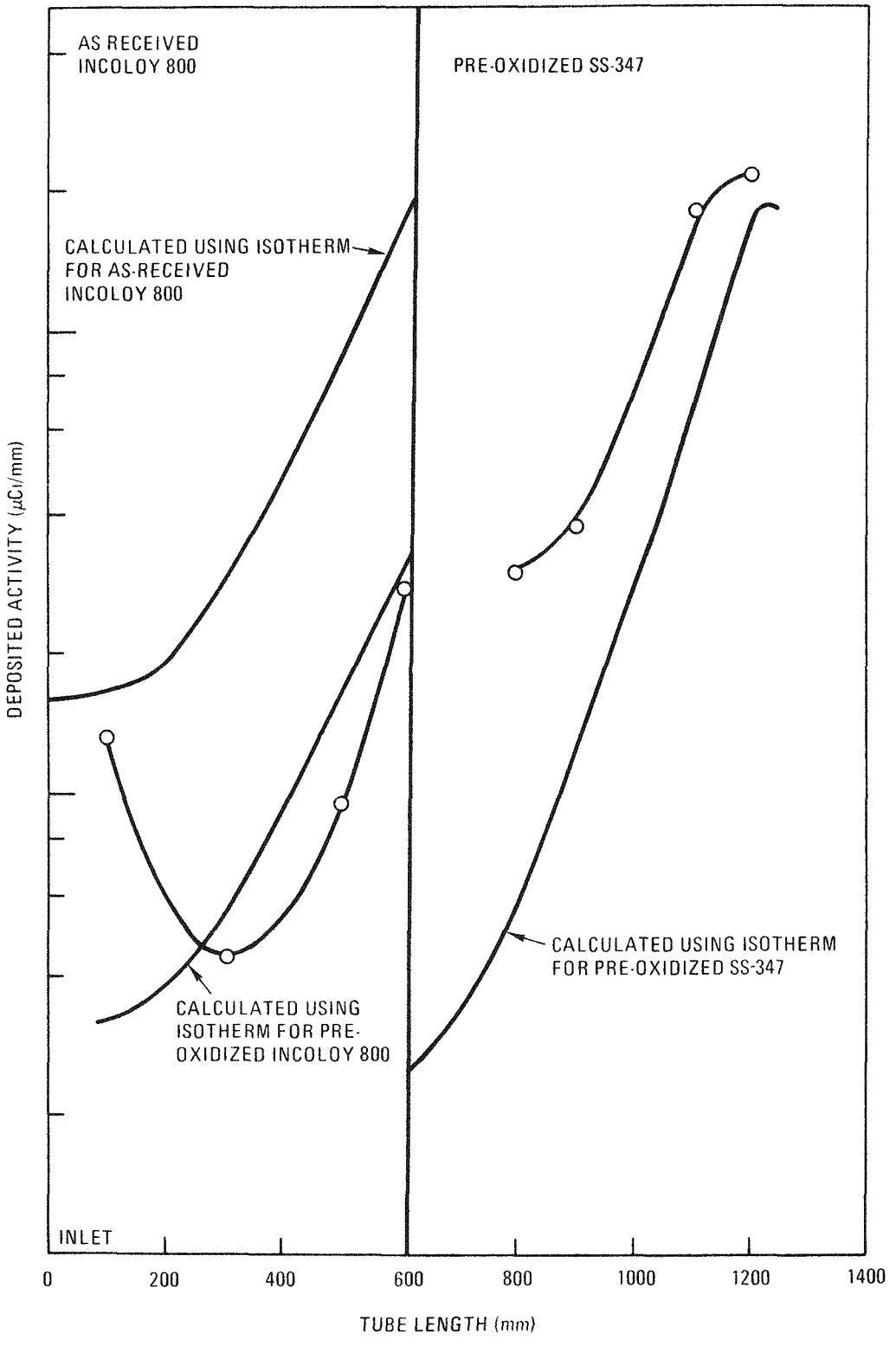

Fig. 4-17. Measured and predicted Cs-137 activity along the length of tube B41 of the CPL-2/1 heat exchanger - recuperator

For this analysis, however, it was assumed that the bare kernel fractional release of I-131 for the duration of the test was 1, i.e., all the iodine born in the bare kernels was released to the coolant. Figures 4-18 and 4-19 show a comparison of the calculated and measured I-131 plateout for tube 2 (as-received Incoloy 800) and tube B31 (as-received Incoloy 800 - as-received SS347), respectively. Two profiles were calculated for both the Incoloy 800 and SS347 tubes using the isotherms for the preoxidized and as-received surfaces. Since the value of the coolant concentration of iodine entering the tubes used in the calculations was arbitrarily chosen, the results can only be judged qualitatively at this time. On this basis it is apparent that the plateout calculated using the isotherms for preoxidized Incoloy 800 or SS347 does not differ greatly from the profiles calculated using the isotherms for as-received Incoloy 800 or SS347. In addition, it appears that the sorption isotherms used in the analysis did exhibit the proper wall temperature dependence given that the shapes of the predicted and measured plateout profiles are in general agreement.

The results of this plateout analysis indicate that the deposition process modeled in PAD is adequate for describing plateout on internal reactor surfaces. However, it is essential to have accurate fission product source terms, reliable wall temperatures, and precise and appropriate sorption isotherms in order to accurately predict the plateout activity levels and distribution.

Analysis of Fission Product Behavior in the Saclay Spitfire Loop Test SSL-1

The SSL-1 test was the first of a series of in-pile tests selected for use in verifying HTGR fission product design methods under the Fission Product Code Validation subtask (Ref. 4-4). Preliminary comparisons of observed cesium release and that predicted using FIPERQ have been reported earlier (Ref. 4-5). This section presents a more detailed review of the input and an assessment of the validation results.

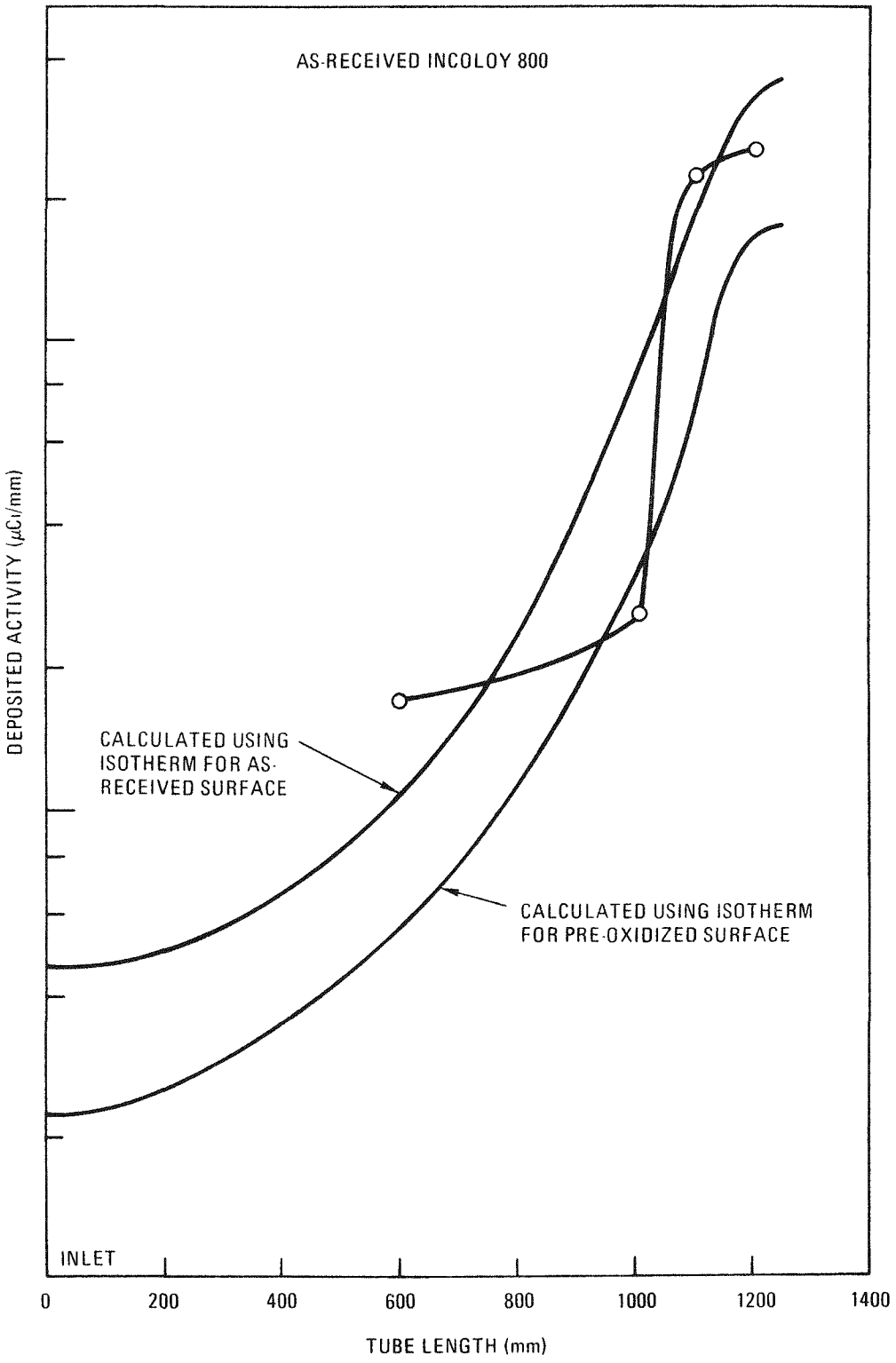

Fig. 4-18. Measured and predicted I-131 activity along the length of tube 2 of the CPL-2/1 heat exchanger - recuperator

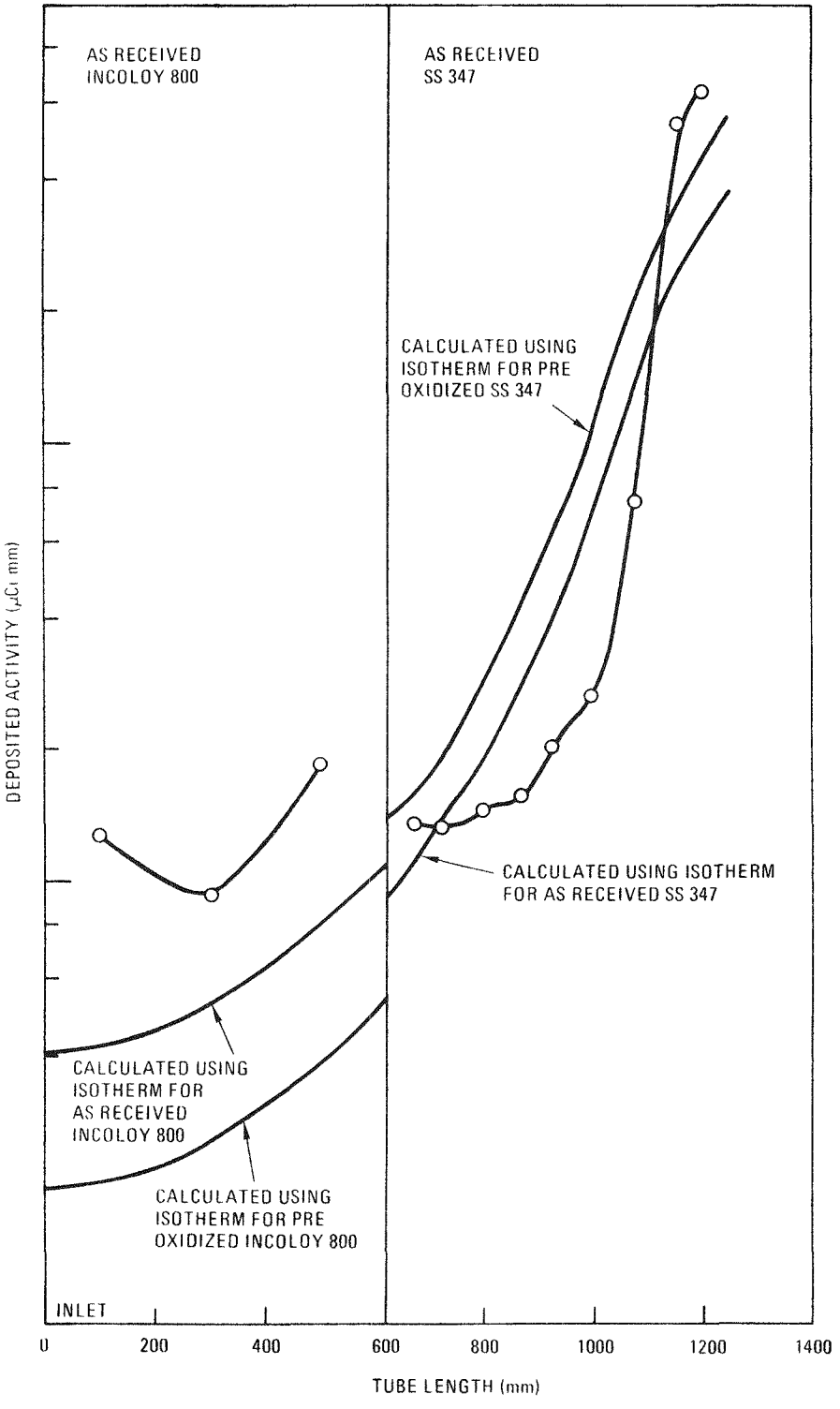

Fig. 4-19. Measured and predicted I-131 activity along the length of tube B31 of the CPL-2/1 heat exchanger - recuperator

Fission Metal Release Calculations. SSL-1 was designed to test the irradiation performance of $(8Th,U)O_2$ fissile (93% enriched uranium) and ThO_2 fertile fuel. The test ran for 120 EFPD at which time the irradiation was stopped due to unexpectedly high fission gas release. The mean operating conditions for the loop are presented in Table 4-4. The CEA carried out a PIE of the fuel element and selected circuit components, in part to ascertain the location of fission products in the loop.

Meaningful comparison of predicted and observed fission metal behavior can be carried out when the following input are well-defined:

1. Fission product source.

2. Fuel and graphite temperatures.

3. Integrated fission metal plateout downstream of the fuel.

4. Reference input data describing metal diffusivity in fuel particle kernel and coating materials, metal diffusivity in graphite, and appropriate sorption isotherms for matrix material and graphite.

The selected input for the FIPERQ analysis of cesium release from SSL-1 are presented below.

Source

SSL-1 was designed as a fuel performance test. As such, a known source of fission metals, i.e., bare kernels, was not included in the fuel element. The lack of a well-defined source proved to be one of the most troublesome aspects of the cesium analysis. To carry out FIPERQ calculations, it was necessary to define the source strength. This was done in three ways:

TABLE 4-4
MEAN OPERATING CONDITIONS FOR THE SSL-1 LOOP TEST

Variable	1[a] (bottom)	2	3	4	5	6	7	8	9 (top)
Axial power factor (APF)	0.74	0.84	0.92	0.98	1.0	0.97	0.92	0.83	0.73
Power (mW/mm^3)[b]	45.9	52.1	57.1	60.8	62.1	60.2	57.1	51.1	45.3
Time-average temperature (K)									
Fuel rod centerline	1403	1442	1465	1482	1477	1449	1400	1328	1235
Fuel rod surface	1295	1315	1330	1337	1329	1304	1264	1206	1131
Graphite fuel hole surface	1212	1224	1234	1235	1226	1202	1165	1114	1064
Graphite coolant hole surface	1168	1172	1177	1175	1164	1141	1106	1061	1003
Helium coolant	918	903	887	871	854	834	822	808	745
He coolant flow in 12-mm hole (mol/s)	2.3								
He coolant pressure [MPa (atm)]	6.08 (60)								

[a] Rod layer

[b] $$\text{Power } (mW/mm^3) = \frac{(\text{mean element power})\ (\text{APF})\ (1.13)}{(\text{No. of rod stacks})\ (\text{volume of single fuel rod stack})}$$

$$= \frac{(14.5\ kW)\ (\text{APF})\ (1.13)\ (10^6\ mW/kW)}{(3)\ (9)\ (50\ mm)\ (195.6\ mm^2)} = 62.05\ (\text{APF})\ mW/mm^3$$

1. By defining the time-dependent particle failure fractions and the fractional release of cesium from failed oxide particles.

2. By assuming total release of cesium from failed oxide particles.

3. By assigning a cesium release fraction derived from the observed axial loading of Cs-137 in the fuel element graphite.

Particle Failure Fractions and Fractional Cesium Release. The EOL fraction of broken fertile particles was assumed to be zero. This result was based upon the observed fission gas release and upon PIE measurements of fertile particles from SSL-1 and other in-pile experiments. Examination of Fig. 4-20, which shows the in-pile $(R/B)_{loop}$ of Kr-85m during the six 20-day cycles of irradiation, revealed the following:

1. The initial $(R/B)_{loop}$ was quite low and well within the design expectations, indicating that contamination in the fuel was low.

2. The $(R/B)_{loop}$ started to rise very quickly during the irradiation such that shortly after the start of the fourth cycle ($\sim$65 EFPD), the $(R/B)_{loop}$ had increased to 1.2×10^{-3}.

3. The $(R/B)_{loop}$ showed a slowly decreasing value in time throughout the remainder of the irradiation.

Since extensive fission gas release was evident as early as the second cycle (>20 EFPD) and the fraction of fissions in the fertile particles was low (<25%) at 65 EFPD when the $(R/B)_{loop}$ had stabilized, it was assumed for the analysis that all particle failure took place in the fissile particles.

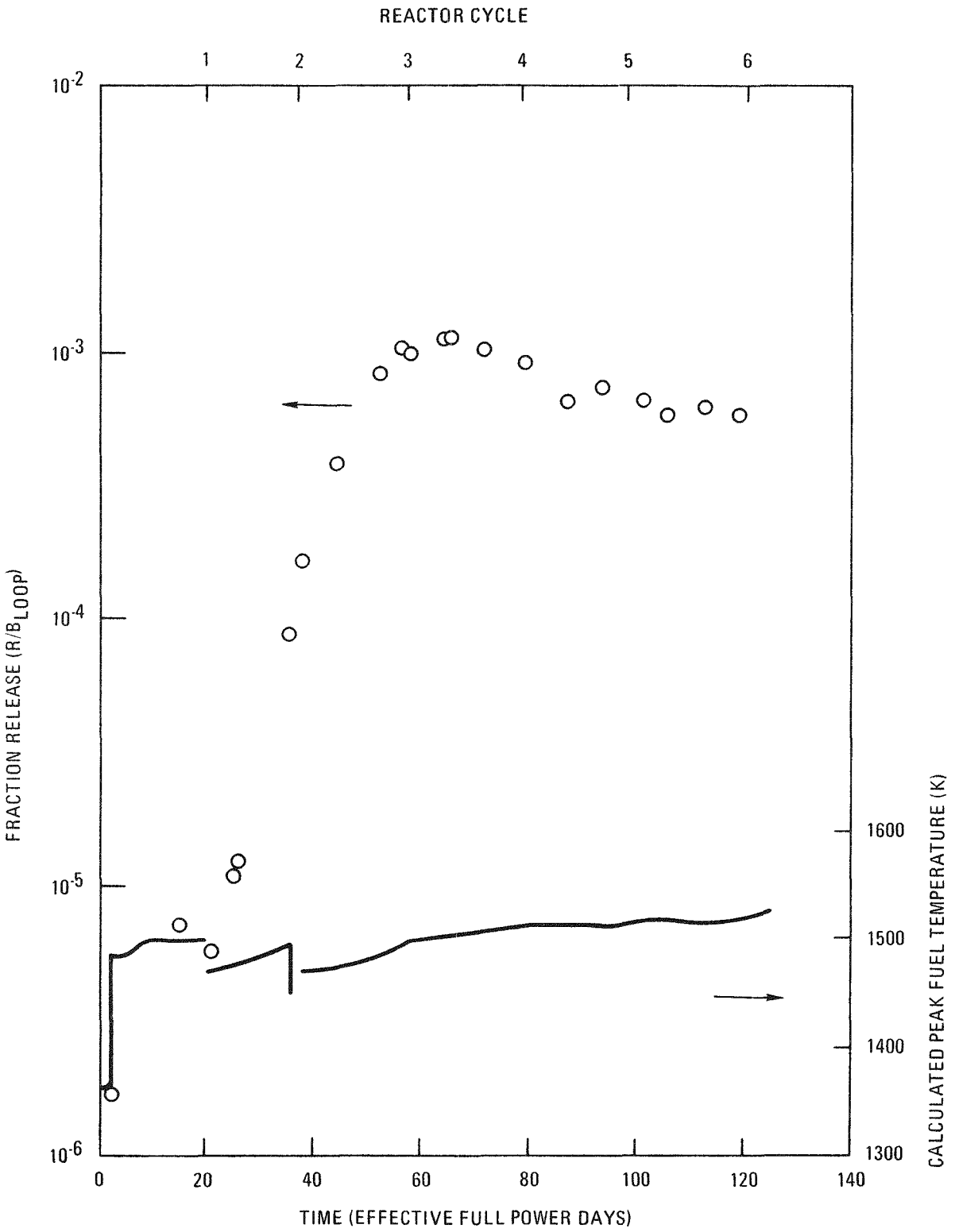

Fig. 4-20. Fission gas release (Kr-85m) and calculated peak fuel temperatures during operation of SSL-1 loop test

The EOL fissile particle failure fraction at each rod layer was determined principally from the R/B measurements carried out on individual fuel rods removed from the fuel body after irradiation. Eighteen of the 27 fuel rods were submitted for postirradiation measurements of R/B at 873 K. This temperature was selected because it was near the maximum attainable with the in-pile furnace used by the CEA. The results were used to assign the fissile particle failure fractions at each rod layer, assuming $(R/B)_{failed} = 5 \times 10^{-3}$ (Kr-85m at 873 K). This value was obtained from "laser-failed*" particles irradiated in SSL-1 and leads to a calculated average EOL failure fraction of ∿3%. Values of $(R/B)_{failed}$ of 2×10^{-2} (1323 K) and 3.4×10^{-2} (1523 K) were also noted by CEA during higher temperature runs (Ref. 4-13). These results are important as they provide the most representative value of $(R/B)_{failed}$ for use in solving for fissile failure fractions.

Metallographic examination of SSL-1 fuel particles from two rods revealed an upper 95% confidence level failure fraction of 2% to 4% based on the relationship between the total particle failures and the number of failed particles observed in a given size particle batch. This value, which includes both fissile and fertile particles, was based on the observation of ∿100 particles.

To further characterize the fraction of broken fissile particles, four SSL-1 fuel rods were mechanically disaggregated and the particles separated from the matrix material. Approximately 100 particles from a fuel rod at level 4 (slightly below the midplane of the fuel element) were selected from gamma-spectrometry analysis to determine the Cs-137/(Zr-95 + Nb-95) ratio. Of the 48 fissile particles counted, three exhibited ratios more than 2σ (95.5% confidence band) below the mean ratio observed (see Table 4-5). These particles were deemed failed. It should be noted that

*Laser-failing is a method used to fail intact particles. A single intact particle, either unirradiated or irradiated, is subjected to a laser beam pulse. The high energy pulse introduces a "pinhole" in the particle coatings which allows fission gases to escape. This particle is then irradiated and the $(R/B)_{failed}$ measured.

TABLE 4-5
SUMMARY OF CESIUM RETENTION DATA FOR 100 PARTICLES IRRADIATED[a] IN SSL-1 FUEL ROD C4

Particle Type	No. of Particles	$\frac{\text{Cs-137}}{\text{Zr-95 + Nb-95}}$ Ratio[b]	Relative Deviation From the Mean (%)	Particle Status	Cesium Release (%)
$(8Th,U)O_2$ fissile	48	9170 (± 1380) (mean)	2σ = 15.1%[c]	45 intact 3 failed[d]	∿1
$(8Th,U)O_2$ fissile[e]	1	7620	16.9	Failed	17
$(8Th,U)O_2$ fissile[e]	1	7290	20.5	Failed	21
$(8Th,U)O_2$ fissile[e]	1	6330	31.0	Failed	31
ThO_2 fertile	52	12925 (± 1230)	(2σ = 9.5%)	52 intact	0

[a] Mean irradiation temperatures, $1337 \leq T \leq 1482$K.

[b] Ratio of counts.

[c] The 2σ values represent the root mean square deviation about the mean. Values for failed particles represent the deviation of the single particle ratio from the particle batch mean.

[d] A particle was deemed failed if the individual particle count ratio was 2σ (15.1% for fissile, 9.5% for fertile) below the respective batch mean.

[e] These three fissile particles were included with the 45 intact fissile particles in the determination of the fissile particle batch mean.

the cesium loss ranged from 17% to 31% for these particles. These results, although derived from a limited number of particles, provide an average fissile failed fraction of ∿6%. A summary of the fuel particle failure fractions determined by the various techniques is presented in Table 4-6.

The preponderance of in-pile and PIE data gathered by CEA lead to a prediction of 3% fissile particles with failed coatings. Having assigned limits to the EOL failure fractions for each rod layer, time-dependent fractions were calculated using Eq. 4-3:

$$f_{u(\text{layer } \ell)}(t) = f_{u(\text{layer } \ell)} \cdot \frac{(R/B)_{loop}(t)}{(R/B)_{loop}(EOL)} \quad , \tag{4-3}$$

where $f_{u(\text{layer } \ell)}(t)$ = fissile failure fraction in fuel rods at rod layer ℓ at time t,

$(R/B)_{loop}(t)$ = fission gas release of the loop at time t,

$(R/B)_{loop}(EOL)$ = fission gas release of the loop at EOL.

This analysis assumed that each rod layer experienced the same fraction of particle failure during each time interval. It is unlikely that this assumption is strictly correct since earlier failure would be expected in the higher flux regions; however, no data are available to permit a more accurate modeling of failure.

Having defined the time-dependent fissile and fertile failure fractions, it was necessary to estimate the fractional cesium release from failed particles. The following assumptions were used:

1. No cesium was released from intact TRISO $(8Th,U)O_2$ fissile or ThO_2 fertile particles. This assumption is used in HTGR design calculations of cesium release (Ref. 4-9).

2. No significant heavy-metal contamination existed in the coatings of SSL-1 fuel particles or the matrix material used

TABLE 4-6
SUMMARY OF EOL FUEL PARTICLE FAILURE FRACTIONS DETERMINED
FROM SSL-1 IN-PILE AND PIE MEASUREMENTS

Method of Measurement	Fissile Failure (%)	Fertile Failure (%)	Comments
In-pile R/B measurement assuming CEA $(R/B)_{failed}$ (Kr-85m at 1373 K) = 2×10^{-2}	7 - 9	0	$(R/B)_{loop,\ fissile}$ confirmed zero fertile particle failure
R/B measurements on individual fuel rods (average of all rods) assuming CEA $(R/B)_{failed}$ (873 K) = 5×10^{-3}	3	--	CEA $(R/B)_{failed}$ determined from measurements of release from laser-failed particles. This is felt to be most reliable measure of failure fraction.
Observation of activity peaks during continuous on-line gamma scan	3	--	Calculation carried out by CEA has large uncertainty
Metallographic examination*	2 - 4 of all particles		Large uncertainty due to limited number of particles examined (100)
Cesium inventory in particles irradiated at rod level 4	6	0	3 failed fissiles in 48 fissile particles counted; 0 failed fertiles in 52 fertile particles counted
*Additional results			
Metallographic examination of particles irradiated in capsule P13S	--	<1	Particles from the same batch were irradiated to significantly higher FIMA and comparable temperature, yet exhibited very low failure

in the rods. This assumption was verified by preirradiation measurements carried out on SSL-1 fuel rods which showed $(R/B)_{Kr-85m} \leq 2 \times 10^{-6}$.

3. Fractional release of cesium from failed oxide particles was defined using the reference design assumption of diffusive and recoil release upon failure, calculated using the COPAR (COated PARticle Release) code (Ref. 4-14). Recoil results in the direct release of a small fraction of fission product atoms formed within the kernel. The fractional release of each isotope is dependent upon the radius of the kernel and the mass of the isotope. Since the recoil range of Cs-137 (6 μm) is short compared to the buffer and coating thickness, no recoil release occurs from intact coated particles. However, when particle failure occurs, cesium atoms recoiled directly into the buffer can subsequently be rapidly released. Diffusion of fission metal atoms is a thermally activated process and the extent of cesium release from particles is dependent upon the temperature of irradiation. At low temperature, where diffusive release is negligible, release of fission products from failed particles is controlled by recoil release; at high temperatures, diffusive release becomes rate controlling. The recoil release fraction is dependent upon the mean recoil distance of the isotope of interest in the kernel material and the kernel radius (Ref. 4-15):

$$F_{recoil} = 3/4 \frac{\rho_i}{r} - \frac{1}{16}\left(\frac{\rho_i}{4}\right)^3 \quad , \qquad (4\text{-}4)$$

where F_{recoil} = recoil release fraction,
ρ_i = recoil range of isotope of mass i (μm),
r = kernel radius (μm).

For the particles irradiated in SSL-1, ρ_{Cs-137} = 6 μm, $\bar{r}$ = 255 μm, and the calculated recoil release fraction is 0.018.

The fractional diffusive release was evaluated using the expression for the diffusion coefficient of cesium in oxide kernels supplied in the summary by Myers and Bell (Ref. 4-16),

$$D = D_o \exp(-Q/RT) \quad , \tag{4-5}$$

where D = diffusion coefficient (m^2/s),
D_o = constant = 2.38 x 10^{-10} (m^2/s),
Q = constant = 268,300 (J/mol-K),
R = gas constant = 8.314 (J/mol),
T = temperature (K).

A diffusive release fraction of 1% was calculated at the peak fuel temperature (rod layer 4) of 1523 K, providing a total calculated release from failed particles in rod layer 4 of 2.8% when the contribution from recoil was included. This value is significantly less than the observed fractional cesium releases of 17%, 21%, and 31% noted for three failed fissile particles detected in fuel at this location during PIE gamma scans (see Table 4-5). The large discrepancy between predicted and observed release is difficult to explain; however, it is possible that when the particle coatings failed, the kernel also underwent fracture or degradation, resulting in higher than expected releases. (Equation 4-5 is applicable to intact kernels only.)

100% Fractional Release of Inventory From Failed Particles. Since preliminary calculations showed that predicted release was significantly underpredicted when using the assumption discussed in the previous section, the more conservative assumption of total cesium release from failed oxide particles was used. While this is not felt to be a true representation of the release behavior, it does provide an upper bound to predicted cesium release from particles with failed coatings. The particle failure fractions derived previously were used with this assumption.

Fractional Release Defined by Axial Cesium Loading in Graphite.

A third estimate of the cesium source was derived from axial and radial gamma scans of the fuel element graphite. During the fuel element PIE, the fuel body was cut into three longitudinal sections, as shown in Fig. 4-21. After removal of the fuel rods, sections A and C were gamma-scanned to determine the inventory of Cs-134, as shown in Fig. 4-22. (Cs-137 was not counted due to the high background activity present in the CEA hot cell facility.) The Cs-137 profile in the fuel body was calculated from the Cs-134 profile using the relative isotope loadings derived from radial profile measurements carried out on a graphite web irradiated at rod layer 4 (see Fig. 4-23). Knowing the relative activities at this location and the axial flux profile, the concentration of Cs-137 at other rod layers was calculated. (Cs-134, being an activation product of Cs-133, exhibits a squared dependence on flux; Cs-137, on the other hand, shows a linear dependence on flux.) The calculated Cs-137 loading is presented in Fig. 4-22.

Having derived the graphite loading, the cesium source at each rod layer was established by equating the FIPERQ-predicted and "observed" Cs-137 loadings. It is worth noting that the use of this method underestimates the source term in the hotter fuel regions because some cesium does diffuse through the graphite into the coolant at the fuel body temperatures present in the axial center of the element. This effect is felt to be small due to the relatively short duration of the experiment.

Fuel and Graphite Temperatures

Temperatures used as input to FIPERQ were calculated by the CEA using (1) measured helium coolant inlet and outlet temperatures, (2) operational fuel element temperatures measured with three thermocouples positioned within the graphite body, and (3) thermal analysis codes. The mean temperatures shown in Table 4-4 are accurate to within ±40 K. No attempt was made by GA to carry out any additional refinement of the thermal data provided.

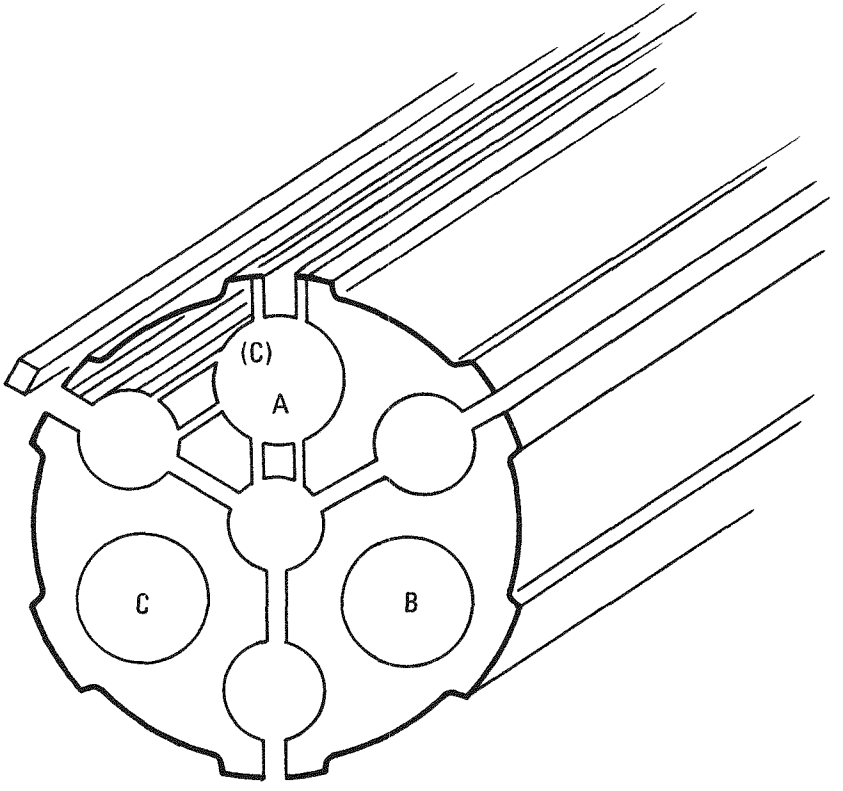

Fig. 4-21. Axial sections from SSL-1 fuel element body (A = fuel rod stack cured in packed bed and B,C = fuel rod stacks cured in place)

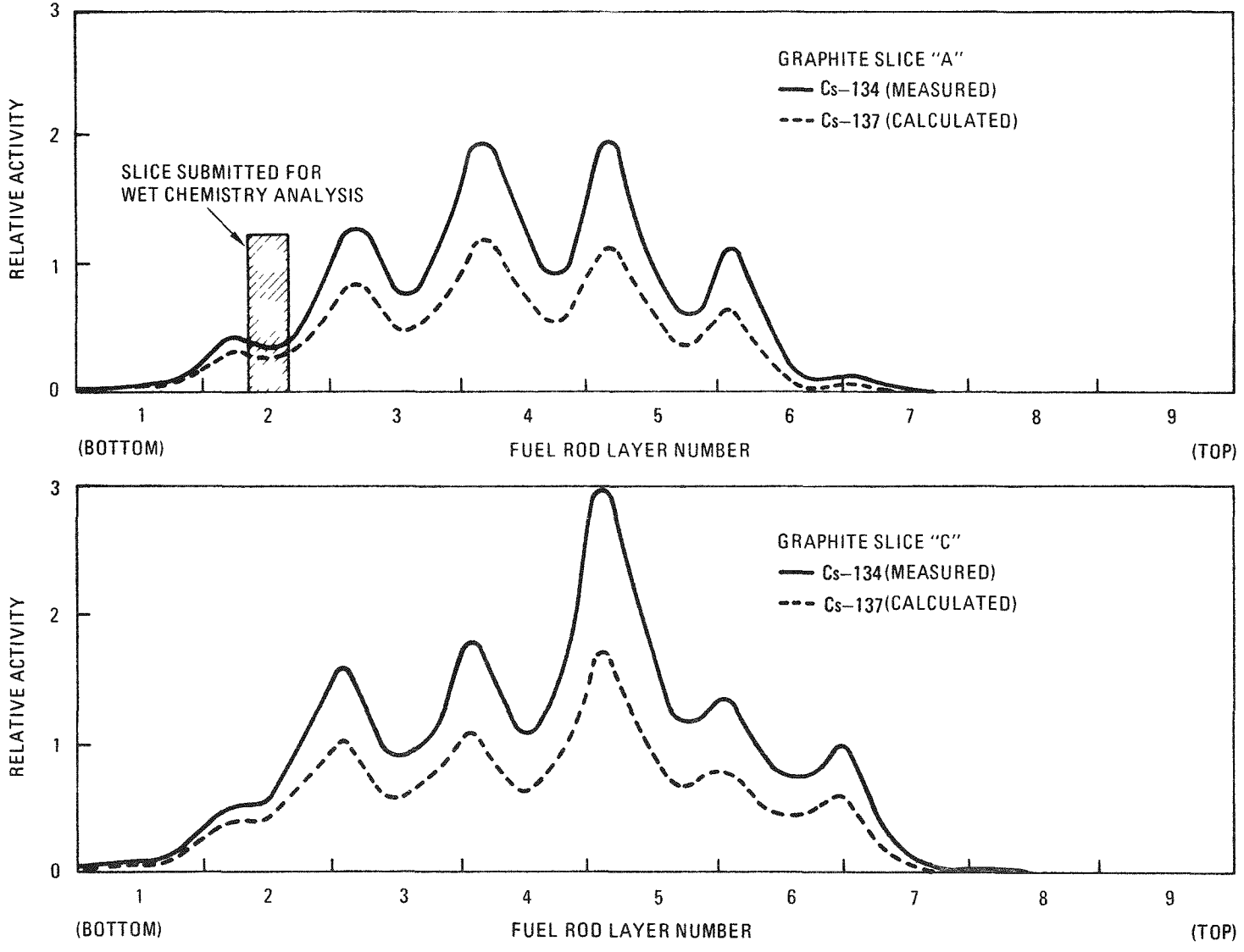

Fig. 4-22. Axial profiles of Cs-134 (measured) and Cs-137 (calculated) in SSL-1 graphite fuel body

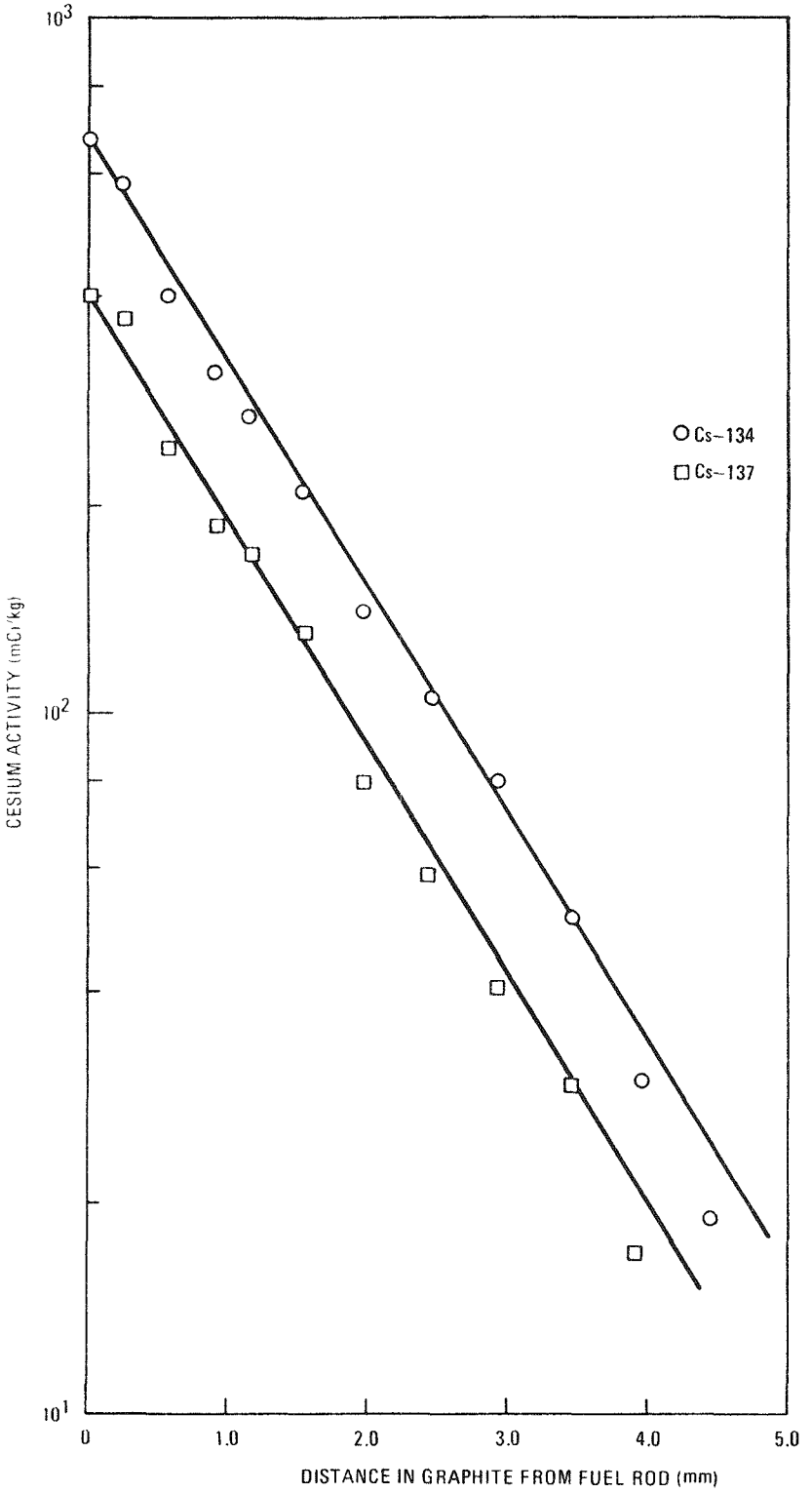

Fig. 4-23. Radial profiles of Cs-134 and Cs-137 in the graphite web adjacent to fuel rod stack C4 in the SSL-1 loop test

Integrated Fission Metal Release

Accurate measurement of the integrated metal release is required to "calibrate" the final release numbers provided by FIPERQ. Portions of the SSL-1 primary coolant circuit downstream of the fuel element were examined to provide a mass balance for cesium in the loop. The SSL-1 fuel element was positioned within an Inconel tube (see Fig. 4-24). Three 15.0-mm ring sections were cut from the tube at two ends and the midpoint. The samples were dissolved in an acid solution and gamma-counted to determine the cesium concentration. This method was used after it was noted that direct gamma scanning of the empty Inconel tube could not be used due to the high background activity of the neutron-activated materials in the tube. The results of the analysis are shown in Fig. 4-25. The straight lines shown represent the first-order least-squares fit of the data points; the equations for these lines were integrated to yield the total cesium plateout on the tube. Integration over the entire length of the tube yielded 9.47 mCi of Cs-137. This value was later summed with other values to provide an estimate of total cesium release. It will be noted that the Cs-137 concentration along the length of the tube exhibited a markedly different behavior than that of Cs-134. Although the concentration of Cs-134 would be expected to be an order of magnitude lower than Cs-137, the reason for a small positive slope of the profile along the tube is not clearly understood. It is possible that because of the early failure of some of the fissile particle coatings, most of the Cs-133 precursor Xe-133 was quickly released to the coolant. In this case, direct release of Cs-134 would be expected to be low and the observed profile would result predominantly from decay of Xe-133 in the helium coolant accompanied by activation of Cs-133 deposited on the Inconel surface. The positive slope may also result in part from uncertainties in the counting measurements.

Adjacent to the Inconel tube was a Hastelloy tube which served as one wall of the double-walled pressure casing separating primary helium coolant from the cooling-moderator water of the Osiris reactor. Since this component was part of the reactor circuit, no PIE measurements of cesium

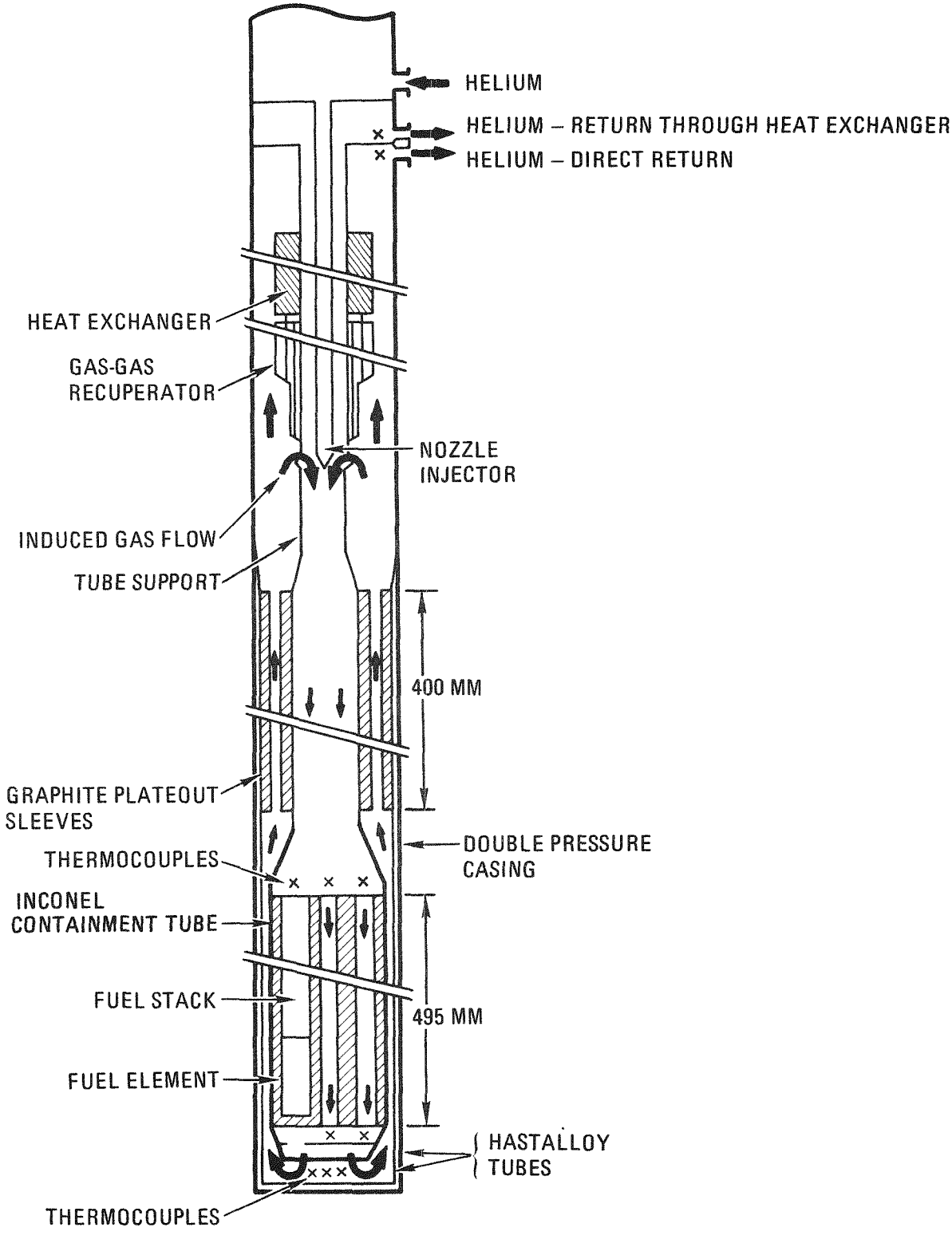

Fig. 4-24. Schematic of Saclay Spitfire Loop SSL-1

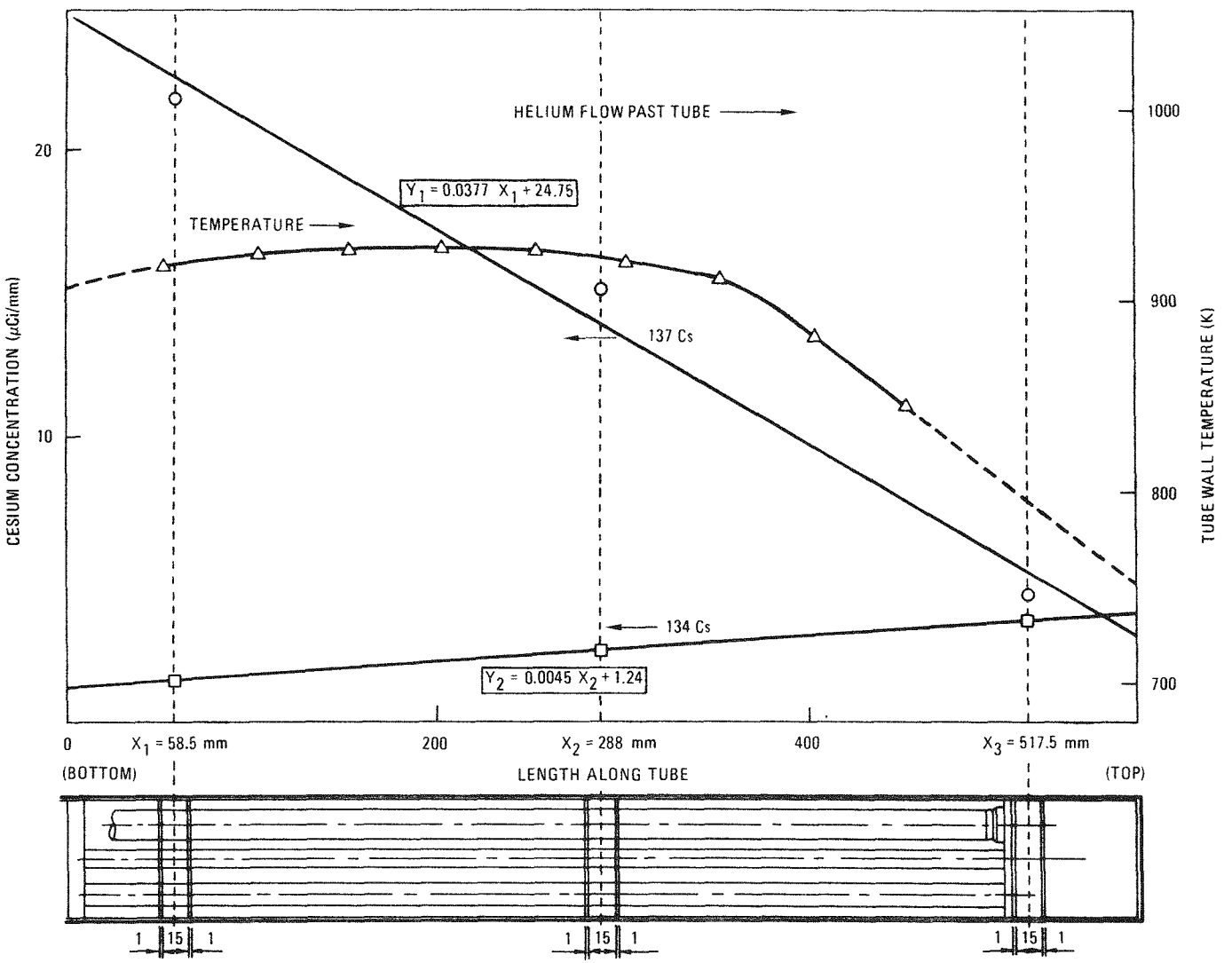

Fig. 4-25. Axial profiles of Cs-134 and Cs-137 and calculated temperatures along the length of the "outer Inconel tube" of the SSL-1 loop test

plateout on the surface were undertaken. As a consequence, it was necessary to estimate this quantity. No temperature measurements were recorded during irradiation for this tube; however, a temperature drop of 150 K between the outer Inconel tube wall and the Hastelloy tube wall was estimated by the CEA. Since PAD code (Ref. 4-12) profile fitting showed that cesium plateout exhibited perfect sink behavior (as opposed to sorption isotherm control), an estimate of inventory was made incorporating the observed axial-dependent plateout on the adjacent Inconel surface and the longer length of Hastelloy tube. This provided a calculated cesium inventory of 10.8 mCi Cs-137.

Two graphite sleeves were positioned in the primary coolant circuit downstream of the fuel element and Inconel tube. These were designed to absorb condensible fission products on high surface area graphite.* The inventory of Cs-137 in the sleeves, 0.32 mCi, was measured by sectioning the sleeves and gamma-counting the graphite dust. No cesium was detectable by gamma-scanning the metal surfaces downstream of the plateout sleeves.

Table 4-7 presents the summary of cesium location and concentrations in the primary circuit. It should be noted that the major contributor to the total release (inventory on the Hastelloy tube surface) is an estimated quantity.

Reference Input Data

All reference input used in this analysis was taken from the summary owrk of Myers and Bell (Ref. 4-16). These data included cesium diffusivity in oxide kernels and P_3JHAN graphite and cesium vapor pressure over GA matrix material and P_3JHAN graphite.

*It should be noted that far less cesium was sorbed in the sleeves than had been expected. It is likely that most of the cesium in the primary coolant plated out on the metal surfaces upstream of the plateout sleeve prior to reaching the sleeve graphite surfaces.

TABLE 4-7
SUMMARY OF Cs-137 RELEASE FROM THE SSL-1 LOOP

	Release (mCi)
Inconel tube (measured)	9.47
Hastalloy tube (estimated)	10.84
Graphite plateout sleeve (measured)	0.32
Biological shielding and other downstream components (neglected)	0
Total	20.6

Results and Discussion

The release at each rod layer was calculated with FIPERQ using the three different source terms. The summed results, shown in Table 4-8, provide a comparison of predicted and measured release. Use of the source term derived from observed particle failure fractions and estimated cesium release from oxide kernels provides a release that is significantly less than that observed. The predicted axial loading of Cs-137 in the graphite fuel element is shown in Fig. 4-26. Note that the loading in this figure has been averaged over discrete rod layers since this is the smallest length modeled by FIPERQ. From these results, it is apparent that the use of a source term obtained using near-reference methods is not appropriate for SSL-1 fuel.

A review of the assumptions used for estimating the above source indicates that cesium release from oxide kernels has been inadequately modeled. This is borne out by the results in Table 4-5, wherein 17%, 21%, and 31% cesium loss from failed particles was observed. This is significantly larger than 2.8% predicted with the COPAR code. The early failure of SSL-1 fissile particles during irradiation indicates that the fissile particles were not representative of normal HTGR fuel. It is possible the oxide kernels in the failed particles underwent degradation that permitted higher than expected cesium releases. However, the limited PIE of the fuel particles did not reveal any significant changes in particles with failed coatings.

Since the source based on diffusive and recoil release did not provide an adequate representation of cesium behavior, a source based on the assumption of total cesium release from failed oxide particles was used. The results in Table 4-8 show that the total release is more closely modeled, although still underpredicted. However, the axial loading of cesium shown in Fig. 4-26 does not correlate well with that measured from the gamma scans. Too much cesium release is ascribed to fuel at the ends of the fuel body, as demonstrated by the significant overprediction of loading in these regions. When the predicted and observed loadings are

TABLE 4-8
COMPARISON OF PREDICTED AND MEASURED[a] Cs-137 RELEASE FROM THE SSL-1 LOOP

Source Description	Release per Rod Layer (mCi)									Total FIPERQ Release (mCi)	"Measured" Release (mCi)
	1 Bottom	2	3	4	5	6	7	8	9 (Top)		
Diffusive/recoil release of inventory from failed particles. Failure at each rod layer determined by PIE R/B measurements.	0.011	0.021	0.020	0.032	0.020	9.3×10^{-3}	5.1×10^{-4}	6.6×10^{-6}	0	0.11	20.6
Total release of inventory from failed oxide particles. Failure at each rod layer determined by PIE R/B measurements.	0.38	0.70	0.67	1.06	0.66	0.31	0.017	2.2×10^{-4}	0	3.80	20.6
Release at each rod layer estimated from PIE measurements carried out on fuel and graphite.	0.026	0.26	0.62	0.70	0.57	0.16	7.9×10^{-3}	0	0	2.34	20.6

[a] The measured release includes a calculated contribution equal to 10.84 mCi (see Table 4-7).

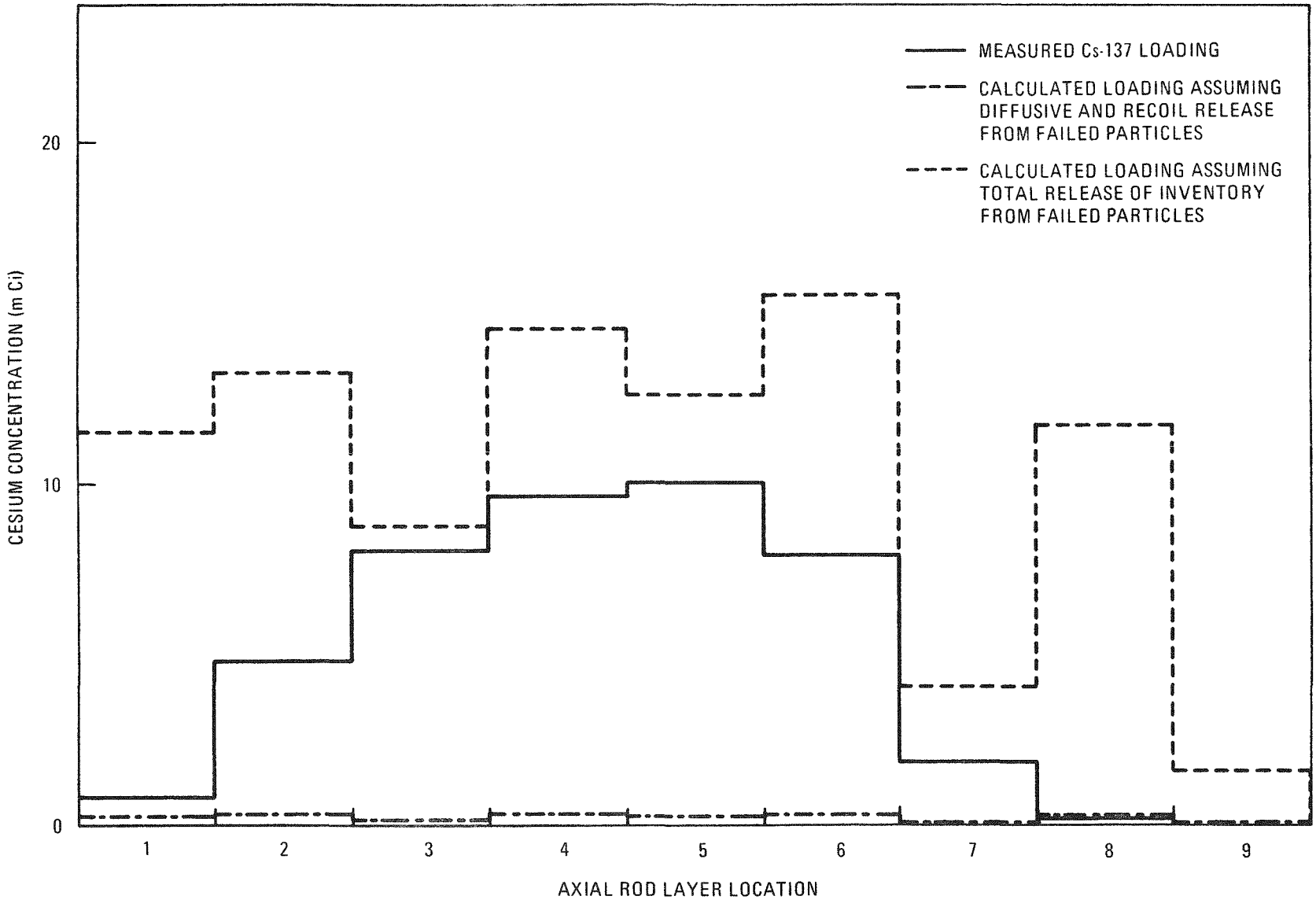

Fig. 4-26. Predicted and measured Cs-137 loading in the SSL-1 fuel body

matched, as was done using the third estimate of the source, predicted release was a factor of ∿9 less than that measured. In view of the lack of correlation between calculated and observed data when the first two source terms were used, a source based on axial cesium loading was used in the analyses discussed below.

The radial profile of Cs-137 in the graphite web at rod layer 4 shows good agreement with the observed profile shape, as demonstrated in Fig. 4-27. The overall magnitudes of the profiles, by definition, are in agreement, although some difference can be expected due to the marked inhomogeneity of fuel loading noted at each rod layer location (see Fig. 4-22). The similarity of the profiles appears to confirm that the Fick's law model used in FIPERQ adequately represents the diffusion of cesium in SSL-1 P_3JHAN graphite. In addition to this comparison, the CEA measured the partition coefficient, ϕ, of cesium at rod layer 4. They obtained a value of 1.0, indicating the cesium loadings per gram of matrix and per gram of graphite were nearly equal. (It should be noted that this is a very difficult measurement to perform, requiring disaggregation of the fuel rod and separation of fuel particles and matrix material. As such, it is prone to large uncertainty.) This compares favorably with the value calculated by FIPERQ of 0.73, indicating that the relative values of vapor pressure derived from the cesium isotherms for GA matrix material and P_3JHAN graphite provide an acceptable value of ϕ.

The sensitivity of the total release, radial profile, and ϕ to changes in the cesium diffusivity in graphite were studied. Previous analysis (Ref. 4-5) has shown that over the relatively short duration of the SSL-1 test, release is highly sensitive to the value of the diffusion coefficient, D_{Cs}, utilized. Since this value has a large associated uncertainty [1σ (log base 10) = 0.66] (Ref. 4-17), the value of D_{Cs} was increased within this uncertainty range to assess the effect of this change upon release. A three-fold increase in D_{Cs} was found to increase the total predicted release by a factor of 5.6. However, the higher diffusion resulted in a predicted radial profile that did not closely agree with the measured profile, as shown in Fig. 4-27. This result would appear to

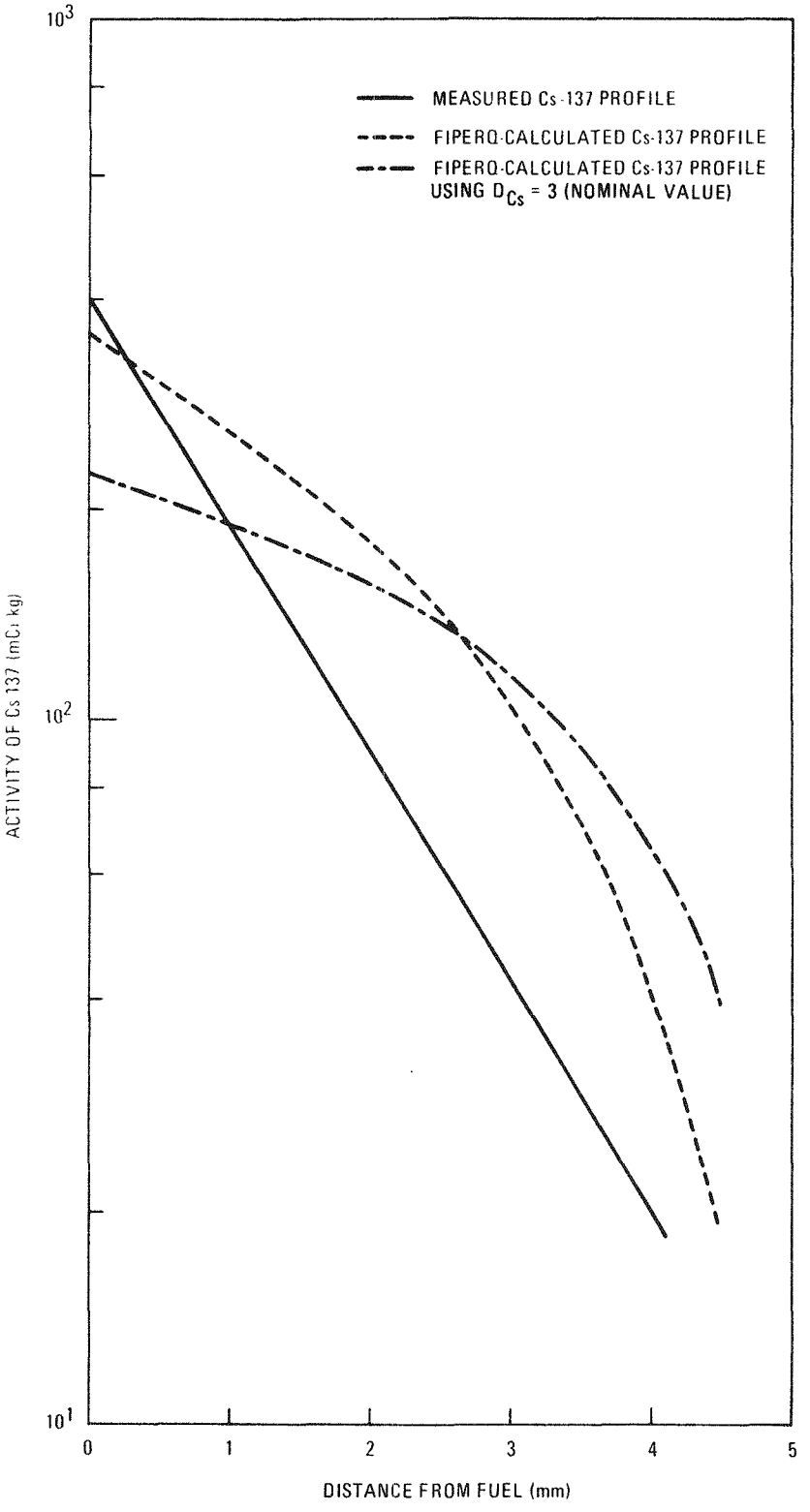

Fig. 4-27. Cesium-137 profile in the graphite web at rod layer 4 of the SSL-1 test

demonstrate that uncertainty in the cesium diffusivity alone cannot account for the large difference noted. No other combination of credible FIPERQ input could be assigned that would result in a satisfactory explanation of the observed experimental data.

Summary

Since SSL-1 represents the first in-pile test subjected to detailed analysis of fission metal release for use in design methods verification studies, the findings of this study are of interest in planning future analysis. The conclusions of this study are as follows:

1. The predicated and observed release showed poorer than expected correlation. Although uncertainty in the reference input data likely accounted for some of the disparity, the measured fission metal behavior was subject to large, essentially unquantifiable uncertainties. This is demonstrated in part by the need to carry out extrapolations and modifications of the measured results in order to make the data suitable for comparison with predictions. Each of these changes introduces uncertainty into the analysis.

2. The fractional cesium release from failed SSL-1 fissile particles was underpredicted by the COPAR code. This is felt to arise in part because of the nonrepresentative nature of the fissile particles irradiated in this test.

3. The Fick's law model used in FIPERQ adequately modeled the single radial profile shape available for analysis. However, no statement regarding the correctness of the predicted cesium loading in graphite can be made due to the large uncertainty in the source.

4. The partition coefficient calculated from PIE measurements was closely modeled by FIPERQ. This provides some assurance

that the sorption isotherms used in this analysis provide the proper loadings at the temperatures and cesium vapor pressures present in this test.

5. Insufficient data were available from the SSL-1 PIE to carry out a rigorous verification of the fission metal reference design methods. The shortcomings of the SSL-1 experimental data base are discussed later in this section in light of planned future work. In the future, more applicable data will be required of a test before it is selected for use in an extensive verification study.

Fission Gas Release Calculations. The half-life dependence of krypton and xenon diffusion in matrix material has been evaluated using in-pile fission gas release data. Values of log $(R/B)_i$ versus the square root of half-life of isotope i for five krypton nuclides and six xenon nuclides at 25 and 120 EPFD of irradiation are presented in Figs. 4-28 and 4-29, respectively. The data at 25 EFPD were selected for analysis since this was the earliest time at which results for all measurable nuclides were available. The latter data were collected just prior to shutdown of the test. A summary of the salient results from these two plots is presented in Table 4-9.

The half-life dependence of krypton diffusion is seen to be slightly greater than 0.5 at both time points. This value is within the scatter band of data reported by Myers and Bell (Ref. 4-18). The similarity of the values at the two time points confirms that no apparent changes affecting fission gas release took place in the fissile particles during irradiation up to 7.3% FIMA. These findings are confirmed by the data on xenon release. In this instance, two estimates of the half-life dependence are presented due to uncertainty associated with the measured value of Xe-135m; at both time points, the Xe-135m release shows significant deviation from the expected behavior. Because of this uncertainty, the least-squares fit of the xenon data has been carried out with and without the Xe-135m data. The inclusion or deletion of these data has only a small impact on the

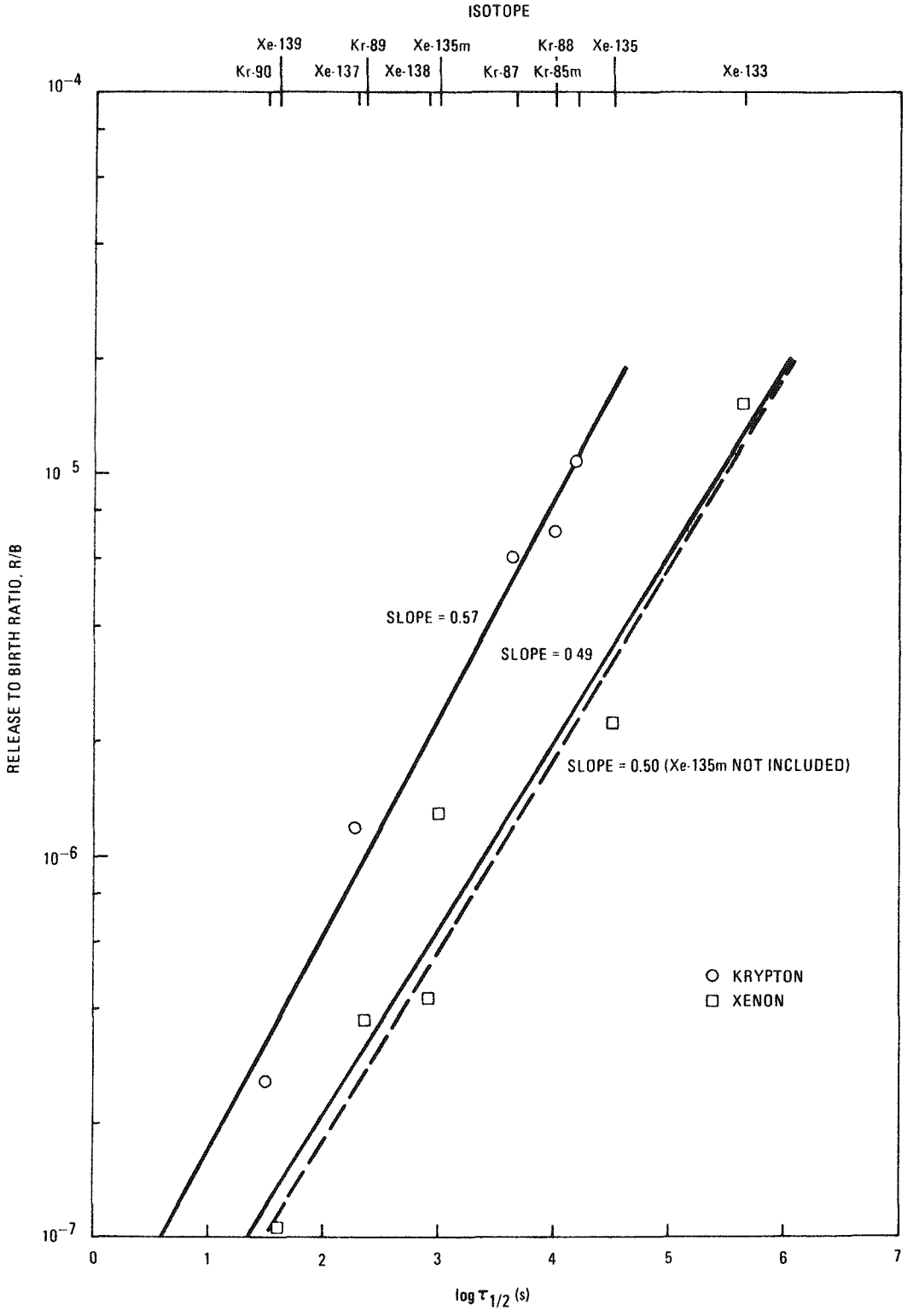

Fig. 4-28. Plot of log $(R/B)_i$ versus $\sqrt{\tau_{i\ 1/2}}$ for krypton and xenon isotopes released from the SSL-1 fuel element at 25 EFPD

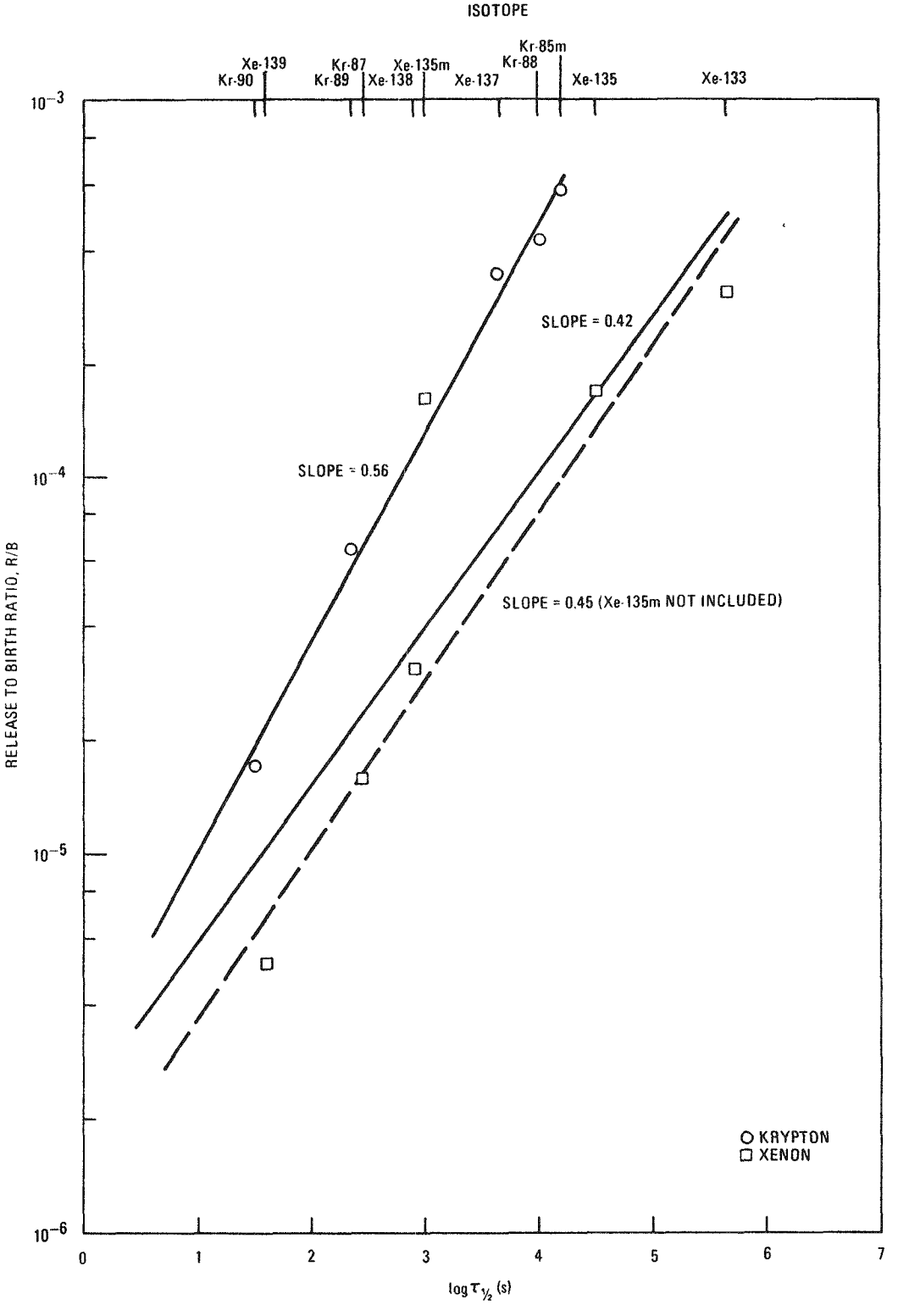

Fig. 4-29. Plot of log $(R/B)_i$ versus $\sqrt{\tau_{i\ 1/2}}$ for krypton and xenon isotopes released from the SSL-1 fuel element at 120 EFPD

TABLE 4-9
SUMMARY OF DATA ON HALF-LIFE DEPENDENCE OF Kr AND Xe DIFFUSION DERIVED FROM THE SSL-1 LOOP

	Time of In-Pile R/B Measurement	
	25 EFPD	120 EFPD
Half-life dependence of Kr diffusion in fuel rods	0.57	0.56
Half-life dependence of Xe diffusion in fuel rods	0.49 (0.50)[a]	0.42 (0.45)[a]
A_{Kr}/A_{Xe}[b]	3.92 (4.40)[a]	4.04 (5.39)[a]

[a] These are values derived without the inclusion of Xe-135m data.

[b] A_{Kr}/A_{Xe} represents the ratio of the fractional release of krypton to that of xenon for isotopes of equal half-lives (hypothetical) of 1 hour.

calculated slope of the data, as shown in Table 4-9. However, the effect is much larger when the value of A_{Kr}/A_{Xe}, the fractional release of krypton to xenon for hypothetical isotopes with half-lives equal to 1 h, is calculated. Based on data in Ref. 4-18 and the assumed volume-average fuel temperature of ∿1473 K, a ratio of ∿3 would be predicted. The results in Table 4-9 show that the measured values are higher than expected, particularly when measurements of Xe-135m R/B are not included. No explanation of this difference is offered; however, it is worth noting that a large uncertainty exists in volume-average fuel temperature (although values greater than 1573 K are unlikely) and the A_{Kr}/A_{Xe} ratio is very sensitive to the krypton and xenon activation energies used as input in the design method (Ref. 4-18). The values may differ for fuel rods cured-in-bed, from which the data in Ref. 4-18 are derived, and fuel rods cured-in-place. Eighteen of 27 fuel rods in SSL-1 were cured by the latter method. Overall, the R/B data from SSL-1 provide confirmation that the fission gas release model used in the design method provides an accurate description of noble gas diffusion in matrix materials. The agreement between predicted and observed behavior is acceptable in view of the uncertainty associated with both data sets.

An analysis of the graphite sectioning data presented in Fig. 4-23 revealed that gaseous precursors did not play an important role in establishing the profiles of Cs-134 and Cs-137 in the graphite web. This can be visualized after reviewing the decay and activation schemes for these isotopes:

$$\text{Xe-133 (5.2 d)} \rightarrow \text{Cs-133 (stable)} + \gamma$$
$$\text{Cs-133} + \eta \rightarrow \text{Cs-134 (2.06 y)}$$
$$\text{Xe-137 (3.84 m)} \rightarrow \text{Cs-137 (30 y)}$$

If the holdup time, T_h, of xenon in graphite were <30 s, the decay of both isotopes would yield flat precursor profiles of differing magnitude (Cs-137 being greater than Cs-134). Since the isotope profiles show similar decreasing concentrations toward the outer boundary of each web, the precursor contributions are seen to be insignificant. If a longer holdup

time were to exist, 30 s < T_h < 650 s, the decay of Xe-137 would provide a precursor profile that was not flat but decreasing toward the outer web boundary; the Xe-133 precursor contribution would still be flat due to its much longer half-life. However, if Xe-137 decay did provide a measurable contribution to the profile, the Cs-137 and Cs-134 profiles would not have identical slopes, a result not found during the sectioning. Analogous reasoning can be used to show that at T_h > 650 s, the precursor contribution of Xe-133 is likewise insignificant. Thus, the combination of Cs-134 and Cs-137 profiles that are both identical and decreasing toward the outer web boundary indicates that metallic diffusion is the controlling release mechanism.

An important parameter in the calculation of fission gas release is the assumed value of $(R/B)_{failed}$. Until recently, $(R/B)_{failed}$ (1373 K) for Kr-85m was assigned a value of 5×10^{3} (Ref. 4-19) for all burnups. Recently the dependence of fission gas release for oxide kernels has been taken into account, and consequently $(R/B)_{failed}$ increases to 2×10^{-2} at burnups greater than 10% FIMA. Analysis of SSL-1 fuel particles, including metallographic and gamma-scan examinations of the fuel during PIE, provided some of the first in-pile confirmation that a value of 2×10^{-2} for failed oxide particles is correct.

Fission Product Plateout Calculations. Although cesium deposition along the Inconel tube was measured by the CEA, the lack of characterization of the metal surfaces and the large uncertainties associated with the calculated metal surface temperatures and the time-dependent source precluded quantitative verification of the fission product plateout design methods with SSL-1 data.

Analysis of Fission Product Behavior in Capsules P13Q, P13R, and P13S

Capsule P13Q was designed to evaluate the performance of LHTGR fresh fuel irradiated in integral graphite bodies under nominal LHTGR operating

conditions. This test, carried out in the Oak Ridge Reactor (ORR), contained three near-isotropic graphite bodies with a fuel - coolant hole pattern that was representative of the geometry envisioned for an LHTGR. A cross-section view of a single body is shown in Fig. 4-30. Each body contained six fuel rods nominally 1.57 cm (0.62 in.) in diameter and 5.35 cm (2.1 in.) long and a number of secondary ("piggy back") fuel particle and graphite specimens. This experiment was the first test of fuel rods fabricated by the cure-in-place process and also contained reference-type TRISO UC_2 and BISO ThO_2 fuel particles and graphite shim particles. A description of the test is given in Ref. 4-20.

Capsules P13R and P13S were two tests in a series to demonstrate the integrity of reference and alternate LHTGR fuels over a wide range of irradiation conditions (Ref. 4-21). The fuel rod samples in the capsules were irradiated in the General Electric Test Reactor (GETR) at design temperatures of 1348, 1573, and 1773 K. One series of fuel rods (cell 1, P13S) was thermal cycled 21 times from its nominal operating temperature of 1348 K to 1773 K. This test was the first attempt to simulate temperature cycling that results from load following and/or control rod pattern changes in the LHTGR.

Fission Metal Release Calculations.

P13Q

The release of Cs-137 from the three fuel bodies was modeled with the FIPERQ code. The same criteria as those required for analysis of metal release from the SSL-1 test are discussed below.

Source. The cesium source strength in the fuel rods was estimated from the EOL particle failure fractions determined from metallographic examinations. The data exhibit considerable scatter, but values of 1% UC_2 fissile failure and 0% ThO_2 fertile failure were assumed to exist throughout the irradiation. Because the in-pile fission gas release was dominated by heavy metal contamination (R/B of Kr-85m at EOL = 3×10^{-6}),

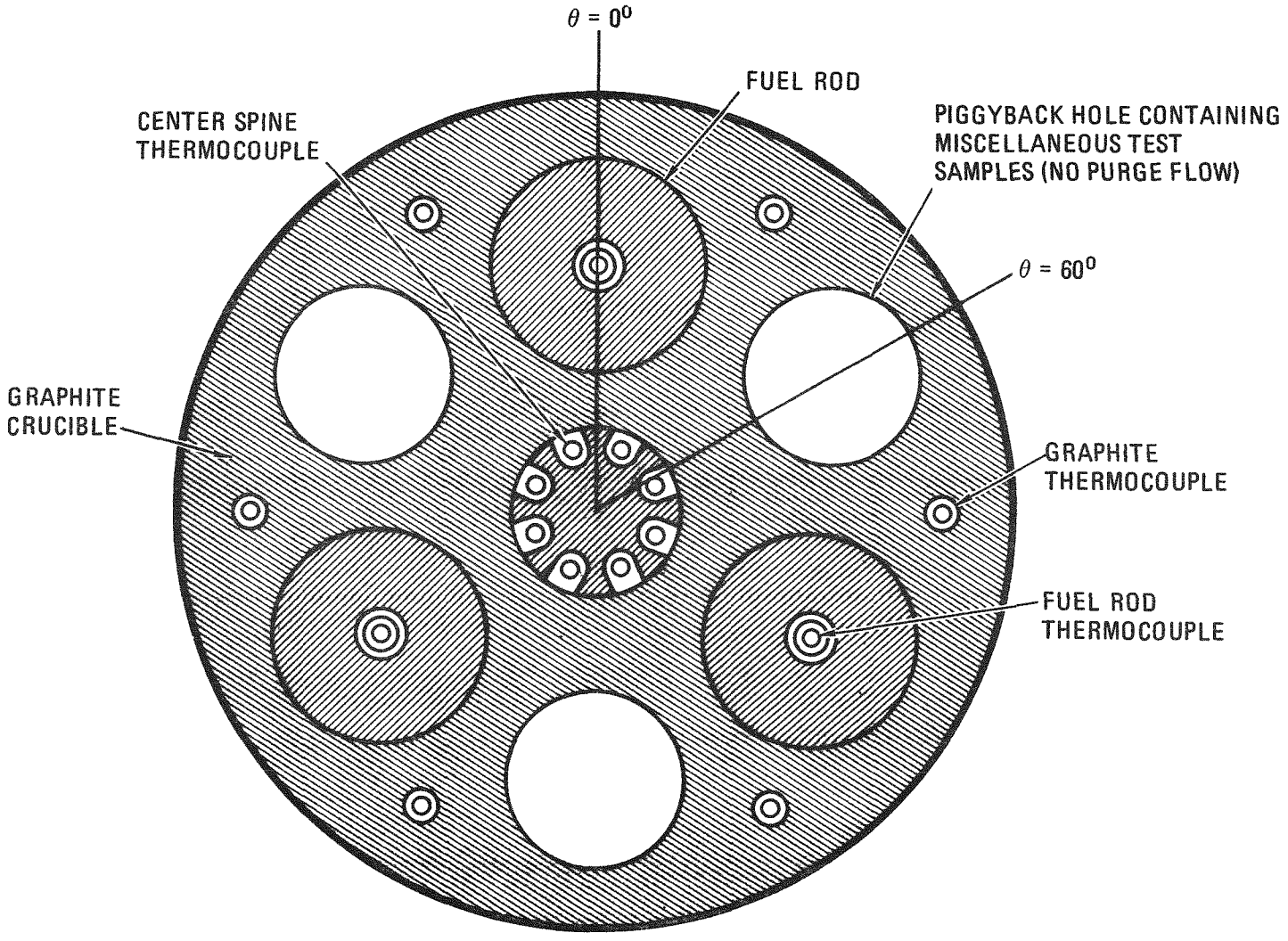

Fig. 4-30. Section through capsule P13Q graphite fuel body

no assessment of the time-dependent failure of the fissile particles could be made. Neglect of this effect results in a slight overprediction of release. In addition to the assignment of fissile failure fraction, the assumption of total release of cesium inventory from failed carbide kernels was used. This input is in keeping with observed cesium release behavior for this type kernel (Ref. 4-16).

Temperature. Because a detailed thermal analysis was not performed, the graphite fuel body temperatures were not clearly defined in each region of the capsule. Therefore, the temperature gradient across the graphite web was estimated from in-pile thermocouple measurements. The surfaces adjacent to the fuel rods were assumed to operate at 1173 K; the graphite coolant hole surfaces were assumed to operate at 1133 K. The fuel temperature was arbitrarily assigned a value of 1373 K. The calculated release is insensitive to this parameter since total release of the cesium inventory from failed particles and rapid diffusion of cesium in matrix material are assumed.

Total Integrated Release. No cesium was detectable on the stainless steel containment tube or in the empty graphite fuel bodies. While this attests to the excellent fuel performance and fission product retention of the fuel, it severely limits the usefulness of capsule data in verifying fission metal release methods. Nevertheless, the predicted fractional release of cesium was compared to the maximum in-pile fractional release that could have taken place and still gone undetected. The latter value was derived from gamma-scan data. These data showed that 10.8 Ci of cesium had been formed in the fuel. In addition, the minimum detectable quantity of cesium deposited on the stainless steel containment tube was estimated to be 0.1 Ci. These results provide a maximum fractional release of 1% that could have gone undetected above the background activity levels.

Reference Input Data. All required reference data were taken from the summary work of Myers and Bell (Ref. 4-16).

Results and Discussion. The FIPERQ calculation of cesium release using a constant source strength and irradiation conditions provided a fractional release to the outer boundary circumference of the fuel body of 0.12%. Since this value is significantly smaller than the minimum detectable release, no quantitative statement regarding the validity of the fission metal release calculations can be made. Since P13Q is felt to be typical of most capsule tests, wherein demonstration of acceptable fission product retention is a major objective, future fission metal design methods verification studies of capsules will be restricted to those instances where high-temperature irradiation has resulted in measurable fission metal release.

P13R and P13S

The graphite crucibles surrounding the individual fuel rods irradiated in these capsules were gamma scanned after irradiation. No cesium was detectable in these crucibles, with the exception of the samples containing fuel thermal cycled between 1348 and 1773 K. Preliminary hand calculations revealed that no verification of the FIPERQ code would be possible with these data. The sensitivity of the gamma-scan measurements did not allow a meaningful comparison of predicted and maximum possible cesium release (see discussion of P13Q above). Although the thermal-cycled samples did exhibit cesium release to the graphite body, no activity on the adjacent stainless steel containment tube was detectable. The large uncertainty associated with the source strength precluded a quantifiable comparison of predicted and measured loading in graphite or release. Therefore, no analysis of release beyond that presented in Ref. 4-21 is provided herein.

Fission Gas Release Calculations.

P13Q

No attempt was made to verify the fission gas release design methods for the following reasons:

1. The in-pile R/B was very low and appeared to be dominated by release from heavy metal contamination.

2. The time-dependent particle failure fractions could not be determined without the use of in-pile R/B measurements.

3. The fuel temperatures were not precisely defined.

4. The measured R/B of the capsule resulted from the accumulated release from all three fuel bodies; i.e., individual fuel bodies were not irradiated in containers.

5. Preliminary review of release data for Kr and Xe isotopes revealed that insufficient data for short-lived isotopes were available for analysis of the half-life dependence of R/B.

In addition, a leak appeared in the bulkhead separating the GA and ORNL capsules (both irradiated in the same ORR position) during irradiation, allowing some mixing of the respective purge gases. This introduced uncertainty in the measured R/B values after failure of the bulkhead seal.

P13R and P13S

A large body of in-pile fission gas release data from each containment cell is available from these capsules. In the past, these data have been used to assign time-dependent failure fractions using an assumed value of $(R/B)_{failed}$. No other experimental means exists to assign the in-pile failure fractions. Because these data are required input for fission gas release calculations, the available data cannot effectively be used to verify fission gas release design methods. The data can, however, be used for verification of fuel performance models, and this work is anticipated under Task 9 at a later date.

No assessment of the half-life dependence of Kr and Xe release during capsule irradiation is presented. The in-pile data provided results that were not in accord with the large body of information available on fission gas release. The disparity between measured and expected behavior arises from the small number of Kr and Xe nuclides detectable (6) and uncertainity associated with the short-lived isotopes.

Fission Metal Plateout Calculations. No data were available from either P13Q, P13R, or P13S to verify the reference design method used to predict fission product distribution and loading on primary circuit components.

Summary. The available data from capsules P13Q, P13R, and P13S did not permit a quantifiable verification of the fission product design methods. This results mainly from the excellent performance and low fission product release exhibited by the fuels irradiated in the capsules. This study was carried out in part to assess the usefulness of capsule data in verification studies. It can be concluded that no further verification effort need be devoted to capsule tests that exhibit the expected low levels of fission product release. In any instance where measurable metal release is noted and coupled with a well-defined source term, fission metal release methods may be verifiable. Fission gas release measurements can best be used to verify fuel performance models. No verification of fission product plateout methods will likely be available from any foreseeable capsule tests.

Appraisal of Potential Tests Based on Progress to Date

As a result of the analyses of fission product behavior carried out under the program, a better understanding of the necessary input from in-pile experiments has been acquired. Experience to date has shown that the single most important requirement is a large body of well-defined data that permits the evaluation of trends in the observed fission product behavior.

It is extremely difficult to arrive at meaningful quantitative assessments when only single measurements of a barrier to release have been examined. The importance of an extensive data base is highlighted by a comparison of the CPL-2/1 and SSL-1 fission metal release calculations. Where the former test provided a nearly complete picture of cesium behavior in the fuel and primary circuit, allowing the evaluation of numerous barriers to release, the SSL-1 analysis was hampered by a lack of PIE data available for comparison with predictions.

Having evaluated five in-pile tests, a ranking of necessary input for verification studies has been assembled. Table 4-10 lists the specific data requirements, in decreasing order of importance, needed to permit verification of the specific design methods. The qualifications put forth in this table have been used to assess the present and potential in-pile and out-of-pile fission product tests that are suitable for use in fission product design methods verification. An evaluation of the available data and an assessment of the overall value of each test are provided in Table 4-11. It should be noted that the length of irradiation was also considered as an important parameter when weighting the likely impact of each test, the longer tests receiving greater weighting. The tests in this table are currently being reviewed to aid selection of the next series of in-pile experiments to be analyzed. It is planned to intermittently amend and update this table to provide a summary of the overall work status for the task.

TASK 300: FISSION PRODUCT DATA ANALYSIS

Fission Product Design Data Review

Introduction and Summary

In the process of updating the Fuel Design Data Manual, fission product transport design data were critically reviewed with the objectives of

TABLE 4-10
REQUIRED EXPERIMENTAL INPUT FOR VERIFICATION OF FISSION PRODUCT DESIGN METHODS

Fission Gas Release Calculations	Fission Metal Release Calculations	Fission Product Plateout Calculations
Experimental operating history data Circulating activity Fuel temperatures Power Time-dependent particle failure fractions Measure of heavy metal contamination	Well-defined source Bare kernels Time-dependent particle failure fractions and metal release from kernel Estimate of total release Filters or plateout probes Gamma-scan measurements Fuel and graphite temperatures Experimental operating history data Power Coolant flow Circulating activity Fission product loading in graphite (radial and/or axial)	Well-defined measure of fission product distribution and activity Estimate of steady-state fission product source in coolant Accurate plateout surface temperatures Applicable sorption isotherms

TABLE 4-11
SUMMARY OF IN-PILE AND OUT-OF-PILE TESTS SUITABLE FOR FISSION PRODUCT DESIGN METHODS VERIFICATION STUDIES

In-Pile Test Description							Fission Gas Release Calculations			Fission Metal Release Calculations								Fission Product Plateout Calculations						
Test	Fuel Type	Enrichment %	Irradiation Time	FIMA	Test Status	Unique Features	Available Data	Percent Complete	Relative Value	Nuclide Data	Source	ϕ	Profiles in Graphite	Integral Release	Other	Percent Complete	Relative Value	Nuclide Data	Source	Plateout Distribution	Plateout Surfaces	Sorption Isotherms	Percent Complete	Relative Value
FSV (reactor)	(4.25 Th,U)C_2 TRISO fissile; ThC_2 TRISO fertile	93	6 months to 6 years	20% fissile 7% fertile	Irradiation and analysis on-going	Operating HTGR	Rise-to-power data on noble gases and iodine release	On-going	High	Cs-134, Cs-137, Sr-89, Sr-90, Ba-140, La-140	Release from contamination and failed particles	No near-term data	No near-term data	Determined from plateout probe measurements	--	0	High	Cs-134, Cs-137, Sr-89, Sr-90, I-131, Ba-140 La-140	Determined from upstream plateout probe data	Determined from difference in upstream and downstream probe results	Variable	Reference values used	0	High
Peach Bottom (reactor)	(5.5 Th,U)C_2 BISO fissile; ThC_2 BISO fertile	93	$\leq$ 900 EFPD	9%	Analysis in progress	Data from operating HTGR to high burnup and fluence	Full-power noble gas and iodine release data	80	High	Cs-134, Cs-137, Sr-90, Ce-144, Ag-110m, Ru-106, Sb-125 and others	Diffusive release from intact BISO particles	0	>50	Determined from probes and integration of plateout data	--	15	High	Cs-134, Cs-137, Sr-90	Determined from probes	Determined from EOL gamma-scan and radiochemistry of destructively removed samples	SS304, I800, C/steel	Reference values used	90	High
CPL-2 (loop)	UO_2(Dragon) TRISO, 4% bare kernels	12	4 tests of 60 EFPD	<1%	Tests complete, analysis in progress	Source well-defined. Extensive body of in-pile and PIE data	R/B data at 5 intervals during irradiation	50	Medium	Cs-134, Cs-137, Sr-90, Sb-125, Ba-140, La-140	Predetermined fraction of bare kernels in hottest fuel rods	2 values	25 - 30	Determined from plateout probe and filter assembly	Recirculation determined from fuel element base plate corrosion	30	High	Cs-134, Cs-137, Sr-89, Sr-90, I-131, Te-129m, Sb-125	Plateout probe with inlet at tube entrance	Large number of plateout profiles from gamma-scans of 125-cm-long tubes	As-received and pre-oxidized I800, SS	Determined from experiments or alloys	25	High
Idylle-03 (loop)	UO_2 (Dragon) TRISO, 2.5% bare kernels	8	262 EFPD	2.25%	Test and Dragon analysis complete, no work yet by GA	Source well-defined. Large body of in-pile and PIE data	Large number of R/B data; detailed analysis performed at CEA	0	Medium	Cs-134, Cs-137, Ag-110m	Predetermined fraction of bare kernels in hottest fuel rod	1 value	4	Determined from graphite-lined plateout probes	--	0	High	Cs-134, Cs-137, Sb-125, I-131, Te-129m, Te-132, Ag-110m	Plateout probe with inlet at tube entrance	1 profile from gamma-scan of 200-cm-long tube	As-received SS	Determined from profiles	0	Medium
SSL-1 (loop)	(8 Th,U)O_2 TRISO fissile; ThO_2 TRISO fertile	93	120 EFPD	7.3% fissile 0.9% fertile	Test and analysis complete	First test subjected to quantitative code verification studies	In-pile R/B data used to define particle failure fractions	100	Medium	Cs-134, Cs-137	Uncertain release from failed fissile particles	1 value	1	Assigned from three plateout measurements, large uncertainty	--	100	Medium	Cs-134, Cs-137	Not well defined	Single profile derived from 3 data points	Inconel	--	No analysis attempted	--
SSL-2 (loop)	UC_2 TRISO fissile; ThO_2 BISO fertile	93	240 EFPD	72% fissile 3.6% fertile	Test complete, analysis in progress	Long (240 day) loop irradiation with reference fuel	In-pile R/B data, likely to be used to define failure fraction	0	Medium	Cs-134, Cs-137	Diffusive release from intact fertile particles	0	1 or more	Derived from gamma-scan measurements of downstream metal surfaces	Diffusive release of Cs from intact BISO particles evident	0	High	Cs-134, Cs-137	Defined by FIPERQ calculations	Single profile available	Inconel	Reference values used	0	Low
Rebise-Q2 (capsule)	(8 Th,U)O_2 BISO (tentative)	93	7 cycles of 30 days	>7%	Test in planning stage	In-pile temperatures and release well-defined; best test of Cs release from BISO particles	Intermittent measurement of total release of long-lived isotopes	--	--	Cs-134, Cs-137	Release from intact BISO particles	--	--	--	--	0	High	Cs-134, Cs-137	Defined by PIE measurements and COPAR code predictions	Measured during PIE	Molybdenum	Reference values used	0	Low
Fuel test elements	Dependent on fuel studied	93 (some LEU)	$\leq$ 900 EFPD	Variable	Irradiation complete, analysis in progress	Wide variety of fuel types tested	In-pile instrumentation (in some cases)	0	Medium	Cs-134, Cs-137 Sr-90	Variable	--	Variable	Estimated from gamma-scan measurements	--	30	Low	--	--	--	--	--	--	--
Fuel performance capsules	Dependent on fuel studied	93 (to date)	Variable	Variable	On-going	Verification of fuel failure models	In-pile R/B, used to define failure fractions	On-going	Low	Cs-134, Cs-137	Low release from failed fissile and intact fertile particles	0	0	No release usually detected	--	50	Low	--	--	--	--	--	--	--
Saphir (loop)	AVR fuel balls	93	14000 h	Low	Irradiation and analysis complete	AVR pebble bed fuel	--	--	--	Cs-134, Cs-137	Variable	--	--	Uncertain	--	0	Low	Cs-134, Cs-137, Sr-89, Ag-111, I-131, Zn-65	Variable	Determined from gamma-scans and radiochemistry	Steel, graphite	--	0	High
Vampire (probe in AVR reactor)	AVR fuel balls	93	~1 month	Low	On-going	Measure of fission product release from operating reactor	Operating R/B data	0	Low	Cs-134, Cs-137	Diffusive release from AVR BISO fuel	--	--	Determined from integration of probe results	--	0	Low	Cs-134. Cs-137	Determined from integration of probe results	Determined from gamma-scans and radiochemistry of probes	Variable	--	0	Medium
Dragon (reactor)	UC_2 TRISO fissile	8	10 yrs	~10%	Test complete, reactor shutdown	Data from operating reactor that used LEU fuel	Operational R/B of numerous noble gases and iodine	0	Medium	Cs-134, Cs-137, Ag-110, Sr-89, Sr-90, and others	Release from intact (Ag) and failed TRISO coated particles	--	Numerous	Variable	Data from test elements available	0	High	Cs-134, Cs-137, Sr-90, Ag-111, I-131, and others	Variable	Determined from gamma-scans and radiochemical analysis	Variable	--	0	High
Comedie (loop)	Variable	Undecided	Variable	Variable	Operational tests beginning	Follow-on to CPL tests	In-pile R/B will be monitored	0	Medium	Cs-134, Cs-137, Sr-89, Sr-90, and others	Variable	Undecided	Undecided	Estimated from gamma-scan measurements	In-situ depressurization	0	High	Cs, Sr and others	Defined by probes and calculations	Precise plateout profiles	Variable	Determined from plateout profiles	0	High
Aida (loop)	Variable	Undecided	Variable	Variable	Loop in planning stage	Follow-on to CPL tests	In-pile R/B will be monitored	0	Medium	Cs-134, Cs-137, Sr-89, Sr-90, I-131 and others	Predetermined fraction of bare kernels	Undecided	Undecided	Plateout probe	--	0	High	Cs, Sr and others	Defined by probes and calculations	Same as CPL	Variable	Comedie loop measurements	0	High
SMOC (loop)	--	--	--	--	Test in early construction	Out-of-pile deposition loop	--	--	--	--	--	--	--	--	--	--	--	Cs and others	Tagged source present in loop	Determined from gamma-scan, radiochemistry and electron microprobe analysis	High-alloy steels	--	0	High

(1) improving the accuracy of the design data, (2) improving the statistical (uncertainty) treatment of the design data, and (3) providing additional (referenceable) supporting data. Areas covered in this review are discussed in the following sections; a summary of the results for each area is given below.

1. Burnup Dependence of R/B for Failed Oxide Fuel Particles. Available data indicate that R/B for failed oxide particles increases with burnup. A burnup dependence equation is presented.

2. Diffusion Coefficient Data for Fission Product Metals in Kernel Materials. Supporting data are presented for assigning diffusion coefficient data and uncertainties for barium, europium, samarium, cerium, and rubidium in carbide and oxide kernels.

3. Diffusion Coefficient Data for Fission Product Metals in Pyrocarbon. Supporting data are presented for assigning diffusion coefficient data and uncertainties for strontium, barium, europium, samarium, cerium, and rubidium in pyrocarbon.

4. Estimation of Upper Limit Concentrations of Selected Fission Product Metals in Pyrocarbon Coatings. Upper limit concentrations of cesium, barium, and europium to be encountered in the pyrocarbon coatings under normal reactor conditions were estimated as an aid in selecting appropriate diffusion coefficient data for these elements in pyrocarbon.

5. Sorption of Fission Product Metals on Fuel Rod Matrix Material. This section provides supporting data for selecting design sorption data for cerium, europium, rubidium, barium, and other elements on fuel rod matrix material.

6. Diffusion Coefficients for Fission Product Metals in Graphite. This section presents new design diffusion coefficient data for

rubidium and barium in graphite and supports treating the diffusion of cerium, europium, and samarium in the same manner as the diffusion of strontium.

7. Sorption of Selected Fission Product Metals on Graphite. This section presents new design isotherms for the sorption of strontium, barium, and rubidium on graphite and supports the assumption that the vapor pressures of cerium, samarium, europium, and other elements are equal to or less than that of strontium.

8. Form of Uncertainty Expressions. This section presents relationships for converting uncertainty expressions to a form applicable to the core design computer codes.

Burnup Dependence of R/B for Failed Oxide Fuel Particles

This section describes the results of an effort to establish the burnup dependence of R/B for failed coated oxide particles. As detailed below, the available data suggest that R/B increases with burnup over the range 0 to 8% FIMA, which is the burnup range of interest for fertile particles.

The available burnup dependence data are given in Fig. 4-31. The data are for Kr-85m at 1100°C (±50°C) and represent several types of failed oxide particles. Included are data for failed ThO_2 particles, which are the reference fertile particles, but these data are relatively uncertain because the fraction of failed particles in the fuel rods tested was not well known.

On the basis of the data in Fig. 4-31, the dependence of R/B on burnup for failed ThO_2 fuel particles at 1100°C is taken to be

$$R/B = 0.0246 \exp[-1.594/(1 + 0.584F)] \quad , \qquad (4\text{-}6)$$

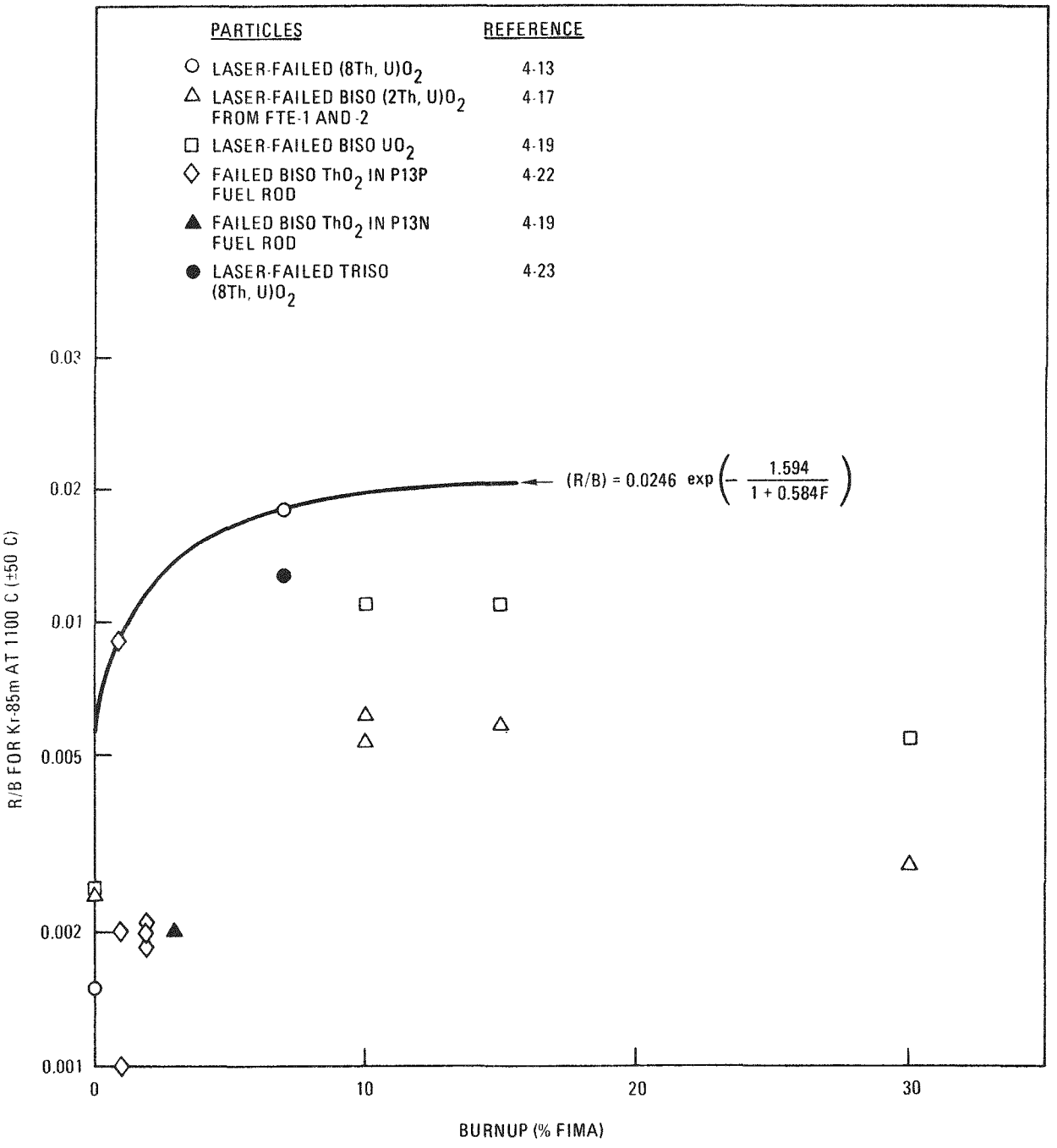

Fig. 4-31. Effect of burnup on R/B for failed coated oxide particles

where F is % FIMA. This equation is represented by the curve in Fig. 4-31; the position of the curve relative to the data shows that Eq. 4-6 is a conservatively high estimate of the data. The R/B value of 0.005 at zero % FIMA, which fixes one end of the curve, was selected on the basis that (1) it is conservatively high, based on the data, and (2) it is the average R/B value found for failed carbide particles (Ref. 4-18). The form of Eq. 4-6, with respect to the F dependence, is the same as was found adequate to describe the burnup dependence for release of long-lived and stable gases from ThO_2 fuel (Ref. 4-18).

Assuming that the exponential dependence on fluence applies at all temperatures, Eq. 4-6 becomes

$$(R/B)_{T,F} = 4.92\ (R/B)_T \exp[-1.594/(1 + 0.584F)] \quad , \qquad (4-7)$$

where $(R/B)_T$ is the R/B value calculated at temperature T for zero % FIMA and $(R/B)_{T,F}$ is the R/B value calculated at temperature T for F % FIMA. Equation 4-7 is assumed to apply to nuclides of Xe, I, Te, Br, and Se, as well as those of Kr.

Diffusion Coefficient Data for Fission Product Metals in Kernel Materials

This section provides supporting data for assigning diffusion coefficient data and uncertainties for strontium, barium, europium, samarium, cerium, and rubidium in kernel material.

Barium Diffusion in Oxide Kernels. A study of the distribution of barium and strontium in UO_2 kernels (Ref. 4-24) indicated that a significant portion of barium is very mobile in contrast to strontium, suggesting that the release of barium is greater than that of strontium. Reduced diffusion coefficients for barium in $(Th,U)O_2$ kernels, presented in Table 4-12, were derived from postirradiation anneal experiments (Ref. 4-23). Reduced diffusion coefficients for strontium derived from these experiments were reported earlier (Ref. 4-25).

TABLE 4-12
KERNEL DIFFUSION COEFFICIENTS FOR BARIUM CALCULATED FROM ANNEALING RELEASE CURVES FOR BISO COATED PARTICLES

Sample Ident.	Particle Characteristics		Irradiation Conditions		Anneal Temp. (°C)	Reduced Diffusion Coefficient (s^{-1})
	Fuel Type	Kernel Diameter (μm)	Irrad. Temp. (°C)	FIMA (%)		
2702-57E[(a)]	$(Th,U)O_2$	240 - 300	1165	3.0	1400	6.9×10^{-10}
2702-57E	$(Th,U)O_2$	240 - 300	1165	3.0	1550	7.7×10^{-9}
2702-57E	$(Th,U)O_2$	240 - 300	1165	3.0	1650	4.7×10^{-7}
3023-99E	$(Th,U)O_2$	300 - 420	1600	2.5	1400	2.0×10^{-9}
3023-99E	$(Th,U)O_2$	300 - 420	1600	2.5	1550	1.2×10^{-8}

[(a)] Sample 2702-57E consists of triplex-coated particles. (Triplex coatings consist of an inner buffer (10 W density) procarbon layer, an isotropic pyrocarbon layer, and an outer granular pyrocarbon layer.)

The data of Table 4-12 are plotted in Fig. 4-32. The least-squares fit to the data is given by the following expression for the reduced diffusion coefficient:

$$D' = 2.16 \times 10^{8} \, e^{-557000/RT} \quad , \tag{4-8}$$

where $D' = D/a^2$ (s^{-1}),

D = diffusion coefficient,

a = radius of the equivalent sphere of the particle or grain through which diffusion occurs.

The activation energy (557000) is in units of J/mol. The associated variance for a single estimated value of the dependent variable in terms of ln D' is

$$S^2 (\ln D') = 80.8 - 28.2 \, (10^4/T) + 2.51 \, (10^4/T)^2 \quad , \tag{4-9}$$

where S is the standard deviation. A line representing Eq. 4-8 is given in Fig. 4-32 with 95% confidence limits calculated using Eq. 4-9.

If Eq. 4-8 for barium diffusion is compared with the reduced diffusion coefficient expression for strontium (Ref. 4-26), the ratio is found to be

$$\frac{D'_{Ba}}{D'_{Sr}} = 0.11 \, e^{4450/T} \quad , \tag{4-10}$$

indicating that the reduced diffusion coefficient for barium in oxide kernels is larger than that for strontium at temperatures below 2016 K. This result is consistent with the observation of Ref. 4-24 as stated above.

Barium Diffusion in Carbide Kernels. Only a few, rather uncertain data on the release of barium from carbide kernels are available from post-irradiation anneal experiments (Ref. 4-23), and these data are only for burnups to 13% FIMA.

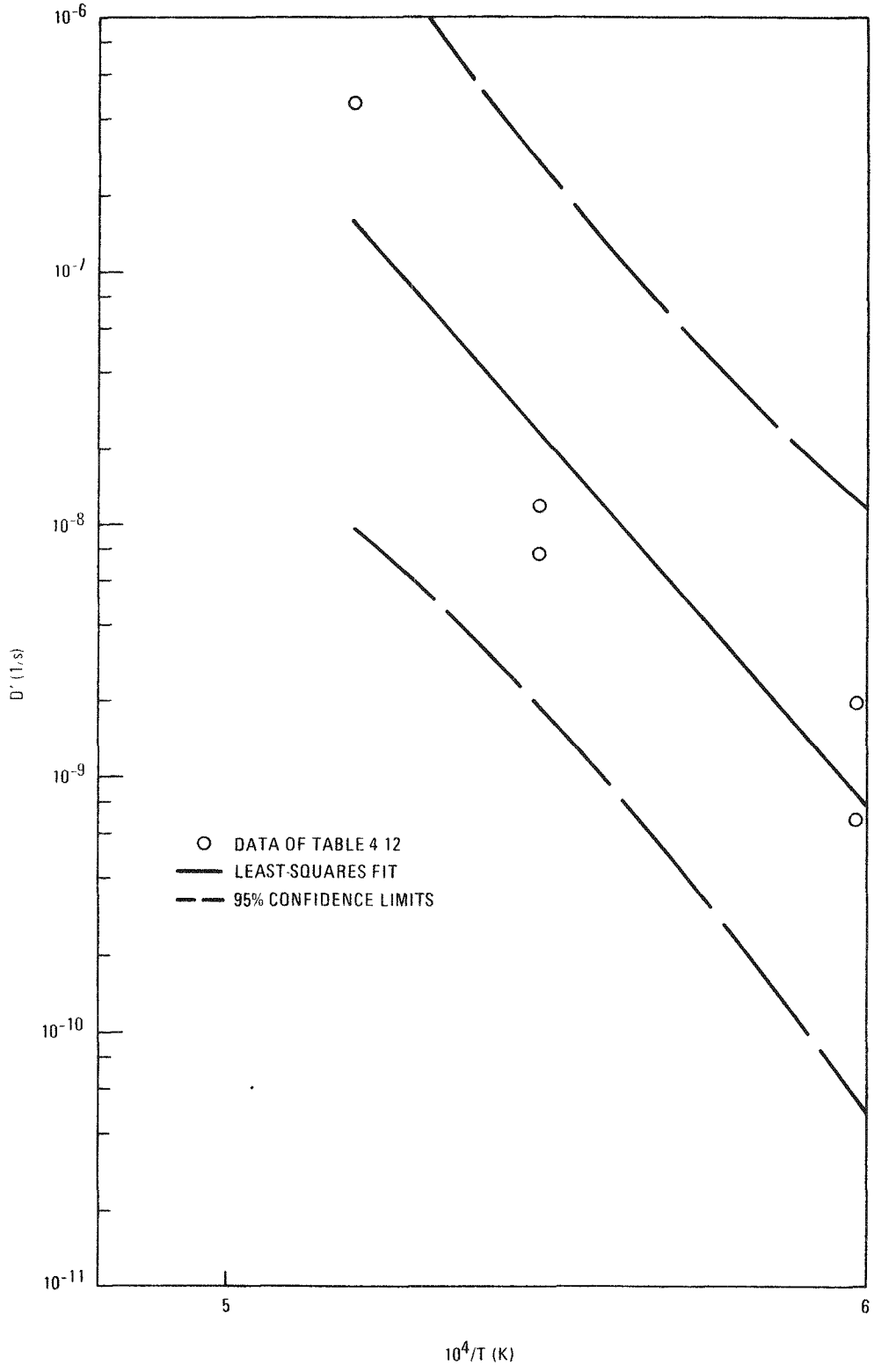

Fig. 4-32. Reduced diffusion coefficients for barium in oxide kernels

In electron microprobe studies on annealed TRISO UC_2 particles (Ref. 4-27), cesium and barium were not detected in the UC_2 kernels, suggesting that barium and cesium exhibit similar release behavior and that both have relatively high mobility in carbide kernels. Earlier electron microprobe studies of TRISO UC_2 particles (Ref. 4-5) showed that cesium is released from UC_2 kernels during irradiation to 63% FIMA at less than 700°C.

On the basis of these observations, it is appropriate to assume that the release of barium, as well as cesium, from coated UC_2 particles under normal reactor conditions is limited only by the coatings (i.e., there is no appreciable holdup of barium and cesium in the kernel).

Strontium Diffusion in Carbide Kernels. Data on the release of strontium from carbide kernels has been presented previously (Ref. 4-26). These data show considerable scatter and are limited to burnups $\lesssim$20% FIMA. Accordingly, in the case of strontium release from carbide kernels over the full range of burnup, the assumption of no appreciable holdup in the kernel is appropriate.

Cerium Diffusion in Oxide Kernels. The data on cerium are limited. Brown and Faircloth (Ref. 4-11) have found roughly the same distribution for strontium and cerium between kernel and coating for coated UO_2 particles. In accord with this information, it can be assumed that the diffusion coefficient for cerium in oxide kernels is equal to that for strontium.

Cerium Diffusion in Carbide Kernels. There are no release data for cerium over the full burnup range of carbide kernels; as for strontium, the assumption of no holdup in the kernel is appropriate.

Europium and Samarium Diffusion in Oxide Kernels. No data on the release of europium or samarium from oxide kernels were found. On the basis of the physical and chemical similarity of europium and samarium to cerium, it is appropriate to treat these two elements the same as cerium

(see above). Accordingly, the diffusion coefficient for europium and samarium in oxide kernels is assumed to be equal to that of strontium.

Europium and Samarium Diffusion in Carbide Kernels. There are apparently no data on the release of europium and samarium over the full burnup range of carbide kernels; as for strontium, the assumption of no holdup in the kernel is appropriate.

Rubidium Diffusion in Oxide Kernels. No data on the release of rubidium from oxide kernels were found. An estimate of the reduced diffusion coefficient for rubidium in oxide kernels is made based on (1) the bond strengths of oxygen with rubidium and cesium, and (2) the reduced diffusion coefficient of cesium in oxide kernels. The bond strengths are 289000 J/mol for cesium and 234000 J/mol for rubidium (Ref. 4-28). Accordingly, the estimated reduced diffusion coefficient for rubidium in oxide kernels is:

$$D'_{Rb}\ (1/s) = \frac{e^{-234000/RT}}{e^{-289000/RT}} \cdot D'_{Cs}$$

$$= e^{55000/RT}\ \ 3.8 \times 10^{-3}\ e^{-268000/RT}$$

$$= 3.8 \times 10^{-3}\ e^{-213000/RT} \quad , \qquad (4\text{-}11)$$

where D'_{Cs} is from Ref. 4-16. The associated variance is taken to be the same as that of cesium (Ref. 4-16), i.e.,

$$S^2\ (\ln D') = 4.90 - 1.47\ (10^4/T) + 0.113\ (10^4/T)^2 \quad , \qquad (4\text{-}12)$$

where S is the standard deviation in ln D'.

Rubidium Diffusion in Carbide Kernels. There are no data on the release of rubidium over the full range of burnup of carbide kernels; as for cesium and strontium, the assumption of no holdup in the kernel is appropriate.

Uncertainty of Diffusion Coefficient Data for Strontium in Oxide Kernels. Based on the data in Ref. 4-26, the variance for a single estimated value of the dependent variable in terms of ln D' is

$$S^2 (\ln D') = 69.2 - 24.5 (10^4/T) + 2.18 (10^4/T)^2 \quad . \qquad (4\text{-}13)$$

Diffusion Coefficient Data for Fission Product Metals in Pyrocarbon

This section provides supporting data for assigning (1) diffusion coefficient data and uncertainties for barium, europium, samarium, cerium, and rubidium in pyrocarbon, and (2) the uncertainty for diffusion coefficient data for strontium in pyrocarbon.

Barium Diffusion in Pyrocarbon. Data on barium diffusion in pyrocarbon have been obtained in experiments using pyrocarbon wafers (Ref. 4-29) and irradiated fuel particles (Ref. 4-30). In the Ref. 4-30 experiments, data were obtained in the temperature range between 1273 and 1973 K for source concentrations of 10^{-2} and 10^{-5} g Ba/g carbon. The derived diffusion coefficients were strongly dependent on the source concentrations, the diffusion coefficients being larger for the larger source concentration. However, as shown in a following section, source concentrations of barium will be less than about 4×10^{-4} g Ba/g carbon under HTGR normal operating conditions. Consequently, the data at the higher source concentration need not be considered here.

The data on barium diffusion in pyrocarbon at the lower source concentration, 10^{-5} g Ba/g carbon, are given in Table 4-13. These data are from chemical and self-diffusion experiments (Ref. 4-29); no distinction between the data from these two types of experiments is made in treating the data.

Postirradiation anneal experiments (Ref. 4-30) were performed with samples of pyrocarbon coated UO_2 particles irradiated to 11% FIMA and UC_2

TABLE 4-13
DATA ON DIFFUSION OF BARIUM IN PYROCARBON

Temp. (K)	D (m^2/s)	Pyrocarbon Type	Reference
1273	1.5×10^{-14}	(a)	Ref. 4-29, Table 4.6, p. 34
1273	2.3×10^{-14}		
1523	1.6×10^{-13}		
1673	3.3×10^{-13}		
1823	1.4×10^{-12}		
1973	2.9×10^{-12}		
1973	2.7×10^{-12}		
1273	2.7×10^{-15}		
1473	4.2×10^{-14}		
1673	4.3×10^{-13}		
1873	2.7×10^{-12}		
1973	7.4×10^{-12}		
1423	1.0×10^{-13}	LTI	Ref. 4-30, Table 5.3, p. 66
1423	1.1×10^{-14}	HTI	
1423	6.0×10^{-14}	LTI	
1773	4.1×10^{-13}	LTI	
1973	4.3×10^{-12}	LTI	

(a) The types of pyrocarbon used in these determinations were granular, isotropic, and laminar.

particles irradiated to 13% FIMA. The temperature range of the experiments was between 1423 and 1973 K. These data are included in Table 4-13.

All the data of Table 4-13 are plotted in Fig. 4-33. From a least-squares fit to the data, the following expression for the diffusion coefficient is derived:

$$D\ (m^2/s) = 2.10 \times 10^{-7}\ e^{-181000/RT} \quad , \qquad (4\text{-}14)$$

where the activation energy is in units of J/mol. The associated variance for a single estimated value of the dependent variable in terms of ln D is:

$$S^2\ (\ln D) = 1.63 - 0.35\ (10^4/T) + 0.028\ (10^4/T)^2 \quad , \qquad (4\text{-}15)$$

where S is the standard deviation. Equation 4-14 and 95% confidence limits calculated using Eq. 4-15 are represented by the solid and dashed lines in Fig. 4-33.

Europium Diffusion in Pyrocarbon. Data on europium diffusion in pyrocarbon have been obtained (Ref. 4-29) over the temperature range 1073 to 1523 K for source concentrations of 1.9×10^{-3} and 6.0×10^{-7} g Eu/g carbon. As shown in a following section, source concentrations of europium will be less than about 5×10^{-6} g Eu/g carbon under HTGR normal operating conditions. Thus, only the lower source concentration data are of present interest. A dependence of the diffusion coefficient on the source concentration, as found in the case of barium, is consistent with the europium data but cannot be substantiated because of the limited number of data. Only two data exist for the lower source concentration: 6.0×10^{-13} at 1523 K and 2.1×10^{-13} at 1273 K.

An estimate of the diffusion coefficient expression, based on the two data at low source concentration, is the following:

$$D\ (m^2/s) = 1.3 \times 10^{-10}\ e^{-68000/RT} \quad , \qquad (4\text{-}16)$$

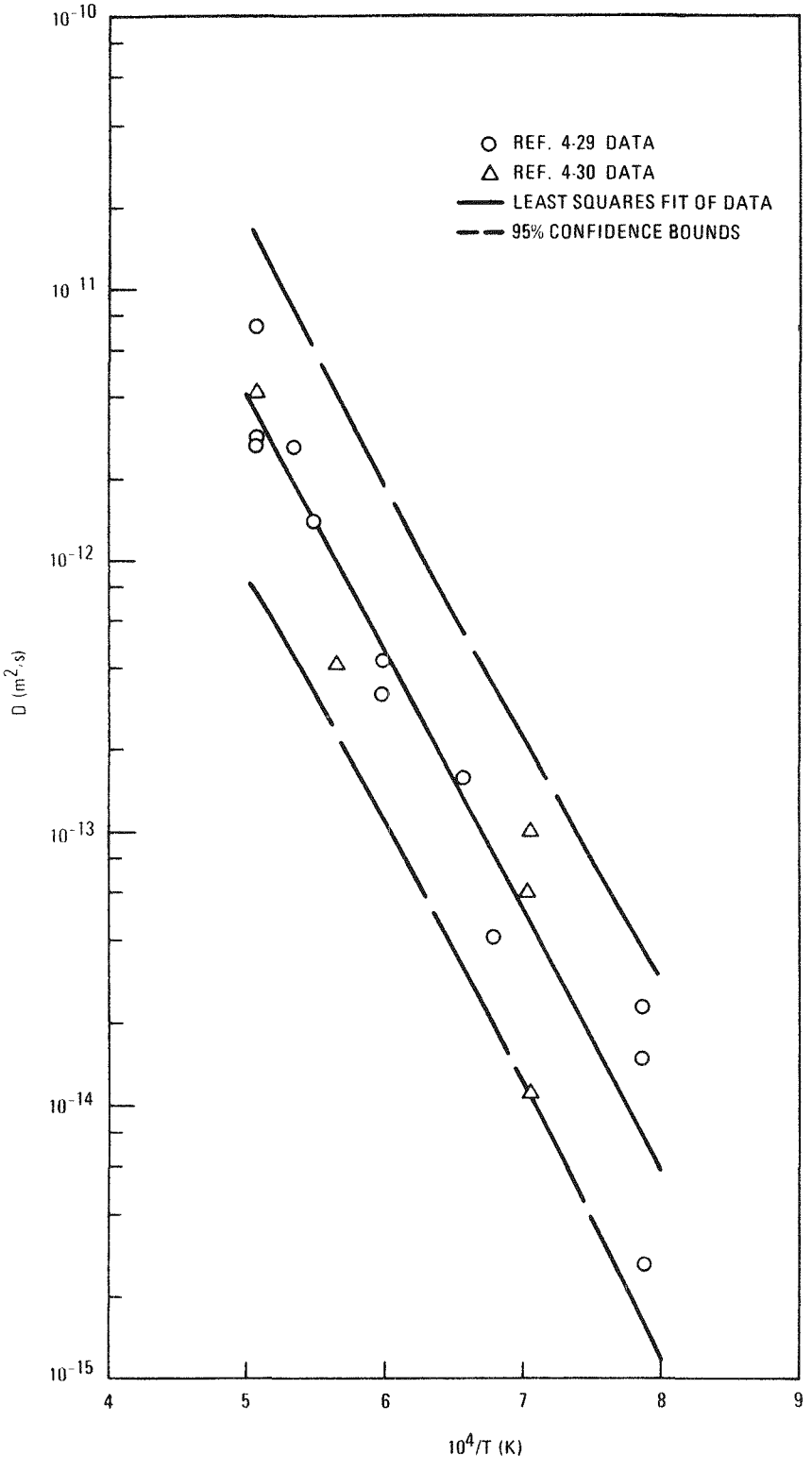

Fig. 4-33. Diffusion coefficients for barium in pyrocarbon

where the activation energy is in J/mol.

The standard deviation is undoubtedly quite large; the following is an estimate of the variance based on assuming the same temperature dependence for high and low source concentrations:

$$S^2 (\ln D) \cong 2.3 \quad . \tag{4-17}$$

Samarium Diffusion in Pyrocarbon. No data on samarium diffusion in pyrocarbon were found. The diffusion coefficient and variance expressions applied to europium (Eqs. 4-16 and 4-17) are assumed to apply to samarium on the basis of the physical and chemical similarity of samarium and europium.

Diffusion of Cerium in Pyrocarbon. Apparently, only one diffusion coefficient value for cerium in pyrocarbon is available. This value, $\sim 3.2 \times 10^{-14}$ m^2/s, was obtained in a postirradiation anneal test at 1423 K on a pyrocarbon (LTI type) coated UC_2 particle irradiated to 13% FIMA (Ref. 4-30).

Other postirradiation anneal tests (Ref. 4-27) conducted in the temperature range 1873 to 2273 K yielded information on the relative release of europium and cerium from TRISO UC_2 particles. (The SiC coating became permeable during the anneals.) In these tests, europium and cerium release fractions were found to be similar, indicating similar diffusion behavior for the two elements in the outer pyrocarbon coating.

The above diffusion coefficient value for cerium in pyrocarbon (3.2×10^{-14} m^2/s) is an order of magnitude smaller than the value predicted using Eq. 4-16, the diffusion coefficient expression for europium. However, this difference cannot be considered significant, given (1) the uncertainty in Eq. 4-16, (2) the approximate nature of the cerium diffusion coefficient value, and (3) the above described observation of similar behavior for the two elements. Accordingly, cerium is conservatively treated by assuming that Eqs. 4-16 and 4-17 apply also to cerium.

Rubidium Diffusion in Pyrocarbon. There are apparently no data on rubidium diffusion in pyrocarbon. Considering the chemical and physical properties of the elements, one would expect that the diffusion behavior of rubidium in relation to that of cesium is like the behavior of strontium in relation to that of barium. In estimating the diffusion coefficient expression for rubidium, this supposition is employed as follows.

The ratio of the diffusion coefficient expressions for strontium to barium is

$$\frac{D_{Sr}}{D_{Ba}} = 11.0\ e^{-16000/RT} \quad , \tag{4-18}$$

where the diffusion coefficient expression for strontium was taken from Ref. 4-26 and that for barium is Eq. 4-14. Then, the diffusion coefficient expression for rubidium becomes

$$D_{Rb} = (D_{Sr}/D_{Ba})D_{Cs} = 5.5 \times 10^{-4}\ e^{-334000/RT} \quad , \tag{4-19}$$

where the diffusion coefficient expression for cesium was taken from Ref. 4-16. The uncertainty associated with D_{Rb} is based on that for cesium (Ref. 4-16) but increased by a factor of 2; thus,

$$S^2\ (\ln D) = 5.42 - 1.05\ (10^4/T) + 0.0927\ (10^4/T)^2 \quad . \tag{4-20}$$

Uncertainty of Diffusion Coefficient Data for Strontium in Pyrocarbon. Based on the data in Table 4-3 of Ref. 4-26, the uncertainty of diffusion coefficient data for strontium in pyrocarbon has been calculated to give the variance for a single estimated value of the dependent variable in terms of ln D as follows:

$$S^2\ (\ln D) = 5.54 - 1.38\ (10^4/T) + 0.112\ (10^4/T)^2 \quad , \tag{4-21}$$

where S is the standard deviation in ln D.

Estimation of Upper Limit Concentrations of Selected Fission Product Metals in Pyrocarbon Coatings

Upper limit concentrations to be encountered in the pyrocarbon coatings of fuel particles in the HTGR under normal operating conditions are estimated as follows:

1. The cesium concentration at the buffer - inner pyrocarbon interface is obtained from measurements of release profiles in post-irradiation anneal tests on irradiated particles (Ref. 4-30). This concentration is an upper limit to the cesium concentration in the pyrocarbon.

2. The upper limit cesium concentration of item (1) is corrected for full burnup of the fuel.

3. The ratio of the inventory of the element of interest to that of cesium is calculated from published nuclide inventories in the fuel (Table 11.1-5 of Ref. 4-31).

The concentration of cesium at the inner surface of the pyrocarbon in fertile particles irradiated to 3.5% FIMA is about 10^{17} atoms Cs/g carbon (from Ref. 4-30). At full burnup of 7.5% FIMA, the estimate of the weight fraction of cesium is taken to be

$$\frac{(7.5/3.5)\ 10^{17}\ (137)}{6.02 \times 10^{23}} \simeq 5 \times 10^{-5}\ \text{g Cs/g carbon} \quad .$$

For fissile particles, the concentration of cesium at the inner surface of the pyrocarbon for particles irradiated to 13% FIMA is $\sim 10^{18}$ atoms Cs/g carbon (from Ref. 4-30). At full burnup of 78% FIMA, the estimate of the weight fraction of cesium is taken to be

$$\frac{(78/13)\ 10^{18}\ (137)}{6.02 \times 10^{23}} \simeq 10^{-3}\ \text{Cs/g carbon} \quad .$$

From Ref. 4-31, the ratios of the mass of barium and europium to that of cesium are 0.36 and 0.005, respectively. Therefore, the estimated upper limit concentrations in the pyrocarbon coatings for fertile and fissile particles for the elements barium and europium are as follows:

	Upper Limit Concentration in Pyrocarbon (g element/g carbon)	
	Fertile Particles	Fissile Particles
Ba	2×10^{-5}	4×10^{-4}
Eu	3×10^{-7}	5×10^{-6}

Sorption of Fission Product Metals on Fuel Rod Matrix Material

This section provides supporting data for assigning sorption isotherms for cerium, europium, samarium, rubidium, barium, and other elements on fuel rod matrix material.

Sorption of Cerium, Europium, and Samarium on Fuel Rod Matrix Material. There are no data for sorption of cerium, europium, and samarium on fuel rod matrix material. Estimates of the sorption isotherms are made by comparing the relative vapor pressure of these elements in a graphite system with those of strontium and barium. The thermodynamic data (Refs. 4-32 and 4-33) necessary to make the comparison are shown in Table 4-14. The relationship between the thermodynamic data and the vapor pressure is also presented in Table 4-14. In Table 4-15, calculated vapor pressures are presented. These data show that the vapor pressures of cerium, europium, and samarium are smaller than those of strontium in the temperature range 1000 to 1600 K. Therefore, as a conservative estimate, cerium, europium, and samarium are assumed to have the same sorption behavior on fuel rod matrix material as strontium.

Sorption of Rubidium on Fuel Rod Matrix Material. There are no data for rubidium sorption on fuel rod matrix material. To estimate the sorption isotherm, use is made of the ratio of rubidium to cesium sorption on

TABLE 4-14
THERMODYNAMIC DATA USEFUL IN CALCULATING VAPOR PRESSURES OF SELECTED FISSION PRODUCT ELEMENTS AND THEIR DICARBIDES [a]

Vapor Species	ΔH_T° (kJ/mol)	ΔS_T° (J/mol·K)	B	A	Ref.
Sr	226	71	11800	8.7	4-32
Ba	234	59	12200	8.1	4-32
Ce	--	--	29500	11.8	4-33
CeC_2	--	--	36700	14.8	4-33
Sm	264	71	13800	8.7	4-32
Eu	222	63	11600	8.3	4-32
EuC_2	--	--	26200	11.7	4-33

[a] $\log P(Pa) = -\frac{B}{T} + A$

$B = \Delta H_T^\circ / 2.303R$

$A = (\Delta S_T^\circ / 2.303R) + 5.006$

$R = 8.314$ J/mol·K

TABLE 4-15
CALCULATED VAPOR PRESSURES OF SELECTED FISSION PRODUCT ELEMENTS AND THEIR DICARBIDES AT SELECTED TEMPERATURES

Temp. (K)	Vapor Pressure (Pa)								
	Sr	Ba	Ce	CeC_2	Ce + CeC_2	Sm	Eu	EuC_2	Eu + EuC_2
1000	7.9×10^{-4}	7.9×10^{-5}	2.0×10^{-18}	1.3×10^{-22}	2.0×10^{-18}	7.9×10^{-6}	5.0×10^{-4}	3.2×10^{-15}	5.0×10^{-4}
1200	7.4×10^{-2}	8.6×10^{-3}	1.6×10^{-13}	1.6×10^{-16}	1.6×10^{-13}	1.6×10^{-3}	4.3×10^{-2}	7.4×10^{-11}	4.3×10^{-2}
1400	1.9×10^{0}	2.4×10^{-1}	5.4×10^{-10}	3.9×10^{-12}	5.4×10^{-10}	7.0×10^{-2}	1.0×10^{0}	9.7×10^{-8}	1.0×10^{0}
1600	$2.1 \times 10^{+1}$	3.0×10^{0}	2.3×10^{-7}	7.3×10^{-9}	2.4×10^{-7}	1.2×10^{0}	$1.1 \times 10^{+1}$	2.1×10^{-5}	1.1×10^{1}

graphite. Thus, the sorption isotherm for rubidium on fuel rod matrix material is determined from the cesium sorption isotherm on fuel rod matrix material corrected by the relationship of the sorption of rubidium to cesium on graphite. The latter relationship is obtained from Ref. 4-34 for sorption on TS-688 graphite and is as follows:

$$\ln C_{Cs} = \frac{\left(-9.0 + \frac{16800}{T}\right) \ln C_{Rb} - \left(12.5 - \frac{21600}{T}\right)}{\left(-14.5 + \frac{24200}{T}\right)} \quad . \qquad (4\text{-}22)$$

The Freundlich isotherm for cesium sorption on fuel rod matrix material is (Ref. 4-16):

$$\ln P_F \text{ (Pa)} = \left(19.3 - \frac{47300}{T}\right) + \left(1.51 + \frac{4340}{T}\right) \ln C_{Cs} \text{ (mmol/kg)} \quad , \qquad (4\text{-}23)$$

where P_F is in units of pascals and C_{Cs} in units of mmol Cs/kg carbon. Equations 4-22 and 4-23 are combined to yield an expression for the pressure P in terms of the concentration of rubidium, C_{Rb}. This expression is simplified to the standard form by reevaluating the constants at temperatures of 1073 and 1273 K with the following result:

$$\ln P_F \text{ (Pa)} = \left(22.1 - \frac{44700}{T}\right) + \left(4.53 + \frac{68}{T}\right) \ln C_{Rb} \text{ (mmol/kg)} \quad . \qquad (4\text{-}24)$$

The transition concentration for rubidium is assumed to be the same as for cesium. Thus,

$$\ln C_t = 3.40 - 6.15 \times 10^{-4} \text{ T (K)} \quad . \qquad (4\text{-}25)$$

The Henrian sorption isotherm for rubidium is based on Eqs. 4-24 and 4-25:

$$\ln P_H \text{ (Pa)} = \left(22.1 - \frac{44700}{T}\right) + \left(3.52 + \frac{68}{T}\right) \ln C_t + \ln C_{Rb} \text{ (mmol/kg)} \quad . \qquad (4\text{-}26)$$

To estimate the uncertainty in the isotherm expressions for rubidium, the assumption is made that the uncertainty in the data establishing the relationship between cesium and rubidium is the same as the uncertainty in the isotherm data for cesium sorption on fuel rod matrix material; thus, for rubidium

$$S^2 (\ln P_F) = 0.84 \tag{4-27}$$

and

$$S^2 (\ln P_H) = 1.52 \quad , \tag{4-28}$$

where S is the standard deviation of $\ln P_i$.

Barium Sorption on Fuel Rod Matrix Material. There are no data for barium sorption on fuel rod matrix material. The isotherm for sorption of strontium on fuel rod matrix material will be taken as an upper limit estimate for barium sorption. This upper limit estimate is based on the fact that strontium vapor pressures are always larger than for barium over graphite at the same sorbate concentration.

Another procedure for estimating the isotherm for barium sorption on fuel rod matrix material was tested and rejected. This procedure assumed that the relation of the isotherm on fuel rod matrix to that on graphite was the same for barium as for strontium. However, this assumption lead to vapor pressures 10^9 times smaller for barium than for strontium over fuel rod matrix material near the transition concentration ($C \sim 20$ mmol/kg) at 1000 K. This was judged to be unreasonable in the absence of any supporting data and therefore the assumption was rejected.

Sorption of Other Elements on Fuel Rod Matrix Material. Under temperature transient conditions, the mobility of certain fission product metallic elements, which are normally immobile, must be considered. These elements are cerium, europium, samarium, zirconium, niobium, molybdenum,

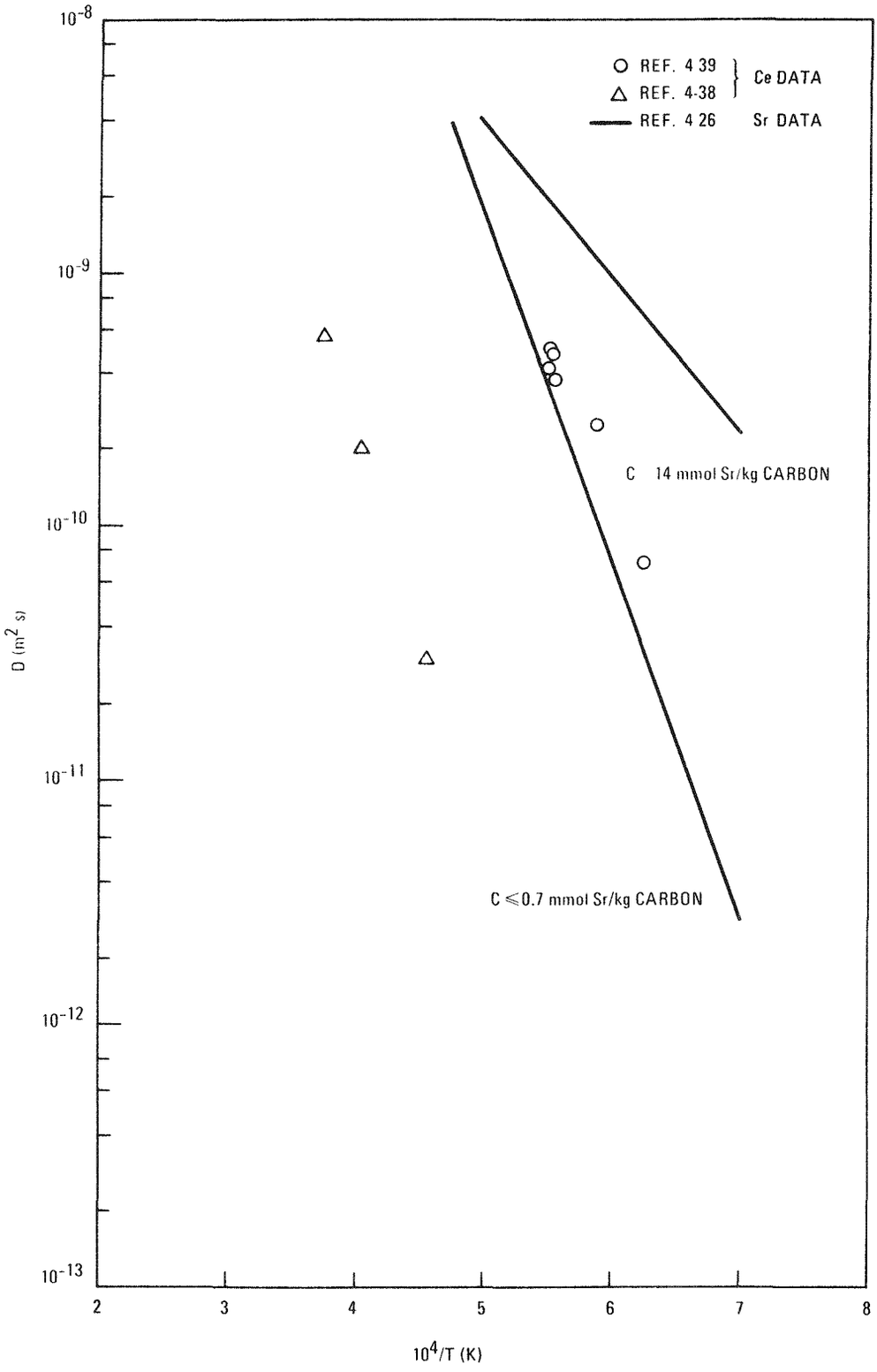

Fig. 4-34. Comparison of diffusion coefficients for cerium and strontium in graphite

strontium is independent of concentration. The concentration of the upper curve, 14 mmol/kg carbon, is the same as the cerium concentration at the surface of the graphite samples in the soaking experiments (Ref. 4-39). In view of the cerium concentration within the graphite, the appropriate curve of strontium diffusion coefficients for comparison with the cerium data of Ref. 4-39 lies between the two curves of Fig. 4-34. Consequently the cerium diffusion coefficients measured in the soaking experiments (Ref. 4-39) are probably not significantly lower than those found for strontium in graphite (Ref. 4-26). By contrast, the cerium data measured using uranium-impregnated graphite (Ref. 4-38) indicate significantly lower diffusion coefficients than either the cerium data of Ref. 4-39 or the strontium curves.

Additional data on europium have been obtained from the fuel test elements FTE-3, -4, and -6 (Ref. 4-40). The diffusion coefficients derived from the profiles in graphite spines for europium range from a factor of five larger to a factor of 180 smaller than the reference diffusion coefficients for strontium diffusion in graphite (Ref. 4-26) within the narrow temperature range 1100 to 1200 K. Seventy-five percent of the europium diffusion coefficients were significantly below the corresponding values for strontium.

The above data suggest that diffusion coefficients for cerium and europium are smaller than those for strontium. However, the data on uranium-impregnated graphite (Refs. 4-35 through 4-38) used non-HTGR type graphites and were obtained with one exception at temperatures beyond the range of interest for HTGRs under normal operating conditions. The soaking experiments (Ref. 4-39) were also on a non-HTGR type graphite. The data from fuel test element analysis have a very large scatter. Accordingly, the prudent choice is to use the diffusion coefficients for strontium to represent those of cerium and europium. This choice would then give upper limit values for cerium and europium. On the basis of physical and chemical similarity, samarium will be treated like cerium and europium.

With these choices, the diffusion coefficient expression for strontium,

$$D\ (m^2/s) = 1.66 \times 10^{-2}\ e^{-268000/RT} \quad , \qquad (4\text{-}29)$$

is used for cerium, europium, and samarium. The activation energy is in units of J/mol. Equation 4-29, which was taken from Table 3-1 of Ref. 4-26, applies to concentrations of $\lesssim$0.7 mmol/kg carbon.

Diffusion of Rubidium in Graphite. There are no data on the diffusion of rubidium in graphite. On the basis of chemical properties, rubidium is expected to behave like cesium. However, from sorption isotherm measurements (Refs. 4-34, 4-41), it is found that rubidium has a higher vapor pressure than cesium over graphite and that cesium readily displaces rubidium on graphite. Cesium migrates in graphite primarily on internal surfaces (Ref. 4-16) and, presumably, rubidium also does. Based on this information, one would expect rubidium to migrate faster than cesium since the bonding of rubidium to surface sites is weaker than for cesium, as indicated by the sorption isotherm measurements.

As an estimate of the upper limit to the diffusion coefficient for rubidium, ten times the diffusion coefficient expression for cesium is recommended. Thus the difussion coefficient expression for rubidium is

$$D\ (m^2/s) = 1.72 \times 10^{-5}\ e^{-148900/RT} \quad , \qquad (4\text{-}30)$$

where the activation energy is in units of J/mol. The diffusion coefficient expression for cesium, used as the basis for Eq. 4-30, is given in Ref. 4-16.

Diffusion of Barium in Graphite. Diffusion coefficient data for barium in graphite have been obtained from experiments with uranium-impregnated samples of AUC graphite (Ref. 4-38), from diffusion spine samples in the Peach Bottom reactor (Ref. 4-40), and from fuel elements in the Pluto Loop A (charge 16) (Ref. 4-42). These data are listed in Table

4-17 and plotted in Fig. 4-35. The data of Table 4-17 and Fig. 4-35 correspond to total diffusant concentrations $\lesssim$0.7 mmol/kg carbon and thus are in the region of concentration in which the diffusion coefficient is independent of concentration [judged by the data on strontium (Ref. 4-26)]. The least-squares fit to the barium data [except for the data of Ref. 4-43 (see below)], shown by the solid line in Fig. 4-35, lies consistently below the strontium line (Ref. 4-26), but the difference in the two lines is not significant. The least-squares fit to the barium data is represented by

$$D\ (m^2/s) = 1.54 \times 10^{-4}\ e^{-243000/RT} \quad , \qquad (4\text{-}31)$$

where the activation energy is in units of J/mol.

Skerker and Zumwalt (Ref. 4-43) have obtained diffusion coefficients for barium in unirradiated H-327 graphite by measuring concentration profiles in thin graphite disks. They gave only analtyical representations of their data, including uncertainties on the activation energies and on the fraction of barium which diffuses by the in-pore path. Consequently, a statistical treatment of their data in combination with the above data is not possible at the present time.

Included in Fig. 4-35 is a plot of the region within which the data of Skerker and Zumwalt fall. [The temperature range of their experiments was approximately 970 to 1450 K (Ref. 4-44).] It can be seen that their data generally lie above the other data and suggest a lower temperature dependence.

The estimated uncertainty of the barium diffusion coefficient data is

$$S^2\ (\ln D) = 32.48 - 4.6\ (10^4/T) + 0.332\ (10^4/T)^2 \quad , \qquad (4\text{-}32)$$

where S is the estimated standard deviation in ln D. This estimated uncertainty is relatively high to account for the data of Skerker and Zumwalt. The 95% confidence bounds derived by using Eq. 4-32 are included in Fig. 4-35.

TABLE 4-17
DIFFUSION COEFFICIENTS FOR BARIUM IN GRAPHITE

Temp. (K)	D (m^2/s)	Graphite	Ref.
1170	3.3×10^{-16}	H-327	4-40
1170	5.8×10^{-16}	H-327	4-40
1164	4.2×10^{-15}	H-327	4-40
1164	4.6×10^{-15}	H-327	4-40
1206	2.6×10^{-14}	H-327	4-40
1206	1.25×10^{-13}	H-327	4-40
1823	2.7×10^{-11}	AUC	4-38
2198	8.0×10^{-10}	AUC	4-38
2473	4.2×10^{-9}	AUC	4-38
2673	1.5×10^{-8}	AUC	4-38
1173	3.6×10^{-15}	HX-30	4-42
1273	3.3×10^{-14}	HX-30	4-42
1393	4.8×10^{-14}	HX-30	4-42
1333	1.9×10^{-14}	HX-30	4-42
$\sim$1673	2.2×10^{-13}	HX-30	4-42
1743	1.3×10^{-13}	HX-30	4-42

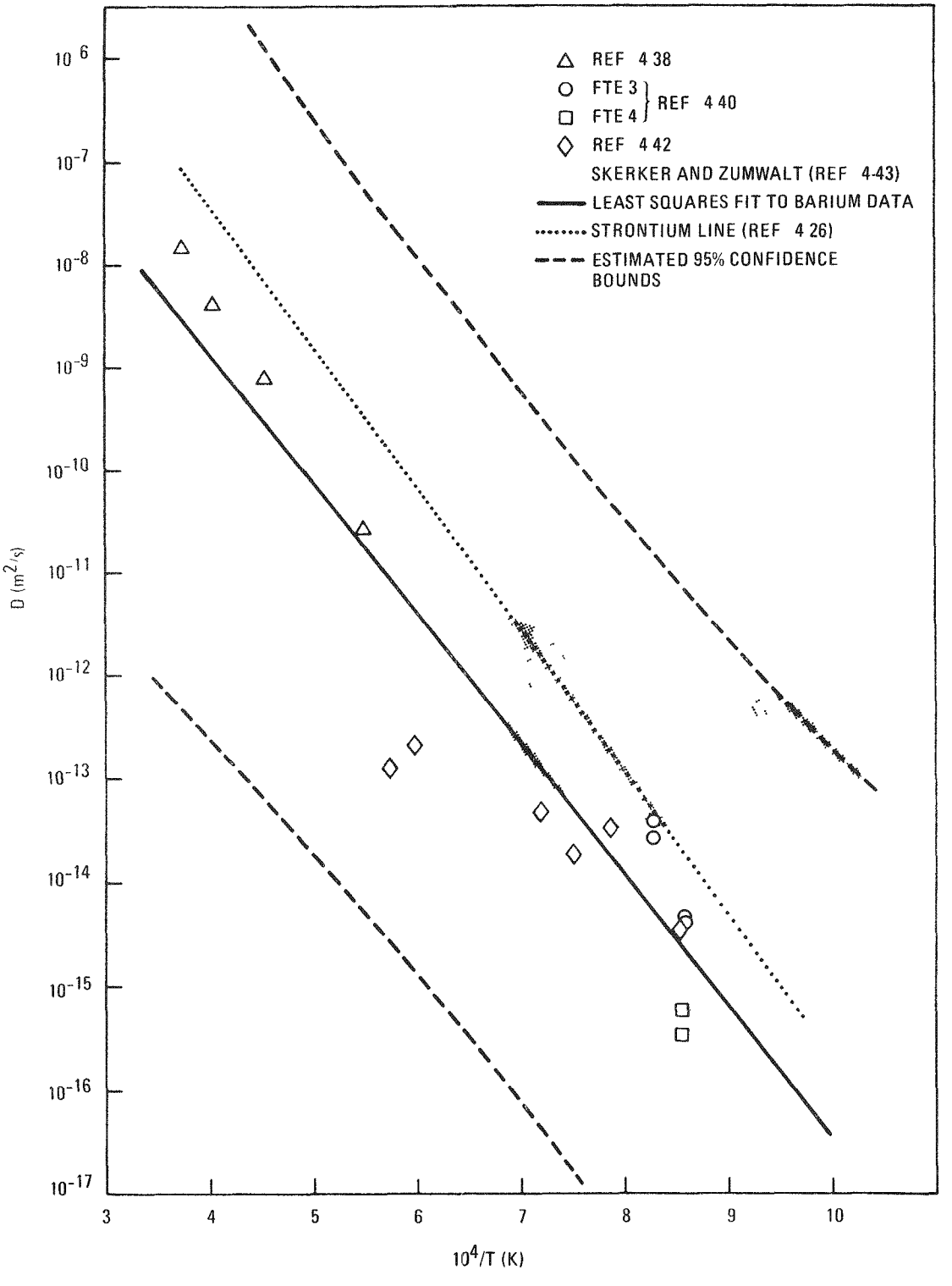

Fig. 4-35. Diffusion coefficients for barium in graphite

Another consideration is that the barium diffusion data of Skerker and Zumwalt were obtained using unirradiated graphite and the data for FTE-3 and -4 were obtained using graphite that had been irradiated to thermal fluences of 0.4 and 1.7 x 10^{25} n/m^2, respectively. Figure 4-35 shows that the data of Skerker and Zumwalt are higher than the FTE-3 data, which in turn are higher than the FTE-4 data. This suggests that the diffusion coefficient for barium in graphite decreases with increasing fluence.

Sorption of Selected Fission Product Metals on Graphite

This section describes the results of a review of sorption data for fission product metals on graphite. New isotherms for the sorption of strontium, barium, and rubidium on graphite and supporting data for the sorption behavior of the other elements are presented.

Sorption of Strontium on Unirradiated Graphite. Most of the data for sorption of strontium on unirradiated graphite apply to H-327 graphite. There are fewer data for sorption on H-451 graphite. These data indicate no significant difference in sorptivity of strontium on H-327 and H-451 graphites.

The data on sorption of strontium on H-327 graphite are presented in Tables 4-18 through 4-20. These data are the results of three experiments (Sr-1, Sr-5, and Sr-6) performed at General Atomic using the mass spectrometric - Knudsen cell method. (For a description of the method see Refs. 4-45 through 4-47.)

The data in Tables 4-18 through 4-20 were derived from experimental (raw) data given in laboratory notebooks (Ref. 4-48). These data apply only to the Freundlich region. All the values of ln P in Tables 4-18 through 4-20 were derived from a fit to the experimental data for each concentration, C. The experimental data were in the form ln P = a - b/T. The standard deviation in P is 5% or less. The values of ln P given in the three tables are within the temperature and concentration ranges of the measurements.

TABLE 4-18

DATA FOR STRONTIUM SORPTION ON UNIRRADIATED H-327 GRAPHITE (EXPERIMENT Sr-1)

conc C' (g Sr/kg carbon)	conc C [(a)] (mmol Sr/kg carbon)	ln C	ln P (Pa)							
			800°C	900°C	1000°C	1100°C	1200°C	1300°C	1400°C	1500°C
4.34	49.32	3.898	-4.65	-2.75	-1.15					
3.66	41.59	3.728	-4.96	-3.01	-1.37	.025				
3.09	35.11	3.559	-5.68	-3.64	-1.92	-.450				
2.72	30.91	3.431	-6.41	-4.26	-2.45	-.903				
2.48	28.18	3.339	-6.66	-4.45	-2.58	-.990				
2.19	24.89	3.214	-6.66	-4.47	-2.62	-1.04				
1.806	20.52	3.022	-6.98	-4.77	-2.91	-1.31				
1.654	18.80	2.934	-7.75	-5.47	-3.54	-1.90				
1.558	17.70	2.874		-5.84	-3.85	-2.15				
1.475	16.76	2.819		-6.16	-4.12	-2.38				
1.320	15.00	2.708		-6.39	-4.36	-2.62	-1.12			
1.191	13.53	2.605		-6.77	-4.73	-3.00	-1.49			
0.941	10.69	2.370		-7.32	-5.22	-3.43	-1.88	-.53		
0.740	8.41	2.129		-8.27	-6.08	-4.22	-2.61	-1.21		
0.641	7.28	1.986			-6.49	-4.60	-2.97	-1.54		
0.533	6.06	1.801			-7.19	-5.22	-3.52	-2.04		
0.495	5.62	1.727			-7.66	-5.64	-3.89	-2.36		
0.464	5.27	1.663			-7.91	-5.87	-4.11	-2.57		
0.414	4.70	1.549			-8.28	-6.22	-4.43	-2.88		
0.360	4.09	1.409			-8.62	-6.54	-4.74	-3.18	-1.80	
0.309	3.51	1.256			-8.97	-6.88	-5.08	-3.50	-2.11	
0.222	2.52	0.925				-7.56	-5.67	-4.02	-2.56	
0.1936	2.20	0.788				-7.97	-6.02	-4.33	-2.84	
0.1629	1.85	0.616				-8.06	-6.14	-4.47	-2.99	
0.1178	1.34	0.292				-8.84	-6.84	-5.09	-3.55	-2.19
0.1035	1.18	0.162				-9.13	-7.12	-5.37	-3.83	-2.46
0.0825	0.937	-0.0645				-9.93	-7.83	-6.00	-4.38	-2.95
0.0756	0.859	-0.152				-10.23	-8.11	-6.26	-4.63	-3.18
0.0704	0.800	-0.223					-8.45	-6.60	-4.97	-3.53
0.0604	0.686	-0.376					-8.91	-7.03	-5.37	-3.90
0.0556	0.632	-0.459					-9.12	-7.26	-5.62	-4.16

TABLE 4-18 (Continued)

conc C' (g Sr/kg carbon)	conc C[(a)] (mmol Sr/kg carbon)	ln C	ln P (Pa) 800°C	900°C	1000°C	1100°C	1200°C	1300°C	1400°C	1500°C
0.0491	0.558	-0.583					-9.64	-7.69	-5.97	-4.46
0.0447	0.508	-0.677					-9.90	-7.95	-6.22	-4.68
0.0381	0.433	-0.837						-8.34	-6.56	-4.99
0.0339	0.385	-0.954						-8.61	-6.84	-5.26
0.0301	0.342	-1.073						-8.93	-7.12	-5.51
0.0261	0.297	-1.215						-9.28	-7.46	-5.86
0.0233	0.265	-1.329						-9.55	-7.70	-6.07
0.0215	0.244	-1.409						-9.71	-7.83	-6.16

(a) C = 1000 C'/88.

TABLE 4-19

DATA FOR SORPTION OF STRONTIUM ON UNIRRADIATED H-327 GRAPHITE (EXPERIMENT Sr-5)

conc C' (g Sr/kg carbon)	conc C[(a)] (mmol Sr/kg carbon)	ln C	ln P(Pa) 1000°C	1100°C	1200°C	1300°C	1400°C	1500°C	1600°C
0.434	4.93	1.596	-7.44	-4.89	-2.69				
0.354	4.02	1.392	-8.10	-5.68					
0.308	3.50	1.253	-8.77	-6.32	-4.20				
0.284	3.23	1.172		-6.46	-4.46				
0.256	2.91	1.068		-7.29	-5.14	-3.25			
0.226	2.57	0.943		-7.40	-5.49				
0.210	2.39	0.870		-7.66	-5.70	-3.99			
0.192	2.18	0.780		-8.02	-6.00	-4.23			
0.166	1.89	0.635		-8.43	-6.39	-4.60			
0.139	1.58	0.457		-8.82	-6.78	-5.00			
0.114	1.30	0.259		-9.15	-7.19	-5.47	-3.96		
0.0924	1.05	0.0488			-8.05	-6.12	-4.43		
0.0679	0.772	-0.259			-8.75	-6.76	-5.02		
0.0562	0.639	-0.448			-9.28	-7.19	-5.35		
0.0455	0.517	-0.660				-7.92	-5.94	-4.18	
0.0310	0.352	-1.043				-8.68	-6.75	-5.04	
0.0251	0.285	-1.254				-9.17	-7.17	-5.38	
0.0172	0.195	-1.632				-10.01	-7.96	-6.15	
0.0116	0.132	-2.026					-8.64	-6.77	
0.00910	0.103	-2.269					-9.08	-7.20	
0.00612	0.0695	-2.666					-9.97	-7.96	
0.00484	0.0550	-2.900						-8.19	-6.62
0.00398	0.0452	-3.096						-8.68	-7.04
0.00282	0.0320	-3.441						-9.35	-7.41

(a) $C = 1000\ C'/88$.

TABLE 4-20
DATA FOR STRONTIUM SORPTION ON UNIRRADIATED H-327 GRAPHITE (EXPERIMENT Sr-6)

Conc C' (g Sr/kg carbon)	Conc c [a] (mmol Sr/kg carbon)	ln C	ln P(Pa) 1000°C	1100°C	1200°C	1300°C	1400°C	1500°C
0.342	3.89	1.357	-6.44	-4.14				
0.284	3.23	1.172	-7.43	-5.13				
0.248	2.82	1.036	-8.26	-5.78				
0.219	2.49	0.912	-8.76	-6.42				
0.202	2.30	0.831	-9.15	-6.86	-4.88			
0.180	2.05	0.716	-9.82	-7.47	-5.44			
0.170	1.93	0.658		-7.64	-5.66	-3.94		
0.148	1.68	0.520		-8.27	-6.30	-4.57		
0.134	1.52	0.421		-8.97	-6.92	-5.14		
0.110	1.25	0.223			-7.35	-5.60	-4.07	
0.0948	1.08	0.0744			-7.92	-6.09	-4.48	
0.0712	0.809	-0.212			-8.62	-6.77	-5.15	
0.0597	0.678	-0.388			-9.33	-7.36	-5.63	-4.09
0.0463	0.526	-0.642				-8.02	-6.29	-4.75
0.0352	0.400	-0.916				-8.92	-7.07	-5.44
0.0244	0.277	-1.283				-9.91	-7.96	-6.24
0.0186	0.211	-1.554					-8.61	-6.82
0.0150	0.170	-1.769					-9.03	-7.27
0.0128	0.145	-1.928					-9.43	-7.62
0.0116	0.132	-2.026					-9.72	-7.84
0.00983	0.112	-2.192					-10.01	-8.20

(a) C = 1000 C'/88.

The grain size of the H-327 graphite used in the three experiments was 44 to 74 μm. However, the data do not need to be corrected for grain size. A study (Ref. 4-49) indicated that for strontium sorption on graphite, the sorptivity is independent of grain size.

The data of Tables 4-18 through 4-20 are shown for selected temperatures in Figs. 4-36 through 4-38, along with the least-squares fit (Ref. 4-50) to all the data of each experiment. The least-squares fits are represented by the following three relations:

1. For data of experiment Sr-1:

$$\ln P\ (\text{Pa}) = \left(20.28 - \frac{41638}{T}\right) + \left(-0.401 + \frac{4298}{T}\right) \ln C\ (\text{mmol/kg}) \qquad (4\text{-}33)$$

2. For data of experiment Sr-5:

$$\ln P\ (\text{Pa}) = \left(21.68 - \frac{43648}{T}\right) + \left(-1.946 + \frac{6748}{T}\right) \ln C\ (\text{mmol/kg}) \qquad (4\text{-}34)$$

3. For data of experiment Sr-6:

$$\ln P\ (\text{Pa}) = \left(20.97 - \frac{42814}{T}\right) + \left(-3.398 + \frac{10026}{T}\right) \ln C\ (\text{mmol/kg}) \qquad (4\text{-}35)$$

Units of P, T, and C are pascal, kelvin, and mmol Sr/kg carbon, respectively. These relations are in the standard form used in core design calculations.

All of the data in Tables 4-18 through 4-20 have been combined to obtain by the least-squares method (Ref. 4-50) the general fit function:

$$\ln P\ (\text{Pa}) = \left(19.38 - \frac{40090}{T}\right) + \left(-0.324 + \frac{4088}{T}\right) \ln C\ (\text{mmol/kg}) \quad . \qquad (4\text{-}36)$$

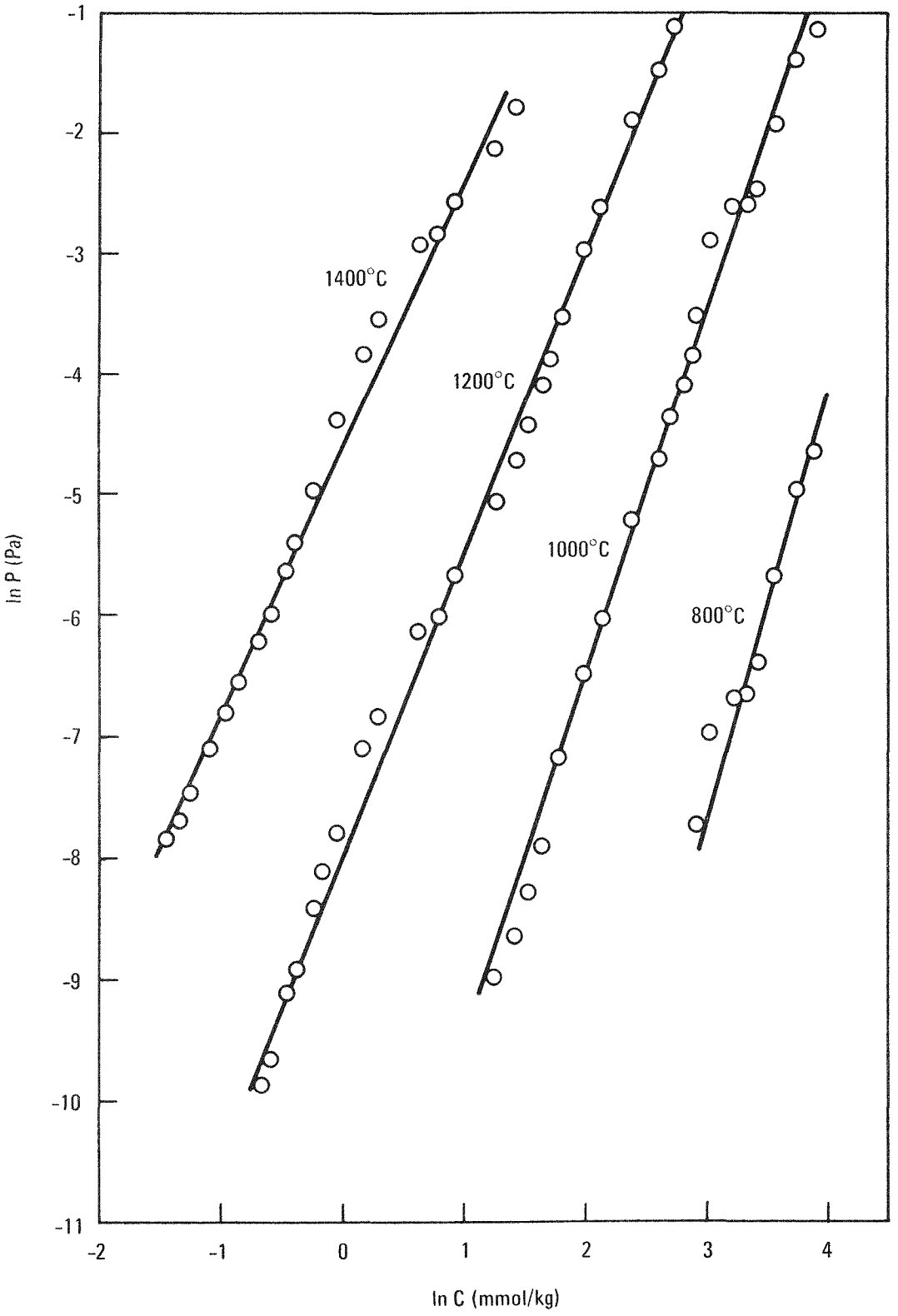

Fig. 4-36. Data and least-squares fit for strontium sorption on H-327 graphite (from experiment Sr-1)

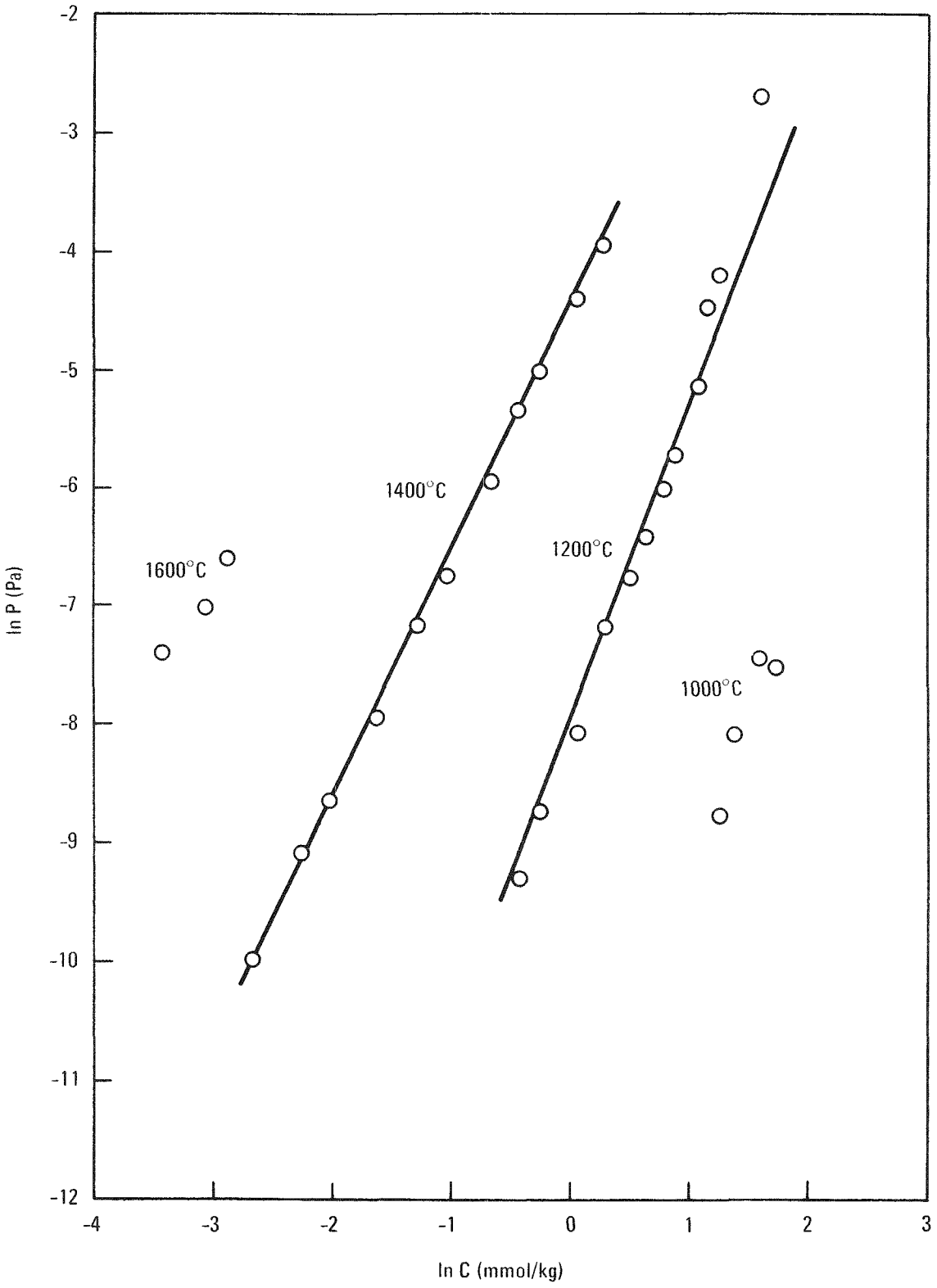

Fig. 4-37. Data and least-squares fit for strontium sorption on H-327 graphite (from experiment Sr-5)

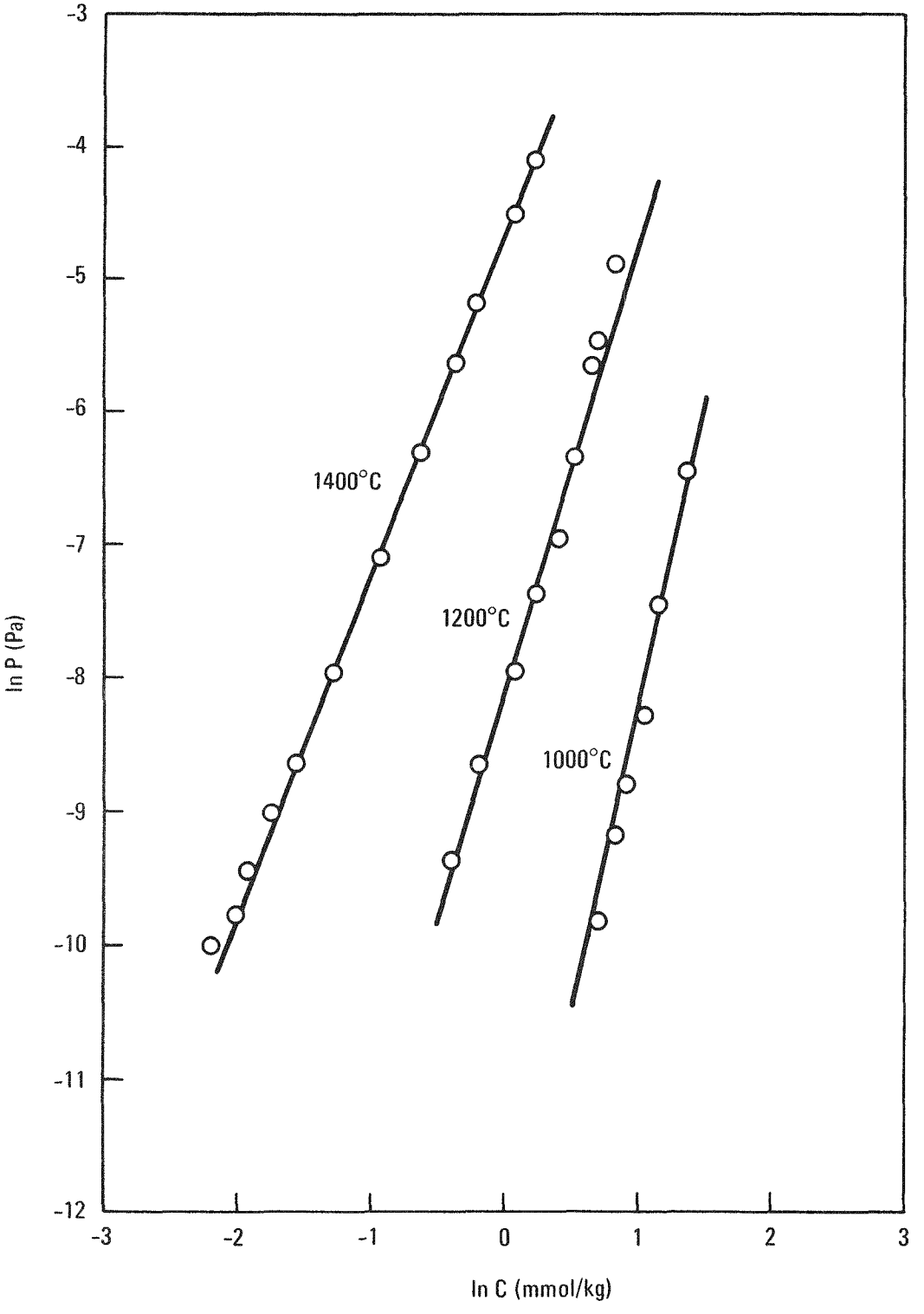

Fig. 4-38. Data and least-squares fit for strontium sorption on H-327 graphite (from experiment Sr-6)

Isotherms for this equation are given in Fig. 4-39 along with isotherms for Eqs. 4-33, 4-34, and 4-35. It can be seen that the isotherms of Eqs. 4-33 and 4-36 are relatively close together, whereas the isotherms of Eqs. 4-34 and 4-35 deviate appreciably from the other two isotherms. This behavior indicates some discord in the data from the three experiments. This behavior also reflects the fact that more data were available for experiment Sr-1; thus, the data of this experiment had a predominant influence in Eq. 4-36.

Isotherm equations were derived earlier (Refs. 4-26, 4-46, and 4-47) from the data for the three experiments. However, Eq. 4-36, compared to the earlier equations, is believed to be a more accurate representation of the data. This equation is based on application of the least-squares method to all the data of the three experiments. None of the earlier equations were based on all the data.

There are no GA data for strontium sorption on graphite in the Henrian regime. The treatment of sorption in the Henrian regimes, introduced previously (Ref. 4-26), will be retained; thus, the transition concentration C_t is given by $\ln C_t = -2.12$ in the Henrian isotherm expression

$$\ln P\ (Pa) = \left(19.38 - \frac{40090}{T}\right) + \left(-1.324 + \frac{4088}{T}\right) \ln C_t + \ln C\ (mmol/kg) \quad .(4\text{-}37)$$

The data for sorption of strontium on H-451 (Ref. 4-25) are listed in Table 4-21 and are compared in Fig. 4-40 with the least-squares fit to the sorption data on H-327 according to Eq. 4-36. There is reasonable agreement between the sorption isotherms for H-327 and H-451 graphites. The H-451 data had some associated experimental problems (Ref. 4-25), so the H-327 data are selected to represent strontium sorption.

Sorption of Strontium on Irradiated Graphite. Sorption data for strontium on irradiated H-451 graphite have been measured (Ref. 4-4) using the mass spectrometric - Knudsen cell method. The graphite sample used had been irradiated to a fluence of 3.7×10^{25} n/m^2. The resulting data are

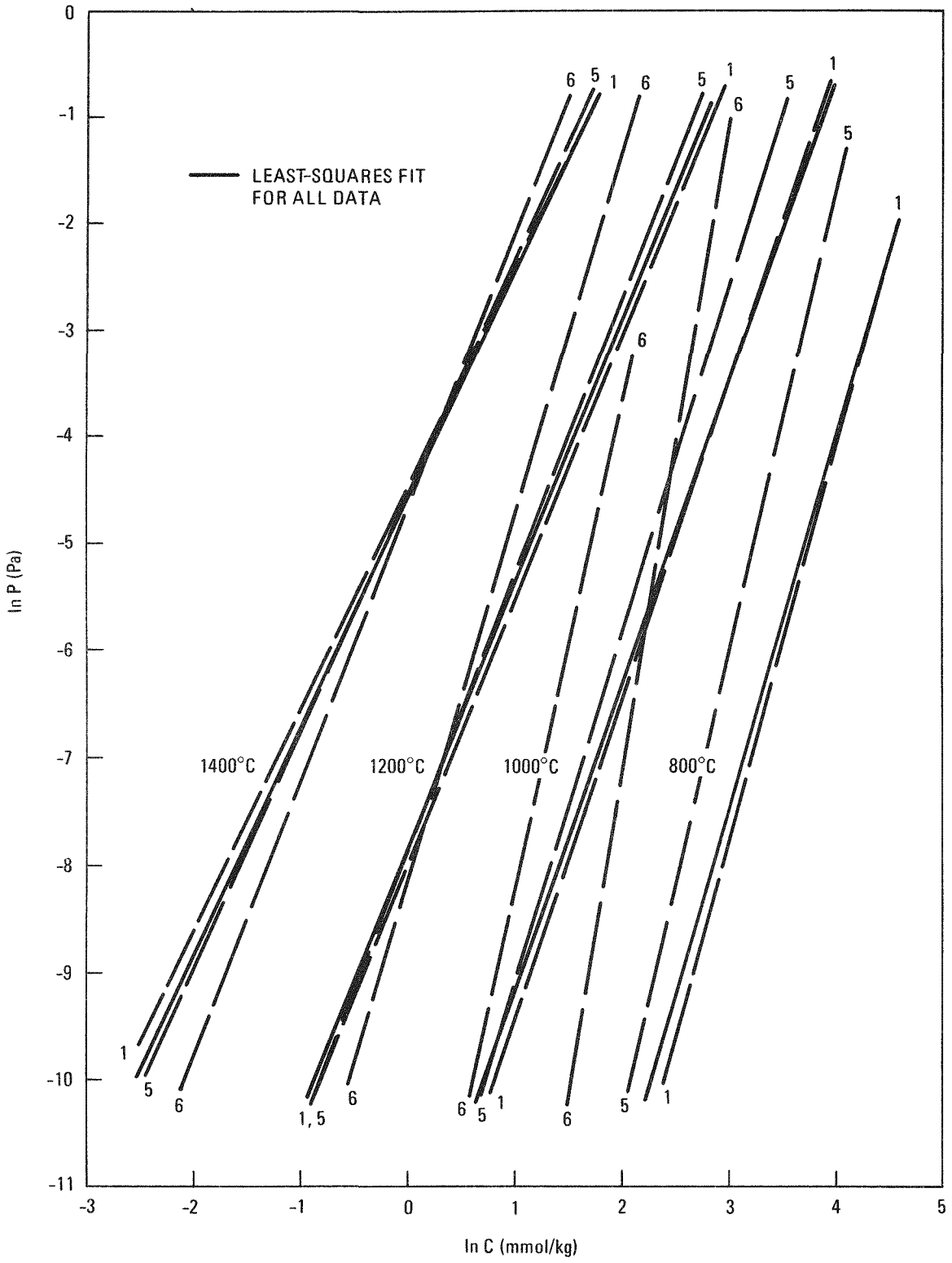

Fig. 4-39. Comparison of least-squares fit for all data with least-squares fit for Sr-1, Sr-5, and Sr-6 data at selected temperatures

TABLE 4-21
DATA FOR STRONTIUM SORPTION ON UNIRRADIATED H-451 GRAPHITE (EXPERIMENT Sr-8)

Conc C' (g Sr/kg carbon)	Conc C[(a)] (mmol Sr/kg carbon)	ln C	ln P (Pa)								
			800°C	900°C	1000°C	1100°C	1200°C	1300°C	1400°C	1500°C	1600°C
8.824	100.3	4.608	-4.39	-2.10							
7.838	89.1	4.489	-3.34	-1.36	0.311						
5.271	59.9	4.093	-3.92	-1.89	-0.178						
3.758	42.7	3.754	-5.44	-3.21	-1.34						
2.790	31.7	3.456	-5.89	-3.66	-1.78	-0.179					
2.083	23.7	3.164		-4.86	-2.89	-1.22					
1.612	18.3	2.908		-5.74	-3.75	-2.05					
1.170	13.3	2.587		-7.16	-5.03	-3.22					
0.9369	10.6	2.365			-6.32	-4.36	-2.66				
0.7462	8.48	2.138			-7.06	-5.07	-3.35				
0.6185	7.03	1.950			-7.72	-5.68	-3.91				
0.4558	5.18	1.645				-6.36	-4.57	-3.00			
0.3610	4.10	1.412				-6.56	-4.82	-3.31			
0.2132	2.42	0.885				-7.46	-5.68	-4.12	-2.75		
0.1359	1.54	0.435					-6.81	-5.20	-3.78		
0.1000	1.14	0.128					-7.86	-6.23	-4.80		
0.0786	0.893	-0.113					-9.12	-7.35	-5.79	-4.41	
0.0598	0.680	-0.386						-8.09	-6.49	-5.08	
0.0546	0.620	-0.477						-9.18	-7.55	-6.11	
0.0455	0.517	-0.660							-8.06	-6.53	-5.16
0.0399	0.453	-0.791							-8.59	-7.00	-5.57
0.0252	0.286	-1.250							-9.17	-7.56	-6.13
0.0148	0.168	-1.783							-9.67	-8.06	-6.63

(a) C = 1000 C'/(88).

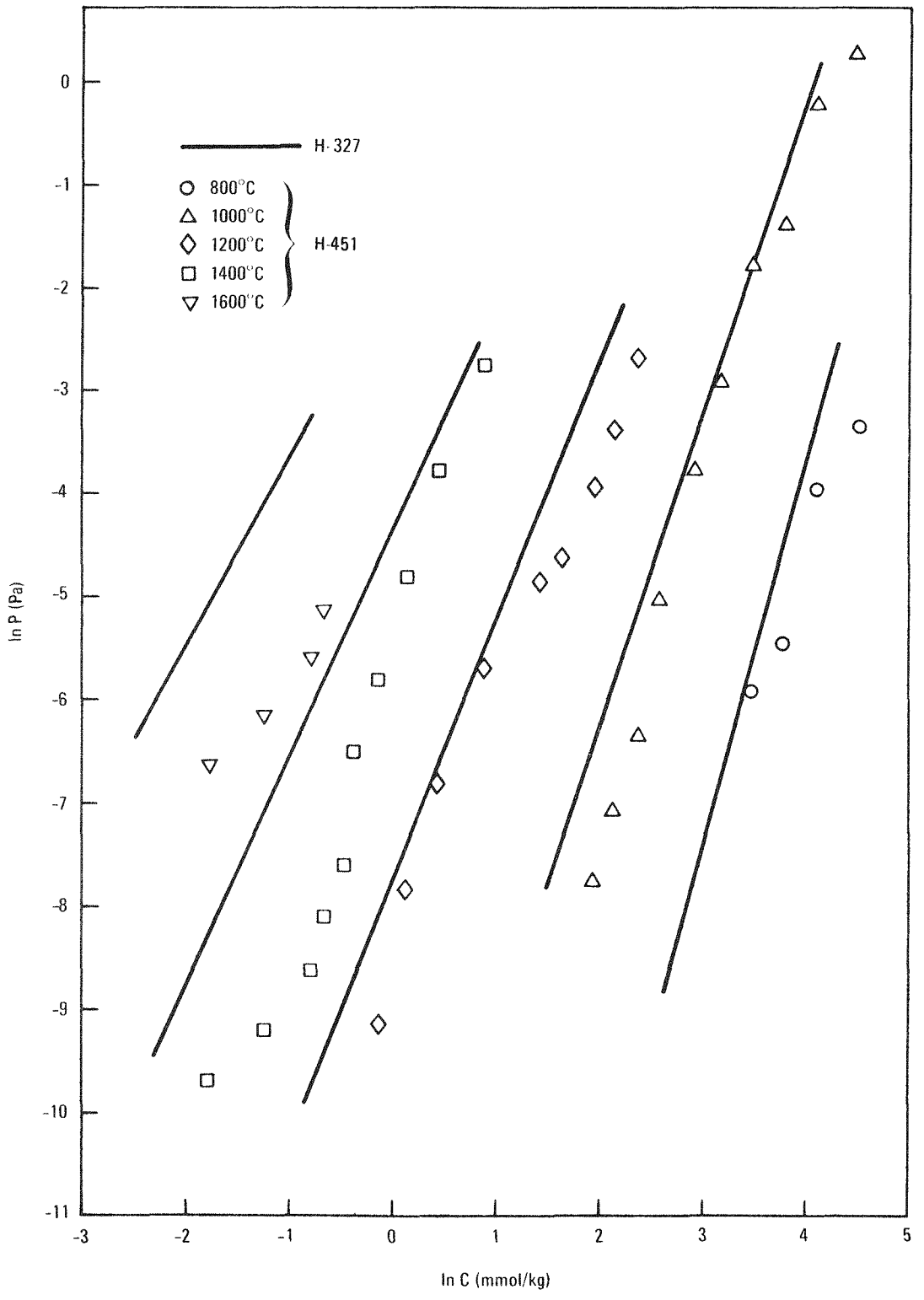

Fig. 4-40. Comparison of strontium data for H-451 graphite with isotherms for H-327 graphite

given in Table 4-22 and plotted in Fig. 4-41 along with the least-squares fit to the data in the Freundlich region and estimates of the Henrian isotherms according to the equations

$$\ln P\ (Pa) = \left(29.62 - \frac{65809}{T}\right) + \left(-2.879 + \frac{9684}{T}\right) \ln C\ (mmol/kg) \qquad (4\text{-}38)$$

for the Freundlich region and

$$\ln P\ (Pa) = \left(29.62 - \frac{65809}{T}\right) + \left(-3.879 + \frac{9684}{T}\right) \ln C_t + \ln C\ (mmol/kg) \qquad (4\text{-}39)$$

for the Henrian region where

$$\ln C_t = 2.473 - 10^{-3}\ T\ (K) \quad . \qquad (4\text{-}40)$$

To combine the data for strontium sorption on unirradiated and irradiated graphite, the assumption is made that the ratio C_i/C is linearly dependent on fluence in the Henrian region. This ratio is the ratio of the sorbate concentration on the irradiated graphite, C_i, to that on the unirradiated graphite, C. This procedure has been previously used in the case of cesium sorption on graphite (Ref. 4-16). The choice of a linear dependence of C_i/C on fluence in the Henrian region leads to a nonlinear dependence in the Freundlich region (Ref. 4-16). The uncertainties introduced by this choice are reflected in increases in the variances for the sorption isotherms.

By use of this procedure in combination with Eq. 4-36, the sorption isotherms for strontium sorption on graphite irradiated to a fluence f (n/m^2) were derived for the Freundlich region:

$$\ln P\ (Pa) = \left(19.38 - \frac{40090}{T}\right) + \left(-0.324 + \frac{4088}{T}\right) \ln C\ (mmol/kg) \quad , \qquad (4\text{-}36)$$

TABLE 4-22
DATA FOR STRONTIUM SORPTION ON IRRADIATED H-451 GRAPHITE (EXPERIMENT Sr-12)

Conc C' (g Sr/kg carbon)	Conc C[(a)] (mmol Sr/kg carbon)	ln C	ln P (Pa)					
			1100°C	1200°C	1300°C	1400°C	1500°C	1600°C
2.301	26.1	3.264	-4.40	-2.49	-0.828			
1.969	22.4	3.108		-3.87	-2.26	-0.837		
1.580	17.95	2.888		-4.76	-3.07	-1.59		
1.282	14.6	2.679		-5.52	-3.65	-2.00		
1.070	12.2	2.498			-4.23	-2.50		
0.8009	9.10	2.208			-4.96	-3.19	-1.62	
0.6964	7.91	2.069			-5.40	-3.56	-1.92	
0.489	5.56	1.715			-6.38	-4.58	-2.97	
0.416	4.73	1.553			-7.06	-5.15	-3.45	
0.318	3.61	1.285				-5.74	-3.99	-2.43
0.228	2.59	0.952				-7.06	-5.32	-3.76
0.170	1.93	0.658				-7.30	-5.46	-3.82
0.112	1.27	0.241				-8.04	-6.19	-4.54

(a) C = 1000 C'/88.

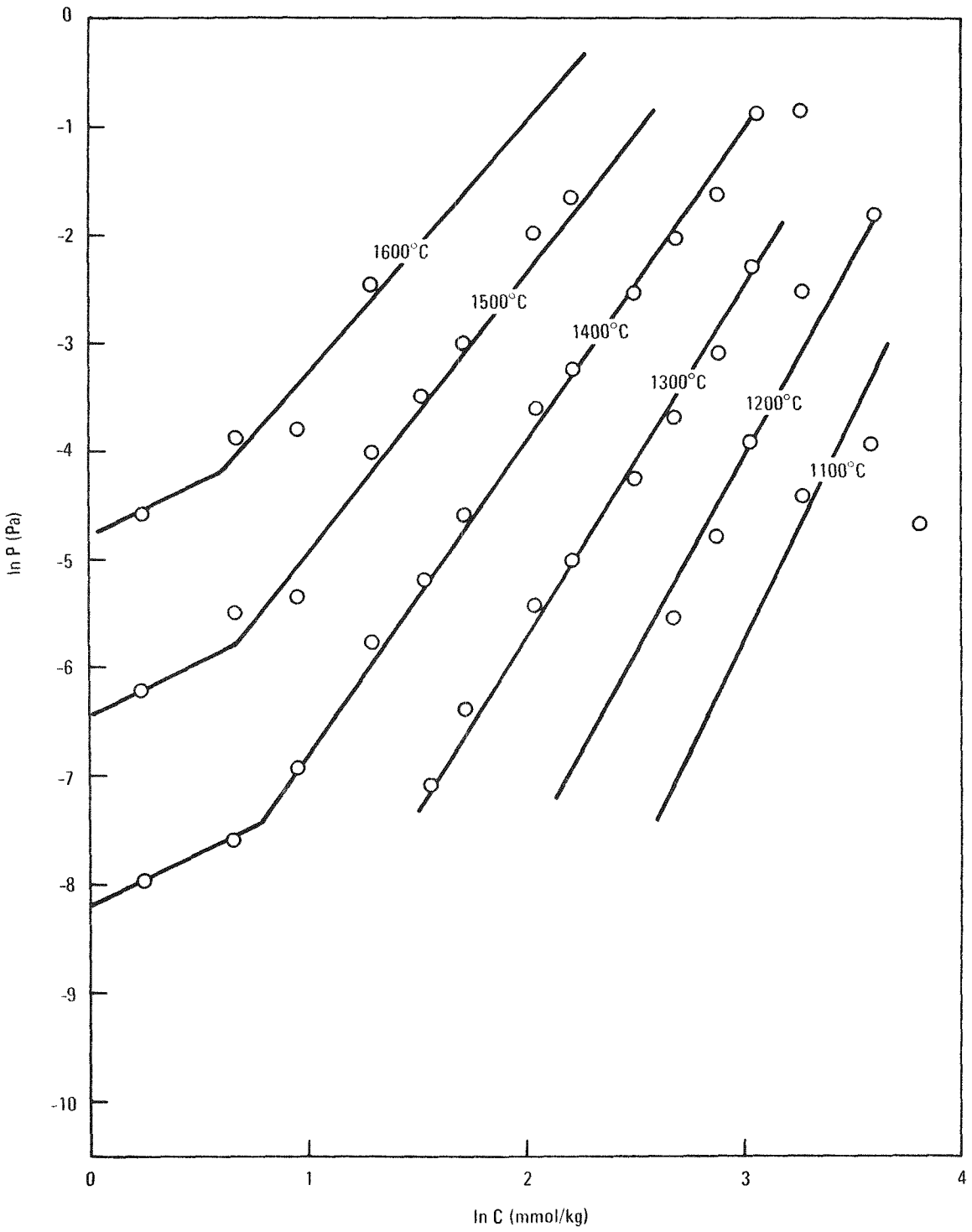

Fig. 4-41. Data and least-squares fit for strontium sorption on irradiated H-451 graphite

where

$$C = \frac{C_i}{1 + \frac{5.133 \times 10^{-28}\ \gamma f\ \exp(13890/T - 6094000/T^2)}{C_i^{(0.976 - 3273/T + 4358000/T^2)}}} \qquad (4\text{-}41)$$

with

$$\gamma^{-1} = 1 + \exp[0.0439(T - 1423)] \qquad (4\text{-}42)$$

and for the Henrian region:

$$\ln P\ (Pa) = \left(19.38 - \frac{40090}{T}\right) + \left(-1.324 + \frac{4088}{T}\right) \ln C_t + \ln C\ (mmol/kg) \quad , \qquad (4\text{-}37)$$

where

$$C = \frac{C_i}{1 + 1.434 \times 10^{-31}\ \gamma f\ (10^4/T)^{13}\ \exp[-1.745\ (10^4/T)]} \qquad (4\text{-}43)$$

and

$$\ln C_t = -2.12 \quad . \qquad (4\text{-}44)$$

The factor γ accounts for the effect of annealing on sorptivity; as the temperature rises, the increase in sorptivity resulting from irradiation is nullified by structural changes induced by the annealing. The actual temperature range in which the annealing becomes effective is uncertain; the parameters in the γ factor are chosen to initiate the annealing effects at a conservatively low temperature.

The uncertainties in the sorption isotherms for strontium as represented by Eqs. 4-36 and 4-37 in combination with Eqs. 4-41 through 4-44 are assigned the same overall values as deduced in the case of cesium (Ref. 4-16). This is reasonable since (1) the same experimental method was used in both cases, (2) the same assumption regarding dependence of sorbate concentration ratio on fluence was made in both cases, and (3) the same concentration and temperature range were involved in both cases. Thus, the variance is given by

$$S^2 (\ln P_i) = 1.48 \quad , \tag{4-45}$$

where S is the estimated standard deviation in $\ln P_i$ with i = H (Henrian region) or F (Freundlich region).

Sorption of Barium on Graphite. Sorption data for barium on unirradiated H-451 graphite were measured at General Atomic in 1973 using the mass spectrometric - Knudsen cell method. The resulting data are given in Tables 4-23 and 4-24. These data were derived from a laboratory notebook (Ref. 4-48) and have not been previously reported.

The data of Tables 4-23 and 4-24 were combined and fitted by use of the least-squares method. The resulting Freundlich expression is:

$$\ln P \text{ (Pa)} = \left(19.37 - \frac{47313}{T}\right) + \left(0.426 + \frac{3728}{T}\right) \ln C \text{ (mmol/kg)} \quad . \tag{4-46}$$

There are no data for barium sorption in the Henrian regime; thus, the transition concentrations are not known for barium. The assumption is made that barium has the same transition concentrations as strontium. Thus, for barium the Henrian isotherm is given by

$$\ln P \text{ (Pa)} = \left(19.37 - \frac{47313}{T}\right) + \left(-0.574 + \frac{3728}{T}\right) \ln C_t + \ln C \text{ (mmol/kg)} \quad , \tag{4-47}$$

TABLE 4-23
DATA FOR BARIUM SORPTION ON UNIRRADIATED H-451 GRAPHITE (EXPERIMENT Ba-1)

Conc C' (g Ba/kg carbon)	Conc C[(a)] (mmol Ba/kg carbon)	ln C	ln P(Pa)						
			1100°C	1200°C	1300°C	1400°C	1500°C	1600°C	1700°C
3.347	24.43	3.196	-4.02	-2.43	-1.04				
2.845	20.77	3.033	-4.57	-3.01	-1.65				
2.391	17.45	2.859		-3.84	-2.39				
1.994	14.55	2.678		-4.66	-3.05	-1.62			
1.640	11.97	2.482		-5.23	-3.56	-2.10			
1.303	9.51	2.252		-5.95	-4.25	-2.75			
1.016	7.42	2.004			-4.73	-3.13	-1.70		
0.842	6.15	1.816			-5.42	-3.76	-2.29		
0.661	4.82	1.574			-6.30	-4.53	-2.96		
0.528	3.85	1.349				-5.27	-3.65		
0.407	2.97	1.089				-6.17	-4.47	-2.95	
0.356	2.60	0.955				-6.58	-4.85	-3.31	
0.292	2.13	0.757				-7.29	-5.44	-3.80	
0.243	1.77	0.573					-6.20	-4.52	-3.00
0.186	1.36	0.306					-6.97	-5.19	-3.58
0.144	1.05	0.0498						-5.87	-4.08
0.0987	0.720	-0.328						-6.73	-4.96
0.0749	0.547	-0.604						-7.25	-5.41
0.0545	0.398	-0.922						-7.84	-5.97

(a) C = 1000 C'/(137).

TABLE 4-24
DATA FOR BARIUM SORPTION ON UNIRRADIATED H-451 GRAPHITE (EXPERIMENT Ba-2)

Conc C' (g Ba/kg carbon)	Conc C[(a)] (mmol Ba/kg carbon)	ln C	ln P (Pa)							
			1100°C	1200°C	1300°C	1400°C	1500°C	1600°C	1700°C	1800°C
3.341	24.38	3.194	-5.98	-4.04	-2.34					
2.732	19.94	2.993	-5.90	-4.18	-2.68	-1.37				
2.254	16.45	2.800		-4.84	-3.28	-1.90				
1.799	13.13	2.575		-5.81	-4.04	-2.49				
1.494	10.91	2.389		-6.29	-4.43	-2.80				
1.050	7.66	2.037			-5.37	-3.71	-2.25			
0.7741	5.65	1.732			-6.14	-4.43	-2.91			
0.5945	4.34	1.468				-5.33	-3.68	-2.20		
0.402	2.93	1.076				-6.39	-4.71	-3.21		
0.3188	2.33	0.845					-5.50	-3.91	-2.49	
0.2239	1.63	0.491					-6.57	-4.80	-3.22	
0.1798	1.31	0.272						-5.59	-3.99	
0.1285	0.938	-0.0641						-6.89	-5.08	-3.45
0.09716	0.709	-0.344							-5.89	-4.24
0.06730	0.491	-0.711							-7.18	-5.53

(a) C = 1000 C'/137.

where

$$\ln C_t = -2.12 \quad . \tag{4-48}$$

Barium, compared to strontium, is known to be more strongly sorbed on graphite (Refs. 4-51 and 4-52). This is consistent with the Freundlich isotherms for strontium, Eq. 4-36, and barium, Eq. 4-46, as shown by the comparison in Fig. 4-42.

There are no data for barium sorption on irradiated graphite. The assumption is made that the changes in barium sorption on graphite as a function of fluence are the same as for strontium; thus Eqs. 4-41, 4-42, and 4-43 are assumed to apply to barium sorption on irradiated graphite.

The uncertainty in the isotherms for barium are taken to be the same as for cesium (see Eq. 4-45); the reasons for this choice are the same as for the case of strontium (see above).

Sorption of Rubidium on Graphite. The sorption isotherm for rubidium is often taken to be the same as that of cesium. This is not reasonable since cesium will readily displace rubidium sorbed on graphite. Accordingly, one would expect the vapor pressure of rubidium to be greater than that of cesium at the same sorbate concentration and temperature.

A reasonable estimate of the rubidium isotherm for H-451 graphite is made as follows. The relation between the sorbate concentrations of cesium and rubidium is determined from data on TS-688 graphite (Ref. 4-34). This relation is combined with the isotherm for cesium sorption on unirradiated H-451 graphite to obtain the estimate for the isotherm of rubidium on H-451 graphite. The data used in this procedure apply to the Freundlich regime.

In the Henrian regime there are no comparable data, and the assumption is made that the transition concentration for rubidium is the same as for cesium.

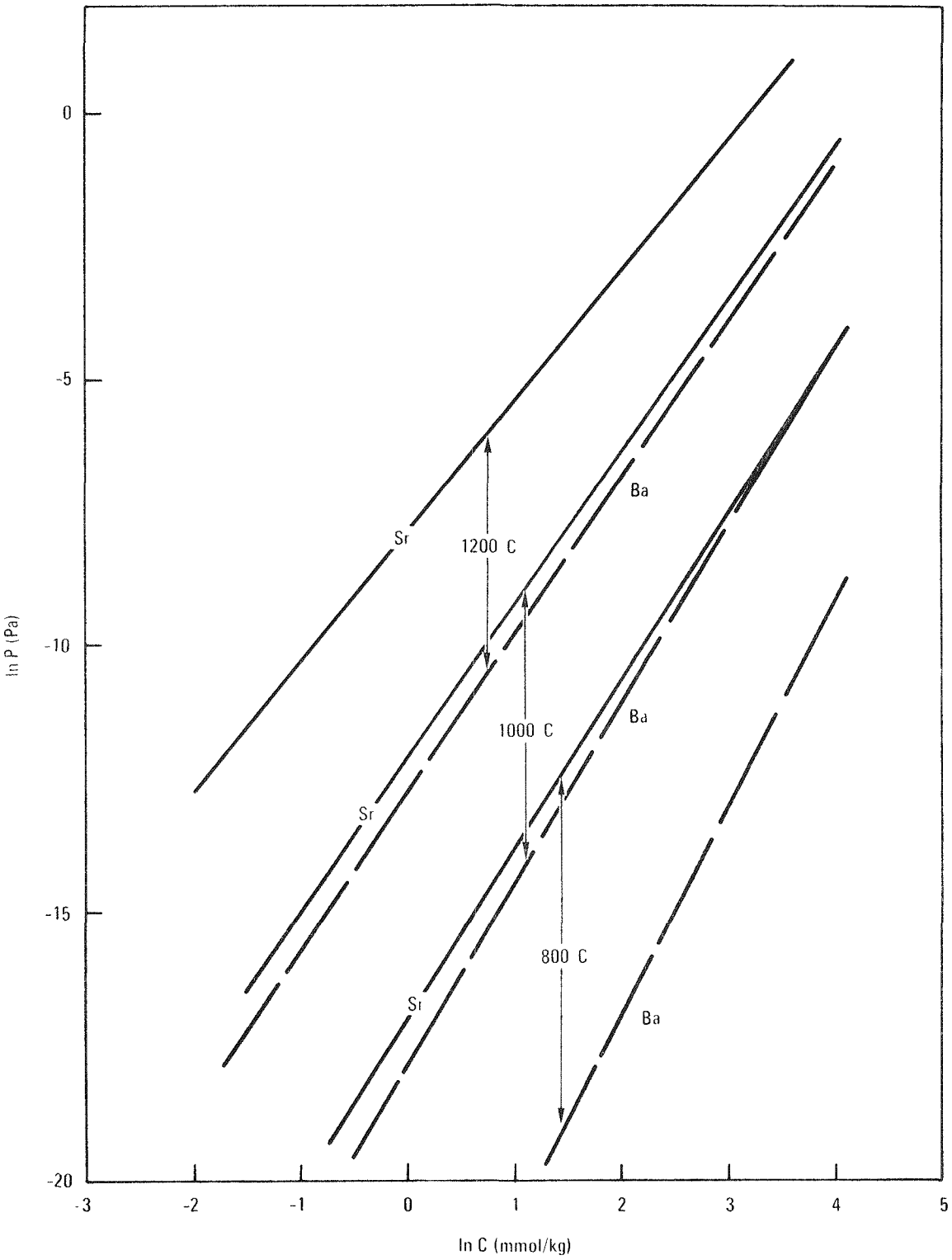

Fig. 4-42. Comparison of strontium and barium 120 isotherms for sorption on H-451 graphite (unirradiated)

From the data on TS-688 (Ref. 4-34), the relation between the sorbate concentrations of cesium and rubidium is found to be

$$\ln C_{Cs} = \frac{\left(-9.0 + \frac{16800}{T}\right) \ln C_{Rb} - \left(12.5 - \frac{21600}{T}\right)}{\left(-14.5 + \frac{24200}{T}\right)} \qquad (4\text{-}49)$$

This equation is combined with the sorption isotherm for cesium on unirradiated H-451 graphite (Ref. 4-16). The resulting expression is then simplified by reevaluating the isotherm constants, A, B, D, and E (Ref. 4-16), to obtain the following isotherm in the standard form:

$$\ln P \text{ (Pa)} = \left(24.39 - \frac{30949}{T}\right) + \left(0.938 + \frac{2664}{T}\right) \ln C \text{ (mmol/kg)} \qquad (4\text{-}50)$$

for the Freundlich regime and

$$\ln P \text{ (Pa)} = \left(24.39 - \frac{30949}{T}\right) + \left(-0.062 + \frac{2664}{T}\right) \ln C_t + \ln C \text{ (mmol/kg)} \qquad (4\text{-}51)$$

for the Henrian regime where

$$\ln C_t = 2.04 - 1.79 \times 10^{-3} \text{ T (K)} \quad . \qquad (4\text{-}52)$$

There are no data for rubidium sorption on irradiated graphite. The assumption is made that the changes in rubidium sorption on graphite as a function of fluence are the same as for cesium; thus, the following equations for cesium (Ref. 4-16) apply to rubidium:

In the Freundlich region,

$$C = \frac{C_i}{1 + \frac{6.55 \times 10^{-29} \gamma f \exp\left(21830/T - 9870000/T^2\right)}{C_i^{\left(-3.663 + 11140/T - 4937000/T^2\right)}}} \qquad (4\text{-}53)$$

with

$$\gamma^{-1} = 1 + \exp[0.0439(T - 1423)] \qquad (4\text{-}54)$$

and in the Henrian region

$$C = \frac{C_i}{1 + 1.025 \times 10^{-31}\ \gamma f\ (10^4/T)^{17}\ \exp[-2.584\ (10^4/T)]} \qquad (4\text{-}55)$$

where the expression for C in the Freundlich and Henrian regions (Eqs. 4-53 and 4-55) are to be combined with Eqs. 4-50 and 4-51, respectively. (See above for definition of f and γ.)

The uncertainty in the isotherms for rubidium is taken to be the same as for cesium (see Eq. 4-45); the reasons for this choice are the same as for the case of strontium (see above).

Sorption of Cerium, Europium, and Samarium on Graphite. There are no data for the sorption of cerium, europium, and samarium on either unirradiated or irradiated graphite. Data on the diffusion of cerium and europium in graphite indicate that these elements generally diffuse more slowly than does strontium (see previous section). On the basis of this result, one might expect these elements to be more strongly sorbed than strontium. Accordingly, it is conservative to assume that cerium and europium (and samarium on the basis of physical and chemical similarity to cerium and europium) have the same sorption behavior as strontium.

Using strontium isotherms for cerium, europium, and samarium yields upper limits to the vapor pressure for these elements; consequently, uncertainties are not given.

Sorption of Other Elements on Graphite. Under temperature transient conditions, the mobility of certain fission product elements, that are normally immobile, needs to be considered. The elements of interest in this

category are: zirconium, niobium, molybdenum, technetium, promethium, neodynmium, praseodymium, yttrium, palladium, tin, lanthanum, ruthenium, and rhodium. There are no sorption data for these elements on graphite, but one can conservatively assume that they have the same sorption isotherms as strontium.

Adoption of the strontium isotherms for these metals yields upper limits to the vapor pressure; consequently, uncertainties are not given.

Form of Uncertainty Expressions

The uncertainty expressions given in the above sections are in the following form:

$$S^2 (\ln D) = A_1 + A_2 (10^4/T) + A_3 (10^4/T)^2 \quad , \tag{4-56}$$

where S is the standard deviation in ln D and A_1, A_2, and A_3 are constants.

A more convenient form for application to core design computer codes is the following:

$$S^2 (\ln D) = a_1 + a_2 [0.7855 - (10^3/T)] + a_3 [0.7855 - (10^3/T)]^2 \quad , \tag{4-57}$$

where a_1, a_2, and a_3 are constants. The relations between the constants of Eqs. 4-56 and 4-57 are as follows:

$$a_3 = 100A_3 \tag{4-58}$$

$$a_2 = -(1.571a_3 + 10A_2) \tag{4-59}$$

$$a_1 = A_1 - 0.7855a_2 - (0.7855)^2 a_3 \tag{4-60}$$

The values of the constants a_i and A_i for i = 1,2,3 are given in Table 4-25.

TABLE 4-25
UNCERTAINTY PARAMETERS FOR FISSION PRODUCT ELEMENTS

Process	Element	A_1	A_2	A_3	a_1	a_2	a_3
Diffusion in pyrocarbon	Sr	5.54	-1.38	0.112	1.61	-3.80	11.2
	Ba	1.63	-0.35	0.028	0.61	-0.90	2.8
	Eu	2.3	0.0	0.0	2.3	0.0	0.0
	Ce	2.3	0.0	0.0	2.3	0.0	0.0
	Sm	2.3	0.0	0.0	2.3	0.0	0.0
	Cs	4.73	-1.05	0.0927	2.20	-4.06	9.27
	Rb	5.42	-1.05	0.0927	2.89	-4.06	9.27
Diffusion in ThO_2	Sr	69.2	-24.5	2.18	11.3	-97.5	218.
	Ba	80.8	-28.2	2.51	13.9	-112.	251.
	Ce	69.2	-24.5	2.18	11.3	-97.5	218.
	Eu	69.2	-24.5	2.18	11.3	-97.5	218.
	Sm	69.2	-24.5	2.18	11.3	-97.5	218.
	Cs	4.90	-1.47	0.113	0.324	-3.05	11.3
	Rb	4.90	-1.47	0.113	0.324	-3.05	11.3
Diffusion in graphite	Sr	(a)	(a)	(a)	0.0798	-0.640	3.16
	Ba	32.48	-4.6	0.332	16.8	-6.16	33.2
	Cs	5.52	-0.809	0.0467	2.05	-0.753	4.67

(a) Values of a_i were calculated directly.

TASK 600: COOLANT IMPURITY/CORE MATERIALS INTERACTION

Subtask 610: Reaction of Coolant Impurities with Fuel Material

Hydrolysis Reaction Rate Studies

Summary. Work on the hydrolysis of exposed irradiated carbide fuel materials and concomitant release of fission gases is presented. In a series of tests, it was shown that the rate of fission gas release during hydrolysis can be used as an effective means of following the rate of the reaction. The reaction rate appears to be first order with respect to the amount of carbide remaining; therefore, an exponential rate law is governing. In a second series of tests, the release of fission gas was used to signal particle rupture due to hydrolysis-induced swelling. These tests indicated that irradiated ThC_2 (2.1% FIMA) is measurably less reactive than unirradiated ThC_2 at temperatures below 600 K.

Introduction. In the HTGR, hydrolysis of exposed carbide fuel consists of two separate steps: (1) transport of water via diffusion through the graphite webs and fuel rod matrix, and (2) chemical reaction with the carbide. In order to simulate these processes, the OXIDE-3 computer code utilizes a model which includes both transport and chemical reaction to calculate the release of fission gases caused by hydrolysis following steam ingress accidents.

Earlier work (Ref. 4-27) on the chemical reactivity of fuel carbides has shown that the chemical reaction of unirradiated ThC_2 is considerably faster than transport of water molecules to the surface. However, Dyck *et al.* (Ref. 4-53) have shown that prior irradiation of uranium monocarbide results in a substantial reduction in the rate of hydrolysis. In a preliminary study at General Atomic, a similar effect was observed for fuel dicarbides. Accordingly, experiments are being conducted to measure the rate of the hydrolysis reaction as a function of irradiation (burnup), temperature, and moisture content. These data can be used to: (1) update and improve the OXIDE computer code calculations of fission gas release and (2)

determine the effects on R/B and fuel element stress of moisture ingress. The experiments are conducted on UC_2, ThC_2, and $(U,Th)C_2$ at burnups of 0 to 75% FIMA in the temperature range 475° to 1275 K and at water vapor concentrations up to 3 kPa (0.03 atm).

Apparatus and Procedure. Two methods are currently being used. In the first method, the release rate of long-lived Kr-85 from irradiated fuel samples having exposed kernels undergoing hydrolysis is used to monitor the effective reaction rate. It is assumed that since the hydrolysis reaction produces multiple disruptions in the carbide lattice, the release of fission gases stored therein should be virtually instantaneous and could therefore be a measure of the reaction rate. This method and results obtained using this method were described in detail in the previous quarterly report (Ref. 4-54).

In the second method, the time-to-failure of laser-drilled particles exposed to moisture is measured. Time-to-failure of irradiated particles is compared directly with that of unirradiated particles. For this method the apparatus consists of a quartz, flow-through furnace liner surrounded by a clamshell furnace. The gas exiting the furnace liner passes through a Cary ionization chamber to determine the concentration of Kr-85. A sudden increase in Kr-85 evolution signals the rupture of the irradiated particle. Verification of coating failure is accomplished visually by simply opening the clamshell furnace for a brief period of time.

Sample Description. Three separate samples of irradiated fuel have been studied. The first type of fuel sample (sample A) consists of small chunks of Peach Bottom (Core 1) compact No. 29 from fuel element D13-05. This compact contained 17 wt % heavy metal in the form of pyrocarbon coated $(Th,U)C_2$ (Th:U = 4.25:1). The burnup is estimated at 4% FIMA, and the fraction of particles which experienced coating failure is greater than 85%. Sample sizes were kept approximately constant by using chunks which had similar gamma activities.

The second type of fuel sample (sample B) consists of microspheres of TRISO coated ThC_2 (batch 4000-242), which had been irradiated in FTE-5 to 2.1% FIMA at an irradiation temperature of 1425 K.

The third type of fuel sample (sample C) consists of TRISO coated UC_2 particles (weak acid resin, batch OR-1694 from ORNL). These particles had been irradiated in capsule P13P and were located in fuel rod 1D-28. The irradiation temperature was 1325 K, and the burnup was estimated at 58% FIMA.

Postirradiation examination of samples B and C indicated that the TRISO coatings were intact. Each particle was laser-drilled three times to provide a pathway for water vapor to reach the reactive carbide. To eliminate hydrolysis prior to the start of the reaction, the laser drilling was conducted under a flow of inert helium and the laser-drilled particles were stored in a glove box under purified argon.

Results and Discussion.

Hydrolysis Reaction Rates Derived From Fission Gas Release Data

Results of the hydrolysis-induced fission gas release tests are given in Table 4-26. The results were reported in part in the previous quarterly report (Ref. 4-54).

Figure 4-43 shows typical data obtained from sample A (Peach Bottom compact material) during the gas release test. In this particular run, the fuel sample was exposed to 2.6 kPa moisture at 885 K; as shown by Fig. 4-43, the response of the Cary 401 electrometer increased rapidly as the hydrolysis began, passed through a maximum, and then declined steadily as the release or chemical reaction approached completion.

In order to transform the raw data into a form suitable for kinetic analysis, the millivolt response from the Cary ionization chamber

TABLE 4-26
EXPERIMENTAL CONDITIONS AND RESULTS FOR HYDROLYSIS-INDUCED FISSION GAS RELEASE FROM IRRADIATED FUEL CARBIDE SAMPLES

Sample[a]	Run Conditions		Experimental Results			
	Temp. (K)	P_{H_2O} (kPa)	Initial Rate ($\times 10^4$ s^{-1})[b]	Initial Validity Range[c]	First-Order Rate Constant[d] ($\times 10^4$ s^{-1})	First-Order Validity Range[c]
A	1162	2.6	8.1	0.1-0.3	14.6	0.2-0.9
A	1085	2.6	6.3	0.01-0.35	9.3	0.16-0.91
A	985	2.6	4.5	0.03-0.3	5.9	0.27-1.0
A	885	2.6	3.8	0.04-0.25	2.8	0.34-0.94
A	859	2.6	2.6	0.02-0.25	1.6	0.45-0.96
A	784	2.6	1.3	0.1-0.5	0.33	0.17-0.55
A	732	2.6	1.0	0.01-0.1	(e)	(e)
A	677	2.6	0.32	0.01-0.10	(e)	(e)
A	572	2.6	0.18	0.02-0.15	(e)	(e)
C	925	1.82	2.6	0.01-0.3	2.8	0.2-0.6
A	1203	0.61	9.3	0.075-0.25	15.7	0.07-0.65
A	1081	0.61	4.0	0.05-0.25	6.1	0.17-0.68
A	973	0.61	6.5	0.1-0.4	11.7	0.3-0.8
A	978	0.61	4.5	0.1-0.25	1.0	0.23-0.80
A	960	0.61	4.9	0.02-0.25	6.0	0.38-0.81
A	859	0.61	2.1	0.04-0.10	0.78	0.37-0.98
A	785	0.61	1.4	0.02-0.20	0.46	0.34-0.85

[a] See text for sample characteristics.

[b] Initial reaction rate in fraction reacted/second.

[c] Fraction of gas released during time interval in which rate expression is valid.

[d] First-order rate constant determined by Guggenheim approximation.

[e] Not applicable since data did not fit first-order rate expression.

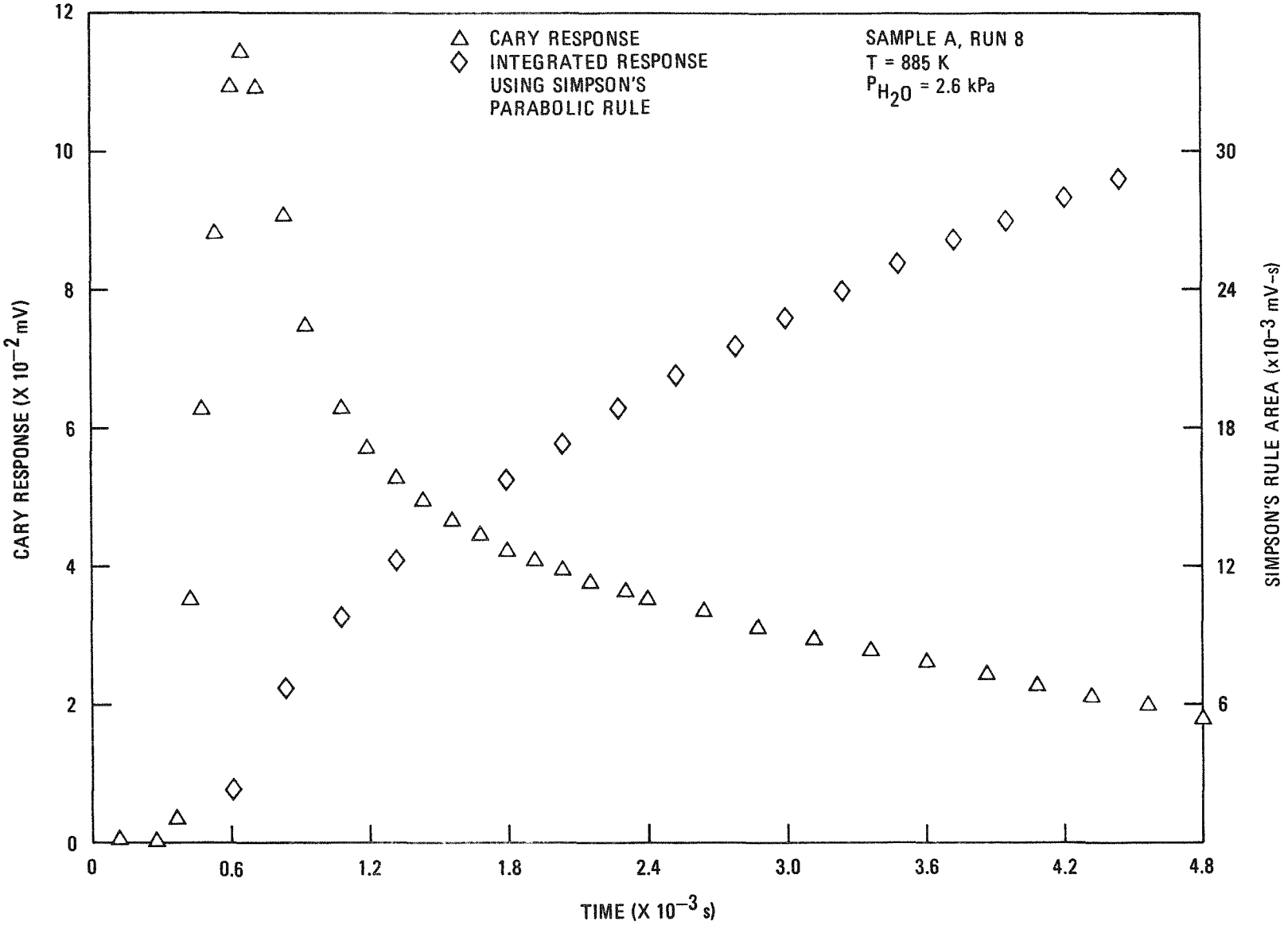

Fig. 4-43. Release of Kr-85 from exposed irradiated $(Th,U)C_2$ during hydrolysis

was integrated using Simpson's parabolic rule. This integrated area, displayed as a function of time, is plotted in Fig. 4-43 along with the raw data.

The apparent fractional gas released can be calculated up to any given time using the equation:

$$\alpha_t = A_t / A_{total} \quad , \tag{4-61}$$

where A_t = Simpson's integrated area up to time t,

A_{total} = total Simpson's area for the duration of the test.

As previously reported (Ref. 4-54), the apparent fraction of fission gas released was found to depend on the hydrolysis temperature. In order to obtain the actual release fraction, α_t was multiplied by a correction factor:

$$\alpha_t^c = \alpha_t \times \frac{\mu Ci \text{ Kr-85 released during hydrolysis}}{\text{total } \mu Ci \text{ Kr-85 in sample}} \quad , \tag{4-62}$$

where the total Kr-85 was obtained by reacting the sample at high temperature to effect total release.

Figure 4-44 shows that the initial portion of the release is linearly dependent on time. That is, the increase in the fraction of gas release, $d\alpha_t^c$, during any small time interval, dt, is a constant:

$$\frac{d\alpha_t^c}{dt} = \text{constant} \quad . \tag{4-63}$$

Figure 4-44 also demonstrates that release rates increase with exposure temperature.

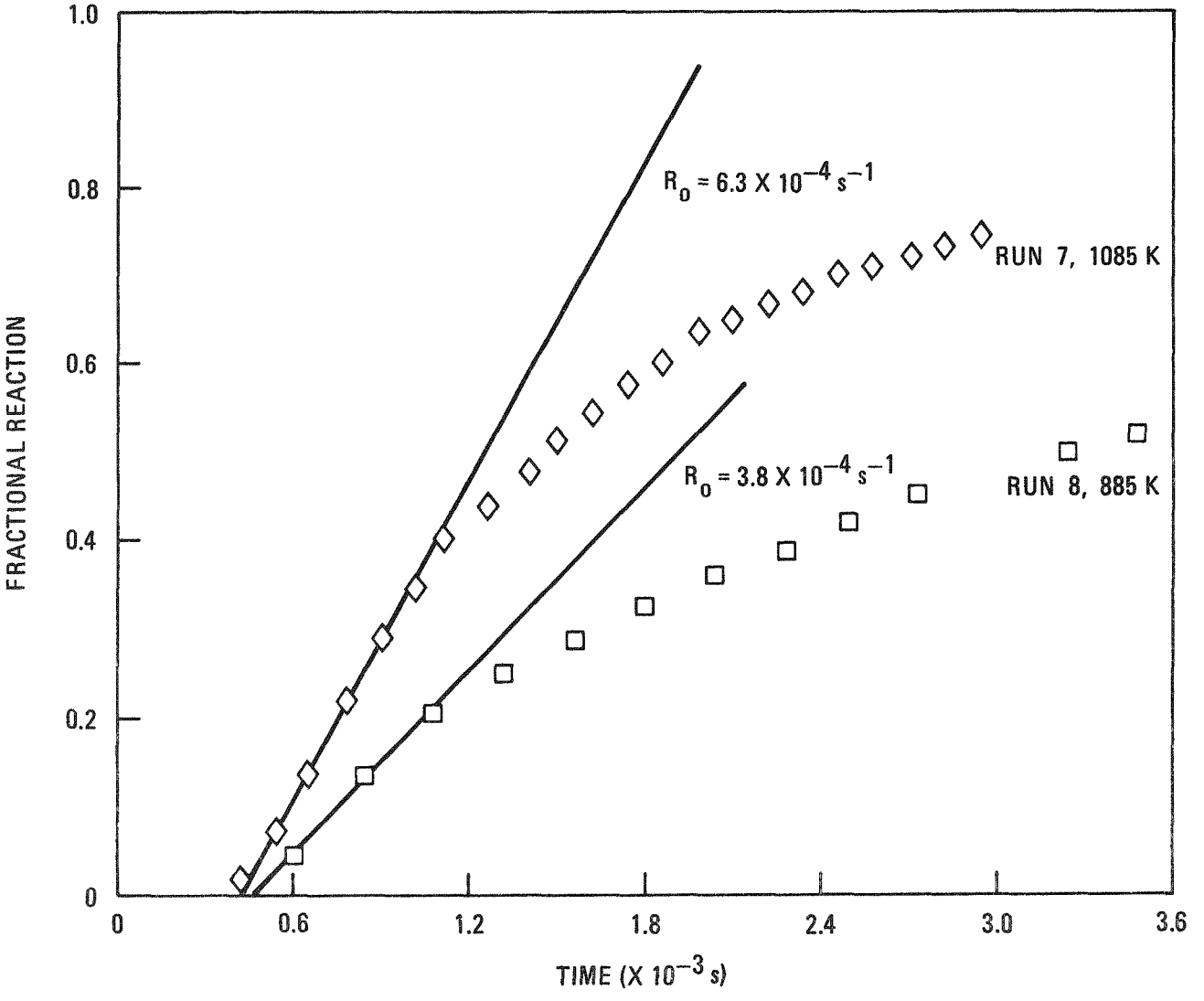

Fig. 4-44. Determination of initial rate of hydrolysis-induced fission gas release in irradiated $(Th,U)C_2$ fuel; P_{H_2O} = 2.6 kPa

After this initial release portion, the release rate begins to decline and appears best fitted to an expression in which the rate is proportional to the amount of reactant remaining:

$$\frac{-dc}{dt} = k_1 c \quad , \tag{4-64}$$

where c is amount of fission gas remaining in the sample. Mathematical analysis of the majority of the experimental runs has indicated that these two kinetic expressions explain greater than 90% of the release behavior exhibited by these α_t^c versus time curves.

In order to calculate k_1, the release rate constant, a method first described by Guggenheim (Ref. 4-55) has been utilized. This method employs any experimental parameter that is a linear function of c. In the present experiments, α_t^c is the fraction of fission gas released. Thus $(1 - \alpha_t^c)$ is the fraction remaining in the sample and should be a linear function of the remaining carbide concentration:

$$(1 - \alpha_t^c) = Ac_t + B \quad , \tag{4-65}$$

where c_t is the true amount of material remaining and A and B are unknown constants.

Combining Eq. 4-65 with the integrated form of Eq. 4-64 results in

$$(1 - \alpha_t^c) = Ac_o \exp(-k_1 t) + B \tag{4-66}$$

and at time $t + \Delta t$,

$$(1 - \alpha_{t+\Delta t}^c) = Ac_o \exp(-k_1 \Delta t) \exp(-k_1 t) + B \quad . \tag{4-67}$$

The difference between Eq. 4-66 and 4-67 is

$$\Delta\alpha_t^c = \alpha_{t+\Delta t}^c - \alpha_t^c = Ac_o\ [1 - \exp(-k_1\Delta t)]\ \exp(-k_1 t) \quad . \qquad (4\text{-}68)$$

Thus, for a constant Δt, $\Delta\alpha_t^c$ varies exponentially in a way similar to the actual material remaining.

Figure 4-45 illustrates the Guggenheim analysis for the two experimental runs of Fig. 4-44. The linearity of the logarithmic plot confirms the assumption of first-order kinetics.

Table 4-26 lists the initial rates of reaction calculated from Eq. 4-63 and the Guggenheim rate constants, k_1, calculated from Eq. 4-68. Also tabulated is the range of gas release, α_t, during which the rate law is valid. There appears to be little, if any, temperature dependence on the validity ranges for both rate laws. The linear expression holds for $0.01 \lesssim \alpha_t \lesssim 0.3$, and the exponential, or Guggenheim expression, is valid when $0.2 \lesssim \alpha_t \lesssim 1$.

The initial reaction rate and the Guggenheim rate constant versus 1/T are given in Figs. 4-46 and 4-47 along with the associated 2σ error bands as calculated by CONFID, a computer code. From the slopes of the lines, apparent activation energies of 37.6 kJ/mol (9 kcal/mole) for the initial reaction rate and 71.1 kJ/mol (17 kcal/mole) for the Guggenheim rate constant are calculated.

One experiment (at 925 K) was performed using a particle from sample C, i.e., an irradiated (58% FIMA) weak acid resin (WAR) particle. As shown in Figs. 4-46 and 4-47, the release rate was very similar to that observed with failed Peach Bottom (Th,U)C_2 material even though the burnup was much greater. It is probable that irradiation does not cause measurable hydrolysis passivation at temperatures above 673 K (see below).

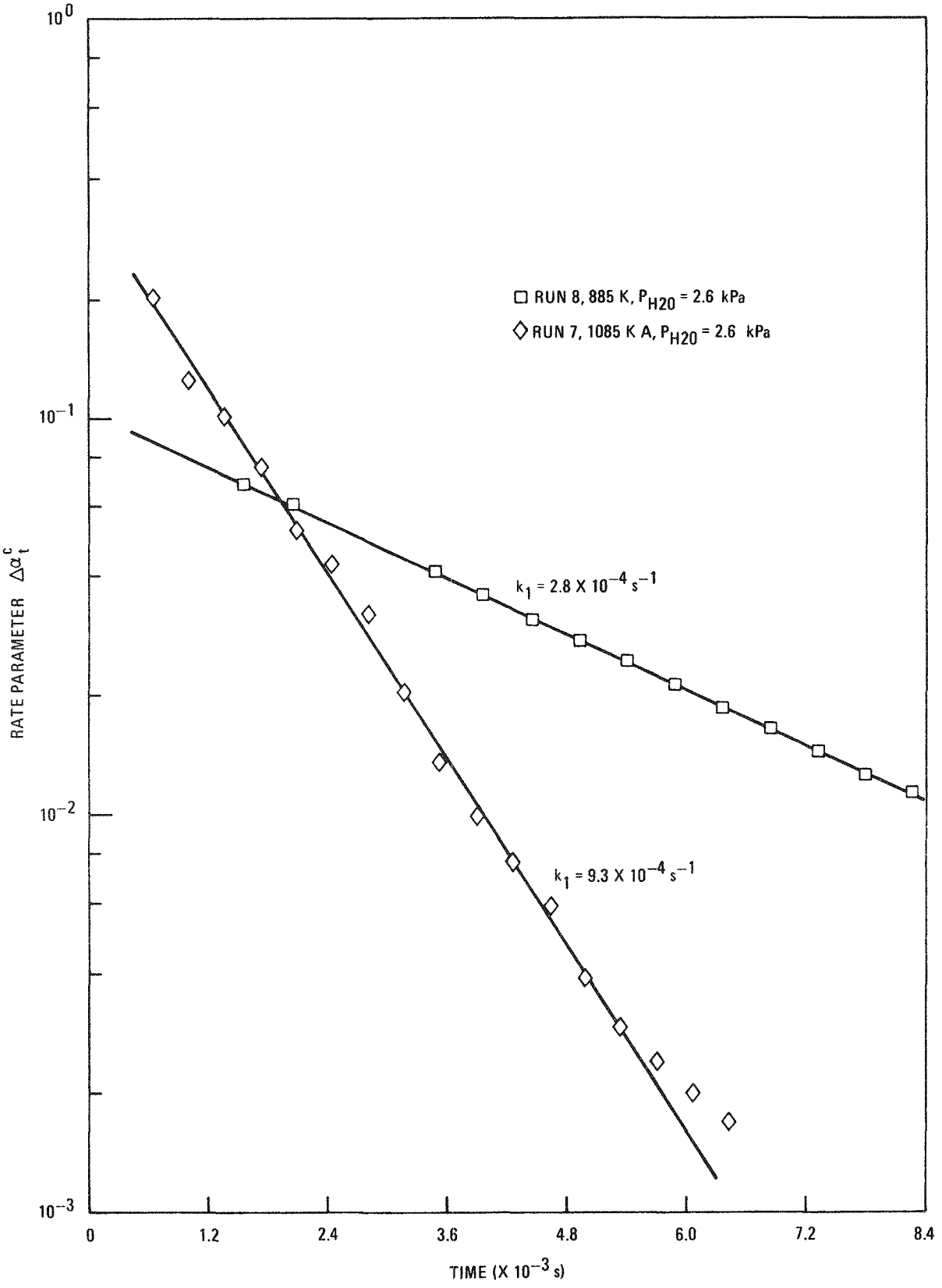

Fig. 4-45. Determination of first-order rate constants by the Guggenheim method

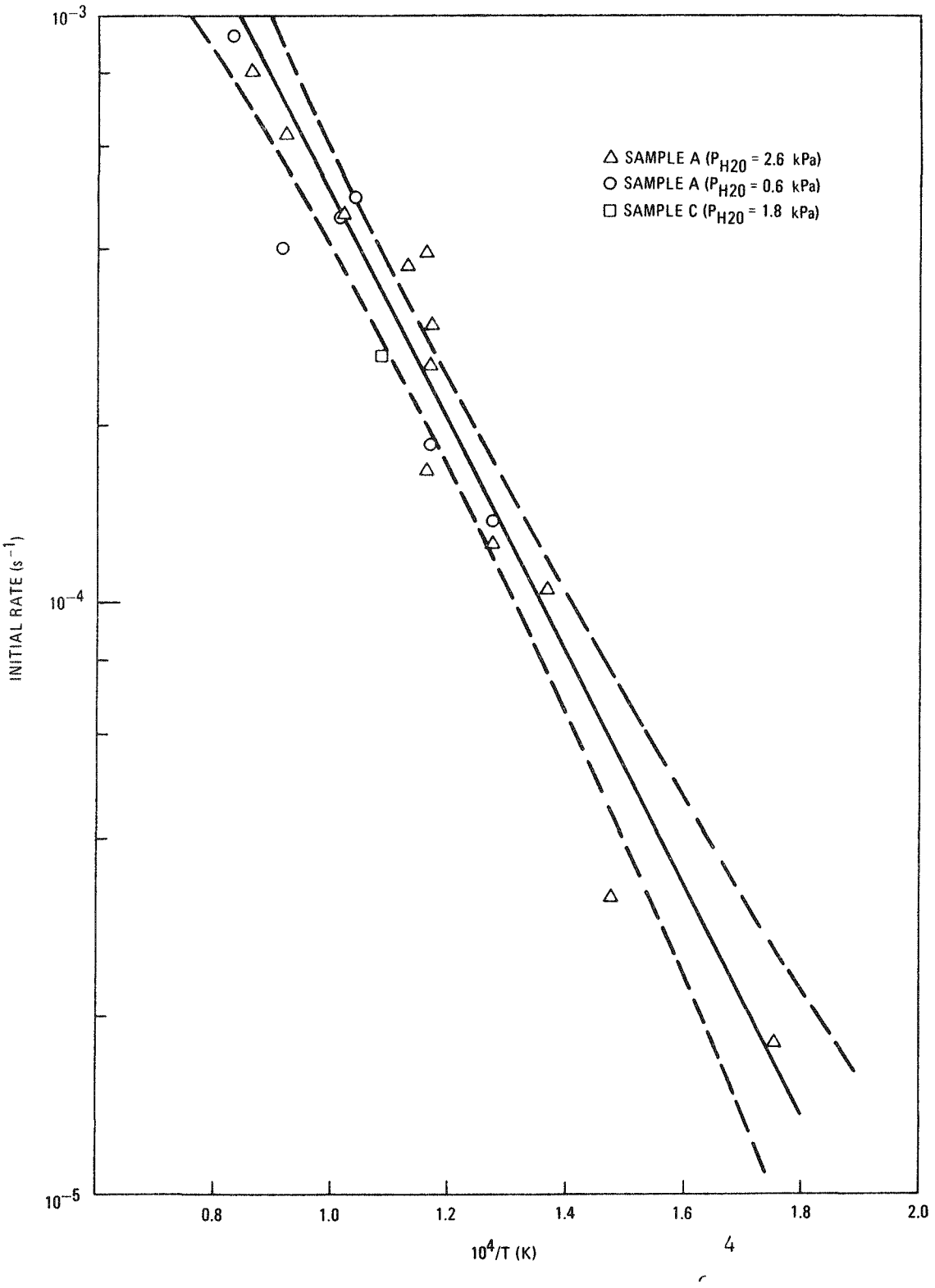

Fig. 4-46. Temperature dependence of initial release rate of Kr-85m from irradiated $(Th,U)C_2$ during hydrolysis

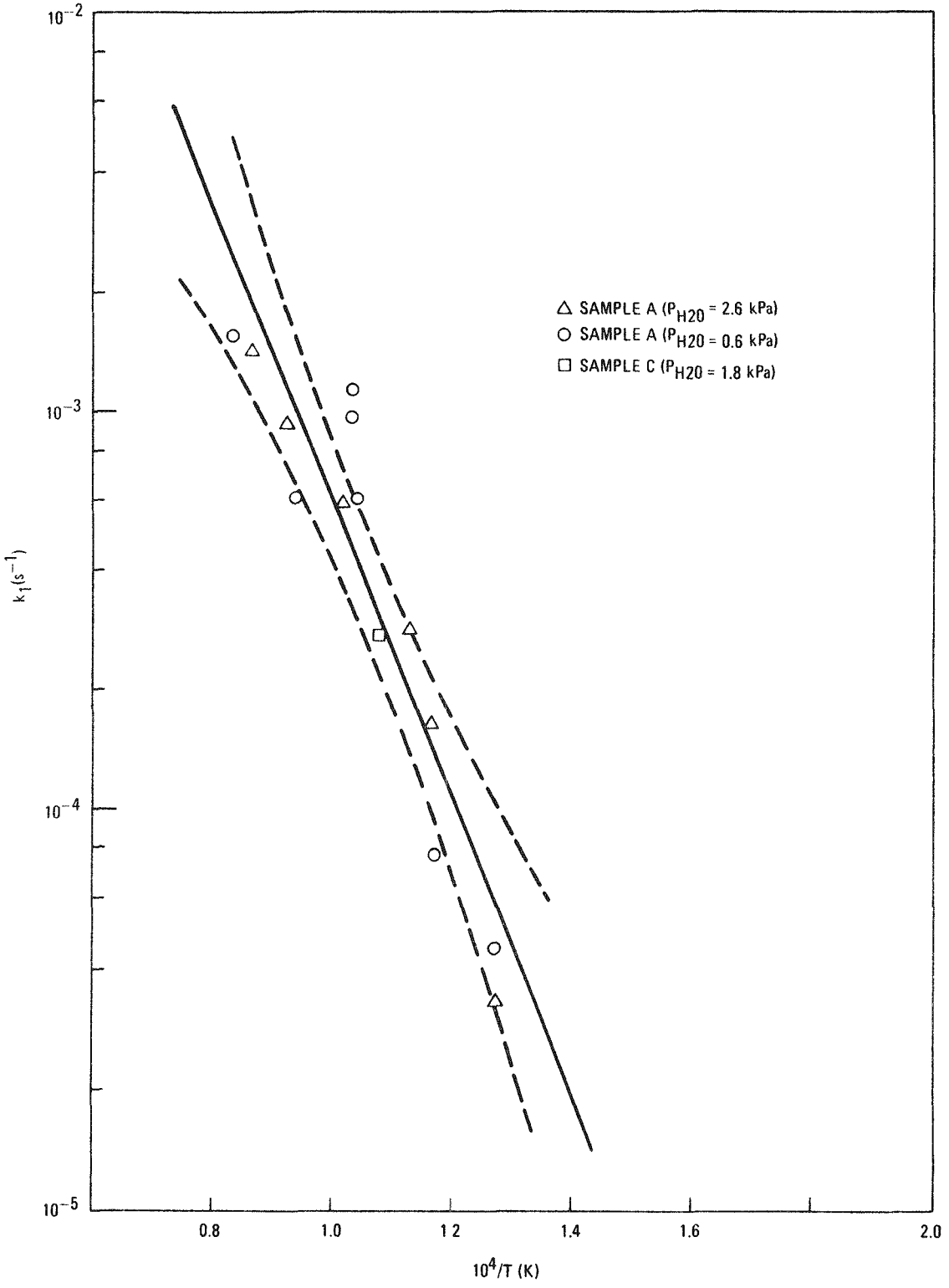

Fig. 4-47. Temperature dependence of Guggenheim reaction rate constant for irradiated $(Th,U)C_2$

Time to Failure

In the time-to-failure experiments, laser-drilled TRISO ThC_2 particles, both unirradiated and irradiated (2.1% FIMA), were used. The irradiated particles were from sample B. It was found that the release of fission gas from the irradiated samples prior to particle rupture was immeasurably small; therefore, only a small amount of kernel hydrolysis is required to cause the coatings of the laser-drilled particles to rupture. Accordingly, it is assumed that the reciprocal of the exposure time necessary to cause particle rupture, T_B^{-1}, is a valid rate parameter similar to the initial rate of reaction discussed above.

Figure 4-48 is a plot of T_B^{-1} versus 1/T for both the irradiated and unirradiated particles. Each data point for the irradiated samples (open circles) represents a measurement on a single particle. Each data point for the unirradiated samples (open triangles) represents a measurement on three particles. Since failure of the unirradiated particles could only be detected visually, in most cases failures occurred within a time span when the experiments were unattended, i.e., at night or during weekends. The number of unirradiated particles which failed within the time span is indicated in each triangle.

Reaction rates for the irradiated particles appear to follow typical inverse temperature dependence (or Arrhenius behavior), having an apparent activation energy of 50 kJ/mol (12 kcal/mole), which is similar to that found in the rate studies described above. The unirradiated samples show little or no temperature dependence, which is indicative of a gas phase mass transport controlled mechanism.

At temperatures above about 973 K, the irradiated particles are more reactive than the unirradiated samples. At below about 600 K, the irradiated particles are less reactive, indicating a passivation effect. In fact, at about 473 K the irradiated particles were about 100 times less reactive. This is remarkable in view of the relatively small burnup (2.1% FIMA) of the irradiated samples.

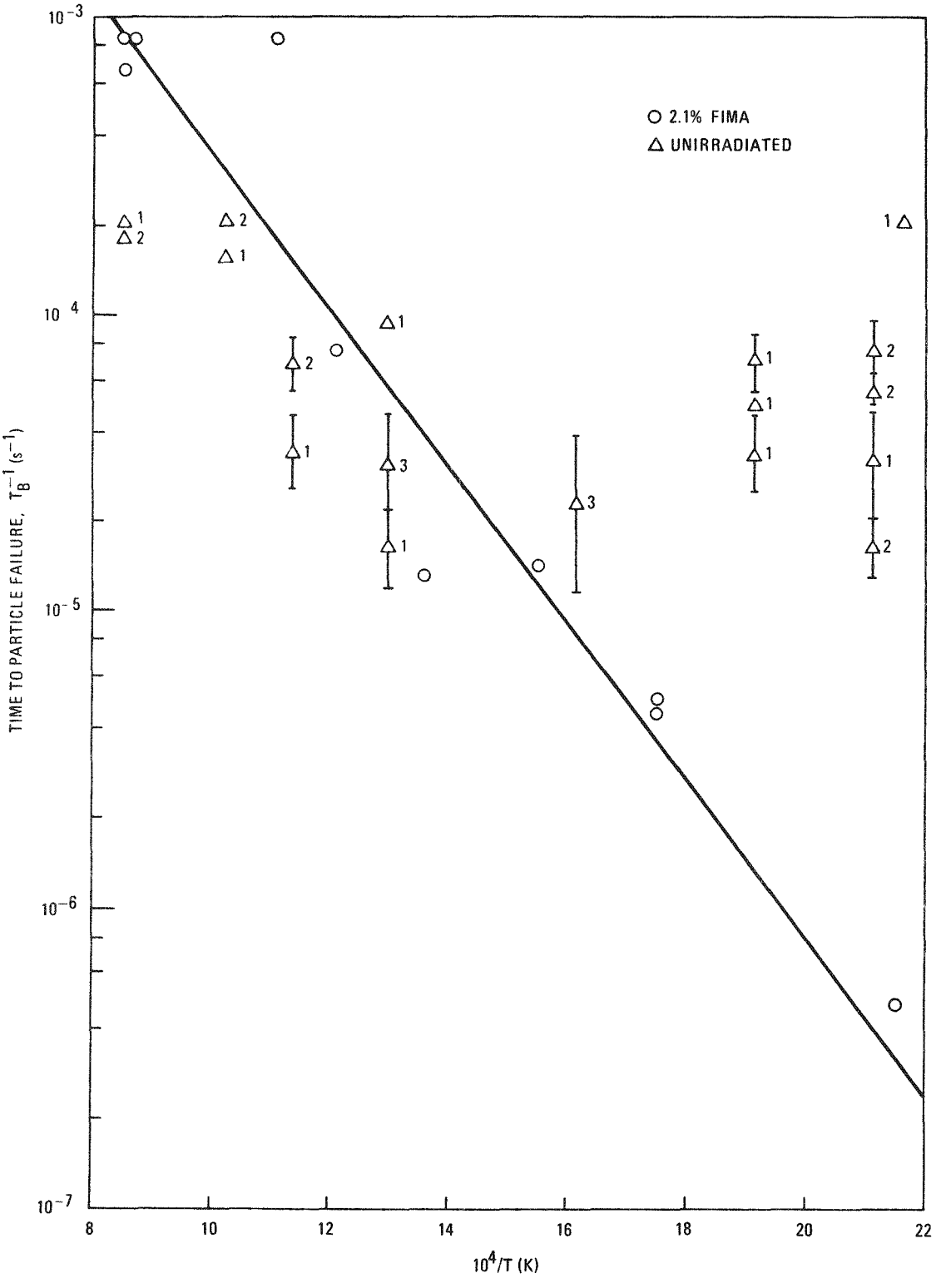

Fig. 4-48. Temperature dependence of time to failure for laser-drilled TRISO coated ThC_2 particles

The apparent low rate of hydrolysis of exposed irradiated fuel at temperatures below 600 K is important from the reactor standpoint because it means that in the event of moisture ingress, fuel hydrolysis is less likely to occur during the cleanup period when the core temperature is about 500 K. It is anticipated that experiments under way on fuel particles having higher burnups will indicate even greater resistance to hydrolysis.

Effect of Fuel Hydrolysis on Fuel Element Design Criteria

Introduction and Summary. A potential consequence of carbide hydrolysis is expansion of the affected fuel. This occurs because the solid products of the hydrolysis reaction are considerably less dense than the original carbide fuel kernels. Fuel expansion can add stress to the graphite fuel elements which could already be stressed due to irradiation and thermal effects and potential seismic events.

Considerable experimental work has been performed to elucidate the effect of fuel expansion on graphite stress. Based on the results of this work and present core design criteria, the amount of graphite stress due to fuel expansion in the large HTGR is expected to be negligible. This is because of (1) the low carbide content in the core and (2) limited fuel temperature peaking so that local particle failure and subsequent conversion of oxide fuel to carbide will be minimized.

Details. Experimental work to elucidate the degree of stress that fuel expansion can cause is covered in Refs. 4-7, 4-54, 4-56, and 4-57. Results indicate that the stress observed is a function of: (1) the degree of hydrolysis or length of exposure, (2) the volume loading of exposed UC_2 or ThC_2, and (3) temperature (with maximum loads observed at around 573 K). The rate of the process is governed totally by mass transport (i.e., diffusion) of water vapor through the surrounding graphite; therefore, the rate of the stress increase should be proportional to water vapor pressure and inversely proportional to total He pressure.

In experiments at 573 K where exposed carbide concentrations simulated 100% failure of all carbide fuel (∿0.6 g ThC_2/cm^3), a maximum graphite stress of around 3.4 MPa (∿500 psi) has been measured. At a fuel failure fraction of ∿10% (∿0.069 g ThC_2/cm^3), which is more representative of a worst-case condition in service, the amount of stress produced was only 0.1 MPa (∿15 psi) or less. Apparently, small amounts of fuel expansion are accommodated by the voidage in the fuel rod, leading to low apparent stress levels.

The amount of graphite stress due to fuel expansion in the lead HTGR is expected to be negligible. This is because of the low carbide content in the core. For example, only two basic fuel kernel types are considered in the high-enriched (HEU) system, carbide, or oxycarbide, fissile and oxide fertile. Only 5% (by weight) of the fuel is fissile UC_2, and the remaining 95% is fertile ThO_2. The low-enriched (LEU) fuel system would likely be all oxide. Therefore, the only possible mechanism for having sufficient exposed carbide to cause measurably increased stress levels is failure of greater than 10% fuel loading locally followed by sufficiently high temperature (>1673 K) to convert the exposed ThO_2 fuel to ThC_2 by the carbothermic reaction.

A design criterion of the Lead Plant core is to limit fuel temperature peaking so that local particle failure and subsequent conversion to carbide will be minimized. Such a criterion is relatively easy to attain, particularly in the LEU core with its low power density, by fuel load and coolant orifice adjustments. Consequently, graphite stress due to hydrolysis-induced fuel expansion is presently deemed to be of little or no consequence in the LHTGR and will therefore have no impact on fuel element design criteria.

With two exceptions, all the work to date in this area has been on mixed beds of ThC_2 kernels and graphite shim particles or laboratory-made (simulated) fuel rods of the same constituents. A small amount of additional work is required to perform proof or validation tests using production-type fuel rods. The rods could be prepared from ThO_2 kernels

with special coatings that would fail and permit the oxide to convert to carbide during an anneal step at ∿2200 K. It is anticipated that the stress levels from hydrolysis of production-type rods would be no greater than levels observed in the mixed bed tests.

TASK 900: FORT ST. VRAIN CHEMISTRY SURVEILLANCE

Fission gas activities and impurity levels in the primary coolant of the Fort St. Vrain reactor are measured at power steps during the rise-to-power program. The measurements are made during steady-state operation at each power step. Through January 1977, steady-state operating conditions had been attained at power steps of 2, 5, 8, 11, 18, 27, and 28%. Since that time, the reactor has operated intermittently, with interruptions due to technical difficulties. The reactor attained a power level around 39% for a brief period of about 2 days in August 1977.

Fission Product Surveillance

Fission gas activities in the primary coolant were measured for each of the above power steps. R/B values were derived from the activity data. The results for power steps through 27% were described in Ref. 4-3.

The primary coolant activity data measured at power levels around 28% are given in Table 4-27. Activity data were measured at the power level around 39%, but these data are not meaningful because steady-state operation was not attained.

The specific activity data of Table 4-27 were used to calculate the steady-state release (R/B) values given in Table 4-28. The calculated fuel temperatures at the steady-state power levels given in Tables 4-27 and 4-28 were 794 K (970°F) at 26.7%, 845 K (1061°F) at 28%, and 886 K (1136°F) at 28.9% power.

The measured R/B values, given in Table 4-28, are low (10^{-6} range) indicating satisfactory retention of fission gases by the fuel and thus

TABLE 4-27
MEASURED STEADY-STATE ACTIVITIES FOR NOBLE GAS ISOTOPES AT VARIOUS POWER LEVELS DURING FSV RISE TO POWER

Date	Time	Power (%)	Gross Circulating Activity (Ci)	Activity in the Primary Coolant by Isotope[a] ($\mu Ci/cm^3 \times 10^4$ STP)						
				Kr-85m	Kr-87	Kr-88	Kr-89	Xe-135	Xe-137	Xe-138
11/22/76	2330	26.7	69	2.6	6.2	5.4	3.8	8.3	3.3	7.3
11/22/76	2336	26.7	59	2.3	5.4	4.6	2.1	7.4	3.5	6.5
Average activity levels			64	2.5	5.8	5.0	3.0	7.9	3.4	6.9
12/15/76	1037	28.0	79	3.3	7.2	6.9	2.3	10.9	3.6	8.2
12/15/76	1055	28.0	68	3.3	6.0	6.0	2.2	9.6	2.2	7.0
Average activity levels			74	3.3	6.6	6.5	2.3	10.3	2.9	7.6
12/17/76	1110	28.9	92	3.9	8.3	7.9	2.9	12.1	4.0	10.3
12/17/76	1130	28.9	85	3.4	7.2	7.2	3.3	11.1	4.4	8.9
Average activity levels			89	3.7	7.8	7.6	3.1	11.6	4.2	9.6

[a] Data corrected for 2.5-min delay time between primary coolant and sampling point.

TABLE 4-28
MEASURED R/B VALUES FOR NOBLE GAS ISOTOPES AT VARIOUS POWER LEVELS DURING FSV RISE TO POWER[a]

Date	Time	Power (%)	R/B x 10^5						
			Kr-85m	Kr-87	Kr-88	Kr-89	Xe-135	Xe-137	Xe-138
11/22/76	2330	26.7	0.39	0.33	0.24	0.08	0.34	0.05	0.12
11/22/76	2336	26.7	0.34	0.29	0.20	0.05	0.33	0.06	0.11
Average R/B values			0.37	0.31	0.22	0.07	0.33	0.06	0.12
12/15/76	1037	28.0	0.47	0.37	0.29	0.07	0.47	0.08	0.14
12/15/76	1055	28.0	0.41	0.31	0.25	0.07	0.41	0.05	0.12
Average R/B values			0.44	0.34	0.27	0.07	0.44	0.07	0.13
12/17/76	1110	28.9	0.54	0.41	0.33	0.06	0.51	0.06	0.16
12/17/76	1130	28.9	0.47	0.36	0.30	0.07	0.47	0.07	0.14
Average R/B values			0.51	0.39	0.31	0.07	0.49	0.07	0.15

[a]Data corrected for 2.5-min delay time between primary coolant and sampling point.

satisfactory performance of the fuel. The data indicate a half-life dependence somewhat less than the square root of half-life. However, the low half-life dependence found was as expected at the low fuel temperatures where recoil-type fission gas release predominates. (See Ref. 4-18 for information on recoil-type release.)

The measured R/B values in Table 4-28 are in good accord with predicted values given in Ref. 4-58, the measured values being slightly lower (by a factor of about two) than the predicted values. The predicted values at 28.6% power are as follows:

Isotope	R/B x 10^5	Isotope	R/B x 10^5
Kr-85m	1.1	Xe-135	0.87
Kr-88	0.90	Xe-137	0.15
Kr-89	0.12	Xe-138	0.29

Coolant Impurity Surveillance

Primary coolant impurity levels were measured and analyzed for each of the above power levels. The results for power levels through 28% are described in Refs. 4-3 and 4-59. Impurity levels were measured at the power level around 39%, but the data are not meaningful because steady-state operation was not attained.

REFERENCES

4-1. Jensen, D. D., et al., "Planning Guide for the Validation of Fission Product Transport Codes," ERDA Report GA-A13386, General Atomic Company, April 15, 1975.

4-2. Haire, M. J., and D. W. McEachern, "Gaseous Radioactivity Levels in the Primary Coolant of an HTGR," General Atomic Report GA-A12946 (GA-LTR-14), October 1, 1974.

4-3. "HTGR Fuels and Core Development Program Quarterly Progress Report for the Period Ending August 31, 1976," ERDA Report GA-A14046, General Atomic Company, September 24, 1976.

4-4. "HTGR Fuels and Core Development Program Quarterly Progress Report for the Period Ending August 31, 1975," ERDA Report GA-A13592, General Atomic Company, September 30, 1975.

4-5. "HTGR Fuels and Core Development Program Quarterly Progress Report for the Period Ending February 28, 1976," ERDA Report GA-A13804, General Atomic Company, March 31, 1976.

4-6. "HTGR Fuels and Core Development Program Quarterly Progress Report for the Period Ending May 31, 1976," ERDA Report GA-A13941, General Atomic Company, June 30, 1976.

4-7. "Fuel Design Data Manual," Issue C, General Atomic Company, to be published.

4-8. Forutanpour, B., and B. Roos, "FIPERX, A FORTRAN V Program for the Solutions of One-Dimensional Linear and Non-Linear Diffusion Problems," USAEC Report GA-9904, Gulf General Atomic, September 1969.

4-9. Alberstein, D., P. D. Smith, and M. J. Haire, "Metallic Fission Product Release from the HTGR Core," General Atomic Report GA-A13258 (GA-LTR-20), May 15, 1975.

4-10. "HTGR Fuels and Core Development Program Quarterly Progress Report for the Period Ending November 30, 1975," ERDA Report GA-A13737, General Atomic Company, December 31, 1976.

4-11. Brown, P. E., and R. L. Faircloth, "Metal Fission Product Behavior in High Temperature Reactor - UO_2 Coated Particle Fuel," J. Nucl. Mater. 59, 29 (1976).

4-12. Vanslager, F. E., and L. D. Mears, "PAD: A Computer Code for Calculating the Plateout Activity Distribution in a Reactor Circuit," Gulf General Atomic Report GA-10460, January 1971.

4-13. Pointud, M., and P. Chenebault, "Emission of Fission Gases by Failed Coated Oxide Fuel Particles," Nucl. Tech., to be published.

4-14. Smith, P. D., et al., "Release of Metallic Fission Products from Multilayered Coated Particles," General Atomic Report GA-A14332, April 1977.

4-15. Zumwalt, L. R., E. E. Anderson, and D. E. Gethard, "Fission-Product Retention Characteristics of Certain (Th,U)C_2 - Graphite Fuels," General Atomic, Division of General Dynamics Report GA-4551, September 17, 1963.

4-16. Myers, B. F., and W. E. Bell, "Cesium Transport Data for HTGR Systems," ERDA Report GA-A13990, General Atomic Company, to be published.

4-17. "HTGR Accident Initiation and Progression Analysis Status Report, Volume V. AIPA Fission Product Source Terms," ERDA Report GA-A13617, General Atomic Company, February 1976.

4-18. Myers, B. F., et al., "The Behavior of Fission Product Gases in HTGR Fuel Material," ERDA Report GA-A13723, General Atomic Company, to be published.

4-19. Burnette, R. D., W. E. Bell, and N. L. Baldwin, "Fission Product Retention Characteristics of HTGR Fuel," in Proceedings of the International Conference on Nuclear Fuels Performance, British Nuclear Energy Society, London, October 15-19, 1973, Paper 16.

4-20. Scott, C. B., and C. A. Young, "Postirradiation Examination of Capsule P13Q," ERDA Report GA-A14174, General Atomic Company, to be published.

4-21. Scott, C. B., D. P. Harmon, and J. F. Holzgraf, "Postirradiation Examination of Capsules P13R and P13S," ERDA Report GA-A13827, General Atomic Company, October 1976.

4-22. Harmon, D. P., and C. B. Scott, "Development and Irradiation Performance of LHTGR Fuel," ERDA Report GA-A13173, General Atomic Company, October 31, 1975.

4-23. Baldwin, N. L., General Atomic Company, private communication.

4-24. Friskney, C. A., and K. A. Simpson, "The Behavior of Fission Product Barium and Strontium in Irradiated UO_2," J. Nucl. Mater. 57, 121 (1975).

4-25. "HTGR Fuels and Core Development Program Quarterly Progress Report for the Period Ending November 30, 1974," USAEC Report GA-A13253, General Atomic Company, January 31, 1975.

4-26. Myers, B. F., and W. E. Bell, "Strontium Transport Data for HTGR Systems," USAEC Report GA-A13168 (GA-LTR-16), General Atomic Company, December 6, 1974.

4-27. "HTGR Fuels and Core Development Program Quarterly Progress Report for the Period Ending November 30, 1976," ERDA Report GA-A14180, General Atomic Company, December 27, 1976.

4-28. Norman, J. H., and H. G. Staley, "Knudsen Cell Measurements to Determine the Stabilities of Gaseous Cesium and Rubidium Oxides," paper presented at the Fourteenth Annual Conference on Mass Spectrometry and Allied Topics, Dallas, Texas, May 22-27, 1966.

4-29. "HTGR Base Program Quarterly Progress Report for the Period Ending May 31, 1968," USAEC Report GA-8662, Gulf General Atomic, June 28, 1968.

4-30. Morgan, M. T., H. J. deNordwall, and R. L. Towns, "Release of Fission Products from Pyrocarbon-Coated HTGR Fuel Particles During Postirradiation Anneals," USAEC Report ORNL-TM-4539, Oak Ridge National Laboratory, December 1974.

4-31. GASSAR-6, General Atomic Standard Safety Analysis Report, August 1, 1975.

4-32. Norman, J. H., "Review of Vapor Pressures and Diffusion Coefficients of Certain HTGR Core Materials and Fission Products for Use in Reactor Accident Calculations," General Atomic Report GA-A12634, May 15, 1974.

4-33. Winchell, P., "Thermodynamic Data for Carbonaceous Systems," USAEC Internal Report GAMD-9335, Gulf General Atomic, November 20, 1970.

4-34. "Public Service Company of Colorado 330-MW(e) High-Temperature Gas-Cooled Reactor Research and Development Program Quarterly Progress Report for the Period Ending March 31, 1966," USAEC Report GA-7086, General Atomic, Division of General Dynamics, May 11, 1966.

4-35. Findlay, J. R., and T. F. Laing, "The Diffusion of Fission Products from Graphite," J. Nucl. Mater. 7, 182 (1962).

4-36. Doyle, L. B., "High Temperature Diffusion of Individual Fission Elements from Uranium Carbide Impregnated Graphite," North American Aviation Report NAA-SR-255, September 11, 1953 (Confidential downgraded to Unclassified 7/2/57).

4-37. Cowan, G. A., and C. J. Arth, "Diffusion of Fission Products at High Temperature from Refractory Matrices," Reactor Technol. 7, 328 (1958).

4-38. Bryant, E. A., et al., "Rates and Mechanisms of the Loss of Fission Products from Uranium-Graphite Fuel Materials," Nucl. Sci. Eng. 15, 288 (1963).

4-39. Faircloth, R. L., F. C. W. Pummery, and B. A. Rolls, "Diffusion of Barium, Strontium and Cerium in Various Grades of Reactor Graphite," in Proceedings of the Symposium on Thermodynamics with Emphasis on Nuclear Materials and Atomic Transport in Solids, Vol. II, International Atomic Energy Agency, Vienna, 1966, pp. 133-152.

4-40. Wallroth, C. F., J. F. Holzgraf, and D. D. Jensen, "Postirradiation Examination and Evaluation of Peach Bottom Fuel Test Element FTE-6," ERDA Report GA-A13943, General Atomic Company, to be published.

4-41. Haire, M. J., and L. R. Zumwalt, "Mixed Sorption Models and Isotherms of Cesium-Rubidium-Graphite System at High Temperatures," Nucl. Sci. Eng. 50, 91 (1973).

4-42. deNordwall, H. J., et al., "Postirradiation Radiochemical Analysis of Pluto Loop A Charge 16," Atomic Energy Research Establishment Report AERE-R 5405, AERE Harwell, June 1967.

4-43. Skerker, A. L., and L. R. Zumwalt, "Fast and Slow Diffusion of Barium in Reactor-Grade Graphite," Trans. Am. Nucl. Soc. 15, 760 (1972).

4-44. Zumwalt, L. R., North Carolina State University, private communication.

4-45. "HTGR Base Program Quarterly Progress Report for the Period Ending February 28, 1967," USAEC Report GA-7801, General Atomic, Division of General Dynamics, April 20, 1967.

4-46. "HTGR Base Program Quarterly Progress Report for the Period Ending May 30, 1969," USAEC Report GA-9372, Gulf General Atomic, June 27, 1969.

4-47. "HTGR Base Program Quarterly Progress Report for the Period Ending August 31, 1970," USAEC Report GA-10288, Gulf General Atomic, September 30, 1970.

4-48. Staley, H. G., General Atomic Company, private communication.

4-49. "HTGR Base Program Quarterly Progress Report for the Period Ending February 28, 1974," USAEC Report GA-A12916, General Atomic Company, March 29, 1974.

4-50. Doring, D. A., "Funfit N-Space Function Fitting," Gulf General Atomic unpublished data, May 1968.

4-51. "Public Service Company of Colorado 330-MW(e) High-Temperature Gas-Cooled Reactor Research and Development Program Quarterly Progress Report for the Period Ending September 30, 1966," USAEC Report GA-7453, General Atomic, Division of General Dynamics, February 7, 1967.

4-52. "Public Service Company of Colorado 330-MW(e) High-Temperature Gas-Cooled Reactor Research and Development Program Quarterly Progress Report for the Period Ending December 31, 1966," USAEC Report GA-7634, General Atomic, Division of General Dynamics, March 20, 1967.

4-53. Dyck, R. W., R. Taylor, and P. G. Boase, "A Study of the Hydrolysis of Uranium Monocarbide, Part I: Reactions in Steam in the Temperature Range 150°C to 2500°C," Atomic Energy of Canada, Ltd. Report AECL-4917, 1975.

4-54. "HTGR Fuels and Core Development Program Quarterly Progress Report for the Period Ending May 31, 1977, "ERDA Report GA-A14418, General Atomic Company, June 1977.

4-55. Guggenheim, E. A., Phil. Mag. 2 (7), 538 (1926).

4-56. "HTGR Fuels and Core Development Program Quarterly Progress Report for the Period Ending August 30, 1974," USAEC Report GA-A13126, General Atomic Company, September 30, 1974.

4-57. "HTGR Fuels and Core Development Program Quarterly Progress Report for the Period Ending May 31, 1975," ERDA Report GA-A13444, General Atomic Company, June 30, 1975.

4-58. Dunn, T. D., and M. J. Haire, "Predictions of the Gaseous Radioactivity Level in the Primary Coolant of Fort St. Vrain During Initial Rise to Power," General Atomic unpublished data, April 1976.

4-59. "HTGR Fuels and Core Development Program Quarterly Progress Report for the Period Ending February 28, 1977," ERDA Report GA-A14298, General Atomic Company, March 1977.

9. HTGR FUEL DEVELOPMENT AND ENGINEERING
189a NO. 00551

TASK 100: FUEL PRODUCT SPECIFICATION

The first draft of the "Technical Support Document for Issue C of the HTGR Fuel Product Specification" has been reviewed by GA and ORNL personnel. ORNL contributions to the document were formally transmitted in a series of working sessions on July 13, 14, and 15. Review comments have been incorporated, and the final draft of the document is being prepared.

TASK 200: ACCELERATED IRRADIATION TESTING

Subtask 210: Fresh Fuel Qualification

Summary

Work on the postirradiation examination (PIE) of capsule P13T was continued during the report period. The P13T thermal analysis was completed and indicated that the time-averaged (over the irradiation lifetime) peak fuel temperatures for fuel rods in crucibles 1, 2, 3, and 4 are 1230°, 1100°, 1050°, and 1045°C, respectively. The design temperatures were 1300°C for crucible 1 and 1100°C for crucibles 2, 3, and 4. It therefore appears that the assumptions made during design of the capsule fuel loadings were correct and that the capsule operated at close to the desired design temperatures.

The P13T fuel rod burnup analysis was also completed. Fuel rod fissile particle burnups ranged from 53 to 75% FIMA, and fertile particle burnups ranged from 0.8 to 3.8% FIMA. The burnup analysis revealed that the cobalt thermal fluence dosimetry previously reported (Ref. 9-1) was

incorrect. After using vanadium as a thermal neutron monitor, a new thermal fluence profile for P13T was developed. At the peak thermal fluence position (fuel rod 2-2), the new thermal fluence of 6.05 n/m^2 is 21% larger than the value reported in Ref. 9-1.

Capsule HT-34 began irradiation in the High Flux Isotope Reactor (HFIR) on July 25, 1977. The capsule contains ThO_2 TRISO particles which are representative of Fort St. Vrain reload 1 test element fertile fuel and were coated in the 240-mm coater. Capsule HT-34 is scheduled to be discharged in December 1977 after receiving five cycles of irradiation.

Capsule P13T

Introduction. Capsule P13T is the ninth in a GA series of LHTGR fuel irradiation tests conducted under the HTGR Fuels and Core Development Program. P13T is a large-diameter capsule containing two cells. Cell 1 is a qualification test of reference fresh fuel [TRISO UC_2 (VSM) and BISO ThO_2 particles] irradiated at 1300°C. Cell 2 is an evaluation test of reference fresh fuel and recycle fissile fuel [TRISO UC_xO_y (WAR) particles] irradiated at 1100°C. A detailed description of the capsule is given in Ref. 9-2. The capsule began irradiation in the E-3 position of the Oak Ridge Reactor (ORR) on May 10, 1975. The capsule was discharged from the core on July 6, 1976. The capsule residence time was 422 calendar days or 363.4 effective full power days. The capsule was irradiated to a peak fast fluence of 8×10^{25} n/m^2 $(E > 29\ fJ)_{HTGR}$.

The postirradiation examination of P13T was started on September 10, 1976. All of the hot cell work on P13T has now been completed. Work is continuing on the analysis of the broad range of data generated by this PIE. Recent results from the thermal and burnup analyses follow.

Thermal Analysis. The P13T experiment was a two-cell, doubly contained and instrumented capsule irradiated in the ORR. Nominal reactor power was 30 MW. Temperature control was achieved by means of He-Ne sweep

gas mixtures in the primary containments of the two cells. Table 9-1 lists the type and location of all thermocouples within the capsule.

The technique employed in the thermal analysis of P13T combined measured data and analytical calculations to determine temperature histories over the entire irradiation period. As indicated in Fig. 9-1, ΔT_{AB} is a measured quantity since thermocouples were located at A and B in each crucible. Furthermore, ΔT_{AB} can be a measure of reactor power from day to day since the geometry is constant and the graphite conductivity will be nearly constant over short periods. Also, if concentric isothermal lines are assumed near the outer edge of the crucible (TAC models show this is true to within 20°C), the temperature at point B is the same as the temperature at the outer edge of the fuel rod hole. This being the case, the peak fuel temperature is then the sum of the temperature at B, the ΔT across the fuel-to-crucible gap, and the ΔT across the fuel rod. A TAC2D (Ref. 9-3) thermal model of a 60° sector of the crucible (dashed lines in Fig. 9-1) was constructed. Four models representing each of the four graphite bodies were run at five time points of the irradiation (beginning of life, quarter life, middle of life, three-quarter life, and end of life) to match measured capsule temperatures as closely as possible. The ΔT_{AB}, ΔT_{gap}, and ΔT_{fuel} values from these TAC runs were then curve fitted as a function of megawatt days. By then combining the daily measured T_B, ΔT_{AB}, and sweep gas mix values with the curve-fitted (or reference) values, it was possible to calculate peak fuel rod temperatures for each day of operation as follows:

$$T_{\substack{\text{fuel}\\\text{peak}}} = T_B \left(\Delta T_{\substack{\text{fuel}\\\text{ref}}}\right)\left(\frac{\Delta T_{AB\ meas}}{\Delta T_{AB\ ref}}\right) + \left(\Delta T_{\substack{\text{gap}\\\text{ref}}}\right)\left(\frac{\Delta T_{AB\ meas}}{\Delta T_{AB\ ref}}\right)\left(\frac{K_{gas\ ref}}{K_{gas\ meas}}\right) \qquad (9\text{-}1)$$

where T_B = daily measured temperature at point B,

$\Delta T_{\substack{\text{fuel}\\\text{ref}}}$ = temperature drop across fuel rod from reference curve fit,

$\Delta T_{\substack{\text{gap}\\\text{ref}}}$ = temperature drop across fuel-crucible gap from reference curve fit,

TABLE 9-1
THERMOCOUPLE ARRANGEMENT WITHIN CAPSULE P13T

Cell	Crucible	T/C[a]	Distance From Bottom of Core (in.)[b]	Location		
				Fuel Rod	Graphite Inner	Graphite Outer
2	4	W32	22.06		X	
		W18	22.06	C		
		W17	22.06	B		
		W16	22.06	A		
		W24[c]	21.81			X
		K23[c]	21.81			X
		W31	20.86		X	
		W30	19.41		X	
	3	W29	16.56		X	
		W22[c]	15.58			X
		K21[c]	15.58			X
		W28	14.60		X	
	2	W27	11.23		X	
		W15	11.23	C		
		W14	11.23	B		
		W13	11.23	A		
		W20[c]	10.98			X
		K19[c]	10.98			X
		W26	10.01		X	
		W25	9.76		X	
1	1	W12	6.20		X	
		W9	6.20			X
		K8	6.20			X
		W11	3.80		X	
		W7[c]	3.80			X
		K6[c]	3.80			X
		W10	2.36		X	
		W5	1.38			X
		K4	1.38			X
		W3	1.16	A		
		W2	1.16	C		
		W1	1.16	B		

[a] W indicates tungsten-rhenium (W3%Re/W25%Re) thermocouples (T/C) and K indicates Chromel/Alumel thermocouples.

[b] 1 in. = 2.54 cm.

[c] Used as starting point temperature in TAC models when calculating peak fuel rod temperatures.

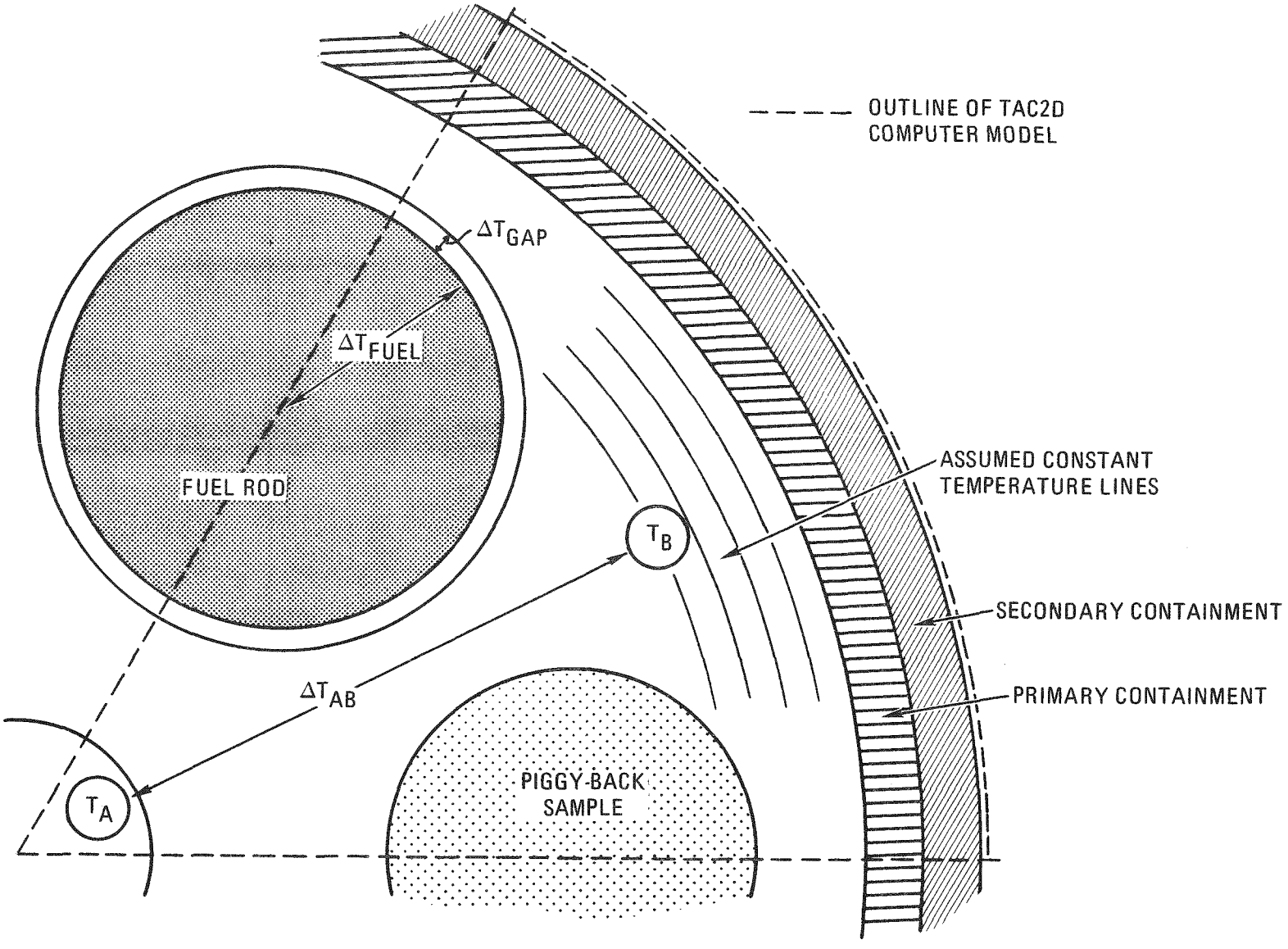

Fig. 9-1. Radial section of P13T capsule

$\Delta T_{AB\ ref} = T_A - T_B$ from reference (TAC-derived) curves,
$\Delta T_{AB\ meas} = T_A - T_B$ daily measured value,
$K_{gas\ ref}$ = gas mix conductivity from reference (TAC-derived) runs,
$K_{gas\ meas}$ = daily measured gas mix conductivity.

Note that $(\Delta T_{AB\ meas}/\Delta T_{AB\ ref})$ corrects for local power variations such as rod bank movement, and $(K_{gas\ ref}/K_{gas\ meas})$ corrects for sweep gas mixture changes.

The TAC models included property variations with temperature and fluence, axial flux variations determined from capsule dosimetry, and as precise a geometrical representation of the actual capsule as was practicable.

It is known that tungsten/rhenium (W/Re) thermocouples decalibrate with neutron exposure (Ref. 9-4). For this reason, six pairs of the two thermocouple types [W/Re and Chromel/Alumel (C/A)] were positioned together at various locations in the capsule so that a determination of this emf loss could be made. Table 9-2 shows the decalibration rates determined for each pair. By applying the decalibration factor of the nearest thermocouple pair to a given W/Re thermocouple, its corrected temperature indication can be calculated. Measured and decalibrated values for a typical W/Re thermocouple that was positioned in a high flux area of the capsule are shown in Fig. 9-2.

The temperature histories (peak fuel, volume-average, and peak graphite temperatures) are plotted as a function of megawatt days in Figs. 9-3 through 9-8. For these graphs, the following definitions apply:

1. Peak fuel temperature is the highest temperature in a fuel rod as calculated by the "hybrid" technique. This is usually not the centerline fuel rod temperature because of the asymmetric configuration of this capsule.

TABLE 9-2
W/Re THERMOCOUPLE DECALIBRATION RATES IN P13T

Thermocouple Pair	Cell	Distance From Bottom of Core (in.)[a]	$\Delta T^{(b)}/\Psi_{th}{}^{(c)}$	=	Decal Factor (^{o}C/unit Ψ_{th})
K4/W5	1	1.38	-112/2.89	=	-38.8
K6/W7	↓	3.80	--		-37.7[d]
K8/W9	↓	6.20	-181/4.95	=	-36.6
K19/W20	2	10.98	--	=	-35.4[e]
K21/W22	↓	15.58	-162/4.08	=	-39.7
K23/W24	↓	21.81	-52/1.67	=	-31.1

[a] 1 in. = 2.54 cm.

[b] ΔT is $(T_{W/Re} - T_K)$ after normalization at BOL.

[c] Ψ_{th} is thermal fluence x 10^{-25} n/m^2.

[d] This pair failed early in life (W7 failed on July 17, 1975); therefore, this decalibration factor is the average of K4/W5 and K8/W9 pairs.

[e] The calculated decalibration factor for this pair was -8.2 $^{o}C/\Psi_{th}$ which does not seem consistent with the other pairs, especially since this pair was in the highest fluence (5.15 x 10^{25} n/m^2) position. Therefore, the average of the other two pairs in cell 2 was used for the K19/W20 pair.

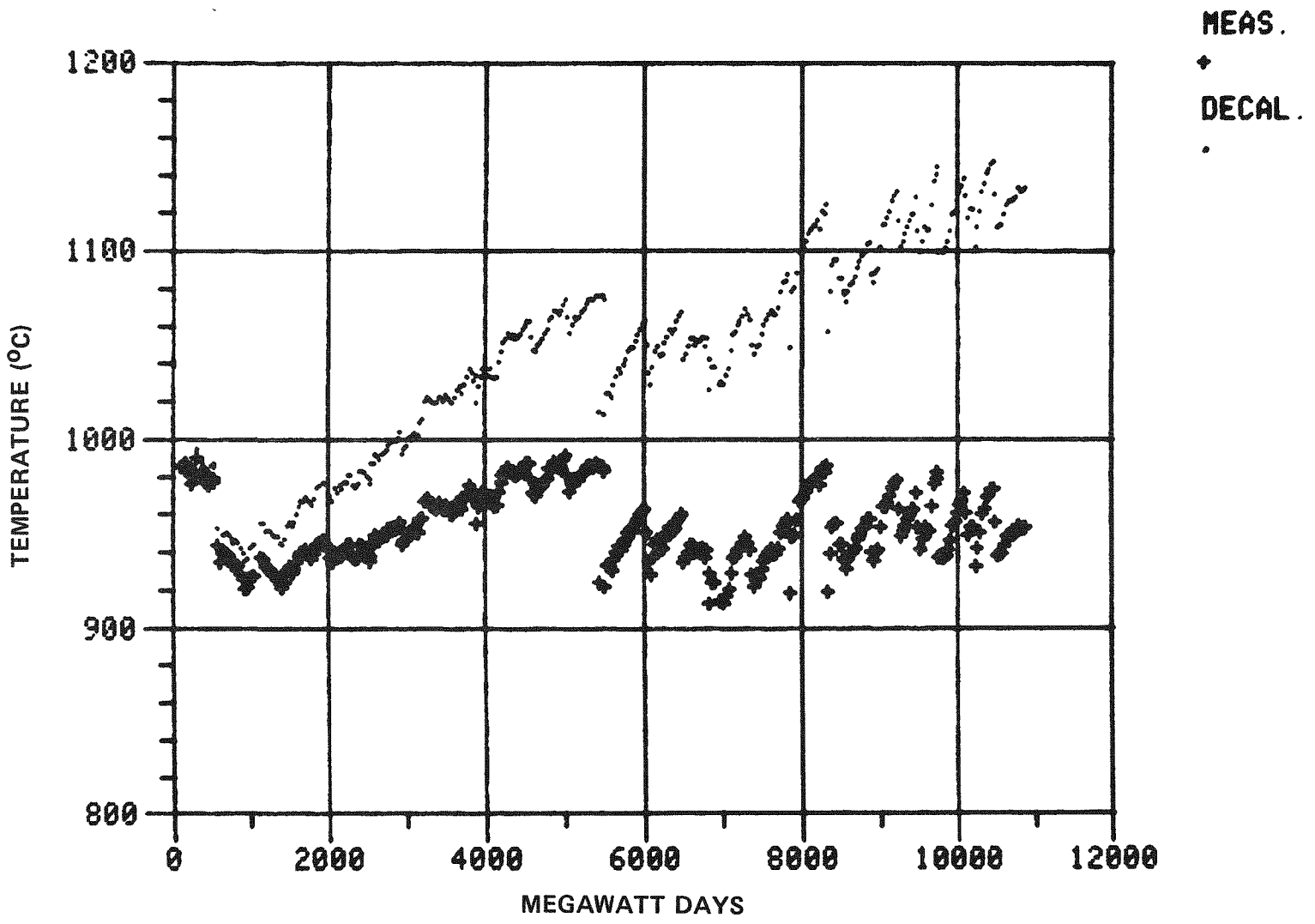

Fig. 9-2. Typical measured and corrected thermocouple readings for thermocouple W27

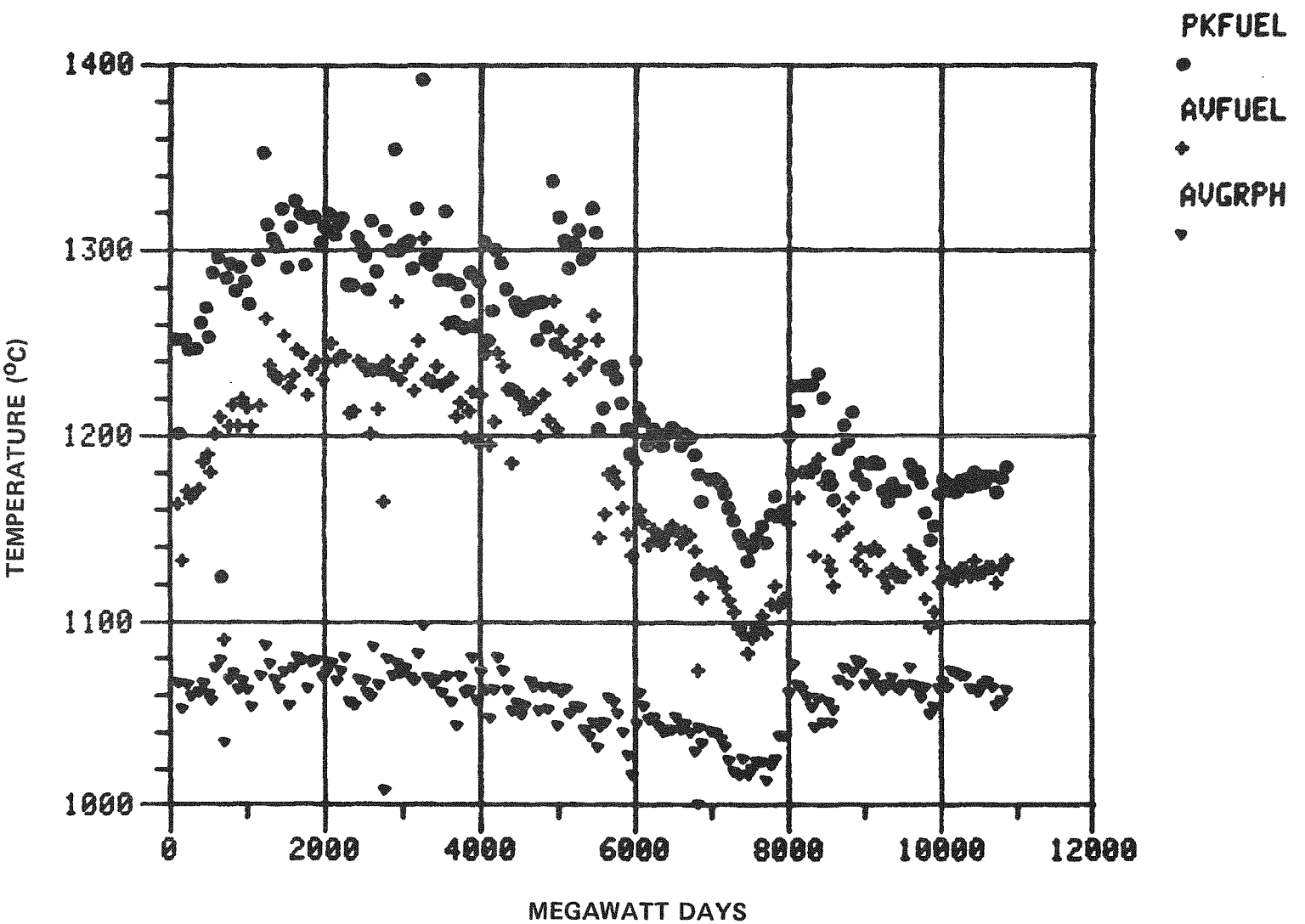

Fig. 9-3. P13T temperature history, crucible 1

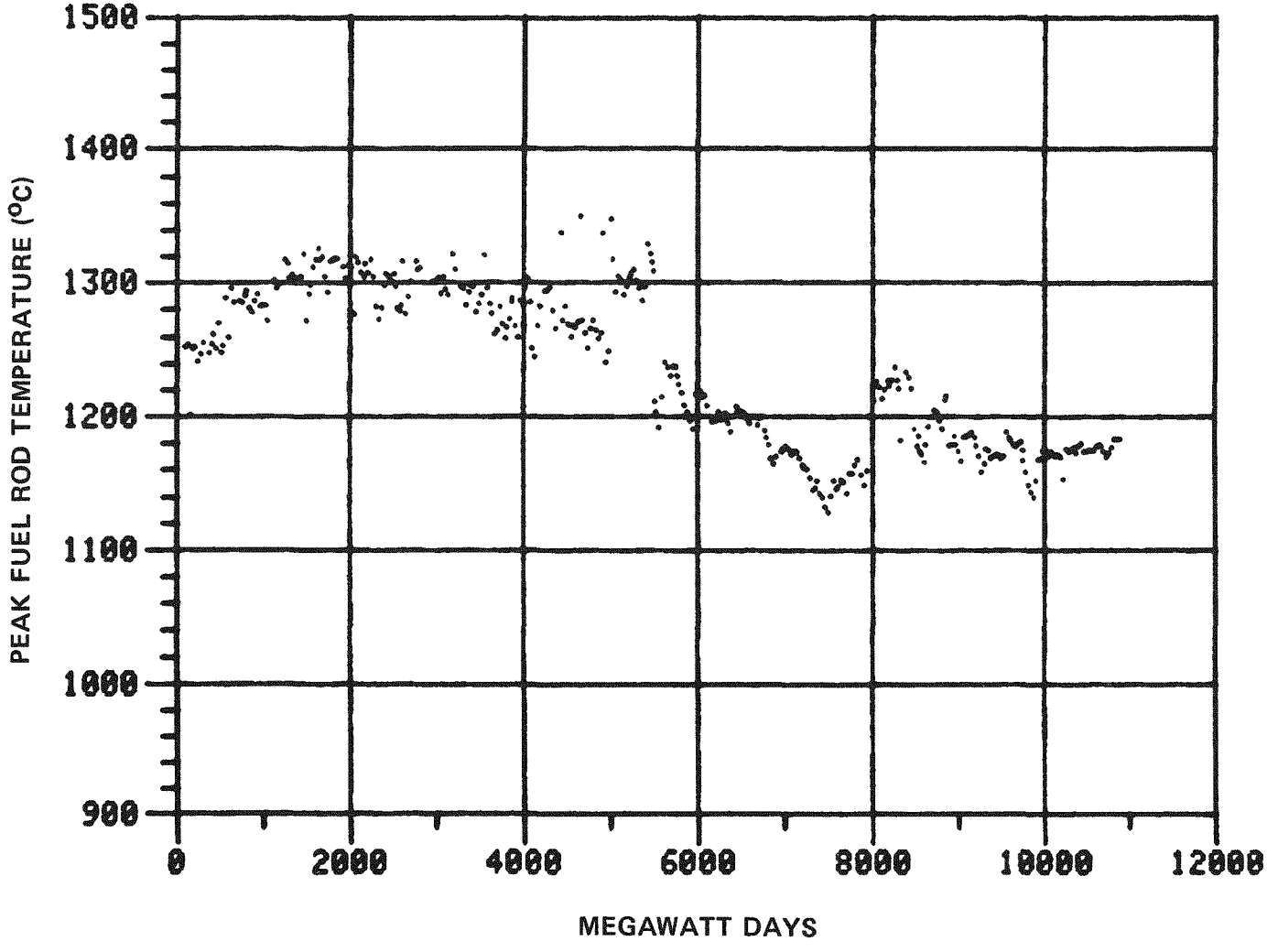

Fig. 9-4. P13T temperature history, rods 1-3A, 1-3B, and 1-3C

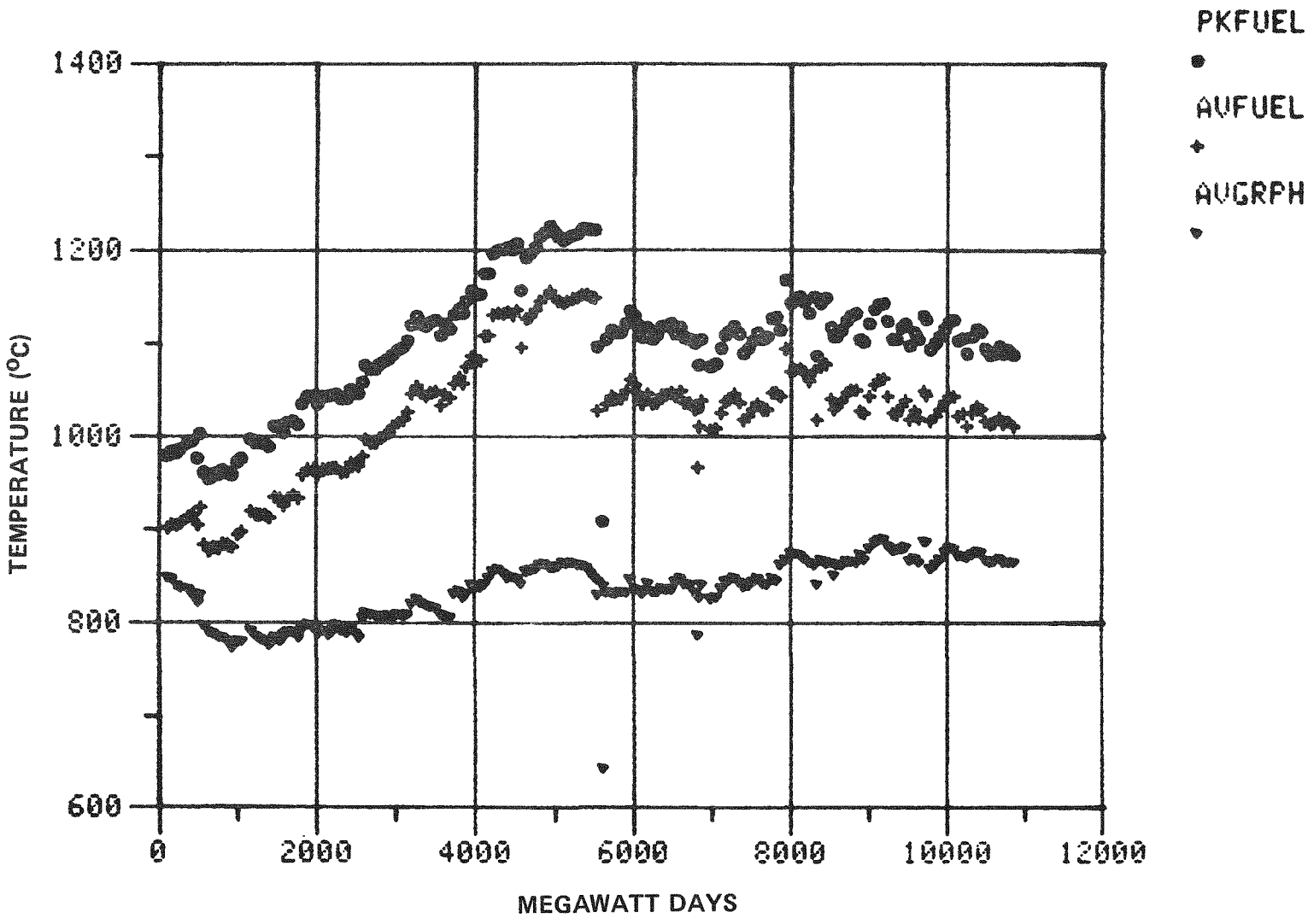

Fig. 9-5. P13T temperature history, crucible 2

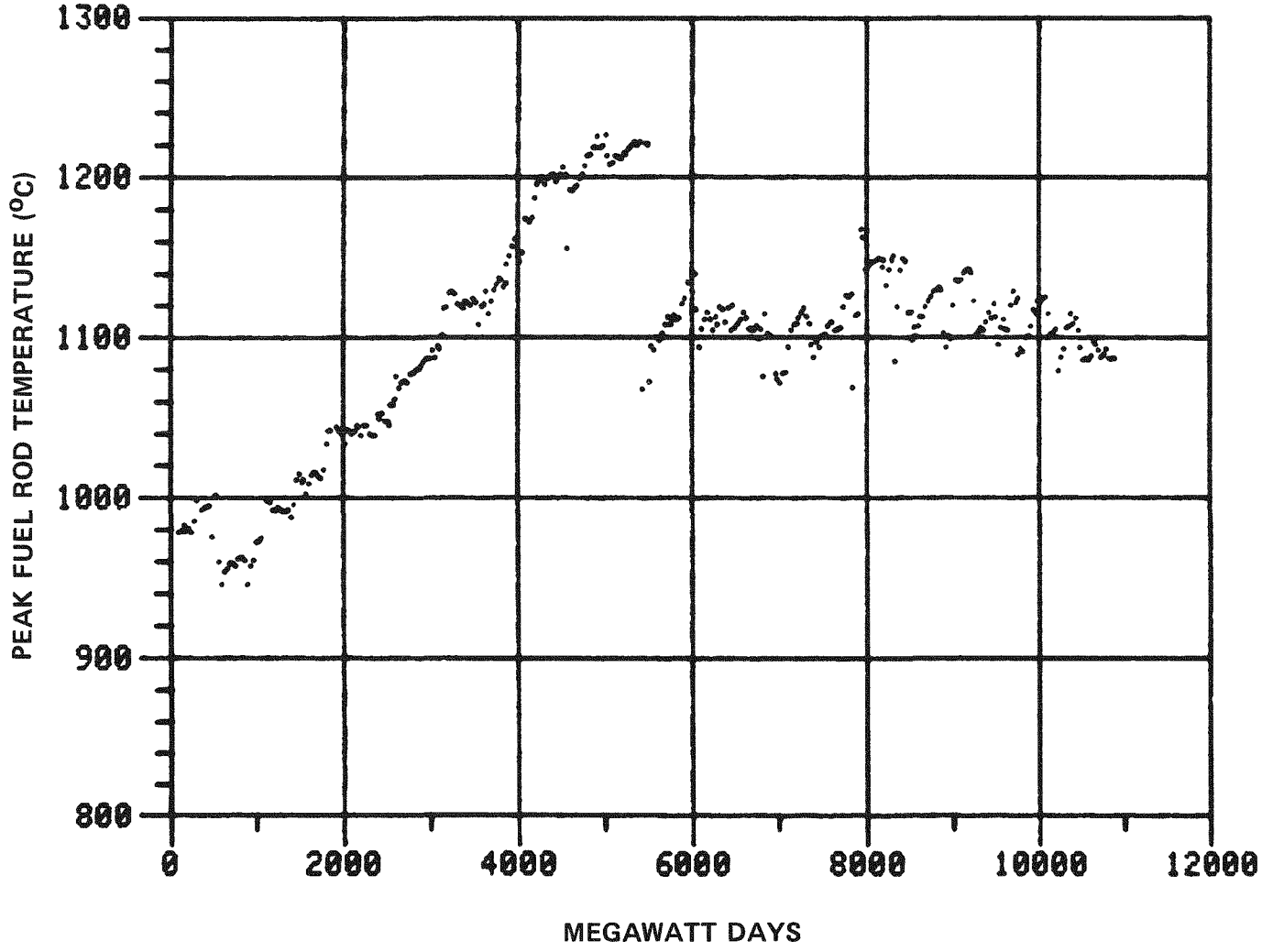

Fig. 9-6. P13T temperature history, rods 2-1A, 2-1B, and 2-1C

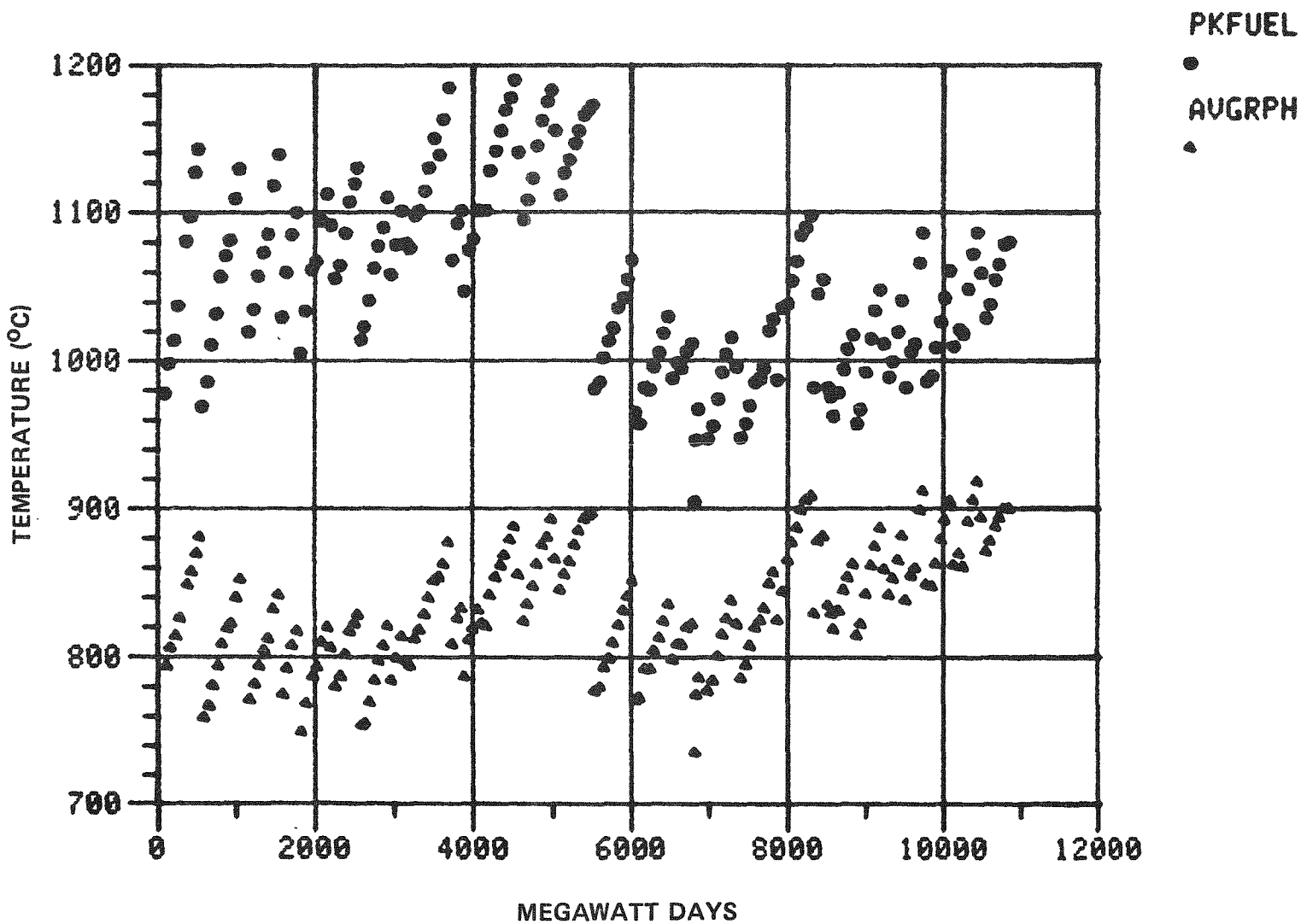

Fig. 9-7. P13T temperature history, crucible 3

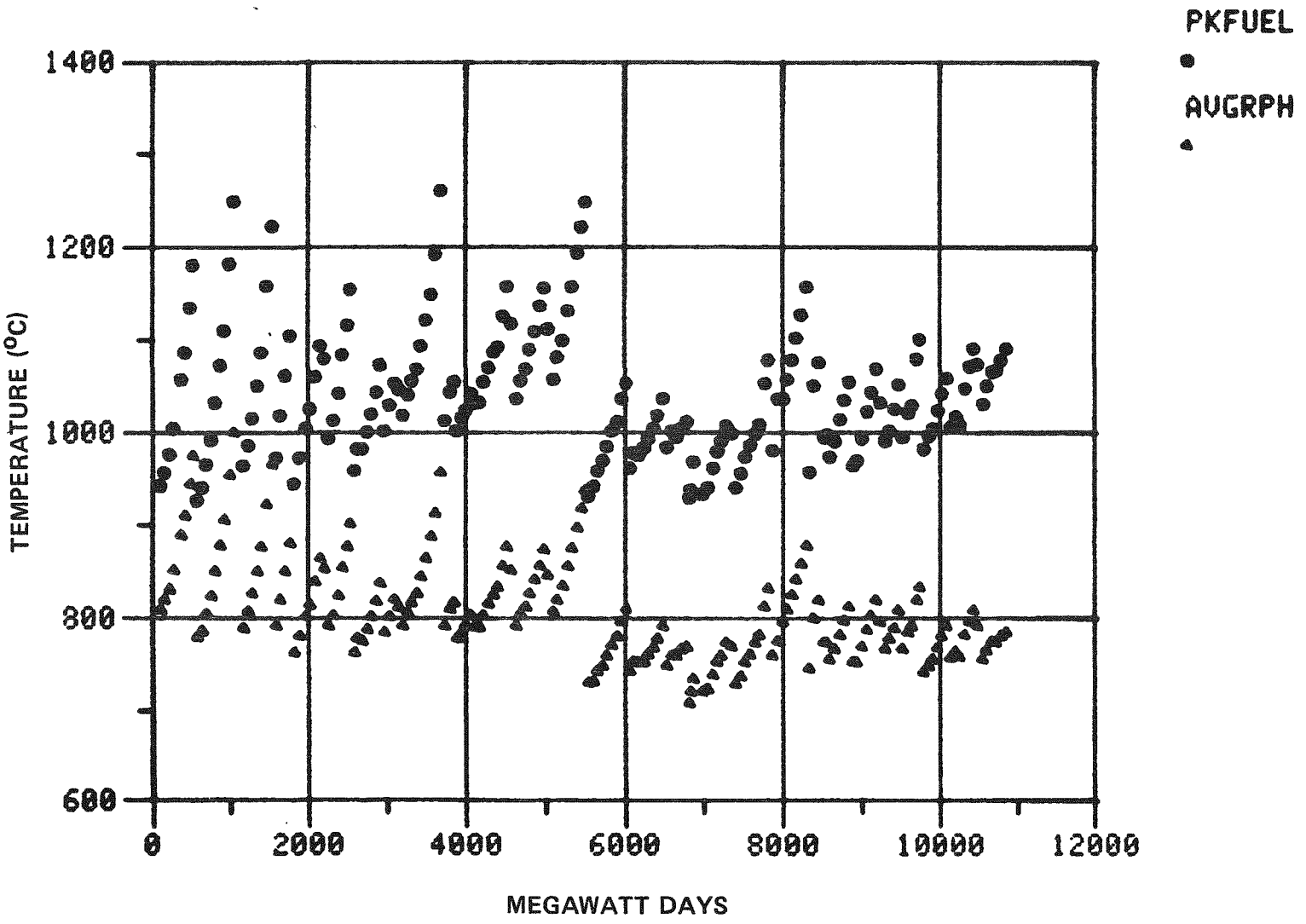

Fig. 9-8. P13T temperature history, crucible 4

2. Average fuel temperature is half the sum of the peak fuel rod and rod surface temperatures.

3. Average graphite temperature is half the sum of the inner and outer graphite crucible temperatures (points A and B in Fig. 9-1).

There is a noticeable discontinuity in all of these plots at ∿5500 MWD. This was due to some condition external to the capsule since all cells were affected. Since the discrepancy occurred at the start of a reactor cycle (cycle 129), it is postulated that a fuel loading change could have caused this effect. Investigation of the cause is continuing.

For crucible 1 temperature histories (Figs. 9-3 and 9-4), all values beyond 5000 MWD are estimates. This was necessary because of the high failure rate of thermocouples in this cell. Only two thermocouples in cell 1 lasted throughout the entire irradiation. It can be seen in Fig. 9-4 that rods 1-3A, 1-3B, and 1-3C operated approximately within ±50°C of the design temperature of 1300°C before the thermocouples began to fail.

Figures 9-5 and 9-6 show the temperature histories for body 2 of cell 2. During the first half of the irradiation, cell 2 was controlled with fuel thermocouple W14. During this time the temperature steadily rose from ∿980° to 1220°C as the fuel-crucible gap in this body increased from 0.0584 to 0.2083 mm (0.0023 to 0.0082 in.). This large gap increase was a result of the high flux at this position in the capsule and the differential shrinkage rates of fuel rod and TS-1240 graphites of which cell 2 was constructed. On December 12, 1975 (coincidentally also the start of cycle 129), control was switched from thermocouple W14 to thermocouple K19. The peak fuel temperature then leveled off at 1100° ± 50°C for the remainder of the experiment.

Figures 9-7 and 9-8 show the operating histories for bodies 3 and 4 of cell 2. Temperatures varied considerably during reactor cycles in these crucibles since they were not controlled as they were in bodies 1 and 2.

The temperature distribution by percentages was also calculated for each fuel rod in P13T. These values for crucibles 1 through 4 are shown in Tables 9-3 through 9-6.

Three of the graphite bodies (1, 2, and 4) contained fuel thermocouples. Figures 9-9 through 9-11 are plots of the differences between the measured (decalibrated) temperatures and the calculated values. Again, cell 1 data were only valid up to ∿5000 MWD due to the thermocouple failures in this cell.

Burnup Analysis. Six samples of fuel particles from the capsule P13T experiment were analyzed in accordance with a standard GA procedure, "Atom Percent Fission in Fissile and Fertile Fuel Particles." The fuel particles were cleaned to remove external contamination; following the cleaning operation each particle was measured for prominent fission products. Total measured fission products to Zr-95 atom ratios were calculated for each sample to reveal any abnormal fuel particles.

The ASTM fission product monitor radiochemical method (which uses Cs-137 as the burnup monitor) was used in the analysis of the fissile and fertile fuel particles. A second fission product monitor method (which uses stable Zr as the burnup monitor) was also used in the analysis of the fissile fuel particles. This second method can not be used effectively in the analysis of fertile fuel particles due to thorium interference. In addition to the fission product monitor methods, the fissile fuel particles were analyzed by a mass spectrometric uranium isotopic analysis method. This method measures burnup through changes in uranium isotopic composition and can be applied only to fuel particles that do not contain thorium and/or U-233 before irradiation; thus, it is not applicable to fertile fuel particles.

Replicate analyses were performed on those particles which met the selection criteria. Initially, the particles were crushed and dissolved in a perchloric acid mixture. These solutions containing fission products and uranium (plus thorium if fertile fuel particles) were separated by an anion

TABLE 9-3
TEMPERATURE (°C) DISTRIBUTION BY PERCENTAGES, CRUCIBLE 1 OF CELL 1

DAYS	PEAK FUEL ROD TEMPERATURES ROD1-1	ROD1-2	ROD1-3	ROD1-4	FUEL ROD SURFACE TEMPERATURES ROD1-1	ROD1-2	ROD1-3	ROD1-4	VOL. AVERAGE FUEL TEMPERATURES ROD1-1	ROD1-2	ROD1-3	ROD1-4
MINIMUM VALUE	967	967	987	1005	970	970	990	1008	969	969	989	1007
1% ARE LESS OR =	1105	1105	1125	1143	1003	1003	1023	1041	1054	1054	1074	1092
5% ARE LESS OR =	1128	1128	1148	1166	1034	1034	1054	1072	1082	1082	1102	1120
10% ARE LESS OR =	1144	1144	1164	1182	1046	1046	1066	1084	1095	1095	1115	1133
20% ARE LESS OR =	1153	1153	1173	1191	1058	1058	1078	1096	1106	1106	1126	1144
30% ARE LESS OR =	1164	1164	1184	1202	1067	1067	1087	1105	1115	1115	1135	1153
40% ARE LESS OR =	1182	1182	1202	1220	1076	1076	1096	1114	1130	1130	1150	1168
50% ARE LESS OR =	1213	1213	1233	1251	1097	1097	1117	1135	1154	1154	1174	1192
60% ARE LESS OR =	1245	1245	1265	1283	1119	1119	1139	1157	1185	1185	1205	1223
70% ARE LESS OR =	1264	1264	1284	1302	1137	1137	1157	1175	1198	1198	1218	1236
80% ARE LESS OR =	1277	1277	1297	1315	1146	1146	1166	1184	1212	1212	1232	1250
90% ARE LESS OR =	1290	1290	1310	1328	1157	1157	1177	1195	1221	1221	1241	1259
95% ARE LESS OR =	1297	1297	1317	1335	1166	1166	1186	1204	1228	1228	1248	1266
99% ARE LESS OR =	1332	1332	1352	1370	1193	1193	1213	1231	1260	1260	1280	1298
MAXIMUM VALUE	1409	1409	1429	1447	1216	1216	1236	1254	1312	1312	1332	1350
AVERAGE VALUE	1215	1215	1235	1253	1100	1100	1120	1138	1157	1157	1177	1195

TABLE 9-4
TEMPERATURE (°C) DISTRIBUTION BY PERCENTAGES, CRUCIBLE 2 OF CELL 2

	PEAK FUEL ROD TEMPERATURES		FUEL ROD SURFACE TEMPERATURES		VOL. AVERAGE FUEL TEMPERATURES	
	ROD2=1	ROD2=2	ROD2=1	ROD2=2	ROD2=1	ROD2=2
MINIMUM VALUE	881	875	731	725	806	800
1% ARE LESS OR =	949	943	793	787	871	865
5% ARE LESS OR =	978	972	823	817	900	894
10% ARE LESS OR =	997	991	840	834	918	912
20% ARE LESS OR =	1047	1041	893	887	969	963
30% ARE LESS OR =	1090	1084	939	933	1014	1008
40% ARE LESS OR =	1103	1097	949	943	1027	1021
50% ARE LESS OR =	1110	1104	961	955	1036	1030
60% ARE LESS OR =	1118	1112	971	965	1044	1038
70% ARE LESS OR =	1126	1120	976	970	1049	1043
80% ARE LESS OR =	1144	1138	991	985	1065	1059
90% ARE LESS OR =	1199	1193	1066	1060	1132	1126
95% ARE LESS OR =	1216	1210	1081	1075	1148	1142
99% ARE LESS OR =	1224	1218	1086	1080	1154	1148
MAXIMUM VALUE	1229	1223	1091	1085	1159	1153
AVERAGE VALUE	1101	1095	952	946	1027	1021

TABLE 9-5
TEMPERATURE (°C) DISTRIBUTION BY PERCENTAGES, CRUCIBLE 3 OF CELL 2

	PEAK FUEL ROD TEMPERATURES		FUEL ROD SURFACE TEMPERATURES		VOL. AVERAGE FUEL TEMPERATURES	
	ROD3=1	ROD3=2	ROD3=1	ROD3=2	ROD3=1	ROD3=2
MINIMUM VALUE	870	866	713	709	791	787
1% ARE LESS OR =	948	944	803	799	887	883
5% ARE LESS OR =	965	961	837	833	899	895
10% ARE LESS OR =	979	975	847	843	916	912
20% ARE LESS OR =	996	992	865	861	932	928
30% ARE LESS OR =	1013	1009	878	874	945	941
40% ARE LESS OR =	1030	1026	889	885	960	956
50% ARE LESS OR =	1051	1047	901	897	976	972
60% ARE LESS OR =	1069	1065	916	912	994	990
70% ARE LESS OR =	1090	1086	934	930	1010	1006
80% ARE LESS OR =	1110	1106	949	945	1031	1027
90% ARE LESS OR =	1141	1137	999	995	1068	1064
95% ARE LESS OR =	1163	1159	1027	1023	1093	1089
99% ARE LESS OR =	1186	1182	1044	1040	1115	1111
MAXIMUM VALUE	1195	1191	1054	1050	1123	1119
AVERAGE VALUE	1054	1050	910	906	982	978

TABLE 9-6
TEMPERATURE (°C) DISTRIBUTION BY PERCENTAGES, CRUCIBLE 4 OF CELL 2

	PEAK FUEL TEMPERATURES				FUEL SURFACE TEMPERATURES				VOL. AVERAGE FUEL TEMPERATURES			
	ROD4-1	ROD4-2	ROD4-3	ROD4-4	ROD4-1	ROD4-2	ROD4-3	ROD4-4	ROD4-1	ROD4-2	ROD4-3	ROD4-4
MINIMUM VALUE	859	854	837	840	733	728	711	714	796	791	774	777
1% ARE LESS OR =	945	940	923	926	805	800	783	786	874	869	852	855
5% ARE LESS OR =	963	958	941	944	815	810	793	796	891	886	869	872
10% ARE LESS OR =	980	975	958	961	830	825	808	811	906	901	884	887
20% ARE LESS OR =	1000	995	978	981	848	843	826	829	925	920	903	906
30% ARE LESS OR =	1016	1011	994	997	862	857	840	843	939	934	917	920
40% ARE LESS OR =	1030	1025	1008	1011	875	870	853	856	950	945	928	931
50% ARE LESS OR =	1048	1043	1026	1029	888	883	866	869	968	963	946	949
60% ARE LESS OR =	1062	1057	1040	1043	903	898	881	884	983	978	961	964
70% ARE LESS OR =	1081	1076	1059	1062	921	916	899	902	999	994	977	980
80% ARE LESS OR =	1102	1097	1080	1083	941	936	919	922	1022	1017	1000	1003
90% ARE LESS OR =	1151	1146	1129	1132	974	969	952	955	1060	1055	1038	1041
95% ARE LESS OR =	1186	1181	1164	1167	1005	1000	983	986	1094	1089	1072	1075
99% ARE LESS OR =	1239	1234	1217	1220	1048	1043	1026	1029	1152	1147	1130	1133
MAXIMUM VALUE	1277	1272	1255	1258	1089	1084	1067	1070	1176	1171	1154	1157
AVERAGE VALUE	1055	1050	1033	1036	896	891	874	877	975	970	953	956

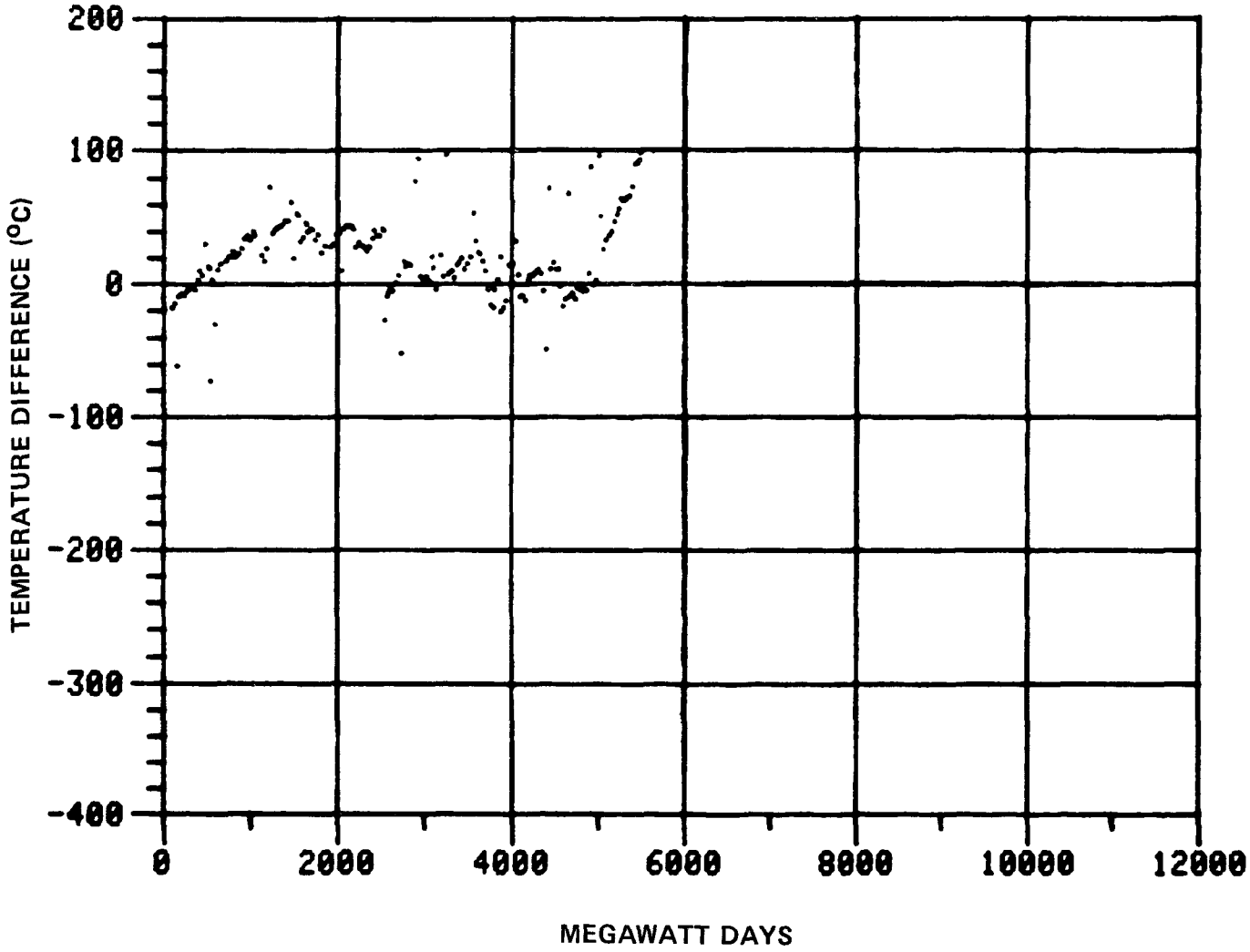

Fig. 9-9. T (calculated) minus T (measured), crucible 1, fuel thermocouple

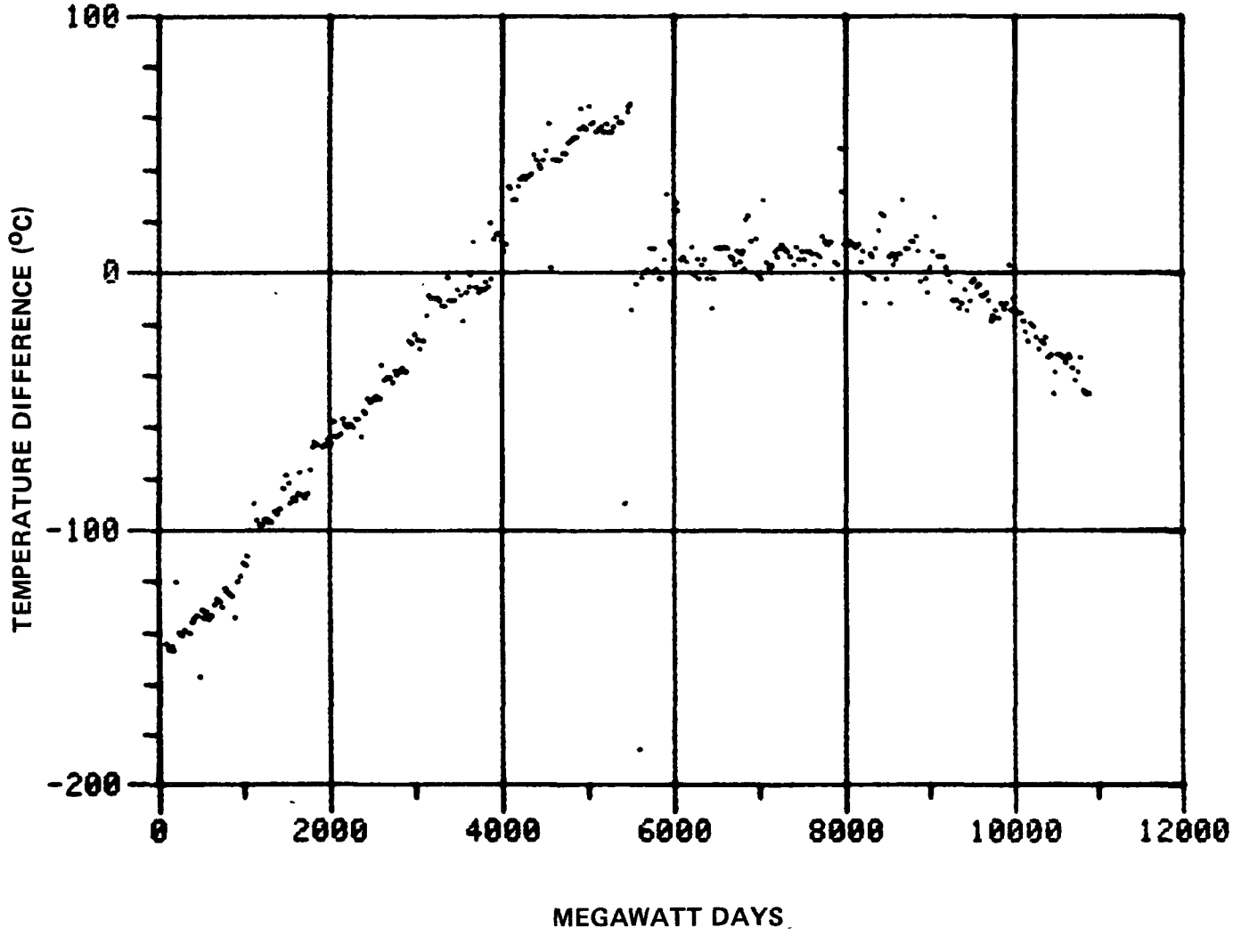

Fig. 9-10. T (calculated) minus T (measured), crucible 2, fuel thermocouple

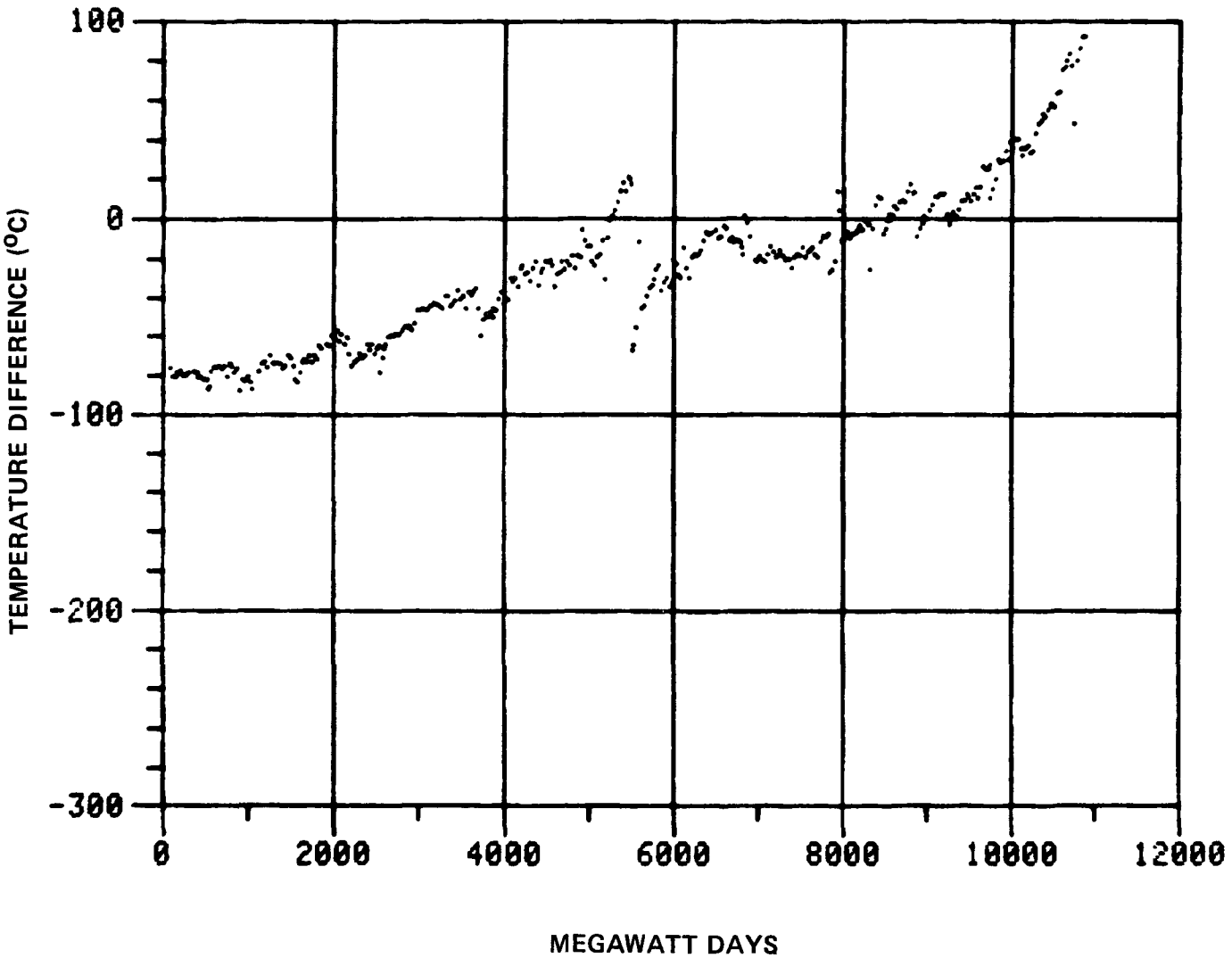

Fig. 9-11. T (calculated) minus T (measured), crucible 4, fuel thermocouple

exchange method. The thorium and uranium fractions were spectrophotometrically analyzed by absorbance of their Arsenazo-III complex. Zirconium fractions were recovered from the fissile fuel particle samples and these fractions were also colorimetrically analyzed. A portion of the uranium fraction from each sample was analyzed by mass spectrometry for uranium isotopic composition.

The mass spectrometric data (atom percent) obtained were then treated in accordance with ASTM Procedure E244, "Atom Percent Fission in Uranium and Plutonium Fuel (Mass Spectrometric Method)." The capture-to-fission ratio for U-235 (α_5 = 0.178) used in these calculations is the previous value determined for capsule P13Q. Burnup values obtained by this method are shown in Table 9-7.

The radiochemical fission product monitor burnup method is essentially ASTM E219, "Atom Percent Fission in Uranium Fuel (Radiochemical Method)." In principle, the number of fissions that have occurred in the fuel particles is determined by measuring the number of atoms of Cs-137 present and dividing by the fractional fission yield (U-233 yield is 6.80% and U-235 yield is 6.27%). The number of fissions is divided by the initial heavy metal atoms. The radiochemical burnup results are shown in Table 9-7.

For long irradiations, the correct Cs-137 concentrations require consideration for decay during as well as after irradiation. An approximate correction was made using the following ASTM recommended equation:

$$N' = N/\{e^{-\lambda t'} - [(1 - e^{-\lambda t})/\lambda t]\} \quad , \tag{9-2}$$

where N' = atoms of Cs-137 corrected for decay during and after irradiation,
N = atoms of Cs-137 at time of measurement,
λ = Cs-137 decay constant (7.3×10^{-10} s^{-1}),
t' = elapsed time from end of irradiation to measurement (s),
t = irradiation time (s).

TABLE 9-7
COMPARISON OF BURNUP DETERMINATIONS FOR CAPSULE IRRADIATION EXPERIMENT P13T

Capsule Position	Batch Number	Type	Percent FIMA ASTM Procedure E244 Case I	Case II	Case III	FISSIN	ASTM Procedure E219 Fiss Cs-137	Fiss Zr
PB 3C1-3	6157-02-026	TRISO[a]	67.14	68.33	67.83		65.6	67.6
							71.0	70.9
							66.0	67.7
		Avg.		67.77		67.95	67.5 ±4.6%	68.7 ±2.8%
PB 4B3-3	6157-02-0260	TRISO[a]	50.46	52.51	51.18		51.3	47.7
							53.1	52.9
							49.9	48.2
		Avg.		51.38		52.04	51.4 ±3.6	49.6 ±6.1
PB 2A-1	6157-02-0270	TRISO[a]	74.96	75.16	75.06		74.3	75.0
							77.3	76.2
							77.1	77.1
		Avg.		74.97		74.63	76.2 ±2.3%	76.1 ±1.7%
PB 4C-3	6542-27-0160	ThO_2 BISO		NA[b]			0.786	
							0.695	
							0.769	
		Avg.				0.85	0.75 ±7.0%	
PB 2A-8	6542-27-0160	ThO_2 BISO		NA			4.12	
							3.96	
							4.15	
		Avg.				4.03	4.08 ±2.7%	
PB 1A-1	6542-27-0160	ThO_2 BISO		NA			1.81	
							2.08	
							1.79	
		Avg.				1.93	1.89 ±8.9%	

[a] TRISO - UC2.930.62.

[b] Not applicable.

In addition to the burnups determined by radiochemistry and mass spectrometric methods, calculated values were obtained via the Sigma 2 FISSIN program. The Sigma 2 FISSIN program calculates burnup (FIMA) for both U-235 and Th at the beginning of each reactor irradiation cycle. The weights of U and Th are also calculated, as well as the final U isotopic inventory. Required inputs are reactor power history, thermal fluence, and U and Th loadings. There is an option to change the initial weight percent U and macroscopic cross-sections which are used in the calculations. These FISSIN-calculated burnup values are included in Table 9-7. The burnups for all P13T fuel rods are given in Table 9-8.

A comparison of mass spectrometric uranium isotopic compositions at the end of irradiation with those computed by the FISSIN program is shown in Table 9-9. The inputted fluences that yielded the corresponding isotopic compositions are included in Table 9-9. For additional comparison between measured and FISSIN-calculated results, Table 9-10 compares the heavy metal compositions (at end of life) that were obtained radiochemically with the calculated values.

Typically a third-order polynomial fit is made on the dosimetry values and thermal and fast fluence profiles are generated. Using the thermal fluence value from this profile, each burnup sample is computed over a range of thermal fluences that bracket this profile value. The FISSIN-computed U isotopic composition is compared with the mass spectrometric U isotopic composition. The fluence value for the FISSIN computation yielding the best match of isotopic composition is then compared with the actual dosimetry fluence value for that location. This action is to verify the validity of the fluence profiles and heavy metal reaction rates.

Although there was excellent agreement between measured burnup results (mass spectrometric and fission product monitor methods) and calculated burnup results (FISSIN program), a problem was observed with the thermal fluence profile previously determined from cobalt dosimetry (Ref. 9-1). In pursuing this problem, it was found that there was a bulkhead of considerable mass located at 0.22 m (8.5 in.) [distance from bottom of core (DFBC)]

TABLE 9-8

EXPOSURES AND BURNUPS FOR P13T FUEL RODS

Fuel Rod	Distance from Bottom of Core (cm)	Thermal Fluence (x 10^{25} n/m^2)	Fast Fluence (x 10^{25} n/m^2) (E > 29 fJ)$_{HTGR}$	Particle EOL Burnups (% FIMA)	
				Fissile	Fertile
1-1	2.03	3.65	3.45	67.7	1.9
1-2	5.08	3.90	4.84	69.1	2.0
1-3	9.65	4.65	6.42	72.2	2.7
1-4	15.75	5.60	7.67	74.7	3.5
2-1	25.37	5.95	8.04	75.3	3.7
2-2	30.38	6.05	7.64	75.5	3.8
3-1	37.06	5.30	6.69	74.0	3.2
3-2	42.06	4.15	5.77	70.3	2.3
4-1	47.75	2.95	4.64	62.7	1.3
4-2	50.80	2.45	4.05	57.8	1.0
4-3	53.85	2.15	3.49	54.1	0.8
4-4	56.90	2.10	2.98	53.4	0.8

TABLE 9-9
COMPARISON OF MASS SPECTROMETRIC URANIUM ISOTOPIC COMPOSITIONS
FOR CAPSULE IRRADIATION EXPERIMENT P13T

Sample	Fertile Fuel Particles (wt %)				Method	Thermal Fluence (n/m^2)
	U-233	U-234	U-235	U-236		
PB 1A-1	86.63	11.69	1.53	0.15	Mass Spec.[(a)] (avg.)	--
(C-2172)	86.78	11.42	1.64	0.16	Sigma 2 (FISSIN code)	3.70×10^{25}
PB 2A-8	78.07	18.07	3.37	0.55	Mass Spec.[(a)] (avg.)	--
(C-2170)	77.89	17.92	3.55	0.63	Sigma 2 (FISSIN code)	6.30×10^{25}
PB 4C-3	92.29	7.01	0.662	0.032	Mass Spec.[(a)]	--
(C-2168-3)	92.53	6.78	0.65	0.032	Sigma 2 (FISSIN code)	2.15×10^{25}

Sample	Fertile Fuel Particles (wt %)				Method	Thermal Fluence (n/m^2)
	U-234	U-235	U-236	U-238		
PB 2A-1	1.22	21.75	55.44	21.60	Mass Spec.	--
(C-2171)	1.27	21.75	54.96	22.02	Sigma 2 (FISSIN code)	5.60×10^{25}
PB 4B3-3	0.97	67.73	19.97	11.32	Mass Spec.	
(C-2169)	0.98	67.64	19.64	11.74	Sigma 2 (FISSIN code)	2.00×10^{25}
PB 3C1-3	1.19	42.80	39.25	16.77	Mass Spec.	--
(C-2167)	1.21	43.10	38.44	17.25	Sigma 2 (FISSIN code)	3.70×10^{25}

[(a)] Normalized to eliminate U-238.

TABLE 9-10
COMPARISON OF MEASURED AND CALCULATED BURNUP RESULTS
FOR CAPSULE IRRADIATION EXPERIMENT P13T

Sample	Fractions	Radiochemistry (%)		Calculated Result From FISSIN Code, Sigma 2 (%)	Thermal Fluence (n/m^2)
PB-1A-1	Th remaining	95.71		95.37	
(C-2172)	U remaining	2.50		2.72	3.70×10^{25}
	U fissioned	1.80		1.89	
	Total	100.01		99.98	
PB 2A-8	Th remaining	92.25		92.25	
(C-2170)	U remaining	3.62		3.59	6.30×10^{25}
	U fissioned	4.13		4.03	
	Total	100.00		99.87	
PB C-3	Th remaining	97.31		97.29	
(C-2168)	U remaining	1.92		1.93	2.15×10^{25}
	U fissioned	.78		.79	
	Total	100.01		100.01	
PB 2A-1	U remaining	23.98	(22.99)[a]	21.24	
(C-2171)	U fissioned	76.02	(72.88)[a]	74.63	5.60×10^{25}
	"U" not recovered	--	(4.13)[a]	--	
	Total		100.00	95.87	
PB 4B3-3	U remaining	48.62	(48.08)[a]	46.88	
(C-2169)	U fissioned	51.38	(50.81)[a]	52.01	2.00×10^{25}
	"U" not recovered	--	(1.11)[a]	--	
	Total		100.00	98.89	
PB 3C1-3	U remaining	32.28	(31.47)[a]	29.54	
(C-2167)	U fissioned	67.71	(66.01)[a]	67.95	3.70×10^{25}
	"U" not recovered	--	(2.51)[a]	--	
	Total		(99.99)	97.49	

[a] Normalization based on Sigma 2 FISSIN code.

(Ref. 9-5). The placement of the V-Co dosimeters at 0.16 m (6.2 in.) (DFBC) and 0.27 m (10.5 in.) (DFBC) was such that they could not indicate the flux depression caused by this bulkhead. There were V-Fe dosimeters located at 0.19 m (7.3 in.) (DFBC) and 0.24 m (9.5 in.) (DFBC); however, they could not reveal the thermal flux depression primarily because Fe is used as a fast neutron monitor. Since both V-Co and V-Fe are essentially pure vanadium (99.4%+), a thermal fluence was determined by measuring the chromium produced in vanadium by the reaction

$$^{51}V(n,\gamma)^{52}V \xrightarrow[3.7\ min]{\lambda} {}^{52}Cr\ (stable) \quad .$$

The stable chromium is measured by atomic absorption spectrophotometry rather than γ-ray spectrometry. The fluences determined by this monitor were in agreement with most of the burnup fluences and the fluence profile indicated the flux depression. After ascertaining that the FISSIN reaction rates and fluences were consistent with the measured values, an explanation was sought for the difference between the burnup fluence at 8.4 mm (0.33 in.) (DFBC) and the extrapolated fluence at this location. The γ-scanning counting data for the outer containment cladding were obtained; since this cladding was 304 SS, both the Fe fast neutron reaction and the Co thermal neutron reaction were produced. These raw cobalt γ-scan counts were given a three-point smooth fit, and the smoothed data were normalized to thermal fluence. Figure 9-12 shows the thermal neutron fluence from γ-scanning results and the thermal neutron fluence from vanadium and burnup results. The fast neutron fluences obtained from γ-scanning the secondary containment and from V-Fe dosimetry are shown in Fig. 9-13. Fast neutron fluence from γ-scanning was also obtained by smoothing and normalization. The bottom dosimeter was located at 50.8 mm (2.0 in.) (DFBC) and the curve had to be extrapolated to 8.4 mm (0.33 in.) (DFBC).

Capsule HT-34

Irradiation capsule HT-34 is part of a continuing cooperation effort between GA and Oak Ridge National Laboratory. The capsule will test TRISO

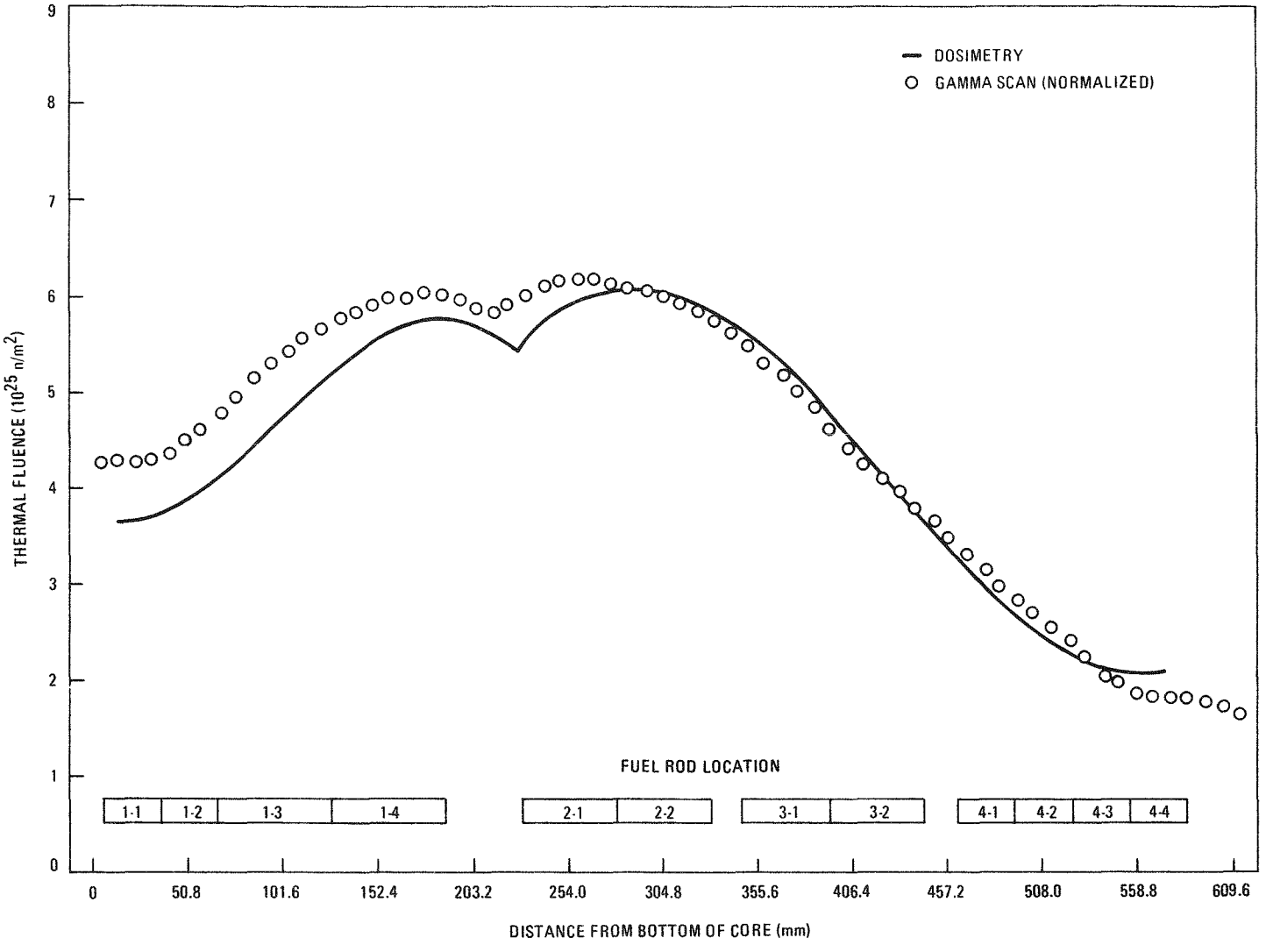

Fig. 9-12. P13T thermal fluence

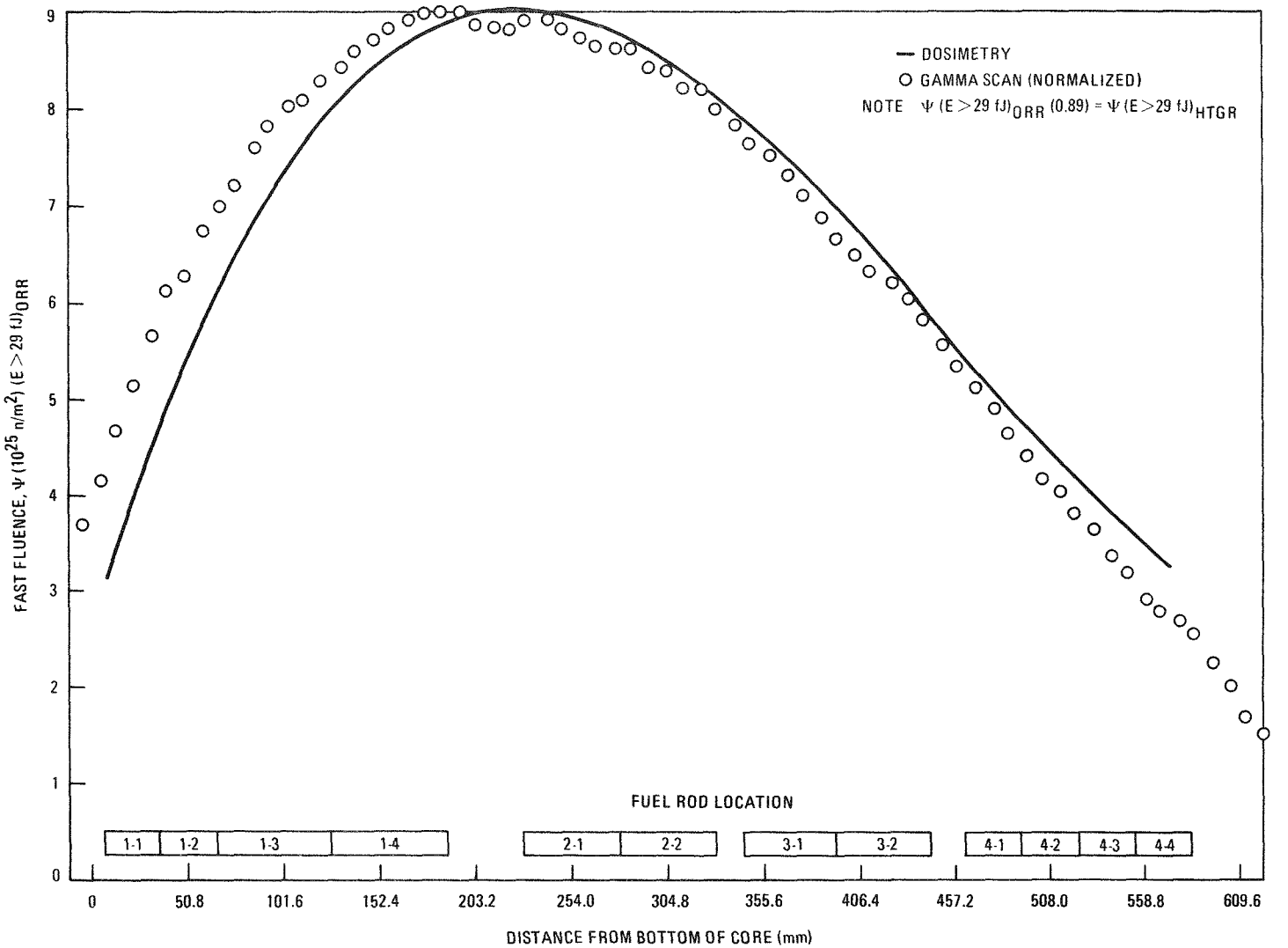

Fig. 9-13. P13T fast fluence $(E > 29\ fJ)_{ORR}$

coated ThO_2 particle fuel which is representative of fuel for Fort St. Vrain reload 1 fuel test elements and is the prime alternate fertile fuel for the LHTGR. Eight TRISO ThO_2 particle batches fabricated in the 240-mm-diameter LHTGR pilot plant coater are being tested in order to characterize the irradiation performance of this type of fuel. A detailed description was given in Ref. 9-5. The samples are being irradiated in the GA half of the uninstrumented capsule in the target facility of the HFIR at ORNL at design peak fuel temperatures of 1200° and 1500°C over a wide range of fluence and burnups. The HT-34 experiment was inserted into the reactor on July 25, 1977 and will be irradiated for five cycles. Reactor and capsule startup occurred on the same day.

The TRISO ThO_2 particle batches were evaluated and the samples for capsule HT-34 were prepared during the spring of 1977. The selection of samples and the irradiation conditions are given in Table 9-11 and a more detailed sample description is presented in Table 9-12. The primary coating variables of the samples were buffer thickness, SiC internal flaw distributions, and OPyC density, coating rate, and diluent gas. The actual batch properties were in good agreement with the design parameters, as discussed in Ref. 9-5, and were acceptable for the irradiation experiment. The test was designed to evaluate the performance of TRISO ThO_2 particles, to characterize the OPyC coating, and to correlate particle failure with the particle performance model. The samples in the 1200°C magazine will reach fluences of approximately 5.3 to 8.3 x 10^{25} n/m^2 $(E > 29\ fJ)_{HTGR}$ and burnups of 5.6 to 9.1% FIMA. The fast fluences and burnups for the high-temperature magazine are 9.4 to 10.4 x 10^{25} n/m^2 $(E > 29\ fJ)_{HTGR}$ and 11.0 to 12.8% FIMA, respectively.

TASK 300: INTEGRAL FUEL SYSTEM TESTING

Subtask 310: Peach Bottom Fuel Test Elements

FTE-6 Thermal Analysis

Introduction. The power generated at any local point within a fuel test element can be established by utilizing precision burnup measurements

TABLE 9-11
DESCRIPTION AND DESIGN IRRADIATION CONDITIONS OF TRISO ThO_2 SAMPLES FOR CAPSULE HT-34

Sample No.	Variables to be Tested					Primary Objective[a]	Th-232 Loading (mg)	Number of Particles	Irradiation Conditions		
			OPyC								
	Buffer Thickness (μm)	SiC Flaw Frequency (%)	Liquid Gradient Density (M/gm^3)	Coating Rate (μm/min)	Diluent Gas				Capsule Position	Fast Fluence ($\times 10^{25}$ n/m^2) ($E > 29fg$)	Burnup (% FIMA)
1200° Magazine											
6252-20-0161-001	83	6	1.98	8.4	H_2	OPyC	23.4	56	2	5.3	5.6
6252-07-0262-001[b]	60	38	1.80	5.0	A_r	Standard	23.4	57	4	5.9	6.2
6252-14-0261-001	27	29	1.97	7.1	H_2	PV	23.4	56	5	6.2	6.5
6252-14-0171-001	35	9	1.97	7.1	H_2	PV	23.4	56	7	6.8	7.1
6252-13-0161-001	57	16	1.79	8.3	H_2	OPyC	23.4	57	8	7.1	7.5
6252-14-0161-001	63	9	1.97	7.6	H_2	OPyC	23.4	57	10	7.6	8.1
6252-15-0161-001	56	12	1.81	5.0	H_2	OPyC	23.4	56	11	7.9	8.5
6252-16-0161-001	57	12	1.96	5.3	H_2	OPyC	23.4	56	13	8.3	9.1
1500° Magazine											
6252-20-0161-002	82	6	1.98	8.0	H_2	PV	33.1	80	15	9.4	11.0
6252-07-0262-002[b]	57	38	1.80	5.6	A_r	Standard	33.1	81	17	9.8	11.5
6252-14-0161-002	62	9	1.97	7.6	H_2	PV	33.1	81	18	9.9	11.7
6252-14-0271-001	86	29	1.97	8.0	H_2	PV	33.1	83	20	10.1	12.1
6252-14-0181-001	91	10	1.97	8.1	H_2	PV	33.1	82	21	10.2	12.2
6252-17-0161-001	80	6	1.95	5.0	H_2	PV	33.1	81	23	10.4	12.5
6252-15-0171-001	84	12	1.81	5.6	H_2	PV	33.1	81	24	10.4	12.6
6252-13-0171-001	79	16	1.79	8.5	H_2	PV	33.1	85	26	10.4	12.8

[a] OPyC - performance of OPyC coating; PV - results to be correlated with particle performance model.

[b] Samples previously irradiated in capsules HT-31 and HT-33.

TABLE 9-12
GENERAL DESCRIPTION[a] OF TRISO ThO_2 PARTICLE SAMPLES FOR CAPSULE HT-34

Batch No.	Kernel Diameter (μm)	Buffer		IPyC		SiC			OPyC							Total Coated Particle			
										Density (Mg/m^3)									
		Thickness (μm)	Density[b] (Mg/m^3)	Thickness (μm)	Liquid Gradient Density[b] (Mg/m^3)	Thickness (μm)	Density (Mg/m^3)	Flaw Content[b,c] (%)	Thickness (μm)	Liquid Gradient	Bulk	BAF_o[b,d]	Accessible Porosity (ml/kg[b,e] OPyC Coatings)	Coating Rate (μm/min)	Coating Diluent Gas	Diameter (μm)	Defective SiC Coating[b,f] (kg Th/kg Th)	Th Contamination[b,g] (kg Th/kg Th)	Fission Gas Release[b,h]
6252-07-0262-001	449	60	1.12	39	1.93	38	3.21	38	45	1.80	1.65	1.027	48	5.0	Ar	816	2.9×10^{-4}	1.1×10^{-5}	1.6×10^{-5}
6252-07-0262-002	449	57	1.12	39	1.93	37	3.21	38	41	1.80	1.65	1.027	48	4.6	Ar	808	2.9×10^{-4}	1.1×10^{-5}	1.6×10^{-5}
6252-13-0161-001	447	57	1.13	32	1.86	43	3.22	16	48	1.79	1.61	1.031	57	8.3	H_2	808	4.3×10^{-4}	4.9×10^{-5}	1.2×10^{-5}
6252-13-0171-001	443	79	1.13	32	1.86	43	3.22	16	49	1.79	1.61	1.031	57	8.5	H_2	848	4.3×10^{-4}	4.9×10^{-5}	1.2×10^{-5}
6252-14-0161-001	448	63	1.10	32	1.84	37	3.22	9	44	1.97	1.76	1.041	57	7.6	H_2	798	2.4×10^{-3}	8.3×10^{-5}	4.2×10^{-5}
6252-14-0161-002	447	62	1.10	32	1.84	37	3.22	9	44	1.97	1.76	1.041	57	7.6	H_2	796	2.4×10^{-3}	8.3×10^{-5}	4.2×10^{-5}
6252-14-0171-001	451	35	1.10	32	1.84	35	3.22	9	41	1.97	1.76	1.041	57	7.1	H_2	736	2.4×10^{-3}	8.3×10^{-5}	4.2×10^{-5}
6252-14-0181-001	445	91	1.10	32	1.84	37	3.22	9	47	1.97	1.76	1.041	57	8.1	H_2	854	2.4×10^{-3}	8.3×10^{-5}	4.2×10^{-5}
6252-14-0261-001	455	27	1.08	35	1.83	35	3.21	29	40	1.97	1.79	1.040	54	7.1	H_2	729	1.1×10^{-3}	6.1×10^{-4}	3.9×10^{-5}
6252-14-0271-001	443	86	1.08	35	1.83	38	3.21	29	45	1.97	1.79	1.040	54	8.0	H_2	849	1.1×10^{-3}	6.1×10^{-4}	3.9×10^{-5}
6252-15-0161-001	450	56	1.07	36	1.85	38	3.22	12	45	1.81	1.68	1.033	21	5.0	H_2	798	4.7×10^{-4}	4.9×10^{-6}	4.0×10^{-6}
6252-15-0171-001	448	84	1.07	36	1.85	39	3.22	12	50	1.81	1.68	1.033	21	5.6	H_2	865	1.9×10^{-4}	4.9×10^{-6}	4.0×10^{-6}
6252-16-0161-001	451	57	1.07	36	1.85	39	3.21	12	48	1.96	1.82	1.048	25	5.3	H_2	813	8.9×10^{-5}	9.8×10^{-6}	2.5×10^{-6}
6252-17-0161-001	451	80	0.93	40	1.79	37	3.22	6	45	1.95	1.80	1.049	28	5.0	H_2	858	1.3×10^{-3}	2.1×10^{-5}	2.1×10^{-5}
6252-20-0161-001	450	83	0.93	40	1.79	36	3.21	6	47	1.98	1.74	1.041	59	8.4	H_2	862	2.9×10^{-3}	2.5×10^{-4}	7.3×10^{-5}
6252-20-0161-002	452	82	0.93	40	1.79	35	3.21	6	45	1.98	1.74	1.041	59	8.0	H_2	854	2.9×10^{-3}	2.5×10^{-4}	7.3×10^{-5}

[a] Mean valves given; valves are for capsule samples except where noted.

[b] Calculated or measured on parent hatch.

[c] Internal flaws measured by visual examination of SiC substrate.

[d] Optical anisotropy measured using a seibersdort optical unit at GA.

[e] The amount of Hy which intrudes into coatings at 67 MPa (10000 psi).

[f] OPyC burned off and particles leached for 24 hours in acid.

[g] Particles leached for 24 hours in acid.

[h] Release rate/birth rate for ,Kr-85m at 1100°C (in linear accelerator).

and fission product profiles obtained through gamma spectroscopy in conjunction with physics code predictions, and by accounting for azimuthal power variations (power tilts) resulting from nonuniform heavy metal loadings. The methods used to calculate the power generation in Peach Bottom fuel test element FTE-6 are presented here. It is anticipated that these methods will be employed for future analyses of fuel test elements, although minor deviations dictated by the idiosyncrasies of each element may be necessary. It is postulated that reliable temperatures to be used in detailed graphite stress, fuel performance, and fission product analyses can be computed using powers determined through the described procedure.

Local Power Generation. The power generated at a given axial location (z) in a given fuel stack (h) of test element x at time point t is given by the equation:

$$P_{x,h,z,t} = (CPF_{x,t})(Tilt_{h,t})(APF_{h,z,t})(\bar{P}_{core,t}) \quad , \tag{9-3}$$

where $CPF_{x,t} = \bar{P}_{x,t}/\bar{P}_{core,t}$ = element average power factor at time t,

$Tilt_{h,t} = \bar{P}_{h,t}/\bar{P}_{x,t}$ = power tilt for fuel stack h at time t,

$APF_{h,z,t} = P_{h,z,t}/\bar{P}_{h,t}$ = axial power factor for axial location z of fuel stack h at time t,

$P_{subscripts}$ = power generated by entity denoted by subscripts.

The manner in which the power tilts, axial power factors, and element average power factor used in the FTE-6 thermal analysis were calculated is discussed below.

Power Tilts. Power tilts for FTE-6 were calculated as a function of fuel hole, core height, and time using the following equation:

$$Tilt_{h,z,t} = \frac{\sum_{i=1}^{4}\left[f_i\ (w_{h,z,t})_i \sum_{j=1}^{4} \phi_{j,t}\ \sigma_{i,j}\right]}{\sum_{i=1}^{4}\left[f_i\ (w_{x,z,t})_i \sum_{j=1}^{4} \phi_{j,t}\ \sigma_{i,j}\right]} \tag{9-4}$$

where $(i = 1,4)$ = four fissionable nuclides (U-233, U-235, Pu-239, Pu-241),

$(j = 1,4)$ = four energy groups for which the GAUGE code computes neutron flux,

f_i = relative power generated by fission of nuclide i,

$\phi_{j,t}$ = neutron flux for energy group j at time t (obtained from GAUGE calculations),

$\sigma_{i,j}$ = fission micro-cross section for nuclide i and energy group j,

$(w_{h,z,t})_i$ = nuclide density at axial position z of fuel hole h at time t,

$(w_{x,z,t})_i$ = element average nuclide density at axial position z at time t.

The element average and local nuclide densities are calculated as follows:

$$\left(w_{x,z,t}\right)_i = \left(w_{x,t}\right)_i \cdot \left(\frac{w_{x,z,t}}{w_{x,t}}\right)_i \cdot \left(\frac{g_{x,z,t=0}}{g_{x,t=0}}\right)_i \tag{9-5}$$

$$\left(w_{h,z,t}\right)_i = \left(w_{x,z,t}\right)_i \cdot \left(\frac{g_{h,z,t=0}}{g_{x,z,t=0}}\right)_i \tag{9-6}$$

where $\left(w_{x,t}\right)_i$ = element average nuclide density at time t,

$\left(\frac{w_{x,z,t}}{w_{x,t}}\right)_i$ = ratio of the element average nuclide density at axial position z and the element average nuclide density. These factors are taken from the normalized axial distributions for various nuclides given in the PIE report on FTE-18 (Ref. 9-6).

$\left(\frac{g_{x,z,t=0}}{g_{x,t=0}}\right)_i$ = ratio of the grams/in. of nuclide i at axial location z and the average grams/in. of nuclide i for the entire element at BOL. For FTE-6, this factor is equal to 1 at all z since the heavy metal within each fuel stack was uniformly distributed.

$\left(\frac{g_{h,z,t=0}}{g_{x,z,t=0}}\right)_i$ = ratio of the grams/in. of nuclide i in fuel stack h at axial position z to the element average grams/in. of nuclide i at axial position z at BOL. Values of this factor for FTE-6 are given in Table 9-13.

TABLE 9-13
RELATIVE HEAVY METAL LOADINGS AT BOL FOR FTE-6

Fuel Holes	Th-232[(a)]	U-235	Pu-239	Pu-241
1 and 2	2.0	1.0	1.0	1.0
3 and 4	0.784	1.0	1.0	1.0
5 and 6	0.761	1.0	1.0	1.0
7 and 8	0.456	1.0	1.0	1.0

[(a)] Th-232 used for U-233.

In calculating the ratios discussed above, the heavy metal contained in the spine was not considered. Since the heat generated in the spine should flow radially outward in all directions, each segment of the element should be influenced relatively the same by the spine samples. In addition, the quantity of heavy metal contained in the spine samples is relatively small compared to the heavy metal contained in the fuel rods. For these reasons, the exclusion of the spine samples in tilt calculations is justified.

The tilt required for Eq. 9-3 is calculated as follows:

$$\text{Tilt}_{h,t} = \frac{\sum_{z=1}^{n} \text{tilt}_{h,z,t}}{n} \quad , \tag{9-7}$$

where n is the number of fuel rods (42) or TREVER nodal points (30) along the fuel element length. The tilts calculated for FTE-6 are given in Table 9-14.

TABLE 9-14
FTE-6 POWER TILTS

Time Point	Time Interval (EFPD)	Hole 1	Hole 3	Hole 5	Hole 7
7	252 - 298	1.00	1.00	1.00	1.00
8	298 - 343	1.005	0.999	0.999	0.997
9	343 - 385	1.019	0.996	0.995	0.989
10	385	1.028	0.994	0.993	0.985
11	385 - 500	1.037	0.992	0.991	0.980
12	500 - 564	1.067	0.986	0.984	0.964
13	564 - 610	1.080	0.983	0.981	0.957
14	610 - 701	1.095	0.979	0.977	0.948
15	701	1.122	0.974	0.971	0.934
16	701 - 748	1.132	0.971	0.968	0.927
17	748 - 788	1.138	0.970	0.967	0.924
18	788 - 818	1.150	0.967	0.964	0.919
19	818 - 835	1.168	0.963	0.960	0.909
20	835 - 858	1.172	0.963	0.959	0.907
21	858 - 890	1.177	0.962	0.957	0.904
22	890 - 897	1.188	0.959	0.955	0.898
23	897	1.192	0.958	0.955	0.896

Axial Power Factors. The axial power factors given in Ref. 9-7 were computed by the FEVER computer code using element average uranium and thorium loadings. The following adjustment to these axial power profiles was made in order to account for the varying thorium-to-uranium ratio from fuel hole to fuel hole:

$$APF_{h,z,t} = APF_{x,z,t} \cdot \frac{tilt_{h,z,t}}{tilt_{h,t}} \quad . \tag{9-8}$$

The revised FEVER power profiles are given in Table 9-15.

A second adjustment, based on PIE gamma scan information, was also made to the FEVER axial power profiles. Approximately every other fuel rod in fuel stacks 1, 3, 5, and 7, as well as the central spine, of FTE-6 were gamma scanned in the hot cell at GA, yielding the counts per minute (cpm) for a variety of nuclides. The cpm for fuel rods which were not scanned were obtained through interpolation. The total cpm for a given nuclide at each axial location corresponding to the center of a fuel rod was obtained for each stack by summing the cpm for the appropriate fuel rod and one-eighth of the cpm for the adjacent spine sample (if any). Axial power profiles were then obtained for each fuel stack by normalizing the cpm at each axial location.

Since Cs-137 and Zr-95 have very long ($\sim$30 years) and very short ($\sim$65 days) half-lives, respectively, it was concluded that the profiles obtained from the cpm of Cs-137 would be equivalent to time-averaged power profiles and the profiles obtained from the cpm of Zr-95 would be equivalent to end-of-life power profiles. Unfortunately, the hot cell scans were taken long after the Peach Bottom reactor had been shut down. Thus, most of the zirconium had decayed away and the rods were not scanned for a sufficient length of time to obtain a large enough Zr-95 peak to avoid large counting errors. Due to the magnitude of these errors ($2\sigma \gtrsim \pm 20\%$), it was decided not to use the Zr-95 profiles. The Cs-137 profiles are given in Table 9-16. Since a considerable quantity of cesium escaped from the fuel rods

TABLE 9-15
FEVER AXIAL POWER PROFILES USED IN FTE-6 THERMAL ANALYSIS

TREVER Node	Fuel Holes 1 and 2			Fuel Holes 3 and 4			Fuel Holes 5 and 6			Fuel Holes 7 and 8		
	0-150[a]	150-450	450-645[b]	0-150	150-450	450-645	0-150	150-450	450-645	0-150	150-450	450-645
1	0.543	0.500	0.447	Same as	0.525	0.495	Same as	0.525	0.496	Same as	0.532	0.512
2	0.607	0.577	0.538	holes 1	0.599	0.585	holes 1	0.600	0.586	holes 1	0.606	0.601
3	0.760	0.724	0.686	and 2	0.744	0.729	and 2	0.744	0.730	and 2	0.750	0.744
4	0.915	0.860	0.806	↓	0.873	0.837	↓	0.873	0.837	↓	0.877	0.847
5	1.020	0.967	0.891		0.976	0.903		0.971	0.903		0.972	0.906
6	1.110	1.060	0.967		1.054	0.958		1.054	0.958		1.052	0.955
7	1.180	1.133	1.041		1.117	1.014		1.117	1.014		1.111	1.005
8	1.230	1.195	1.097		1.170	1.056		1.170	1.055		1.163	1.043
9	1.255	1.246	1.142		1.214	1.089		1.214	1.088		1.204	1.070
10	1.270	1.274	1.190		1.239	1.126		1.238	1.125		1.228	1.105
11	1.285	1.293	1.231		1.252	1.154		1.251	1.153		1.240	1.127
12	1.285	1.299	1.253		1.257	1.173		1.256	1.171		1.245	1.145
13	1.280	1.303	1.274		1.262	1.193		1.261	1.191		1.250	1.164
14	1.276	1.301	1.278		1.260	1.198		1.259	1.197		1.248	1.170
15	1.250	1.290	1.281		1.252	1.204		1.252	1.202		1.241	1.177
16	1.230	1.272	1.276		1.239	1.205		1.238	1.203		1.228	1.180
17	1.195	1.244	1.266		1.214	1.202		1.214	1.200		1.205	1.179
18	1.160	1.215	1.251		1.190	1.193		1.189	1.192		1.182	1.172
19	1.130	1.177	1.229		1.155	1.179		1.155	1.178		1.150	1.163
20	1.090	1.133	1.207		1.117	1.167		1.117	1.166		1.112	1.153
21	1.040	1.073	1.162		1.069	1.147		1.069	1.147		1.068	1.142
22	0.995	1.030	1.111		1.030	1.110		1.030	1.110		1.030	1.109
23	0.935	0.965	1.061		0.971	1.072		0.971	1.072		0.973	1.076
24	0.865	0.912	1.001		0.922	1.025		0.922	1.025		0.926	1.033
25	0.810	0.837	0.933		0.853	0.967		0.853	0.968		0.858	0.979
26	0.745	0.764	0.865		0.784	0.909		0.784	0.910		0.789	0.924
27	0.675	0.697	0.788		0.719	0.841		0.720	0.842		0.726	0.859
28	0.615	0.720	0.703		0.644	0.762		0.645	0.764		0.652	0.783
29	0.550	0.553	0.620		0.580	0.683		0.581	0.685		0.588	0.706
30	0.595	0.587	0.623		0.622	0.701		0.622	0.703		0.632	0.728

[a] All times are in EFPD and correspond to the number of effective full power days during which FTE-6 was in the core.

[b] FTE-6 went into the core at 252 EFPD and came out at 897 EFPD (EOL), for a total residency time of 645 EFPD.

TABLE 9-16
FTE-6 AXIAL POWER PROFILES, Cs-137 PLUS SPINE

Fuel Rod Ident.	Core Height		Spine (cpm)	Stack 1		Stack 3		Stack 5		Stack 7		cpm/mean Stacks 3,5,7	cpm/mean Stacks 1,3,5,7
	Bottom	Top		cpm	cpm/mean	cpm	cpm/mean	cpm	cpm/mean	cpm	cpm/mean		
1-1	664	714	0	673	0.482	758(a)	0.526	717(a)	0.506	656(a)	0.504	0.512	0.504
1-2	714	763	0	785	0.563	859	0.596	847	0.598	749	0.576	0.590	0.583
1-3	763	813	0	888	0.637	960(a)	0.666	976(a)	0.689	842(a)	0.647	0.667	0.659
1-4	813	862	0	1005	0.720	1062	0.737	1106	0.781	936	0.720	0.746	0.739
1-5	862	912	0	1105	0.792	1158(a)	0.804	1160(a)	0.819	1053(a)	0.809	0.811	0.860
1-6	912	961	87.5	1204	0.863	1266	0.879	1225	0.865	1182	0.909	0.854	0.879
1-7	961	1011	112.5	1257	0.901	1321(a)	0.917	1245(a)	0.879	1221(a)	0.939	0.912	0.909
1-8	1011	1061	0	1292	0.926	1359	0.943	1247	0.880	1243	0.956	0.926	0.926
1-9	1061	1110	0	1309	0.938	1359(a)	0.943	1269(a)	0.896	1232(a)	0.947	0.929	0.931
1-10	1110	1159	0	1313	0.941	1360	0.944	1292	0.912	1221	0.939	0.932	0.934
1-11	1159	1209	0	1448	1.038	1496(a)	1.038	1424(a)	1.005	1326(a)	1.019	1.026	1.025
1-12	1209	1258	0	1585	1.136	1633	1.133	1556	1098	1432	1.101	1.111	1.117
1-13	1258	1308	25	1659	1.189	1706(a)	1.184	1632(a)	1.152	1498(a)	1.152	1.163	1.169
1-14	1308	1357	75	1740	1.247	1781	1.236	1711	1.208	1566	1.204	1.216	1.224
2-1	1154	1504	19	1749	1.254	1740(a)	1.208	1674(a)	1.182	1652(a)	1.270	1.220	1.228
2-2	1504	1554	56	1756	1.259	1748	1.213	1693	1.195	1640	1.261	1.223	1.232
2-3	1554	1603	151	1760	1.262	1763(a)	1.223	1719(a)	1.214	1611(a)	1.238	1.225	1.234
2-4	1603	1653	170.5	1757	1.260	1768	1.227	1736	1.226	1595	1.218	1.229	1.233
2-5	1653	1702	170.5	1755	1.258	1775(a)	1.232	1759(a)	1.242	1549(a)	1.171	1.222	1.231
2-6	1702	1752	170.5	1742	1.249	1775(a)	1.232	1759(a)	1.242	1512	1.162	1.212	1.221
2-7	1752	1801	170.5	1762	1.263	1781	1.236	1781	1.257	1556(a)	1.196	1.230	1.238
2-8	1801	1851	170.5	1721	1.234	1719	1.193	1692	1.194	1600	1.230	1.206	1.213
2-9	1851	1900	45	1656	1.187	1685(a)	1.169	1661(a)	1.173	1491(a)	1.146	1.163	1.169
2-10	1900	1950	0	1607	1.152	1661	1.153	1640	1.158	1392	1.070	1.127	1.133
2-11	1950	1999	52.5	1662	1.191	1683(a)	1.168	1686(a)	1.190	1499(a)	1.152	1.170	1.175
2-12	1999	2049	37.5	1707	1.224	1697	1.178	1723	1.216	1597	1.228	1.207	1.211
2-13	2049	2098	69.0	1703	1.221	1695(a)	1.176	1726(a)	1.218	1586(a)	1.219	1.204	1.208
2-14	2098	2148	31.0	1683	1.206	1684	1.169	1720	1.214	1566	1.204	1.196	1.198
3-1	2244	2294	133.5	1568	1.124	1595(a)	1.107	1599(a)	1.129	1490(a)	1.145	1.127	1.126
3-2	2294	2343	503.5	1577	1.130	1613	1.119	1619	1.143	1499	1.152	1.138	1.136
3-3	2343	2393	508.5	1545	1.107	1583(a)	1.099	1592(a)	1.124	1460(a)	1.122	1.115	1.113
3-4	2393	2443	492	1501	1.076	1552	1.077	1562	1.103	1420(a)	1.092	1.091	1.087
3-5	2943	2492	441	1428	1.024	1484(a)	1.030	1470(a)	1.038	1381(a)	1.062	1.043	1.038
3-6	2492	2542	441	1369	0.981	1423	0.987	1384	0.977	1347	1.036	1.000	0.995
3-7	2542	2591	315	1313	0.941	1377(a)	0.956	1360(a)	0.960	1281(a)	0.985	0.967	0.960
3-8	2591	2641	108.5	1250	0.896	1321	0.917	1326	0.936	1206(a)	0.927	0.927	0.919
3-9	2641	2690	184	1172	0.840	1282(a)	0.890	1241(a)	0.876	1115	0.857	0.974	0.865
3-10	2690	2739	308	1115	0.799	1250	0.867	1163	0.821	1047(a)	0.805	0.831	0.823
3-11	2739	2789	0	966	0.692	1062(a)	0.737	1041(a)	0.735	925	0.711	0.728	0.719
3-12	1789	2839	0	867	0.621	912	0.633	956	0.675	873(a)	0.671	0.660	0.650
3-13	2839	2888	0	838	0.601	909(a)	0.631	920(a)	0.649	820	0.630	0.637	0.628
3-14	2888	2938	0	803	0.575	905	0.628	883	0.623	777	0.597	0.616	0.606

(a) Interpolated.

in fuel stack 1 during irradiation, the Cs-137 profile for this stack is not representative of the axial power shape. A time-averaged power profile based on the Cs-137 profiles for fuel stacks 3, 5, and 7 was computed for fuel stack 1 using the following approach:

$$APF_z = \frac{\sum_{i=1}^{3} cpm_{i,z}}{3} - \frac{cpm_{spine,z}}{8} \cdot \frac{\left(tilt_{h,z}/tilt_h\right)_{h=1}}{\frac{1}{3}\sum_{i=1}^{3}\left(tilt_{i,z}/tilt_i\right)}$$

$$+ \frac{cpm_{spine,z}}{8} \quad , \qquad (9\text{-}9)$$

where (i=1,3) = fuel stacks 3, 5, and 7,

cpm = counts per minute of Cs-137,

$tilt_{y,z}$ = power tilt for fuel stack y at axial location z (see section on power tilts),

$tilt_y$ = average power tilt for fuel stack y (see section on power tilts).

Through interpolation of the Cs-137 profiles given in Table 9-16, power profiles consisting of 30 points corresponding to the 30 TREVER nodes were obtained. These profiles, given in Table 9-17, were used to correct the FEVER axial power profiles using the approach outlined below.

1. A time-averaged axial power profile based on the FEVER profiles (Table 9-15) was calculated for each fuel stack.

2. The ratio of the gamma scan Cs-137 axial power factor and the FEVER time-averaged power factor was calculated at each TREVER node:

$$f_{h,z} = \frac{\left(APF_{h,z}\right)_{Cs\text{-}137}}{\left(APF_{h,z}\right)_{time\ avg.\ FEVER}} \quad . \qquad (9\text{-}10)$$

TABLE 9-17
FTE-6 TIME-AVERAGED POWER PROFILES AS DETERMINED FROM HOT CELL GAMMA SCANS FOR Cs-137[a]

TREVER Node	Fuel Hole 1	Fuel Hole 3	Fuel Hole 5	Fuel Hole 7
1	0.500	0.541	0.526	0.520
2	0.608	0.639	0.654	0.619
3	0.720	0.737	0.781	0.720
4	0.821	0.835	0.838	0.850
5	0.894	0.910	0.876	0.933
6	0.929	0.943	0.884	0.954
7	0.940	0.944	0.906	0.942
8	1.040	1.040	1.007	1.021
9	1.158	1.154	1.121	1.122
10	1.238	1.228	1.199	1.196
11	1.255	1.209	1.185	1.268
12	1.261	1.219	1.206	1.247
13	1.260	1.227	1.226	1.217
14	1.254	1.232	1.242	1.179
15	1.260	1.235	1.254	1.190
16	1.223	1.187	1.189	1.210
17	1.165	1.159	1.164	1.098
18	1.192	1.168	1.191	1.154
19	1.223	1.177	1.217	1.224
20	1.208	1.170	1.215	1.206
21	1.125	1.110	1.132	1.147
22	1.116	1.107	1.132	1.134
23	1.075	1.076	1.102	1.091
24	1.006	1.012	1.013	1.051
25	0.948	0.962	0.963	0.994
26	0.883	0.911	0.922	0.910
27	0.814	0.875	0.841	0.824
28	0.691	0.735	0.734	0.710
29	0.613	0.632	0.665	0.656
30	0.579	0.628	0.627	0.602

[a] These profiles were used in the TREVER analysis of FTE-6.

3. These factors were then used to adjust each FEVER axial power profile:

$$APF_{h,z,t} = (APF_{h,z,t})_{FEVER} \cdot f_{h,z} \quad . \tag{9-11}$$

These calculations are performed within the TREVER code.

In addition to the hot cell work, FTE-6 was also gamma scanned at the Peach Bottom reactor site shortly after removal from the core. Because of the arrangement of the gamma scanning equipment, the collimator did not see the entire element but only part or all of fuel holes 1, 4, 5, and 8 and the spine. Since the profiles obtained from the cpm of various nuclides are therefore not representative of the element average power profile and since the uncertainty as to where the cpm recorded by the collimator were coming from makes it impossible to adjust these profiles to a usable form, it was decided that the Peach Bottom gamma scans for FTE-6 would not be used in the thermal analysis.

Element Average Power Factor. The element average power factor for FTE-6 calculated by GAUGE was corrected using burnup measurements for spine sample TS6-5. The calculations performed to obtain this correction are outlined below.

	FIMA at Location of Spine Sample TS6-5	
	Calculated[a]	Measured
Fissile	30.35%	34.26%
Fertile	0.58%	0.69%[b]

[a] Based on GAUGE-FEVER predictions.

[b] From slightly different core location (i.e., 2586 mm) but adjusted to core location of finite sample via FEVER code prediction.

The composite FIMA is given by the equation:

$$F_c = xF_1 + (1 - x)\, F_2 \quad , \tag{9-12}$$

where F_1 = fissile FIMA,
F_2 = fertile FIMA,
x = U/(Th+U) at BOL (atomic ratio).

The heavy metal loadings at the axial location of TS6-5 (2684 mm) were:

Fuel Holes	U_o (g/rod)	Th_o (g/rod)	
1 and 2	0.6557	4.973	
3 and 4	0.6557	1.950	
5 and 6	0.6557	1.892	
7 and 8	0.6557	1.133	
Total	5.2454	19.396	(for 8 holes)

$$x = 5.2454/25.1414 = 0.2086$$

The above calculation assumed that the quantity of heavy metal contained by the spine at this location is small compared to heavy metal contained in the fuel rods. Therefore,

$$(F_c)_{calc} = 0.2086\ (30.35) + (1 - 0.2086)\ (0.58) = 6.79$$

$$(F_c)_{meas} = 0.2086\ (34.26) + (1 - 0.2086)\ (0.69) = 7.69$$

$$\frac{(F_c)_{calc}}{(F_c)_{meas}} - 1 = \frac{6.79}{7.69} - 1 = -0.117$$

Since the burnup is directly related to the power, this can also be expressed as

$$\frac{(CPF_x)_{GAUGE}\ (APF_{x,z})_{FEVER}}{(CPF_x)_{actual}\ (APF_{x,z})_{Cs-137}} - 1 = -0.117 \quad , \tag{9-13}$$

where $(CPF_x)_{GAUGE}$ = the time-averaged element average power factor predicted by GAUGE,

$(APF_{x,z})_{FEVER}$ = the time-averaged element average axial power factor at the location of TS6-5 as calculated by FEVER,

$(CPF_x)_{actual}$ = the actual time-averaged element average power factor,

$(APF_{x,z})_{Cs-137}$ = element average axial power factor at axial location of TS6-5 as determined from the hot cell gamma scans via linear regression of neighboring fuel rods.

Rearranging the above equation yields

$$\frac{(CPF_x)_{actual}}{(CPF_x)_{GAUGE}} = \frac{1}{0.883} \cdot \frac{(APF_{x,z})_{FEVER}}{(APF_{x,z})_{Cs-137}} \quad .$$

At a core height of 2684 mm (location of TS6-5),

$$(APF_{x,z})_{FEVER} = 0.753$$

$$(APF_{x,z})_{Cs-137} = 0.849$$

therefore,

$$\frac{(CPF_x)_{actual}}{(CPF_x)_{GAUGE}} = \frac{1}{0.883}\left(\frac{0.753}{0.849}\right) = 1.004$$

The element average power factor at each time point appearing in Eq. 9-3 ($CPF_{x,t}$) is obtained by multiplying the element average power factors calculated by GAUGE by 1.004:

$$(CPF_{x,t}) = 1.004\ (CPF_{x,t})_{GAUGE} \quad .$$

TASK 400: OUT-OF-PILE PARTICLE TESTING AND EVALUATION

Subtask 430: Isothermal Postirradiation Heating

Summary and Conclusions

Eighty-eight unbonded irradiated TRISO $(Th/U)C_2$ (FSV fissile A fuel) particles were heated from 1100° to 2400°C over an 8-h period in the first of a series of tests designed to demonstrate HTGR fuel particle performance during an unrestricted core heatup event. Cesium release fractions increased from 10^{-4} to 0.99 in the temperature range 1900° to 2400°C. Krypton-85 release fractions increased from 10^{-4} to 1 in the temperature range 2100° to 2400°C. Radiographic observations showed that the fission product release was not related to pressure vessel failure but occurred by diffusion through intact OPyC layers after the SiC layer was depleted in Si at the high temperatures.

FSV performance models, which predict 100% failure at 1700°C, and LHTGR models, which predict 100% failure at 2000°C, are extremely conservative relative to the test results. If this trend continues, the test program will show conclusively that HTGR fuel performance models, used in reactor safety and licensing studies, are conservative.

Introduction

Models used to predict LHTGR fuel particle coating failure during reactor operation were published in late 1974 (Ref. 9-8). The models conservatively account for all known coating failure mechanisms and are applicable to normal reactor operation and conditions predicted for hypothetical, unrestricted core heatup events evaluated during reactor safety and licensing studies. The models were evaluated by NRC in late 1976 (Ref. 9-9). The NRC developed interim models that are more conservative than those given in Ref. 9-8 and recommended that a statistically significant data base be developed to support the GA models. A series of tests was subsequently planned to demonstrate HTGR fuel particle performance under

conditions predicted for hypothetical unrestricted core heatup events. The major objective of the tests is to show that fuel failure models, used to predict performance in the safety and licensing studies, are conservative.

An operating reactor would be scrammed at the onset of an unrestricted core heatup, and fuel temperatures would eventually rise beyond normal operating temperatures because of fission product decay heat. These conditions will be obtained in core heatup simulation tests by heating irradiated samples out-of-pile using temperature ramps typical of those predicted for a core heatup. The initial phase of the core heatup simulation test program will extend through mid-CY-79 and will concentrate on TRISO UC_2 - TRISO ThO_2 performance.

A series of preliminary tests is being conducted prior to starting the initial phase to develop the required experimental methods. The preliminary tests will include unbonded, irradiated TRISO $(Th/U)C_2$ (FSV fissile A fuel), TRISO WAR $UC_{3.0}O_{0.5}$, and BISO ThO_2 fuel particles. Results of the TRISO $(Th/U)C_2$ test are given in this report.

Test Sample

Eighty-eight irradiated particles from TRISO $(Th/U)C_2$ batch CU6A-6328 were tested. The particles were selected from FSV production material (FSV fissile A fuel) and irradiated in capsule F-30 to a kernel burnup of 18.2% FIMA and fast neutron exposure of 9.1×10^{25} n/m^2 $(E > 29\ fJ)_{HTGR}$ at 1243°C (Ref. 9-10), which is representative of the most severe conditions expected for 6-year FSV fissile fuel.

Test Procedure

Unbonded particles were retrieved from the GA hot cell and characterized by gamma ray spectroscopy and X-radiography to assure that all particles in the test sample survived irradiation. The gamma counting data were then used as a basis for predicting the Kr-85 inventory in the test particles. Following characterization, the particles were heated from

∿100° to ∿2400°C over a period of 8 h, which represents the most rapid temperature ramp expected during an unrestricted core heatup in a LHTGR having a power density of 8.3 W/cm^3. Performance was evaluated by monitoring Cs-137 and Kr-85 release as a function of time and temperature.

The test was conducted in a resistance-heated graphite tube (King) furnace. The furnace configuration is shown schematically in Fig. 9-14. Forty-four particles were placed in each of two H-451 graphite sample containers. The two graphite containers were placed in a single open-ended Ta tube that extended through the furnace. While at temperature, a continuous flow of He (50 cm^3/min) was maintained through the Ta tube. A mullite tube was placed at 1100°C on the downstream side of the Ta tube to collect Cs released during testing. The mullite tube was changed at approximately 200°C intervals during the test.

Fission product gases released during testing were swept up by the flowing He, passed through a series of traps to remove tritium and Rn, and then analyzed for Kr-85. The tritium trap consists of hot (500°C) cuprous oxide to convert tritium to water and a desiccant to remove the water; activated charcoal held in dry ice and alcohol was used to trap Rn. The gases were then passed through two ionization chambers (A and B) and finally collected in a liquid N_2 cold trap. The cold trap was changed at approximately 200°C intervals and analysed for Kr-85 by gamma counting. Results from the ionization chambers were used to obtain a continuous measure of Kr-85 release.

After the test was completed, all coated particles were radiographed to determine the operating coating failure mechanism and gamma counted to confirm metallic fission product release results.

Results

Temperature Versus Time. The variation in temperature with time during the core heatup simulation tests of the irradiated FSV fissile A

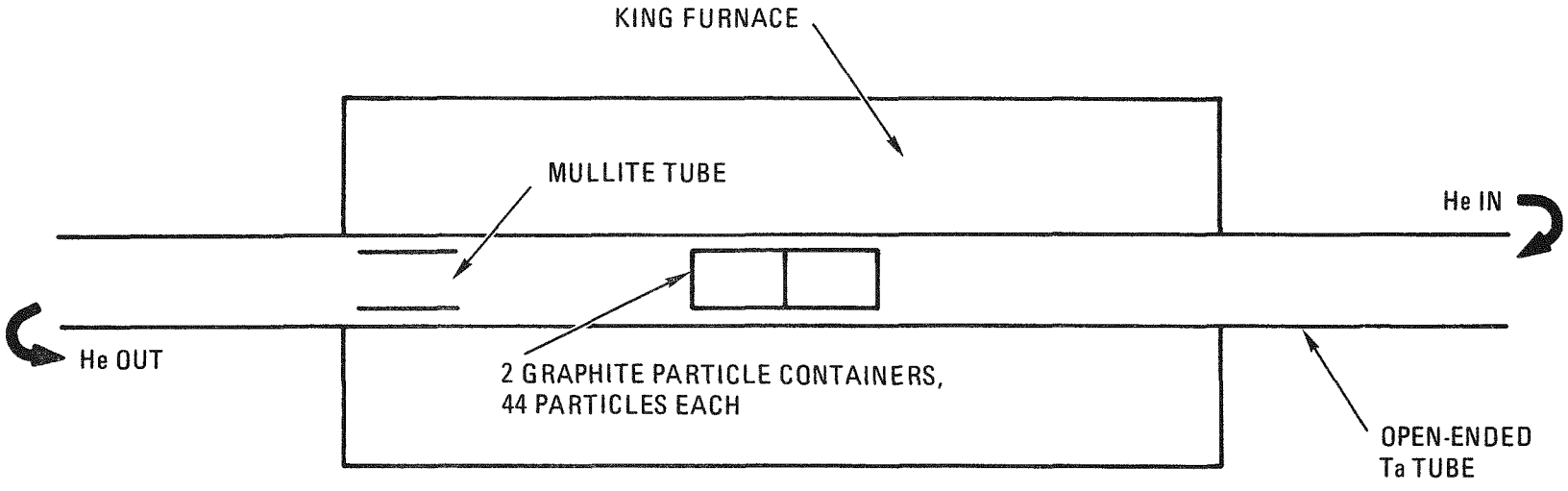

Fig. 9-14. Schematic drawing of furnace used for core heatup simulation testing

fuel is shown in Fig. 9-15. The temperature ramp was obtained using a programmable controller and satisfies the goal of a linear rise in temperature from 1100° to 2400°C over an 8-h period.

Radiographic Observations. All particles were radiographed before and after heating. Two particles appeared to have burst and three particles were not visible in the post-heating radiographs, leading to the conclusion that 5 of 88 particles suffered pressure vessel failure during testing.

Photomicrographs of radiographs of typical particles are shown before and after testing in Fig. 9-16. Although resolution is poor because the radiographs were shot through the 65-mil (1651 μm) thick H-451 graphite particle containers, the kernel, SiC, and OPyC layers are visible in the radiographs taken prior to the core heatup simulation tests (Fig. 9-16a). Post-heating radiographs (Fig. 9-16b) showed that the kernels expanded during heating, the OPyC layer remained intact on 83 of the original 88 particles, and the SiC layer was depleted in Si on 82 of the 83 particles with intact OPyC layers.

It will be shown later that 100% Cs-137 and 100% Kr-85 release occurred during this test. The radiographic results suggest that the majority of the fission product release occurred by diffusion through the OPyC layer after Si was lost from the SiC layer, rather than by pressure vessel failure of the IPyC, SiC, and OPyC layers.

Fission Product Release. Release of Kr-85 was monitored using ionization chambers and liquid N_2 cold traps. The ionization chambers were calibrated prior to these tests with known Kr-85 sources. Ionization chamber A was set up to follow peaks of activity associated with release of Kr-85 from single particles or groups of particles. The response of ionization chamber B was integrated electronically and compared with Kr-85 release data collected from the liquid N_2 cold traps. The ionization chamber data indicated 5.7 times more Kr-85 release than the liquid N_2 cold traps after completion of testing. The discrepancy increased with time from the point that detectable gas release occurred. Since past experience has shown that

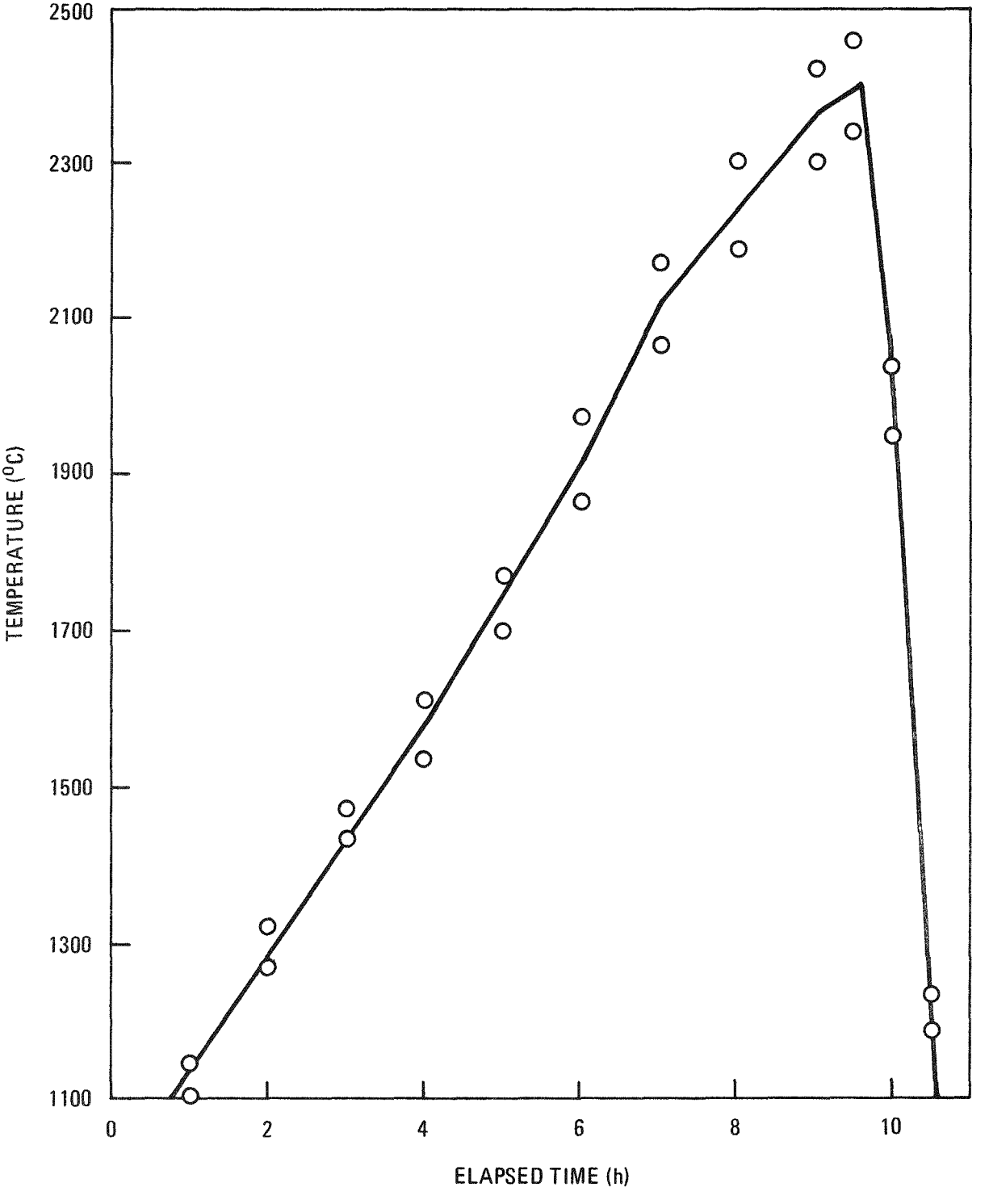

Fig. 9-15. Variation in temperature with time during core heatup simulation testing of 88 irradiated particles from batch CU6A-6328

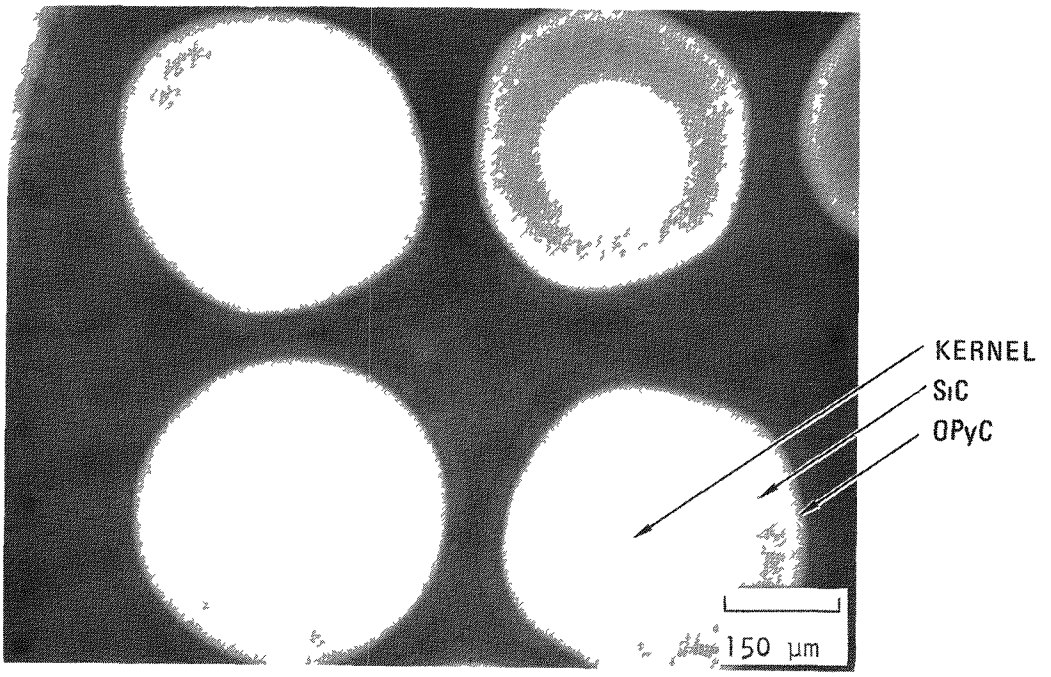

(a)

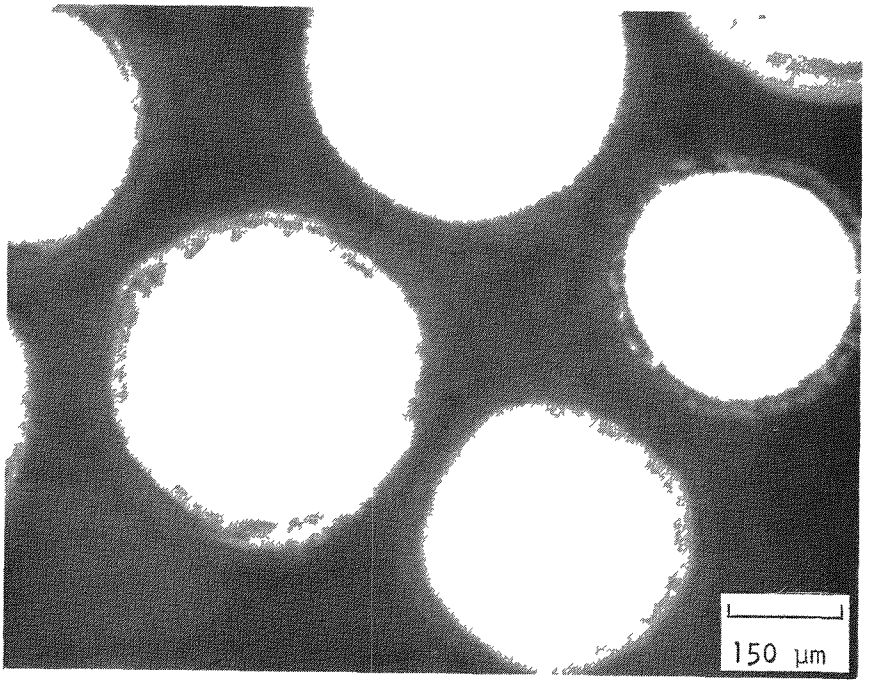

(b)

Fig. 9-16. Contact X-radiographs of irradiated FSV fissile A fuel particles (CU6A-6328): (a) prior to core heatup simulation testing, (b) after core heatup simulation testing

the liquid N_2 traps are nearly 100% effective for Kr-85 and the N_2 trap data indicated 100% Kr-85 release at the conclusion of the test, it was concluded that the ionization chamber data were clouded by the presence of tritium or Rn not removed by their respective trapping systems. The ionization chamber data were therefore used qualitatively to define the form of the curve used to connect the periodic Kr-85 release datum obtained from liquid N_2 cold traps.

The response of ionization chamber A is shown as a function of time in Fig. 9-17. The variation in test temperature with time is also shown in the figure. The ionization chamber response increased steadily with time from about 6.7 to 9.4 h into the test. No individual peaks were observed, indicating that the rate of release of Kr-85 from failed particles was slow relative to the increase in failure fraction with time. The ionization chamber response peaked just before the maximum temperature was reached. Based on liquid N_2 cold trap data, approximately 45% of the Kr-85 was released as the sample temperature was reduced from 2400°C to room temperature. It will be assumed that all Kr-85 detected while cooling the samples to room temperature was released at 2400°C.

The variation in the Cs-137 release fraction with temperature is shown in Fig. 9-18. The Cs release fraction was negligible up to 1920°C and then increased from $\sim 10^{-4}$ to 0.023 between 1920° and 2130°C and to 0.99 at 2400°C. The loss of Si from the SiC layer shown in Fig. 9-16 therefore began between 1920° and 2130°C. The frequency of metallic fission product release sampling will be increased in future tests to reduce the uncertainty in the temperature at which Si loss and Cs release begin.

The Kr-85 release fraction is also shown as a function of temperature in Fig. 9-18. The individual datum were obtained from liquid N_2 cold traps. The line connecting the data points was based on ionization chamber results showing that gaseous release did not begin until 2100°C. The Kr-85 release lagged behind the Cs release, which supports the radiographic evidence that release occurred by diffusion through the OPyC layers after the SiC layer was degraded.

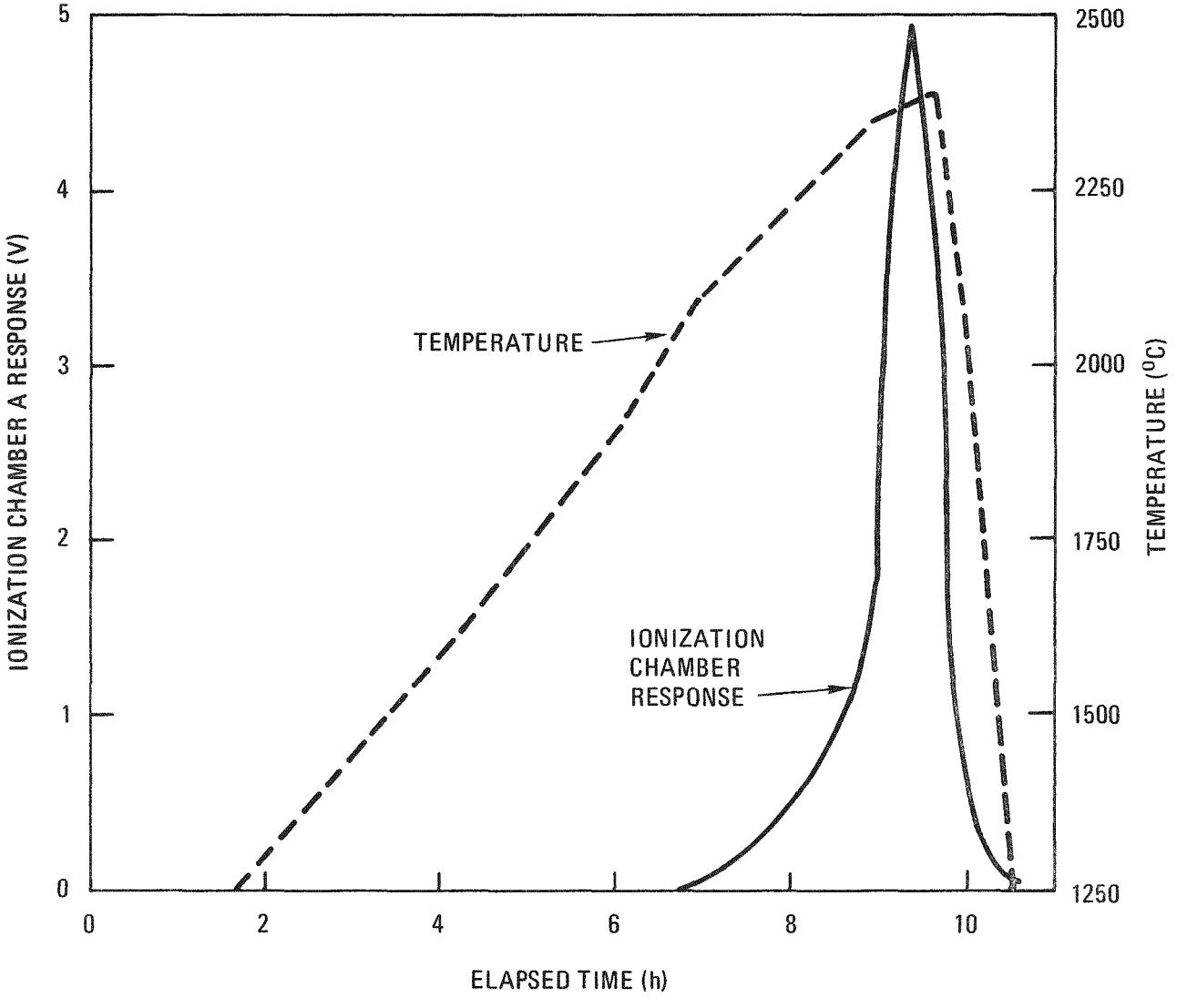

Fig. 9-17. Ionization chamber response and variation with temperature with time during core heatup simulation testing of 88 irradiated particles from batch CU6A-6328

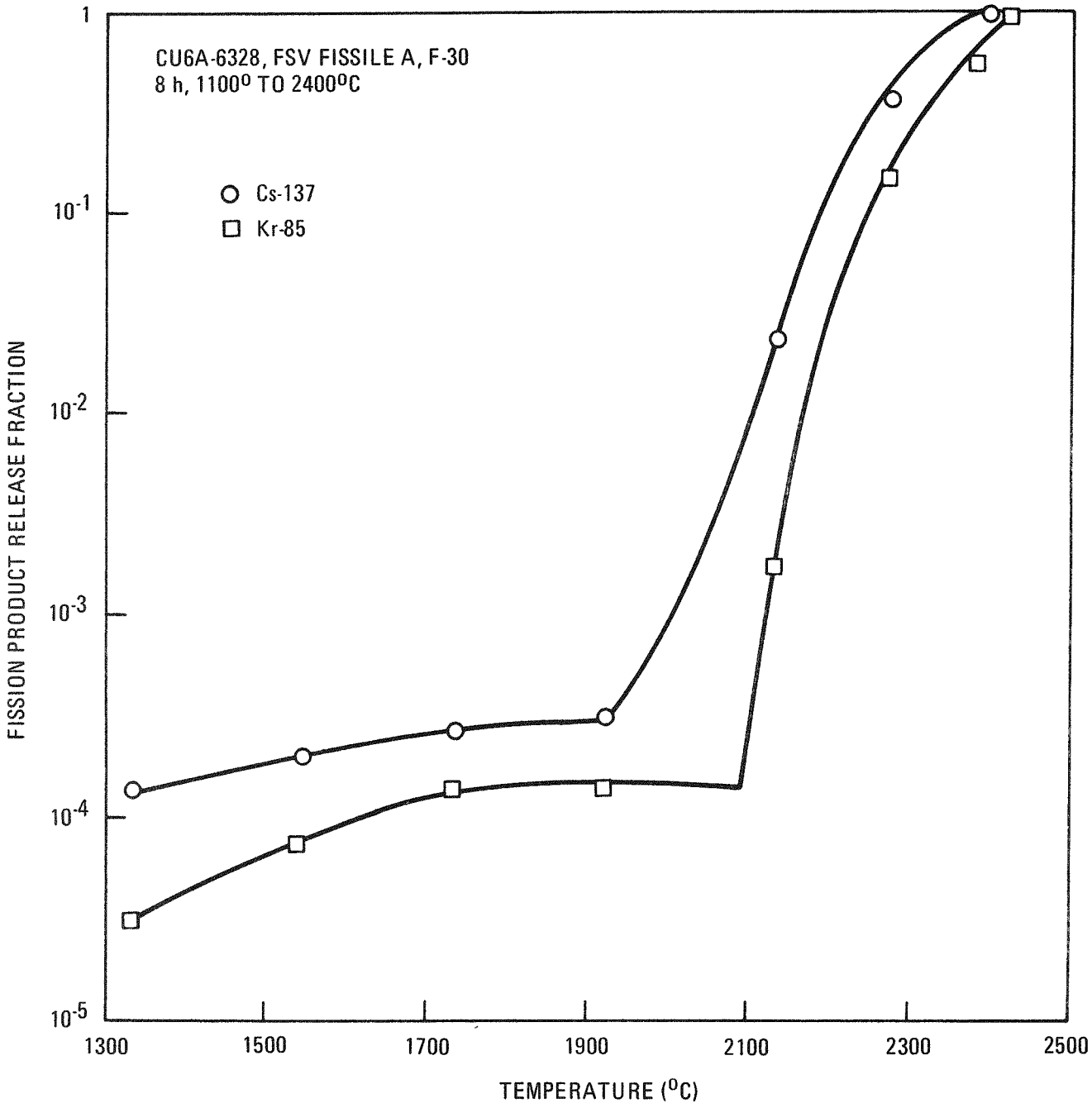

Fig. 9-18. Fractional Cs and Kr release versus temperature measured during an 8-h ramp test conducted with 88 particles from CU6A-6328

The fuel particles and crucibles were gamma counted before and after testing as part of the standard test procedure. These data yielded the release fractions shown in Table 9-18. The Cs data are consistent with mullite tube Cs release fractions. The only other metallic fission product collected on the mullite tubes was Eu-154. The mullite tube data suggested only 13% release compared to the 90% release obtained by counting particles before and after testing. Europium data will be evaluated as the core heatup simulation tests continue to determine if the mullite tube release fractions can be used to characterize Eu-154 release. One interesting observation is that all Ce-144 released from the coated particles during the 8-h ramp test was retained by the H-451 graphite sample holders.

Discussion

The results presented allow the first direct comparison between HTGR fuel performance models and experimental observations of fuel behavior during a simulated, unrestricted core heatup. The original FSV design studies assumed 100% failure at 1700°C during hypothetical design accidents. LHTGR performance models would suggest the initiation of failure at 1600° to 1800°C and 100% failure at 2000°C. Assuming that the Kr-85 release fraction is equivalent to the coating failure fraction, the results of this initial test show the fuel performance models to be extremely conservative. The very positive results lead to the belief that the core heatup simulation test program will confirm that LHTGR fuel performance models (Ref. 9-8) are conservative and will justify the adoption of more realistic performance models.

TASK 600: FUEL DESIGN AND PERFORMANCE MODELS

Subtask 620: Emperical Fuel Performance Models

Introduction

LEU* and MEU** 1/1 $(Th/U)O_2$ and UO_2 are being evaluated as possible fissile fuels for HTGRs. Data required to predict kernel migration

*<20% enriched with U-235.
**∿20% enriched with U-235.

TABLE 9-18
METALLIC FISSION PRODUCT RELEASE FRACTIONS CAUSED BY CORE HEATUP SIMULATION TESTS OF TRISO $(Th/U)C_2$ PARTICLES FROM BATCH CU6A-6328[a]

Nuclide	Release Fraction
Ru-106	0.29
Sb-125	0.97
Cs-134	>0.99
Cs-137	>0.99
Ce-144	0.97[b]
Eu-154	0.90

[a] 8-h temperature ramp, 1100° to 2400°C.

[b] All Ce was retained by the H-451 graphite sample holders.

distances for these kernels as a function of time, temperature, and temperature gradient are provided in this discussion.

Kernel Migration Coefficient

The kinetics of LEU and MEU oxide kernel migration are described by the kernel migration coefficient, which is defined as

$$KMC = \left(\frac{dx}{dt}\right)(T)^2\left(\frac{dT}{dx}\right)^{-1} = \beta\, e^{-\Delta H/RT} \quad , \tag{9-14}$$

where KMC = kernel migration coefficient ($m^2 \cdot K/s$),
(dx/dt) = kernel migration rate (m/s),
T = temperature (K),
dT/dx = temperature gradient (K/m),
β = pre-exponential constant ($m^2 \cdot K/s$),
ΔH = apparent activation energy (J/mol),
R = gas constant (8.313 J/mol·K).

UO_2 Kernel Migration Coefficient. GA and ORNL have obtained KMC data for HEU* UO_2 from in-pile irradiation experiments. KMC data have also been collected for LEU UO_2 during studies conducted to characterize fuel performance for the Dragon reactor. There is no significant difference in KMC values obtained from HEU and LEU UO_2 (Ref. 9-11). KMC values obtained by GA will therefore be used to describe HEU, MEU, and LEU kernel migration. The variation in UO_2 KMC with inverse temperature (K) is given in Fig. 9-19. The best estimate for UO_2 KMC is

$$UO_2 \text{ KMC } (m^2 \cdot K/s) = 0.265 \times 10^{-7} \exp\left(\frac{-6.78 \times 10^4}{8.313T}\right) \quad . \tag{9-15}$$

An estimate of KMC values at the 5% and 95% confidence levels can be obtained from the product of the correlation parameter at 5% (C_5) or 95%

*$\sim$93% enriched with U-235.

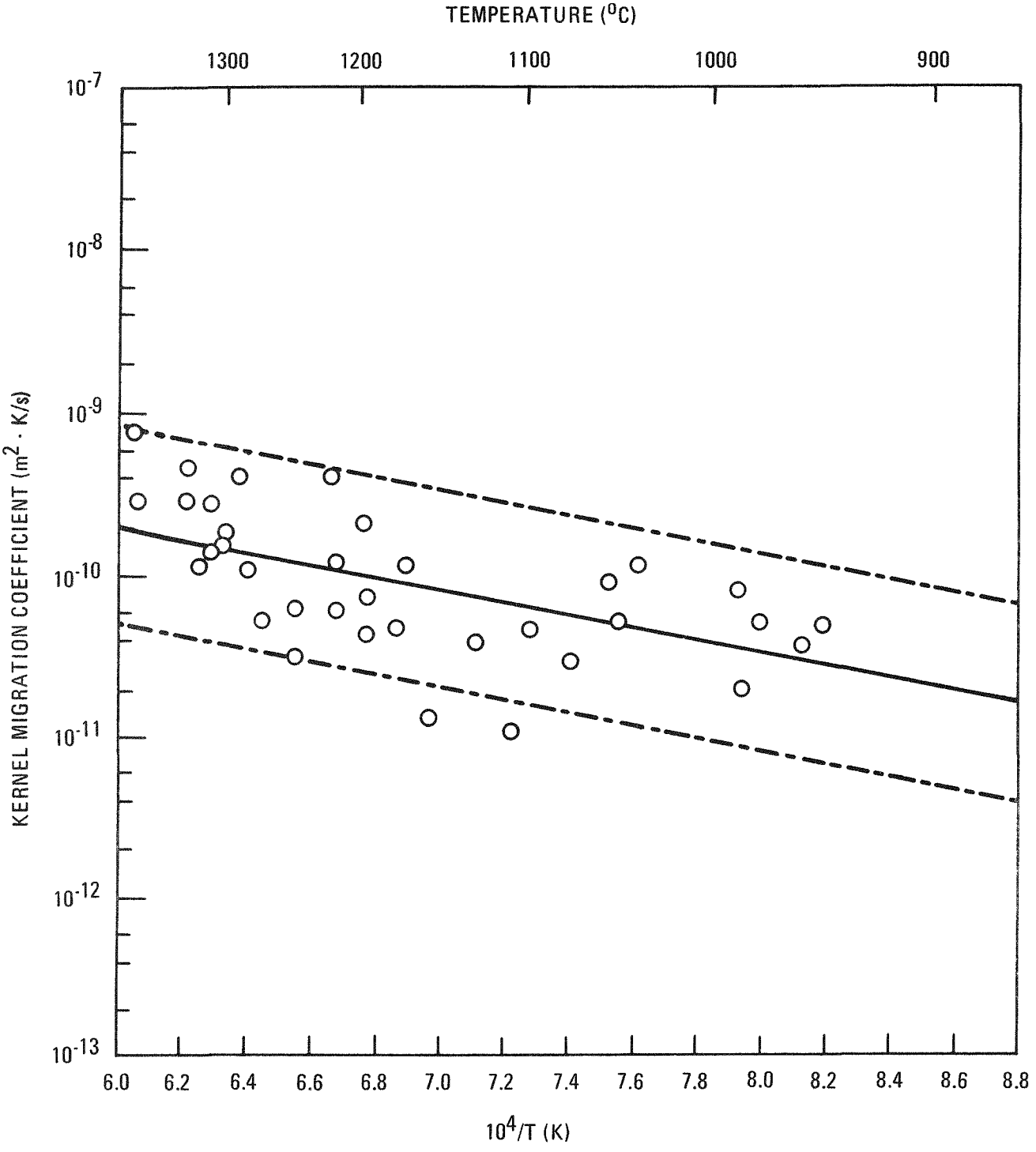

Fig. 9-19. Variation in UO_2 KMC with inverse temperature (K)

(C_{95}) confidence and the best estimate for KMC. The value of C_5 for UO_2 is 0.254; the value of C_{95} for UO_2 is 3.94.

(Th/U)O_2 Kernel Migration Coefficient. There are no available LEU or MEU 1/1 (Th/U)O_2 KMC data. In-pile HEU (Th/U)O_2 KMC data have been collected by GA and ORNL (Refs. 9-12 through 9-15). The bulk of the data were obtained from HRB irradiation tests conducted by investigators at ORNL. The data base includes kernels having Th/U ratios in the range 8/1 to 1/1. Given the observation that HEU and LEU UO_2 KMC values are similar, it is assumed that LEU and MEU KMC values for the mixed oxide equal HEU KMC values. The scatter in the mixed oxide data made it impossible to identify a relationship between Th/U ratio and KMC; therefore, all available mixed oxide data were combined to obtain

$$(Th/U)O_2 \text{ KMC } (m^2 \cdot K/s) = 0.172 \times 10^{-4} \exp\left(\frac{-1.55 \times 10^5}{8.313T}\right) . \qquad (9\text{-}16)$$

The (Th/U)O_2 KMC data are shown in Fig. 9-20 as a function of inverse temperature. Correlation parameters can also be used to estimate mixed oxide KMC values at the 5% or 95% confidence level. The value of C_5 for (Th/U)O_2 is 0.204; the value of C_{95} is 4.90.

FUEL PERFORMANCE MODELS FOR BISO ThO_2 FUEL AT TEMPERATURES EXCEEDING 2000°C

Introduction and Summary

Fuel failure predictions originally developed to estimate fuel performance in an operating HTGR predicted 100% failure of BISO ThO_2 fertile fuel any time that HTGR operating temperatures exceed 2000°C (Ref. 9-8). Recent modifications that removed all conservatism and introduced uncertainties in the models (see discussion under last section in Task 9, "Uncertainties in HTGR Fuel Performance Models") provide a method for estimating performance at temperatures less than or equal to 2000°C; however, the failure values vary with the confidence level of the prediction from 10% to 100% at 2000°C. The method described in this section provides

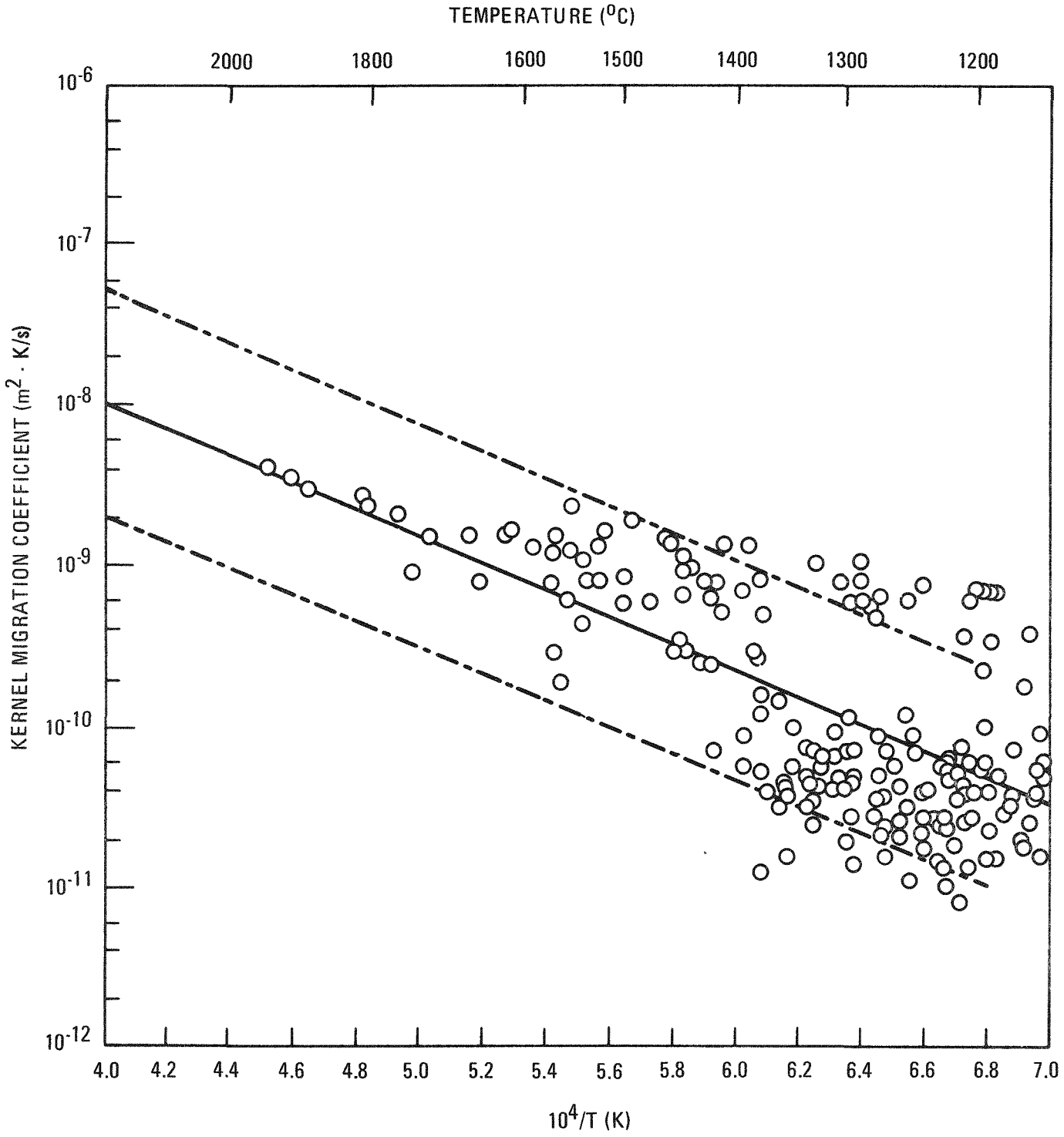

Fig. 9-20. Variation in $(Th/U)O_2$ KMC with inverse temperature

a means for extrapolating BISO fertile fuel performance estimates to temperatures greater than 2000°C until an estimate of 100% failure is reached.

The prediction of BISO ThO_2 fuel failure for temperatures exceeding 2000°C is based on PyC annealing data that show a reduction in PyC fracture strength with annealing time for heating temperatures that exceed the PyC deposition temperature. Estimated failure at temperatures exceeding 2000°C is independent of fuel age or exposure but varies with the confidence level of the estimate. The steps used to estimate failure at confidence level x for temperatures exceeding 2000°C are given later in this discussion.

Current Model

The model now available provides a nominal value and confidence bounds for BISO ThO_2 fuel failure at temperatures $\leq$2000°C. Failure can be estimated as a function of fluence, burnup, and temperature for a given confidence level using input from Ref. 9-8 and from the work reported under "Uncertainties in HTGR Fuel Performance Models." Predicted failure values at the 95%, 50%, and 5% confidence levels* are given as a function of fast neutron exposure at 1800° and 2000°C in Table 9-19. Failure at temperatures between 1800° and 2000°C is estimated by interpolating linearly between the 1800° and 2000°C data. As shown in Table 9-19, estimates for failure at 2000°C indicate less than 100% failure for confidence levels less than 95%. Certain safety-related design studies are conducted for conditions that could lead to operating temperatures exceeding 2000°C. In order to be applicable in safety calculations, fuel failure models must be extended to operating temperatures that result in failure predictions of 100% at all confidence levels.

Estimation of BISO Fuel Performance at Temperatures Greater than 2000°C

BISO ThO_2 particles have not been tested at temperatures exceeding 2000°C. The performance estimates provided below are therefore based on

*There is a 90% probability that the true failure value lies between failure values predicted at the 5% and 95% confidence levels.

TABLE 9-19
PREDICTED FAILURE OF BISO ThO_2 FERTILE FUEL

Fast Neutron Exposure (10^{25} n/m^2) (E ≥ 29 fJ)HTGR	Failure (%)					
	5% Confidence Level(a)		50% Confidence Level		95% Confidence Level(a)	
	1800°C	2000°C	1800°C	2000°C	1800°C	2000°C
0	0	10	0	55	0	100
1.0	0.006	10	0.034	55	0.063	100
2.0	0.013	10	0.069	55	0.125	100
3.0	0.019	10	0.103	55	0.188	100
4.0	0.025	10	0.138	55	0.250	100
5.0	0.031	10	0.172	55	0.313	100
5.5	0.134	10	0.737	55	1.34	100
6.0	0.537	10	2.95	55	5.37	100
6.5	1.30	10	7.16	55	13.01	100
7.0	1.93	10	10.63	55	19.32	100
7.5	3.24	10	17.79	55	32.35	100
8.0	4.39	10	24.16	55	43.92	100

(a)There is a 90% probability that the true failure value lies between the values given at the 5% and 95% confidence levels.

indirect evidence. (Tests at temperatures exceeding 2000°C will be conducted in the near future.)

Data describing the effects of annealing and irradiation on the strength of PyC provide the most rational basis for performance estimates at temperatures >2000°C. It has been shown that irradiation of unrestrained PyC strips at temperatures as high as 1600°C (Ref. 9-16) causes dimensional changes as well as increases in PyC density and apparent crystallite height. The combination of these (or possible unknown) phenomena causes an increase in Young's modulus and a possible increase in fracture strength. The data show conclusively that fracture strength is not reduced under the irradiation conditions described in Ref. 9-16. According to Kaae of General Atomic, similar results are expected for restrained PyC.

Annealing studies on unirradiated PyC with as-deposited properties similar to those discussed above have been conducted to determine the effects on mechanical properties and structure (Refs. 9-17 and 9-18). After annealing for 1 h at temperatures in the range 1400° to 1900°C (Ref. 9-17), there is a small increase in density, an increase in apparent crystallite height, a decrease in Young's modulus (the effect is more pronounced as the PyC density increases), and a decrease in PyC fracture stress. The variation in fracture stress with annealing temperature is shown in Fig. 9-21. Thin film transmission electron microscopy of a PyC sample having an as-deposited density of 2.04 g/cm^3 showed that cracks parallel to the carbon layer planes developed during annealing at 1900°C. Studies of densification, crystallite height change, and dimensional change occurring during annealing at temperatures as high as 2800°C (Ref. 9-18) showed that the trends developed at temperatures less than 1900°C were continued in the higher temperature studies. Transmission electron microscopy of a sample having an as-deposited density of 2.04 g/cm^3 showed more cracking after annealing for 2 h at 2800°C than the sample heated 2 h at 1900°C. Although strengths were not measured, these data suggest that the strength of these PyC coatings would have continued to decrease with increased annealing in the temperature range 1900° to 2800°C.

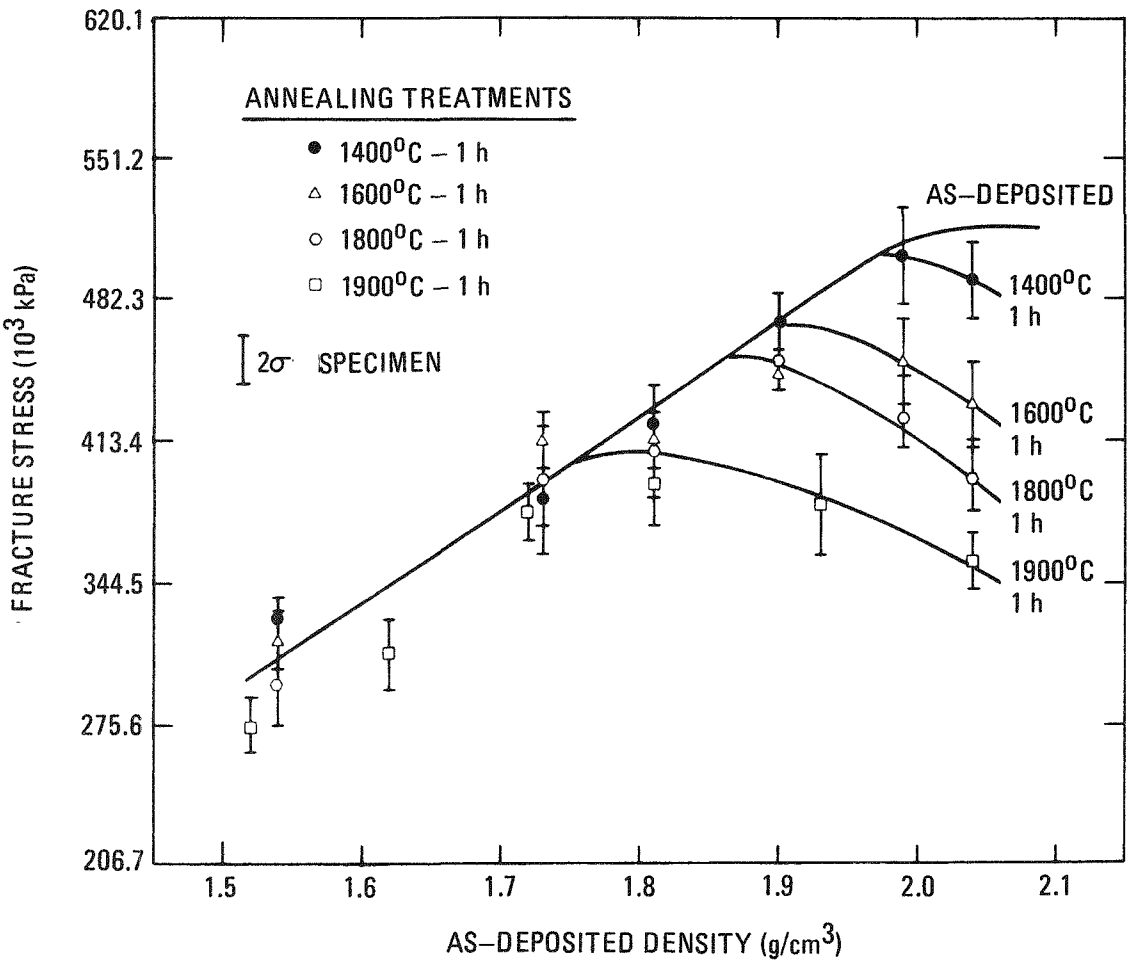

Fig. 9-21. Variation of PyC fracture stress as a function of as-deposited density for various annealing temperatures

The discussion presented shows that current BISO ThO_2 failure models cannot be extrapolated directly in order to estimate fuel failure at temperatures exceeding 2000°C. There is also no indication that irradiation at temperatures as high as 1600°C decreases PyC strength thereby contributing to increases in failure. The data do show, however, that high-temperature annealing causes a reduction in PyC strength that could contribute to failure of the outer PyC layer on BISO fuel. The circumstances leading to HTGR core operation at temperatures exceeding 2000°C involve a hypothetical accident. In these cases, the core would be scrammed and temperatures exceeding 2000°C would be experienced without a significant fast neutron flux. The conditions would therefore be similar to the high-temperature annealing studies which will be used as the basis for performance models at temperatures greater than 2000°C.

During irradiation, the density of PyC coatings of the type used as the OPyC layer on BISO fuel particles increases to greater than 2.0 g/cm^3. Data showing the effect of annealing temperature on the strength of PyC strips with densities of 1.99 and 2.04 g/cm^3 (Ref. 9-17) are plotted in Fig. 9-22 and extrapolated to 2800°C assuming that the failure stress decreases linearly with increasing annealing temperature. The strength of the PyC coatings in a fresh core or segment (density = 1.80 to 1.95 g/cm^3) is 60,000 to 65,000 psi (390 to 449 kPa) (Ref. 9-17). For purposes of performance prediction, it will be arbitrarily assumed that 100% failure occurs at operating temperatures less than or equal to the temperature (based on Fig. 9-22) that would result in a decrease in PyC failure stress of 50%, or approximately 2600°C.

The steps used to estimate failure at temperatures exceeding 2000°C are described below. Two ground rules that were followed are: (1) failure for $T \geq 2000°C$ is independent of fuel age, neutron exposure, or kernel burnup, and (2) failure at $T \geq 2000°C$ varies with the confidence level of the failure estimate. The steps used for confidence level x are:

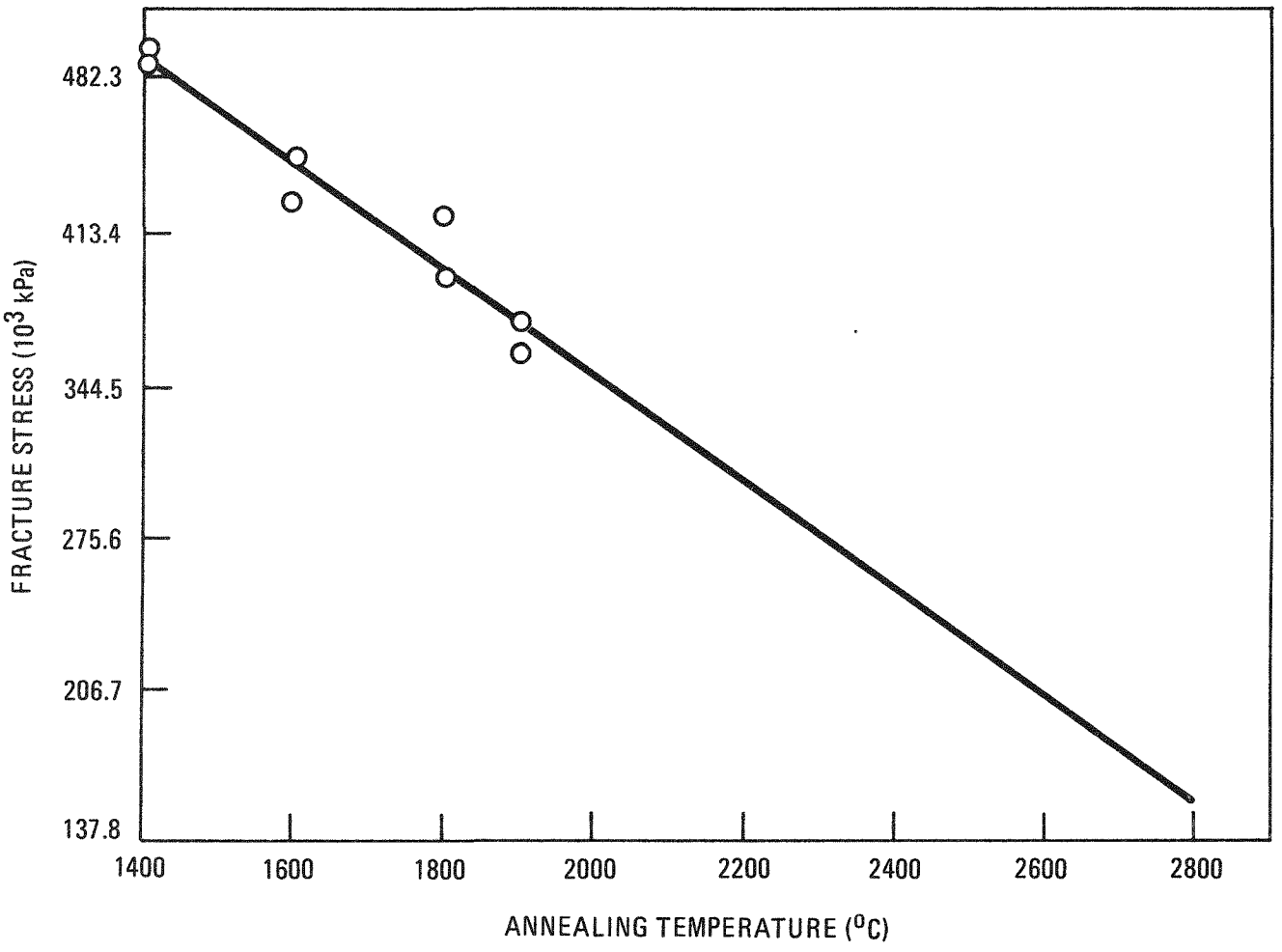

Fig. 9-22. PyC fracture stress versus annealing temperature for PyC coatings having as-deposited densities in the range 1.99 to 2.04 Mg/m^3

1. Linearly extrapolate failure predictions at 1800° and 2000°C for fuel experiencing 7.5% FIMA and a fast neutron fluence of 8×10^{25} n/m^2 $(E > 29\ fJ)_{HTGR}$ to 100% failure.

2. Determine the temperature for 100% failure.

3. If the temperature for 100% failure is less than 2600°C, use the extrapolated variation in failure with temperature to define failure at confidence level x for $T \geq 2000$°C independent of fuel age.

4. If the temperature of 100% failure is greater than 2600°C, assume failure at confidence level x increases linearly from the value currently predicted at 2000°C to 100% at 2600°C independent of fuel age.

Examples of predicted failure in the temperature range 2000° to 2600°C are given in Fig. 9-23 at the 5%, 50%, and 95% confidence levels.

UNCERTAINTIES IN HTGR FUEL PERFORMANCE MODELS

Introduction and Summary

Models used to predict fuel particle coating failure that would lead to gaseous fission product release in an operating LHTGR are given in Ref. 9-8. The phenomena treated are: (1) fuel particles having missing or defective coatings, (2) kernel migration, (3) pressure vessel failure, and (4) failure of TRISO coated fuel particles from fission product - SiC interactions. The failure rates given in Ref. 9-8 represent performance estimates made during the time period January to July 1974. No uncertainties are given. A fifth phenomenon that causes fission gas release is the presence of heavy metal exposed during fuel particle and fuel rod fabrication. The purpose of the discussion in this section is to provide estimates for uncertainties in the failure models.

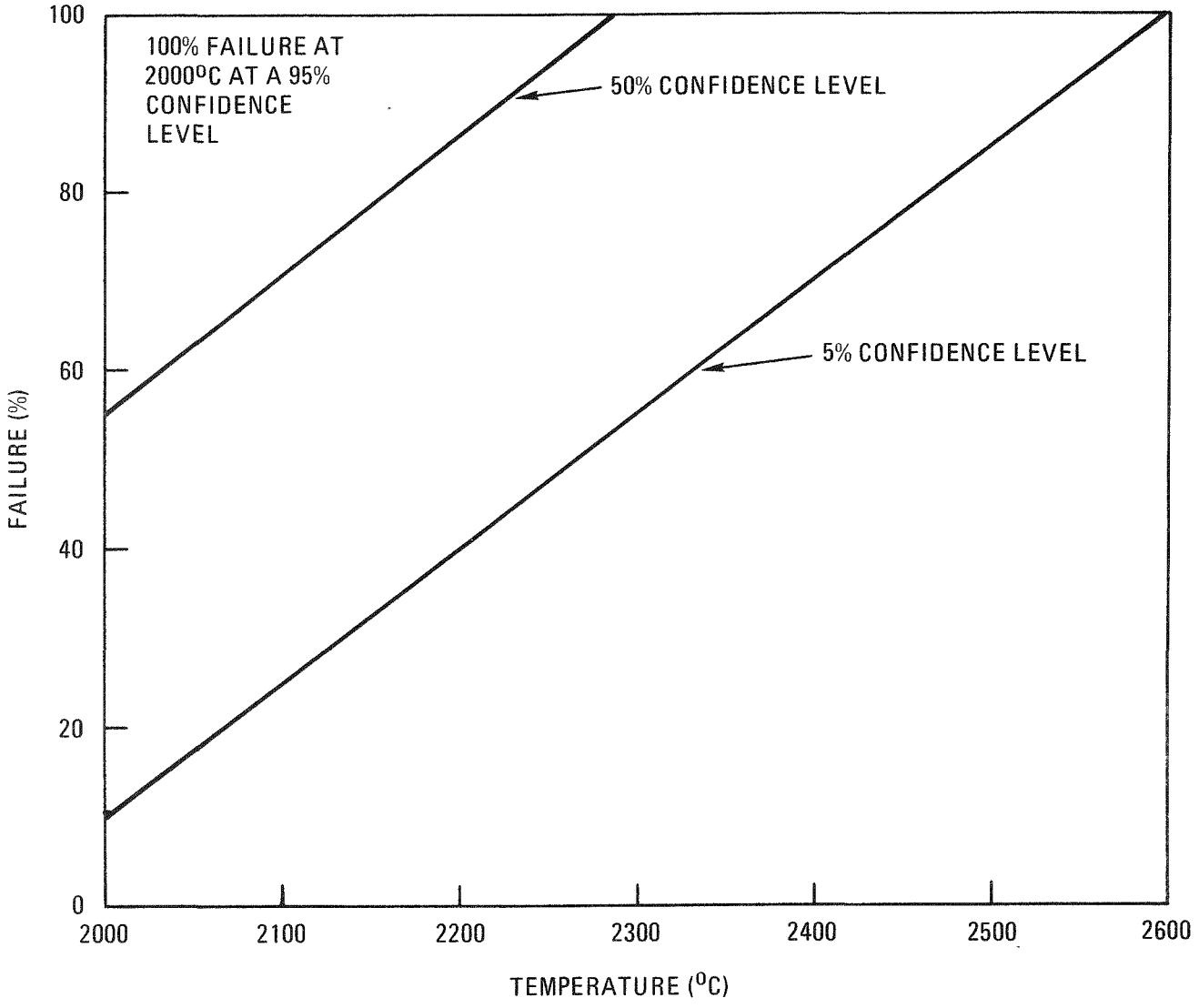

Fig. 9-23. Examples of estimated failure of BISO ThO_2 fuel particles as a function of confidence level in the temperature range 2000° to 2600°C

With the exception of data describing fuel kernel migration, failure predictions given in Ref. 9-8 are conservative estimates for fuel performance that were based on available irradiation or out-of-pile heating data. In the treatment of the performance estimates discussed below, all conservatisms are removed in order to provide a "best estimate" and 5% or 95% confidence limits for estimated fuel performance during LHTGR operation. The uncertainties provided apply to fuel fabricated to the HTGR Fuel Product Specification (Ref. 9-19).

The uncertainties are given in terms of correlation parameters at 5% (C_5), 50% (C_{50}), or 95% (C_{95}) confidence levels. Correlation parameters are tabulated for TRISO UC_2 fissile and BISO ThO_2 fertile fuels in Tables 9-20 and 9-21, respectively.

Approach

The performance model uncertainty estimates are provided in the form of correlation parameters (C). These parameters are defined so that

$$f_{i,x} = (C_{i,x})(F_i) \quad , \tag{9-17}$$

where F_i = failure estimate for mechanism i based on Ref. 9-8,
$c_{i,x}$ = correlation parameter at confidence level x for mechanism i,
$f_{i,x}$ = failure estimate for mechanism i at confidence level x.

Correlation parameters will be given for calculation of the most probable (50% confidence) failure fraction ($C_{i,50}$), and the 95% ($C_{i,95}$), and 5% ($C_{i,5}$) confidence limits for failure. There is a 90% probability that failure is bounded by $(C_{i,5})(F_i)$ and $(C_{i,95})(F_i)$.

TABLE 9-20
CORRELATION PARAMETERS FOR COATING FAILURE MECHANISMS THAT LEAD TO FISSION GAS RELEASE FROM TRISO UC_2 FISSILE FUEL

Failure Mechanism	Base Case Value	Correlation Parameter		
		C_5	C_{50}	C_{95}
Fission gas release from actinide metal exposed during fuel fabrication	3×10^{-5} R/B, Kr-85m at 1100°C	0.67	1.0	1.33
Missing or defective coatings				
Fraction present	2×10^{-3}[a]	0.412	0.75	1.365
Failure probability at peak burnup	1.0[a]	0.5	0.7	1.0
Pressure vessel failure	0 - 100%[a]	0.10	0.55	1.0
Kernel migration coefficient	Eq. 9-20	0.351	1.0	2.850
SiC - fission product reactions				
Rate of thinning	Eq. 9-23	0.46	1.0	2.18
Failure at T = 1600°C	0 - 100%[a]	1.0	1.0	1.0

[a]Values predicted using models in Ref. 9-8.

TABLE 9-21
CORRELATION PARAMETERS FOR COATING FAILURE MECHANISMS THAT LEAD TO FISSION GAS RELEASE FROM BISO ThO_2 FERTILE FUEL

Failure Mechanism	Base Case Value	Correlation Parameter		
		C_5	C_{50}	C_{95}
Fission gas release from actinide metal exposed during fuel fabrication	3×10^{-5} R/B Kr-85m at 1100°C	0.67	1.0	1.33
Missing or defective coatings				
Fraction present	2×10^{-3}[a]	0.275	0.50	0.91
Failure probability at peak burnup	1.0[a]	1.0	1.0	1.0
Pressure vessel failure	0 - 100%[a]	0.10	0.55	1.0
Kernel migration				
KMC	Eq. 9-21	0.24	1.0	4.22
θ	Eq. 9-22	0.32	1.0	3.12
Burnup limit on incubation period	2% FIMA	1.0	1.0	1.0

[a] Values predicted using models in Ref. 9-8.

Model Uncertainties

Fission Gas Release From Heavy Metal Exposed During Fuel Particle and Fuel Rod Fabrication

Based on requirements in Ref. 9-19, the best estimate for fission gas release from heavy metal exposed during fuel fabrication is assumed equal to 3×10^{-5} R/B for Kr-85m at 1100°C. The standard deviation in fission gas release values measured on rods from a single lot during FSV production was 3×10^{-5}. Fission gas release measurements will be made on ∿25 rods per segment during LHTGR fabrication. Assuming the standard deviation obtained during FSV fabrication, the uncertainty in the average fission gas release will be 0.6×10^{-5}. Given this uncertainty in the average value, C_{95} will be assumed equal to 1.33 and C_5 will be assumed equal to 0.67.

Failure of Fuel Particles Having Missing or Defective Coatings

The HTGR Fuel Product Specification (Ref. 9-19) allows for the presence of a small fraction of fuel particles having missing or defective coatings. Failure of these particles is estimated in Ref. 9-8 using

$$f_D = W \frac{(BU)}{BU_{max}} \leq W \quad , \tag{9-18}$$

where f_D = failure fraction due to fuel having missing or defective coatings,

W = fraction of fuel in a LHTGR core having missing or defective coatings (assumed equal to 2×10^{-3} for both fissile and fertile fuel in Ref. 9-8),

BU = kernel burnup (% FIMA),

BU_{max} = maximum kernel burnup (7.5% FIMA for fertile fuel; 78% FIMA for fissile fuel).

Two assumptions are made in Eq. 9-18: (1) the value for W, and (2) that all particles having missing or defective coatings fail at peak

burnup. Correlation parameters will be given for both assumptions. This results in an expression of the form

$$f_D = (C_f W)\left[C_{BU}\left(\frac{BU}{BU_{max}}\right)\right] \leq W \quad , \tag{9-19}$$

where C_f = correlation parameter describing the probability of having a defect fraction (C_f W),

C_{BU} = correlation parameter describing the probability that all fuel having missing or defective coatings will fail at peak burnup.

LHTGR fuel product specifications (Ref. 9-19) are written to assure that BISO fertile fuel with missing or defective buffer coating fractions exceeding 1×10^{-3} are rejected. The fraction specified for missing or defective outer PyC coatings is also 1×10^{-3}. In order to meet these limits, expected values will have to be less than 1×10^{-3} for each layer and the probability of exceeding a total of 2×10^{-3} missing or defective coatings will be negligible. In addition, the specification on exposed Th limits the fraction of missing outer PyC layers to less than 1×10^{-4}. The most probable fraction of fertile fuel having missing or defective coatings will therefore be assumed to be 1×10^{-3}. The probability density function for the range of possible segment or core average defect fractions will be assumed to have a nominal value of 1×10^{-3} and a standard deviation of 0.5×10^{-3}. The 95% confidence limit for missing or defective coatings on fertile fuel is therefore 1.82×10^{-3}. The value assumed in Ref. 9-8 is 2×10^{-3}. Relative to Ref. 9-8, $C_{f,95}$ is therefore 0.91 and $C_{f,50}$ is 0.5. Using the basic assumption of a log normal distribution [expected = $(C_{95})/x = (C_5)(x)$], $C_{f,5} = 0.275$. These C values result in 95%, 50%, and 5% confidence levels for segment average defect fractions in fertile fuel of 1.82×10^{-3}, 1×10^{-3}, or 0.55×10^{-3}.

The assumption that all fertile fuel particles having missing or defective coatings fail at peak HTGR burnup (7.5% FIMA) is reasonable since

the particles in question have no buffer or OPyC layer. Values for $C_{BU,95}$, $C_{BU,50}$, and $C_{BU,5}$ are therefore assumed to be 1.

Reference 9-19 requires that the total fraction of TRISO fuel having missing or defective coatings is less than 3×10^{-3}. Using the approach used for BISO ThO_2, the most probable value for missing or defective TRISO coatings in a segment is assumed to be 1.5×10^{-3}. The probability density distribution is described by a most probable value of 1.5×10^{-3} and a standard deviation of 0.75×10^{-3}. The 95% confidence and nominal values for TRISO defect fractions in a segment are therefore 2.73×10^{-3} and 1.5×10^{-3}, respectively. Assuming a log normal distribution, the 5% confidence value for defect fractions would be 0.824×10^{-3}. The value for defect fractions used in Ref. 9-8 is 2×10^{-3}. Therefore, relative to Ref. 9-8, $C_{f,95} = 1.365$, $C_{f,50} = 0.75$, and $C_{f,5} = 0.412$ can be used to describe the range of defect fractions that could exist in any single segment or core.

TRISO coatings contain multiple structural coating layers. It is therefore improbable that a single defective layer implies total particle failure for every coated particle having a missing or defective coating. Recent irradiation results have in fact shown that 95% to 100% of the particles in a batch with 100% OPyC failure can survive (Ref. 9-14). To estimate C_{BU}, it will be assumed that there are equal quantities of each type of coating defect. Values for $C_{BU,95}$, $C_{BU,50}$, and $C_{BU,5}$ are given in Table 9-22 along with the assumptions made in generating them.

TABLE 9-22
VALUES FOR C_{BU} AT 95%, 50%, AND 5% CONFIDENCE LEVELS

Confidence Level	Percent Failure of Particles Having Indicated Missing or Defective Coating			
	Buffer + IPyC	SiC	OPyC	C_{BU}
95	100	100	100	1
50	100	100	10	0.7
5	50	100	0	0.5

Pressure Vessel Failure

Both BISO and TRISO pressure vessel failure models (Ref. 9-8) show 0.5% failure in fuel irradiated to peak burnup and fast neutron fluence at 1250°C. The design goal is zero failure under average conditions, which is achieved by demonstrating less than 0.1% failure at peak burnup and fluence. The margin (0.4%) is present to account for a small quantity of "off specification" fuel that may be present in an HTGR segment or core because of limited Quality Control sampling. The predictions given in Ref. 9-8 are therefore considered representative of a 95% confidence level ($C_{\text{pressure vessel},95} = 1$).

Estimates of the lower limit for pressure vessel failure are based on observations of unbonded TRISO UC_2 and BISO ThO_2 irradiation results from capsules P13R and P13S (Ref. 9-14). The failure fraction observed in ∿7000 BISO ThO_2 particles having properties that meet current specification limits is 0.06%. No failures leading to fission gas release were observed in ∿2000 TRISO UC_2 particles having properties that meet current specification requirements. Based on Ref. 9-8, the predicted pressure vessel failure level for both fuel types was 0.5%. The pressure vessel correlation parameter at a 5% confidence level is therefore assumed equal to 0.10.

The correlation parameter at a 50% confidence level is assumed to be midway between $C_{\text{pressure vessel},5}$ and $C_{\text{pressure vessel},95}$, or $C_{\text{pressure vessel},50} = 0.55$.

Kernel Migration - UC_2

The best estimate for the UC_2 kernel migration coefficient is (Ref. 9-8)

$$\text{KMC } (m^2 \cdot K/s) = 0.62 \exp\left(\frac{-3.11 \times 10^5}{8.313T}\right) \quad . \tag{9-20}$$

Correlation parameters for UC_2 KMC were determined at the midrange of the experimental data. The values are $C_5 = 0.351$, $C_{50} = 1$, and $C_{95} = 2.850$.

The predicted failure fraction due to UC_2 kernel migration equals the probability that a migrating kernel has penetrated the buffer layer and is in contact with the IPyC. The distribution of buffer thicknesses in TRISO UC_2 is described by an average of 110 μm and a standard deviation of 18.1 μm.

Kernel Migration - ThO_2

The ThO_2 KMC data in Ref. 9-8 have been superceded by results of recent ThO_2 kernel migration studies (Ref. 9-20). The ThO_2 kernel migration coefficient is

$$KMC\ (m^2 \cdot K/s) = 0.39\ \exp\left(\frac{-2.96 \times 10^5}{8.313T}\right) \quad . \tag{9-21}$$

Correlation parameters are $C_5 = 0.24$, $C_{50} = 1$, and $C_{95} = 4.22$.

Experimental results indicate an incubation period during which no ThO_2 migration occurs. The incubation period (Ref. 9-20) at constant temperature is given by

$$\theta(sec) = 4.7 \times 10^{-4}\ \exp\left(\frac{3.16 \times 10^5}{8.313T}\right) \quad . \tag{9-22}$$

Correlation parameters are $C_5 = 0.32$, $C_{50} = 1$, and $C_{95} = 3.12$. It is also assumed that ThO_2 migration begins when kernel burnups reach 2% FIMA, even if the incubation period is not exceeded. No uncertainty is assumed for the burnup limit ($C_5 = C_{50} = C_{95} = 1$).

Predicted, migration-induced BISO ThO_2 failure fractions equal the probability that a migrating kernel penetrates the buffer layer and contacts the PyC. Accounting for a 5% decrease in particle diameter caused by

fast neutron - PyC interactions, the distribution of buffer thicknesses will have an average value of 74 μm and a standard deviation of 16.1 μm.

SiC - Fission Product Reactions - TRISO UC_2

Two methods are used to predict TRISO UC_2 coating failure during reactor operation. During normal operation, the rate of decrease in SiC thickness ($\dot{x}$) is given by(Ref. 9-21):

$$\dot{x}\ (\mu m/h) = 4.2 \times 10^{7} \exp\left(\frac{-3.283 \times 10^{5}}{8.313T}\right) \quad . \tag{9-23}$$

Correlation parameters for $\dot{x}$ are $C_5 = 0.46$, $C_{50} = 1$, and $C_{95} = 2.18$. The predicted failure fraction equals the probability that the SiC thickness is reduced by 50%. The distribution of SiC thicknesses is described by an average value of 35 μm and a standard deviation of 5.0 μm.

The second method is applied at temperatures in the range 1600° to 2000°C. The model provided in Ref. 9-8 is conservative; however, the current data base is not sufficient to warrant the assignment of uncertainties. Correlation parameters are therefore assumed to be 1 at all confidence levels.

REFERENCES

9-1. "HTGR Fuels and Core Development Program Quarterly Progress Report for the Period Ending February 28, 1977," ERDA Report GA-A14298, General Atomic Company, March 1977.

9-2. Young, C. A., and D. P. Harmon, "Preirradiation Report of Fuel Materials for P13T Capsule Irradiation," ERDA Report GA-A13343, General Atomic Company, April 1976.

9-3. Peterson, J. F., "TAC2D - A General Purpose Two-Dimensional Heat Transfer Computer Code - User's Manual," USAEC Report GA-8868, Gulf General Atomic, September 1969.

9-4. Sandefur, N. L., J. S. Steibel, and R. J. Grenda, "EMF Drift of Chromel/Alumel and W-3% Re/W-25% Re Thermocouples Measured In-Pile to High Neutron Exposures," Gulf General Atomic Report Gulf-GA-A12501, May 24, 1973.

9-5. "HTGR Fuels and Core Development Program Quarterly Progress Report for the Period Ending May 31, 1977," ERDA Report GA-A14418, General Atomic Company, June 1977.

9-6. Wallroth, C. F., et al., "Postirradiation Examination and Evaluation of Peach Bottom Molded Fuel Test Element FTE-18," General Atomic Report GA-A13699, June 1, 1976.

9-7. Schwartz, M. H., "Peach Bottom Core II Physics Analysis," General Atomic unpublished data, November 19, 1975.

9-8. Smith, C. L., "Fuel Particle Behavior Under Normal and Transient Conditions," ERDA Report GA-A12971 (GA-LTR-15), General Atomic Company, October 1, 1974.

9-9. Tokar, M., "Evaluation of High-Temperature Gas-Cooled Reactor Fuel Particle Coating Failure Models and Data," NUREG-0111 (NRC-8), November 1976.

9-10. Scott, C. B., and D. P. Harmon, "Postirradiation Examination of Capsule F-30," General Atomic Report GA-A13208, April 1, 1975.

9-11. Hick, H., et al., "Summary of a Round Table Discussion on Amoeba Mechanisms in Oxide Fuel Particles," Dragon Project Report DP-919, February 1975.

9-12. Lindemer, T. B., and R. L. Pearson, "Kernel Migration for HTGR Fuels from the System Th-U-Pu-C-O-N," J. Am. Ceram. Soc. 60, 5 (1977).

9-13. Lindemer, T. B., and R. A. Olstad, "HTGR Fuel Kernel Migration Data for the Th-U-C-O System as of April 1, 1974," ERDA Report ORNL-TM-4493, Oak Ridge National Laboratory, June 1974.

9-14. Scott, C. B., D. P. Harmon, and J. F. Holzgraf, "Postirradiation Examination of Capsules P13R and P13S," ERDA Report GA-A13827, General Atomic Company, October 8, 1976.

9-15. General Atomic Notebook, unpublished data.

9-16. Kaae, J. L., "Mechanical Properties of Isotropic Pyrolytic Carbons," J. Nucl. Mater. 46, 121 (1973).

9-17. Kaae, J. L., "The Effect of Annealing on the Microstructures and the Mechanical Properties of Poorly Crystalline Isotropic Pyrolytic Carbons," Carbon 10, 691 (1972).

9-18. Stevens, D. W., "Annealing of Isotropic Pyrolytic Carbons Formed Below 1500°C," Gulf General Atomic Report GA-10448, June 13, 1971.

9-19. "HTGR Fuel Product Specification," General Atomic Report GA-A13464, January 1976.

9-20. Smith, C. L., "Migration of ThO_2 Kernels Under the Influence of a Temperature Gradient," General Atomic Report GA-A14058, November 1976.

9-21. Smith, C. L., "SiC-Fission Product Reactions in TRISO UC_2 and WAR UC_xO_y Fissile Fuel, Part 1: Kinetics of Reactions in a Thermal Gradient," General Atomic Report GA-A14313, to be published.

11. GRAPHITE DEVELOPMENT
189a NO. 00552

Graphites that will satisfy the requirements for LHTGR components are being developed and evaluated. Characterization and irradiation studies to establish reference and backup grades for fuel elements, core support components, and side reflectors are in progress. Support technology is being developed to provide data for design and safety analyses. Development of control materials is included in the long-range program but no work is being funded during FY-77.

Preliminary characterization of graphites for core support structures and side reflectors is under way. This work was aimed at completing a preliminary characterization data set, which will permit the selection of reference grades for these components. Upon selection of the reference grades, an in-depth characterization program will commence. The in-depth study will cover variations of properties within logs, from log to log within lots, and from lot to lot.

The irradiation work has been suspended during FY-77 due to the temporary closing of the Oak Ridge Reactor (ORR). Capsule OG-5 will be assembled during FY-77 for insertion in the ORR in early FY-78.

Support technology studies include generic studies of the mechanical behavior of graphites, verification of stress calculation methods, and the effects of oxidation on the strength and integrity of the core and core support blocks.

TASK 100: FABRICATION AND OPERATION OF IRRADIATION CAPSULES

Capsule OG-5

Assembly of capsule OG-5 will be resumed in the final quarter of FY-77 in preparation for insertion in the ORR in FY-78.

TASK 200: GRAPHITE SPECIMEN PREPARATION AND PROPERTY MEASUREMENTS FOR CAPSULE IRRADIATIONS

Capsule OG-5

Specimen preparation for capsule OG-5 is complete, thus completing milestone 3 of Task 11. The principal material will be H-451 graphite from lots 426 (used in capsule OG-3), 440 (different coke blend than lot 426), and 478 (production lot for Fort St. Vrain reload segment).

Dimensional Change of Nuclear Graphites

The irradiation-induced dimensional changes in H-327 and H-451 graphites were reported previously (Ref. 11-1). Design curves of dimensional change were fit through the three-dimensional space of dimensional change, fast neutron fluence, and irradiation temperature. These computer-fit design curves have proven quite satisfactory; however, the statistical uncertainty in the calculated curves has been difficult to establish. Consequently, the code STAT*FIT has been generated to provide function fitting with enhanced statistical capabilities.

Changes in the treatment of the difference between the calculated dimensional change value and the experimentally observed value (residual) at each data point are as follows:

1. If r_i is the residual value at the i^{th} data point (i.e., r_i = data value - value of fitting function), the overall standard deviation of the fit is calculated by the formula

$$S = \left[\sum_{i=1}^{m} r_i^2/(m - n) \right]^{1/2} , \qquad (11\text{-}1)$$

where m is the number of data points and n is the number of coefficients in the fitting function. This is the statistically correct form [the old version used m instead of (m - n) in the denominator].

2. A standard deviation value S_i is calculated at each data point. This value represents the standard deviation of the fitting function f(x) assuming the underlying model (form of the fitting function) is correct. This value is used to calculate lower and upper 95% confidence limits $F(x_i) \pm tS_i$, where t is the upper 97.5 percentile limit of the student's "t" distribution with (m - n) degrees of freedom and x_i is the vector of independent variables at the i^{th} data point.

3. The solution algorithm for the least-squares coefficients has been changed from the Gram-Schmidt orthogonalization procedure in FUNFIT to a direct solution approach based on Householder transformations in the independent variable space.

The STAT*FIT program has been operated and compared to previous computer fits to a constant data bank with excellent results. In addition, estimates of uncertainty in the design curves correlate very well with the raw data. For example, calculated dimensional change for H-451 in the radial direction at 1203 K (930°C) and 8.5 x 10^{25} n/m^2 $(E > 29\ fJ)_{HTGR}$ was -0.716% with 95% confidence limits of -0.61% and -0.75%. All experimentally observed data at these conditions fell within the confidence limits.

The dimensional change caused by neutron irradiation of grade HLM graphite has been estimated for design purposes. The estimate is based upon the behavior observed in H-451 and other nuclear graphites. A polynomial design curve (Eq. 11-2) was derived based on the coefficient of thermal expansion of the HLM graphite:

$$\varepsilon = (C_1 + C_2T + C_3T^2 + C_4T^3 + C_5T^4)\phi$$
$$+ (C_6 + C_7T + C_8T^2 + C_9T^3 + C_{10}T^4)\phi^2$$
$$+ (C_{11} + C_{12}T + C_{13}T^2 + C_{14}T^3 + C_{15}T^4)\phi^3 \qquad (11\text{-}2)$$

where ε is the irradiation-induced strain in percent, T is the irradiation temperature (°C), ϕ is the fast neutron fluence (x 10^{25} n/m^2) (E > 29 fJ)$_{HTGR}$, and the values of C are as follows:

$$C_1 = -0.19966 + 0.26560\ \alpha$$
$$C_2 = -3.2850 \times 10^{-3} - 8.4980 \times 10^{-4}\ \alpha$$
$$C_3 = 1.2940 \times 10^{-5} + 4.6200 \times 10^{-7}\ \alpha$$
$$C_4 = -1.5849 \times 10^{-8} + 8.5200 \times 10^{-10}\ \alpha$$
$$C_5 = 5.4264 \times 10^{-12} - 5.3060 \times 10^{-13}\ \alpha$$
$$C_6 = -3.6691 \times 10^{-1} + 4.8520 \times 10^{-2}\ \alpha$$
$$C_7 = 2.0980 \times 10^{-3} - 2.5498 \times 10^{-4}\ \alpha$$
$$C_8 = -4.0010 \times 10^{-6} + 4.5600 \times 10^{-7}\ \alpha$$
$$C_9 = 2.8737 \times 10^{-9} - 3.2980 \times 10^{-10}\ \alpha$$
$$C_{10} = -6.9838 \times 10^{-13} + 9.2520 \times 10^{-14}\ \alpha$$
$$C_{11} = -8.3248 \times 10^{-4} + 7.9160 \times 10^{-4}\ \alpha$$
$$C_{12} = 3.1936 \times 10^{-5} - 1.0158 \times 10^{-5}\ \alpha$$
$$C_{13} = -1.3160 \times 10^{-7} + 3.2494 \times 10^{-8}\ \alpha$$
$$C_{14} = 1.6506 \times 10^{-10} - 3.3902 \times 10^{-11}\ \alpha$$
$$C_{15} = -5.4538 \times 10^{-14} + 9.2860 \times 10^{-15}\ \alpha$$

In the above, α is the average thermal expansivity between 22° and 500°C (x 10^{-6} $°C^{-1}$).

Coefficients C_1 through C_{15} were calculated for each orientation of HLM graphite from the coefficient of thermal expansivity of the graphite. The coefficients C_1 through C_{15} were then substituted in Eq. 11-2 to generate a design surface in the same manner as done for H-451 and H-327 graphites.

TASK 300: CHARACTERIZATION OF CANDIDATE GRAPHITES FOR PROPERTIES AND PURITY

Replaceable Fuel and Reflector Elements

Continued research and testing of H-327 graphite has generated a larger data base than originally reported for Fort St. Vrain design. Large portions of these additional data have not been reported in the open literature. These data have been assimulated to create a common data base for H-327 design. Previously unpublished data are presented in tabular form.* The H-327 data are summarized by property below.

Bulk Density

The data utilized for design is taken from QA acceptance tests of H-327 graphite logs produced for Fort St. Vrain. Data for Fort St. Vrain reloads are given in Table 11-1. The following data used for design were taken from Table 11-1: $N = 524$, $\bar{X} = 1.77$ Mg/m^3, and $S = 0.02$ Mg/m^3.

Chemical Purity

In addition to the QA acceptance data of Table 11-1, the chemical purity of H-327 production logs was determined by GA. The results of chemical characterization of the graphite are given in Tables 11-2 and 11-3. Quality Assurance data of an order of H-327 graphite for reload 2 are given in Table 11-4. Design data were based on the above data and are given in Table 11-5. Other chemical analysis at GA reported sulfur levels of approximately 1 ppm and a lithium content of <10 ppb for H-327 graphite.

Ultimate Tensile Strength

Most of the strength test results on H-327 graphite have been reported previously. The axial ultimate tensile strength (UTS) results are summarized in Table 11-6 and the radial UTS results are summarized in Table

*Tables appear at the end of Task 11.

11-7. Previously unreported results of characterization of an H-327 log used for a fuel test element are presented in Table 11-8. Quality Assurance acceptance test results for FSV production graphite are listed in Table 11-9.

Elastic Modulus

The elastic modulus data were taken from the same source as the ultimate tensile strength data. The data are summarized in Table 11-10.

Thermal Properties

The thermal expansivity of H-327 graphite has been discussed earlier (Ref. 11-9). Thermal conductivity design data were reported in the reports on the OG-series irradiation capsules.

Side Reflector Graphites

Great Lakes Carbon Corporation's grade HLM, an extruded graphite 1.14 m in diameter by 1.83 m long, is under investigation as a candidate graphite for side reflector blocks. One-half of an HLM log (6484-78) has been characterized and the results reported in Refs. 11-10 and 11-11. This log was a standard GLCC commercial production log. A second "special production" log (6484-148) has been purchased from GLCC and characterization tests have begun. The special log was manufactured under more controlled conditions than the regular commercial grade. The special HLM log is being characterized in the same manner as the first log.

Thermal expansivity measurements on specimens from HLM log 6484-78 have been completed and the results are given in Table 11-11. The mean coefficient of thermal expansion between 295 and 773 K was found to be 2.47 x 10^{-6} K^{-1} in the axial orientation and 2.85 x 10^{-6} K^{-1} in the radial direction.

The ultimate tensile, flexural, and compressive strengths of the special HLM log (6484-148) have been determined. The data are given in Tables 11-12 through 11-14. Comparison of the two HLM logs at the axial midlength center location revealed that the special log (6484-148) was stronger in tension (10.4 versus 6.8 MPa), bend (19.1 versus 13.8 MPa), and compression (42.7 versus 35.3 MPa). The special log was generally stronger at all locations tested.

Core Support Floor Graphites

Union Carbide's (UC) grade PGX is under investigation as a candidate graphite for core support floor blocks. Grade PGX is a molded graphite 1.14 m in diameter by 1.83 m long. Characterization results have been reported for logs 6484-112 and 6484-138 (Refs. 11-10 and 11-11).

Measurements of compressive stress-strain properties have been completed on log 6484-138. The ultimate compressive strength of log 6484-138 was slightly lower than measured on the previous log 6484-112. Test data are reported in Table 11-15.

Thermal conductivity values measured from log 6484-112 are given in Table 11-16. The mean values of the room temperature thermal conductivity at the midlength center of the PGX log were 87 W/m-K axially and 94 W/m-K in the radial direction.

Additional data on PGX graphite were made available by UC. The data were taken from many logs (billets) of varying size; however, the range and standard deviation reported for some property values were useful in evaluation of GA characterization data. The UC data are presented in Table 11-17.

Core Support Post and Seat Graphites

Stackpole Carbon's (SC) grade 2020 and GLCC's grade H-440N are candidate materials for core support post and seat components. Grades 2020 and

H-440N are medium-grained isostatically molded graphites. Grade 2020 is manufactured as logs 254 mm in diameter by 1.83 m long and GLCC has the capability of producing logs of the same size. Grade 2020 is the prime candidate at this time and, therefore, is receiving more attention. The first prototype log of grade H-440N was found to be weak. Work has been suspended on H-440N until additional material of higher strength is delivered.

Characterization results of 2020 graphite logs 6799-00, 6484-110, 6484-137, 6484-139, and 6484-140 have been reported in part (Refs. 11-10 and 11-12). Thermal expansivity data from log 6484-110 are given in Table 11-18. The mean coefficient of thermal expansion between 295 and 773 K was found to be 3.2×10^{-6} K^{-1} radially and 3.4×10^{-6} K^{-1} in the axial direction of 2020 graphite.

In addition to tensile and flexural strengths reported earlier (Ref. 11-10), the ultimate compressive strengths (UCS) were measured for 2020 logs 6484-139 and 6484-140. The mean compressive strength of log 6484-139 was approximately 72 MPa, slightly lower than the UCS of 78 MPa measured on log 6484-110. The UCS measured on log 6484-140 was approximately 82 MPa, slightly higher than the other values. Test data are given in Tables 11-19 and 11-20.

The purity data of 2020 logs 6484-139 and 6484-140 are given in Tables 11-21 through 11-23.

TASK 400: FRACTURE MECHANICS

No work funded under this subtask in FY-77.

TASK 500: FATIGUE BEHAVIOR OF GRAPHITE

Fatigue testing of irradiated H-451 graphite was completed with the testing of axial specimens of H-451 graphite irradiated successively in

capsules OG-1, OG-2, and OG-3 to 8.5 x 10^{25} n/m^2 $(E > 29\ fJ)_{HTGR}$ at 1173 to 1243 K (900° to 970°C).

The specimens were cylinders measuring 5.1 mm in diameter by 11.2 mm long and were tested at ambient temperature in uniaxial loading. Ten specimens were tensile tested to failure in the fatigue machine and 32 were fatigue tested at 7 Hz using a reversed stress (tension-compression) cycle (R = -1). Eight specimens were tested at each of four stress levels until they failed or reached 100,000 cycles without failure.

The tensile test data and fatigue data are listed in Tables 11-24 and 11-25. The corresponding S-N plot (logarithm of the maximum stress versus the logarithm of the number of cycles to failure) is shown in Fig. 11-1. Run-outs beyond 100,000 cycles are shown as open circles. Tensile data and first cycle failures are plotted at N = 0.25. The stresses are normalized by dividing by the mean (irradiated) tensile strength. The data were analyzed statistically and lower tolerance limits are included in the plot.

The fatigue stress limits for survival to 100,000 cycles, normalized by dividing by the mean unirradiated tensile strength, are plotted against the fast neutron fluence in Fig. 11-2 for H-451 graphite irradiated in the OG-series capsules. Both the stress limits for 50% specimen survival and the 99/95 lower tolerance limits are included in the plot. The median survival stress shows a steady increase with fluence which results both from the irradiation-induced increase in tensile strength and the irradiation-induced reduction in the downward slope of the S-N curve. The lower tolerance limit also increases with fluence except for the highest fluence point, where increased data scatter reduces the limit. The increased scatter may be caused by slight warpage of the highly irradiated specimens, which interferes with accurate uniaxial alignment.

The improved fatigue resistance of the irradiated specimens may be caused by the reduction in the mobility of basal dislocations. Fatigue in graphite has many points in common with fatigue in metals, and it seems probable that the fatigue crack advance involves limited plastic flow at

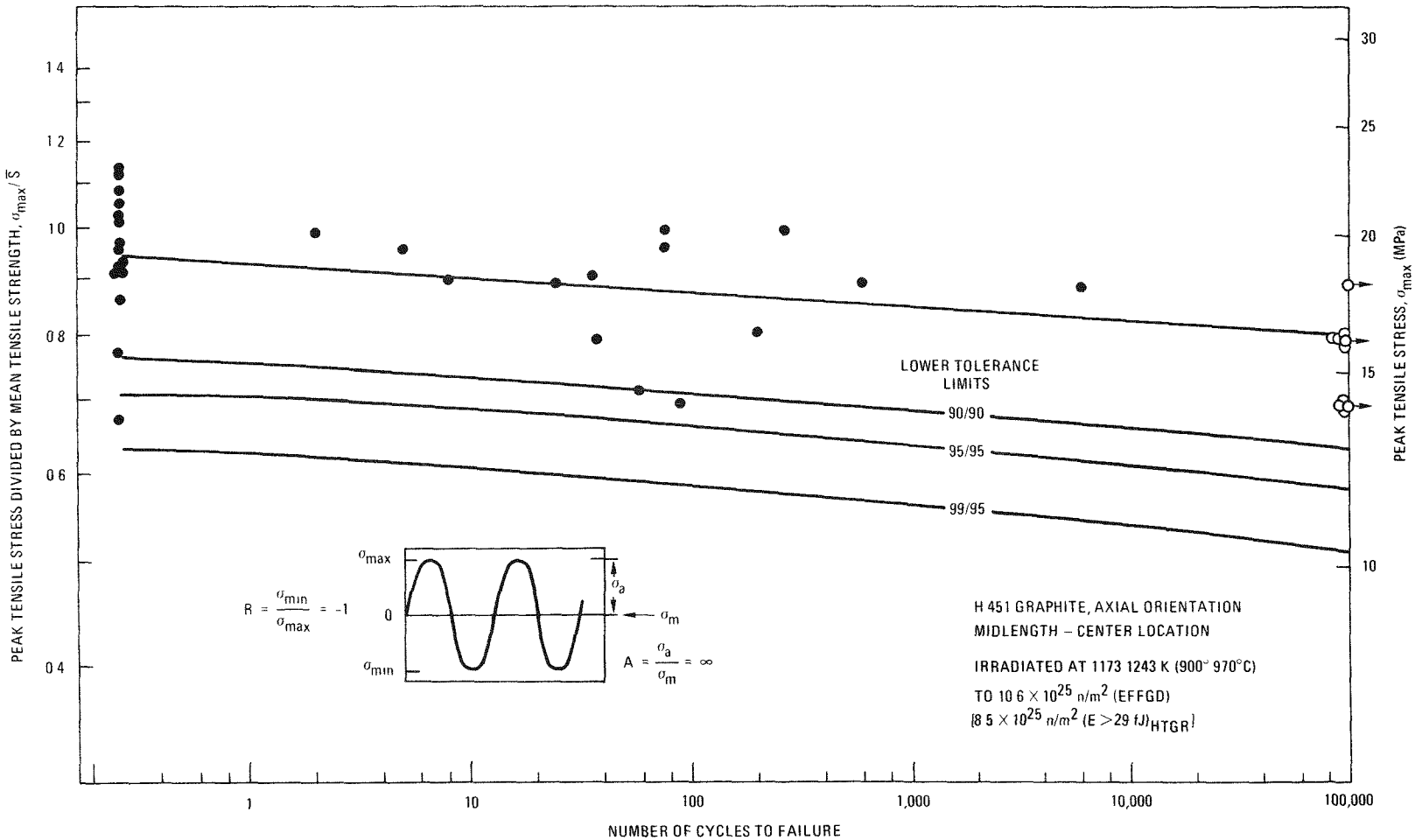

Fig. 11-1. Ambient temperature fatigue test data for H-451 graphite, axial orientation, irradiated to 8.5 x 10^{25} n/m^2 (E > 29 fJ)$_{HTGR}$ at 1173 to 1243 K (900° to 970°C). Log-log plot of normalized peak stress versus the number of cycles to failure, with stress ratio, R = -1. Lower x/y tolerance limits represent the limits above which x% of all observations would fall, with y% confidence. Open circles represent run-outs.

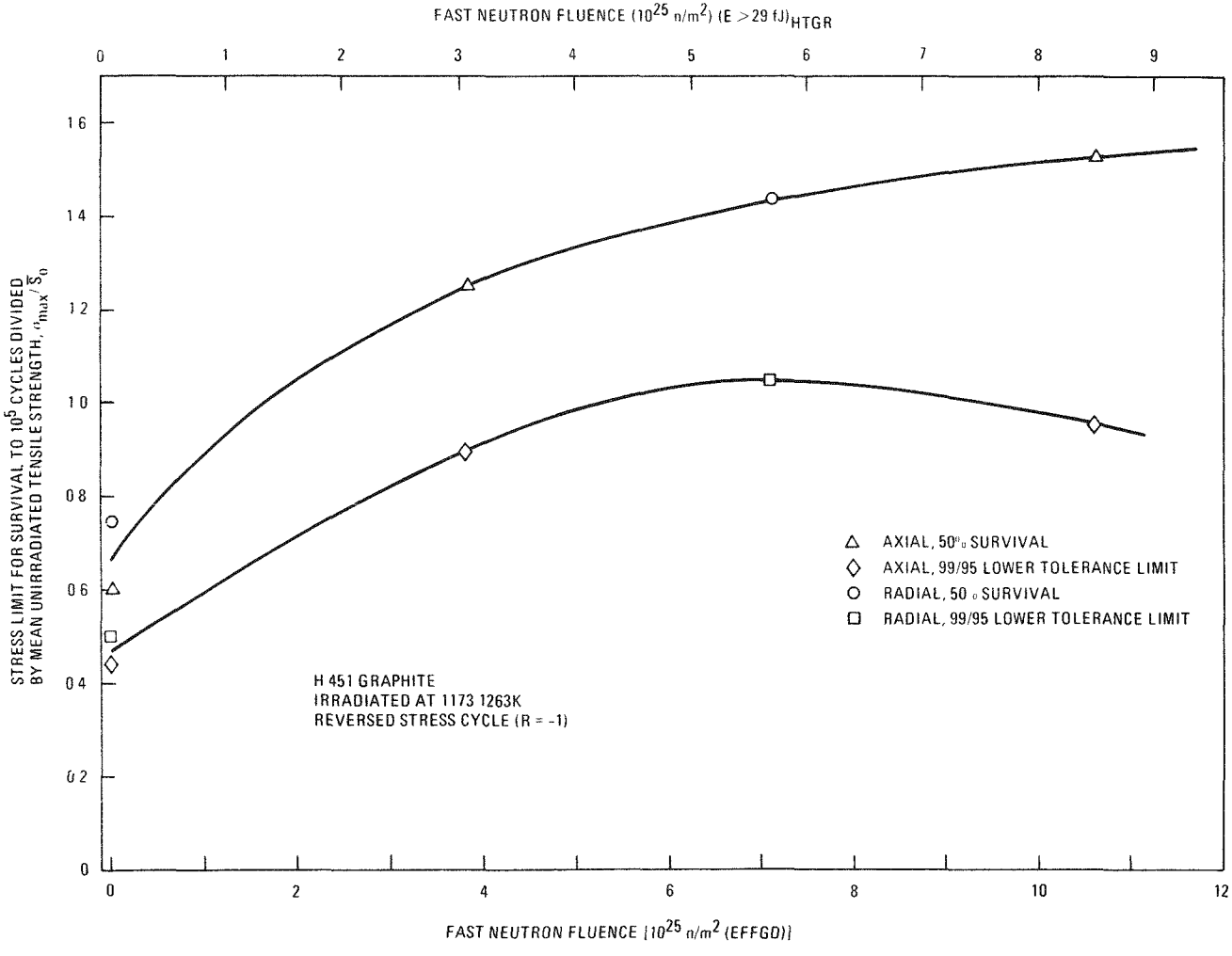

Fig. 11-2. Fatigue stress limits for survival of H-451 graphite to 10^5 cycles, normalized to the unirradiated tensile strength, versus the fast neutron fluence at an irradiation temperature of 1173 to 1263 K (900° to 990°C)

the crack tip. A process such as irradiation, which reduces dislocation mobility, would be expected to improve fatigue resistance.

To conclude the work on H-451 graphite, a series of tests is being run on unirradiated radial specimens. The specimens measure 12.7 mm in diameter by 25.4 mm long. The first set of tests was made in a tension-compression cycle (R = -1). The baseline tensile strengths (measured in the fatigue machine) are shown in Table 11-26 and the fatigue data are given in Table 11-27. The S-N curve is given in Fig. 11-3. The data show a somewhat higher fatigue stress limit than the corresponding tests on axial material (Ref. 11-13) (75% of the mean tensile strength for 50% survival to 100,000 cycles, compared with 60% of the mean tensile strength for axial specimens). Further tests are in progress.

TASK 600: RDT AND ASTM GRAPHITE STANDARDS

This section concerns the writing of RDT graphite standards for HTGR graphite component materials. ASTM standard work on nuclear graphite will be monitored and progress will be reported. The ASTM work is by industry concensus and as such is not a part of the Task 11 scope.

RDT Standard E6-1

Standard E6-1 (draft 5) on core graphites for LHTGRs has been rewritten after consultation with the ERDA Tech. Lead. A final draft was submitted for approval. This completes milestone 11 of Task 11.

ASTM Standard C781-00 (information only, not part of work scope)

ASTM Standard C781-00, which is a recommended practice for testing nuclear graphite, has been approved by full ASTM society vote and will be published in 1978.

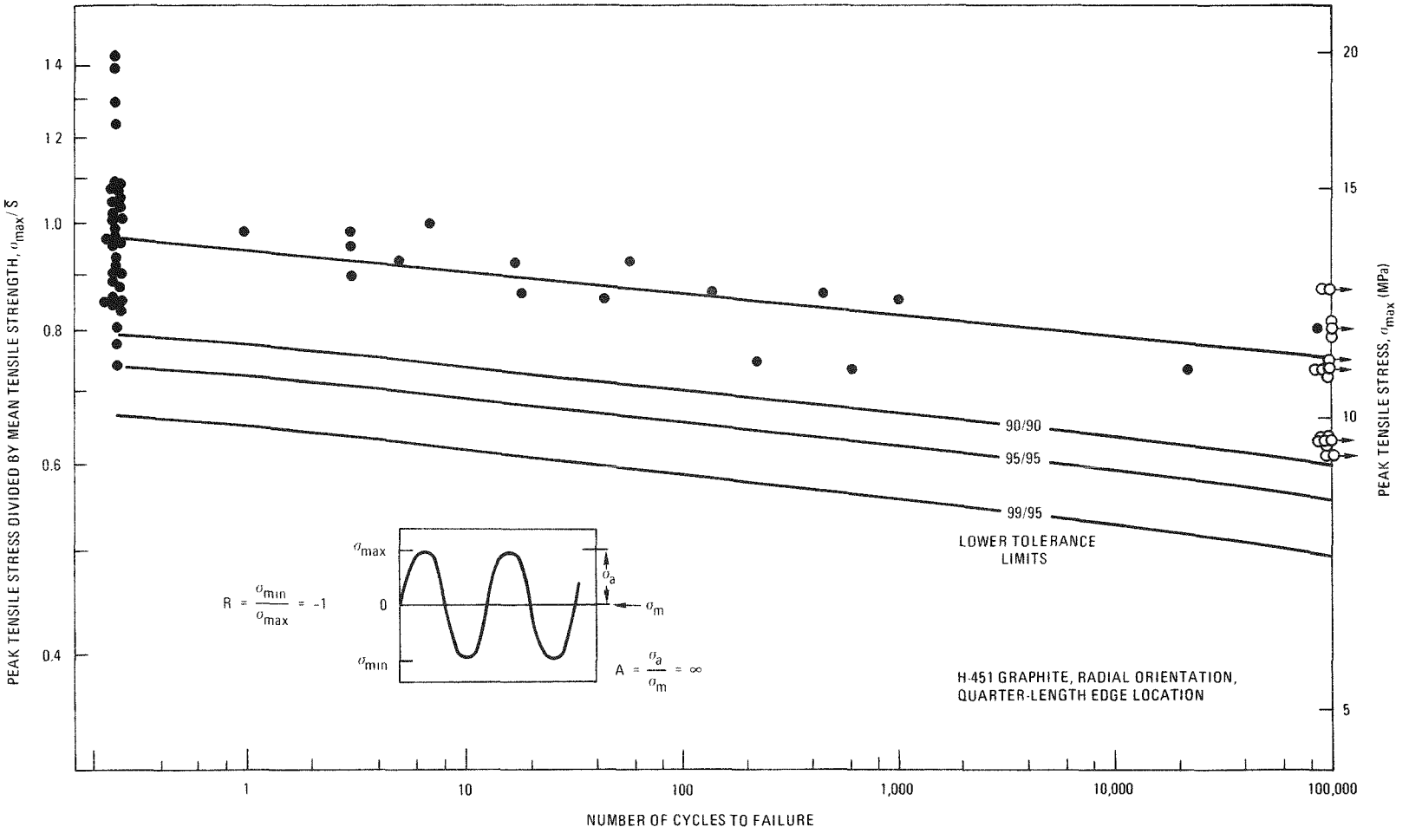

Fig. 11-3. Ambient temperature fatigue test data for unirradiated H-451 graphite, radial orientation. Log-log plot of normalized peak stress versus the number of cycles to failure, with stress ratio, R = -1. Lower x/y tolerance limits represent the limits above which x% of all observations would fall, with y% confidence. Open circles represent run-outs.

TASK 700: IRRADIATION-INDUCED CREEP IN GRAPHITE

This work is funded at ORNL.

TASK 800: STRUCTURAL INTEGRITY OF GRAPHITE BLOCKS

A program is under way to verify the accuracy of structural design methods and the data used to predict deformation and stresses in the core graphite blocks. Current work is concerned with the evaluation of fuel test elements from Peach Bottom. The results of primary loading, strip cutting, and ring closure tests are being analyzed. In conjunction with this work, preliminary design criteria have been postulated. These design criteria for graphite will be the basis for future work to verify and confirm them as realistic criteria for designing the HTGR fuel elements. This work is being coordinated with similar work for core support graphite being carried out by the Joint ACI-ASME Working Group on Core Support Structure. The work of the ACI-ASME committee is by industry concensus. GA is a member of this group and participates in the work of the committee.

The failure criteria described below, when combined with appropriate safety factors in the final design criteria, are intended to prevent structural failure due to overloading of the replaceable fuel and reflector elements.

Preliminary Multiaxial Failure Criteria

A multiaxial failure criterion, which is the basis for the effective stress definition, is defined. The maximum effective stress σ_{eff} will be computed for test, normal, upset, emergency, and faulted loads and compared to the allowable tensile stress. Mechanical replica tests are also allowed to determine the strength limits for nonuniformly stressed components.

Effective Stress

The effective stress, σ_{eff}, which provides a measure of the damage and failure of graphite components under multiaxially stressed conditions, is

defined by a piece-wise continuous function;

$$\frac{\sigma_{eff}^2}{2E_o W_1} = \frac{W(\sigma_{ij})}{W_1} \quad \text{for } I_1 \geq 0 \text{ and } I_2 \geq 0$$

$$= \frac{W(\sigma_{ij})}{W_2} \quad \text{for } I_1 \leq 0 \text{ and } I_2 \geq 0$$

$$= \frac{W(\sigma_{ij}) + f(\sigma_{ij})}{W_3} \quad \text{for } I_2 < 0 \quad , \tag{11-3}$$

where σ_{ij} is the stress tensor in a Cartesian coordinate system x_i; i,j = 1,2,3; x_3 is assumed to be the anisotropic axis of a transversely isotropic graphite; $\sqrt{2E_o W_1}$ and $\sqrt{2E_o W_2}$ are the failure stresses under uniaxial tensile and compressive loadings, respectively; and

$$I_1 = \sigma_{11} + \sigma_{22} + m\sigma_{33} \quad ,$$

$$I_2 = \sigma_{11}\sigma_{22} + m\sigma_{33}\,(\sigma_{11} + \sigma_{22}) - \sigma_{12}^2 - m^*(\sigma_{13}^2 + \sigma_{23}^2) \quad ;$$

$$W = [I_1^2 - 2(1 + \nu)\, I_2]/2E \quad ;$$

$$f = \left[\nu\left(1 - \frac{W_3}{\sqrt{W_1 W_2}}\right) I_1^2 + \frac{1}{2}\left(\frac{W_3}{W_1} - \frac{W_3}{W_2}\right) I_1 \sqrt{\frac{4EW}{1 + \nu} - \frac{1 - \nu}{1 + \nu} I_1^2}\right] \Bigg/ 2E \quad ;$$

where E and ν are Young's modulus and Poisson's ratio measured in the isotropic plane, m and m* are material constants, and $W_3 = 2(1 + \nu)\, W_1 W_2\, (W_1 + W_2 + 2\nu\sqrt{W_1 W_2})^{-1}$.

The failure surface can be obtained by equating the effective stress to the uniaxial tensile failure stress, $\sqrt{2E_o W_1}$. The effective stress is defined as a piece-wise continuous function in terms of the invariants I_1 and I_2, which allows more flexibility in fitting experimental data than

would be allowed by a smooth quadratic function. Because the strain energy, W, is used, the inverse proportionality between the strength and the square root of Young's modulus is assumed.

Fatigue Limit

The fatigue limit is established by the S - log N relation under uniaxial loading conditions (S is the applied stress and N is the fatigue life). The effective stress defined in the previous section can be used to replace the uniaxial tensile stress S in the S - log N relation to define the fatigue limit for multiaxial stressed components. Miner's rule can be applied to estimate the cumulative damage to the specimen under various loading conditions.

Strength Limits Under Nonuniform Stress Conditions

The failure criteria equating the maximum effective stress calculated by the linear elasticity theory to the uniaxial tensile strength is usually too conservative for components under nonuniform stresses. In such cases, the fracture strength of a component may also be obtained by testing a true replica under a stress distribution simulating the service conditions. This completes milestone 13 of Task 11.

TASK 900: CONTROL MATERIALS DEVELOPMENT

No work funded under this subtask in FY-77.

TASK 1000: GRAPHITE OXIDATION STUDIES

Summary

Work is reported on the oxidation rates of PGX and Stackpole (SC) 2020 graphites and on the determination of oxidation profiles in H-451 graphite. Although this work is incomplete, an interim report is provided for preliminary design calculations. The initial tests indicate the rate of oxidation of SC 2020 graphite is about three times higher than the rate of H-451

graphite. The oxidation kinetics of H-451 graphite are well characterized (Refs. 11-10 and 11-14). The oxidation rate of PGX is greatly enhanced by its high impurity content and it is about 1000 times more reactive than H-451. The measured oxidation profiles of H-451 graphite closely matched predicted profiles.

Rate Constants (PGX and SC 2020)

Introduction

A study is under way to identify the rates of oxidation of PGX and SC 2020 graphites when exposed to steam-helium mixtures at high temperatures. The experimental program is divided into three phases: (1) identification of the intrinsic chemical characteristics of each graphite type through investigations conducted in the chemical-kinetics-limited temperature regime, (2) identification of mass transport parameters through experimentation in the in-pore diffusion temperature region utilizing the developed chemical-kinetics-limited rate parameters, and (3) oxidation of large samples of sufficient size to minimize extrapolation to reactor geometries. Preliminary data from phase 1 for PGX and SC 2020 and from phase 2 for H-451 graphite are reported herein. The preliminary data are required to provide approximations of the rate of oxidation and of the diffusion parameter for early design considerations. Updating of these preliminary results will follow.

Reaction Rate of SC 2020

Stackpole 2020 is a fine-grain, isostatically molded artificial graphite made by Stackpole Carbon Company. Stackpole 2020 is relatively uniform (compared to PGX) in many of its physical and chemical properties. The tentative model recommended for rate of oxidation calculations of SC 2020 is the same expression as that used for H-451 graphite oxidation (Ref. 11-14) multiplied by a factor of three.

The rate equation for thermally induced oxidation is:

$$R(s^{-1}) = \frac{F_b K_1 P_{H_2O}}{1 + K_2 P_{H_2}^{0.75} + K_3 P_{H_2O}} \quad . \qquad (11\text{-}4)$$

The recommended Langmuir-Hinshelwood constants for this equation are:

$K_1 = 0.33 \exp(-195000/RT)$ $\quad (s\text{-}Pa^{-1})$

$K_2 = 7.9 \times 10^{-8} \exp(119700/RT)$ $\quad (Pa^{-0.75})$

$K_3 = 1.3 \times 10^{-9} \exp(131400/RT)$ $\quad (Pa^{-1})$

P_{H_2O}, P_{H_2} = partial pressure of steam and hydrogen, respectively $\quad (Pa)$

It is suggested that use be made of the generalized burnoff factor as given by the OXIDE code (Ref. 11-15):

$$F_b = 0.447 + 0.8094b - 0.3221b^2 + 0.0681b^3 - 0.00613b^4$$
$$+ 12.32 \times 10^{-6} b^5 + 2.89 \times 10^{-5} b^6 - 1.15 \times 10^{-6} b^7 \quad , \qquad (11\text{-}5)$$

where b is the percent burnoff. In Fig. 11-4, the recommended chemical parameters for SC 2020 are compared with the current data base at 1% burnoff. Using an approximation of the diffusion parameters, m, or torosity/porosity of 0.003 (see discussion under Oxidation Profile of H-451 Graphite) and solving the differential expression for transport into a solid cylinder (Refs. 11-16 and 11-17), a theoretical in-pore diffusion controlled rate was calculated for 1% burnoff (dashed line). As the data base is expanded, improved correlation is anticipated.

Reaction Rate for PGX Graphite

Grade PGX graphite is a molded artificial graphite produced in large sizes by Union Carbide Company. The physical properties and chemical

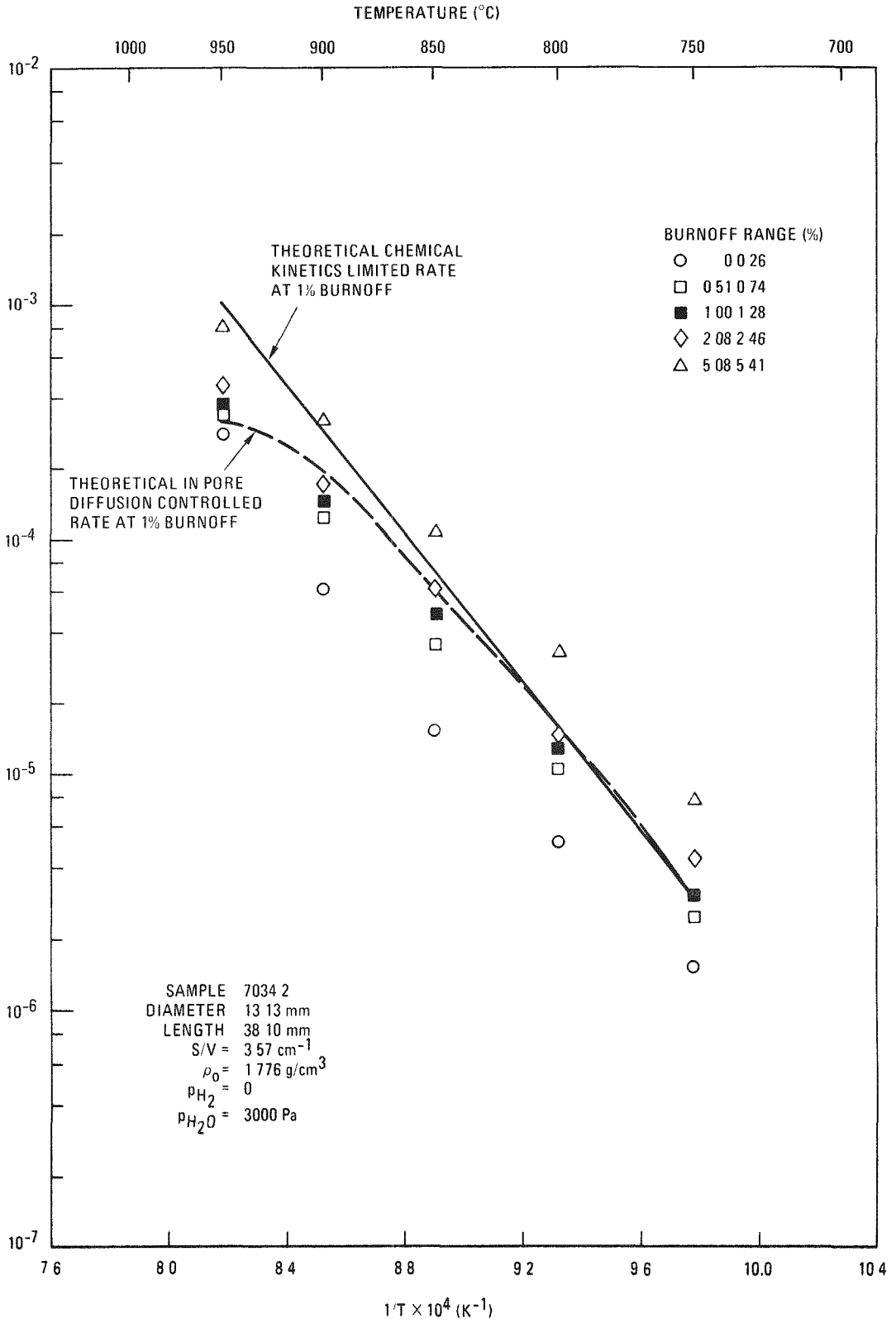

Fig. 11-4. Steam oxidation rate of Stackpole 2020 graphite

impurities vary significantly with respect to position in the log. Samples examined in this preliminary study of the rate of oxidation were obtained from a central region in both the axial and radial directions. As an interim measure, PGX is assumed to obey the Langmuir-Hinshelwood type equation, used for H-451 graphite (Eq. 11-4), multiplied by a factor of 1000. The recommended constants are as follows:

$$K_1 = 1.1 \times 10^{2} \exp(-195000/RT) \qquad (s\text{-}Pa^{-1})$$

$$K_2 = 7.9 \times 10^{-8} \exp(119700/RT) \qquad (Pa^{-0.75})$$

$$K_3 = 1.3 \times 10^{-9} \exp(131400/RT) \qquad (Pa^{-1})$$

$$F_b = \text{same as Eq. 11-5}$$

The calculated reaction rates using the recommended constants are compared with experimental results given in Fig. 11-5. At low temperatures the agreement with the raw data is fair. At temperatures >1130 K the data deviate from the predicted line. PGX graphite is so reactive that mass transport across the diffuse layer (i.e., zone 3) is apparently controlling and causing the deviation. Among the potential causes for this high chemical activity is the high impurity content of PGX. The spectrochemical analysis of the log of PGX from which these samples were taken indicated levels of 40 to 400 ppm Fe (Ref. 11-10). Because of its high impurity content, it must be recognized that the chemical reactivity of PGX may not follow the traditional Langmuir-Hinshelwood reaction kinetics model. This is because the catalyzed reactions are controlled by the chemical state of the catalytic impurities (for example, Fe, Fe_3C, FeO, Fe_2O_3) which in turn is controlled by temperature and the oxidizing potential of the gaseous atmosphere and carbon environment. Consequently, the recommended rate equation is regarded as preliminary and will be updated in the near future.

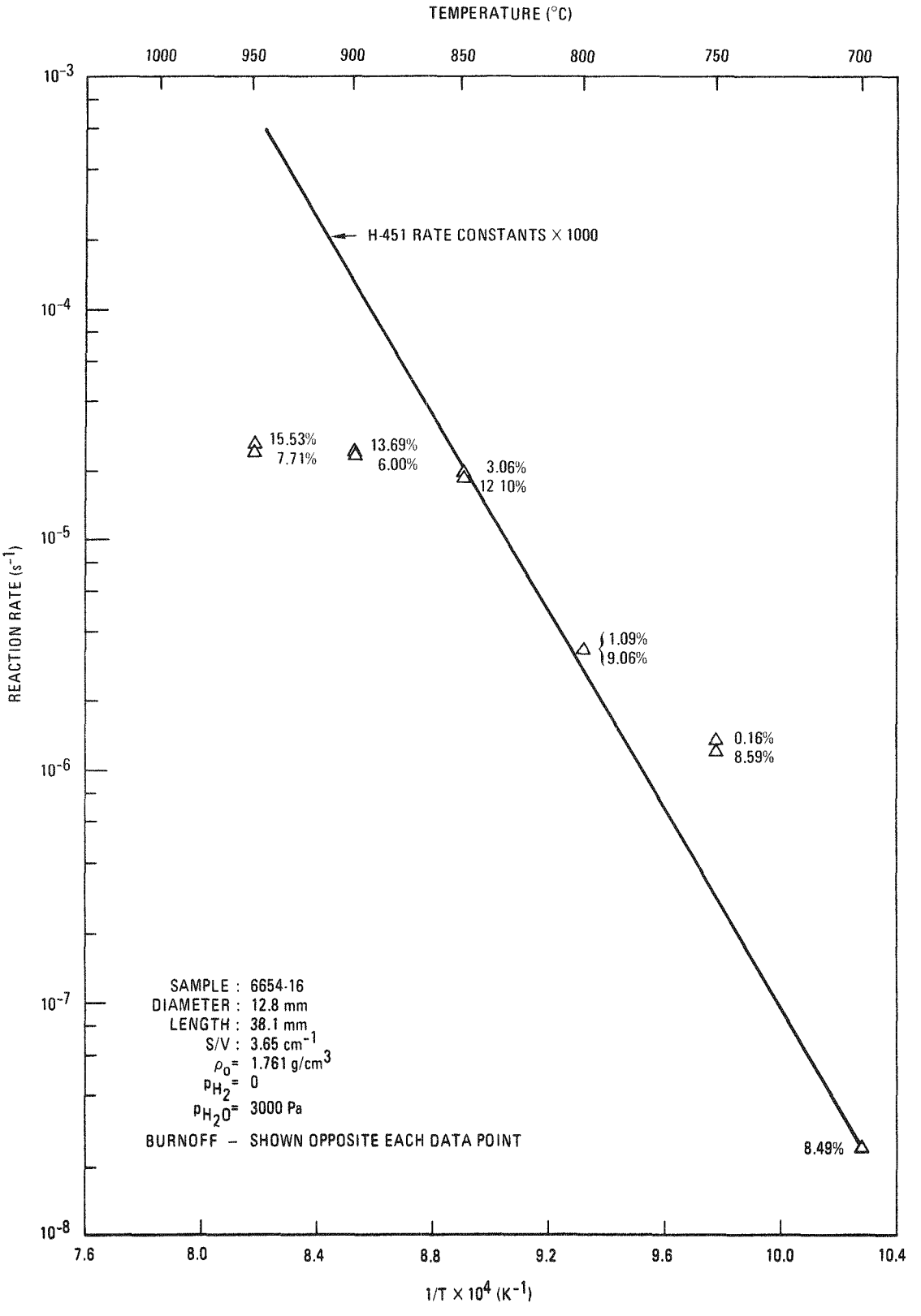

Fig. 11-5. Steam oxidation rate of PGX graphite versus reciprocal temperature

Oxidation Profile of H-451 Graphite

Because of the porous nature of graphite, the rate of oxidation by steam is dependent upon in-pore diffusion of the reactants and their products and also dependent upon the intrinsic chemical reactivity of the graphite. The dependence on diffusion and chemical activity leads to concentration gradients of the reactants and products, which ultimately lead to burnoff gradients.

To estimate the profiles of the burnoff gradients, intrinsic mass transport parameters of graphite must be correlated with the constituents of the oxidizing atmosphere. The theory of diffusion-controlled reactions has been treated by Thiele, Wheeler (Refs. 11-16, 11-17), and others. Application of this theory to graphites was proposed notably by Wicke and later by Dodson (Ref. 11-18). The basis of these proposed theories is that in a volume element of material, the difference in rates of diffusion inward and outward from the volume element is equal to the rate of oxidation. A general solution given by Dodson for this relationship is:

$$\frac{d^2c}{dx^2} = \frac{K_v}{Z} \cdot C \quad , \tag{11-6}$$

where K_v = intrinsic volumetric rate constant,
Z = effective in-pore diffusion coefficient,
C = concentration of oxidizing species,
x = distance.

For convenience, early in the theoretical work Dodson introduces:

$$\frac{Z}{K_v} = L^2 \quad , \tag{11-7}$$

where L is the diffusion length or depth of oxidation and Z is given by $mD_{1,2}$, where $D_{1,2}$ is the ordinary gas phase diffusion coefficient for water

in He and m is a correction term for the porous medium, or the torosity/porosity ratio, ε/q^2.

The H-451 samples tested were cylindrical in shape. Dodson's specific solution for this configuration is:

$$\frac{d^2C}{dr^2} + 1/r \frac{dC}{dr} - \frac{C}{L^2} = 0 \quad . \tag{11-8}$$

The boundary conditions are $C - C_o$ at $r = r_o$, and $dC/dr = 0$ at $r = 0$; i.e., the diffuse layer between the sample and the bulk phase is assumed to be nonlimiting. The solution in terms of the modified Bessel function of zero order is:

$$C = C_o \frac{I_o(r/L)}{I_o(r_o/L)} \quad . \tag{11-9}$$

Assuming that the chemical-kinetics-limited rate constants hold, rates of reaction were calculated for various depths using partial pressure of water as given by the solution for C/C_o (Eq. 11-9). In calculations of L (or $\sqrt{K_v/m\ D_{1,2}}$), K_v was obtained from the Langmuir-Hinshelwood rate equation and rate constants determined and reported previously (Ref. 11-14). A range of values for the transport parameter, m, was tried to obtain the best data fit. A value of m = 0.003 was found to correlate the oxidation profile quite well; this is the same value recently determined at GA for ATJ graphite (Ref. 11-19). In addition, a value of 0.004 for m was determined for H-451 graphite in a separate experiment on fuel hydrolysis (Ref. 11-11). Burnoffs were calculated by integrating reaction rates over the time of oxidation.

Experimentally, burnoff was determined from density measurements. The density values were obtained by placing the cylindrical specimen in a high-speed precision lathe and cutting the sample at fixed depths and length. The fine granules obtained by this cutting technique was vacuumed into filter paper and weighed. From the volume and weight of each cut, density

profiles were determined. The density profiles were then converted to burnoff profiles. In Fig. 11-6, the calculated burnoffs obtained by the method described above are compared with the burnoffs determined by the lathe technique. The data and theoretical estimate correlate quite well, indicating the use of the value 0.003 for oxidized H-451 graphite is correct.

Oxidation Profile Test

A test plan, "Test Plan for Oxidation/Strength Tests on 2020 and H-451 Graphite" has been written and the equipment is available to commence testing. This completes milestone 16 of Task 11.

REFERENCES

11-1. Price, R. J., and L. A. Beavan, "Final Report on Graphite Irradiation Test OG-3," ERDA Report GA-A14211, General Atomic Company, January 1977.

11-2. Engle, G. B., et al., "Development Status of Near-Isotropic Graphites for Large HTGRs," ERDA Report GA-A12944, General Atomic Company, June 1, 1974.

11-3. "Public Service Company of Colorado 330-MW(e) High-Temperature Gas-Cooled Reactor Research and Development Program Quarterly Progress Report for the Period Ending September 30, 1969," USAEC Report GA-9720, Gulf General Atomic, October 29, 1969.

11-4. "Public Service Company of Colorado 330-MW(e) High-Temperature Gas-Cooled Reactor Research and Development Program Quarterly Progress Report for the Period Ending December 31, 1969," USAEC Report GA-9875, Gulf General Atomic, January 30, 1970.

11-5. "Public Service Company of Colorado 330-MW(e) High-Temperature Gas-Cooled Reactor Research and Development Program Quarterly Progress Report for the Period Ending March 31, 1970," USAEC Report GA-10010, Gulf General Atomic, April 30, 1970.

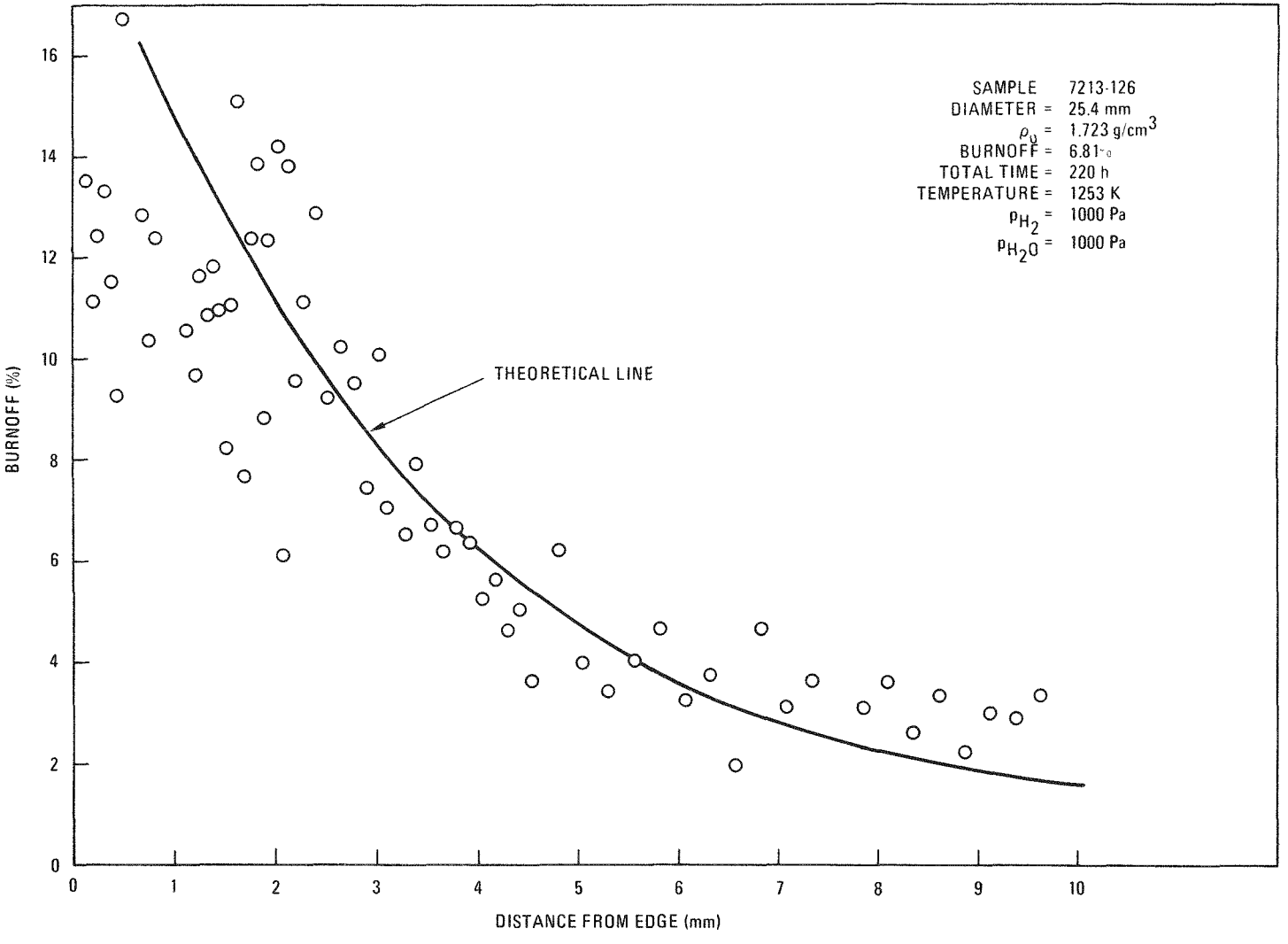

Fig. 11-6. Oxidation profile of H-451 graphite

11-6. "Public Service Company of Colorado 330-MW(e) High-Temperature Gas-Cooled Reactor Research and Development Program Quarterly Progress Report for the Period Ending September 30, 1970," USAEC Report GA-10313, Gulf General Atomic, October 30, 1970.

11-7. "Public Service Company of Colorado 330-MW(e) High-Temperature Gas-Cooled Reactor Research and Development Program Quarterly Progress Report for the Period Ending March 31, 1971," USAEC Report GA-10560, Gulf General Atomic, April 30, 1971.

11-8. Price, R. J., and L. A. Beavan, "Final Report on Graphite Irradiation Test OG-2," ERDA Report GA-A13556, General Atomic Company, December 15, 1975.

11-9. Price, R. J., "Strength of Graphite Webs in Fort St. Vrain Fuel Elements," General Atomic Report GA-A14201, November 1976.

11-10. "HTGR Fuels and Core Development Program Quarterly Progress Report for the Period Ending May 31, 1977," ERDA Report GA-A14418, General Atomic Company, May 1977.

11-11. "HTGR Fuels and Core Development Program Quarterly Progress Report for the Period Ending November 30, 1976," ERDA Report GA-A14180, General Atomic Company, November 1976.

11-12. Engle, G. B., "Properties of Unirradiated HTGR Core Support and Permanent Side Reflector Graphites: PGX, HLM, 2020, and H-440N," ERDA Report GA-A14328, General Atomic Company, May 1977.

11-13. "HTGR Fuels and Core Development Program Quarterly Progress Report for the Period Ending November 30, 1975," ERDA Report GA-A13737, General Atomic Company, December 31, 1975.

11-14. "HTGR Fuels and Core Development Program Quarterly Progress Report for the Period Ending August 31, 1976," ERDA Report GA-A14046, General Atomic Company, September 24, 1976.

11-15. Peroomian, M. B., A. W. Barsell, and J. C. Saeger, "OXIDE-3: A Computer Code for Analysis of HTGR Steam or Air Ingress Accidents," General Atomic Report GA-A12493, (GA-LTR-7), January 15, 1974.

11-16. Thiele, E. W., "Relation Between Catalytic Activity and Size of Particle," Ind. Eng. Chem. 31, (7) 916 (1936).

11-17. Wheeler, A., "Reaction Rates and Selectivity in Catalyst Pores," in Adv. In Catalysis, Vol. III, Academic Press, New York, 1951.

11-18. Dodson, M. H., "The Depth of Oxidation of Graphite: A Theoretical Approach," UKAEA Development and Engineering Report 148 (CA), 1960.

11-19. Burnette, R. D., et al., "Studies of the Rate of Oxidation of ATJ Graphite by Steam" paper presented at the 13th Biennial Carbon Conference, Irvine, California, July 18, 1977.

TABLE 11-1
PROPERTIES OF H-327 GRAPHITE, FORT ST. VRAIN RELOAD 1
[Density (Mg/m^3), tensile strength (psi), impurity content (ppm)]

SERIAL NUMBER	FURNACE RUN	GRADE	LOG LOCATION	DENSITY	RESISTIVITY	TENSILE STRENGTH	ASH CONTENT	BORON CONTENT	IRON CONTENT	VANADIUM CONTENT	TITANIUM CONTENT
10.	2504	A	22.3	1.80	18.F	1415.	0.	.0	.0	.0	.0
114.	2504	A	10.2	1.75	17.3	2139.	0.	.0	.0	.0	.0
119.	2504	A	23.1	1.79	17.4	2065.	60.	.0	.0	.0	.0
121.	2504	A	16.1	1.73	18.7	1947.	0.	.0	.0	.0	.0
266.	2504	A	15.1	1.80	17.0	1212.	33.	.7	.0	.0	.0
318.	3215	A	15.2	1.73	15.4	2101.	0.	.0	.0	.0	.0
356.	3215	A	11.1	1.76	10.2	1838.	0.	.0	.0	.0	.0
435.	2504	A	21.1	1.77	17.3	1443.	90.	.0	.0	.0	.0
460.	2504	A	18.2	1.80	17.2	1756.	0.	.0	.0	.0	.0
469.	2504	A	15.2	1.80	18.5	2105.	0.	.0	.0	.0	.0
473.	2504	A	20.3	1.81	17.9	1718.	217.	.4	.0	.0	.0
492.	2504	A	21.2	1.80	18.5	1528.	0.	.0	.0	.0	.0
519.	3215	A	8.2	1.78	18.0	2204.	0.	.0	.0	.0	.0
527.	3372-C	A	8.3	1.73	17.7	2307.	0.	.0	.0	.0	.0
634.	2504	A	24.2	1.79	18.8	1177.	0.	.0	.0	.0	.0
645.	2504	A	19.5	1.82	18.0	1825.	29.	.5	.0	.0	.0
674.	2504	A	21.3	1.81	19.4	2281.	0.	.0	.0	.0	.0
681.	2504	A	10.3	1.82	19.2	1373.	0.	.0	.0	.0	.0
947.	2504	A	23.2	1.73	18.8	2565.	0.	.0	.0	.0	.0
1202.	3215	A	14.3	1.76	15.4	2652.	0.	.0	.0	.0	.0
1236.	3343-C	A	7.1	1.75	15.6	1717.	0.	.0	.0	.0	.0
1356.	2504	A	16.3	1.80	16.7	2237.	0.	.0	.0	.0	.0
1383.	3322-C	A	5.3	1.77	17.2	1631.	0.	.0	.0	.0	.0
1422.	2504	A	23.1	1.81	17.0	1051.	0.	.0	.0	.0	.0
1432.	3343-C	A	6.2	1.73	16.7	1789.	0.	.0	.0	.0	.0
1500.	3322-C	A	7.1	1.78	17.5	1733.	0.	.0	.0	.0	.0
1580.	3322-C	A	1.3	1.79	16.6	1084.	127.	.0	.0	.0	.0
1631.	2504	A	25.1	1.76	19.5	1544.	229.	.0	.0	.0	.0
1657.	2504	A	25.3	1.80	17.5	1891.	237.	.4	.0	.0	.0
1668.	3215	A	1.1	1.72	15.9	1325.	247.	1.2	.0	.0	.0
1683.	2504	A	22.2	1.81	18.0	1658.	0.	.0	.0	.0	.0
2210.	2504	A	23.3	1.79	18.7	2017.	0.	.0	.0	.0	.0
2226.	2504	A	25.2	1.82	17.1	2190.	0.	.0	.0	.0	.0
2251.	3343-C	A	5.3	1.78	15.3	1804.	0.	.0	.0	.0	.0
2305.	2504	A	17.2	1.82	16.1	1681.	0.	.0	.0	.0	.0
2331.	2504	A	17.1	1.79	21.0	1606.	0.	.0	.0	.0	.0
2471.	2504	A	24.1	1.80	17.9	2175.	0.	.0	.0	.0	.0
2494.	2504	A	13.2	1.77	13.5	1044.	0.	.0	.0	.0	.0
2559.	3343-C	A	8.3	1.75	15.8	1528.	0.	.0	.0	.0	.0
2612.	3343-C	A	9.1	1.74	15.4	1357.	0.	.0	.0	.0	.0
2617.	3322-C	A	14.2	1.79	17.4	1128.	0.	.0	.0	.0	.0
2655.	2504	A	21.1	1.73	18.1	1380.	0.	.0	.0	.0	.0
2744.	2504	A	15.3	1.73	17.8	1850.	57.	.0	.0	.0	.0
2971.	2504	A	20.2	1.73	17.6	2050.	0.	.0	.0	.0	.0
2972.	2504	A	24.3	1.73	18.0	1461.	0.	.0	.0	.0	.0
2977.	2504	A	17.3	1.74	13.0	1525.	0.	.0	.0	.0	.0
2375.	2504	A	19.1	1.80	18.3	1712.	0.	.0	.0	.0	.0
2376.	3215	A	13.1	1.76	14.4	2273.	203.	.0	.0	.0	.0
4001.	3322-C	A	7.3	1.71	19.8	1103.	0.	.0	.0	.0	.0
4002.	3372-C	A	13.3	1.72	19.5	1530.	0.	.0	.0	.0	.0
4003.	3322-C	A	14.1	1.72	18.2	1037.	0.	.0	.0	.0	.0
4005.	3323-C	A	5.2	1.73	19.2	1964.	401.	1.0	11.4	8.2	43.9
4007.	3343-C	A	1.3	1.72	17.8	1508.	177.	.0	.0	.0	.0
4009.	3371-C	A	7.1	1.72	19.1	1435.	0.	.0	.0	.0	.0

TABLE 11-1 (Continued)

SERIAL NUMBER	FURNACE RUN	GRADE	LOG LOCATION	DENSITY	RESISTIVITY	TENSILE STRENGTH	ASH CONTENT	BORON CONTENT	IRON CONTENT	VANADIUM CONTENT	TITANIUM CONTENT
4010.	3322-C	A	10.2	1.75	18.7	1484.	0.	.0	.0	.0	.0
4011.	3371-C	A	5.2	1.74	17.2	1231.	46.	1.1	.0	.0	.0
4013.	3309-C	A	12.1	1.74	18.7	1681.	223.	.0	.0	.0	.0
4014.	3371-C	A	7.2	1.72	18.6	1013.	0.	.0	.0	.0	.0
4015.	3371-C	A	2.3	1.73	19.9	1437.	0.	.0	.0	.0	.0
4018.	3322-C	A	10.1	1.74	17.9	1598.	0.	.0	.0	.0	.0
4020.	3343-C	A	3.3	1.71	17.8	1230.	107.	.0	.0	.0	.0
4021.	3343-C	A	16.3	1.73	18.8	1142.	78.	.0	.0	.0	.0
4022.	3322-C	A	4.2	1.76	18.9	1853.	0.	.0	.0	.0	.0
4023.	3322-C	A	13.3	1.75	18.8	1726.	0.	.0	.0	.0	.0
4024.	3329-C	A	10.2	1.74	17.7	1539.	0.	.0	.0	.0	.0
4026.	3322-C	A	10.3	1.74	17.9	1546.	0.	.0	.0	.0	.0
4027.	3343-C	A	15.2	1.73	18.1	1302.	0.	.0	.0	.0	.0
4029.	3372-C	A	8.2	1.76	18.0	1462.	0.	.0	.0	.0	.0
4030.	3347-C	A	3.1	1.76	18.3	1396.	0.	.0	.0	.0	.0
4031.	3322-C	A	18.3	1.77	18.8	1670.	134.	.0	.0	.0	.0
4034.	3309-C	A	8.1	1.76	17.4	1163.	53.	.0	.0	.0	.0
4036.	3303-C	A	6.2	1.75	18.6	1630.	71.	.0	.0	.0	.0
4045.	3309-C	A	1.1	1.77	18.3	1595.	185.	1.4	.0	.0	.0
4046.	3307-C	A	4.3	1.77	18.1	1649.	137.	.0	.0	.0	.0
4047.	3371-C	A	3.1	1.77	19.3	1349.	0.	.0	.0	.0	.0
4048.	3307-C	A	1.2	1.73	17.8	1178.	151.	.0	.0	.0	.0
4049.	3371-C	A	9.2	1.76	18.4	1641.	0.	.0	.0	.0	.0
4050.	3372-C	A	6.1	1.76	18.9	1521.	0.	.0	.0	.0	.0
4051.	3371-C	A	4.3	1.76	19.6	1410.	0.	.0	.0	.0	.0
4053.	3215	A	16.3	1.75	17.4	1552.	151.	.0	.0	.0	.0
4054.	3307-C	A	7.3	1.76	17.6	1574.	192.	.0	.0	.0	.0
4055.	3307-C	A	4.1	1.78	18.4	1703.	739.	.0	.0	.0	.0
4057.	3372-C	A	7.3	1.78	17.2	1509.	0.	.0	.0	.0	.0
4058.	3329-C	A	6.1	1.78	18.0	2064.	0.	.0	.0	.0	.0
4059.	3371-C	A	6.2	1.75	18.2	1381.	0.	.0	.0	.0	.0
4060.	3343-C	A	1.1	1.75	17.2	2049.	257.	2.1	.0	.0	.0
4064.	3372-C	A	9.2	1.75	15.5	1478.	0.	.0	.0	.0	.0
4065.	3307-C	A	12.3	1.73	19.8	1277.	49.	.0	.0	.0	.0
4066.	3307-C	A	7.2	1.74	18.7	1866.	324.	.0	.0	.0	.0
4068.	3372-C	A	10.1	1.74	17.4	1987.	0.	.0	.0	.0	.0
4070.	3307-C	A	6.2	1.74	18.3	1864.	297.	.0	.0	.0	.0
4073.	3307-C	A	9.2	1.75	17.3	1502.	201.	.0	.0	.0	.0
4074.	3371-C	A	3.2	1.74	18.3	2073.	0.	.0	.0	.0	.0
4075.	3371-C	A	1.1	1.7	10.7	2370.	95.	1.1	.0	.0	.0
4078.	3307-C	A	10.1	1.77	18.6	1924.	175.	.0	.0	.0	.0
4080.	3372-C	A	12.1	1.76	18.4	1546.	0.	.0	.0	.0	.0
4087.	3309-C	A	12.2	1.74	18.5	1291.	120.	.0	.0	.0	.0
4087.	3329-C	A	6.2	1.77	18.6	1583.	0.	.0	.0	.0	.0
4094.	3372-C	A	1.2	1.76	18.7	2076.	0.	.0	.0	.0	.0
4095.	3372-C	A	15.3	1.75	17.6	1816.	0.	.0	.0	.0	.0
4096.	3372-C	A	5.1	1.75	16.5	1252.	364.	.0	18.3	15.1	38.8
4097.	3329-C	A	9.1	1.75	17.0	1908.	297.	2.3	.0	.0	.0
4099.	3307-C	A	13.2	1.75	17.3	1744.	97.	1.3	.0	.0	.0
4101.	3343-C	A	2.2	1.76	18.1	1239.	0.	.0	.0	.0	.0
4102.	3371-C	A	2.2	1.74	17.4	2723.	0.	.0	.0	.0	.0
4103.	3372-C	A	1.3	1.76	16.9	1749.	49.	.0	.0	.0	.0
4104.	3329-C	A	3.2	1.73	16.9	1605.	0.	.0	.0	.0	.0
4105.	3343-C	A	11.1	1.75	15.6	1414.	0.	.0	.0	.0	.0

TABLE 11-1 (Continued)

SERIAL NUMBER	FURNACE RUN	GRADE	LOG LOCATION	DENSITY	RESISTIVITY	TENSILE STRENGTH	ASH CONTENT	BORON CONTENT	IRON CONTENT	VANADIUM CONTENT	TITANIUM CONTENT
4106.	3372-C	A	15.1	1.74	17.6	1886.	0.	.0	.0	.0	.0
4107.	3372-C	A	7.1	1.75	15.7	2068.	0.	.0	.0	.0	.0
4109.	3372-C	A	1.1	1.74	17.6	1633.	55.	1.9	.0	.0	.0
4128.	3372-C	A	15.3	1.76	17.3	1505.	0.	.0	.0	.0	.0
4129.	3372-C	A	10.2	1.76	16.9	1690.	0.	.0	.0	.0	.0
4130.	3303-C	A	8.3	1.75	18.3	1610.	40.	.0	.0	.0	.0
4131.	3372-C	A	7.2	1.76	16.2	1676.	0.	.0	.0	.0	.0
4133.	3303-C	A	2.1	1.77	13.2	1736.	82.	.0	.0	.0	.0
4140.	3347-C	A	5.2	1.74	16.1	1699.	175.	1.0	.0	.0	.0
4147.	3371-C	A	10.2	1.74	15.9	1990.	0.	.0	.0	.0	.0
4152.	3215	A	4.1	1.74	16.6	1402.	0.	.0	.0	.0	.0
4153.	3215	A	7.1	1.77	17.2	1542.	0.	.0	.0	.0	.0
4155.	3307-C	A	14.1	1.74	18.0	1685.	34.	.0	.0	.0	.0
4156.	3371-C	A	10.3	1.75	17.2	2270.	0.	.0	.0	.0	.0
4157.	3372-C	A	12.3	1.72	17.8	1621.	0.	.0	.0	.0	.0
4169.	3371-C	A	10.1	1.75	13.9	1530.	0.	1.3	.0	.0	.0
4170.	3372-C	A	4.2	1.73	17.6	2059.	0.	.0	.0	.0	.0
4175.	3215	A	14.1	1.74	15.1	1953.	0.	.0	.0	.0	.0
4196.	3215	A	10.3	1.73	18.2	1235.	0.	.0	.0	.0	.0
4214.	3215	A	6.1	1.72	17.7	1709.	0.	.0	.0	.0	.0
4215.	3215	A	5.1	1.74	17.3	1477.	277.	.0	.0	.0	.0
4217.	3215	A	7.3	1.73	18.0	1737.	0.	.0	.0	.0	.0
4222.	3215	A	12.1	1.75	16.2	2325.	0.	.0	.0	.0	.0
4237.	3215	A	15.1	1.74	15.1	2281.	52.	.4	.0	.0	.0
4242.	3215	A	2.2	1.74	17.5	1719.	0.	.0	.0	.0	.0
4243.	3215	A	10.2	1.75	17.2	1317.	0.	.0	.0	.0	.0
4244.	3215	A	3.1	1.75	17.1	1656.	0.	.0	.0	.0	.0
4267.	3343-C	A	3.2	1.74	16.7	2032.	0.	.0	.0	.0	.0
4273.	3215	A	17.2	1.71	16.4	1301.	147.	2.3	.0	.0	.0
4349.	3343-C	A	14.2	1.73	16.8	1451.	0.	.0	.0	.0	.0
4350.	3343-C	A	2.2	1.75	17.4	1507.	0.	.0	.0	.0	.0
4379.	3215	A	4.3	1.72	18.2	2025.	0.	.0	.0	.0	.0
4391.	3215	A	7.3	1.73	16.8	1219.	0.	.0	.0	.0	.0
4423.	3215	A	1.2	1.74	15.8	2039.	0.	.0	.0	.0	.0
4426.	3372-C	A	7.2	1.75	17.4	1627.	0.	.0	.0	.0	.0
4455.	3372-C	A	9.3	1.74	18.3	1167.	0.	.0	.0	.0	.0
4459.	3371-C	A	15.1	1.77	16.9	1312.	0.	.0	.0	.0	.0
4461.	3307-C	A	13.1	1.73	18.8	1332.	105.	.0	.0	.0	.0
4462.	3372-C	A	15.2	1.77	15.8	2113.	0.	.0	.0	.0	.0
4467.	3371-C	A	1.3	1.77	17.5	1579.	0.	.0	.0	.0	.0
4465.	3371-C	A	1.2	1.78	18.0	1919.	0.	.0	.0	.0	.0
4467.	3327-C	A	9.1	1.77	17.4	1499.	65.	.9	.0	.0	.0
4469.	3372-C	A	2.2	1.77	16.4	1647.	0.	.0	.0	.0	.0
4471.	3442-C	A	11.5	1.73	17.3	1940.	57.	.0	.0	.0	.0
4477.	3442-C	A	14.1	1.78	20.2	2271.	283.	.0	.0	.0	.0
4474.	3442-C	A	11.1	1.73	18.9	1433.	248.	.0	.0	.0	.0
4476.	3371-C	A	11.2	1.79	19.4	1892.	0.	.0	.0	.0	.0
4477.	3309-C	A	9.3	1.74	17.6	1577.	55.	.0	.0	.0	.0
4482.	3442-C	A	10.1	1.79	18.1	1524.	264.	.0	.0	.0	.0
4483.	3442-C	A	14.5	1.73	16.0	2048.	47.	.0	.0	.0	.0
4485.	3442-C	A	5.1	1.77	17.7	1977.	43.	.4	.0	.0	.0
4486.	3442-C	A	7.1	1.77	20.2	2195.	51.	.0	.0	.0	.0
4487.	3442-C	A	16.5	1.80	17.3	1848.	425.	.6	99.2	12.2	47.0
4491.	3442-C	A	8.2	1.77	17.7	1840.	129.	.0	.0	.0	.0

TABLE II-1 (Continued)

SERIAL NUMBER	FURNACE RUN	GRADE	LOG LOCATION	DENSITY	RESISTIVITY	TENSILE STRENGTH	ASH CONTENT	BORON CONTENT	IRON CONTENT	VANADIUM CONTENT	TITANIUM CONTENT
4499.	3309-C	A	2.3	1.76	19.7	1363.	53.	.0	.0	.0	.0
4501.	3309-C	A	8.2	1.76	18.0	1768.	0.	.0	.0	.0	.0
4502.	3309-C	A	9.1	1.76	18.2	1619.	55.	.0	.0	.0	.0
4504.	3307-C	A	5.3	1.77	18.3	1819.	213.	.0	.0	.0	.0
4505.	3372-C	A	4.1	1.77	17.3	2237.	0.	.0	.0	.0	.0
4507.	3343-C	A	3.3	1.76	16.9	1530.	0.	.0	.0	.0	.0
4508.	3343-C	A	14.1	1.72	16.4	1956.	0.	.0	.0	.0	.0
4509.	3372-C	A	5.2	1.77	16.1	2151.	257.	3.3	.0	.0	.0
4511.	3322-C	A	7.2	1.75	16.4	1533.	0.	.0	.0	.0	.0
4512.	3322-C	A	13.2	1.78	17.0	2018.	27.	1.2	.0	.0	.0
4522.	3442-C	A	5.3	1.76	19.1	1528.	43.	.0	.0	.0	.0
4523.	3371-C	A	10.1	1.77	15.9	2241.	0.	.0	.0	.0	.0
4525.	3371-C	A	9.1	1.76	18.3	1865.	53.	.9	.0	.0	.0
4527.	3372-C	A	6.2	1.76	16.4	1911.	0.	.0	.0	.0	.0
4531.	3372-C	A	11.2	1.77	17.1	2363.	0.	.0	.0	.0	.0
4532.	3329-C	A	5.1	1.77	17.5	1788.	294.	.0	.0	.0	.0
4537.	3372-C	A	6.3	1.76	15.7	2302.	0.	.0	.0	.0	.0
4538.	3343-C	A	4.2	1.77	16.1	1939.	0.	.0	.0	.0	.0
4537.	3371-C	A	16.3	1.77	15.5	1753.	117.	.0	.0	.0	.0
4539.	3309-C	A	7.2	1.76	17.9	2335.	20.	.0	.0	.0	.0
4542.	3329-C	A	13.2	1.73	17.0	2458.	79.	4.4	.0	.0	.0
4544.	3215	A	17.3	1.79	18.1	2257.	0.	.0	.0	.0	.0
4545.	3215	A	5.3	1.77	17.4	1791.	0.	.0	.0	.0	.0
4549.	3215	A	12.2	1.79	17.1	1282.	0.	.0	.0	.0	.0
4553.	3307-C	A	3.2	1.77	17.9	1654.	229.	.0	.0	.0	.0
4554.	3343-C	A	6.3	1.77	16.8	1567.	0.	.0	.0	.0	.0
4555.	3371-C	A	11.1	1.77	17.3	1246.	0.	.0	.0	.0	.0
4557.	3307-C	A	4.2	1.77	17.0	2049.	277.	.0	.0	.0	.0
4563.	3307-C	A	11.1	1.77	20.3	1355.	161.	.0	.0	.0	.0
4574.	3307-C	A	11.2	1.73	19.7	1192.	0.	.0	.0	.0	.0
4575.	3309-C	A	10.3	1.76	18.9	1513.	75.	.0	.0	.0	.0
4577.	3371-C	A	11.3	1.78	13.4	1810.	0.	.0	.0	.0	.0
4578.	3371-C	A	5.1	1.73	15.5	2042.	56.	.0	.0	.0	.0
4579.	3329-C	A	15.3	1.79	15.7	2449.	0.	.0	.0	.0	.0
4580.	3215	A	7.1	1.78	18.7	2052.	0.	.0	.0	.0	.0
4584.	3372-C	A	10.2	1.78	18.5	2425.	0.	.0	.0	.0	.0
4585.	3343-C	A	10.2	1.80	15.6	1245.	0.	.0	.0	.0	.0
4588.	3371-C	A	4.1	1.79	15.7	2358.	0.	.0	.0	.0	.0
4590.	3307-C	A	14.2	1.77	15.7	2058.	29.	.0	.0	.0	.0
4591.	3309-C	A	5.3	1.78	17.2	2023.	45.	.0	.0	.0	.0
4597.	3307-C	A	2.3	1.77	17.0	1610.	133.	.0	.0	.0	.0
4601.	3215	A	9.3	1.81	15.4	1752.	181.	.0	.0	.0	.0
4629.	3215	A	15.1	1.73	13.0	1439.	0.	.0	.0	.0	.0
4642.	3329-C	A	14.1	1.73	18.0	2250.	0.	.0	.0	.0	.0
4645.	3215	A	5.2	1.77	17.1	1600.	0.	.0	.0	.0	.0
4647.	3215	A	10.2	1.78	17.1	1370.	0.	.0	.0	.0	.0
4673.	3215	A	6.3	1.80	15.9	2247.	0.	.0	.0	.0	.0
4698.	3215	A	7.2	1.76	16.1	2581.	0.	.0	.0	.0	.0
4709.	3215	A	3.2	1.77	16.6	1347.	0.	.0	.0	.0	.0
4731.	3442-C	A	8.1	1.79	22.4	1284.	285.	.0	.0	.0	.0
4732.	3442-C	A	6.2	1.77	17.4	1353.	59.	.0	.0	.0	.0
4735.	3442-C	A	3.5	1.76	17.5	1909.	59.	.0	.0	.0	.0
4748.	3442-C	A	6.5	1.81	13.1	2063.	61.	.0	.0	.0	.0
4749.	3442-C	A	9.2	1.75	17.0	2319.	36.	.0	.0	.0	.0

TABLE 11-1 (Continued)

SERIAL NUMBER	FURNACE RUN	GRADE	LOG LOCATION	DENSITY	RESISTIVITY	TENSILE STRENGTH	ASH CONTENT	BORON CONTENT	IRON CONTENT	VANADIUM CONTENT	TITANIUM CONTENT
4876.	3215	A	10.1	1.76	16.1	1944.	0.	.0	.0	.0	.0
4887.	3215	A	8.1	1.76	15.5	1994.	0.	.0	.0	.0	.0
4895.	3215	A	9.2	1.77	15.4	1767.	0.	.0	.0	.0	.0
5063.	3215	A	15.3	1.80	15.9	2090.	0.	.0	.0	.0	.0
5085.	3343-C	A	4.3	1.73	16.3	1878.	0.	.0	.0	.0	.0
5086.	3343-C	A	8.1	1.76	15.6	1083.	0.	.0	.0	.0	.0
5088.	3322-C	A	14.2	1.81	16.8	2104.	0.	.0	.0	.0	.0
5089.	3215	A	1.3	1.81	15.2	1659.	180.	.0	.0	.0	.0
5090.	3215	A	9.1	1.82	15.2	2266.	196.	1.0	.0	.0	.0
5130.	3215	A	5.2	1.80	15.5	2020.	241.	.5	.0	.0	.0
5141.	3343-C	A	14.3	1.77	16.0	1309.	0.	.0	.0	.0	.0
5143.	3215	A	8.3	1.73	15.9	1440.	0.	.0	.0	.0	.0
5176.	3215	A	3.3	1.77	16.2	1992.	0.	.0	.0	.0	.0
5222.	3442-C	A	6.3	1.77	17.2	2163.	51.	.0	.0	.0	.0
5223.	3468-C	A	12.2	1.80	18.7	1269.	194.	.0	.0	.0	.0
5227.	3442-C	A	10.5	1.73	15.7	1368.	95.	.0	.0	.0	.0
5229.	3442-C	A	4.4	1.76	16.7	2257.	38.	.0	.0	.0	.0
5230.	3442-C	A	2.4	1.81	16.5	2087.	55.	.0	.0	.0	.0
5231.	3442-C	A	4.3	1.76	17.2	2521.	51.	.0	.0	.0	.0
5234.	3442-C	A	11.6	1.73	16.5	1871.	70.	.0	.0	.0	.0
5236.	3442-C	A	9.4	1.78	17.1	1895.	50.	.0	.0	.0	.0
5241.	3442-C	A	13.5	1.77	16.9	1275.	58.	.0	.0	.0	.0
5243.	3442-C	A	11.4	1.77	17.5	2018.	57.	.0	.0	.0	.0
5244.	3442-C	A	10.2	1.73	16.8	1595.	128.	.0	.0	.0	.0
5246.	3442-C	A	10.1	1.78	22.1	2009.	242.	.0	.0	.0	.0
5247.	3468-C	A	10.2	1.79	16.5	1659.	217.	.3	.0	.0	.0
5248.	3442-C	A	10.4	1.75	17.3	1113.	230.	.0	.0	.0	.0
5252.	3468-C	A	12.1	1.78	17.3	2057.	285.	.0	.0	.0	.0
5253.	3442-C	A	10.4	1.78	16.1	2323.	43.	.0	.0	.0	.0
5254.	3442-C	A	4.1	1.80	17.2	1623.	44.	.0	.0	.0	.0
5255.	3468-C	A	13.3	1.78	18.0	2571.	199.	.5	.0	.0	.0
5259.	3442-C	A	14.3	1.82	15.7	2081.	265.	.0	.0	.0	.0
5260.	3442-C	A	12.5	1.78	16.7	1807.	133.	.0	.0	.0	.0
5264.	3468-C	A	10.1	1.77	17.5	1828.	392.	.5	21.1	24.4	42.0
5269.	3442-C	A	8.8	1.77	18.3	1378.	40.	.0	.0	.0	.0
5271.	3442-C	A	2.3	1.77	17.5	1661.	57.	.0	.0	.0	.0
5272.	3442-C	A	5.4	1.77	18.9	1750.	44.	.1	.0	.0	.0
5273.	3468-C	A	16.1	1.76	16.5	2226.	260.	.0	.0	.0	.0
5274.	3468-C	A	13.1	1.75	15.4	1528.	289.	.0	.0	.0	.0
5279.	3442-C	A	11.4	1.79	17.5	1478.	65.	.0	.0	.0	.0
5285.	3442-C	A	13.2	1.80	20.5	1948.	240.	.8	.0	.0	.0
5283.	3442-C	A	2.2	1.73	16.1	2076.	44.	.0	.0	.0	.0
5291.	3442-C	A	11.2	1.80	15.4	2691.	46.	.0	.0	.0	.0
5293.	3442-C	A	7.3	1.77	17.0	1713.	59.	.0	.0	.0	.0
5296.	3442-C	A	3.4	1.79	15.3	2405.	155.	.0	.0	.0	.0
5297.	3442-C	A	7.4	1.78	17.9	1963.	52.	.0	.0	.0	.0
5298.	3442-C	A	4.2	1.78	15.9	2462.	107.	.0	.0	.0	.0
5233.	3442-C	A	3.2	1.79	15.3	2084.	43.	.0	.0	.0	.0
5300.	3442-C	A	15.2	1.79	19.1	2078.	105.	.0	.0	.0	.0
5302.	3442-C	A	15.5	1.79	16.0	2533.	330.	.0	35.8	10.7	35.0
5307.	3442-C	A	3.1	1.79	15.4	1395.	221.	.0	.0	.0	.0
5309.	3442-C	A	9.5	1.81	17.6	1677.	43.	.0	.0	.0	.0
5311.	3442-C	A	11.3	1.78	17.5	1607.	51.	.0	.0	.0	.0
5315.	3442-C	A	13.3	1.79	17.0	2378.	197.	1.0	.0	.0	.0

TABLE 11-1 (Continued)

SERIAL NUMBER	FURNACE RUN	GRADE	LOG LOCATION	DENSITY	RESISTIVITY	TENSILE STRENGTH	ASH CONTENT	BORON CONTENT	IRON CONTENT	VANADIUM CONTENT	TITANIUM CONTENT
5319.	3402-C	A	3.3	1.77	17.0	2124.	54.	.0	.0	.0	.0
5320.	3408-C	A	12.3	1.79	17.8	2217.	104.	.0	.0	.0	.0
5326.	3402-C	A	1.5	1.81	15.1	1913.	423.	.0	91.4	8.6	44.4
5327.	3402-C	A	10.6	1.79	18.1	2078.	47.	.0	.0	.0	.0
5333.	3403-C	A	10.3	1.80	17.8	2027.	265.	.0	.0	.0	.0
5334.	3408-C	A	15.1	1.76	19.1	1949.	277.	.0	.0	.0	.0
5335.	3403-C	A	10.3	1.73	17.9	1334.	203.	.0	.0	.0	.0
5336.	3408-C	A	13.2	1.79	17.8	1728.	90.	.0	.0	.0	.0
5339.	3402-C	A	1.4	1.76	17.9	1412.	71.	.0	.0	.0	.0
5340.	3408-C	A	10.2	1.74	18.1	2201.	291.	.0	.0	.0	.0
5341.	3309-C	A	3.2	1.75	17.1	2084.	66.	.0	.0	.0	.0
5342.	3309-C	A	3.3	1.73	18.4	1600.	29.	.0	.0	.0	.0
5343.	3307-C	A	13.3	1.75	18.2	1602.	27.	.0	.0	.0	.0
5344.	3329-C	A	3.3	1.74	17.8	1794.	0.	.0	.0	.0	.0
5347.	3327-C	A	11.1	1.76	17.5	1464.	0.	.0	.0	.0	.0
5349.	3322-C	A	12.2	1.75	17.2	1955.	0.	.0	.0	.0	.0
5350.	3371-C	A	14.3	1.74	18.0	1139.	0.	.0	.0	.0	.0
5351.	3329-C	A	15.1	1.75	18.0	1621.	0.	.0	.0	.0	.0
5353.	3309-C	A	13.2	1.76	17.7	2447.	213.	1.0	.0	.0	.0
5354.	3329-C	A	9.2	1.75	18.1	2031.	0.	.0	.0	.0	.0
5355.	3442-C	A	7.5	1.79	16.9	2266.	71.	.0	.0	.0	.0
5361.	3371-C	A	4.2	1.77	17.3	2272.	0.	.0	.0	.0	.0
5362.	3303-C	A	9.2	1.78	16.0	1033.	0.	.0	.0	.0	.0
5363.	3329-C	A	2.1	1.77	15.5	1684.	0.	.0	.0	.0	.0
5367.	3343-C	A	7.2	1.77	15.5	1183.	0.	.0	.0	.0	.0
5368.	3309-C	A	10.1	1.81	16.6	2189.	194.	.0	.0	.0	.0
5370.	3309-C	A	11.3	1.76	18.0	2273.	68.	.0	.0	.0	.0
5371.	3329-C	A	10.1	1.77	16.6	2123.	57.	1.0	.0	.0	.0
5372.	3307-C	A	11.3	1.76	18.4	2251.	43.	.0	.0	.0	.0
5377.	3309-C	A	3.2	1.76	17.1	1521.	47.	.0	.0	.0	.0
5378.	3307-C	A	13.3	1.78	18.3	1781.	53.	.0	.0	.0	.0
5379.	3309-C	A	11.2	1.78	17.6	1792.	145.	.0	.0	.0	.0
5380.	3303-C	A	15.2	1.75	17.2	1664.	309.	.0	.0	.0	.0
5381.	3329-C	A	7.3	1.79	17.4	1614.	0.	.0	.0	.0	.0
5382.	3309-C	A	5.2	1.76	18.6	2459.	66.	.3	.0	.0	.0
5383.	3371-C	A	13.3	1.77	16.1	1127.	0.	.0	.0	.0	.0
5384.	3327-C	A	11.3	1.73	16.8	1703.	0.	.0	.0	.0	.0
5392.	3309-C	A	6.3	1.77	17.4	2020.	65.	.0	.0	.0	.0
5393.	3307-C	A	15.2	1.76	17.6	1853.	22.	.0	.0	.0	.0
5394.	3329-C	A	15.2	1.75	16.5	1728.	0.	.0	.0	.0	.0
5395.	3309-C	A	11.1	1.77	16.0	1535.	197.	.0	.0	.0	.0
5396.	3309-C	A	10.2	1.77	16.9	1745.	54.	.0	.0	.0	.0
5399.	3307-C	A	1.1	1.77	17.5	1305.	321.	1.3	.0	.0	.0
5404.	3309-C	A	8.2	1.78	16.8	1088.	50.	.0	.0	.0	.0
5406.	3303-C	A	1.3	1.91	17.7	2235.	195.	.0	.0	.0	.0
5408.	3307-C	A	15.1	1.77	18.1	2125.	28.	.0	.0	.0	.0
5409.	3327-C	A	11.2	1.79	17.5	1610.	0.	.0	.0	.0	.0
5410.	3322-C	A	1.1	1.79	16.1	1712.	722.	1.6	.0	.0	.0
5411.	3309-C	A	12.3	1.78	18.0	1723.	169.	.0	.0	.0	.0
5412.	3307-C	A	9.7	1.76	18.5	1951.	156.	.0	.0	.0	.0
5413.	3307-C	A	13.1	1.77	17.4	2175.	70.	.0	.0	.0	.0
5414.	3329-C	A	12.1	1.77	16.3	1860.	0.	.0	.0	.0	.0
5415.	3309-C	A	3.1	1.76	17.3	1550.	46.	.0	.0	.0	.0
5416.	3307-C	A	3.3	1.75	17.6	1340.	181.	.0	.0	.0	.0

TABLE 11-1 (Continued)

SERIAL NUMBER	FURNACE RUN	GRADE	LOG LOCATION	DENSITY	RESISTIVITY	TENSILE STRENGTH	ASH CONTENT	BORON CONTENT	IRON CONTENT	VANADIUM CONTENT	TITANIUM CONTENT
5417.	3307-C	A	2.2	1.78	16.1	1837.	284.	.0	.0	.0	.0
5418.	3309-C	A	7.3	1.75	17.6	2065.	29.	.0	.0	.0	.0
5419.	3307-C	A	16.2	1.78	17.5	2079.	18.	.0	.0	.0	.0
5420.	3307-C	A	10.3	1.77	18.6	1402.	97.	.0	.0	.0	.0
5421.	3371-C	A	8.1	1.76	18.2	1518.	0.	.0	.0	.0	.0
5422.	3303-C	A	15.1	1.78	17.1	1157.	360.	.0	.0	.0	.0
5423.	3309-C	A	4.2	1.75	17.4	1855.	35.	.0	.0	.0	.0
5424.	3303-C	A	16.3	1.78	13.0	1713.	234.	.0	.0	.0	.0
5426.	3329-C	A	6.3	1.78	18.4	1864.	0.	.0	.0	.0	.0
5427.	3322-C	A	15.2	1.77	18.0	1904.	0.	.0	.0	.0	.0
5428.	3307-C	A	6.3	1.77	18.3	1654.	201.	.0	.0	.0	.0
5429.	3307-C	A	5.1	1.77	19.0	1339.	336.	.0	19.0	13.1	63.3
5430.	3372-C	A	8.1	1.76	17.6	1403.	0.	.0	.0	.0	.0
5431.	3307-C	A	2.1	1.76	18.0	1488.	239.	.0	.0	.0	.0
5433.	3309-C	A	4.1	1.75	18.5	2370.	31.	.0	.0	.0	.0
5452.	3368-C	A	15.2	1.74	17.3	2149.	233.	.0	.0	.0	.0
5578.	3302-C	A	7.2	1.78	17.0	1566.	47.	.0	.0	.0	.0
5563.	3343-C	A	10.3	1.78	15.4	1571.	0.	.0	.0	.0	.0
5670.	3343-C	A	8.2	1.84	15.8	1683.	0.	.0	.0	.0	.0
5671.	3371-C	A	9.2	1.77	17.0	2109.	0.	.0	.0	.0	.0
5672.	3309-C	A	14.2	1.79	16.0	2342.	251.	.0	.0	.0	.0
5673.	3372-C	A	14.2	1.73	15.8	1562.	0.	.0	.0	.0	.0
5674.	3343-C	A	16.1	1.75	16.3	1692.	238.	1.0	.0	.0	.0
5675.	3307-C	A	1.3	1.78	17.9	1939.	174.	.0	.0	.0	.0
5676.	3322-C	A	5.1	1.78	15.9	2460.	161.	.0	.0	.0	.0
5677.	3372-C	A	13.2	1.73	17.0	1759.	33.	.3	.0	.0	.0
5678.	3329-C	A	7.2	1.77	17.1	2081.	0.	.0	.0	.0	.0
5679.	3309-C	A	14.3	1.77	18.4	1077.	195.	.0	.0	.0	.0
5680.	3343-C	A	12.3	1.78	13.6	1410.	0.	.0	.0	.0	.0
5690.	3329-C	A	4.3	1.80	16.8	2353.	0.	.0	.0	.0	.0
5691.	3309-C	A	7.1	1.77	18.6	1847.	43.	.0	.0	.0	.0
5692.	3329-C	A	10.1	1.78	16.7	2345.	0.	.0	.0	.0	.0
5694.	3309-C	A	1.1	1.78	15.9	1911.	291.	2.8	.0	.0	.0
5695.	3347-C	A	4.1	1.80	16.1	1773.	0.	.0	.0	.0	.0
5696.	3309-C	A	15.3	1.77	17.0	1575.	294.	.0	.0	.0	.0
5697.	3329-C	A	11.2	1.78	18.8	2383.	0.	.0	.0	.0	.0
5698.	3322-C	A	12.1	1.80	14.8	2468.	0.	.0	.0	.0	.0
5700.	3343-C	A	1.2	1.77	15.8	1698.	0.	.0	.0	.0	.0
5701.	3309-C	A	16.1	1.77	17.6	2475.	386.	.7	42.8	9.1	69.0
5702.	3372-C	A	9.3	1.78	15.9	2337.	0.	.0	.0	.0	.0
5707.	3322-C	A	4.1	1.78	15.5	2086.	0.	.0	.0	.0	.0
5703.	3372-C	A	14.3	1.80	15.4	2544.	0.	.0	.0	.0	.0
5709.	3329-C	A	16.1	1.77	16.9	2551.	134.	1.3	.0	.0	.0
5710.	3343-C	A	13.2	1.78	16.1	1133.	43.	1.1	.0	.0	.0
5715.	3372-C	A	10.3	1.78	16.8	2259.	0.	.0	.0	.0	.0
5716.	3343-C	A	5.1	1.78	15.4	1573.	400.	.0	75.1	14.9	20.6
5717.	3322-C	A	3.1	1.79	16.4	1997.	0.	.0	.0	.0	.0
5713.	3372-C	A	14.1	1.80	16.1	1420.	0.	.0	.0	.0	.0
5719.	3343-C	A	15.1	1.80	14.7	1918.	0.	.0	.0	.0	.0
5720.	3372-C	A	3.1	1.81	15.2	2259.	0.	.0	.0	.0	.0
5721.	3343-C	A	12.2	1.78	15.4	1485.	0.	.0	.0	.0	.0
5722.	3329-C	A	4.3	1.81	16.3	2219.	0.	.0	.0	.0	.0
5723.	3372-C	A	2.1	1.81	15.7	1854.	0.	.0	.0	.0	.0
5724.	3371-C	A	9.3	1.78	15.9	2340.	58.	.0	.0	.0	.0

TABLE 11-1 (Continued)

SERIAL NUMBER	FURNACE RUN	GRADE	LOC LOCATION	DENSITY	RESISTIVITY	TENSILE STRENGTH	ASH CONTENT	BORON CONTENT	IRON CONTENT	VANADIUM CONTENT	TITANIUM CONTENT
5725.	3303-C	A	2.2	1.73	15.7	2490.	62.	.0	.0	.0	.0
5726.	3372-C	A	9.1	1.81	15.2	2369.	0.	2.5	.0	.0	.0
5727.	3367-C	A	15.3	1.81	17.1	2311.	27.	.0	.0	.0	.0
5728.	3372-C	A	11.1	1.80	15.3	2386.	0.	.0	.0	.0	.0
5730.	3343-C	A	2.1	1.80	15.1	1336.	0.	.0	.0	.0	.0
5731.	3343-C	A	15.3	1.79	15.2	1258.	0.	.0	.0	.0	.0
5733.	3329-C	A	16.2	1.77	17.3	1709.	0.	.0	.0	.0	.0
5734.	3329-C	A	9.3	1.81	16.1	1724.	215.	.0	.0	.0	.0
5735.	3329-C	A	10.3	1.81	15.0	2544.	0.	.0	.0	.0	.0
5737.	3371-C	A	12.1	1.79	15.9	2052.	0.	.0	.0	.0	.0
5738.	3372-C	A	13.1	1.79	15.9	1695.	74.	.0	.0	.0	.0
5745.	3309-C	A	9.1	1.77	17.3	1839.	184.	2.3	.0	.0	.0
5746.	3307-C	A	9.1	1.79	15.5	1515.	302.	.3	.0	.0	.0
5747.	3329-C	A	1.3	1.80	15.2	1998.	241.	.0	.0	.0	.0
5751.	3322-C	A	9.3	1.79	15.0	1966.	0.	.0	.0	.0	.0
5752.	3327-C	A	12.3	1.78	15.3	1961.	0.	.0	.0	.0	.0
5761.	3303-C	A	4.3	1.79	17.4	1234.	31.	.0	.0	.0	.0
5762.	3371-C	A	15.3	1.79	16.8	1501.	0.	.0	.0	.0	.0
5763.	3329-C	A	7.1	1.79	15.5	2478.	0.	.0	.0	.0	.0
5771.	3371-C	A	6.1	1.78	17.1	1170.	0.	.0	.0	.0	.0
5772.	3367-C	A	3.6	1.73	16.9	1401.	229.	.0	.0	.0	.0
5773.	3307-C	A	3.1	1.77	17.1	1569.	317.	.0	.0	.0	.0
5774.	3307-C	A	10.2	1.77	16.7	1834.	167.	.0	.0	.0	.0
5775.	3309-C	A	1.2	1.75	17.3	1471.	55.	.0	.0	.0	.0
5776.	3329-C	A	5.3	1.77	18.2	1762.	0.	.0	.0	.0	.0
5777.	3343-C	A	12.1	1.76	15.3	1690.	0.	.0	.0	.0	.0
5778.	3307-C	A	3.1	1.75	18.3	1341.	329.	.0	.0	.0	.0
5779.	3307-C	A	6.1	1.75	19.3	1614.	727.	.0	.0	.0	.0
5780.	3372-C	A	15.2	1.76	16.2	1727.	0.	.0	.0	.0	.0
5781.	3329-C	A	11.3	1.77	16.2	2107.	0.	.0	.0	.0	.0
5782.	3329-C	A	8.3	1.77	17.4	2115.	0.	.0	.0	.0	.0
5783.	3329-C	A	3.1	1.79	15.8	1519.	0.	.0	.0	.0	.0
5784.	3372-C	A	13.1	1.77	17.4	1729.	23.	.0	.0	.0	.0
5785.	3309-C	A	5.1	1.76	17.6	1371.	56.	.0	.0	.0	.0
5786.	3372-C	A	11.3	1.77	17.1	1437.	0.	.0	.0	.0	.0
5787.	3329-C	A	4.1	1.75	16.0	1580.	0.	.0	.0	.0	.0
5788.	3329-C	A	1.2	1.72	17.3	1736.	0.	.0	.0	.0	.0
5789.	3343-C	A	13.3	1.75	16.7	1685.	0.	.0	.0	.0	.0
5790.	3322-C	A	3.2	1.75	15.2	1291.	111.	2.6	.0	.0	.0
5791.	3307-C	A	8.2	1.76	17.7	1198.	275.	.0	.0	.0	.0
5795.	3371-C	A	14.2	1.70	20.3	1303.	0.	.0	.0	.0	.0
5796.	3329-C	A	13.3	1.71	21.4	1557.	0.	.0	.0	.0	.0
5797.	3322-C	A	5.1	1.73	19.4	1359.	0.	.0	.0	.0	.0
5798.	3307-C	A	12.2	1.73	20.0	1328.	89.	.0	.0	.0	.0
5799.	3372-C	A	4.3	1.74	17.4	1487.	0.	.0	.0	.0	.0
5800.	3329-C	A	2.2	1.75	17.6	1792.	0.	.0	.0	.0	.0
5801.	3371-C	A	2.1	1.77	15.8	1934.	0.	.0	.0	.0	.0
5802.	3322-C	A	2.3	1.75	16.9	2125.	0.	.0	.0	.0	.0
5803.	3329-C	A	12.2	1.74	17.5	2375.	0.	.0	.0	.0	.0
5804.	3371-C	A	5.3	1.75	16.8	1667.	0.	.0	.0	.0	.0
5805.	3329-C	A	14.3	1.76	15.7	1623.	0.	.0	.0	.0	.0
5806.	3309-C	A	14.1	1.75	17.2	1654.	292.	.0	.0	.0	.0
5307.	3329-C	A	1.2	1.77	16.2	1432.	0.	.0	.0	.0	.0
5808.	3307-C	A	5.2	1.77	17.6	1967.	260.	.5	.0	.0	.0

TABLE 11-1 (Continued)

SERIAL NUMBER	FURNACE RUN	GRADE	LOG LOCATION	DENSITY	RESISTIVITY	TENSILE STRENGTH	ASH CONTENT	BORON CONTENT	IRON CONTENT	VANADIUM CONTENT	TITANIUM CONTENT
5809.	3307-C	A	10.1	1.75	18.1	1579.	82.	.7	.0	.0	.0
5810.	3329-C	A	14.2	1.76	17.0	1624.	0.	.0	.0	.0	.0
5811.	3307-C	A	7.1	1.76	17.3	1317.	345.	.0	.0	.0	.0
5812.	3329-C	A	15.3	1.77	16.3	1974.	0.	.0	.0	.0	.0
5813.	3307-C	A	11.2	1.78	17.7	1559.	119.	.0	.0	.0	.0
5814.	3343-C	A	13.1	1.75	16.0	1445.	200.	.0	.0	.0	.0
5815.	3371-C	A	7.3	1.70	18.2	1470.	0.	.0	.0	.0	.0
5816.	3309-C	A	13.3	1.77	17.6	1416.	297.	.0	.0	.0	.0
5817.	3329-C	A	12.3	1.78	16.1	1773.	0.	.0	.0	.0	.0
5818.	3329-C	A	2.1	1.74	16.9	2043.	0.	.0	.0	.0	.0
5819.	3322-C	A	14.1	1.73	14.8	2359.	0.	.0	.0	.0	.0
5820.	3329-C	A	16.1	1.77	16.8	1570.	75.	.5	.0	.0	.0
5821.	3329-C	A	11.1	1.79	16.3	2128.	0.	.0	.0	.0	.0
5826.	3322-C	A	8.1	1.73	16.4	1387.	0.	.0	.0	.0	.0
5829.	3329-C	A	13.1	1.76	16.8	2380.	128.	.0	.0	.0	.0
5830.	3307-C	A	3.3	1.76	17.6	1294.	237.	.0	.0	.0	.0
5837.	3442-C	A	12.6	1.78	16.4	1711.	115.	.0	.0	.0	.0
5838.	3442-C	A	6.1	1.79	18.0	1477.	210.	.0	.0	.0	.0
5839.	3442-C	A	14.6	1.79	16.7	2099.	137.	.0	.0	.0	.0
5841.	3442-C	A	4.5	1.79	17.5	1338.	67.	.0	.0	.0	.0
5844.	3442-C	A	4.6	1.77	17.6	1461.	51.	.0	.0	.0	.0
5848.	3329-C	A	3.3	1.74	16.6	1699.	0.	.0	.0	.0	.0
5850.	3442-C	A	15.6	1.84	15.2	1731.	143.	.0	.0	.0	.0
5854.	3442-C	A	15.3	1.82	16.7	1604.	210.	.0	.0	.0	.0
5855.	3442-C	A	5.6	1.82	16.3	2489.	50.	.0	.0	.0	.0
5856.	3442-C	A	2.6	1.79	17.7	2232.	43.	.0	.0	.0	.0
5857.	3442-C	A	15.1	1.81	21.0	1739.	140.	.0	.0	.0	.0
5863.	3442-C	A	16.3	1.81	16.0	1376.	158.	.0	.0	.0	.0
5864.	3442-C	A	5.2	1.80	18.5	1163.	32.	.0	.0	.0	.0
5866.	3442-C	A	2.5	1.79	18.3	1162.	103.	.0	.0	.0	.0
5875.	3442-C	A	8.3	1.78	17.8	1912.	48.	.0	.0	.0	.0
5378.	3442-C	A	9.3	1.78	16.7	1506.	87.	.0	.0	.0	.0
5881.	3442-C	A	1.6	1.82	15.5	1696.	36.	.4	.0	.0	.0
5888.	3442-C	A	16.2	1.80	20.3	1638.	277.	1.0	.0	.0	.0
5889.	3442-C	A	9.5	1.80	18.2	1202.	238.	1.1	.0	.0	.0
5890.	3442-C	A	10.3	1.80	16.5	1131.	50.	.0	.0	.0	.0
5892.	3442-C	A	13.1	1.81	20.0	1172.	281.	.0	.0	.0	.0
5895.	3215	A	4.2	1.82	14.9	2325.	0.	.0	.0	.0	.0
5897.	3442-C	A	15.4	1.77	14.9	2027.	47.	.0	.0	.0	.0
5901.	3442-C	A	16.6	1.79	18.0	1814.	202.	.0	.0	.0	.0
5905.	3442-C	A	14.4	1.80	18.5	1080.	68.	.0	.0	.0	.0
5909.	3442-C	A	2.1	1.82	16.4	1673.	115.	.0	.0	.0	.0
6049.	3215	A	14.2	1.75	17.2	1794.	0.	.0	.0	.0	.0
6050.	3215	A	11.3	1.75	17.8	1432.	0.	.0	.0	.0	.0
6051.	3215	A	11.2	1.74	18.1	2175.	0.	.0	.0	.0	.0
6052.	3215	A	17.3	1.73	17.5	1739.	0.	.0	.0	.0	.0
6053.	3307-C	A	14.3	1.75	17.7	2156.	32.	.0	.0	.0	.0
6054.	3309-C	A	1.3	1.81	17.7	2235.	196.	.0	.0	.0	.0
6055.	3309-C	A	13.1	1.75	17.2	1503.	295.	.0	.0	.0	.0
6056.	3329-C	A	8.1	1.75	16.3	1778.	0.	.0	.0	.0	.0
6057.	3329-C	A	2.3	1.80	15.2	1748.	0.	.0	.0	.0	.0
6059.	3329-C	A	10.3	1.82	15.7	1910.	0.	.0	.0	.0	.0
6060.	3322-C	A	6.2	1.80	16.4	1987.	0.	.0	.0	.0	.0
6061.	3322-C	A	2.2	1.78	16.0	2260.	0.	.0	.0	.0	.0

TABLE 11-1 (Continued)

SERIAL NUMBER	FURNACE RUN	GRADE	LOG LOCATION	DENSITY	RESISTIVITY	TENSILE STRENGTH	ASH CONTENT	BORON CONTENT	IRON CONTENT	VANADIUM CONTENT	TITANIUM CONTENT
6062.	3322-C	A	7.2	1.75	18.1	1387.	0.	.0	.0	.0	.0
6063.	3322-C	A	9.3	1.73	18.1	1864.	121.	.0	.0	.0	.0
6064.	3372-C	A	3.3	1.76	17.8	1523.	0.	.0	.0	.0	.0
6065.	3372-C	A	8.3	1.73	18.3	1835.	0.	.0	.0	.0	.0
6066.	3393-C	A	16.2	1.77	16.8	1263.	0.	.0	.0	.0	.0
6067.	3393-C	A	11.3	1.77	17.7	1429.	0.	.0	.0	.0	.0
6068.	3323-C	A	4.2	1.77	16.5	1213.	0.	.0	.0	.0	.0
6069.	3371-C	A	12.2	1.76	17.3	2270.	0.	.0	.0	.0	.0
6070.	3371-C	A	13.2	1.73	16.9	2326.	57.	.9	.0	.0	.0
6071.	3371-C	A	14.1	1.77	16.6	1827.	0.	.0	.0	.0	.0
6072.	3371-C	A	16.2	1.76	17.0	1626.	0.	.0	.0	.0	.0
6073.	3371-C	A	3.3	1.77	16.4	2829.	0.	.0	.0	.0	.0
6074.	3371-C	A	15.2	1.77	17.9	1693.	0.	.0	.0	.0	.0
6076.	3442-C	A	12.2	1.78	17.1	1457.	74.	.0	.0	.0	.0
6077.	3442-C	A	14.2	1.73	21.2	1535.	73.	.0	.0	.0	.0
6078.	3442-C	A	3.3	1.79	17.4	1549.	51.	.0	.0	.0	.0
6079.	3442-C	A	5.5	1.80	16.8	2110.	222.	.0	.0	.0	.0
6080.	3442-C	A	7.5	1.80	16.9	1540.	60.	.0	.0	.0	.0
6081.	3442-C	A	8.4	1.73	16.1	1977.	55.	.0	.0	.0	.0
6082.	3442-C	A	12.4	1.80	14.1	1714.	60.	.0	.0	.0	.0
6083.	3442-C	A	13.4	1.79	15.4	1683.	122.	.0	.0	.0	.0
6084.	3442-C	A	13.6	1.78	16.9	1445.	104.	.0	.0	.0	.0
6090.	3469-C	A	16.3	1.77	17.8	2002.	170.	.0	.0	.0	.0
226.	2504	B	18.3	1.84	18.7	709.	0.	.0	.0	.0	.0
2234.	2504	B	16.1	1.79	18.2	917.	0.	.0	.0	.0	.0
4005.	3371-C	B	9.3	1.72	18.6	856.	0.	.0	.0	.0	.0
4008.	3393-C	B	9.1	1.73	18.3	837.	105.	1.7	.0	.0	.0
4025.	3393-C	B	7.3	1.72	18.9	825.	0.	.0	.0	.0	.0
4457.	3371-C	B	6.3	1.79	18.2	671.	0.	.0	.0	.0	.0
5267.	3442-C	B	10.3	1.79	17.2	943.	63.	.0	.0	.0	.0
5355.	3442-C	B	1.2	1.77	16.4	920.	207.	.0	.0	.0	.0
5736.	3393-C	B	10.1	1.79	15.9	921.	0.	.0	.0	.0	.0
5792.	3372-C	B	12.2	1.74	17.1	922.	0.	.0	.0	.0	.0
5794.	3372-C	B	2.3	1.69	21.8	892.	0.	.0	.0	.0	.0
5977.	3442-C	B	1.1	1.80	15.6	802.	71.	.5	.0	.0	.0
6075.	3442-C	B	1.3	1.80	16.6	943.	55.	.0	.0	.0	.0
5285.	3442-C	C	12.1	1.79	18.7	2530.	762.	.0	****	21.3	17.2
5286.	3442-C	C	9.1	1.78	20.2	2357.	517.	.5	****	19.5	30.6

TABLE 11-2

STATISTICAL DATA ON IMPURITIES IN H-327 GRAPHITE

(Logs Selected from Various Stages in Fuel Block Production Schedules)

Production Period	Impurity, Max/Min/Mean Content and Standard Deviation (ppm)																			
	Total Ash				Boron				Iron				Titanium				Vanadium			
	$\bar{x}$	σ	Max	Min	$\bar{x}$	σ	Max	Min	$\bar{x}$	σ	Max	Min	$\bar{x}$	σ	Max	Min	$\bar{x}$	σ	Max	Min
First three graphitizing runs, 3/69 (approx 70 logs)	56.1	53.8	408	16.0	0.5	0.48	4.6	0.1	9.92	16.37	80.0	1.0	4.35	7.72	33.4	0.2	1.22	1.54	8.7	0.1
Log 42/2034, from mid-schedule, May 1969	60[a]				0.5				6.0				<1.0				<0.5			
Logs from late stage of graphitization schedule, August 1970, Sept. 1970	199 192				ND[b] ND[b]				80.0 20.0				8.0 20.0				10.0 10.0			

[a] Accuracy -25% to +35% 1 σ.

[b] Not detected, less than 0.5 ppm.

TABLE 11-3

SPECTROCHEMICAL ANALYSIS OF H-327 GRAPHITE

Log No.	Position	Element Concentration (ppm) [a]									
		Al	B	Cu	Fe	Mg	Si	Ti	V	Mn	Ash [b]
10-2/694	End Edge	1.0	ND [c]	ND	ND	2.0	<10.0	4.0	ND	ND	21
3-1/705	End Edge	1.0	1.0	ND	ND	2.0	<10.0	8.0	ND	ND	38
2-2/739	End Edge	1.0	2.0	ND	ND	2.0	10.0	10.0	ND	ND	55
7-2/744	End Edge	4.0	2.0	ND	2.0	6.0	20.0	8.0	ND	ND	77
12-2/769	End Edge	1.0	1.0	1.0	1.0	4.0	20.0	10.0	ND	ND	55
12-2/956	End Edge	4.09	1.0	1.0	2.0	4.0	20.0	10.0	ND	ND	472
12-1/958	End Edge	ND	1.0	ND	2.0	1.0	20.0	20.0	ND	ND	317
8-2/1058	End Edge	1.0	1.0	ND	ND	4.0	20.0	10.0	ND	ND	72
4-2/1959	End Edge	6.0	ND	1.0	10.0	10.0	80.0	10.0	ND	ND	77
4-2/2479	End Edge	4.0	1.0	1.0	1.0	6.0	20.0	10.0	ND	ND	65
3-1/2482	End Edge	2.0	1.0	2.0	2.0	2.0	<10.0	6.0	ND	ND	47
42/1960	End Edge	20.0	10.0	<1.0	2.0	2.0	<10.0	6.0	ND	ND	62
10/9977C	End Center	2.0	ND	ND	1.0	2.0	<10.0	6.0	ND	ND	
12-1	Mid Length Edge	4.0	4.0	ND	1.0	4.0	20.0	8.0	ND	ND	
	Mid Length Ctr	1.0	ND	ND	1.0	4.0	10.0	ND	ND	ND	
0001/1743	QC Edge Slab	4.0	ND	ND	ND	ND	10.0	ND	ND	ND	< 43
0001/2820	QC Edge Slab	4.0	ND	ND	ND	ND	20.0	ND	ND	ND	54
0018/1787	QC Edge Slab	2.0	ND	ND	6.0	ND	40.0	4.0	ND	ND	< 37
0018/2511	QC Edge Slab	ND	ND	ND	ND	ND	ND	1.0	ND	ND	61
0175/615	QC Edge Slab	ND	ND	ND	ND	ND	10.0	ND	ND	ND	< 32
0175/2520	QC Edge Slab	4.0	4.0	ND	8.0	ND	20.0	ND	ND	ND	< 35
9974	QC Edge Slab	1.0	4.0	ND	2.0	ND	10.0	ND	ND	10.0	14
9987	QC Edge Slab	ND	ND	ND	1.0	ND	10.0	ND	ND	<10.0	21
9990	QC Edge Slab	ND	ND	ND	1.0	ND	10.0	ND	ND	<10.0	93
0060	QC Edge Slab	ND	ND	ND	1.0	ND	10.0	ND	ND	<10.0	93
Sensitivity, Min Content Detectable		1.0	0.5	1.0	1.0	1.0	10.0	1.0	0.5	10.0	

(a) Accuracy -25% to +35% = 1 σ; for 90% confidence x 1.5.

(b) Ash content determined by Great Lakes Carbon Corporation.

(c) Not detected.

TABLE 11-4
PROPERTIES OF H-327 GRAPHITE, FORT ST. VRAIN RELOAD 2
[Density (Mg/m^3), tensile strength (psi), impurity content (ppm)]

SERIAL NUMBER	FURNACE RUN	GRADE	LOG LOCATION	DENSITY	RESISTIVITY	TENSILE STRENGTH	ASH CONTENT	BORON CONTENT	IRON CONTENT	VANADIUM CONTENT	TITANIUM CONTENT
5442.	3670-C	A	1.1	1.74	18.0	1420.	410.	.0	41.5	15.0	66.0
5550.	3670-C	A	2.1	1.77	17.8	1830.	166.	.0	.0	.0	.0
5551.	3670-C	A	3.1	1.79	17.3	1910.	83.	.0	.0	.0	.0
5574.	3670-C	A	1.3	1.76	17.3	2010.	236.	.0	.0	.0	.0
5460.	3670-C	A	2.3	1.76	17.4	1570.	231.	.3	.0	.0	.0
5588.	3670-C	A	3.3	1.76	17.7	2150.	65.	.0	.0	.0	.0
5653.	4017-C	A	1.1	1.80	20.8	2633.	233.	.7	.0	.0	.0
5601.	4019-C	A	1.2	1.78	18.4	2388.	272.	.0	.0	.0	.0
5760.	4017-C	B	1.3	1.80	18.0	0.	0.	.0	.0	.0	.0
5656.	4017-C	A	2.1	1.81	20.7	2052.	0.	.0	.0	.0	.0
5667.	4017-C	B	2.2	1.84	20.6	0.	0.	.0	.0	.0	.0
5556.	4017-C	B	2.3	1.79	19.4	0.	0.	.0	.0	.0	.0
5529.	4017-C	A	3.1	1.78	22.9	1756.	0.	.0	.0	.0	.0
5549.	4017-C	B	3.2	1.79	20.8	0.	0.	.0	.0	.0	.0
5898.	4017-C	B	3.3	1.82	19.6	0.	0.	.0	.0	.0	.0
7003.	4017-C	A	4.1	1.81	21.5	2204.	0.	.0	.0	.0	.0
4730.	4017-C	B	4.2	1.79	19.6	0.	0.	.0	.0	.0	.0
5654.	4017-C	B	4.3	1.80	17.7	0.	0.	.0	.0	.0	.0
5459.	4017-C	A	5.1	1.78	21.8	1881.	39.	.4	.0	.0	.0
5840.	4017-C	B	5.2	1.79	18.8	0.	0.	.0	.0	.0	.0
5663.	4017-C	B	5.3	1.80	18.6	0.	0.	.0	.0	.0	.0
5623.	4017-C	A	6.1	1.79	22.8	1930.	0.	.0	.0	.0	.0
5699.	4017-C	B	6.2	1.79	22.1	0.	0.	.0	.0	.0	.0
5544.	4017-C	B	6.3	1.78	19.3	0.	0.	.0	.0	.0	.0
5470.	4017-C	A	7.1	1.78	22.1	2041.	0.	.0	.0	.0	.0
5561.	4017-C	B	7.2	1.78	19.6	0.	0.	.0	.0	.0	.0
5398.	4017-C	B	7.3	1.77	19.4	0.	0.	.0	.0	.0	.0
5587.	4017-C	B	8.1	1.78	22.6	0.	0.	.0	.0	.0	.0
5611.	4017-C	B	8.2	1.78	18.9	0.	0.	.0	.0	.0	.0
5455.	4017-C	B	8.3	1.79	20.6	0.	0.	.0	.0	.0	.0
5453.	4017-C	A	9.1	1.78	22.8	1202.	225.	.7	.0	.0	.0
5636.	4017-C	A	9.2	1.78	18.7	2384.	244.	.0	.0	.0	.0
5531.	4017-C	B	9.3	1.77	20.4	0.	0.	.0	.0	.0	.0
5657.	4017-C	B	10.1	1.80	21.8	0.	0.	.0	.0	.0	.0
5450.	4017-C	B	10.2	1.78	19.8	0.	0.	.0	.0	.0	.0
5602.	4017-C	B	10.3	1.78	19.4	0.	0.	.0	.0	.0	.0
7004.	4017-C	B	11.1	1.78	18.9	0.	0.	.0	.0	.0	.0
5757.	4017-C	B	11.2	1.81	17.9	0.	0.	.0	.0	.0	.0
4741.	4017-C	B	11.3	1.78	19.7	0.	0.	.0	.0	.0	.0
5661.	4017-C	B	12.1	1.80	22.6	0.	0.	.0	.0	.0	.0
5576.	4017-C	B	12.2	1.78	19.1	0.	0.	.0	.0	.0	.0
5744.	4017-C	B	12.3	1.80	20.3	0.	0.	.0	.0	.0	.0
5508.	4017-C	A	13.1	1.76	23.5	2121.	84.	.6	.0	.0	.0
5647.	4017-C	A	13.2	1.82	18.0	2552.	214.	.4	.0	.0	.0
5444.	4017-C	B	13.3	1.78	19.8	0.	0.	.0	.0	.0	.0
5577.	4017-C	B	14.1	1.77	23.7	0.	0.	.0	.0	.0	.0
5443.	4017-C	B	14.2	1.77	19.8	0.	0.	.0	.0	.0	.0
4494.	4017-C	B	14.3	1.78	19.8	0.	0.	.0	.0	.0	.0
5648.	4017-C	B	15.1	1.80	18.0	0.	0.	.0	.0	.0	.0
5582.	4017-C	B	15.2	1.77	19.6	0.	0.	.0	.0	.0	.0
5284.	4017-C	B	15.3	1.81	18.4	0.	0.	.0	.0	.0	.0
5436.	4017-C	A	16.1	1.79	21.5	1358.	39.	.0	.0	.0	.0
5754.	4017-C	A	16.2	1.79	18.2	2598.	171.	.5	.0	.0	.0
5553.	4017-C	A	16.3	1.79	21.5	2207.	0.	.0	.0	.0	.0

TABLE 11-4 (Continued)

SERIAL NUMBER	FURNACE RUN	GRADE	LOG LOCATION	DENSITY	RESISTIVITY	TENSILE STRENGTH	ASH CONTENT	BORON CONTENT	IRON CONTENT	VANADIUM CONTENT	TITANIUM CONTENT
5475.	4017-C	A	1.4	1.78	21.8	1864.	0.	.0	.0	.0	.0
5668.	4017-C	A	1.5	1.81	20.4	2243.	189.	.0	.0	.0	.0
5711.	4017-C	A	1.6	1.80	21.1	2470.	247.	.7	.0	.0	.0
7005.	4017-C	A	2.4	1.78	21.3	1782.	0.	.0	.0	.0	.0
7006.	4017-C	A	2.5	1.77	22.6	2506.	0.	.0	.0	.0	.0
5629.	4017-C	A	2.6	1.90	20.6	2461.	0.	.0	.0	.0	.0
5275.	4017-C	A	3.4	1.77	22.5	1322.	0.	.0	.0	.0	.0
5607.	4017-C	A	3.5	1.77	22.7	2769.	0.	.0	.0	.0	.0
5283.	4017-C	A	3.6	1.79	21.7	2723.	0.	.0	.0	.0	.0
5896.	4017-C	A	4.4	1.82	20.7	1744.	0.	.0	.0	.0	.0
5249.	4017-C	A	4.5	1.78	22.6	2355.	0.	.0	.0	.0	.0
5548.	4017-C	A	4.6	1.76	22.3	1862.	0.	.0	.0	.0	.0
5448.	4017-C	B	5.4	1.77	20.3	0.	0.	.0	.0	.0	.0
5743.	4017-C	A	5.5	1.79	22.0	2327.	34.	.4	.0	.0	.0
5530.	4017-C	A	5.6	1.78	21.2	2178.	0.	.0	.0	.0	.0
5555.	4017-C	A	6.4	1.78	19.8	2022.	32.	.0	.0	.0	.0
5447.	4017-C	A	6.5	1.76	22.9	2201.	0.	.0	.0	.0	.0
5666.	4017-C	A	6.6	1.92	20.3	2493.	0.	.0	.0	.0	.0
5627.	4017-C	A	7.4	1.80	18.6	2313.	164.	.0	.0	.0	.0
5684.	4017-C	A	7.5	1.82	20.9	2571.	0.	.0	.0	.0	.0
5626.	4017-C	A	7.6	1.79	21.1	2081.	0.	.0	.0	.0	.0
7007.	4017-C	A	8.4	1.79	20.8	2197.	0.	.0	.0	.0	.0
5616.	4017-C	A	8.5	1.77	22.7	1916.	0.	.0	.0	.0	.0
5619.	4017-C	A	8.6	1.78	22.7	1678.	0.	.0	.0	.0	.0
5598.	4017-C	A	9.4	1.77	19.8	2223.	0.	.0	.0	.0	.0
5632.	4017-C	A	9.5	1.77	22.1	1683.	232.	.5	.0	.0	.0
5628.	4017-C	A	9.6	1.79	21.0	2442.	221.	.0	.0	.0	.0
5753.	4017-C	A	10.4	1.82	19.1	1950.	0.	.0	.0	.0	.0
5686.	4017-C	A	10.5	1.82	20.0	2343.	0.	.0	.0	.0	.0
5528.	4017-C	B	10.6	1.82	19.5	0.	0.	.0	.0	.0	.0
5435.	4017-C	A	11.4	1.81	21.0	1358.	0.	.0	.0	.0	.0
5504.	4017-C	A	11.5	1.78	22.3	1981.	0.	.0	.0	.0	.0
5523.	4017-C	B	11.6	1.77	18.7	0.	0.	.0	.0	.0	.0
5518.	4017-C	A	12.4	1.78	19.9	2564.	0.	.0	.0	.0	.0
5613.	4017-C	A	12.5	1.78	22.7	1637.	0.	.0	.0	.0	.0
5823.	4017-C	B	12.6	1.79	18.5	0.	0.	.0	.0	.0	.0
5552.	4017-C	B	13.4	1.79	19.1	0.	0.	.0	.0	.0	.0
5650.	4017-C	A	13.5	1.91	19.0	2435.	286.	.0	.0	.0	.0
5741.	4017-C	B	13.6	1.77	22.8	0.	0.	.0	.0	.0	.0
5517.	4017-C	A	14.4	1.80	20.2	1655.	71.	.0	.0	.0	.0
5446.	4017-C	A	14.5	1.75	20.3	1324.	0.	.0	.0	.0	.0
5501.	4017-C	B	14.6	1.77	23.1	0.	0.	.0	.0	.0	.0
5473.	4017-C	A	15.4	1.80	20.0	1538.	0.	.0	.0	.0	.0
5758.	4017-C	A	15.5	1.82	20.8	2351.	0.	.0	.0	.0	.0
5390.	4017-C	A	15.6	1.80	22.8	1780.	0.	.0	.0	.0	.0
5706.	4017-C	A	16.4	1.92	19.2	2413.	263.	.0	.0	.0	.0
5757.	4017-C	A	16.5	1.80	21.4	2801.	263.	.0	.0	.0	.0
7008.	4017-C	B	16.6	1.91	19.5	0.	0.	.3	.0	.0	.0
7009.	4022-C	A	1.1	1.73	17.4	2603.	77.	.8	.0	.0	.0
7010.	4022-C	A	1.2	1.78	17.2	1385.	50.	.0	.0	.0	.0
5833.	4022-C	B	1.3	1.75	18.7	0.	0.	.0	.0	.0	.0
5568.	4022-C	B	2.1	1.77	18.4	0.	0.	.0	.0	.0	.0
5532.	4022-C	B	2.2	1.77	17.9	0.	0.	.0	.0	.0	.0
5527.	4022-C	B	2.3	1.78	18.4	0.	0.	.0	.0	.0	.0

TABLE 11-4 (Continued)

SERIAL NUMBER	FURNACE RUN	GRADE	LOG LOCATION	DENSITY	RESISTIVITY	TENSILE STRENGTH	ASH CONTENT	BORON CONTENT	IRON CONTENT	VANADIUM CONTENT	TITANIUM CONTENT
4745.	4022-C	B	3.1	1.74	18.6	0.	0.	.0	.0	.0	.0
5683.	4022-C	B	3.2	1.79	17.0	0.	0.	.0	.0	.0	.0
5468.	4022-C	B	3.3	1.78	18.1	0.	0.	.0	.0	.0	.0
5545.	4022-C	B	4.1	1.77	18.5	0.	0.	.0	.0	.0	.0
5562.	4022-C	B	4.2	1.78	18.4	0.	0.	.0	.0	.0	.0
7014.	4022-C	B	4.3	1.74	18.9	0.	0.	.0	.0	.0	.0
5610.	4022-C	A	5.1	1.84	17.1	2661.	151.	.1	.0	.0	.0
5646.	4022-C	A	5.2	1.78	14.2	2727.	118.	.0	.0	.0	.0
5742.	4022-C	A	5.3	1.78	17.2	2711.	92.	.0	.0	.0	.0
5547.	4022-C	B	6.1	1.78	18.6	0.	0.	.0	.0	.0	.0
7015.	4022-C	B	6.2	1.77	18.4	0.	0.	.0	.0	.0	.0
5490.	4022-C	B	6.3	1.76	19.0	0.	0.	.0	.0	.0	.0
5749.	4022-C	B	7.1	1.80	17.7	0.	0.	.0	.0	.0	.0
5641.	4022-C	B	7.2	1.78	17.7	0.	0.	.0	.0	.0	.0
5834.	4022-C	B	7.3	1.76	18.7	0.	0.	.0	.0	.0	.0
5831.	4022-C	B	8.1	1.76	18.6	0.	0.	.0	.0	.0	.0
5445.	4022-C	B	8.2	1.78	19.3	0.	0.	.0	.0	.0	.0
5437.	4022-C	B	8.3	1.78	18.8	0.	0.	.0	.0	.0	.0
5356.	4022-C	A	9.1	1.79	17.9	2178.	48.	.0	.0	.0	.0
5520.	4022-C	A	9.2	1.77	17.0	2337.	91.	.0	.0	.0	.0
5581.	4022-C	B	9.3	1.77	18.7	0.	0.	.0	.0	.0	.0
4484.	4022-C	B	10.1	1.76	18.6	0.	0.	.0	.0	.0	.0
5647.	4022-C	B	10.2	1.78	17.4	0.	0.	.0	.0	.0	.0
5503.	4022-C	B	10.3	1.77	18.5	0.	0.	.0	.0	.0	.0
5765.	4022-C	B	11.1	1.80	18.2	0.	0.	.0	.0	.0	.0
5569.	4022-C	B	11.2	1.79	18.1	0.	0.	.0	.0	.0	.0
5835.	4022-C	B	11.3	1.78	18.1	0.	0.	.0	.0	.0	.0
5461.	4022-C	B	12.1	1.77	18.6	0.	0.	.0	.0	.0	.0
7018.	4022-C	B	12.2	1.80	17.7	0.	0.	.0	.0	.0	.0
5592.	4022-C	B	12.3	1.77	17.7	0.	0.	.0	.0	.0	.0
5465.	4022-C	A	13.1	1.76	18.2	1888.	66.	1.2	.0	.0	.0
5467.	4022-C	A	13.2	1.78	18.8	1869.	84.	.0	.0	.0	.0
5511.	4022-C	A	13.3	1.76	17.3	2643.	108.	.0	.0	.0	.0
5659.	4022-C	B	14.1	1.80	17.3	0.	0.	.0	.0	.0	.0
5643.	4022-C	B	14.2	1.77	17.8	0.	0.	.0	.0	.0	.0
5525.	4022-C	B	14.3	1.79	18.1	0.	0.	.0	.0	.0	.0
5661.	4022-C	B	15.1	1.80	17.2	0.	0.	.0	.0	.0	.0
4729.	4022-C	B	15.2	1.76	17.6	0.	0.	.0	.0	.0	.0
5825.	4022-C	B	15.3	1.78	18.0	0.	0.	.0	.0	.0	.0
7019.	4022-C	A	16.1	1.78	17.5	2114.	181.	.0	.0	.0	.0
5484.	4022-C	A	16.2	1.75	17.9	1614.	192.	1.2	.0	.0	.0
5822.	4022-C	B	16.3	1.78	17.7	0.	0.	.0	.0	.0	.0
5586.	4022-C	B	1.4	1.77	17.9	0.	0.	.0	.0	.0	.0
7011.	4022-C	A	1.5	1.77	17.4	2249.	259.	.0	.0	.0	.0
5385.	4022-C	A	1.6	1.79	18.5	1651.	251.	.5	.0	.0	.0
5572.	4022-C	B	2.4	1.76	18.5	0.	0.	.0	.0	.0	.0
5524.	4022-C	B	2.5	1.79	18.8	0.	0.	.0	.0	.0	.0
7012.	4022-C	B	2.6	1.79	17.5	0.	0.	.0	.0	.0	.0
5614.	4022-C	B	3.4	1.77	18.6	0.	0.	.0	.0	.0	.0
5454.	4022-C	B	3.5	1.77	18.8	0.	0.	.0	.0	.0	.0
7013.	4022-C	B	3.6	1.77	18.9	0.	0.	.0	.0	.0	.0
5495.	4022-C	B	4.4	1.78	18.6	0.	0.	.0	.0	.0	.0
5469.	4022-C	B	4.5	1.78	18.9	0.	0.	.0	.0	.0	.0
5575.	4022-C	B	4.6	1.78	18.5	0.	0.	.0	.0	.0	.0

TABLE 11-4 (Continued)

SERIAL NUMBER	FURNACE RUN	GRADE	LOG LOCATION	DENSITY	RESISTIVITY	TENSILE STRENGTH	ASH CONTENT	BORON CONTENT	IRON CONTENT	VANADIUM CONTENT	TITANIUM CONTENT
4747.	3577-C	A	7.1	1.78	15.2	1607.	0.	.0	.0	.0	.0
5687.	3577-C	A	7.2	1.78	15.2	1389.	0.	.0	.0	.0	.0
5226.	3577-C	A	7.3	1.82	15.3	1509.	0.	.0	.0	.0	.0
5870.	3577-C	A	8.1	1.80	16.0	1503.	0.	.0	.0	.0	.0
5281.	3577-C	A	8.2	1.79	17.6	2315.	0.	.0	.0	.0	.0
5756.	3577-C	A	8.3	1.81	16.2	1905.	0.	.0	.0	.0	.0
5867.	3577-C	A	9.1	1.81	17.8	1998.	116.	.7	.0	.0	.0
5902.	3577-C	A	9.2	1.83	17.5	1825.	217.	.0	.0	.0	.0
6099.	3577-C	A	9.3	1.78	17.2	2291.	0.	.0	.0	.0	.0
4480.	3577-C	A	10.1	1.77	15.8	1646.	0.	.0	.0	.0	.0
5261.	3577-C	A	10.2	1.80	15.8	2300.	0.	.0	.0	.0	.0
5662.	3577-C	A	10.3	1.81	16.2	1898.	0.	.0	.0	.0	.0
5451.	3577-C	A	11.1	1.78	18.0	2199.	0.	.0	.0	.0	.0
5599.	3577-C	A	11.2	1.79	16.6	2524.	0.	.0	.0	.0	.0
5295.	3577-C	A	11.3	1.78	17.3	2000.	0.	.0	.0	.0	.0
5486.	3577-C	A	12.1	1.78	15.6	1369.	0.	.0	.0	.0	.0
5401.	3577-C	A	12.2	1.81	16.7	2158.	0.	.0	.0	.0	.0
5748.	3577-C	A	12.3	1.78	15.9	2465.	0.	.0	.0	.0	.0
5262.	3577-C	A	13.1	1.81	19.9	2194.	179.	.0	.0	.0	.0
5615.	3577-C	A	13.2	1.79	19.2	2082.	59.	.7	.0	.0	.0
5620.	3577-C	A	13.3	1.79	18.5	2140.	60.	.5	.0	.0	.0
5638.	3577-C	A	14.1	1.79	16.7	2287.	0.	.0	.0	.0	.0
5742.	3577-C	A	14.2	1.81	15.9	2154.	0.	.0	.0	.0	.0
5635.	3577-C	A	14.3	1.79	15.9	1990.	0.	.0	.0	.0	.0
5440.	3577-C	A	15.1	1.78	17.5	1694.	0.	.0	.0	.0	.0
5505.	3577-C	A	15.2	1.76	17.8	1991.	0.	.0	.0	.0	.0
5606.	3577-C	A	15.3	1.79	16.8	2152.	0.	.0	.0	.0	.0
5664.	3577-C	A	16.1	1.81	18.3	2732.	260.	.0	.0	.0	.0
5239.	3577-C	A	16.2	1.78	17.4	2184.	132.	.5	.0	.0	.0
5289.	3577-C	A	16.3	1.79	15.5	2639.	0.	.0	.0	.0	.0
5434.	3577-C	A	1.4	1.79	18.4	1774.	0.	.0	.0	.0	.0
5887.	3577-C	A	1.5	1.82	15.9	2005.	296.	.0	.0	.0	.0
5280.	3577-C	A	1.6	1.79	16.6	1203.	53.	.7	.0	.0	.0
4481.	3577-C	A	2.4	1.78	17.4	1984.	0.	.0	.0	.0	.0
5886.	3577-C	A	2.5	1.83	15.9	1913.	0.	.0	.0	.0	.0
4739.	3577-C	A	2.6	1.80	18.7	1803.	0.	.0	.0	.0	.0
5322.	3577-C	A	3.4	1.80	16.1	2183.	0.	.0	.0	.0	.0
4752.	3577-C	A	3.5	1.78	18.2	1683.	0.	.0	.0	.0	.0
5651.	3577-C	A	3.6	1.81	20.0	2607.	0.	.0	.0	.0	.0
5538.	3577-C	A	4.4	1.80	18.2	2159.	0.	.0	.0	.0	.0
5755.	3577-C	A	4.5	1.81	17.6	1685.	0.	.0	.0	.0	.0
5277.	3577-C	A	4.6	1.79	17.5	1402.	0.	.0	.0	.0	.0
5439.	3577-C	A	5.4	1.78	17.6	1253.	49.	.7	.0	.0	.0
5310.	3577-C	A	5.5	1.80	17.5	2366.	0.	.0	.0	.0	.0
5588.	3577-C	A	5.6	1.82	18.7	2376.	0.	.0	.0	.0	.0
5714.	3577-C	A	6.4	1.83	17.2	1977.	0.	.0	.0	.0	.0
7000.	3577-C	A	6.5	1.81	17.3	2085.	0.	.0	.0	.0	.0
5705.	3577-C	A	6.6	1.82	19.7	2136.	0.	.0	.0	.0	.0
5760.	3577-C	A	7.4	1.82	17.9	1507.	0.	.0	.0	.0	.0
7001.	3577-C	A	7.5	1.78	19.1	2039.	0.	.0	.0	.0	.0
7002.	3577-C	A	7.6	1.87	16.6	2350.	0.	.0	.0	.0	.0
5403.	3577-C	A	8.4	1.80	18.5	2300.	0.	.0	.0	.0	.0
5608.	3577-C	A	8.5	1.81	17.7	2379.	0.	.0	.0	.0	.0
5449.	3577-C	A	8.6	1.82	20.1	1315.	0.	.0	.0	.0	.0

TABLE 11-4 (Continued)

SERIAL NUMBER	FURNACE RUN	GRADE	LOG LOCATION	DENSITY	RESISTIVITY	TENSILE STRENGTH	ASH CONTENT	BORON CONTENT	IRON CONTENT	VANADIUM CONTENT	TITANIUM CONTENT
5759.	4022-C	A	5.4	1.81	17.9	2594.	225.	.8	.0	.0	.0
5516.	4022-C	B	5.5	1.77	18.9	0.	0.	.0	.0	.0	.0
5637.	4022-C	B	5.6	1.79	18.4	0.	0.	.0	.0	.0	.0
5874.	4022-C	B	6.4	1.79	17.4	0.	0.	.0	.0	.0	.0
5624.	4022-C	B	6.5	1.77	19.4	0.	0.	.0	.0	.0	.0
5441.	4022-C	B	6.6	1.76	19.7	0.	0.	.0	.0	.0	.0
5832.	4022-C	B	7.4	1.75	19.3	0.	0.	.0	.0	.0	.0
5471.	4022-C	B	7.5	1.77	19.3	0.	0.	.0	.0	.0	.0
5304.	4022-C	B	7.6	1.77	18.0	0.	0.	.0	.0	.0	.0
5526.	4022-C	B	8.4	1.79	18.3	0.	0.	.0	.0	.0	.0
5509.	4022-C	B	8.5	1.75	20.0	0.	0.	.0	.0	.0	.0
5579.	4022-C	B	8.6	1.77	19.6	0.	0.	.0	.0	.0	.0
7016.	4022-C	B	9.4	1.78	18.4	0.	0.	.0	.0	.0	.0
5907.	4022-C	A	9.5	1.80	17.4	2003.	260.	.3	.0	.0	.0
5593.	4022-C	A	9.6	1.78	19.1	2580.	270.	.6	.0	.0	.0
5458.	4022-C	B	10.4	1.78	18.3	0.	0.	.0	.0	.0	.0
5836.	4022-C	B	10.5	1.77	18.3	0.	0.	.0	.0	.0	.0
5660.	4022-C	B	10.6	1.79	18.1	0.	0.	.0	.0	.0	.0
7017.	4022-C	B	11.4	1.79	18.0	0.	0.	.0	.0	.0	.0
5681.	4022-C	B	11.5	1.79	18.0	0.	0.	.0	.0	.0	.0
5499.	4022-C	B	11.6	1.77	18.4	0.	0.	.0	.0	.0	.0
5507.	4022-C	B	12.4	1.76	18.1	0.	0.	.0	.0	.0	.0
5665.	4022-C	B	12.5	1.80	18.1	0.	0.	.0	.0	.0	.0
5554.	4022-C	B	12.6	1.79	18.6	0.	0.	.0	.0	.0	.0
5625.	4022-C	A	13.4	1.77	18.6	2076.	121.	.7	.0	.0	.0
5563.	4022-C	B	13.5	1.78	19.0	0.	0.	.0	.0	.0	.0
5633.	4022-C	B	13.6	1.79	17.8	0.	0.	.0	.0	.0	.0
5876.	4022-C	B	14.4	1.80	17.5	0.	0.	.0	.0	.0	.0
5573.	4022-C	B	14.5	1.77	18.6	0.	0.	.0	.0	.0	.0
5456.	4022-C	B	14.6	1.77	19.0	0.	0.	.0	.0	.0	.0
5515.	4022-C	B	15.4	1.78	17.4	0.	0.	.0	.0	.0	.0
5658.	4022-C	B	15.5	1.78	17.6	0.	0.	.0	.0	.0	.0
5474.	4022-C	B	15.6	1.76	18.8	0.	0.	.0	.0	.0	.0
5510.	4022-C	B	16.4	1.76	18.1	0.	0.	.0	.0	.0	.0
5558.	4022-C	A	16.5	1.77	18.6	1927.	279.	.5	.0	.0	.0
5389.	4022-C	A	16.6	1.79	17.6	2151.	278.	.0	.0	.0	.0
5391.	3577-C	A	1.1	1.80	17.7	1758.	193.	.5	.0	.0	.0
5290.	3577-C	A	1.2	1.81	18.8	1364.	208.	.0	.0	.0	.0
5853.	3577-C	A	1.3	1.82	16.1	1578.	0.	.0	.0	.0	.0
5594.	3577-C	A	2.1	1.77	17.4	1475.	0.	.0	.0	.0	.0
5617.	3577-C	A	2.2	1.79	17.7	1648.	0.	.0	.0	.0	.0
6097.	3577-C	A	2.3	1.77	17.9	1339.	0.	.0	.0	.0	.0
5388.	3577-C	A	3.1	1.80	16.1	1225.	0.	.0	.0	.0	.0
5584.	3577-C	A	3.2	1.79	16.9	2657.	0.	.0	.0	.0	.0
4493.	3577-C	A	3.3	1.78	17.1	1770.	0.	.0	.0	.0	.0
4492.	3577-C	A	4.1	1.79	17.0	1864.	0.	.0	.0	.0	.0
5522.	3577-C	A	4.2	1.79	18.0	1847.	0.	.0	.0	.0	.0
5305.	3577-C	A	4.3	1.79	15.1	2201.	0.	.0	.0	.0	.0
5712.	3577-C	A	5.1	1.81	18.1	2239.	275.	.7	.0	.0	.0
5652.	3577-C	A	5.2	1.80	18.0	2150.	220.	.0	.0	.0	.0
5884.	3577-C	A	5.3	1.82	17.5	2215.	149.	.0	.0	.0	.0
5536.	3577-C	A	6.1	1.78	19.2	2247.	0.	.0	.0	.0	.0
5491.	3577-C	A	6.2	1.77	18.4	2086.	0.	.0	.0	.0	.0
6098.	3577-C	A	6.3	1.78	17.6	1958.	0.	.0	.0	.0	.0

TABLE 11-4 (Continued)

SERIAL NUMBER	FURNACE RUN	GRADE	LOG LOCATION	DENSITY	RESISTIVITY	TENSILE STRENGTH	ASH CONTENT	BORON CONTENT	IRON CONTENT	VANADIUM CONTENT	TITANIUM CONTENT
5560.	3577-C	A	9.4	1.79	18.4	1899.	0.	.0	.0	.0	.0
5642.	3577-C	A	9.5	1.81	17.6	2488.	193.	.7	.0	.0	.0
5871.	3577-C	A	9.6	1.80	18.2	1337.	192.	.0	.0	.0	.0
5541.	3577-C	A	10.4	1.78	18.1	2375.	0.	.0	.0	.0	.0
5317.	3577-C	A	10.5	1.81	18.3	1304.	0.	.0	.0	.0	.0
5901.	3577-C	A	10.6	1.83	16.8	1554.	0.	.0	.0	.0	.0
5604.	3577-C	A	11.4	1.79	18.1	1974.	0.	.0	.0	.0	.0
5537.	3577-C	A	11.5	1.78	19.3	2436.	0.	.0	.0	.0	.0
5600.	3577-C	A	11.6	1.79	17.8	2690.	0.	.0	.0	.0	.0
5514.	3577-C	A	12.4	1.79	18.0	2041.	0.	.0	.0	.0	.0
5880.	3577-C	A	12.5	1.81	18.1	2037.	0.	.0	.0	.0	.0
5685.	3577-C	A	12.6	1.80	17.0	2195.	0.	.0	.0	.0	.0
5869.	3577-C	A	13.4	1.81	16.6	2369.	135.	.0	.0	.0	.0
5542.	3577-C	A	13.5	1.80	17.5	2432.	0.	.0	.0	.0	.0
5498.	3577-C	A	13.6	1.78	17.7	1329.	0.	.0	.0	.0	.0
5631.	3577-C	A	14.4	1.79	17.5	2029.	0.	.0	.0	.0	.0
5899.	3577-C	A	14.5	1.83	17.4	2170.	0.	.0	.0	.0	.0
5713.	3577-C	A	14.6	1.80	17.9	2434.	0.	.0	.0	.0	.0
5303.	3577-C	A	15.4	1.80	17.5	2626.	0.	.0	.0	.0	.0
5485.	3577-C	A	15.5	1.77	18.4	1955.	0.	.0	.0	.0	.0
5583.	3577-C	A	15.6	1.77	18.1	1388.	0.	.0	.0	.0	.0
5564.	3577-C	A	16.4	1.76	17.8	2382.	0.	.0	.0	.0	.0
5492.	3577-C	A	16.5	1.77	19.2	1639.	262.	.4	.0	.0	.0
5483.	3577-C	A	16.6	1.76	20.3	1587.	0.	.0	.0	.0	.0

TABLE 11-5
CHEMICAL PURITY OF H-327 GRAPHITE
(in ppm)

Data Source	Ash			Boron			Iron		
	N	$\bar{X}$	S	N	$\bar{X}$	S	N	$\bar{X}$	S
FSV reload QA - Table 11-1	65	172	87	57	1.15	0.8	11	78	63
FSV reload QA - Table 11-4	267	145	104	31	0.6	0.2			
Characterization - Table 11-2	22	84	105	25	1.6	2	26	2	2
Characterization - Table 11-3	70	56	50	70	0.5	0.5	70	10	16
Characterization - Table 11-3	3	150	78				3	35	

TABLE 11-6
AXIAL ULTIMATE TENSILE STRENGTH OF H-327 GRAPHITE
(in MPa)

Data Source	Midlength Center			Midlength Edge			End Center			End Edge		
	N	$\bar{X}$	S	N	$\bar{X}$	S	N	$\bar{X}$	S	N	$\bar{X}$	S
Characterization - Ref. 11-2	(a)	11.2	1.34	(a)	16.5	1.52	(a)	15.0	1.77	(a)	15.9	1.22
QA acceptance - Table 11-9	2938	11.9	2.43									
Characterization - Refs. 11-3 through 11-7	17	9.4	2.20	16	15.8	2.13	17	12.0	3.75	17	16.3	1.89
OG experiment - Ref. 11-8	8	9.1	1.09	10	15.1	2.02						
FTE experiment - Table 11-8	16	13.6	1.14	32	16.7	1.24	16	14.7	2.44	32	15.6	1.20

(a) Unknown.

TABLE 11-7
RADIAL ULTIMATE TENSILE STRENGTH OF H-327 GRAPHITE
(in MPa)

Data Source	Midlength Center			Midlength Edge			End Center			End Edge		
	N	$\bar{X}$	S	N	$\bar{X}$	S	N	$\bar{X}$	S	N	$\bar{X}$	S
Characterization - Ref. 11-2	(a)	6.4	0.77	(a)	8.9	0.90	(a)	9.3	1.74	(a)	9.7	1.05
Characterization - Refs. 11-3 through 11-7	18	6.1	1.10	15	7.9	1.17	17	9.2	2.19	17	9.5	0.96
OG experiment - Ref. 11-2	13	5.6	1.97	19	9.9	1.38						
Web strength test - Ref. 11-8	25	8.4	0.67	25	9.5	0.92						

(a) Unknown.

TABLE 11-8
TENSILE PROPERTIES OF H-327 GRAPHITE
LOG 6484-147 — FUEL TEST ELEMENT LOG
RADIAL, MID-RADIUS

LOT NO. SPEC. DIA. 12.8 MM
LOG NO. 6484-147 SPEC. LENGTH 70. MM
LOG DENSITY MG/M**3

SPECIMEN NUMBER	ORIENTATION	LOCATION	DENSITY (MG/M**3)	YOUNGS MODULUS (GPA)	PERMANENT SET (PCT)	FRACTURE STRAIN (PCT)	TENSILE STRENGTH (MPA)
6484-147-01A	RAD	MR	1.758	4.6	.025	.325	10.3
-02A	RAD	MR					10.3
-03A	RAD	MR	1.761	4.5	.026	.355	10.1
-04A	RAD	MR					10.0
-05A	RAD	MR	1.755	4.3	.030	.261	8.4
-06A	RAD	MR					10.1
-07A	RAD	MR	1.764	4.5	.025	.297	9.7
-08A	RAD	MR					10.9
-01B	RAD	MR					10.1
-02B	RAD	MR					8.3
-03B	RAD	MR					5.7
-04B	RAD	MR					9.3
-05B	RAD	MR					9.2
-06B	RAD	MR					10.1
-07B	RAD	MR					10.1
-08B	RAD	MR					10.5
-01C	RAD	MR					6.5
-02C	RAD	MR					4.8
-03C	RAD	MR					7.2
-04C	RAD	MR					6.3
-05C	RAD	MR					8.0
-06C	RAD	MR					8.6
-07C	RAD	MR					8.4
-08C	RAD	MR					5.5
-01D	RAD	MR	1.728	3.9	.040	.270	8.0
-02D	RAD	MR					3.8
-03D	RAD	MR	1.743				6.1
-04D	RAD	MR					8.3
-05D	RAD	MR	1.749	4.1	.035	.241	7.7
-06D	RAD	MR					9.5
-07D	RAD	MR	1.759	4.9	.025	.311	10.4
-08D	RAD	MR					6.7
-01E	RAD	MR					7.7
-02E	RAD	MR					4.3
-03E	RAD	MR					8.6
-04E	RAD	MR					6.8
-05E	RAD	MR					7.6
-06E	RAD	MR					9.3
-07E	RAD	MR					9.0
-08E	RAD	MR					8.2
-01F	RAD	MR					8.8
-02F	RAD	MR					6.5
-03F	RAD	MR					6.9
-04F	RAD	MR					7.7

TABLE 11-8 (Continued)
RADIAL, MID-RADIUS

-05F RAD	MR					7.3
-06F RAD	MR					9.6
-07F RAD	MR					8.6
-08F RAD	MR					7.8
-01G RAD	MR					9.3
-02G RAD	MR					8.3
-03G RAD	MR					7.8
-04G RAD	MR					7.9
-05G RAD	MR					10.0
-06G RAD	MR					10.0
-07G RAD	MR					9.8
-08G RAD	MR					9.4
-01H RAD	MR	1.758	4.7	.025	.324	10.5
-02H RAD	MR					8.0
-03H RAD	MR	1.761	4.6	.031	.281	9.3
-04H RAD	MR					10.0
-05H RAD	MR	1.761	4.3	.031	.253	8.3
-06H RAD	MR					10.2
-07H RAD	MR	1.771	4.4	.016	.283	10.0
-08H RAD	MR					10.0
MEAN		1.756	4.4	.028	.291	8.5
			(.64 MPSI)			(1229.PSI)
STD. DEV.		.011	.3	.006	.035	1.6
			(.04 MPSI)			(236.PSI)

TABLE 11-8 (Continued)
TANGENTIAL, CENTER

LOT NO. SPEC. DIA. 12.8 MM
LOG NO. 6484-147 SPEC. LENGTH 70. MM
LOG DENSITY MG/M**3

SPECIMEN NUMBER	ORIENTATION	LOCATION	DENSITY (MG/M**3)	YOUNGS MODULUS (GPA)	PERMANENT SET (PCT)	FRACTURE STRAIN (PCT)	TENSILE STRENGTH (MPA)
6484-147-09A	TAN	C	1.752	4.8	.028	.302	10.3
-10A	TAN	C					9.5
-11A	TAN	C	1.756	5.0	.035	.362	11.6
-12A	TAN	C					11.6
-09B	TAN	C					8.9
-10B	TAN	C					6.2
-11B	TAN	C					9.0
-12B	TAN	C					9.5
-09C	TAN	C					5.6
-10C	TAN	C					8.6
-11C	TAN	C					7.5
-12C	TAN	C					7.4
-09D	TAN	C	1.738	4.2	.043	.218	7.1
-10D	TAN	C					8.8
-11D	TAN	C	1.741	3.9	.040	.228	7.1
-12D	TAN	C					7.0
-09E	TAN	C					6.6
-10E	TAN	C					8.4
-11E	TAN	C					6.5
-12E	TAN	C					6.5
-09F	TAN	C					7.8
-10F	TAN	C					8.5
-11F	TAN	C					6.4
-12F	TAN	C					5.5
-09G	TAN	C					6.4
-10G	TAN	C					2.8
-11G	TAN	C					6.5
-12G	TAN	C					7.4
-09H	TAN	C	1.754	4.6	.039	.265	8.8
-10H	TAN	C					9.9
-11H	TAN	C	1.757	4.9	.031	.311	10.3
-12H	TAN	C					10.3
MEAN			1.750	4.6 (.66 MPSI)	.036	.281	7.9 (1152.PSI)
STD. DEV.			.008	.4 (.06 MPSI)	.006	.055	1.9 (278.PSI)

TABLE 11-8 (Continued)
TANGENTIAL, EDGE

LOT NO. SPEC. DIA. 12.8 MM
LOG NO. 6484-147 SPEC. LENGTH 70. MM
LOG DENSITY MG/M**3

SPECIMEN NUMBER	ORIENTATION	LOCATION	DENSITY (MG/M**3)	YOUNGS MODULUS (GPA)	PERMANENT SET (PCT)	FRACTURE STRAIN (PCT)	TENSILE STRENGTH (MPA)
6484-147-13A	TAN	E	1.764	4.9	.026	.321	10.9
-14A	TAN	E					10.8
-15A	TAN	E	1.780	5.1	.024	.350	11.9
-16A	TAN	E					11.4
-17A	TAN	E	1.777	5.0	.026	.306	10.9
-18A	TAN	E					11.5
-19A	TAN	E	1.765	5.2	.025	.332	11.4
-20A	TAN	E					11.0
-13B	TAN	E					11.2
-14B	TAN	E					11.0
-15B	TAN	E					11.5
-16B	TAN	E					10.7
-17B	TAN	E					11.3
-18B	TAN	E					11.1
-19B	TAN	E					11.7
-20B	TAN	E					11.7
-13C	TAN	E					9.9
-14C	TAN	E					10.9
-15C	TAN	E					11.4
-16C	TAN	E					11.7
-17C	TAN	E					12.1
-18C	TAN	E					11.7
-19C	TAN	E					12.0
-20C	TAN	E					11.0
-13D	TAN	E	1.766	4.8	.026	.331	10.7
-14D	TAN	E					10.9
-15D	TAN	E	1.776	5.2	.025	.285	10.7
-16D	TAN	E					12.0
-17D	TAN	E	1.779	5.2	.026	.341	11.9
-18D	TAN	E					11.7
-19D	TAN	E	1.663	5.3	.022	.368	12.5
-20D	TAN	E					10.4
-13E	TAN	E					11.0
-14E	TAN	E					11.6
-15E	TAN	E					11.5
-16E	TAN	E					11.4
-17E	TAN	E					11.7
-18E	TAN	E					11.5
-19E	TAN	E					12.0
-20E	TAN	E					11.3
-13F	TAN	E					10.6
-14F	TAN	E					10.1
-15F	TAN	E					11.6
-16F	TAN	E					11.3

TABLE 11-8 (Continued)
TANGENTIAL, EDGE

-17F TAN	E					11.7
-18F TAN	E					11.2
-19F TAN	E					11.1
-20F TAN	E					11.7
-13G TAN	E					10.3
-14G TAN	E					10.5
-15G TAN	E					12.5
-16G TAN	E					11.3
-17G TAN	E					10.7
-18G TAN	E					11.3
-19G TAN	E					12.5
-20G TAN	E					11.4
-13H TAN	E	1.772	5.0	.025	.300	10.6
-14H TAN	E					9.9
-15H TAN	E	1.770	5.2	.024	.330	11.4
-16H TAN	E					11.8
-17H TAN	E	1.778	5.2	.010	.304	11.2
-18H TAN	E					12.1
-19H TAN	E	1.666	5.3	.020	.290	11.1
-20H TAN	E					11.7
MEAN		1.755	5.1	.023	.321	11.3
			(.74 MPSI)			(1638.PSI)
STD. DEV.		.043	.2	.005	.025	.6
			(.02 MPSI)			(86.PSI)

TABLE 11-8 (Continued)
AXIAL, CENTER

LOT NO. SPEC. DIA. 12.8 MM
LOG NO. 6484-147 SPEC. LENGTH 70. MM
LOG DENSITY MG/M**3

SPECIMEN NUMBER	ORIENTATION	LOCATION	DENSITY (MG/M**3)	YOUNGS MODULUS (GPA)	PERMANENT SET (PCT)	FRACTURE STRAIN (PCT)	TENSILE STRENGTH (MPA)
6484-147-21A	AX	C	1.756	10.3	.006	.159	12.0
-24A	AX	C					10.6
-27A	AX	C					13.7
-30A	AX	C					11.9
-33A	AX	C	1.756	11.0	.006	.187	14.9
-36A	AX	C					12.7
-39A	AX	C					14.2
-42A	AX	C					18.4
-21B	AX	C					11.2
-24B	AX	C					11.7
-27B	AX	C					13.1
-30B	AX	C					11.8
-33B	AX	C					12.4
-36B	AX	C					13.0
-39B	AX	C					13.6
-42B	AX	C					13.5
-21C	AX	C	1.741	9.8	.009	.140	10.9
-24C	AX	C					13.3
-27C	AX	C					13.4
-30C	AX	C					14.1
-33C	AX	C	1.745	10.5	.010	.194	14.4
-36C	AX	C					12.0
-39C	AX	C					15.0
-42C	AX	C					13.5
-21D	AX	C					13.4
-24D	AX	C					13.4
-27D	AX	C					12.4
-30D	AX	C					14.4
-33D	AX	C					13.4
-36D	AX	C					15.3
-39D	AX	C					14.8
-42D	AX	C					13.7
-21F	AX	C	1.752	11.2	.007	.220	17.2
-24F	AX	C					14.6
-27F	AX	C					17.5
-30F	AX	C					12.4
-33F	AX	C	1.758	12.1	.011	.203	16.9
-36F	AX	C					13.7
-39F	AX	C					15.8
-42F	AX	C					18.2
-21E	AX	C					12.7
-24E	AX	C					13.7
-27E	AX	C					15.5
-30E	AX	C					13.4

TABLE 11-8 (Continued)
AXIAL, CENTER

-33E	AX	C					11.0
-36E	AX	C					14.6
-39E	AX	C					14.2
-42E	AX	C					14.7
MEAN			1.751	10.8 (1.57 MPSI)	.008	.184	13.8 (2001.PSI)
STD. DEV.			.007	.8 (.12 MPSI)	.002	.029	1.8 (263.PSI)

TABLE 11-8 (Continued)
AXIAL, EDGE

LOT NO. SPEC. DIA. 12.8 MM
LOG NO. 6484-147 SPEC. LENGTH 70. MM
LOG DENSITY MG/M**3

SPECIMEN NUMBER	ORIENTATION	LOCATION	DENSITY (MG/M**3)	YOUNGS MODULUS (GPA)	PERMANENT SET (PCT)	FRACTURE STRAIN (PCT)	TENSILE STRENGTH (MPA)
6484-147-22A	AX	E	1.760	11.0	.008	.174	14.1
-23A	AX	E					14.4
-25A	AX	E					14.1
-26A	AX	E					13.7
-28A	AX	E	1.760	10.8	.008	.164	13.4
-29A	AX	E					16.5
-31A	AX	E					15.8
-32A	AX	E					15.8
-34A	AX	E	1.766	10.7	.008	.171	13.5
-35A	AX	E					15.3
-37A	AX	E					15.3
-38A	AX	E					16.9
-40A	AX	E	1.766	11.7	.006	.202	16.8
-41A	AX	E					14.6
-43A	AX	E					16.2
-44A	AX	E					16.1
-22B	AX	E					15.0
-23B	AX	E					15.7
-25B	AX	E					14.8
-26B	AX	E					14.1
-28B	AX	E					16.4
-29B	AX	E					16.8
-31B	AX	E					16.7
-32B	AX	E					17.0
-34B	AX	E					16.0
-35B	AX	E					17.7
-37B	AX	E					18.2
-38B	AX	E					17.2
-40B	AX	E					18.0
-41B	AX	E					18.7
-43B	AX	E					17.6
-44B	AX	E					16.4
-22C	AX	E					16.1
-23C	AX	E					16.9
-25C	AX	E					16.2
-26C	AX	E					16.6
-28C	AX	E					16.6
-29C	AX	E					17.0
-31C	AX	E					15.8
-32C	AX	E					15.7
-34C	AX	E					15.7
-35C	AX	E					17.5
-37C	AX	E					17.9
-38C	AX	E					18.8

TABLE 11-8 (Continued)
AXIAL, EDGE

-40C	AX	E					18.1
-41C	AX	E					17.5
-43C	AX	E					18.3
-44C	AX	E					16.6
-22D	AX	E	1.745	10.7	.005	.192	15.4
-23D	AX	E					16.3
-25D	AX	E					14.0
-26D	AX	E					16.8
-28D	AX	E	1.760	11.3	.004	.204	16.2
-29D	AX	E					16.1
-31D	AX	E					14.2
-32D	AX	E					16.3
-34D	AX	E	1.766	12.1	.005	.222	18.6
-35D	AX	E					18.2
-37D	AX	E					17.5
-38D	AX	E					17.8
-40D	AX	E	1.772	11.9	.006	.213	18.0
-41D	AX	E					16.9
-43D	AX	E					15.1
-44D	AX	E					14.7
-22E	AX	E					15.9
-23E	AX	E					15.8
-25E	AX	E					14.7
-26E	AX	E					16.6
-28E	AX	E					15.9
-29E	AX	E					13.0
-31E	AX	E					16.5
-32E	AX	E					16.6
-34E	AX	E					17.9
-35E	AX	E					17.8
-37E	AX	E					17.9
-38E	AX	E					17.2
-40E	AX	E					18.3
-41E	AX	E					18.5
-43E	AX	E					17.7
-44E	AX	E					15.5
-22F	AX	E	1.758	11.9	.009	.218	17.5
-23F	AX	E					15.8
-25F	AX	E					17.0
-26F	AX	E					15.5
-28F	AX	E	1.768	11.5	.005	.175	15.4
-29F	AX	E					16.3
-31F	AX	E					14.8
-32F	AX	E					15.0
-34F	AX	E	1.772	11.5	.010	.212	16.8
-35F	AX	E					15.5
-37F	AX	E					15.5
-38F	AX	E					16.8
-40F	AX	E	1.776	11.9	.006	.224	18.3
-41F	AX	E					15.0
-43F	AX	E					16.1
-44F	AX	E					17.0
	MEAN		1.764	11.4	.007	.198	16.3
				(1.65 MPSI)			(2366.PSI)
	STD. DEV.		.008	.5	.002	.022	1.3
				(.07 MPSI)			(194.PSI)

TABLE 11-9

ULTIMATE TENSILE STRENGTH OF FORT ST. VRAIN INITIAL CORE H-327 GRAPHITE
(Strength in psi)

SERIAL #	STRENGTH	LOCATION	SERIAL #	STRENGTH	LOCATION	SERIAL #	STRENGTH	LOCATION
1	1600.	7- 1-2	95	1790.	1-10-4	192	1804.	3-18-5
3	1070.	2-17-6	96	1782.	2-11-3	195	2180.	3-33-2
11	1340.	1-27-6	99	1940.	5- 5-1	199	1950.	5- 4-6
15	1450.	7- 1-6	100	1920.	2-36-4	201	1742.	5- 7-5
16	1390.	7-24-6	101	1680.	2-28-6	203	1818.	7-11-2
18	1045.	7-16-2	102	1640.	1-31-4	204	1278.	7-17-4
22	1673.	4-35-2	104	1650.	6-31-1	205	1300.	7-10-1
23	1530.	4-32-4	105	1823.	6-31-6	209	1620.	1-29-3
24	1620.	7- 3-3	106	1810.	7- 7-1	211	1792.	1-28-4
25	1011.	7-12-1	108	1570.	6- 8-4	212	1740.	4-32-3
26	1040.	4-22-5	111	1580.	1-35-2	213	1688.	5-12-5
27	1200.	4-29-5	112	1890.	7-16-1	215	2038.	5-35-1
30	1530.	2-28-2	124	1609.	4- 9-3	217	1405.	1- 7-3
32	1665.	2-11-2	125	1380.	2-12-4	218	1650.	4- 7-5
33	1170.	7- 8-1	126	2002.	5-10-1	219	1485.	3-27-6
34	1201.	3-13-5	127	2120.	6-33-3	220	1302.	2-24-3
36	1755.	7-33-3	129	2100.	4-29-2	227	1474.	5-23-3
40	1178.	2-30-3	133	1634.	6- 7-3	228	1760.	1-25-3
41	1330.	5- 9-3	134	1920.	6-19-1	229	1460.	7-12-5
43	1420.	7- 3-5	137	2571.	2- 3-6	232	2500.	3- 9-3
46	1700.	5-12-4	140	2040.	3-32-3	235	1855.	6- 6-3
47	1405.	1-28-5	142	2205.	4- 9-5	238	1425.	6- 8-2
48	2082.	4- 8-3	143	2163.	4- 8-1	239	1304.	3- 5-2
52	1761.	6- 5-5	144	2456.	2- 6-6	242	1267.	6-10-2
55	1595.	7- 2-1	148	1646.	3-17-6	244	1417.	1- 7-6
57	1450.	2-13-6	149	1680.	2-11-6	246	1455.	5-16-1
59	2185.	7-30-5	151	1940.	6-11-1	250	1135.	6- 8-3
60	2340.	2-24-2	152	1930.	7-22-6	251	1277.	3- 3-3
65	1575.	7- 3-6	154	2580.	3-27-2	254	1120.	1- 9-6
67	2465.	1-29-4	155	2400.	7- 6-1	255	2170.	3-25-6
68	2265.	3-21-6	157	2040.	3-29-5	256	1670.	3-37-3
73	1890.	7-14-3	161	2440.	2- 4-6	257	2080.	3- 6-3
75	1190.	2-31-5	162	2850.	4- 3-4	258	1447.	5-23-4
76	1670.	6-31-5	164	1290.	6-24-2	260	1090.	3-11-1
78	1626.	1-12-5	166	2130.	4-15-2	264	1715.	2-31-4
80	1570.	2-11-4	169	1934.	3-15-1	265	1533.	1-18-3
81	1330.	6-16-3	170	2297.	2-16-4	267	2180.	4-31-6
83	1070.	5- 2-5	172	2015.	5- 8-3	268	1021.	2-36-5
84	1364.	1-16-6	173	2050.	6- 6-1	270	1520.	6-37-5
85	1887.	2-14-6	175	1590.	6- 4-6	271	1462.	4-19-6
88	1885.	7- 3-2	182	1858.	4-12-6	272	1102.	2- 4-2
89	1572.	6-21-2	185	1536.	6-14-6	273	1350.	6-27-5
91	1500.	3-18-2	189	1955.	6- 1-3	274	1570.	6-30-6
93	2320.	3-12-1	190	1990.	2-22-1	276	1510.	6- 4-4
94	2008.	3-28-4	191	2042.	2-13-3	279	1400.	4-28-1

TABLE 11-9 (Continued)

SERIAL #	STRENGTH	LOCATION	SERIAL #	STRENGTH	LOCATION	SERIAL #	STRENGTH	LOCATION
280	1575.	2-24-5	371	2050.	3-37-5	462	1900.	5-13-5
284	1828.	7- 8-3	373	2180.	5-25-3	463	1710.	3-18-6
285	1775.	5-13-4	374	1992.	7-12-2	465	1628.	7-19-4
286	1191.	1-17-4	375	1017.	3-35-1	467	2058.	7-21-5
287	1630.	3- 9-4	376	2040.	7-37-6	469	1715.	4-10-1
289	1740.	6- 2-4	380	1980.	7- 4-6	471	1625.	3-15-5
290	1910.	7-19-2	383	1500.	3- 1-3	473	1520.	4- 2-5
291	1760.	3-27-4	387	1908.	2-19-3	478	1575.	2-28-4
292	1537.	4- 3-2	388	2154.	7-19-1	483	1276.	6-23-3
294	1770.	3-15-4	391	1996.	4-31-1	486	1990.	3- 1-5
298	1409.	1- 4-5	393	1920.	5-15-2	487	1567.	4-16-1
304	2075.	4- 8-5	396	1350.	4- 4-5	488	1775.	1-35-6
305	1460.	4-18-5	397	1102.	7-30-2	489	1578.	6- 7-4
306	1570.	3- 2-2	399	2360.	3-19-3	494	1799.	6-10-4
307	1878.	4- 6-3	400	2140.	1-15-2	496	1670.	1-30-6
308	1920.	3- 4-5	401	1868.	5-32-2	502	1820.	2- 7-6
309	1520.	5-34-6	402	1890.	6-12-1	504	1910.	6-22-3
310	1870.	2- 1-6	403	1690.	6-12-4	507	1460.	7-30-3
312	1865.	5-12-2	408	2030.	7-31-5	509	1750.	4- 9-4
313	1370.	7- 9-3	409	1390.	3-33-1	510	1276.	5-36-2
320	1539.	5-19-5	411	2470.	5-21-3	511	2045.	2-12-3
321	2355.	7-12-3	415	1680.	1-36-5	513	1960.	1-27-4
323	1990.	7- 5-5	418	2075.	4-34-3	514	1990.	5-30-4
324	2270.	2-13-2	419	2740.	2-25-5	515	2000.	7-25-6
325	1970.	2-16-3	420	1736.	3-29-4	517	1650.	5-32-1
326	2340.	5- 5-3	421	1412.	2- 2-5	518	1608.	1- 8-5
331	1650.	4-19-4	424	1800.	7-25-4	520	1808.	4-12-4
333	1913.	4-25-1	427	1551.	7-33-4	522	1779.	2-27-3
334	1350.	2-23-5	428	1425.	4- 3-1	523	1725.	4-12-2
335	2103.	3-13-1	430	1463.	5-28-4	529	1572.	5- 5-2
337	2000.	5- 3-6	432	1652.	5-14-6	530	1499.	4-18-1
338	2290.	7-11-6	433	1365.	2-12-1	532	1618.	1-25-5
342	2510.	5- 4-3	437	1640.	1-30-2	536	1826.	7-18-2
343	2220.	7-10-3	438	1550.	4-11-4	537	2130.	5-10-4
344	1332.	6-21-5	443	1388.	2-18-3	538	1485.	2- 4-5
347	2200.	7-15-6	445	1850.	5-34-3	539	1990.	5-27-5
351	1270.	3- 4-3	448	1845.	6-26-5	540	1780.	6- 9-4
355	1650.	5-19-4	449	1764.	2-17-4	541	2120.	2-21-4
358	1694.	7-16-5	454	1300.	3-30-4	542	1625.	5-15-1
361	1850.	4- 7-2	455	1890.	1- 5-6	544	2440.	3-27-5
365	1985.	2-21-1	456	1850.	5- 4-1	545	1985.	3-12-2
366	1525.	5-11-5	457	1520.	3-10-6	548	1800.	1- 6-4
367	1470.	6- 3-5	458	1002.	2- 1-2	551	2070.	5-10-3
368	1720.	2-25-4	459	1838.	4-33-1	552	1315.	6- 5-6
370	2121.	7-11-5	461	2160.	1-16-2	553	1930.	6-15-1

TABLE 11-9 (Continued)

SERIAL #	STRENGTH	LOCATION	SERIAL #	STRENGTH	LOCATION	SERIAL #	STRENGTH	LOCATION
555	1790.	6- 2-5	671	1895.	6-24-6	749	1900.	7-29-4
556	2060.	5-33-6	672	1630.	1-23-6	750	2045.	5-37-2
560	1990.	3-11-2	673	2710.	1-13-5	751	1725.	2-22-4
565	2190.	6- 9-5	675	1345.	1-32-2	752	1422.	7- 7-4
568	2155.	3-34-1	679	1960.	5-31-1	753	1353.	2-16-1
574	1180.	1-21-1	681	1900.	6-17-4	755	2080.	2-34-1
577	1616.	1- 3-3	682	1860.	1-23-2	756	1382.	5-27-1
580	1735.	7- 3-4	683	1500.	4-28-6	758	2190.	2-31-6
581	1905.	6- 3-3	684	1570.	2-18-6	759	1978.	4-14-3
583	1970.	7-31-3	687	1690.	2-27-2	763	2361.	4-16-4
584	1480.	3-14-5	688	2560.	1-28-6	765	1960.	5-22-6
587	1300.	2- 3-1	692	2285.	4-24-1	766	2115.	6-28-5
589	1545.	6-36-4	693	1335.	5-27-3	767	1315.	7-37-3
590	1210.	6-16-2	697	1550.	3- 9-6	768	1302.	4- 5-4
596	1600.	3-14-1	700	1805.	7-36-3	770	1360.	3-19-5
599	1685.	5-35-6	702	1305.	6-36-2	771	2038.	2-10-6
605	1355.	6-24-5	703	1830.	5-11-1	773	1475.	6-28-2
610	1403.	3-35-2	704	1930.	4-28-2	774	1170.	1-24-1
612	1070.	7-15-1	706	1820.	5-24-4	776	1500.	1-16-4
613	2100.	6-36-3	707	2040.	6-23-1	778	1480.	3-32-2
614	2153.	6-13-1	708	1532.	4- 1-6	780	1730.	1-30-5
617	1955.	2-19-4	709	2020.	7-20-3	781	1790.	5-24-6
620	1880.	5-34-1	710	1540.	6-30-1	782	1650.	5-32-6
623	1055.	2-25-2	711	1670.	7- 4-1	783	2285.	5-19-6
625	1130.	4-16-2	714	1570.	7-31-4	784	1720.	7-20-6
626	1650.	4-24-6	715	2310.	7-18-1	785	1154.	4-21-6
628	1605.	3-30-6	716	2150.	5-10-6	786	1045.	1-11-6
631	1364.	4-12-3	719	1663.	5-16-5	787	1080.	1-18-1
635	1655.	6-37-6	720	2250.	3-29-2	788	1245.	5-30-5
638	1181.	6-31-2	722	1815.	6-26-4	791	1870.	4- 5-6
639	1570.	3-31-1	723	2040.	4-22-6	792	1230.	2-15-4
641	1375.	7-17-5	725	1722.	7- 3-1	794	1775.	7-10-4
642	1482.	1-33-2	726	1650.	5-27-6	798	1230.	3-32-4
647	1320.	6-18-6	727	2075.	6- 8-5	799	1220.	2-21-3
649	1240.	7- 4-3	729	1710.	1-20-3	800	2150.	1- 2-1
654	1750.	2-32-3	731	1970.	7-33-6	801	1140.	3-25-3
655	1130.	1-36-3	732	1240.	1- 5-5	803	2020.	4-27-1
656	1401.	7-23-3	733	1405.	2-17-5	805	1340.	2-33-6
658	2060.	4-32-5	735	1050.	1-32-5	806	1875.	1-36-6
661	1694.	4-33-6	736	1885.	6-15-5	807	1790.	1-20-1
662	1450.	6-14-4	737	1930.	3-31-6	809	2025.	1-37-1
664	1520.	2-31-2	741	1765.	3-24-2	811	1435.	5- 8-1
666	1440.	6- 5-4	743	1540.	4-17-4	812	1915.	2- 4-4
667	1556.	6-13-3	746	1905.	6-33-4	815	1285.	5-12-6
670	1440.	7-13-6	748	1165.	5-23-5	817	1620.	5-23-6

TABLE 11-9 (Continued)

SERIAL #	STRENGTH	LOCATION	SERIAL #	STRENGTH	LOCATION	SERIAL #	STRENGTH	LOCATION
818	2040.	5-30-6	883	1300.	5- 7-1	955	1485.	7-26-3
819	1505.	3-21-2	887	1725.	5-14-1	957	1970.	4-25-6
820	2260.	1-35-3	888	1285.	2- 2-2	961	1585.	1-29-2
821	1755.	7-31-1	890	1560.	2-10-4	962	1980.	1- 8-6
823	1970.	3- 1-4	891	1485.	2-17-1	963	1560.	2-28-1
824	2115.	5-33-2	892	1720.	4-29-6	964	1605.	7-19-3
825	1390.	3-21-3	893	1005.	7-37-1	965	1560.	6-28-3
826	2145.	3- 7-1	894	1915.	7- 2-2	966	1560.	5-16-3
827	1325.	1-10-3	896	1700.	6- 1-4	967	1895.	1-12-6
830	1930.	6-34-3	897	1240.	6- 7-2	969	1045.	7-14-1
831	1240.	2-22-2	898	1560.	1-22-1	970	1915.	3-16-1
832	1485.	7-27-3	899	1410.	5-11-3	972	1870.	6-30-5
834	1939.	3-13-2	901	1340.	7-25-5	974	1563.	7-18-5
836	1640.	2-36-2	902	1415.	2- 9-3	975	1925.	3-29-3
838	1670.	2-34-2	903	1490.	7-36-6	977	2140.	4- 2-3
839	1445.	2- 4-3	904	1552.	7-28-3	978	1980.	5-31-4
841	1930.	2-16-6	906	1295.	3-24-5	979	1295.	5-31-6
842	1498.	6-16-5	910	1635.	3- 4-2	980	1550.	1-10-2
843	1340.	5-22-4	912	1940.	5-22-3	981	1700.	4-13-6
844	1335.	1-35-5	914	1450.	7-14-6	982	2480.	7-27-4
845	1970.	4-20-6	917	1000.	7-34-6	985	2245.	1-23-5
847	1200.	3-16-3	919	1250.	1- 5-1	986	1870.	1-24-2
848	1220.	6-19-2	921	1800.	2-29-1	987	1501.	6- 6-4
849	1950.	5- 9-1	923	1290.	1-16-1	988	2165.	4-24-3
850	1095.	3-25-2	924	1620.	4-37-2	989	1930.	5- 8-5
853	1275.	7-20-5	925	1310.	4-34-5	990	1710.	6-22-4
854	1235.	3-22-6	927	1900.	5-20-4	992	1765.	4-24-4
855	1410.	7-19-6	928	1690.	2-32-1	993	2025.	5-17-5
857	1250.	6-27-1	929	1910.	5-37-6	994	1766.	4- 3-3
858	1140.	5- 4-4	930	1170.	4- 8-6	998	1470.	1-26-2
861	1130.	4-27-3	931	1305.	6- 8-1	999	1730.	3-37-4
862	1080.	3-22-5	932	1020.	7-22-2	1002	1462.	3-11-3
864	1430.	2- 2-3	933	1200.	3-19-4	1004	1698.	6-22-5
866	1815.	4- 6-6	934	1370.	2-31-3	1006	2095.	4-35-5
867	1700.	7- 5-1	935	1900.	1-20-5	1007	1860.	3-31-2
868	1345.	7-27-6	936	1660.	6-24-3	1008	1690.	4-25-5
869	1770.	4-20-5	937	1600.	1-23-3	1011	1410.	2-15-2
872	1570.	2-24-6	938	1564.	5-10-5	1014	2115.	4-28-3
873	1420.	6-18-4	939	1535.	5- 1-4	1015	2130.	4- 4-3
874	1210.	5- 8-6	940	1735.	3-13-6	1018	2095.	4-18-6
875	1940.	2-14-3	942	2060.	1-19-3	1019	1380.	2-30-2
877	1450.	7-22-4	948	2100.	2-13-4	1020	1930.	6-30-2
879	1785.	4-37-4	949	1794.	6-16-1	1021	1910.	7-21-6
880	1725.	2-26-6	950	1660.	2- 9-4	1023	2285.	3-29-1
882	1000.	7-25-2	951	1780.	7-25-1	1024	2020.	5-28-3

TABLE 11-9 (Continued)

SERIAL #	STRENGTH	LOCATION	SERIAL #	STRENGTH	LOCATION	SERIAL #	STRENGTH	LOCATION
1028	2040.	1-22-3	1120	1972.	1-18-4	1195	1348.	3-14-3
1029	1560.	6-14-2	1121	2160.	2-29-5	1199	1480.	4-30-5
1030	1910.	4-15-1	1124	1495.	5-31-2	1200	1868.	6-31-4
1032	1728.	6-17-1	1127	2230.	2-34-3	1204	2320.	2- 3-5
1033	2250.	7- 4-2	1131	1391.	1-15-4	1206	2310.	4-14-1
1034	2290.	6-19-4	1132	1890.	7-23-4	1210	2180.	3-32-6
1035	1460.	4-17-6	1133	1240.	1-25-2	1211	1415.	5-16-2
1038	1430.	6-26-2	1135	2029.	2-10-5	1212	2336.	7-15-3
1039	2080.	7-36-2	1136	2149.	2-17-3	1214	1780.	4- 6-4
1042	1900.	2- 6-3	1139	2100.	5- 6-4	1215	2070.	5-17-6
1043	1835.	3- 5-1	1141	1775.	4-20-3	1223	2315.	3-10-2
1044	1868.	1- 3-2	1142	1708.	4- 4-6	1224	1750.	2-29-3
1047	2065.	3-24-3	1143	2070.	4- 9-6	1225	2070.	7-36-5
1048	1770.	4-30-6	1144	2520.	5-32-3	1226	2180.	1- 7-2
1049	2060.	3-18-1	1147	2443.	5- 5-5	1228	1930.	3-18-4
1050	1835.	7-17-6	1148	2200.	2-33-1	1232	1855.	1-24-4
1053	1455.	5- 3-5	1149	2010.	3- 9-2	1234	1970.	4-16-6
1054	1880.	3-17-1	1153	2210.	2-13-5	1235	2145.	3-33-5
1055	1740.	6-17-6	1154	1511.	3-16-4	1237	1602.	4- 1-3
1057	1851.	3- 8-1	1155	1920.	7- 2-3	1238	2020.	7-14-2
1058	2420.	6-33-5	1157	2100.	7- 6-3	1240	1792.	6-34-6
1060	2285.	3-24-6	1158	1902.	6-12-2	1241	2480.	3-31-5
1062	2188.	7-21-2	1159	2280.	2-23-2	1242	1536.	2- 1-3
1063	2328.	7-26-4	1160	1348.	4-20-4	1243	1630.	3-15-3
1064	2220.	6-30-4	1161	2041.	2-10-2	1244	1810.	6-26-6
1065	2380.	1-20-6	1163	1970.	5-33-5	1246	2070.	2-37-1
1066	1905.	7-28-2	1166	2410.	1-11-5	1248	2040.	3-34-2
1067	1946.	3- 2-5	1168	1741.	7-30-6	1249	1850.	4-22-1
1068	1018.	2-23-4	1171	1456.	1-36-1	1251	1920.	3- 8-3
1069	1997.	6-10-5	1173	2170.	5- 1-3	1252	1650.	4- 2-4
1075	2040.	3-28-3	1174	1570.	5- 6-5	1253	2220.	7- 5-4
1086	1064.	3-25-5	1175	1831.	1-12-4	1255	1790.	7-27-2
1089	1545.	6- 6-6	1176	1508.	7-29-5	1258	2060.	1-31-3
1090	1890.	1- 1-1	1177	1310.	5-36-3	1259	1600.	4-11-1
1092	2010.	6-34-2	1178	1982.	7- 5-6	1260	1825.	1- 1-6
1095	1630.	4-22-2	1179	1558.	6-34-4	1261	2306.	7-26-6
1099	2582.	2- 5-6	1182	2150.	1-22-4	1262	1865.	2-27-4
1100	1580.	6- 6-5	1183	1757.	4-10-6	1263	2320.	5- 6-6
1101	1075.	4-13-5	1184	2065.	2-15-6	1264	2170.	5- 5-4
1102	2100.	6- 9-6	1186	2380.	7-28-1	1265	2170.	6- 6-2
1108	2178.	4-10-3	1187	1938.	5- 2-1	1268	2230.	3-15-6
1110	1350.	5-14-2	1188	2140.	7-14-4	1269	2040.	3-21-5
1111	1291.	2-29-2	1192	1865.	5-32-4	1270	1060.	2- 2-1
1116	1325.	6-10-6	1193	2190.	2- 6-1	1271	1700.	3-10-4
1117	1510.	7-22-5	1194	2262.	2-24-1	1273	1660.	7-13-2

TABLE 11-9 (Continued)

SERIAL #	STRENGTH	LOCATION	SERIAL #	STRENGTH	LOCATION	SERIAL #	STRENGTH	LOCATION
1278	1465.	7-10-2	1384	1340.	6-23-2	1477	1675.	1-37-4
1279	1560.	7-16-6	1387	1490.	3- 9-5	1478	1575.	6-20-2
1281	2118.	5-12-3	1388	1425.	5-25-6	1486	1784.	6-35-5
1282	2605.	1-10-1	1390	2000.	2-12-6	1489	2185.	1-13-2
1296	2236.	4-36-4	1391	1875.	1-12-2	1494	1505.	4-19-1
1299	1814.	1-36-4	1392	1720.	4- 7-3	1497	2000.	6- 4-5
1300	1626.	2- 7-3	1395	1360.	6-31-3	1507	1290.	5- 1-2
1301	1535.	2- 5-4	1397	1545.	5-18-4	1508	2035.	5- 6-1
1305	2250.	2- 8-3	1399	1675.	3-12-6	1515	1405.	5-28-6
1306	1754.	3-19-1	1401	1453.	3-26-1	1516	1325.	7- 8-6
1307	1305.	3-36-3	1403	1583.	4-33-4	1519	1872.	1- 3-4
1310	1920.	5- 2-4	1407	2428.	4-19-3	1520	2200.	1- 5-3
1311	1645.	7-28-5	1409	1509.	5-19-1	1529	1580.	1- 4-2
1315	1912.	7-25-3	1410	1778.	6-18-5	1532	1650.	1-15-3
1317	1990.	3- 7-6	1412	1968.	1-25-1	1535	1750.	2- 8-5
1319	1600.	1-30-4	1414	1270.	4-20-2	1537	1785.	3-14-6
1321	2440.	4-36-5	1417	1690.	3-36-5	1539	1520.	1-37-5
1324	1410.	1-28-2	1418	1525.	2-11-1	1544	1340.	4- 5-3
1326	1355.	2- 7-2	1419	1565.	4-24-2	1545	1492.	1- 7-4
1327	1730.	3-12-4	1420	1880.	6-12-5	1547	2340.	1-31-2
1329	1108.	2-15-5	1421	1100.	3- 8-2	1548	1795.	5-37-3
1331	1420.	7-10-5	1425	2330.	4- 7-6	1555	1779.	5-18-5
1336	1885.	2- 3-4	1427	1935.	5-37-4	1556	1448.	3-26-3
1337	1427.	6-18-2	1430	1865.	4-11-2	1557	1380.	6-11-4
1345	1512.	3- 5-4	1431	2100.	3-37-2	1563	1185.	7-29-3
1346	1165.	4-17-5	1440	1392.	3- 5-5	1568	1620.	3-26-2
1348	2580.	5-11-2	1441	2092.	2-26-3	1569	2200.	5-23-2
1349	1934.	2- 5-5	1443	2338.	7- 6-2	1570	2085.	1- 4-3
1350	1935.	1- 9-5	1445	1810.	4- 1-4	1571	2250.	5-36-4
1352	1520.	5-37-5	1446	1381.	7-17-3	1574	1355.	7-17-2
1353	1810.	5-22-1	1448	1404.	7- 9-5	1579	1690.	7- 7-3
1357	1125.	6- 4-1	1449	1430.	1-14-3	1581	1650.	4-19-2
1358	2178.	5- 7-6	1450	2230.	3-17-3	1584	1222.	2-29-4
1360	1490.	4- 1-2	1451	1535.	1-35-1	1585	1602.	5-35-4
1361	1632.	4-36-1	1453	1890.	6- 1-5	1587	2130.	4-31-5
1363	1040.	4-37-1	1454	1436.	4- 7-4	1588	2190.	6-11-3
1364	1870.	6- 7-1	1458	1220.	3-29-6	1589	2065.	4- 5-5
1367	1345.	6- 4-3	1459	1710.	6-21-6	1590	1690.	1- 8-3
1368	1522.	5- 6-2	1460	1223.	2-22-3	1593	2160.	2-28-3
1370	1777.	4-14-6	1466	1200.	5- 7-2	1598	1935.	7-37-4
1371	1445.	3- 2-6	1467	1570.	3-14-2	1599	1292.	7-30-1
1374	1340.	5-15-5	1468	2200.	1-17-2	1602	1248.	5-11-6
1377	1310.	7-24-3	1469	1914.	7-31-2	1603	1200.	1-24-6
1378	1134.	3-33-4	14 0	1820.	2-14-2	1604	1828.	7-26-5
1379	1600.	5-23-1	1471	1235.	1-33-4	1606	1629.	1- 3-3

TABLE 11-9 (Continued)

SERIAL #	STRENGTH	LOCATION	SERIAL #	STRENGTH	LOCATION	SERIAL #	STRENGTH	LOCATION
1609	2005.	7-24-5	1713	1820.	4-30-3	1780	2135.	5-15-4
1611	1382.	4-16-3	1714	2100.	4-17-2	1781	1620.	6-11-2
1612	1830.	7-18-6	1715	2380.	1-32-3	1782	1960.	3- 5-6
1614	1500.	5-35-2	1717	2440.	4-32-2	1783	1960.	6-20-3
1619	1800.	5-34-2	1718	2290.	2- 1-4	1784	2693.	5-24-5
1621	1743.	2-16-2	1719	1665.	1-13-1	1787	2030.	4- 4-1
1624	1200.	3-17-4	1720	1685.	6-25-4	1789	1510.	2- 7-4
1625	1130.	6-10-3	1722	1630.	3-36-6	1792	2170.	1-33-5
1628	1640.	2-32-4	1723	1638.	2- 1-5	1793	1765.	4-14-2
1629	1030.	2-11-5	1724	1760.	5-34-4	1794	1710.	1-31-1
1630	1502.	1-23-1	1726	1790.	1-33-3	1795	1790.	6- 2-1
1633	1513.	6-30-3	1727	1420.	3- 8-4	1796	1040.	5-18-2
1634	2042.	3-34-4	1731	2155.	4-20-1	1797	1820.	6-25-5
1644	1320.	6-37-3	1732	1515.	4-12-1	1798	1195.	5-24-1
1645	2410.	2-24-4	1734	2075.	2-16-5	1799	1545.	2-22-6
1649	1585.	6-10-1	1735	1828.	6-20-5	1801	1810.	6-33-1
1652	2248.	1-26-1	1736	1606.	3- 6-6	1804	1195.	2-14-1
1658	1798.	3-17-5	1737	1775.	6-13-2	1805	1742.	6-18-1
1659	1312.	6-24-1	1739	1178.	2-33-3	1806	1560.	7-22-3
1661	1515.	7-34-2	1741	1765.	2- 5-3	1811	1640.	1-34-6
1662	1580.	3-19-6	1742	2053.	5- 8-2	1813	1005.	4- 9-2
1665	1965.	3-12-3	1743	2100.	2-19-5	1814	1085.	1- 4-1
1669	1980.	3-28-6	1745	1215.	2-12-5	1817	1945.	3-18-3
1670	2100.	1-32-1	1746	1650.	3- 6-1	1818	2080.	2-21-2
1672	2235.	7- 1-3	1748	2165.	3-26-6	1822	1724.	6-21-4
1673	1480.	7-13-3	1750	1630.	4-33-3	1825	1850.	2-25-3
1674	1850.	5-11-4	1752	2330.	3- 7-3	1827	1680.	4-31-3
1676	1563.	4-35-4	1753	1640.	6- 2-3	1829	1440.	5- 4-2
1677	1292.	3- 5-3	1754	2090.	6-27-2	1830	1346.	2- 9-2
1678	1780.	5-35-3	1755	1768.	1- 7-1	1831	1725.	1-34-3
1681	2265.	5-34-5	1757	1985.	7-23-1	1832	1340.	7- 8-2
1682	1960.	2-32-6	1759	1794.	6- 9-1	1835	1930.	1- 4-4
1689	1925.	4-19-5	1762	2360.	3- 7-2	1837	1425.	7-36-4
1690	2310.	2- 5-2	1763	1818.	7- 6-4	1840	1490.	1-12-3
1692	1957.	5-33-6	1764	1580.	6-15-4	1844	1525.	4-25-4
1693	2265.	7-20-1	1765	2238.	6- 7-5	1845	1054.	6-34-1
1694	2080.	3- 4-1	1766	1785.	1- 3-1	1848	2100.	5- 9-5
1699	1970.	5-12-1	1767	2120.	4-15-5	1850	2040.	5- 3-4
1701	1999.	7-13-1	1769	2180.	4- 6-5	1853	1400.	5-31-3
1703	1143.	3-30-3	1770	2315.	4- 1-5	1859	1260.	1-31-6
1706	2090.	2- 8-1	1771	1180.	4- 3-6	1861	1874.	3-17-2
1707	2298.	1-18-6	1772	2250.	3-11-5	1863	1982.	4-34-2
1710	1820.	3- 6-4	1773	1905.	7-18-3	1865	1160.	3-22-2
1711	1530.	1-17-1	1774	1975.	1- 6-3	1866	1645.	1- 9-4
1712	1640.	2- 9-1	1778	1965.	2-23-6	1868	1390.	2-37-2

TABLE 11-9 (Continued)

SERIAL #	STRENGTH	LOCATION	SERIAL #	STRENGTH	LOCATION	SERIAL #	STRENGTH	LOCATION
1869	1280.	2- 4-1	1974	1545.	3-22-1	2060	1750.	6- 1-2
1872	1540.	5-22-2	1977	1920.	6- 5-2	2068	1705.	5-21-2
1876	1700.	6- 3-4	1979	1005.	6-35-6	2080	1280.	4-35-1
1878	1955.	7- 9-2	1980	1600.	1-30-1	2083	1079.	4-24-5
1879	2100.	3- 7-5	1982	1665.	1- 1-5	2084	1687.	1-15-5
1883	1185.	6-37-4	1983	2275.	7- 9-1	2086	1510.	6-17-2
1884	1835.	3-24-1	1984	1725.	1-29-5	2087	1192.	2-25-1
1885	1745.	4-37-3	1985	2400.	4- 5-1	2088	1067.	1-22-6
1887	1530.	4-21-2	1987	2125.	3-35-3	2089	1225.	3-24-4
1888	1710.	1-16-3	1988	2080.	7-13-4	2090	1055.	1- 2-6
1889	1994.	1-11-1	1989	2430.	4-17-1	2102	1570.	1-21-4
1890	1880.	4-13-2	1990	2250.	2-18-5	2103	1233.	2-37-6
1893	1390.	7-24-2	1993	2420.	5-27-4	2104	1350.	4-22-4
1894	1440.	4-35-6	1994	1940.	6-22-6	2106	2282.	2- 3-2
1900	1058.	6-19-6	1995	2095.	2-37-3	2110	2230.	6-35-1
1902	1800.	4- 6-2	1996	1158.	1-14-1	2113	1910.	7-23-2
1903	1890.	7- 5-3	1998	1820.	6-13-4	2114	1839.	5- 6-3
1904	2140.	5- 3-2	2000	1765.	3-15-2	2116	1910.	6- 9-2
1905	2100.	2-30-5	2001	1635.	7-33-1	2117	1574.	2-37-4
1907	1350.	2- 6-5	2006	1610.	7-37-5	2118	1835.	7-20-2
1908	1980.	6- 5-3	2007	2035.	4-37-5	2119	2055.	2- 5-1
1909	1240.	1- 9-2	2008	1290.	5-17-3	2120	1710.	2-28-5
1912	1685.	5-25-5	2009	1504.	3-30-2	2122	2090.	2-23-1
1913	1025.	4- 8-4	2017	2390.	4-15-6	2129	1710.	4- 2-6
1914	1780.	6-15-3	2018	2340.	5-14-5	2131	2250.	7- 2-5
1918	1400.	7-18-4	2019	2520.	3-33-3	2133	2270.	2-14-5
1922	1624.	1-27-1	2020	2230.	4-21-1	2134	2380.	5-33-3
1923	1512.	6-17-3	2021	1245.	5- 3-3	2136	1660.	3-37-6
1929	1835.	6- 1-1	2022	2480.	6-33-6	2137	2390.	6-26-1
1930	1695.	6-20-6	2025	1435.	1-19-2	2138	1330.	1- 5-2
1931	1430.	4- 4-2	2026	2150.	7-34-1	2141	2058.	7- 1-5
1933	1710.	1-31-5	2027	1805.	6-20-1	2142	2245.	6- 3-6
1935	1865.	2-23-3	2029	1820.	3-27-3	2143	2105.	6- 5-1
1940	1670.	5-33-1	2030	2340.	3- 2-1	2151	2050.	5-25-1
1942	1740.	3-34-3	2031	1210.	3-22-3	2152	1640.	1-11-2
1944	1530.	6-11-5	2033	1950.	5-30-3	2154	2510.	3-35-5
1949	1940.	7-17-1	2035	2289.	2-17-2	2155	2355.	7- 8-5
1950	1302.	1-18-2	2036	1438.	5- 1-1	2156	1945.	3- 4-6
1952	1070.	6-25-1	2037	1440.	5-25-4	2157	1735.	5-36-1
1954	1656.	3-25-1	2038	2135.	7- 8-4	2158	1000.	1-10-6
1961	1390.	3-32-5	2039	2210.	6-35-4	2159	2410.	2-33-2
	1413.	5-25-2	2040	2025.	4-27-6	2162	1280.	1- 2-3
	1105.	1-24-3	2044	1830.	7-13-5	2164	1420.	1-37-6
	1585.	1- 8-1	2048	1557.	5-27-2	2165	1100.	6-28-4
		1-15-	2050	1333.	6-26-3	2169	1650.	1-21-

TABLE 11-9 (Continued

SERIAL #	STRENGTH	LOCATION	SERIAL #	STRENGTH	LOCATION	SERIAL #	STRENGTH	LOCATION
2170	1240.	1-34-2	2282	1160.	5-18-6	2395	1240.	2-26-2
2174	1050.	6-22-2	2284	1575.	6-36-1	2396	1283.	4-18-2
2175	1250.	6-21-3	2285	2005.	1-32-4	2397	2090.	6-14-3
2176	1160.	5-30-1	2287	1115.	3-31-4	2398	1680.	3- 9-1
2179	2180.	7-21-3	2288	2340.	1-29-6	2399	1780.	2- 9-6
2181	1610.	7-36-1	2291	1392.	7-12-6	2400	1620.	4-33-5
2184	1100.	7- 7-6	2295	1031.	6-27-6	2401	1400.	3-16-5
2185	1425.	6-20-4	2296	2130.	4- 6-1	2402	1100.	6-23-4
2187	1500.	1-17-6	2297	1070.	5- 7-4	2403	1930.	6-22-1
2191	1780.	3-22-4	2299	1840.	2-19-1	2405	1562.	5- 7-3
2195	1609.	3-26-5	2301	1840.	7-11-3	2407	1448.	4-10-2
2197	1772.	1-37-3	2302	1920.	1-27-2	2409	1402.	6- 9-3
2199	1730.	7-15-5	2306	1970.	4-32-6	2410	2050.	4- 9-1
2204	2180.	6-14-5	2309	2110.	4-17-3	2413	1800.	1- 6-6
2206	1784.	3- 3-5	2311	1520.	7-14-5	2415	1730.	5- 8-4
2209	1360.	1-21-3	2316	1740.	2-30-1	2416	1220.	4-29-1
2212	2060.	7-24-1	2322	1350.	6-12-3	2417	1236.	3-21-4
2213	1560.	7-29-6	2336	1350.	3-10-1	2418	1985.	7-12-4
2215	2140.	1-34-1	2337	2130.	4-10-5	2421	1310.	1- 6-1
2217	1820.	2-30-4	2339	2220.	5-13-6	2422	2228.	1-28-1
2219	2265.	4-11-6	2340	1470.	4-31-2	2423	1270.	3- 8-6
2222	1615.	1-32-6	2347	1360.	7-19-5	2424	1585.	1- 3-6
2223	1338.	2-25-6	2348	2026.	1-14-5	2426	1555.	7- 7-2
2227	1100.	6-19-3	2349	1322.	7-33-2	2427	1388.	3-28-2
2228	1140.	3- 3-6	2350	1600.	1-25-6	2429	1620.	1-14-2
2230	1200.	7-10-6	2351	1200.	4-18-4	2430	1760.	2-22-5
2233	2190.	1-11-3	2352	1575.	5-17-1	2435	2005.	4-37-6
2235	2405.	6-33-2	2353	1780.	6-35-2	2436	1915.	4-28-4
2236	2140.	1- 7-5	2360	1630.	3-36-1	2440	1755.	3- 3-4
2238	1804.	6-28-6	2363	1820.	2- 6-4	2442	1410.	2- 1-1
2240	1405.	5-31-5	2364	1830.	5- 4-5	2444	2460.	1-14-6
2242	2070.	3-27-1	2365	2182.	3-16-6	2445	1960.	2-15-3
2243	1012.	2-10-1	2368	1499.	7-21-4	2447	1665.	2-18-4
2247	1900.	1-16-5	2371	1200.	6-36-5	2448	1470.	5-20-3
2252	1775.	2-16-2	2372	1785.	1-19-5	2450	1988.	3- 1-2
2255	1670.	4-10-4	2373	1211.	2- 8-4	2451	2010.	2-19-2
2256	1690.	3- 8-5	2374	1240.	3- 2-4	2452	1815.	1- 2-2
2260	1915.	1-10-5	2375	2132.	3- 2-3	2454	1241.	3- 1-6
2263	1443.	1- 3-5	2377	1545.	5-36-5	2455	2000.	5-22-5
2264	1619.	1-14-4	2378	2092.	2-14-4	2456	2125.	5-28-2
2269	1729.	4-27-4	2385	1520.	1-21-6	2458	1665.	3-32-1
2271	1030.	6-14-1	2387	1872.	7-26-1	2459	1275.	3-34-6
2273	1260.	2- 6-2	2388	1270.	6- 7-6	2460	1565.	7-33-5
2275	1835.	2-33-5	2390	1402.	4-34-1	2463	2585.	6-12-6
			2392	1365.	4-36-3	2464	2190.	7-28-6

TABLE 11-9 (Continued)

SERIAL #	STRENGTH	LOCATION	SERIAL #	STRENGTH	LOCATION	SERIAL #	STRENGTH	LOCATION
2465	1880.	6-27-3	2543	1144.	3-10-3	2670	1700.	6-28-1
2467	1080.	5-19-3	2544	1355.	6-27-4	2673	1774.	6-34-5
2469	1300.	3- 6-2	2545	1570.	6- 2-2	2674	1120.	7-28-4
2472	1890.	2-26-1	2546	1530.	5-24-?	2675	1280.	4-12-5
2473	2345.	2-34-4	2547	1210.	7-11-1	2676	1381.	4-36-2
2474	2220.	6- 3-2	2548	1485.	1-17-5	2677	1380.	5- 9-4
2476	2130.	5- 9-6	2549	1330.	4-25-3	2680	1733.	5-24-3
2477	2310.	1- 1-3	2551	1209.	3-10-5	2682	1470.	5- 5-6
2478	2580.	2-36-6	2555	1940.	6-37-2	2683	1420.	1- 5-4
2481	2170.	2-21-5	2556	1660.	7-29-2	2685	1820.	2-21-6
2483	2630.	6-23-5	2558	1450.	7-27-5	2686	1890.	7- 9-4
2484	1893.	7-34-5	2560	1470.	6-13-6	2688	1314.	7-29-1
2485	2310.	5-21-4	2561	1370.	6-36-6	2690	1210.	7-23-5
2487	2435.	7-24-4	2563	1285.	2-18-1	2692	1565.	3-36-4
2488	2177.	3-11-4	2564	1250.	5-14-4	2693	1415.	1- 8-4
2489	1890.	4- 1-1	2565	1130.	6-19-5	2694	1970.	1- 6-2
2490	1434.	2-27-5	2570	2165.	4-13-4	2697	1608.	5-20-6
2495	1255.	2-27-1	2579	1140.	4-28-5	2700	1360.	7-31-6
2497	1616.	5- 2-6	2583	1150.	7-20-4	2702	1080.	1-23-4
2498	1885.	1-19-1	2590	1430.	7-34-3	2703	1350.	5-28-5
2499	1321.	1-29-1	2591	1905.	4-34-6	2704	1335.	1-19-6
2500	2780.	7- 6-6	2592	1355.	3-26-4	2705	1805.	5- 2-3
2501	1750.	1- 8-2	2593	2125.	1-26-3	2706	1315.	5-14-3
2502	2400.	4-31-4	2595	1820.	3-14-4	2713	1980.	2-36-1
2503	1665.	4-14-4	2598	1510.	1-20-4	2715	1710.	2-29-6
2504	1110.	4-27-2	2600	1275.	1- 9-1	2716	1568.	5-20-2
2505	1490.	2-12-2	2606	1470.	3-13-4	2717	1510.	2- 7-5
2506	1826.	2-37-5	2608	1380.	3-21-1	2718	2240.	4-35-3
2507	1802.	5-19-2	2625	1150.	3-30-5	2719	2080.	6-25-2
2511	1355.	7- 2-4	2626	1430.	7-37-2	2720	1813.	2- 3-3
2512	2240.	6-23-6	2635	2170.	7- 7-5	2722	1950.	1-17-3
2515	1660.	5-36-6	2639	1358.	3-31-3	2723	1735.	1-26-6
2519	1325.	4-13-1	2640	1382.	5-18-1	2727	1325.	1-11-4
2521	2042.	4- 3-5	2642	1790.	5-21-1	2728	1570.	3-35-4
2522	1495.	4-11-3	2644	1472.	1-30-3	2730	1890.	2-27-6
2523	1655.	3-11-6	2645	1493.	2-34-6	2731	1525.	4-32-1
2526	2065.	2-30-6	2646	2080.	6-15-6	2733	2020.	1-28-3
2528	2470.	3-35-6	2647	1455.	6-24-4	2734	1630.	4-34-4
2529	1430.	4-33-2	2650	1664.	2- 8-6	2735	1475.	5-21-6
2530	1540.	4-29-3	2651	1950.	7- 9-6	2736	1470.	4-21-4
2531	1147.	1- 4-6	2661	1135.	1- 2-5	2738	1953.	7- 4-4
2533	1190.	3- 6-5	2664	1300.	5-20-5	2739	1570.	1- 6-5
2535	1795.	3- 4-4	2665	1779.	6-21-1	2740	2750.	2-19-6
253	1693.	2-31-1	2666	1670.	3-34-5	2743	1775.	1- 9-3
	1455	2- 3-4	2668	1340.	7-27-1	2753	1734.	4- 2-1

TABLE 11-9 (Continued)

SERIAL #	STRENGTH	LOCATION	SERIAL #	STRENGTH	LOCATION	SERIAL #	STRENGTH	LOCATION
2755	2100.	3-28-5	2841	2065.	3-25-4	2933	1485.	4-22-3
2758	1980.	7-21-1	2842	1455.	5-15-3	2935	1408.	5-17-4
2759	1410.	6-25-6	2843	1965.	5- 1-6	2936	1994.	6- 8-6
2760	2376.	5-13-2	2846	2105.	3-36-2	2939	1848.	4-18-3
2761	1920.	1- 1-2	2850	1580.	1-33-1	2940	1483.	2-13-1
2762	1265.	3- 1-1	2851	1340.	1-25-4	2942	1705.	5-35-5
2764	1715.	5-30-2	2852	1808.	1-15-1	2943	1626.	6- 3-1
2767	1340.	5-21-5	2855	2280.	4- 2-2	2944	1941.	3- 3-2
2768	1678.	5-16-6	2857	2560.	4-36-6	2946	1841.	3-13-3
2769	1285.	1-15-6	2858	2005.	1-12-1	2952	1507.	4- 5-2
2770	2100.	2- 9-5	2860	1170.	7-34-4	4108	2205.	1-27-5
2773	1675.	7- 5-2	2861	1610.	7-16-3	4278	1996.	2-33-4
2774	1770.	1-20-2	2863	1390.	1- 2-4	4304	1531.	5-18-3
2775	1780.	1-27-3	2865	1590.	2-10-3	4312	1388.	3-37-1
2776	1470.	1-26-4	2866	1395.	1-26-5	4318	2083.	5-13-3
2777	1620.	7- 4-5	2869	1560.	6-15-2	4329	1849.	6-16-4
2781	1590.	1-13-6	2873	1341.	3-28-1	4361	2262.	2- 8-2
2782	1130.	7-26-2	2874	1892.	5- 9-2	4381	1879.	6-17-5
2783	1890.	2-15-1	2875	1892.	3-12-5	4387	1580.	7-23-6
2784	1832.	4-30-2	2876	1730.	7-30-4	4430	1892.	5- 3-1
2786	1425.	3-19-2	2879	1470.	5-32-5	4572	1906.	3-30-1
2787	2018.	2-26-5	2880	1045.	1-21-5	4715	1785.	3- 3-1
2789	2560.	5- 2-2	2882	1925.	1-33-6	4716	1361.	4-15-4
2792	1960.	1-35-4	2883	1714.	1-19-4	4764	1898.	4-25-2
2795	1315.	5-13-1	2884	1277.	1- 1-4	4817	1960.	6- 2-6
2796	1465.	6-16-6	2885	1783.	4-27-5	4834	1969.	4- 8-2
2798	1564.	5-17-2	2891	2070.	1-22-5	4837	1395.	2-32-5
2799	1244.	6-11-6	2892	1326.	1-37-2	4925	2368.	1-34-4
2802	2210.	5-28-1	2893	1587.	1-36-2	4928	1639.	4- 6-5
2803	1624.	2-26-4	2904	1770.	7- 1-4	4983	1525.	5-37-1
2804	2138.	3- 7-4	2907	1980.	2-36-3	4987	1491.	7-15-4
2805	1684.	2- 7-1	2908	1535.	4-29-4	5003	1124.	7-16-4
2808	1868.	5- 1-5	2910	1625.	2- 2-6	5007	1429.	1-34-5
2810	1430.	4- 7-1	2911	2155.	2-34-5	5115	2315.	7- 2-6
2812	1710.	7- 6-5	2912	1939.	3-16-2	5152	1851.	4-13-3
2813	1888.	4-21-5	2913	1701.	7-11-4	5154	1546.	1-24-5
2815	1530.	1-18-5	2915	1420.	6- 1-6	5178	2176.	1-13-4
2820	1180.	4- 4-4	2919	1969.	6-13-5	5198	2019.	5-10-2
2826	1038.	6-35-3	2920	1701.	5-33-4	5205	2666.	5-16-4
2828	1475.	7- 1-1	2921	1265.	5-20-1	5217	2300.	6-18-3
2832	2460.	6-25-3	2923	1790.	7-22-1	5891	2124.	4-30-1
2833	1460.	4-14-5	2924	2290.	4-11-5	6004	2124.	6-37-1
2836	1820.	1-22-2	2928	1640.	4-30-4			
2838	1489.	4-21-3	2929	1650.	6- 4-2			
			2931	1750.	7-15-2			

TABLE 11-10
ELASTIC MODULUS FOR H-327 GRAPHITE
(in GPa)

Data Source	Midlength Center			Midlength Edge			End Center			End Edge		
	N	$\bar{X}$	S	N	$\bar{X}$	S	N	$\bar{X}$	S	N	$\bar{X}$	S
Axial Orientation												
Ref. 11-2	(a)	10.3	2.76	(a)	12.1	4.14	(a)	10.3	2.07	(a)	11.7	4.88
Refs. 11-3 through 11-7	14	9.0	3.45	14	11.0	4.14	16	9.0	2.07	16	11.0	4.14
Ref. 11-8	8	9.0	0.83	10	13.3	1.72						
Table 11-9	2	10.1	0.49	4	11.5	0.63	4	11.1	0.74	8	11.4	0.48
Radial Orientation												
Ref. 11-2	(a)	4.0	1.31	(a)	4.5	1.86	(a)	4.8	1.93	(a)	4.6	1.65
Refs. 11-3 through 11-7	15	3.6	0.97	12	4.2	1.67	15	4.1	1.59	15	4.2	0.85
Ref. 11-8	10	4.4	0.55									
Table 11-9	2	4.0	0.21	4	5.1	0.22	4	4.8	0.17	8	5.1	0.14

(a) Unknown.

TABLE 11-11

THERMAL EXPANSIVITY OF HLM GRAPHITE

LOT NUMBER: LOG NUMBER: 6484-78

ORIENTATION	LOG LOCATION	SPECIMEN NUMBER	THERMAL EXPANSIVITY (10EXP-6/K) 295K-773K (22C-500C)	295K-1173K (22C-900C)
AXIAL	END-CENTER	SLAB1 14B	2.55	3.01
		14A	2.57	3.04
		22A	2.47	2.91
		22B	2.38	2.82
		SL.1 84A	2.42	2.82
		84B	2.35	2.77
		92A	2.57	2.99
		92B	2.44	2.88
		MEAN:	2.47	2.90
		STD. DEV:	.09	.10
AXIAL	END-MIDRADIUS	SL.1 34A	2.47	2.92
		34B	2.34	2.77
		44A	2.67	3.10
		44B	2.42	2.90
		SL.1 106A	2.71	3.12
		106B	2.49	2.97
		116A	2.57	3.00
		116B	2.32	2.81
		MEAN:	2.50	2.95
		STD. DEV:	.14	.13
AXIAL	END-EDGE	SL.1 54A	2.25	2.71
		54B	2.12	2.61
		64A	2.49	2.94
		64B	2.23	2.77
		126A	2.19	2.60
		126B	2.63	3.07
		136A	2.26	2.72
		136B	2.19	2.64
		MEAN:	2.29	2.76
		STD. DEV:	.17	.17

TABLE 11-11 (Continued)

THERMAL EXPANSIVITY OF HLM GRAPHITE

LOT NUMBER: LOG NUMBER: 6484-78

ORIENTATION	LOG LOCATION	SPECIMEN NUMBER	THERMAL EXPANSIVITY (10EXP-6/K) 295K-773K (22C-500C)	295K-1173K (22C- 900C)
AXIAL	MIDLENGTH-CENTER	SL.6158A	2.38	2.77
		158B	2.36	2.75
		172A	2.51	2.93
		172B	2.61	3.01
		MEAN:	2.46	2.86
		STD. DEV:	.12	.13
		228A	2.52	2.89
		228B	2.60	2.98
		240A	2.57	3.01
		240B	2.67	3.14
		MEAN:	2.59	3.01
		STD. DEV:	.06	.10
AXIAL	MIDLENGTH-MIDRAD	SL.6178A	2.55	2.97
		178B	2.20	2.67
		188A	2.46	2.86
		188B	2.53	2.98
		248A	2.54	2.97
		248B	2.45	3.03
		258A	2.41	2.90
		258B	2.64	3.10
		MEAN:	2.51	3.00
		STD. DEV:	.10	.08
AXIAL	MIDLENGTH-EDGE	SL.6198A	2.36	2.81
		198B	2.43	2.93
		208A	2.51	3.00
		208B	2.38	2.88
		268A	2.47	2.94
		268B	2.59	3.01
		278A	2.47	2.94
		278B	2.38	2.88
		MEAN:	2.45	2.92
		STD. DEV:	.08	.06

TABLE 11-11 (Continued)

THERMAL EXPANSIVITY OF HLM GRAPHITE

LOT NUMBER: LOG NUMBER: 6484-78

ORIENTATION	LOG LOCATION	SPECIMEN NUMBER	THERMAL EXPANSIVITY (10EXP-6/K) 295K-773K (22C-500C)	295K-1173K (22C- 900C)
RADIAL	END-CENTER	SL.1 11A	2.85	3.30
		11B	2.92	3.31
		37A	2.99	3.43
		37B	3.11	3.60
		MEAN:	2.96	3.41
		STD. DEV:	.11	.14
		167A	2.96	3.35
		167B	2.74	3.21
		193A	2.75	3.23
		193B	2.59	3.11
		MEAN:	2.76	3.22
		STD. DEV:	.15	.10
RADIAL	END-MIDRADIUS	SL.167A	2.90	3.37
		67B	2.90	3.31
		93A	2.93	3.37
		93B	2.72	3.22
		223A	2.87	3.24
		223B	2.77	3.30
		249A	2.96	3.44
		249B	2.90	3.46
		MEAN:	2.87	3.34
		STD. DEV:	.08	.09
RADIAL	END-EDGE	119A	3.09	3.59
		119B	2.78	3.33
		145A	2.89	3.40
		145B	2.69	3.27
		275A	3.18	3.69
		275B	3.03	3.63
		301A	3.31	3.78
		301B	2.88	3.35
		MEAN:	2.98	3.50
		STD. DEV:	.21	.19

TABLE 11-11 (Continued)

THERMAL EXPANSIVITY OF HLM GRAPHITE

LOT NUMBER: LOG NUMBER: 6484-78

ORIENTATION	LOG LOCATION	SPECIMEN NUMBER	THERMAL EXPANSIVITY (10EXP-6/K) 295K-773K (22C-500C)	295K-1173K (22C- 900C)
RADIAL	MIDLENGTH-CENTER	SL.6323A	2.46	2.98
		323B	2.76	3.22
		349A	2.69	3.15
		349B	2.81	3.27
		479A	2.92	3.32
		479B	2.65	3.14
		491A	2.72	3.24
		491B	2.73	3.25
		MEAN:	2.72	3.20
		STD. DEV:	.13	.11
RADIAL	MIDLENGTH-MIDRAD	SL.6379A	2.82	3.29
		379B	2.73	3.19
		405A	2.57	3.09
		405B	2.79	3.26
		509A	2.69	3.19
		509B	2.92	3.38
		535A	2.87	3.34
		535B	3.05	3.57
		MEAN:	2.80	3.29
		STD. DEV:	.15	.15
RADIAL	MIDLENGTH-EDGE	SL.6431A	2.91	3.42
		431B	2.63	3.15
		457A	3.03	3.51
		457B	2.79	3.28
		561A	2.66	3.11
		561B	2.83	3.33
		587A	3.09	3.61
		587B	2.83	3.35
		MEAN:	2.85	3.35
		STD. DEV:	.16	.17

TABLE 11-12

TENSILE PROPERTIES OF HLM GRAPHITE

LOT NO. SPEC. DIA. 12.8 MM
LOG NO. 6484-148 SPEC. LENGTH 70. MM
LOG DENSITY MG/M**3

SPECIMEN NUMBER	ORIENTATION	LOCATION	DENSITY (MG/M**3)	YOUNGS MODULUS (GPA)	PERMANENT SET (PCT)	FRACTURE STRAIN (PCT)	TENSILE STRENGTH (MPA)
1AC-E- 10A	AX	EC	1.793	8.0	.009	.185	11.6
- 12A	AX	EC	1.794	8.7	.013	.152	10.4
- 22A	AX	EC	1.795	9.5	.015	.165	11.0
- 24A	AX	EC	1.793	8.4	.020	.156	10.3
- 06A	AX	EC					12.9
- 08B	AX	EC					11.6
- 10B	AX	EC					12.7
- 12B	AX	EC					11.7
- 18A	AX	EC					10.7
- 20B	AX	EC					11.5
- 22B	AX	EC					13.0
- 24B	AX	EC					13.3
1BC-E-106B	AX	EC	1.799	8.8	.019	.157	10.3
-108B	AX	EC	1.800	8.8	.020	.180	11.1
- 96B	AX	EC	1.794	8.5	.024	.180	10.7
- 94B	AX	EC	1.798	8.8	.021	.164	10.4
-102A	AX	EC					10.5
-104B	AX	EC					11.0
-106A	AX	EC					11.4
-108A	AX	EC					11.7
1BC-E- 90A	AX	EC					11.1
- 92B	AX	EC					9.4
- 94A	AX	EC					12.0
- 96A	AX	EC					12.2
MEAN			1.796	8.7 (1.26 MPSI)	.018	.167	11.3 (1646.PSI)
STD. DEV.			.003	.4 (.06 MPSI)	.005	.013	1.0 (141.PSI)

TABLE 11-12 (Continued)

TENSILE PROPERTIES OF HLM GRAPHITE

LOT NO. SPEC. DIA. 12.8 MM
LOG NO. 6484-148 SPEC. LENGTH 70. MM
LOG DENSITY MG/M**3

SPECIMEN NUMBER	ORIENTATION	LOCATION	DENSITY (MG/M**3)	YOUNGS MODULUS (GPA)	PERMANENT SET (PCT)	FRACTURE STRAIN (PCT)	TENSILE STRENGTH (MPA)
1AC-E- 05	RAD	EC	1.798	8.4	.020	.221	12.4
- 09	RAD	EC	1.798	8.2	.018	.250	13.5
- 25	RAD	EC	1.798	7.8	.019	.267	14.0
- 29	RAD	EC	1.796	7.8	.024	.261	13.6
- 03	RAD	EC					14.8
- 07	RAD	EC					13.4
- 11	RAD	EC					14.4
- 23	RAD	EC					13.7
- 27	RAD	EC					14.1
- 31	RAD	EC					14.4
1BC-E-113	RAD	EC	1.799	8.2	.022	.229	12.7
117	RAD	EC	1.795	8.1	.021	.245	13.3
133	RAD	EC	1.797	8.2	.020	.253	13.5
137	RAD	EC	1.797	7.8	.023	.235	12.7
111	RAD	EC					10.5
115	RAD	EC					9.9
1BC-E-119	RAD	EC					11.8
-131	RAD	EC					14.0
-135	RAD	EC					13.2
-139	RAD	EC					11.6
MEAN			1.797	8.1 (1.17 MPSI)	.021	.245	13.1 (1897.PSI)
STD. DEV.			.001	.2 (.03 MPSI)	.002	.016	1.3 (188.PSI)

TABLE 11-12 (Continued)

TENSILE PROPERTIES OF HLM GRAPHITE

LOT NO. SPEC. DIA. 12.8 MM
LOG NO. 6484-148 SPEC. LENGTH 70. MM
LOG DENSITY MG/M**3

SPECIMEN NUMBER	ORIENTATION	LOCATION	DENSITY (MG/M**3)	YOUNGS MODULUS (GPA)	PERMANENT SET (PCT)	FRACTURE STRAIN (PCT)	TENSILE STRENGTH (MPA)
1AY-E- 30B	AX	EM	1.810	9.1	.010	.170	11.7
- 34A	AX	EM	1.806	9.5	.018	.174	11.5
- 46B	AX	EM	1.804	8.7	.007	.178	12.2
- 54A	AX	EM	1.803	9.5	.021	.187	11.8
- 30A	AX	EM					12.5
- 34B	AX	EM					12.0
- 42A	AX	EM					12.6
- 42B	AX	EM					12.8
- 46A	AX	EM					12.3
- 54B	AX	EM					12.7
1BY-E-114B	AX	EM	1.805	9.0	.015	.225	13.8
-118A	AX	EM	1.807	8.6	.020	.234	13.7
-130B	AX	EM	1.808	9.4	.020	.207	12.7
-138A	AX	EM	1.806	9.4	.016	.184	12.2
-114A	AX	EM					13.0
-118B	AX	EM					13.0
1BY-E-126A	AX	EM					12.4
-126B	AX	EM					13.4
-130A	AX	EM					13.2
-138B	AX	EM					14.2
MEAN			1.806	9.2 (1.33 MPSI)	.016	.195	12.7 (1839.PSI)
STD. DEV.			.002	.4 (.05 MPSI)	.005	.024	.7 (105.PSI)

TABLE 11-12 (Continued)

TENSILE PROPERTIES OF HLM GRAPHITE

LOT NO. SPEC. DIA. 12.8 MM
LOG NO. 6484-148 SPEC. LENGTH 70. MM
LOG DENSITY MG/M**3

SPECIMEN NUMBER	ORIENTATION	LOCATION	DENSITY (MG/M**3)	YOUNGS MODULUS (GPA)	PERMANENT SET (PCT)	FRACTURE STRAIN (PCT)	TENSILE STRENGTH (MPA)
1AY-E- 45	RAD	EM	1.807	7.8	.020	.289	14.1
- 49	RAD	EM	1.807	7.8	.023	.269	13.7
- 63	RAD	EM	1.805	8.1	.020	.275	14.4
- 67	RAD	EM	1.803	7.8	.019	.258	13.9
- 43	RAD	EM					14.4
- 47	RAD	EM					13.8
- 51	RAD	EM					12.7
- 61	RAD	EM					13.6
- 65	RAD	EM					14.7
- 69	RAD	EM					14.2
1BY-E-153	RAD	EM	1.804	8.2	.017	.182	11.0
-157	RAD	EM	1.808	8.6	.018	.205	12.4
-171	RAD	EM	1.806	8.1	.017	.170	10.4
-175	RAD	EM	1.807	8.1	.019	.209	12.0
-151	RAD	EM					12.5
-155	RAD	EM					11.8
1BY-E-159	RAD	EM					12.0
-169	RAD	EM					11.5
-173	RAD	EM					8.0
-177	RAD	EM					9.2
MEAN			1.806	8.1 (1.17 MPSI)	.019	.232	12.5 (1815.PSI)
STD. DEV.			.002	.3 (.04 MPSI)	.002	.046	1.8 (265.PSI)

TABLE 11-12 (Continued)

TENSILE PROPERTIES OF HLM GRAPHITE

LOT NO. SPEC. DIA. 12.8 MM
LOG NO. 6484-148 SPEC. LENGTH 70. MM
LOG DENSITY MG/M**3

SPECIMEN NUMBER	ORIENTATION	LOCATION	DENSITY (MG/M**3)	YOUNGS MODULUS (GPA)	PERMANENT SET (PCT)	FRACTURE STRAIN (PCT)	TENSILE STRENGTH (MPA)
1AE-E- 60B	AX	EE	1.810	9.4	.020	.220	13.9
- 64A	AX	EE	1.808	9.8	.010	.209	14.8
- 76B	AX	EE	1.808	9.1	.015	.210	13.8
- 84A	AX	EE	1.802	9.7	.018	.254	15.8
- 60A	AX	EE					12.5
- 64B	AX	EE					14.7
- 72A	AX	EE					12.8
- 72B	AX	EE					13.8
- 76A	AX	EE					13.7
- 84B	AX	EE					14.4
1BE-E-144B	AX	EE	1.803	8.9	.018	.237	14.1
-148A	AX	EE	1.806	8.8	.018	.228	13.9
-160B	AX	EE	1.816	9.2	.014	.269	16.5
-168A	AX	EE	1.806	9.7	.018	.208	13.9
-144A	AX	EE					16.3
-148B	AX	EE					15.4
1BE-E-156A	AX	EE					14.8
-156B	AX	EE					14.7
-160A	AX	EE					14.2
-168B	AX	EE					13.2
MEAN			1.807	9.3 (1.35 MPSI)	.016	.229	14.4 (2082.PSI)
STD. DEV.			.004	.4 (.06 MPSI)	.003	.023	1.1 (153.PSI)

TABLE 11-12 (Continued)

TENSILE PROPERTIES OF HLM GRAPHITE

LOT NO. SPEC. DIA. 12.8 MM
LOG NO. 6484-148 SPEC. LENGTH 70. MM
LOG DENSITY MG/M**3

SPECIMEN NUMBER	ORIENTATION	LOCATION	DENSITY (MG/M**3)	YOUNGS MODULUS (GPA)	PERMANENT SET (PCT)	FRACTURE STRAIN (PCT)	TENSILE STRENGTH (MPA)
1AE-E- 81	RAD	EE	1.810	6.7	.022	.258	12.9
- 85	RAD	EE	1.809	7.6	.016	.274	13.8
- 99	RAD	EE	1.804	7.5	.024	.263	13.0
-103	RAD	EE	1.806	7.6	.024	.245	12.7
- 79	RAD	EE					13.8
- 83	RAD	EE					15.9
- 87	RAD	EE					14.4
- 97	RAD	EE					14.0
-101	RAD	EE					12.1
-105	RAD	EE					12.0
1BE-E-189	RAD	EE	1.806	8.0	.016	.255	13.7
193	RAD	EE	1.805	7.9	.019	.256	13.6
207	RAD	EE	1.812	8.2	.020	.203	11.6
211	RAD	EE	1.814	7.7	.020	.235	12.6
187	RAD	EE					12.8
191	RAD	EE					13.1
1BE-E-195	RAD	EE					13.2
-205	RAD	EE					12.5
-209	RAD	EE					12.8
-213	RAD	EE					12.1
MEAN			1.808	7.7 (1.11 MPSI)	.020	.249	13.1 (1906.PSI)
STD. DEV.			.004	.5 (.07 MPSI)	.003	.022	1.0 (143.PSI)

TABLE 11-12 (Continued)

TENSILE PROPERTIES OF HLM GRAPHITE

LOT NO. SPEC. DIA. 12.8 MM
LOG NO. 6484-148 SPEC. LENGTH 70. MM
LOG DENSITY MG/M**3

SPECIMEN NUMBER	ORIENTATION	LOCATION	DENSITY (MG/M**3)	YOUNGS MODULUS (GPA)	PERMANENT SET (PCT)	FRACTURE STRAIN (PCT)	TENSILE STRENGTH (MPA)
6AC-M- 10B	AX	MLC	1.817	9.4	.011	.145	10.3
- 12B	AX	MLC	1.817	9.5	.016	.112	8.2
- 22A	AX	MLC	1.811	9.4	.018	.198	12.4
- 24A	AX	MLC	1.817	8.8	.016	.113	8.0
- 06B	AX	MLC					10.6
- 08B	AX	MLC					10.4
- 10A	AX	MLC					11.8
- 12A	AX	MLC					12.9
- 18A	AX	MLC					7.6
- 20A	AX	MLC					12.3
- 22B	AX	MLC					12.8
- 24B	AX	MLC					11.8
6BC-M- 94B	AX	MLC	1.820	8.9	.019	.130	8.6
- 96A	AX	MLC	1.819	8.6	.013	.201	12.6
- 98A	AX	MLC	1.823	8.5	.020	.121	8.2
6BC-M-106B	AX	MLC	1.813	9.0	.014	.127	9.0
- 92A	AX	MLC					9.6
- 94A	AX	MLC					12.2
- 96B	AX	MLC					9.1
- 98B	AX	MLC					8.9
-104B	AX	MLC					10.2
-106A	AX	MLC					12.1
MEAN			1.817	9.0 (1.31 MPSI)	.016	.143	10.4 (1514.PSI)
STD. DEV.			.004	.4 (.06 MPSI)	.003	.036	1.8 (261.PSI)

TABLE 11-12 (Continued)

TENSILE PROPERTIES OF HLM GRAPHITE

LOT NO. SPEC. DIA. 12.8 MM
LOG NO. 6484-148 SPEC. LENGTH 70. MM
LOG DENSITY MG/M**3

SPECIMEN NUMBER	ORIENTATION	LOCATION	DENSITY (MG/M**3)	YOUNGS MODULUS (GPA)	PERMANENT SET (PCT)	FRACTURE STRAIN (PCT)	TENSILE STRENGTH (MPA)
6AC-M- 07	RAD	MLC	1.815	7.9	.023	.213	11.9
- 11	RAD	MLC	1.817	7.9	.024	.227	12.4
- 25	RAD	MLC	1.815	8.3	.025	.203	11.3
- 29	RAD	MLC	1.816	8.0	.021	.179	10.3
- 05	RAD	MLC					10.7
- 09	RAD	MLC					10.7
- 13	RAD	MLC					11.8
- 23	RAD	MLC					13.2
- 27	RAD	MLC					13.2
- 31	RAD	MLC					12.3
6BC-M-115	RAD	MLC	1.818	8.1	.016	.214	12.0
-119	RAD	MLC	1.819	7.5	.023	.183	10.0
-133	RAD	MLC	1.818	8.1	.020	.214	12.0
6BC-M-137	RAD	MLC	1.819	7.9	.019	.195	11.0
-113	RAD	MLC					10.0
-117	RAD	MLC					10.6
-121	RAD	MLC					9.2
-131	RAD	MLC					12.1
-135	RAD	MLC					11.7
-139	RAD	MLC					9.9
	MEAN		1.817	8.0 (1.16 MPSI)	.021	.203	11.3 (1641.PSI)
	STD. DEV.		.002	.2 (.03 MPSI)	.003	.017	1.1 (163.PSI)

TABLE 11-12 (Continued)

TENSILE PROPERTIES OF HLM GRAPHITE

LOT NO. SPEC. DIA. 12.8 MM
LOG NO. 6484-148 SPEC. LENGTH 70. MM
LOG DENSITY MG/M**3

SPECIMEN NUMBER	ORIENTATION	LOCATION	DENSITY (MG/M**3)	YOUNGS MODULUS (GPA)	PERMANENT SET (PCT)	FRACTURE STRAIN (PCT)	TENSILE STRENGTH (MPA)
6AY-M- 30B	AX	MLM	1.801	9.5	.013	.166	11.4
- 34A	AX	MLM	1.808	9.6	.017	.205	13.1
- 46B	AX	MLM	1.802	9.2	.013	.150	10.8
- 52A	AX	MLM	1.802	9.1	.015	.144	10.0
- 30A	AX	MLM					12.8
- 34B	AX	MLM					11.8
- 42A	AX	MLM					13.3
- 42B	AX	MLM					13.4
- 46A	AX	MLM					11.3
- 52B	AX	MLM					11.7
6BY-M-112B	AX	MLM	1.814	8.8	.016	.148	10.0
116A	AX	MLM	1.815	9.2	.014	.152	10.4
128B	AX	MLM	1.805	9.0	.019	.160	10.5
6BY-M-134A	AX	MLM	1.805	9.4	.016	.136	9.6
-112A	AX	MLM					10.0
-116B	AX	MLM					12.6
-124A	AX	MLM					11.9
-124B	AX	MLM					11.5
-128A	AX	MLM					9.0
-134B	AX	MLM					11.7
MEAN			1.807	9.2 (1.34 MPSI)	.015	.158	11.3 (1643.PSI)
STD. DEV.			.005	.2 (.04 MPSI)	.002	.021	1.3 (187.PSI)

TABLE 11-12 (Continued)

TENSILE PROPERTIES OF HLM GRAPHITE

LOT NO.
LOG NO. 6484-148
LOG DENSITY MG/M**3

SPEC. DIA. 12.8 MM
SPEC. LENGTH 70. MM

SPECIMEN NUMBER	ORIENTATION	LOCATION	DENSITY (MG/M**3)	YOUNGS MODULUS (GPA)	PERMANENT SET (PCT)	FRACTURE STRAIN (PCT)	TENSILE STRENGTH (MPA)
6AY-M- 45	RAD	MLM	1.803	7.4	.026	.265	13.0
- 49	RAD	MLM	1.804	7.5	.024	.239	12.1
- 63	RAD	MLM	1.804	7.4	.026	.255	12.4
- 67	RAD	MLM	1.805	7.5	.023	.262	12.8
- 43	RAD	MLM					10.0
- 47	RAD	MLM					13.2
- 51	RAD	MLM					12.6
- 61	RAD	MLM					12.4
- 65	RAD	MLM					12.6
- 69	RAD	MLM					12.5
6BY-M-153	RAD	MLM	1.818	8.3	.019	.199	11.3
-157	RAD	MLM	1.816	8.3	.023	.209	11.4
-171	RAD	MLM	1.812	8.2	.020	.162	9.8
6BY-M-175	RAD	MLM	1.811	8.1	.019	.214	12.3
-151	RAD	MLM					12.8
-155	RAD	MLM					11.0
-159	RAD	MLM					11.5
-169	RAD	MLM					10.8
-173	RAD	MLM					11.3
-177	RAD	MLM					11.7
MEAN			1.809	7.8 (1.13 MPSI)	.022	.226	11.9 (1723.PSI)
STD. DEV.			.006	.4 (.06 MPSI)	.003	.036	1.0 (141.PSI)

TABLE 11-12 (Continued)

TENSILE PROPERTIES OF HLM GRAPHITE

LOT NO. SPEC. DIA. 12.8 MM
LOG NO. 6484-148 SPEC. LENGTH 70. MM
LOG DENSITY MG/M**3

SPECIMEN NUMBER	ORIENTATION	LOCATION	DENSITY (MG/M**3)	YOUNGS MODULUS (GPA)	PERMANENT SET (PCT)	FRACTURE STRAIN (PCT)	TENSILE STRENGTH (MPA)
6AE-M- 60B	AX	MLE	1.790	9.1	.014	.230	14.1
- 64A	AX	MLE	1.790	9.1	.018	.230	13.9
- 76B	AX	MLE	1.793	9.3	.015	.219	14.3
- 84A	AX	MLE	1.793	9.7	.015	.204	13.5
- 60A	AX	MLE					12.9
- 64B	AX	MLE					14.8
- 72A	AX	MLE					15.1
- 72B	AX	MLE					12.7
- 76A	AX	MLE					13.5
- 84B	AX	MLE					11.4
6BE-M-142B	AX	MLE	1.805	9.0	.014	.217	13.3
146A	AX	MLE	1.803	8.9	.015	.241	14.3
158B	AX	MLE	1.801	9.0	.021	.235	13.8
6BE-M-164A	AX	MLE	1.796	9.5	.015	.222	14.4
-142A	AX	MLE					13.3
-146B	AX	MLE					13.8
-154A	AX	MLE					12.6
-154B	AX	MLE					14.9
-158A	AX	MLE					14.7
-164B	AX	MLE					13.3
MEAN			1.796	9.2 (1.33 MPSI)	.016	.225	13.7 (1991.PSI)
STD. DEV.			.006	.3 (.04 MPSI)	.002	.012	.9 (132.PSI)

TABLE 11-12 (Continued)

TENSILE PROPERTIES OF HLM GRAPHITE

LOT NO. SPEC. DIA. 12.8 MM
LOG NO. 6484-148 SPEC. LENGTH 70. MM
LOG DENSITY MG/M**3

SPECIMEN NUMBER	ORIENTATION	LOCATION	DENSITY (MG/M**3)	YOUNGS MODULUS (GPA)	PERMANENT SET (PCT)	FRACTURE STRAIN (PCT)	TENSILE STRENGTH (MPA)
6AE-M- 81	RAD	MLE	1.791	6.8	.030	.295	12.5
- 85	RAD	MLE	1.789	6.8	.026	.256	11.8
- 99	RAD	MLE	1.792	6.8	.024	.285	12.9
-103	RAD	MLE	1.791	7.0	.027	.266	12.0
- 79	RAD	MLE					12.2
- 83	RAD	MLE					12.9
- 87	RAD	MLE					13.4
- 97	RAD	MLE					11.4
-101	RAD	MLE					12.4
-105	RAD	MLE					11.5
6BE-M-189	RAD	MLE	1.808	7.6	.024	.250	12.5
-193	RAD	MLE	1.807	7.7	.021	.218	11.4
-207	RAD	MLE	1.803	7.9	.017	.268	14.1
6BE-M-211	RAD	MLE	1.803	7.7	.018	.260	13.4
-187	RAD	MLE					14.1
-191	RAD	MLE					13.6
-195	RAD	MLE					13.4
-205	RAD	MLE					13.2
-209	RAD	MLE					13.6
-213	RAD	MLE					13.3
MEAN			1.798	7.3 (1.06 MPSI)	.023	.262	12.8 (1854.PSI)
STD. DEV.			.008	.5 (.07 MPSI)	.004	.023	.9 (125.PSI)

TABLE 11-12 (Continued)

TENSILE PROPERTIES OF HLM GRAPHITE

LOT NO. SPEC. DIA. 12.8 MM
LOG NO. 6484-148 SPEC. LENGTH 70. MM
LOG DENSITY MG/M**3

SPECIMEN NUMBER	ORIENTATION	LOCATION	DENSITY (MG/M**3)	YOUNGS MODULUS (GPA)	PERMANENT SET (PCT)	FRACTURE STRAIN (PCT)	TENSILE STRENGTH (MPA)
12AC-B- 10B	AX	EC	1.823	9.1	.015	.198	12.4
- 12B	AX	EC	1.819	9.2	.018	.196	12.5
- 22B	AX	EC	1.827	9.1	.018	.243	14.6
- 24B	AX	EC	1.820	9.8	.013	.195	13.1
- 06A	AX	EC					11.1
- 08B	AX	EC					12.3
- 10A	AX	EC					11.1
- 12A	AX	EC					12.5
- 18A	AX	EC					13.5
- 20B	AX	EC					12.9
- 22A	AX	EC					12.7
- 24A	AX	EC					12.1
12BC-B- 94B	AX	EC	1.821	9.4	.017	.206	12.8
- 96B	AX	EC	1.820	9.1	.015	.188	12.6
-106B	AX	EC	1.820	8.9	.011	.182	11.8
-108B	AX	EC	1.811	9.0	.020	.165	10.7
- 90A	AX	EC					12.4
- 92B	AX	EC					12.1
- 94A	AX	EC					11.6
- 96A	AX	EC					11.2
-102A	AX	EC					11.3
-104B	AX	EC					12.3
-106A	AX	EC					12.5
-108A	AX	EC					11.0
MEAN			1.820	9.2 (1.33 MPSI)	.016	.197	12.2 (1772.PSI)
STD. DEV.			.004	.3 (.04 MPSI)	.003	.022	.9 (129.PSI)

TABLE 11-12 (Continued)

TENSILE PROPERTIES OF HLM GRAPHITE

LOT NO. SPEC. DIA. 12.8 MM
LOG NO. 6484-148 SPEC. LENGTH 70. MM
LOG DENSITY MG/M**3

SPECIMEN NUMBER	ORIENTATION	LOCATION	DENSITY (MG/M**3)	YOUNGS MODULUS (GPA)	PERMANENT SET (PCT)	FRACTURE STRAIN (PCT)	TENSILE STRENGTH (MPA)
12AC-B- 05	RAD	EC	1.825	8.3	.024	.243	13.4
- 09	RAD	EC	1.825	8.3	.017	.259	14.4
- 23	RAD	EC	1.825	8.4	.020	.261	14.4
- 27	RAD	EC	1.822	8.3	.020	.255	14.3
- 03	RAD	EC					13.4
- 07	RAD	EC					14.8
- 11	RAD	EC					14.5
- 21	RAD	EC					15.4
12AC-B- 25	RAD	EC					14.4
- 29	RAD	EC					14.7
12BC-B-113	RAD	EC	1.817	7.9	.017	.224	12.5
-117	RAD	EC	1.818	8.1	.020	.224	12.7
-131	RAD	EC	1.820	7.8	.016	.199	11.4
-135	RAD	EC	1.821	8.7	.021	.213	12.2
-111	RAD	EC					12.5
-115	RAD	EC					12.3
-119	RAD	EC					13.1
-129	RAD	EC					11.7
-133	RAD	EC					13.1
-137	RAD	EC					12.0
MEAN			1.822	8.2 (1.19 MPSI)	.019	.235	13.4 (1936.PSI)
STD. DEV.			.003	.3 (.04 MPSI)	.003	.023	1.2 (172.PSI)

TABLE 11-12 (Continued)

TENSILE PROPERTIES OF HLM GRAPHITE

LOT NO. SPEC. DIA. 12.8 MM
LOG NO. 6484-148 SPEC. LENGTH 70. MM
LOG DENSITY MG/M**3

SPECIMEN NUMBER	ORIENTATION	LOCATION	DENSITY (MG/M**3)	YOUNGS MODULUS (GPA)	PERMANENT SET (PCT)	FRACTURE STRAIN (PCT)	TENSILE STRENGTH (MPA)
12AY-B- 30B	AX	EM	1.818	9.0	.016	.130	9.1
- 34A	AX	EM	1.815	9.7	.011	.184	12.8
- 46B	AX	EM	1.818	10.2	.016	.186	13.1
- 54A	AX	EM	1.816	9.8	.015	.185	12.7
- 30A	AX	EM					11.0
- 34B	AX	EM					13.3
- 42A	AX	EM					14.6
- 42B	AX	EM					13.5
12AY-B- 46A	AX	EM					14.4
- 54B	AX	EM					13.6
12BY-B-114B	AX	EM	1.823	9.4	.021	.228	13.8
-118A	AX	EM	1.746	7.3	.024	.152	8.5
-130B	AX	EM	1.821	9.5	.023	.251	15.4
-138A	AX	EM	1.814	9.7	.020	.231	14.7
-114A	AX	EM					13.1
-118B	AX	EM					10.6
-126A	AX	EM					13.3
-126B	AX	EM					14.3
-130A	AX	EM					13.0
-138B	AX	EM					14.6
MEAN			1.809	9.3 (1.35 MPSI)	.018	.193	13.0 (1881.PSI)
STD. DEV.			.026	.9 (.13 MPSI)	.004	.041	1.8 (268.PSI)

TABLE 11-12 (Continued)

TENSILE PROPERTIES OF HLM GRAPHITE

LOT NO. SPEC. DIA. 12.8 MM
LOG NO. 6484-148 SPEC. LENGTH 70. MM
LOG DENSITY MG/M**3

SPECIMEN NUMBER	ORIENTATION	LOCATION	DENSITY (MG/M**3)	YOUNGS MODULUS (GPA)	PERMANENT SET (PCT)	FRACTURE STRAIN (PCT)	TENSILE STRENGTH (MPA)
12AY-B- 45	RAD	EM	1.828	8.0	.029	.259	13.4
- 49	RAD	EM	1.813	7.9	.025	.269	13.7
- 63	RAD	EM	1.817	7.9	.029	.245	12.8
- 67	RAD	EM	1.808	7.7	.014	.231	12.4
- 43	RAD	EM					13.4
- 47	RAD	EM					13.1
- 51	RAD	EM					12.2
- 61	RAD	EM					13.1
12AY-B- 65	RAD	EM					11.5
- 69	RAD	EM					12.4
12BY B-153	RAD	EM	1.822	8.7	.025	.240	13.6
-157	RAD	EM	1.827	8.8	.021	.208	12.3
-171	RAD	EM	1.821	8.1	.031	.256	14.1
-175	RAD	EM	1.818	8.4	.021	.212	12.3
-151	RAD	EM					10.1
-155	RAD	EM					14.6
-159	RAD	EM					16.0
-169	RAD	EM					15.4
-173	RAD	EM					15.1
-177	RAD	EM					15.8
MEAN			1.819	8.2 (1.19 MPSI)	.024	.240	13.4 (1939.PSI)
STD. DEV.			.007	.4 (.06 MPSI)	.006	.022	1.5 (217.PSI)

TABLE 11-12 (Continued)

TENSILE PROPERTIES OF HLM GRAPHITE

LOT NO. SPEC. DIA. 12.8 MM
LOG NO. 6484-148 SPEC. LENGTH 70. MM
LOG DENSITY MG/M**3

SPECIMEN NUMBER	ORIENTATION	LOCATION	DENSITY (MG/M**3)	YOUNGS MODULUS (GPA)	PERMANENT SET (PCT)	FRACTURE STRAIN (PCT)	TENSILE STRENGTH (MPA)
12AE-B- 60B	AX	EE	1.738	5.8	.029	.202	9.0
- 64A	AX	EE	1.804	9.5	.014	.235	15.2
- 76B	AX	EE	1.802	10.0	.013	.227	14.9
- 84A	AX	EE	1.806	10.5	.016	.230	15.2
- 60A	AX	EE					13.8
- 64B	AX	EE					14.8
- 72A	AX	EE					16.1
- 72B	AX	EE					16.4
12AE-B- 76A	AX	EE					13.8
- 84B	AX	EE					13.1
12BE-B-144B	AX	EE	1.819	9.4	.016	.221	14.2
-148A	AX	EE	1.815	8.7	.017	.264	14.9
-160B	AX	EE	1.821	9.4	.014	.231	14.9
-168A	AX	EE	1.809	9.7	.016	.236	15.1
-144A	AX	EE					11.2
-148B	AX	EE					13.2
-156A	AX	EE					11.4
-156B	AX	EE					15.1
-160A	AX	EE					15.6
-168B	AX	EE					12.0
	MEAN		1.802	9.1 (1.32 MPSI)	.017	.231	14.0 (2029.PSI)
	STD. DEV.		.027	1.4 (.21 MPSI)	.005	.017	1.9 (272.PSI)

TABLE 11-12 (Continued)

TENSILE PROPERTIES OF HLM GRAPHITE

LOT NO. SPEC. DIA. 12.8 MM
LOG NO. 6484-148 SPEC. LENGTH 70. MM
LOG DENSITY MG/M**3

SPECIMEN NUMBER	ORIENTATION	LOCATION	DENSITY (MG/M**3)	YOUNGS MODULUS (GPA)	PERMANENT SET (PCT)	FRACTURE STRAIN (PCT)	TENSILE STRENGTH (MPA)
12AE-B- 81	RAD	EE	1.806	6.8	.024	.236	11.4
- 85	RAD	EE	1.807	7.2	.026	.203	10.2
- 99	RAD	EE	1.806	7.0	.027	.273	12.7
-103	RAD	EE	1.805	7.3	.032	.254	12.0
- 79	RAD	EE					12.4
- 83	RAD	EE					12.3
- 87	RAD	EE					13.7
- 97	RAD	EE					6.3
12AE-B-101	RAD	EE					11.8
-105	RAD	EE					11.5
12BE-B-189	RAD	EE	1.815	7.8	.017	.269	14.4
-193	RAD	EE	1.818	8.2	.025	.286	15.0
-207	RAD	EE	1.816	8.1	.019	.247	13.7
-211	RAD	EE	1.814	8.1	.020	.269	14.7
-187	RAD	EE					13.0
-191	RAD	EE					15.1
-195	RAD	EE					14.8
-205	RAD	EE					13.8
-209	RAD	EE					13.4
-213	RAD	EE					15.5
MEAN			1.811	7.6 (1.10 MPSI)	.024	.255	12.9 (1869.PSI)
STD. DEV.			.006	.6 (.08 MPSI)	.005	.026	2.1 (308.PSI)

TABLE 11-13

FLEXURAL PROPERTIES OF HLM GRAPHITE

LOT NO. SPEC. DIA. 6.4 MM
LOG NO. 6484-148 SPEC. LENGTH 51. MM
LOG DENSITY MG/M**3

SPECIMEN NUMBER	ORIENTATION	LOCATION	DENSITY (MG/M**3)	MODULUS OF RUPTURE (MPA) (UNCORRECTED)	FLEXURAL STRENGTH (MPA) (CORRECTED)
1AE	56A	AX	EE	24.1	21.2
	56B	AX	EE	25.2	22.1
	58A	AX	EE	24.4	21.5
	58B	AX	EE	20.5	18.5
	62A	AX	EE	23.2	20.6
	62B	AX	EE	24.0	21.2
	68A	AX	EE	24.0	21.2
	68B	AX	EE	28.1	24.2
	70A	AX	EE	29.5	25.1
	70B	AX	EE	26.0	22.7
1BE	128A	AX	EE	22.8	20.3
	128B	AX	EE	27.3	23.6
	130A	AX	EE	24.7	21.7
	130B	AX	EE	26.9	23.3
	134A	AX	EE	26.9	23.3
	134B	AX	EE	25.8	22.6
	140A	AX	EE	26.1	22.7
	140B	AX	EE	26.1	22.8
	142A	AX	EE	25.8	22.5
	142B	AX	EE	26.5	23.1
	MEAN			25.4 MPA (3682. PSI)	22.2 MPA (3223. PSI)
	STD. DEV.			2.0 MPA (293. PSI)	1.5 MPA (216. PSI)

TABLE 11-13 (Continued)

FLEXURAL PROPERTIES OF HLM GRAPHITE

LOT NO. SPEC. DIA. 6.4 MM
LOG NO. 64R4-148 SPEC. LENGTH 51. MM
LOG DENSITY MG/M**3

SPECIMEN NUMBER	ORIENTATION	LOCATION	DENSITY (MG/M**3)	MODULUS OF RUPTURE (MPA) (UNCORRECTED)	FLEXURAL STRENGTH (MPA) (CORRECTED)
1AY	36A	AX	EM	24.3	21.4
	36B	AX	EM	23.2	20.5
	38A	AX	EM	19.7	17.8
	38B	AX	EM	21.6	19.4
	42A	AX	EM	24.6	21.6
	42B	AX	EM	23.0	20.4
	48A	AX	EM	19.1	17.3
	48B	AX	EM	25.6	22.3
	50A	AX	EM	25.5	22.3
	50B	AX	EM	23.5	20.8
1BY	108A	AX	EM	18.9	17.2
	108B	AX	EM	24.5	21.5
	110A	AX	EM	26.3	22.8
	110B	AX	EM	22.9	20.3
	114A	AX	EM	24.0	21.2
	114B	AX	EM	26.1	22.7
	120A	AX	EM	26.2	22.8
	120B	AX	EM	24.4	21.5
	122A	AX	EM	25.3	22.1
	122B	AX	EM	26.8	23.2
	MEAN			23.8 MPA (3448. PSI)	21.0 MPA (3040. PSI)
	STD. DEV.			2.4 MPA (343. PSI)	1.8 MPA (262. PSI)

TABLE 11-13 (Continued)

FLEXURAL PROPERTIES OF HLM GRAPHITE

LOT NO. SPEC. DIA. 6.4 MM
LOG NO. 6484-148 SPEC. LENGTH 51. MM
LOG DENSITY MG/M**3

SPECIMEN NUMBER	ORIENTATION	LOCATION	DENSITY (MG/M**3)	MODULUS OF RUPTURE (MPA) (UNCORRECTED)	FLEXURAL STRENGTH (MPA) (CORRECTED)
1AC	12A	AX	EC	18.8	17.0
	12B	AX	EC	23.4	20.5
	10A	AX	EC	23.5	20.6
	10B	AX	EC	19.6	17.7
	16A	AX	EC	23.6	20.7
	16B	AX	EC	18.5	16.8
	24A	AX	EC	22.6	19.9
	24B	AX	EC	22.0	19.5
	26A	AX	EC	21.0	18.7
	26B	AX	EC	21.0	18.7
	32A	AX	EC	23.2	20.4
	32B	AX	EC	18.9	17.0
1BC	8AA	AX	EC	23.8	20.8
	8AB	AX	EC	17.5	15.9
	86A	AX	EC	22.7	20.0
	86B	AX	EC	26.2	22.6
	80A	AX	EC	20.7	18.5
	80B	AX	EC	21.2	18.8
	96A	AX	EC	24.7	21.5
	96B	AX	EC	24.3	21.2
1BC	102A	AX	EC	20.3	18.2
	102B	AX	EC	21.3	18.9
	104A	AX	EC	22.6	20.0
	104B	AX	EC	19.2	17.3
	MEAN			21.7 MPA (3145. PSI)	19.2 MPA (2788. PSI)
	STD. DEV.			2.2 MPA (324. PSI)	1.7 MPA (247. PSI)

TABLE 11-13 (Continued)

FLEXURAL PROPERTIES OF MLM GRAPHITE

LOT NO. SPEC. DIA. 6.4 MM
LOG NO. 6484-148 SPEC. LENGTH 51. MM
LOG DENSITY MG/M**3

SPECIMEN NUMBER	ORIENTATION	LOCATION	DENSITY (MG/M**3)	MODULUS OF RUPTURE (MPA) (UNCORRECTED)	FLEXURAL STRENGTH (MPA) (CORRECTED)
6AE	200A	AX	MLE	24.6	21.6
	200B	AX	MLE	25.4	22.2
	202A	AX	MLE	23.9	21.1
	202B	AX	MLE	27.6	23.8
	206A	AX	MLE	26.8	23.2
	206B	AX	MLE	26.2	22.8
	212A	AX	MLE	21.6	19.3
	212B	AX	MLE	18.8	17.1
	214A	AX	MLE	21.5	19.2
	214B	AX	MLE	24.6	21.6
6BE	270A	AX	MLE	23.7	20.9
	270B	AX	MLE	26.3	22.8
	272A	AX	MLE	26.3	22.8
	272B	AX	MLE	24.3	21.4
	276A	AX	MLE	25.5	22.3
	276B	AX	MLE	24.5	21.5
	280A	AX	MLE	23.6	20.9
	280B	AX	MLE	24.4	21.4
	282A	AX	MLE	23.8	21.0
	282B	AX	MLE	21.3	19.1
	MEAN			24.2 MPA (3515. PSI)	21.3 MPA (3091. PSI)
	STD. DEV.			2.1 MPA (311. PSI)	1.6 MPA (235. PSI)

TABLE 11-13 (Continued)

FLEXURAL PROPERTIES OF HLM GRAPHITE

LOT NO.
LOG NO. A484-148
LOG DENSITY MG/M**3

SPEC. DIA. 6.4 MM
SPEC. LENGTH 51. MM

SPECIMEN NUMBER	ORIENTATION	LOCATION	DENSITY (MG/M**3)	MODULUS OF RUPTURE (MPA) (UNCORRECTED)	FLEXURAL STRENGTH (MPA) (CORRECTED)
6AY	180A AX	MLM		22.4	20.0
	180B AX	MLM		21.3	19.1
	182A AX	MLM		25.1	22.0
	182B AX	MLM		21.5	19.3
	196A AX	MLM		20.6	18.6
	196B AX	MLM		25.6	22.3
	192A AX	MLM		22.5	20.0
	192B AX	MLM		21.9	19.6
	194A AX	MLM		16.9	15.6
	194B AX	MLM		22.1	19.8
6BY	250A AX	MLM		23.0	20.4
	250B AX	MLM		20.8	18.7
	252A AX	MLM		24.9	21.8
	252B AX	MLM		23.3	20.7
	256A AX	MLM		24.2	21.3
	256B AX	MLM		25.7	22.4
	262A AX	MLM		19.7	17.8
	262B AX	MLM		20.1	18.2
	264A AX	MLM		17.6	16.1
	264B AX	MLM		19.7	17.8
	MEAN			21.9 MPA (3181. PSI)	19.6 MPA (2839. PSI)
	STD. DEV.			2.5 MPA (358. PSI)	1.9 MPA (279. PSI)

TABLE 11-13 (Continued)

FLEXURAL PROPERTIES OF HLM GRAPHITE

LOT NO. SPEC. DIA. 6.4 MM
LOG NO. 6484-148 SPEC. LENGTH 51. MM
LOG DENSITY MG/M**3

SPECIMEN NUMBER	ORIENTATION	LOCATION	DENSITY (MG/M**3)	MODULUS OF RUPTURE (MPA) (UNCORRECTED)	FLEXURAL STRENGTH (MPA) (CORRECTED)
6AC	154A	AX	MLC	23.1	20.5
	154B	AX	MLC	18.9	17.2
	156A	AX	MLC	18.9	17.2
	156B	AX	MLC	20.3	18.2
	160A	AX	MLC	26.0	22.6
	160B	AX	MLC	18.6	16.4
	174A	AX	MLC	22.9	20.3
	174B	AX	MLC	18.4	16.8
	176A	AX	MLC	20.8	18.7
	176B	AX	MLC	17.6	16.1
	168A	AX	MLC	27.4	23.6
	168B	AX	MLC	20.0	18.0
6BC	224A	AX	MLC	21.6	19.3
	224B	AX	MLC	23.2	20.5
	226A	AX	MLC	16.9	15.5
	226B	AX	MLC	22.3	19.9
	232A	AX	MLC	18.0	16.4
	232B	AX	MLC	25.2	22.0
	236A	AX	MLC	22.7	20.1
	236B	AX	MLC	22.5	19.9
6BC	238A	AX	MLC	21.1	18.9
	238B	AX	MLC	25.3	22.0
	244A	AX	MLC	21.9	19.5
	244B	AX	MLC	20.2	18.2
	MEAN			21.4 MPA (3101. PSI)	19.1 MPA (2766. PSI)
	STD. DEV.			2.8 MPA (410. PSI)	2.2 MPA (317. PSI)

TABLE 11-13 (Continued)

FLEXURAL PROPERTIES OF HLM GRAPHITE

LOT NO. SPEC. DIA. 6.4 MM
LOG NO. 6480-148 SPEC. LENGTH 51. MM
LOG DENSITY MG/M**3

SPECIMEN NUMBER	ORIENTATION	LOCATION	DENSITY (MG/M**3)	MODULUS OF RUPTURE (MPA) (UNCORRECTED)	FLEXURAL STRENGTH (MPA) (CORRECTED)
12AE	340A	AX	EE	23.7	20.9
	340B	AX	EF	22.5	20.0
	342A	AX	EE	23.0	20.4
	342B	AX	EE	25.3	22.1
	346A	AX	EE	28.2	24.1
	346B	AX	EF	24.8	21.7
	352A	AX	EE	25.6	22.3
	352B	AX	EE	28.0	24.0
	354A	AX	EE	27.4	23.6
	354B	AX	EE	27.7	23.8
12BE	412A	AX	EE	26.2	22.8
	412B	AX	EE	26.2	22.8
	414A	AX	EF	28.2	24.1
	414B	AX	EE	23.7	20.9
	418A	AX	EF	26.4	22.9
	418B	AX	EE	26.8	23.2
	424A	AX	EE	24.7	21.7
	424B	AX	EE	25.1	21.9
	426A	AX	EF	27.6	23.7
	426B	AX	EE	23.3	20.6
	MEAN			25.7 MPA (3730. PSI)	22.4 MPA (3245. PSI)
	STD. DEV.			1.8 MPA (267. PSI)	1.3 MPA (194. PSI)

TABLE 11-13 (Continued)

FLEXURAL PROPERTIES OF HLM GRAPHITE

LOT NO. SPEC. DIA. 6.4 MM
LOG NO. 6484-148 SPEC. LENGTH 51. MM
LOG DENSITY MG/M**3

SPECIMEN NUMBER	ORIENTATION	LOCATION	DENSITY (MG/M**3)	MODULUS OF RUPTURE (MPA) (UNCORRECTED)	FLEXURAL STRENGTH (MPA) (CORRECTED)
12AY	320A	AX	EM	23.6	20.9
	320B	AX	EM	22.7	20.2
	322A	AX	EM	25.0	21.9
	322B	AX	EM	23.2	20.6
	326A	AX	EM	28.5	24.5
	326B	AX	EM	23.7	21.0
	332A	AX	EM	26.1	22.8
	332B	AX	EM	22.7	20.2
	334A	AX	EM	23.7	21.0
	334B	AX	EM	23.7	21.0
12BY	392A	AX	EM	23.8	21.1
	392B	AX	EM	25.8	22.5
	394A	AX	EM	21.0	18.9
	394B	AX	EM	13.7	12.8
	398A	AX	EM	27.0	23.4
	398B	AX	EM	26.0	22.7
	404A	AX	EM	26.3	22.9
	404B	AX	EM	28.9	24.7
	406A	AX	EM	28.3	24.3
	406B	AX	EM	25.4	22.2
	MEAN			24.5 MPA (3546. PSI)	21.5 MPA (3116. PSI)
	STD. DEV.			3.3 MPA (479. PSI)	2.6 MPA (372. PSI)

TABLE 11-13 (Continued)

FLEXURAL PROPERTIES OF HLM GRAPHITE

LOT NO. SPEC. DIA. 6.4 MM
LOG NO. 6484-148 SPEC. LENGTH 51. MM
LOG DENSITY MG/M**3

SPECIMEN NUMBER	ORIENTATION	LOCATION	DENSITY (MG/M**3)	MODULUS OF RUPTURE (MPA) (UNCORRECTED)	FLEXURAL STRENGTH (MPA) (CORRECTED)
12AC	294A	AX	EC	22.0	19.7
	294B	AX	EC	25.6	22.3
	296A	AX	EC	26.8	23.2
	296B	AX	EC	22.9	20.3
	300A	AX	EC	26.0	22.6
	300B	AX	EC	22.6	20.1
	310A	AX	EC	28.6	24.5
	310B	AX	EC	24.3	21.3
	312A	AX	EC	24.9	21.8
	312B	AX	EC	27.9	24.0
	316A	AX	EC	26.4	23.0
	316B	AX	EC	18.3	16.7
12BC	368A	AX	EC	22.5	20.0
	368B	AX	EC	21.9	19.5
	366A	AX	EC	20.2	18.3
	366B	AX	EC	23.1	20.5
	372A	AX	EC	24.8	21.8
	372B	AX	EC	23.7	21.0
	384A	AX	EC	21.6	19.4
	384B	AX	EC	22.0	19.6
12BC	382A	AX	EC	25.4	22.2
	382B	AX	EC	24.1	21.2
	388A	AX	EC	23.7	21.0
	388B	AX	EC	25.3	22.1
	MEAN			23.9 MPA (3473. PSI)	21.1 MPA (3058. PSI)
	STD. DEV.			2.4 MPA (349. PSI)	1.8 MPA (262. PSI)

TABLE 11-13 (Continued)

FLEXURAL PROPERTIES OF HLM GRAPHITE

LOT NO. SPEC. DIA. 6.4 MM
LOG NO. 6484-148 SPEC. LENGTH 51. MM
LOG DENSITY MG/M**3

SPECIMEN NUMBER	ORIENTATION	LOCATION	DENSITY (MG/M**3)	MODULUS OF RUPTURE (MPA) (UNCORRECTED)	FLEXURAL STRENGTH (MPA) (CURRECTED)
1AE	111 RAD	EE		23.3	20.0
	115 RAD	EE		26.6	22.2
	117 RAD	EE		23.9	20.4
	121 RAD	EE		23.4	20.1
	123 RAD	EE		25.6	21.5
	127 RAD	EE		20.3	17.8
	141 RAD	EE		23.6	20.2
	143 RAD	EE		24.0	20.5
	147 RAD	EE		23.7	20.3
	149 RAD	EE		20.7	18.1
1BE	267 RAD	EE		25.0	21.2
	271 RAD	EE		19.8	17.5
	273 RAD	EE		25.3	21.4
	277 RAD	EE		25.1	21.2
	279 RAD	EE		24.1	20.6
	293 RAD	EE		24.1	20.6
	297 RAD	EE		23.3	20.0
	299 RAD	EE		22.8	19.7
	303 RAD	EE		23.0	19.8
	305 RAD	EE		24.5	20.8
	MEAN			23.6 MPA (3424. PSI)	20.2 MPA (2930. PSI)
	STD. DEV.			1.7 MPA (251. PSI)	1.2 MPA (174. PSI)

TABLE 11-13 (Continued)

FLEXURAL PROPERTIES OF HLM GRAPHITE

LOT NU. SPEC. DIA. 6.4 MM
LOG NU. 6484-148 SPEC. LENGTH 51. MM
LOG DENSITY MG/M**3

SPECIMEN NUMBER	ORIENTATION	LOCATION	DENSITY (MG/M**3)	MODULUS OF RUPTURE (MPA) (UNCORRECTED)	FLEXURAL STRENGTH (MPA) (CURRECTED)
1AY	59 RAD	EM		23.8	20.5
	63 RAD	EM		20.7	18.3
	65 RAD	EM		26.7	22.5
	69 RAD	EM		21.0	18.5
	71 RAD	EM		24.1	20.8
	85 RAD	EM		24.5	21.1
	89 RAD	EM		24.7	21.2
	91 RAD	EM		24.8	21.3
	95 RAD	EM		24.1	20.8
	97 RAD	EM		21.5	18.9
1BY	215 RAD	EM		24.8	21.3
	219 RAD	EM		23.0	20.0
	221 RAD	EM		25.1	21.5
	225 RAD	EM		25.1	21.5
	227 RAD	EM		20.7	18.3
	241 RAD	EM		25.2	21.6
	245 RAD	EM		19.3	17.2
	247 RAD	EM		19.4	17.3
	251 RAD	EM		23.2	20.2
	253 RAD	EM		24.6	21.1
	MEAN			23.3 MPA (3381. PSI)	20.2 MPA (2928. PSI)
	STD. DEV.			2.1 MPA (309. PSI)	1.5 MPA (223. PSI)

TABLE 11-13 (Continued)

FLEXURAL PROPERTIES OF HLM GRAPHITE

LOT NO. SPEC. DIA. 6.4 MM
LOG NO. 6484-148 SPEC. LENGTH 51. MM
LOG DENSITY MG/M**3

SPECIMEN NUMBER	ORIENTATION	LOCATION	DENSITY (MG/M**3)	MODULUS OF RUPTURE (MPA) (UNCORRECTED)	FLEXURAL STRENGTH (MPA) (CORRECTED)
1AC	7 RAD	EC		23.4	20.6
	9 RAD	EC		24.1	21.0
	13 RAD	EC		23.0	20.2
	15 RAD	EC		22.1	19.6
	19 RAD	EC		24.5	21.4
	33 RAD	EC		24.3	21.2
	35 RAD	EC		21.3	19.0
	39 RAD	EC		24.9	21.7
	41 RAD	EC		23.7	20.8
	45 RAD	EC		25.2	21.8
1BC	163 RAD	EC		25.4	22.0
	165 RAD	EC		21.7	19.3
	169 RAD	EC		24.6	21.4
	171 RAD	EC		25.4	22.0
	175 RAD	EC		19.1	17.3
	189 RAD	EC		20.4	18.3
	191 RAD	EC		23.7	20.8
	195 RAD	EC		24.9	21.7
	197 RAD	EC		26.6	22.8
	201 RAD	EC		29.0	24.4
	MEAN			23.9 MPA (3464. PSI)	20.9 MPA (3026. PSI)
	STD. DEV.			2.2 MPA (322. PSI)	1.6 MPA (235. PSI)

TABLE 11-13 (Continued)

FLEXURAL PROPERTIES OF HLM GRAPHITE

LOT NO.
LOG NO. 6484-148
LOG DENSITY MG/M**3

SPEC. DIA. 6.4 MM
SPEC. LENGTH 51. MM

SPECIMEN NUMBER	ORIENTATION	LOCATION	DENSITY (MG/M**3)	MODULUS OF RUPTURE (MPA) (UNCORRECTED)	FLEXURAL STRENGTH (MPA) (CORRECTED)
6AE	423 RAD	MLE		19.9	17.4
	427 RAD	MLE		22.7	19.4
	429 RAD	MLE		15.8	14.3
	433 RAD	MLE		21.9	18.9
	435 RAD	MLE		20.9	18.2
	449 RAD	MLE		22.1	19.0
	453 RAD	MLE		19.9	17.4
	455 RAD	MLE		21.7	18.8
	459 RAD	MLE		21.1	18.3
	461 RAD	MLE		22.4	19.2
6BE	553 RAD	MLE		21.6	18.6
	557 RAD	MLE		21.4	18.5
	559 RAD	MLE		20.0	17.5
	563 RAD	MLE		21.2	18.4
	565 RAD	MLE		23.7	20.1
	579 RAD	MLE		22.6	19.4
	583 RAD	MLE		22.6	19.3
	585 RAD	MLE		18.3	16.2
	586 RAD	MLE		21.3	18.4
	591 RAD	MLE		22.4	19.2
	MEAN			21.2 MPA (3071. PSI)	18.3 MPA (2659. PSI)
	STD. DEV.			1.8 MPA (256. PSI)	1.3 MPA (188. PSI)

TABLE 11-13 (Continued)

FLEXURAL PROPERTIES OF HLM GRAPHITE

LOT NO. SPEC. DIA. 6.4 MM
LOG NO. 6484-148 SPEC. LENGTH 51. MM
LOG DENSITY MG/M**3

SPECIMEN NUMBER	ORIENTATION	LOCATION	DENSITY (MG/M**3)	MODULUS OF RUPTURE (MPA) (UNCORRECTED)	FLEXURAL STRENGTH (MPA) (CORRECTED)
6AY	371 RAD	MLM		22.7	19.6
	375 RAD	MLM		23.6	20.3
	377 RAD	MLM		22.8	19.7
	381 RAD	MLM		21.5	18.8
	383 RAD	MLM		22.6	19.6
	397 RAD	MLM		22.4	19.5
	401 RAD	MLM		22.6	19.6
	403 RAD	MLM		22.7	19.6
	407 RAD	MLM		24.2	20.7
	409 RAD	MLM		20.5	18.1
6BY	501 RAD	MLM		22.3	19.4
	505 RAD	MLM		19.4	17.2
	507 RAD	MLM		23.0	19.9
	511 RAD	MLM		22.3	19.4
	513 RAD	MLM		20.6	18.2
	527 RAD	MLM		25.6	21.6
	531 RAD	MLM		22.5	19.5
	533 RAD	MLM		22.8	19.7
	537 RAD	MLM		25.5	21.6
	539 RAD	MLM		20.5	18.0
	MEAN			22.5 MPA (3265. PSI)	19.5 MPA (2830. PSI)
	STD. DEV.			1.5 MPA (225. PSI)	1.1 MPA (159. PSI)

TABLE 11-13 (Continued)

FLEXURAL PROPERTIES OF HLM GRAPHITE

LOT NO. SPEC. DIA. 6.4 MM
LOG NO. 6484-148 SPEC. LENGTH 51. MM
LOG DENSITY MG/M**3

SPECIMEN NUMBER	ORIENTATION	LOCATION	DENSITY (MG/M**3)	MODULUS OF RUPTURE (MPA) (UNCORRECTED)	FLEXURAL STRENGTH (MPA) (CORRECTED)
6AC	319 RAD	MLC		26.4	22.3
	321 RAD	MLC		22.0	19.2
	325 RAD	MLC		23.3	20.2
	327 RAD	MLC		22.4	19.5
	331 RAD	MLC		22.4	19.6
	345 RAD	MLC		21.9	19.2
	347 RAD	MLC		23.3	20.2
	351 RAD	MLC		22.2	19.4
	353 RAD	MLC		27.5	23.0
	357 RAD	MLC		22.1	19.3
6BC	471 RAD	MLC		21.7	19.1
	473 RAD	MLC		24.8	21.3
	475 RAD	MLC		23.9	20.6
	477 RAD	MLC		17.0	15.4
	481 RAD	MLC		25.7	21.9
	483 RAD	MLC		22.5	19.6
	485 RAD	MLC		23.8	20.6
	487 RAD	MLC		22.9	19.9
	489 RAD	MLC		23.6	20.4
	493 RAD	MLC		24.0	20.7
	MEAN			23.2 MPA (3362. PSI)	20.1 MPA (2910. PSI)
	STD. DEV.			2.1 MPA (311. PSI)	1.5 MPA (224. PSI)

TABLE 11-13 (Continued)

FLEXURAL PROPERTIES OF HLM GRAPHITE

LOT NO. SPEC. DIA. 6.4 MM
LOG NO. 6484-148 SPEC. LENGTH 51. MM
LOG DENSITY MG/M**3

SPECIMEN NUMBER	ORIENTATION	LOCATION	DENSITY (MG/M**3)	MODULUS OF RUPTURE (MPA) (UNCORRECTED)	FLEXURAL STRENGTH (MPA) (CORRECTED)
12AE	709 RAD	EE		22.8	19.7
	713 RAD	EE		23.6	20.2
	715 RAD	EE		21.4	18.7
	719 RAD	EE		22.6	19.5
	721 RAD	EE		21.5	18.7
	735 RAD	EE		22.9	19.7
	739 RAD	EE		22.5	19.4
	741 RAD	EE		22.1	19.1
	745 RAD	EF		21.1	18.4
	747 RAD	EE		23.9	20.4
12BE	865 RAD	EE		25.5	21.4
	869 RAD	EE		27.8	22.8
	871 RAD	EF		26.8	22.3
	875 RAD	EE		23.3	20.0
	877 RAD	EF		27.9	23.0
	891 RAD	EE		24.4	20.7
	895 RAD	EE		26.1	21.8
	897 RAD	EE		26.4	22.0
	901 RAD	EE		20.7	18.1
	903 RAD	EE		24.1	20.5
	MEAN			23.9 MPA (3462. PSI)	20.3 MPA (2948. PSI)
	STD. DEV.			2.2 MPA (321. PSI)	1.5 MPA (214. PSI)

TABLE 11-13 (Continued)

FLEXURAL PROPERTIES OF HLM GRAPHITE

LOT NO.
LOG NO. 6484-148
LOG DENSITY MG/M**3

SPEC. DIA. 6.4 MM
SPEC. LENGTH 51. MM

SPECIMEN NUMBER	ORIENTATION	LOCATION	DENSITY (MG/M**3)	MODULUS OF RUPTURE (MPA) (UNCORRECTED)	FLEXURAL STRENGTH (MPA) (CORRECTED)
12AY	657 RAD	EM		26.9	22.8
	661 RAD	EM		25.5	21.8
	663 RAD	EM		23.2	20.2
	667 RAD	EM		26.2	22.3
	669 RAD	EM		26.1	22.2
	683 RAD	EM		22.7	19.9
	687 RAD	EM		20.0	17.8
	689 RAD	EM		19.0	17.1
	693 RAD	EM		23.0	20.0
	695 RAD	EM		23.5	20.5
12BY	813 RAD	EM		27.2	23.0
	817 RAD	EM		27.0	22.8
	819 RAD	EM		25.1	21.6
	823 RAD	EM		24.1	20.8
	825 RAD	EM		24.8	21.4
	839 RAD	EM		24.7	21.3
	843 RAD	EM		22.5	19.7
	845 RAD	EM		22.2	19.5
	849 RAD	EM		20.9	18.5
	851 RAD	EM		24.6	21.2
	MEAN			24.0 MPA (3478. PSI)	20.7 MPA (3005. PSI)
	STD. DEV.			2.3 MPA (334. PSI)	1.6 MPA (239. PSI)

TABLE 11-13 (Continued)

FLEXURAL PROPERTIES OF HLM GRAPHITE

LOT NO. SPEC. DIA. 6.4 MM
LOG NO. 6484-148 SPEC. LENGTH 51. MM
LOG DENSITY MG/M**3

SPECIMEN NUMBER	ORIENTATION	LOCATION	DENSITY (MG/M**3)	MODULUS OF RUPTURE (MPA) (UNCORRECTED)	FLEXURAL STRENGTH (MPA) (CORRECTED)
12AC	601 RAD	EC		24.2	21.0
	605 RAD	EC		25.2	21.6
	607 RAD	EC		26.7	22.6
	611 RAD	EC		26.1	22.2
	613 RAD	EC		26.7	22.6
	627 RAD	EC		24.8	21.3
	631 RAD	EC		25.8	22.0
	633 RAD	EC		27.4	23.0
	637 RAD	EC		25.1	21.6
	639 RAD	EC		28.3	23.6
12BC	757 RAD	EC		20.3	18.1
	761 RAD	EC		22.4	19.6
	763 RAD	EC		27.0	22.8
	767 RAD	EC		21.9	19.3
	769 RAD	EC		23.7	20.6
	783 RAD	EC		25.9	22.1
	787 RAD	EC		25.7	22.0
	789 RAD	EC		22.5	19.7
	793 RAD	EC		20.4	18.1
	795 RAD	EC		24.3	21.0
	MEAN			24.7 MPA (3586. PSI)	21.2 MPA (3081. PSI)
	STD. DEV.			2.3 MPA (327. PSI)	1.6 MPA (230. PSI)

TABLE 11-14

COMPRESSIVE PROPERTIES OF HLM GRAPHITE

LOT NO. SPEC. DIA. 12.8 MM
LOG NO. 6484-148 SPEC. LENGTH 25. MM
LOG DENSITY MG/M**3

SPECIMEN NUMBER	ORIENTATION	LOCATION	DENSITY (MG/M**3)	YOUNGS MODULUS (GPA)	PERMANENT SET (PCT)	FRACTURE STRAIN (PCT)	COMPR. STRENGTH (MPA)
1AC F 6C	AX	EC		4.9	.140	2.267	44.2
8C	AX	EC		4.7	.200	2.343	43.1
10C	AX	EC		4.1	.211	2.368	40.6
12C	AX	EC		4.9	.140	2.277	43.6
1BC E102C	AX	EC		4.1	.200	2.236	40.6
104C	AX	EC		4.2	.160	2.157	39.9
106C	AX	EC		4.3	.180	2.225	40.1
108C	AX	EC		4.2	.221	2.286	40.7
MEAN				4.4	.184	2.272	41.6
				(.64 MPSI)			(6036.PSI)
STD. DEV.				.4	.031	.068	1.7
				(.06 MPSI)			(253.PSI)
1AC F 3C	RAD	EC		4.5	.120	1.936	43.1
7P	RAD	EC		4.5	.150	2.175	44.3
11B	RAD	EC		4.7	.180	2.345	45.3
23B	RAD	EC		4.7	.200	2.358	45.9
1BC E111P	RAD	EC		4.7	.150	2.035	44.4
113P	RAD	EC		4.6	.170	2.404	46.0
119B	RAD	EC		4.5	.160	2.350	45.2
131B	RAD	EC		4.1	.151	2.238	45.2
MEAN				4.5	.160	2.230	44.9
				(.66 MPSI)			(6517.PSI)
STD. DEV.				.2	.024	.170	1.0
				(.03 MPSI)			(141.PSI)

TABLE 11-14 (Continued)

COMPRESSIVE PROPERTIES OF HLM GRAPHITE

LOT NO. SPEC. DIA. 12.8 MM
LOG NO. 6484-148 SPEC. LENGTH 25. MM
LOG DENSITY MG/M**3

SPECIMEN NUMBER	ORIENTATION	LOCATION	DENSITY (MG/M**3)	YOUNGS MODULUS (GPA)	PERMANENT SET (PCT)	FRACTURE STRAIN (PCT)	COMPR. STRENGTH (MPA)
1AY F 30C	AX	EM		5.0	.120	1.959	41.7
34C	AX	EM		4.5	.130	2.155	38.7
42C	AX	EM		5.0	.100	1.963	42.7
46C	AX	EM		5.3	.180	2.188	44.1
1BY F114C	AX	EM		5.1	.210	2.382	44.1
118C	AX	EM		4.7	.100	2.022	42.3
126C	AX	EM		4.8	.160	2.084	45.1
130C	AX	EM		4.6	.201	2.379	47.2
MEAN				4.9 (.71 MPSI)	.150	2.144	43.2 (6272.PSI)
STD. DEV.				.3 (.04 MPSI)	.044	.166	2.5 (367.PSI)
1AY F 43R	RAD	EM		4.5	.180	2.382	45.4
47R	RAD	EM		4.5	.180	2.447	45.7
51R	RAD	EM		4.7	.160	2.661	47.7
61R	RAD	EM		5.0	.270	2.450	47.4
1BY F151C	RAD	EM		4.9	.160	1.989	44.0
155F	RAD	EM		4.9	.130	2.022	44.9
159R	RAD	EM		4.9	.190	2.293	45.7
169R	RAD	EM		4.8	.170	2.783	49.7
MEAN				4.8 (.69 MPSI)	.171	2.378	46.3 (6717.PSI)
STD. DEV.				.2 (.03 MPSI)	.022	.278	1.8 (266.PSI)

TABLE 11-14 (Continued)

COMPRESSIVE PROPERTIES OF HLM GRAPHITE

LOT NO. SPEC. DIA. 12.8 MM
LOG NO. 6484-148 SPEC. LENGTH 25. MM
LOG DENSITY MG/M**3

SPECIMEN NUMBER	ORIENTATION	LOCATION	DENSITY (MG/M**3)	YOUNGS MODULUS (GPA)	PERMANENT SET (PCT)	FRACTURE STRAIN (PCT)	COMPR. STRENGTH (MPA)
1AE E 60C	AX	EE		5.4	.170	1.848	41.7
64C	AX	EE		5.2	.170	2.224	46.3
72C	AX	EE		5.4	.180	2.117	45.0
76C	AX	EE		5.4	.160	1.820	43.2
1BE E144C	AX	EE		5.3	.170	2.272	44.7
148C	AX	EE		5.1	.210	2.355	44.4
156C	AX	EE		5.5	.150	2.069	47.2
160C	AX	EE		5.8	.191	1.987	48.7
	MEAN			5.4 (.78 MPSI)	.175	2.086	45.1 (6545.PSI)
	STD. DEV.			.3 (.04 MPSI)	.039	.194	2.2 (319.PSI)
1AE F 79E	RAD	EE		4.4	.220	2.562	45.8
83B	RAD	EE		4.4	.190	2.305	45.1
87B	RAD	EE		4.6	.190	2.209	44.4
97B	RAD	EE		4.6	.150	2.278	45.8
1BE F187B	RAD	EE		4.6	.170	2.555	48.2
191B	RAD	EE		4.6	.170	2.289	46.0
195B	RAD	EE		4.8	.180	2.480	46.8
205B	RAD	EE		4.2	.200	3.118	49.6
	MEAN			4.5 (.66 MPSI)	.184	2.477	46.4 (6736.PSI)
	STD. DEV.			.2 (.03 MPSI)	.021	.294	1.7 (246.PSI)

TABLE 11-14 (Continued)

COMPRESSIVE PROPERTIES OF HLM GRAPHITE

LOT NO. SPEC. DIA. 12.8 MM
LOG NO. 6484-148 SPEC. LENGTH 25. MM
LOG DENSITY MG/M**3

SPECIMEN NUMBER	ORIENTATION	LOCATION	DENSITY (MG/M**3)	YOUNGS MODULUS (GPA)	PERMANENT SET (PCT)	FRACTURE STRAIN (PCT)	COMPR. STRENGTH (MPA)
6AC M 10C	AX	MLC		4.6	.180	2.967	42.1
8C	AX	MLC		5.0	.200	1.963	41.8
12C	AX	MLC		4.9	.229	2.022	41.6
18C	AX	MLC		4.4	.180	2.368	43.3
6BC M 92C	AX	MLC		4.6	.170	2.151	43.1
94C	AX	MLC		4.7	.170	2.378	44.7
96C	AX	MLC		4.7	.211	2.019	42.9
98C	AX	MLC		4.4	.220	2.144	41.8
	MEAN			4.7	.195	2.126	42.7
				(.68 MPSI)			(6187.PSI)
	STD. DEV.			.2	.023	.177	1.1
				(.03 MPSI)			(153.PSI)
6AC M 5B	RAD	MLC		4.1	.220	2.761	41.6
9B	RAD	MLC		4.4	.250	2.562	45.1
13B	RAD	MLC		4.5	.210	2.213	44.0
23B	RAD	MLC		4.4	.200	2.227	42.6
6BC M113B	RAD	MLC		4.7	.240	2.072	42.9
117B	RAD	MLC		4.2	.220	2.264	41.9
121B	RAD	MLC		4.5	.180	2.760	43.3
131B	RAD	MLC		4.3	.250	3.164	47.2
	MEAN			4.4	.221	2.345	43.6
				(.64 MPSI)			(6323.PSI)
	STD. DEV.			.2	.025	.364	1.8
				(.03 MPSI)			(267.PSI)

TABLE 11-14 (Continued)

COMPRESSIVE PROPERTIES OF HLM GRAPHITE

LOT NO. SPEC. DIA. 12.0 MM
LOG NO. 6484-148 SPEC. LENGTH 25. MM
LOG DENSITY MG/M**3

SPECIMEN NUMBER	ORIENTATION	LOCATION	DENSITY (MG/M**3)	YOUNGS MODULUS (GPA)	PERMANENT SET (PCT)	FRACTURE STRAIN (PCT)	COMPR. STRENGTH (MPA)
6AY M 30C	AX	MLM		5.1	.190	1.972	40.7
34C	AX	MLM		4.8	.170	2.206	41.8
42C	AX	MLM		4.7	.200	1.967	39.2
46C	AX	MLM		4.6	.190	1.825	39.0
6BY M112C	AX	MLM		4.6	.180	1.979	40.3
116C	AX	MLM		4.6	.200	2.167	39.9
124C	AX	MLM		4.6	.130	1.866	41.5
128C	AX	MLM		4.8	.170	1.705	38.7
	MEAN			4.7	.179	1.964	40.1
				(.69 MPSI)			(5821.PSI)
	STD. DEV.			.2	.023	.171	1.1
				(.03 MPSI)			(167.PSI)
6AY M 43E	RAD	MLM		4.2	.220	2.295	42.4
47E	RAD	MLM		4.1	.200	2.313	43.6
51E	RAD	MLM		3.9	.180	2.446	43.6
61E	RAD	MLM		3.9	.210	2.495	43.1
6BY M151E	RAD	MLM		4.4	.190	2.549	44.0
155E	RAD	MLM		4.7	.220	2.438	44.1
159E	RAD	MLM		4.4	.180	1.974	41.3
169E	RAD	MLM		4.3	.190	2.202	42.7
	MEAN			4.2	.197	2.339	43.1
				(.61 MPSI)			(6248.PSI)
	STD. DEV.			.3	.017	.187	.9
				(.04 MPSI)			(137.PSI)

TABLE 11-14 (Continued)

COMPRESSIVE PROPERTIES OF HLM GRAPHITE

LOT NO. SPEC. DIA. 12.8 MM
LOG NO. 6484-148 SPEC. LENGTH 25. MM
LOG DENSITY MG/M**3

SPECIMEN NUMBER	ORIENTATION	LOCATION	DENSITY (MG/M**3)	YOUNGS MODULUS (GPA)	PERMANENT SET (PCT)	FRACTURE STRAIN (PCT)	COMPR. STRENGTH (MPA)
6AE M 6CC	AX	MLE		4.9	.170	2.081	41.0
64C	AX	MLE		5.0	.170	1.761	40.2
72C	AX	MLE		4.7	.210	1.787	38.7
76C	AX	MLE		5.0	.200	1.842	40.0
6BE M142C	AX	MLE		5.0	.130	1.734	41.3
146C	AX	MLE		5.0	.210	1.920	42.0
154C	AX	MLE		5.0	.170	1.824	41.2
158C	AX	MLE		5.0	.170	1.742	39.5
	MEAN			5.0	.179	1.856	40.5
				(.72 MPSI)			(5871.PSI)
	STD. DEV.			.1	.027	.116	1.1
				(.02 MPSI)			(159.PSI)
6AE M 79E	RAD	MLE		3.5	.230	2.612	42.5
83E	RAD	MLE		3.8	.260	2.954	44.3
87P	RAD	MLE		3.7	.210	2.313	41.8
97P	RAD	MLE		3.9	.200	2.464	43.3
6BE M167P	RAD	MLE		4.1	.250	2.659	43.3
191P	RAD	MLE		4.4	.200	2.773	46.6
195P	RAD	MLE		4.5	.170	2.793	42.2
2056	RAD	MLE		4.2	.240	2.865	46.4
	MEAN			4.0	.220	2.584	43.8
				(.58 MPSI)			(6354.PSI)
	STD. DEV.			.3	.030	.282	1.8
				(.05 MPSI)			(267.PSI)

TABLE 11-14 (Continued)

COMPRESSIVE PROPERTIES OF HLM GRAPHITE

LOT NO. SPEC. DIA. 12.8 MM
LOG NO. 6484-148 SPEC. LENGTH 25. MM
LOG DENSITY MG/M**3

SPECIMEN NUMBER	ORIENT-ATION	LOCA-TION	DENSITY (MG/M**3)	YOUNGS MODULUS (GPA)	PERM-ANENT SET (PCT)	FRAC-TURE STRAIN (PCT)	COMPR. STRENGTH (MPA)
12AC B 6C	AX	EC		5.0	.150	2.332	46.6
8C	AX	EC		4.8	.200	2.515	48.9
10C	AX	EC		5.4	.200	2.265	46.9
12C	AX	EC		4.8	.130	2.262	45.4
12BC B 90C	AX	EC		5.2	.170	2.230	45.4
92C	AX	EC		5.4	.160	1.753	44.9
94C	AX	EC		5.3	.200	1.742	42.3
96C	AX	EC		5.1	.180	2.310	45.4
MEAN				5.1 (.74 MPSI)	.174	2.176	45.7 (6632.PSI)
STD. DEV.				.2 (.03 MPSI)	.026	.279	1.9 (275.PSI)
12AC B 3E	RAD	EC		4.7	.140	2.203	46.3
7E	RAD	EC		4.8	.210	2.335	47.5
11E	RAD	EC		4.4	.240	2.216	44.9
21E	RAD	EC		4.4	.200	2.441	49.1
12BC B111E	RAD	EC		4.4	.190	2.324	45.4
115E	RAD	EC		4.6	.190	1.857	44.3
119E	RAD	EC		4.8	.160	2.168	46.5
129E	RAD	EC		4.8	.183	2.470	47.3
MEAN				4.7 (.68 MPSI)	.189	2.227	46.4 (6723.PSI)
STD. DEV.				.2 (.03 MPSI)	.030	.213	1.6 (232.PSI)

TABLE 11-14 (Continued)

COMPRESSIVE PROPERTIES OF HLM GRAPHITE

LOT NO. SPEC. DIA. 12.8 MM
LOG NO. 6464-148 SPEC. LENGTH 25. MM
LOG DENSITY MG/M**3

SPECIMEN NUMBER	ORIENTATION	LOCATION	DENSITY (MG/M**3)	YOUNGS MODULUS (GPA)	PERMANENT SET (PCT)	FRACTURE STRAIN (PCT)	COMPR. STRENGTH (MPA)
12AX B 30C	AX	EM		4.4	.170	1.584	36.8
34C	AX	EM		5.5	.170	2.149	47.9
42C	AX	EM		4.8	.150	2.097	44.0
46C	AX	EM		5.2	.220	2.323	45.3
12BY B114C	AX	EM		5.5	.270	2.076	46.1
118C	AX	EM		5.4	.170	1.874	46.5
126C	AX	EM		5.3	.150	1.656	44.4
130C	AX	EM		5.3	.140	1.406	40.2
MEAN				5.1	.180	1.896	43.9
				(.75 MPSI)			(6367.PSI)
STD. DEV.				.4	.044	.319	3.7
				(.06 MPSI)			(533.PSI)
12AY B 43B	RAD	EM		4.4	.220	2.622	47.7
47B	RAD	EM		4.4	.170	2.255	45.6
51B	RAD	EM		4.4	.200	2.135	44.6
61B	RAD	EM		4.2	.230	2.427	43.7
12BY B151F	RAD	EM		4.5	.260	2.302	46.4
155B	RAD	EM		5.0	.150	2.435	48.3
159B	RAD	EM		4.7	.170	2.148	46.2
169B	RAD	EM		5.3	.180	2.191	47.4
MEAN				4.6	.197	2.314	46.2
				(.66 MPSI)			(6706.PSI)
STD. DEV.				.3	.037	.169	1.6
				(.05 MPSI)			(227.PSI)

TABLE 11-14 (Continued)

COMPRESSIVE PROPERTIES OF HLM GRAPHITE

LOT NO. SPEC. DIA. 12.8 MM
LOG NO. 6484-148 SPEC. LENGTH 25. MM
LOG DENSITY MG/M**3

SPECIMEN NUMBER	ORIENTATION	LOCATION	DENSITY (MG/M**3)	YOUNGS MODULUS (GPA)	PERMANENT SET (PCT)	FRACTURE STRAIN (PCT)	COMPR. STRENGTH (MPA)
12AE B 60C	AX	EE		2.9	.260	2.288	36.6
64C	AX	EE		5.7	.170	1.820	45.2
72C	AX	EF		5.2	.120	1.624	40.6
76C	AX	EE		5.6	.180	1.946	43.9
12BE B144C	AX	EF		5.1	.130	1.922	43.4
148C	AX	FF		5.4	.140	2.169	47.5
156C	AX	EE		5.5	.180	2.067	46.3
160C	AX	EE		6.7	.270	2.024	45.4
	MEAN			5.3	.181	1.975	43.6
				(.76 MPSI)			(6321.PSI)
	STD. DEV.			1.1	.056	.203	3.5
				(.16 MPSI)			(507.PSI)
12AE B 79E	RAD	EE		4.2	.220	2.617	46.6
83E	RAD	EF		4.1	.260	2.802	46.4
87E	RAD	EE		3.7	.220	2.737	44.2
97E	RAD	EF		3.5	.220	3.044	47.0
12BE B187E	RAD	EE		4.9	.190	2.065	45.0
191E	RAD	FF		4.7	.160	2.528	47.5
195E	RAD	EE		4.9	.190	2.526	48.4
205E	RAD	EF		5.0	.170	2.367	49.3
	MEAN			4.4	.206	2.586	46.8
				(.63 MPSI)			(6789.PSI)
	STD. DEV.			.6	.029	.294	1.7
				(.08 MPSI)			(243.PSI)

TABLE 11-15

COMPRESSIVE PROPERTIES OF PGX GRAPHITE

LOT NO. SPEC. DIA. 12.8 MM
LOG NO. 6484-13A SPEC. LENGTH 25. MM
LOG DENSITY MG/M**3

SPECIMEN NUMBER	ORIENTATION	LOCATION	DENSITY (MG/M**3)	YOUNGS MODULUS (GPA)	PERMANENT SET (PCT)	FRACTURE STRAIN (PCT)	COMPR. STRENGTH (MPA)
1AC F 6C	AX	FC		2.9	.265	1.968	36.5
E 8C	AX	EC		2.6	.317	2.640	38.0
E10C	AX	EC		3.0	.269	2.372	37.2
E12C	AX	EC		3.0	.244	2.435	39.2
1BC E102C	AX	EC		2.6	.396	2.451	35.8
E104C	AX	EC		2.6	.261	2.280	36.5
E106C	AX	EC		3.1	.296	2.345	37.5
E108C	AX	EC		3.1	.265	2.476	39.6
MEAN				2.9 (.41 MPSI)	.289	2.371	37.5 (5444.PSI)
STD. DEV.				.2 (.03 MPSI)	.049	.195	1.3 (195.PSI)
1AC F 3B	RAD	FC		3.7	.186	1.750	37.2
E 7B	RAD	EC		3.6	.334	1.984	37.9
E11B	RAD	EC		3.4	.245	1.974	37.9
E23B	RAD	EC		3.9	.236	1.936	39.3
1BC E111B	RAD	EC		3.4	.222	1.685	34.2
E115B	RAD	EC		3.3	.232	2.054	37.3
E119B	RAD	EC		3.0	.290	2.025	35.1
E131B	RAD	EC		3.6	.214	1.878	37.3
MEAN				3.5 (.51 MPSI)	.245	1.911	37.0 (5370.PSI)
STD. DEV.				.3 (.04 MPSI)	.046	.132	1.6 (233.PSI)

TABLE 11-15 (Continued)

COMPRESSIVE PROPERTIES OF PGX GRAPHITE

LOT NO. SPEC. DIA. 12.8 MM
LOG NO. 6484-138 SPEC. LENGTH 25. MM
LOG DENSITY MG/M**3

SPECIMEN NUMBER	ORIENTATION	LOCATION	DENSITY (MG/M**3)	YOUNGS MODULUS (GPA)	PERMANENT SET (PCT)	FRACTURE STRAIN (PCT)	COMPR. STRENGTH (MPA)
1AY F30C	AX	FM		3.2	.237	2.157	36.8
E34C	AX	EM		3.2	.281	2.400	38.6
F42C	AX	EM		2.8	.209	2.400	37.9
E46C	AX	EM		2.6	.327	2.322	36.0
1BY E114C	AX	EM		3.1	.264	2.368	37.5
E118C	AX	EM		3.1	.344	2.457	38.2
E126C	AX	EM		3.0	.319	2.496	39.4
E130C	AX	EM		3.2	.233	2.255	39.6
MEAN				3.0 (.44 MPSI)	.277	2.357	38.0 (5511.PSI)
STD. DEV.				.2 (.03 MPSI)	.049	.110	1.2 (178.PSI)
1AY F43B	RAD	FM		3.3	.219	1.923	34.8
E47B	RAD	EM		3.2	.247	1.943	34.4
E51B	RAD	EM		3.3	.225	1.856	35.3
E61B	RAD	EM		2.9	.195	1.924	33.4
1BY E151B	RAD	EM		3.0	.276	1.966	34.3
E155B	RAD	EM		3.5	.223	2.085	37.2
E159B	RAD	EM		3.3	.234	1.998	35.5
E169B	RAD	EM		3.1	.263	2.283	35.8
MEAN				3.2 (.46 MPSI)	.235	1.997	35.1 (5086.PSI)
STD. DEV.				.2 (.03 MPSI)	.026	.133	1.1 (166.PSI)

TABLE 11-15 (Continued)

COMPRESSIVE PROPERTIES OF PGX GRAPHITE

LOT NO.
LOG NO. 64R4-138
LOG DENSITY MG/M**3

SPEC. DIA. 12.8 MM
SPEC. LENGTH 25. MM

SPECIMEN NUMBER	ORIENTATION	LOCATION	DENSITY (MG/M**3)	YOUNGS MODULUS (GPA)	PERMANENT SET (PCT)	FRACTURE STRAIN (PCT)	COMPR. STRENGTH (MPA)
1AE E60C	AX	EE		3.1	.229	2.110	37.3
E64C	AX	EE		3.1	.230	2.398	38.4
E72C	AX	EE		3.1	.250	2.260	36.8
E76C	AX	EE		3.0	.251	2.517	38.0
1BE E144C	AX	EE		2.9	.268	2.339	36.7
E148C	AX	EE					
E156C	AX	EE		3.1	.300	2.307	38.4
E160C	AX	EE		3.5	.293	2.353	41.1
	MEAN			3.1 (.45 MPSI)	.260	2.326	38.1 (5526.PSI)
	STD. DEV.			.2 (.03 MPSI)	.028	.125	1.5 (216.PSI)
1AE F79B	RAD	FE		3.2	.249	1.939	35.4
E83B	RAD	EE		3.5	.244	1.894	35.5
E87B	RAD	EE		3.4	.269	1.900	34.8
E97B	RAD	EE		3.5	.248	2.038	36.8
1BE E187B	RAD	EE		2.9	.301	2.132	35.1
E191B	RAD	EE		2.7	.347	2.105	34.1
E195B	RAD	EE		3.2	.270	2.080	36.5
E205B	RAD	EE		3.1	.261	2.259	38.6
	MEAN			3.2 (.46 MPSI)	.274	2.043	35.8 (5198.PSI)
	STD. DEV.			.3 (.04 MPSI)	.035	.127	1.4 (205.PSI)

TABLE 11-15 (Continued)

COMPRESSIVE PROPERTIES OF PGX GRAPHITE

LOT NO. SPEC. DIA. 12.8 MM
LOG NO. 6494-13B SPEC. LENGTH 25. MM
LOG DENSITY MG/M**3

SPECIMEN NUMBER	ORIENTATION	LOCATION	DENSITY (MG/M**3)	YOUNGS MODULUS (GPA)	PERMANENT SET (PCT)	FRACTURE STRAIN (PCT)	COMPR. STRENGTH (MPA)
6AC	M10C	AX	MLC	2.9	.251	2.280	35.1
	M 8C	AX	MLC	2.6	.275	2.204	33.0
	M12C	AX	MLC	3.0	.310	2.317	36.7
	M18C	AX	MLC	2.8	.345	2.201	35.6
6BC	M92C	AX	MLC	2.8	.293	2.072	34.7
	M94C	AX	MLC				
	M96C	AX	MLC	2.5	.581	2.577	35.9
	M98C	AX	MLC	2.6	.796	3.035	37.5
	MEAN			2.8 (.40 MPSI)	.407	2.384	35.5 (5151.PSI)
	STD. DEV.			.2 (.02 MPSI)	.204	.326	1.4 (208.PSI)
6AC	M 5B	RAD	MLC	3.6	.227	1.797	35.1
	M 9B	RAD	MLC	3.3	.197	1.841	35.1
	M13B	RAD	MLC	3.4	.267	1.945	34.4
	M23B	RAD	MLC	3.2	.198	1.922	35.3
6BC	M113B	RAD	MLC	3.3	.235	1.879	34.4
	M117B	RAD	MLC	3.0	.235	1.902	33.9
	M121B	RAD	MLC	3.3	.244	1.689	33.2
	M131B	RAD	MLC	3.1	.253	1.880	34.1
	MEAN			3.3 (.47 MPSI)	.232	1.857	34.4 (4995.PSI)
	STD. DEV.			.2 (.02 MPSI)	.025	.082	.7 (103.PSI)

TABLE 11-15 (Continued)

COMPRESSIVE PROPERTIES OF PGX GRAPHITE

LOT NO. SPEC. DIA. 12.8 MM
LOG NO. 6484-138 SPEC. LENGTH 25. MM
LOG DENSITY MG/M**3

SPECIMEN NUMBER		ORIENTATION	LOCATION	DENSITY (MG/M**3)	YOUNGS MODULUS (GPA)	PERMANENT SET (PCT)	FRACTURE STRAIN (PCT)	COMPR. STRENGTH (MPA)
6AY	M30C	AX	MLM		3.1	.270	2.666	40.3
	M34C	AX	MLM		3.1	.210	2.480	36.7
	M42C	AX	MLM		3.2	.267	2.394	38.8
	M46C	AX	MLM		3.2	.299	2.413	38.6
6BY	M112C	AX	MLM		2.8	.301	2.401	37.9
	M116C	AX	MLM					32.3
	M124C	AX	MLM		3.4	.211	2.161	39.8
	M128C	AX	MLM		2.7	.422	2.368	37.3
		MEAN			3.1	.283	2.412	37.7
					(.45 MPSI)			(5468.PSI)
		STD. DEV.			.2	.072	.150	2.5
					(.04 MPSI)			(359.PSI)
6AY	M43B	RAD	MLM		3.6	.148	1.817	37.5
	M47B	RAD	MLM		3.7	.216	1.978	37.9
	M51B	RAD	MLM		3.7	.167	1.909	37.2
	M61B	RAD	MLM		3.4	.286	2.007	36.5
6BY	M151B	RAD	MLM		3.7	.294	2.005	37.7
	M155B	RAD	MLM		3.6	.238	2.070	38.0
	M159B	RAD	MLM		3.8	.220	2.032	38.4
	M169B	RAD	MLM		3.7	.219	2.054	37.8
		MEAN			3.7	.224	1.984	37.6
					(.53 MPSI)			(5456.PSI)
		STD. DEV.			.1	.051	.084	.6
					(.01 MPSI)			(83.PSI)

TABLE 11-15 (Continued)

COMPRESSIVE PROPERTIES OF PGX GRAPHITE

LOT NO. SPEC. DIA. 12.8 MM
LOG NO. 6484-13A SPEC. LENGTH 25. MM
LOG DENSITY MG/M**3

SPECIMEN NUMBER		ORIENTATION	LOCATION	DENSITY (MG/M**3)	YOUNGS MODULUS (GPA)	PERMANENT SET (PCT)	FRACTURE STRAIN (PCT)	COMPR. STRENGTH (MPA)
6AE	M60C	AX	MLE		3.2	.351	2.712	40.3
	M64C	AX	MLE		3.2	.238	2.319	38.7
	M72C	AX	MLE		3.3	.280	2.432	39.1
	M76C	AX	MLE		3.3	.290	2.634	40.3
6BE	M142C	AX	MLE		3.4	.284	2.353	38.5
	M146C	AX	MLE		3.0	.261	2.338	38.2
	M154C	AX	MLE		3.2	.407	2.815	40.7
	M158C	AX	MLE		3.1	.268	2.193	38.2
		MEAN			3.2	.297	2.474	39.2
					(.47 MPSI)			(5692.PSI)
		STD. DEV.			.1	.055	.219	1.0
					(.02 MPSI)			(149.PSI)
6AE	M79B	RAD	MLE		3.9	.200	1.869	37.7
	M83B	RAD	MLE		3.7	.166	2.164	40.3
	M87B	RAD	MLE		3.9	.239	2.008	38.9
	M97B	RAD	MLE		4.2	.201	2.190	41.1
6BE	M187B	RAD	MLE		3.4	.291	2.113	37.9
	M191B	RAD	MLE		3.6	.252	1.978	36.3
	M195B	RAD	MLE		3.6	.293	1.789	36.0
	M205B	RAD	MLE		3.5	.189	1.853	36.8
		MEAN			3.7	.229	1.996	38.1
					(.54 MPSI)			(5530.PSI)
		STD. DEV.			.3	.048	.151	1.9
					(.04 MPSI)			(269.PSI)

TABLE 11-15 (Continued)

COMPRESSIVE PROPERTIES OF PGX GRAPHITE

LOT NO.
LOG NO. 6484-138
LOG DENSITY MG/M**3

SPEC. DIA. 12.8 MM
SPEC. LENGTH 25. MM

SPECIMEN NUMBER	ORIENTATION	LOCATION	DENSITY (MG/M**3)	YOUNGS MODULUS (GPA)	PERMANENT SET (PCT)	FRACTURE STRAIN (PCT)	COMPR. STRENGTH (MPA)
12AC	B 6C	AX	EC	2.9	.241	2.290	36.8
	B 8C	AX	EC	2.7	.280	2.337	36.0
	B10C	AX	EC	2.6	.352	2.639	37.5
	B12C	AX	EC	3.0	.306	2.346	38.2
12BC	B90C	AX	EC	2.6	.300	2.606	37.1
	B92C	AX	EC	2.9	.255	2.421	37.6
	B94C	AX	EC	3.0	.265	2.393	38.4
	B96C	AX	EC	2.7	.254	2.404	38.0
	MEAN			2.8 (.40 MPSI)	.282	2.429	37.5 (5433.PSI)
	STD. DEV.			.2 (.02 MPSI)	.036	.127	.8 (115.PSI)
12AC	B 3B RAD		EC	3.8	.243	1.931	38.4
	B 7B RAD		EC	3.6	.230	2.200	39.9
	B11B RAD		EC	3.8	.211	1.991	38.2
	B21B RAD		EC	3.8	.181	1.799	36.7
12BC	B111B RAD		EC	3.7	.236	2.086	38.3
	B115B RAD		EC	3.3	.294	2.130	38.5
	B119B RAD		EC	3.1	.253	2.094	36.8
	B129B RAD		EC	3.4	.225	1.950	36.8
	MEAN			3.6 (.52 MPSI)	.234	2.022	38.0 (5505.PSI)
	STD. DEV.			.3 (.04 MPSI)	.033	.129	1.1 (164.PSI)

TABLE 11-15 (Continued)

COMPRESSIVE PROPERTIES OF PGX GRAPHITE

LOT NO. SPEC. DIA. 12.8 MM
LOG NO. 6484-138 SPEC. LENGTH 25. MM
LOG DENSITY MG/M**3

SPECIMEN NUMBER		ORIENTATION	LOCATION	DENSITY (MG/M**3)	YOUNGS MODULUS (GPA)	PERMANENT SET (PCT)	FRACTURE STRAIN (PCT)	COMPR. STRENGTH (MPA)
12AY	B30C	AX	EM		3.0	.351	2.732	39.1
	B34C	AX	EM		2.7	.295	2.575	37.1
	B42C	AX	EM		2.8	.260	2.576	37.5
	B46C	AX	EM		2.6	.335	2.644	37.2
12BY	B114C	AX	EM		3.1	.227	2.409	40.5
	B118C	AX	EM		2.8	.227	2.458	38.6
	B126C	AX	EM		2.9	.264	2.422	37.4
	B130C	AX	EM		2.9	.266	2.472	37.8
		MEAN			2.9	.278	2.536	38.2
					(.41 MPSI)			(5536.PSI)
		STD. DEV.			.1	.046	.115	1.2
					(.02 MPSI)			(171.PSI)
12AY	B43B	RAD	EM		3.7	.276	2.199	38.7
	B47B	RAD	EM		3.9	.209	2.036	39.1
	B51B	RAD	EM		3.8	.218	1.777	37.5
	B61B	RAD	EM		3.7	.206	2.003	37.5
12BY	B151B	RAD	EM		3.1	.283	2.037	35.6
	B155B	RAD	EM		3.3	.293	2.058	36.5
	B159B	RAD	EM		3.1	.332	2.238	37.1
	B169B	RAD	EM		3.1	.244	2.056	35.4
		MEAN			3.5	.258	2.050	37.2
					(.50 MPSI)			(5393.PSI)
		STD. DEV.			.3	.045	.139	1.3
					(.05 MPSI)			(193.PSI)

TABLE 11-15 (Continued)

COMPRESSIVE PROPERTIES OF PGX GRAPHITE

LOT NO.
LOG NO. 6484-138
LOG DENSITY MG/M**3

SPEC. DIA. 12.8 MM
SPEC. LENGTH 25. MM

SPECIMEN NUMBER		ORIENTATION	LOCATION	DENSITY (MG/M**3)	YOUNGS MODULUS (GPA)	PERMANENT SET (PCT)	FRACTURE STRAIN (PCT)	COMPR. STRENGTH (MPA)
12AE	A60C	AX	FE		2.8	.409	2.440	36.1
	A64C	AX	EE		3.0	.225	2.359	37.9
	A72C	AX	EE		2.9	.205	2.433	37.2
	A76C	AX	EE		2.6	.379	2.605	36.8
12AE	A144C	AX	EE		2.8	.267	2.279	37.2
	A148C	AX	EE		3.0	.325	2.569	39.6
	A156C	AX	EE		2.6	.382	2.349	36.2
	A160C	AX	EE		2.9	.348	2.117	34.8
	MEAN				2.8 (.41 MPSI)	.318	2.394	37.0 (5363.PSI)
	STD. DEV.				.1 (.02 MPSI)	.077	.157	1.4 (205.PSI)
12AE	A79B	RAD	EF		3.5	.218	1.947	35.8
	A83B	RAD	EE		3.5	.283	1.898	35.8
	A87B	RAD	EE		3.0	.388	2.169	35.6
	A97B	RAD	EE		3.6	.250	1.983	36.3
12BE	A187B	RAD	EE		2.9	.222	2.294	37.8
	B191B	RAD	EE		3.3	.243	2.133	38.5
	A195B	RAD	EE		3.2	.371	2.094	36.8
	B205B	RAD	EE		3.2	.243	2.197	37.5
	MEAN				3.3 (.48 MPSI)	.277	2.089	36.8 (5334.PSI)
	STD. DEV.				.2 (.04 MPSI)	.066	.136	1.1 (156.PSI)

TABLE 11-16

THERMAL CONDUCTIVITY OF PGX GRAPHITE

LOT NUMBER: LOG NUMBER: 6484-112

ORIENTATION	LOCATION	SPECIMEN NUMBER	THERMAL CONDUCTIVITY (W/M-K) AT: 295K (22C)	473K (200C)	673K (400C)	873K (600C)	1073K (800C)
AXIAL	MLC	M-90A	88.3	81.2	65.7	55.9	47.7
		M-90B	86.1	81.7	64.6	54.4	47.4
		M-90C	85.9	86.2	74.3	62.4	54.5
		M-90D	83.6	86.4	67.7	60.3	54.7
		M-90E	92.3	84.9	67.2	58.4	49.9
		M-90F	96.3	86.4	69.5	62.5	55.3
		M-90G	86.7	74.3	60.1	53.0	43.2
		M-90H	85.4	70.8	57.2	52.2	42.0
		M-90I	91.4	72.4	58.7	50.2	44.6
		M-90J	82.6	76.3	63.0	52.8	43.1
		M-90K	84.5	81.2	65.4	55.0	47.0
		M-90L	82.9	76.7	63.3	53.0	44.6
		MEAN:	87.2	79.9	64.7	55.8	47.8
		STD. DEV:	4.2	5.6	4.8	4.1	4.8
RADIAL	MLC	M-123A	89.0	81.9	67.7	56.3	46.5
		M-123B	92.6	84.0	69.9	54.0	48.5
		M-123C	95.5	82.2	69.6	56.6	50.0
		M-123D	99.7	81.5	67.1	56.1	50.5
		M-123E	93.9	80.6	62.1	52.3	41.1
		M-123F	99.4	92.5	74.1	62.1	52.7
		M-123G	91.1	86.3	70.8	58.7	47.2
		M-123H	88.5	75.3	57.4	47.2	39.8
		M-123I	98.3	86.8	68.6	56.5	45.1
		M-123J	88.9	86.2	63.6	54.8	45.7
		M-123K	96.4	77.4	62.9	53.1	44.6
		M-123L	98.3	90.3	75.3	64.2	54.5
		MEAN:	94.3	83.7	67.4	56.0	47.2
		STD. DEV:	4.2	5.0	5.2	4.4	4.4

TABLE 11-17
PROPERTY DATA FOR GRADE PGX GRAPHITE

	Bulk Density (Mg/m^3)	Specific Resistance ($\times 10^{-4}$ ohm-in.)	Elastic Modulus (GPa)	Fluxural Strength (MPa)	Tensile Strength (MPa)	Compressive Strength (MPa)	CTE, ($\times 10^{-6}$/K)	Ash, (ppm)	Iron, (ppm)
	Billet Size 36-in. diameter by 72 in. long								
With grain									
Maximum	1.78	13.81	8.52	16.10	13.04	48.95	2.41	6400	2900
Minimum	1.74	10.58	7.25	13.04	10.36	42.23	2.02	4000	2300
Mean	1.76	12.58	7.92	14.98	11.42	45.62	2.25	5500	2600
Std. dev.	0.014	1.48	0.43	0.86	0.82	2.63	0.16	1300	300
No. of billets	3	3	3	3	3	3	3	3	3
Specimens/billet	4	4	4	4	4	2	2	1	1
Total specimen	12	12	12	12	12	6	6	3	3
Against grain									
Maximum	1.84	16.80	6.47	13.77	10.28	46.02	2.82		
Minimum	1.72	12.10	5.70	12.10	8.71	41.54	2.45		
Mean	1.77	14.77	6.05	12.84	9.67	44.27	2.70		
Std. dev.	0.030	1.93	0.31	0.50	0.49	2.09	0.18		
No. of billets	3	3	3	3	3	3	3		
Specimens/billet	4	4	4	4	4	2	2		
Total specimen	12	12	12	12	12	6	6		

TABLE 11-17 (Continued)

	Bulk Density (Mg/m^3)	Specific Resistance (x 10^{-4} ohm-in.)	Elastic Modulus (GPa)	Fluxural Strength (MPa)	Tensile Strength (MPa)	Compressive Strength (MPa)	CTE, (x 10^{-6}/K)	Ash, (ppm)	Iron, (ppm)
Billet Size 45-in. diameter by 72 in. long									
With grain									
Maximum	1.77	12.71	8.25	14.14	11.16	41.71	2.49	6000	3600
Minimum	1.71	10.38	6.86	10.51	6.67	31.03	2.13	4200	800
Mean	1.74	12.37	7.58	12.40	8.96	36.94	2.25	5100	2500
Std. dev.	0.019	0.94	0.49	1.19	1.37	3.14	0.12	700	1300
No. of billets	5	5	5	5	5	5	5	5	5
Specimens/billet	3 - 8	3 - 8	3 - 8	3 - 8	3 - 8	2 - 8	2 - 4	0 - 1	0 - 1
Total specimen	23	23	19	23	22	16	11	4	4
Against grain									
Maximum	1.77	15.73	8.07	16.01	11.12	43.95	2.73		
Minimum	1.71	10.89	5.17	8.76	6.01	26.54	2.20		
Mean	1.75	13.93	6.59	12.28	9.02	38.68	2.54		
Std. dev.	0.020	1.48	0.90	1.98	1.38	4.82	0.18		
No. of billets	5	5	5	5	5	5	5		
Specimens/billet	3 - 8	3 - 8	3 - 8	3 - 8	3 - 8	2 - 8	2 - 4		
Total specimen	24	24	20	24	23	17	11		

TABLE 11-17 (Continued)

	Bulk Density (Mg/m^3)	Specific Resistance (x 10^{-4} ohm-in.)	Elastic Modulus (GPa)	Fluxural Strength (MPa)	Tensile Strength (MPa)	Compressive Strength (MPa)	CTE, (x 10^{-6}/K)	Ash, (ppm)	Iron, (ppm)
Billet Size 50-in. diameter by 72 in. long									
With grain									
Maximum	1.81	13.61	8.60	15.50	11.77	44.30	2.36	9600	2900
Minimum	1.74	11.69	7.22	9.91	7.64	38.61	2.19	1000	600
Mean	1.77	12.72	7.23	12.94	10.02	41.50	2.26	5500	2000
Std. dev.	0.018	0.51	0.26	1.56	1.09	1.41	0.06	2560	790
No. of billets	10	10	10	10	10	10	10	10	10
Specimens/billet	4	4	4	4	4	2	2	1	1
Total specimen	40	40	40	40	40	20	20	10	10
Against grain									
Maximum	1.81	15.02	7.43	14.82	10.60	47.75	2.81		
Minimum	1.76	13.00	6.65	9.96	8.37	39.82	2.44		
Mean	1.78	14.16	6.88	12.25	9.37	42.29	2.68		
Std. dev.	0.013	0.49	0.19	1.28	0.60	3.08	0.10		
No. of billets	10	10	10	10	10	10	10		
Specimens/billet	4	4	4	4	4	2	2		
Total specimen	40	40	40	40	40	20	20		

TABLE 11-17 (Continued)

	Bulk Density (Mg/m^3)	Specific Resistance (x 10^{-4} ohm-in.)	Elastic Modulus (GPa)	Fluxural Strength (MPa)	Tensile Strength (MPa)	Compressive Strength (MPa)	CTE, (x 10^{-6}/K)	Ash, (ppm)	Iron, (ppm)
Billet Size 67-in. diameter by 72 in. long									
With grain									
Maximum	1.79	8.77	8.32	13.98	11.60	46.19	1.82	4000	2600
Minimum	1.78	7.92	7.40	7.92	6.72	35.68	1.74	800	300
Mean	1.79	8.36	7.85	11.19	9.09	40.68	1.77	2400	1450
Std. dev.	0.005	0.43	0.46	2.35	1.82	5.69	0.04	2262	1626
No. of billets	1	1	1	1	1	1	1	1	1
Specimens/billet	8	8	8	8	8	4	4	2	2
Total Specimen	8	8	8	8	8	4	4	2	2
Against grain									
Maximum	1.79	9.88	7.38	12.36	10.67	41.54	2.24		
Minimum	1.77	8.80	6.74	9.40	8.16	38.78	2.16		
Mean	1.78	9.38	7.06	10.88	9.41	40.29	2.21		
Std. dev.	0.008	0.51	0.24	1.01	0.91	1.30	0.04		
No. of billets	1	1	1	1	1	1	1		
Specimens/billet	8	8	8	8	8	4	4		
Total Specimen	8	8	8	8	8	4	4		

TABLE 11-18

THERMAL EXPANSIVITY OF 2020 GRAPHITE

LOT NUMBER: LOG NUMBER: 6484-110

ORIENTATION	LOG LOCATION	SPECIMEN NUMBER	THERMAL EXPANSIVITY (10EXP-6/K) 295K-773K (22C-500C)	295K-1173K (22C- 900C)
RADIAL	END	SL.1 11A	3.20	3.73
		11B	3.57	4.26
		11C	3.24	3.76
		37A	3.26	3.81
		37B	3.16	3.69
		37C	3.23	3.71
		MEAN:	3.28	3.83
		STD. DEV:	.15	.22
RADIAL	MIDLENGTH	SL.6 115A	3.20	3.71
		115B	2.99	3.59
		115C	3.26	3.78
		141A	3.13	3.70
		141B	3.19	3.72
		141C	3.16	3.69
		167A	3.13	3.62
		167B	3.25	3.75
		167C	3.18	3.69
		193A	3.11	3.59
		193B	3.13	3.67
		193C	3.26	3.75
		MEAN:	3.17	3.69
		STD. DEV:	.08	.06

TABLE 11-18 (Continued)

THERMAL EXPANSIVITY OF 2020 GRAPHITE

LOT NUMBER: LOG NUMBER: 6484-110

ORIENTATION	LOG LOCATION		SPECIMEN NUMBER	THERMAL EXPANSIVITY (10EXP-6/K) 295K-773K (22C-500C)	295K-1173K (22C-900C)
AXIAL	END	SL.1	8A	3.27	3.85
			8B	3.41	3.92
			16A	3.57	4.04
			16B	3.47	3.94
			24A	3.37	3.89
			24B	3.51	4.00
			38A	3.28	3.82
			38B	3.23	3.74
			46A	3.49	4.02
			46B	3.25	3.83
			62A	3.50	3.96
			62B	3.09	3.67
			MEAN:	3.37	3.89
			STD. DEV:	.15	.12
AXIAL	MIDLENGTH	SL. 6	72A	3.37	3.87
			72B	3.48	3.97
			80A	3.56	4.04
			80B	3.38	3.89
			88A	3.38	3.94
			88B	3.35	3.86
			102A	3.44	3.93
			102B	3.50	3.97
			110A	3.39	3.87
			110B	3.44	3.91
			126A	3.53	3.97
			126B	3.24	3.72
			MEAN:	3.42	3.91
			STD. DEV:	.09	.08

TABLE 11-19

COMPRESSIVE PROPERTIES OF 7627 GRAPHITE

LOT NO. SPEC. DIA. 12.9 MM
LOG NO. 6464-139 SPEC. LENGTH 25. MM
LOG DENSITY MG/M**3

SPECIMEN NUMBER	ORIENTATION	LOCATION	DENSITY (MG/M**3)	YOUNGS MODULUS (GPA)	PERMANENT SET (PCT)	FRACTURE STRAIN (PCT)	COMPR. STRENGTH (MPA)
1A	L6C AX	END		6.9	.1[illegible]0	1.834	68.8
	L8C AX	END		6.1	.110	2.021	67.1
	L12C AX	END		5.6	.103	2.274	71.9
	L14C AX	END		6.4	.140	2.476	78.0
1B	L30C AX	END		6.5	.1[illegible]9	2.312	75.0
	L32C AX	END		6.2	.099	2.028	69.8
	L36C AX	END		5.6	.120	2.356	72.9
	L38C AX	END		6.1	.100	2.163	75.0
	MEAN			6.2	.110	2.183	72.3
				(.90 MPSI)			(10487.PSI)
	STD. DEV.			.4	.014	.212	3.7
				(.06 MPSI)			(531.PSI)
1A	L5B RAD	END		6.1	.100	1.732	68.8
	L9B RAD	END		7.3	.109	2.164	77.1
	L13B RAD	END		6.7	.120	1.789	62.3
	L23B RAD	END		6.7	.070	1.896	73.0
1B	L41B RAD	END		6.9	.090	1.955	74.4
	L45B RAD	END		6.9	.111	2.077	75.9
	L49B RAD	END		7.3	.100	2.025	74.8
	L59B RAD	END		6.7	.080	1.741	64.1
	MEAN			7.1	.097	1.922	71.3
				(1.03 MPSI)			(10342.PSI)
	STD. DEV.			.7	.017	.161	5.6
				(.11 MPSI)			(809.PSI)

TABLE 11-19 (Continued)

COMPRESSIVE PROPERTIES OF ?C2? GRAPHITE

LOT NO. SPEC. DIA. 12.8 MM
LOG NO. E4o4-139 SPEC. LENGTH ?5. MM
LOG DENSITY MG/M**3

SPECIMEN NUMBER	ORIENTATION	LOCATION	DENSITY (MG/M**3)	YOUNGS MODULUS (GPA)	PERMANENT SET (PCT)	FRACTURE STRAIN (PCT)	COMPR. STRENGTH (MPA)
6A	L5?C AX	ML		6.0	.14?	2.425	74.6
	L54C AX	ML		5.5	.151	2.132	66.4
	L56C AX	ML		6.2	.1??	2.143	74.4
	L6?C AX	ML		6.5	.15?	2.?86	74.?
6B	L74C AX	ML		6.4	.18?	2.?4?	67.8
	L78C AX	ML		6.1	.17?	2.528	75.8
	L8?C AX	ML		6.5	.181	2.5?5	77.4
	L84C AX	ML		6.9	.17?	2.2?4	74.?
	MEAN			6.3	.155	2.25?	7?.?
				(.?1 MPSI)			(1?593.PSI)
	STD. DEV.			.4	.?27	.196	3.9
				(.?6 MPSI)			(559.PSI)
5A	L77B RAD	ML		5.3	.?2?	2.273	75.7
	L81B RAD	ML		6.3	.16?	2.143	65.5
	L85B RAD	ML		6.6	.141	2.?21	71.6
	L95B RAD	ML		4.8	.?7?	1.777	57.1
6B	L113B RAD	ML		6.6	.1?1	2.125	73.3
	L117B RAD	ML		6.?	.19?	2.344	72.7
	L121B RAD	ML		6.7	.12?	1.96?	71.9
	L131B RAD	ML		6.7	.1??	1.871	67.5
	MEAN			6.6	.115	2.?64	69.4
				(.96 MPSI)			(1??67.PSI)
	STD. DEV.			.4	.?5?	.194	5.9
				(.?? MPSI)			(861.PSI)

TABLE 11-20

COMPRESSIVE PROPERTIES OF 2020 GRAPHITE

LOT NO. SPEC. DIA. 12.8 MM
LOG NO. 64c4-14? SPEC. LENGTH ?5. MM
LOG DENSITY MG/M**?

SPECIMEN NUMBER	ORIENTATION	LOCATION	DENSITY (MG/M**3)	YOUNGS MODULUS (GPA)	PERMANENT SET (PCT)	FRACTURE STRAIN (PCT)	COMPR. STRENGTH (MPA)
1A	L6C AX	END		9.1	.?3?	1.846	84.2
	L8C AX	END		7.2	.152	1.712	70.9
	L12C AX	END		7.6	.?9?	1.84?	77.7
	L14C AX	END		7.2	.142	1.693	74.7
1B	L3?C AX	END		6.8	.111	1.9??	8?.9
	L32C AX	END		6.9	.?7?	?.?55	84.?
	L36C AX	END		6.6	.2?4	2.16?	82.?
	L38C AX	END		7.1	.?92	1.963	85.4
	MEAN			7.3 (1.?6 MPSI)	.111	1.897	8?.? (11598.PSI)
	STD. DEV.			.8 (.?1 MPSI)	.?54	.?62	5.1 (743.PSI)
1A	L5B RAD	END		7.9	.14?	1.?0?	85.4
	L9B RAD	END		6.7	.?81	1.63?	76.1
	L13B RAD	END		8.1	.?6?	1.581	77.5
	L23B RAD	END		6.3	.17?	1.925	88.1
1B	L41B RAD	END		7.2	.?7?	1.842	83.4
	L45B RAD	END		7.4	.12?	1.952	62.3
	L49B RAD	END		7.2	.1??	1.94?	83.4
	L59B RAD	END		7.2	.?7?	1.863	84.7
	MEAN			7.5 (1.?9 MPSI)	.1?2	1.831	82.6 (11982.PSI)
	STD. DEV.			.5 (.?8 MPSI)	.?39	.143	4.? (583.PSI)

TABLE 11-20 (Continued)

COMPRESSIVE PROPERTIES OF 2020 GRAPHITE

LOT NO.
LOG NO. 6484-147
LOG DENSITY MG/M**3

SPEC. DIA. 12.8 MM
SPEC. LENGTH 25. MM

SPECIMEN NUMBER	ORIENTATION	LOCATION	DENSITY (MG/M**3)	YOUNGS MODULUS (GPA)	PERMANENT SET (PCT)	FRACTURE STRAIN (PCT)	COMPR. STRENGTH (MPA)
6A	L50C	AX	ML	6.5	.080	1.952	82.2
	L54C	AX	ML	7.2	.111	2.258	86.0
	L56C	AX	ML	6.8	.101	1.755	73.6
	L60C	AX	ML	6.5	.080	2.226	84.4
6B	L74C	AX	ML	6.7	.100	2.033	83.2
	L78C	AX	ML	6.6	.112	2.091	84.3
	L80C	AX	ML	7.0	.080	2.081	83.6
	L84C	AX	ML	7.1	.111	1.994	81.6
	MEAN			6.8	.097	2.049	82.3
				(.99 MPSI)			(11942.PSI)
	STD. DEV.			.2	.015	.159	3.8
				(.4 MPSI)			(549.PSI)
6A	L77B	RAD	ML	7.9	.120	1.792	81.6
	L81B	RAD	ML	6.9	.090	2.126	90.2
	L85B	RAD	ML	6.9	.080	2.368	93.7
	L95B	RAD	ML	6.9	.090	1.729	76.5
6B	L113B	RAD	ML	7.2	.140	2.262	86.1
	L117B	RAD	ML	7.4	.100	1.995	84.5
	L121B	RAD	ML	7.6	.090	1.892	82.7
	L131B	RAD	ML	7.9	.150	1.771	80.6
	MEAN			7.3	.095	1.992	84.5
				(1.06 MPSI)			(12255.PSI)
	STD. DEV.			.4	.027	.239	5.5
				(.06 MPSI)			(796.PSI)

TABLE 11-21
SUMMARY OF GRADE 2020 IMPURITIES

Log	Impurity (ppm)										
	Ash	S	Al	B	Ba	Ca	Fe	Li	Si	Ti	V
6484-139											
Mean	735	3.5	8.9	2	58	130	8	<1	60	29	16
Std-dev.	80	2	4.7	--	7	80	4	--	--	16	7
6484-140											
Mean	1560	3.5	64	4.4	25	175	200	<1	190	42	20
Std. dev.	135	3	92	0.8	9	124	--	--	48	7	--

TABLE 11-22
SPECTROCHEMICAL REPORT FOR 2020 GRAPHITE, LOG 6484-139

LAB. NO. 46243 — REPORT TO: G ENGLE — DATE: 6-7-77
SAMPLE: GRAPHITE 6484-139-L-3 — PROJECT NO. 3224146005 — DILUTION: 1.0000 — PLATE NO. 77-040

ELEMENT	CONCENTRATION, PPM	ELEMENT	CONCENTRATION, PPM	ELEMENT	CONCENTRATION, PPM
AG	< .50	AL	20.00	B	2.00
BA	60.00	BE	< .50	BI	< 2.00
CA	400.00	CD	< 10.00	CE	< 80.00
CO	< 4.00	CR	< 10.00	CS	< 100.00
CU	< 1.00	DY	< 20.00	ER	< 6.00
EU	< 10.00	FE	10.00	GD	< 10.00
HF	< 20.00	HO	< 10.00	IN	< 1.00
K	< 10.00	LA	< 10.00	LI	< 1.00
LU	< .50	MG	1.00	MN	< 1.00
MO	< 1.00	NA	< 10.00	NB	< 6.00
ND	< 200.00	NI	< 4.00	P	< 100.00
PB	< 6.00	PR	< 100.00	RB	< 40.00
SB	< 8.00	SC	< 1.00	SI	60.00
SM	< 100.00	SN	< 6.00	SR	< 40.00
TA	< 40.00	TB	< 40.00	TI	40.00
TL	< 20.00	TM	< 4.00	V	20.00
W	< 40.00	YB	< 10.00	ZN	< 20.00
ZR	< .50				

LAB. NO. 46243 — REPORT TO: G ENGLE — DATE: 6-7-77
SAMPLE: GRAPHITE 6484-139-L-10 — PROJECT NO. 3224146005 — DILUTION: 1.0000 — PLATE NO. 77-040

ELEMENT	CONCENTRATION, PPM	ELEMENT	CONCENTRATION, PPM	ELEMENT	CONCENTRATION, PPM
AG	< .50	AL	10.00	B	2.00
BA	60.00	BE	< .50	BI	< 2.00
CA	200.00	CD	< 10.00	CE	< 80.00
CO	< 4.00	CR	< 10.00	CS	< 100.00
CU	< 1.00	DY	< 20.00	ER	< 6.00
EU	< 10.00	FE	10.00	GD	< 10.00
HF	< 20.00	HO	< 10.00	IN	< 1.00
K	< 10.00	LA	< 10.00	LI	< 1.00
LU	< .50	MG	< .50	MN	< 1.00
MO	< 1.00	NA	< 10.00	NB	< 6.00
ND	< 200.00	NI	< 4.00	P	< 100.00
PB	< 6.00	PR	< 100.00	RB	< 40.00
SB	< 8.00	SC	< 1.00	SI	60.00
SM	< 100.00	SN	< 6.00	SR	< 40.00
TA	< 40.00	TB	< 40.00	TI	20.00
TL	< 20.00	TM	< 4.00	V	20.00
W	< 40.00	YB	< 10.00	ZN	< 20.00
ZR	< .50				

CONCENTRATION BASED ON ORGINAL SAMPLE BEFORE DILUTION WITH DILUENT
> MEANS GREATER THAN
< MEANS LESS THAN THE SENSITIVITYOF THE SPECTROGRAPHIC PROCEDURE USED
RESULTS ARE CORRECT WITHIN A FACTOR OF 40% , (ONE STANDARD DEVIATION)

TABLE 11-22 (Continued)

LAB. NO. 46243 — REPORT TO: G ENGLE — DATE: 6-7-77
SAMPLE: GRAPHITE 6484-139-L-16 — PROJECT NO. 3224146005 — DILUTION: 1.0000 — PLATE NO. 77-040

ELEMENT	CONCENTRATION, PPM	ELEMENT	CONCENTRATION, PPM	ELEMENT	CONCENTRATION, PPM
AG	< .50	AL	< 1.00	B	2.00
BA	60.00	BE	< .50	BI	< 2.00
CA	100.00	CD	< 10.00	CE	< 80.00
CO	< 4.00	CR	< 10.00	CS	< 100.00
CU	< 1.00	DY	< 20.00	ER	< 6.00
EU	< 10.00	FE	< 1.00	GD	< 10.00
HF	< 20.00	HO	< 10.00	IN	< 1.00
K	< 10.00	LA	< 10.00	LI	< 1.00
LU	< .50	MG	< .50	MN	< 1.00
MO	< 1.00	NA	< 10.00	NB	< 6.00
ND	< 200.00	NI	< 4.00	P	< 100.00
PB	< 6.00	PR	< 100.00	RB	< 40.00
SB	< 8.00	SC	< 1.00	SI	60.00
SM	< 100.00	SN	< 6.00	SR	< 40.00
TA	< 40.00	TB	< 40.00	TI	2.00
TL	< 20.00	TM	< 4.00	V	< .50
W	< 40.00	YB	< 10.00	ZN	< 20.00
ZR	< .50				

LAB. NO. 46243 — REPORT TO: G ENGLE — DATE: 6-7-77
SAMPLE: GRAPHITE 6484-139-L-21 — PROJECT NO. 3224146005 — DILUTION: 1.0000 — PLATE NO. 77-040

ELEMENT	CONCENTRATION, PPM	ELEMENT	CONCENTRATION, PPM	ELEMENT	CONCENTRATION, PPM
AG	< .50	AL	10.00	B	2.00
BA	60.00	BE	< .50	BI	< 2.00
CA	200.00	CD	< 10.00	CE	< 80.00
CO	< 4.00	CR	< 10.00	CS	< 100.00
CU	< 1.00	DY	< 20.00	ER	< 6.00
EU	< 10.00	FE	8.00	GD	< 10.00
HF	< 20.00	HO	< 10.00	IN	< 1.00
K	< 10.00	LA	< 10.00	LI	< 1.00
LU	< .50	MG	1.00	MN	< 1.00
MO	< 1.00	NA	< 10.00	NB	< 6.00
ND	< 200.00	NI	< 4.00	P	< 100.00
PB	< 6.00	PR	< 100.00	RB	< 40.00
SB	< 8.00	SC	< 1.00	SI	60.00
SM	< 100.00	SN	< 6.00	SR	< 40.00
TA	< 40.00	TB	< 40.00	TI	20.00
TL	< 20.00	TM	< 4.00	V	20.00
W	< 40.00	YB	< 10.00	ZN	< 20.00
ZR	< .50				

CONCENTRATION BASED ON ORGINAL SAMPLE BEFORE DILUTION WITH DILUENT
> MEANS GREATER THAN
< MEANS LESS THAN THE SENSITIVITYOF THE SPECTROGRAPHIC PROCEDURE USED
RESULTS ARE CORRECT WITHIN A FACTOR OF 40% , (ONE STANDARD DEVIATION)

TABLE 11-22 (Continued)

LAB. NO. 46243 REPORT TO: G ENGLE DATE: 6-7-77
SAMPLE: GRAPHITE 6484-139-L-28 PROJECT NO. 3224146005 DILUTION: 1.0000 PLATE NO. 77-040

ELEMENT	CONCENTRATION, PPM	ELEMENT	CONCENTRATION, PPM	ELEMENT	CONCENTRATION, PPM
AG	< .50	AL	10.00	B	2.00
BA	60.00	BE	< .50	BI	< 2.00
CA	100.00	CD	< 10.00	CE	< 80.00
CO	< 4.00	CR	< 10.00	CS	< 100.00
CU	< 1.00	DY	< 20.00	ER	< 6.00
EU	< 10.00	FE	8.00	GD	< 10.00
HF	< 20.00	HO	< 10.00	IN	< 1.00
K	< 10.00	LA	< 10.00	LI	< 1.00
LU	< .50	MG	4.00	MN	< 1.00
MO	< 1.00	NA	< 10.00	NB	< 6.00
ND	< 200.00	NI	< 4.00	P	< 100.00
PB	< 6.00	PR	< 100.00	RB	< 40.00
SB	< 8.00	SC	20.00	SI	60.00
SM	< 100.00	SN	< 6.00	SR	< 40.00
TA	< 40.00	TB	< 40.00	TI	< 1.00
TL	< 20.00	TM	< 4.00	V	10.00
W	< 40.00	YB	< 10.00	ZN	< 20.00
ZR	< .50				

LAB. NO. 46243 REPORT TO: G ENGLE DATE: 6-7-77
SAMPLE: GRAPHITE 6484-139-L-34 PROJECT NO. 3224146005 DILUTION: 1.0000 PLATE NO. 77-040

ELEMENT	CONCENTRATION, PPM	ELEMENT	CONCENTRATION, PPM	ELEMENT	CONCENTRATION, PPM
AG	< .50	AL	10.00	B	2.00
BA	60.00	BE	< .50	BI	< 2.00
CA	100.00	CD	< 10.00	CE	< 80.00
CO	< 4.00	CR	< 10.00	CS	< 100.00
CU	< 1.00	DY	< 20.00	ER	< 6.00
EU	< 10.00	FE	10.00	GD	< 10.00
HF	< 20.00	HO	< 10.00	IN	< 1.00
K	< 10.00	LA	< 10.00	LI	< 1.00
LU	< .50	MG	< .50	MN	< 1.00
MO	< 1.00	NA	< 10.00	NB	< 6.00
ND	< 200.00	NI	< 4.00	P	< 100.00
PB	< 6.00	PR	< 100.00	RB	< 40.00
SB	< 8.00	SC	< 1.00	SI	60.00
SM	< 100.00	SN	< 6.00	SR	< 40.00
TA	< 40.00	TB	< 40.00	TI	20.00
TL	< 20.00	TM	< 4.00	V	20.00
W	< 40.00	YB	< 10.00	ZN	< 20.00
ZR	< .50				

CONCENTRATION BASED ON ORGINAL SAMPLE BEFORE DILUTION WITH DILUENT
> MEANS GREATER THAN
< MEANS LESS THAN THE SENSITIVITYOF THE SPECTROGRAPHIC PROCEDURE USED
RESULTS ARE CORRECT WITHIN A FACTOR OF 40% , (ONE STANDARD DEVIATION)

TABLE 11-22 (Continued)

LAB. NO. 46243 — REPORT TO: G ENGLE — DATE: 6-7-77
SAMPLE: GRAPHITE 6484-139-L-39 — PROJECT NO. 3224146005 — DILUTION: 1.0000 — PLATE NO. 77-040

ELEMENT	CONCENTRATION, PPM	ELEMENT	CONCENTRATION, PPM	ELEMENT	CONCENTRATION, PPM
AG	< .50	AL	10.00	B	2.00
BA	60.00	BE	< .50	BI	< 2.00
CA	100.00	CD	< 10.00	CE	< 80.00
CO	< 4.00	CR	< 10.00	CS	< 100.00
CU	< 1.00	DY	< 20.00	ER	< 6.00
EU	< 10.00	FE	10.00	GD	< 10.00
HF	< 20.00	HO	< 10.00	IN	< 1.00
K	< 10.00	LA	< 10.00	LI	< 1.00
LU	< .50	MG	< .50	MN	< 1.00
MO	< 1.00	NA	< 10.00	NB	< 6.00
ND	< 200.00	NI	< 4.00	P	< 100.00
PB	< 6.00	PR	< 100.00	RB	< 40.00
SB	< 8.00	SC	< 1.00	SI	60.00
SM	< 100.00	SN	< 6.00	SR	< 40.00
TA	< 40.00	TB	< 40.00	TI	40.00
TL	< 20.00	TM	< 4.00	V	20.00
W	< 40.00	YB	< 10.00	ZN	< 20.00
ZR	< .50				

LAB. NO. 46243 — REPORT TO: G ENGLE — DATE: 6-7-77
SAMPLE: GRAPHITE 6484-139-L-57 — PROJECT NO. 3224146005 — DILUTION: 1.0000 — PLATE NO. 77-040

ELEMENT	CONCENTRATION, PPM	ELEMENT	CONCENTRATION, PPM	ELEMENT	CONCENTRATION, PPM
AG	< .50	AL	10.00	B	2.00
BA	60.00	BE	< .50	BI	< 2.00
CA	100.00	CD	< 10.00	CE	< 80.00
CO	< 4.00	CR	< 10.00	CS	< 100.00
CU	< 1.00	DY	< 20.00	ER	< 6.00
EU	< 10.00	FE	10.00	GD	< 10.00
HF	< 20.00	HO	< 10.00	IN	< 1.00
K	< 10.00	LA	< 10.00	LI	< 1.00
LU	< .50	MG	1.00	MN	< 1.00
MO	< 1.00	NA	< 10.00	NB	< 6.00
ND	< 200.00	NI	< 4.00	P	< 100.00
PB	< 6.00	PR	< 100.00	RB	< 40.00
SB	< 8.00	SC	< 1.00	SI	60.00
SM	< 100.00	SN	< 6.00	SR	< 40.00
TA	< 40.00	TB	< 40.00	TI	40.00
TL	< 20.00	TM	< 4.00	V	20.00
W	< 40.00	YB	< 10.00	ZN	< 20.00
ZR	< .50				

CONCENTRATION BASED ON ORGINAL SAMPLE BEFORE DILUTION WITH DILUENT
> MEANS GREATER THAN
< MEANS LESS THAN THE SENSITIVITYOF THE SPECTROGRAPHIC PROCEDURE USED
RESULTS ARE CORRECT WITHIN A FACTOR OF 40% , (ONE STANDARD DEVIATION)

TABLE 11-22 (Continued)

LAB. NO. 46243 REPORT TO: G ENGLE DATE: 6-7-77
SAMPLE: GRAPHITE 6484-139-L-58 PROJECT NO. 3224146005 DILUTION: 1.0000 PLATE NO. 77-040

ELEMENT	CONCENTRATION, PPM	ELEMENT	CONCENTRATION, PPM	ELEMENT	CONCENTRATION, PPM
AG	< .50	AL	10.00	B	2.00
BA	60.00	BE	< .50	BI	< 2.00
CA	100.00	CD	< 10.00	CE	< 80.00
CO	< 4.00	CR	< 10.00	CS	< 100.00
CU	< 1.00	DY	< 20.00	ER	< 6.00
EU	< 10.00	FE	10.00	GD	< 10.00
HF	< 20.00	HO	< 10.00	IN	< 1.00
K	< 10.00	LA	< 10.00	LI	< 1.00
LU	< .50	MG	1.00	MN	< 1.00
MO	< 1.00	NA	< 10.00	NB	< 6.00
ND	< 200.00	NI	< 4.00	P	< 100.00
PB	< 6.00	PR	< 100.00	RB	< 40.00
SB	< 8.00	SC	< 1.00	SI	60.00
SM	< 100.00	SN	< 6.00	SR	< 40.00
TA	< 40.00	TB	< 40.00	TI	40.00
TL	< 20.00	TM	< 4.00	V	20.00
W	< 40.00	YB	< 10.00	ZN	< 20.00
ZR	< .50				

LAB. NO. 46243 REPORT TO: G ENGLE DATE: 6-7-77
SAMPLE: GRAPHITE 6484-139-L-64 PROJECT NO. 3224146005 DILUTION: 1.0000 PLATE NO. 77-040

ELEMENT	CONCENTRATION, PPM	ELEMENT	CONCENTRATION, PPM	ELEMENT	CONCENTRATION, PPM
AG	< .50	AL	10.00	B	2.00
BA	60.00	BE	< .50	BI	< 2.00
CA	100.00	CD	< 10.00	CE	< 80.00
CO	< 4.00	CR	< 10.00	CS	< 100.00
CU	< 1.00	DY	< 20.00	ER	< 6.00
EU	< 10.00	FE	10.00	GD	< 10.00
HF	< 20.00	HO	< 10.00	IN	< 1.00
K	< 10.00	LA	< 10.00	LI	< 1.00
LU	< .50	MG	< .50	MN	< 1.00
MO	< 1.00	NA	< 10.00	NB	< 6.00
ND	< 200.00	NI	< 4.00	P	< 100.00
PB	< 6.00	PR	< 100.00	RB	< 40.00
SB	< 8.00	SC	< 1.00	SI	60.00
SM	< 100.00	SN	< 6.00	SR	< 40.00
TA	< 40.00	TB	< 40.00	TI	40.00
TL	< 20.00	TM	< 4.00	V	20.00
W	< 40.00	YB	< 10.00	ZN	< 20.00
ZR	< .50				

CONCENTRATION BASED ON ORGINAL SAMPLE BEFORE DILUTION WITH DILUENT
> MEANS GREATER THAN
< MEANS LESS THAN THE SENSITIVITYOF THE SPECTROGRAPHIC PROCEDURE USED
RESULTS ARE CORRECT WITHIN A FACTOR OF 40% , (ONE STANDARD DEVIATION)

TABLE 11-22 (Continued)

LAB. NO. 46243 — REPORT TO: G ENGLE — DATE: 6-7-77
SAMPLE: GRAPHITE 6484-139-L-75 — PROJECT NO. 3224146005 — DILUTION: 1.0000 — PLATE NO. 77-040

ELEMENT	CONCENTRATION, PPM	ELEMENT	CONCENTRATION, PPM	ELEMENT	CONCENTRATION, PPM
AG	< .50	AL	10.00	B	2.00
BA	60.00	BE	< .50	BI	< 2.00
CA	100.00	CD	< 10.00	CE	< 80.00
CO	< 4.00	CR	< 10.00	CS	< 100.00
CU	< 1.00	DY	< 20.00	ER	< 6.00
EU	< 10.00	FE	8.00	GD	< 10.00
HF	< 20.00	HO	< 10.00	IN	< 1.00
K	< 10.00	LA	< 10.00	LI	< 1.00
LU	< .50	MG	1.00	MN	< 1.00
MO	< 1.00	NA	< 10.00	NB	< 6.00
ND	< 200.00	NI	< 4.00	P	< 100.00
PB	< 6.00	PR	< 100.00	RB	< 40.00
SB	< 8.00	SC	< 1.00	SI	60.00
SM	< 100.00	SN	< 6.00	SR	< 40.00
TA	< 40.00	TB	< 40.00	TI	40.00
TL	< 20.00	TM	< 4.00	V	20.00
W	< 40.00	YB	< 10.00	ZN	< 20.00
ZR	< .50				

LAB. NO. 46243 — REPORT TO: G ENGLE — DATE: 6-7-77
SAMPLE: GRAPHITE 6484-139-L-76 — PROJECT NO. 3224146005 — DILUTION: 1.0000 — PLATE NO. 77-040

ELEMENT	CONCENTRATION, PPM	ELEMENT	CONCENTRATION, PPM	ELEMENT	CONCENTRATION, PPM
AG	< .50	AL	< 1.00	B	2.00
BA	60.00	BE	< .50	BI	< 2.00
CA	100.00	CD	< 10.00	CE	< 80.00
CO	< 4.00	CR	< 10.00	CS	< 100.00
CU	< 1.00	DY	< 20.00	ER	< 6.00
EU	< 10.00	FE	< 1.00	GD	< 10.00
HF	< 20.00	HO	< 10.00	IN	< 1.00
K	< 10.00	LA	< 10.00	LI	< 1.00
LU	< .50	MG	< .50	MN	< 1.00
MO	< 1.00	NA	< 10.00	NB	< 6.00
ND	< 200.00	NI	< 4.00	P	< 100.00
PB	< 6.00	PR	< 100.00	RB	< 40.00
SB	< 8.00	SC	< 1.00	SI	60.00
SM	< 100.00	SN	< 6.00	SR	< 40.00
TA	< 40.00	TB	< 40.00	TI	40.00
TL	< 20.00	TM	< 4.00	V	10.00
W	< 40.00	YB	< 10.00	ZN	< 20.00
ZR	< .50				

CONCENTRATION BASED ON ORGINAL SAMPLE BEFORE DILUTION WITH DILUENT
> MEANS GREATER THAN
< MEANS LESS THAN THE SENSITIVITYOF THE SPECTROGRAPHIC PROCEDURE USED
RESULTS ARE CORRECT WITHIN A FACTOR OF 40% , (ONE STANDARD DEVIATION)

TABLE 11-22 (Continued)

LAB. NO. 46243 REPORT TO: G ENGLE DATE: 6-7-77
SAMPLE: GRAPHITE 6484-139-L-82 PROJECT NO. 3224146005 DILUTION: 1.0000 PLATE NO. 77-040

ELEMENT	CONCENTRATION, PPM	ELEMENT	CONCENTRATION, PPM	ELEMENT	CONCENTRATION, PPM
AG	< .50	AL	< 1.00	B	2.00
BA	60.00	BE	< .50	BI	< 2.00
CA	100.00	CD	< 10.00	CE	< 80.00
CO	< 4.00	CR	< 10.00	CS	< 100.00
CU	< 1.00	DY	< 20.00	ER	< 6.00
EU	< 10.00	FE	< 1.00	GD	< 10.00
HF	< 20.00	HO	< 10.00	IN	< 1.00
K	< 10.00	LA	< 10.00	LI	< 1.00
LU	< .50	MG	< .50	MN	< 1.00
MO	< 1.00	NA	< 10.00	NB	< 6.00
ND	< 200.00	NI	< 4.00	P	< 100.00
PB	< 6.00	PR	< 100.00	RB	< 40.00
SB	< 8.00	SC	< 1.00	SI	60.00
SM	< 100.00	SN	< 6.00	SR	< 40.00
TA	< 40.00	TB	< 40.00	TI	40.00
TL	< 20.00	TM	< 4.00	V	20.00
W	< 40.00	YB	< 10.00	ZN	< 20.00
ZR	< .50				

LAB. NO. 46243 REPORT TO: G ENGLE DATE: 6-7-77
SAMPLE: GRAPHITE 6484-139-L-93 PROJECT NO. 3224146005 DILUTION: 1.0000 PLATE NO. 77-040

ELEMENT	CONCENTRATION, PPM	ELEMENT	CONCENTRATION, PPM	ELEMENT	CONCENTRATION, PPM
AG	< .50	AL	10.00	B	2.00
BA	60.00	BE	< .50	BI	< 2.00
CA	100.00	CD	< 10.00	CE	< 80.00
CO	< 4.00	CR	< 10.00	CS	< 100.00
CU	< 1.00	DY	< 20.00	ER	< 6.00
EU	< 10.00	FE	10.00	GD	< 10.00
HF	< 20.00	HO	< 10.00	IN	< 1.00
K	< 10.00	LA	< 10.00	LI	< 1.00
LU	< .50	MG	< .50	MN	< 1.00
MO	< 1.00	NA	< 10.00	NB	< 6.00
ND	< 200.00	NI	< 4.00	P	< 100.00
PB	< 6.00	PR	< 100.00	RB	< 40.00
SB	< 8.00	SC	< 1.00	SI	60.00
SM	< 100.00	SN	< 6.00	SR	< 40.00
TA	< 40.00	TB	< 40.00	TI	40.00
TL	< 20.00	TM	< 4.00	V	20.00
W	< 40.00	YB	< 10.00	ZN	< 20.00
ZR	< .50				

CONCENTRATION BASED ON ORGINAL SAMPLE BEFORE DILUTION WITH DILUENT
> MEANS GREATER THAN
< MEANS LESS THAN THE SENSITIVITYOF THE SPECTROGRAPHIC PROCEDURE USED
RESULTS ARE CORRECT WITHIN A FACTOR OF 40% , (ONE STANDARD DEVIATION)

TABLE 11-22 (Continued)

LAB. NO. 46243 — REPORT TO: G ENGLE — DATE: 6-7-77
SAMPLE: GRAPHITE 6484-139-L-111 — PROJECT NO. 3224146005 — DILUTION: 1.0000 — PLATE NO. 77-040

ELEMENT	CONCENTRATION, PPM	ELEMENT	CONCENTRATION, PPM	ELEMENT	CONCENTRATION, PPM
AG	< .50	AL	10.00	B	2.00
BA	40.00	BE	< .50	BI	< 2.00
CA	100.00	CD	< 10.00	CE	< 80.00
CO	< 4.00	CR	< 10.00	CS	< 100.00
CU	< 1.00	DY	< 20.00	ER	< 6.00
EU	< 10.00	FE	8.00	GD	< 10.00
HF	< 20.00	HO	< 10.00	IN	< 1.00
K	< 10.00	LA	< 10.00	LI	< 1.00
LU	< .50	MG	< .50	MN	< 1.00
MO	< 1.00	NA	< 10.00	NB	< 6.00
ND	< 200.00	NI	< 4.00	P	< 100.00
PB	< 6.00	PR	< 100.00	RB	< 40.00
SB	< 8.00	SC	< 1.00	SI	60.00
SM	< 100.00	SN	< 6.00	SR	< 40.00
TA	< 40.00	TB	< 40.00	TI	40.00
TL	< 20.00	TM	< 4.00	V	20.00
W	< 40.00	YB	< 10.00	ZN	< 20.00
ZR	< .50				

LAB. NO. 46243 — REPORT TO: G ENGLE — DATE: 6-7-77
SAMPLE: GRAPHITE 6484-139-L-129 — PROJECT NO. 3224146005 — DILUTION: 1.0000 — PLATE NO. 77-040

ELEMENT	CONCENTRATION, PPM	ELEMENT	CONCENTRATION, PPM	ELEMENT	CONCENTRATION, PPM
AG	< .50	AL	10.00	B	2.00
BA	40.00	BE	< .50	BI	< 2.00
CA	100.00	CD	< 10.00	CE	< 80.00
CO	< 4.00	CR	< 10.00	CS	< 100.00
CU	< 1.00	DY	< 20.00	ER	< 6.00
EU	< 10.00	FE	10.00	GD	< 10.00
HF	< 20.00	HO	< 10.00	IN	< 1.00
K	< 10.00	LA	< 10.00	LI	< 1.00
LU	< .50	MG	< .50	MN	< 1.00
MO	< 1.00	NA	< 10.00	NB	< 6.00
ND	< 200.00	NI	< 4.00	P	< 100.00
PB	< 6.00	PR	< 100.00	RB	< 40.00
SB	< 8.00	SC	< 1.00	SI	60.00
SM	< 100.00	SN	< 6.00	SR	< 40.00
TA	< 40.00	TB	< 40.00	TI	2.00
TL	< 20.00	TM	< 4.00	V	< .50
W	< 40.00	YB	< 10.00	ZN	< 20.00
ZR	< .50				

CONCENTRATION BASED ON ORGINAL SAMPLE BEFORE DILUTION WITH DILUENT
> MEANS GREATER THAN
< MEANS LESS THAN THE SENSITIVITYOF THE SPECTROGRAPHIC PROCEDURE USED
RESULTS ARE CORRECT WITHIN A FACTOR OF 40% , (ONE STANDARD DEVIATION)

TABLE 11-23
SPECTROCHEMICAL REPORT FOR 2020 GRAPHITE, LOG 6484-140

LAB. NO. 46244 — REPORT TO: G ENGLE — DATE: 7-11-77
SAMPLE: 6484-140-L 3 GRAPHITE — PROJECT NO. 3224146005 — DILUTION: 1.0000 — PLATE NO. 77-050

ELEMENT	CONCENTRATION, PPM	ELEMENT	CONCENTRATION, PPM	ELEMENT	CONCENTRATION, PPM
AG	< .50	AL	80.00	B	4.00
BA	40.00	BE	< .50	BI	< 2.00
CA	100.00	CD	< 10.00	CE	< 80.00
CO	< 4.00	CR	< 10.00	CS	< 100.00
CU	< 1.00	DY	< 20.00	ER	< 6.00
EU	< 10.00	FE	200.00	GD	< 10.00
HF	< 20.00	HO	< 10.00	IN	< 1.00
K	20.00	LA	< 10.00	LI	< 1.00
LU	< .50	MG	1.00	MN	1.00
MO	< 1.00	NA	< 10.00	NB	< 6.00
ND	< 200.00	NI	< 4.00	P	< 100.00
PB	< 6.00	PR	< 100.00	RB	< 40.00
SB	< 8.00	SC	< 1.00	SI	200.00
SM	< 100.00	SN	< 6.00	SR	< 40.00
TA	< 40.00	TB	< 40.00	TI	60.00
TL	< 20.00	TM	< 4.00	V	20.00
W	< 40.00	YB	< 10.00	ZN	< 20.00
ZR	< .50				

LAB. NO. 46244 — REPORT TO: G ENGLE — DATE: 7-11-77
SAMPLE: 6484-140-L10 GRAPHITE — PROJECT NO. 3224146005 — DILUTION: 1.0000 — PLATE NO. 77-050

ELEMENT	CONCENTRATION, PPM	ELEMENT	CONCENTRATION, PPM	ELEMENT	CONCENTRATION, PPM
AG	< .50	AL	400.00	B	4.00
BA	40.00	BE	< .50	BI	< 2.00
CA	600.00	CD	< 10.00	CE	< 80.00
CO	< 4.00	CR	< 10.00	CS	< 100.00
CU	< 1.00	DY	< 20.00	ER	< 6.00
EU	< 10.00	FE	200.00	GD	< 10.00
HF	< 20.00	HO	< 10.00	IN	< 1.00
K	20.00	LA	< 10.00	LI	1.00
LU	< .50	MG	1.00	MN	20.00
MO	< 1.00	NA	< 10.00	NB	< 6.00
ND	< 200.00	NI	< 4.00	P	< 100.00
PB	< 6.00	PR	< 100.00	RB	< 40.00
SB	< 8.00	SC	< 1.00	SI	< 10.00
SM	< 100.00	SN	< 6.00	SR	< 40.00
TA	< 40.00	TB	< 40.00	TI	60.00
TL	< 20.00	TM	< 4.00	V	20.00
W	< 40.00	YB	< 10.00	ZN	< 20.00
ZR	< .50				

CONCENTRATION BASED ON ORGINAL SAMPLE BEFORE DILUTION WITH DILUENT
> MEANS GREATER THAN
< MEANS LESS THAN THE SENSITIVITYOF THE SPECTROGRAPHIC PROCEDURE USED
RESULTS ARE CORRECT WITHIN A FACTOR OF 40% . (ONE STANDARD DEVIATION)

TABLE 11-23 (Continued)

LAB. NO. 46244 — REPORT TO: G ENGLE — DATE: 7-11-77
SAMPLE: 6484-140-L16 GRAPHITE — PROJECT NO. 3224146005 — DILUTION: 1.0000 — PLATE NO. 77-050

ELEMENT	CONCENTRATION, PPM	ELEMENT	CONCENTRATION, PPM	ELEMENT	CONCENTRATION, PPM
AG	< .50	AL	80.00	B	6.00
BA	40.00	BE	< .50	BI	< 2.00
CA	200.00	CD	< 10.00	CE	< 80.00
CO	< 4.00	CR	< 10.00	CS	< 100.00
CU	< 1.00	DY	< 20.00	ER	< 6.00
EU	< 10.00	FE	200.00	GD	< 10.00
HF	< 20.00	HO	< 10.00	IN	< 1.00
K	10.00	LA	< 10.00	LI	< 1.00
LU	< .50	MG	1.00	MN	< 1.00
MO	< 1.00	NA	< 10.00	NB	< 6.00
ND	< 200.00	NI	< 4.00	P	< 100.00
PB	< 6.00	PR	< 100.00	RB	< 40.00
SB	< 8.00	SC	< 1.00	SI	200.00
SM	< 100.00	SN	< 6.00	SR	< 40.00
TA	< 40.00	TB	< 40.00	TI	40.00
TL	< 20.00	TM	< 4.00	V	20.00
W	< 40.00	YB	< 10.00	ZN	< 20.00
ZR	< .50				

LAB. NO. 46244 — REPORT TO: G ENGLE — DATE: 7-11-77
SAMPLE: 6484-140-L21 GRAPHITE — PROJECT NO. 3224146005 — DILUTION: 1.0000 — PLATE NO. 77-050

ELEMENT	CONCENTRATION, PPM	ELEMENT	CONCENTRATION, PPM	ELEMENT	CONCENTRATION, PPM
AG	< .50	AL	60.00	B	4.00
BA	20.00	BE	< .50	BI	< 2.00
CA	200.00	CD	< 10.00	CE	< 80.00
CO	< 4.00	CR	< 10.00	CS	< 100.00
CU	< 1.00	DY	< 20.00	ER	< 6.00
EU	< 10.00	FE	200.00	GD	< 10.00
HF	< 20.00	HO	< 10.00	IN	< 1.00
K	10.00	LA	< 10.00	LI	< 1.00
LU	< .50	MG	< .50	MN	< 1.00
MO	< 1.00	NA	< 10.00	NB	< 6.00
ND	< 200.00	NI	< 4.00	P	< 100.00
PR	< 6.00	PR	< 100.00	RB	< 40.00
SB	< 8.00	SC	< 1.00	SI	200.00
SM	< 100.00	SN	< 6.00	SR	< 40.00
TA	< 40.00	TB	< 40.00	TI	40.00
TL	< 20.00	TM	< 4.00	V	20.00
W	< 40.00	YB	< 10.00	ZN	< 20.00
ZR	< .50				

CONCENTRATION BASED ON ORGINAL SAMPLE BEFORE DILUTION WITH DILUENT
> MEANS GREATER THAN
< MEANS LESS THAN THE SENSITIVITYOF THE SPECTROGRAPHIC PROCEDURE USED
RESULTS ARE CORRECT WITHIN A FACTOR OF 40% , (ONE STANDARD DEVIATION)

TABLE 11-23 (Continued)

LAB. NO. 46244 REPORT TO: G ENGLE DATE: 7-11-77
SAMPLE: 6484-140-L28-GRAPHITE PROJECT NO. 3224146005 DILUTION: 1.0000 PLATE NO. 77-050

ELEMENT	CONCENTRATION, PPM	ELEMENT	CONCENTRATION, PPM	ELEMENT	CONCENTRATION, PPM
AG	< .50	AL	20.00	B	4.00
BA	40.00	BE	< .50	BI	< 2.00
CA	200.00	CD	< 10.00	CE	< 80.00
CO	< 4.00	CR	< 10.00	CS	< 100.00
CU	< 1.00	DY	< 20.00	ER	< 6.00
EU	< 10.00	FE	200.00	GD	< 10.00
HF	< 20.00	HO	< 10.00	IN	< 1.00
K	10.00	LA	< 10.00	LI	< 1.00
LU	< .50	MG	1.00	MN	< 1.00
MO	< 1.00	NA	< 10.00	NB	< 6.00
ND	< 200.00	NI	< 4.00	P	< 100.00
PB	< 6.00	PR	< 100.00	RB	< 40.00
SB	< 8.00	SC	< 1.00	SI	200.00
SM	< 100.00	SN	< 6.00	SR	< 40.00
TA	< 40.00	TB	< 40.00	TI	40.00
TL	< 20.00	TM	< 4.00	V	20.00
W	< 40.00	YB	< 10.00	ZN	< 20.00
ZR	< .50				

LAB. NO. 46244 REPORT TO: G ENGLE DATE: 7-11-77
SAMPLE: 6484-140-L34 GRAPHITE PROJECT NO. 3224146005 DILUTION: 1.0000 PLATE NO. 77-050

ELEMENT	CONCENTRATION, PPM	ELEMENT	CONCENTRATION, PPM	ELEMENT	CONCENTRATION, PPM
AG	< .50	AL	20.00	B	4.00
BA	20.00	BE	< .50	BI	< 2.00
CA	200.00	CD	< 10.00	CE	< 80.00
CO	< 4.00	CR	< 10.00	CS	< 100.00
CU	< 1.00	DY	< 20.00	ER	< 6.00
EU	< 10.00	FE	200.00	GD	< 10.00
HF	< 20.00	HO	< 10.00	IN	< 1.00
K	10.00	LA	< 10.00	LI	< 1.00
LU	< .50	MG	1.00	MN	1.00
MO	< 1.00	NA	< 10.00	NB	< 6.00
ND	< 200.00	NI	< 4.00	P	< 100.00
PB	< 6.00	PR	< 100.00	RB	< 40.00
SB	< 8.00	SC	< 1.00	SI	200.00
SM	< 100.00	SN	< 6.00	SR	< 40.00
TA	< 40.00	TB	< 40.00	TI	40.00
TL	< 20.00	TM	< 4.00	V	20.00
W	< 40.00	YB	< 10.00	ZN	< 20.00
ZR	< .50				

CONCENTRATION BASED ON ORGINAL SAMPLE BEFORE DILUTION WITH DILUENT
> MEANS GREATER THAN
< MEANS LESS THAN THE SENSITIVITYOF THE SPECTROGRAPHIC PROCEDURE USED
RESULTS ARE CORRECT WITHIN A FACTOR OF 40% , (ONE STANDARD DEVIATION)

TABLE 11-23 (Continued)

LAB. NO. 46244 — REPORT TO: G ENGLE — DATE: 7-11-77
SAMPLE: 6484-140-L39 GRAPHITE — PROJECT NO. 3224146005 — DILUTION: 1.0000 — PLATE NO. 77-050

ELEMENT	CONCENTRATION, PPM	ELEMENT	CONCENTRATION, PPM	ELEMENT	CONCENTRATION, PPM
AG	< .50	AL	40.00	B	4.00
BA	20.00	BE	< .50	BI	< 2.00
CA	200.00	CD	< 10.00	CE	< 80.00
CO	< 4.00	CR	< 10.00	CS	< 100.00
CU	< 1.00	DY	< 20.00	ER	< 6.00
EU	< 10.00	FE	200.00	GD	< 10.00
HF	< 20.00	HO	< 10.00	IN	< 1.00
K	10.00	LA	< 10.00	LI	< 1.00
LU	< .50	MG	1.00	MN	< 1.00
MO	< 1.00	NA	< 10.00	NB	< 6.00
ND	< 200.00	NI	< 4.00	P	< 100.00
PB	< 6.00	PR	< 100.00	RB	< 40.00
SB	< 8.00	SC	< 1.00	SI	200.00
SM	< 100.00	SN	< 6.00	SR	< 40.00
TA	< 40.00	TB	< 40.00	TI	40.00
TL	< 20.00	TM	< 4.00	V	20.00
W	< 40.00	YB	< 10.00	ZN	< 20.00
ZR	< .50				

LAB. NO. 46244 — REPORT TO: G ENGLE — DATE: 7-11-77
SAMPLE: 6484-140-L57 GRAPHITE — PROJECT NO. 3224146005 — DILUTION: 1.0000 — PLATE NO. 77-050

ELEMENT	CONCENTRATION, PPM	ELEMENT	CONCENTRATION, PPM	ELEMENT	CONCENTRATION, PPM
AG	< .50	AL	40.00	B	4.00
BA	20.00	BE	< .50	BI	< 2.00
CA	200.00	CD	< 10.00	CE	< 80.00
CO	< 4.00	CR	< 10.00	CS	< 100.00
CU	< 1.00	DY	< 20.00	ER	< 6.00
EU	< 10.00	FE	200.00	GD	< 10.00
HF	< 20.00	HO	< 10.00	IN	< 1.00
K	< 10.00	LA	< 10.00	LI	< 1.00
LU	< .50	MG	1.00	MN	< 1.00
MO	< 1.00	NA	< 10.00	NB	< 6.00
ND	< 200.00	NI	< 4.00	P	< 100.00
PB	< 6.00	PR	< 100.00	RB	< 40.00
SB	< 8.00	SC	< 1.00	SI	200.00
SM	< 100.00	SN	< 6.00	SR	< 40.00
TA	< 40.00	TB	< 40.00	TI	40.00
TL	< 20.00	TM	< 4.00	V	20.00
W	< 40.00	YB	< 10.00	ZN	< 20.00
ZR	< .50				

CONCENTRATION BASED ON ORGINAL SAMPLE BEFORE DILUTION WITH DILUENT
> MEANS GREATER THAN
< MEANS LESS THAN THE SENSITIVITYOF THE SPECTROGRAPHIC PROCEDURE USED
RESULTS ARE CORRECT WITHIN A FACTOR OF 40% + (ONE STANDARD DEVIATION)

TABLE 11-23 (Continued)

LAB. NO. 46244 — REPORT TO: G ENGLE — DATE: 7-11-77
SAMPLE: 6484-140-L58 GRAPHITE — PROJECT NO. 3224146005 — DILUTION: 1.0000 — PLATE NO. 77-050

ELEMENT	CONCENTRATION, PPM	ELEMENT	CONCENTRATION, PPM	ELEMENT	CONCENTRATION, PPM
AG	< .50	AL	40.00	B	4.00
BA	20.00	BE	< .50	BI	< 2.00
CA	200.00	CD	< 10.00	CE	< 80.00
CO	< 4.00	CR	< 10.00	CS	< 100.00
CU	< 1.00	DY	< 20.00	ER	< 6.00
EU	< 10.00	FE	200.00	GD	< 10.00
HF	< 20.00	HO	< 10.00	IN	< 1.00
K	< 10.00	LA	< 10.00	LI	< 1.00
LU	< .50	MG	1.00	MN	< 1.00
MO	< 1.00	NA	< 10.00	NB	< 6.00
ND	< 200.00	NI	< 4.00	P	< 100.00
PB	< 6.00	PR	< 100.00	RB	< 40.00
SB	< 8.00	SC	< 1.00	SI	200.00
SM	< 100.00	SN	< 6.00	SR	< 40.00
TA	< 40.00	TB	< 40.00	TI	40.00
TL	< 20.00	TM	< 4.00	V	20.00
W	< 40.00	YB	< 10.00	ZN	< 20.00
ZR	< .50				

LAB. NO. 46244 — REPORT TO: G ENGLE — DATE: 7-11-77
SAMPLE: 6484-140-L64 GRAPHITE — PROJECT NO. 32241460055 — DILUTION: 1.0000 — PLATE NO. 77-050

ELEMENT	CONCENTRATION, PPM	ELEMENT	CONCENTRATION, PPM	ELEMENT	CONCENTRATION, PPM
AG	< .50	AL	60.00	B	4.00
BA	20.00	BE	< .50	BI	< 2.00
CA	100.00	CD	< 10.00	CE	< 80.00
CO	< 4.00	CR	< 10.00	CS	< 100.00
CU	< 1.00	DY	< 20.00	ER	< 6.00
EU	< 10.00	FE	200.00	GD	< 10.00
HF	< 20.00	HO	< 10.00	IN	< 1.00
K	< 10.00	LA	< 10.00	LI	< 1.00
LU	< .50	MG	< .50	MN	4.00
MO	< 1.00	NA	< 10.00	NB	< 6.00
ND	< 200.00	NI	< 4.00	P	< 100.00
PB	< 6.00	PR	< 100.00	RB	< 40.00
SB	< 8.00	SC	< 1.00	SI	200.00
SM	< 100.00	SN	< 6.00	SR	< 40.00
TA	< 40.00	TB	< 40.00	TI	40.00
TL	< 20.00	TM	< 4.00	V	20.00
W	< 40.00	YB	< 10.00	ZN	< 20.00
ZR	< .50				

CONCENTRATION BASED ON ORGINAL SAMPLE BEFORE DILUTION WITH DILUENT
> MEANS GREATER THAN
< MEANS LESS THAN THE SENSITIVITYOF THE SPECTROGRAPHIC PROCEDURE USED
RESULTS ARE CORRECT WITHIN A FACTOR OF 40% , (ONE STANDARD DEVIATION)

TABLE 11-22 (Continued)

LAB. NO. 46244 — REPORT TO: G ENGLE — DATE: 7-11-77
SAMPLE: 6484-140-L75 GRAPHITE — PROJECT NO. 32241460055 — DILUTION: 1.0000 — PLATE NO. 77-050

ELEMENT	CONCENTRATION, PPM	ELEMENT	CONCENTRATION, PPM	ELEMENT	CONCENTRATION, PPM
AG	< .50	AL	20.00	B	4.00
BA	20.00	BE	< .50	BI	< 2.00
CA	100.00	CD	< 10.00	CE	< 80.00
CO	< 4.00	CR	< 10.00	CS	< 100.00
CU	< 1.00	DY	< 20.00	ER	< 6.00
EU	< 10.00	FE	200.00	GD	< 10.00
HF	< 20.00	HO	< 10.00	IN	< 1.00
K	< 10.00	LA	< 10.00	LI	< 1.00
LU	< .50	MG	< .50	MN	< 1.00
MO	< 1.00	NA	< 10.00	NB	< 6.00
ND	< 200.00	NI	< 4.00	P	< 100.00
PB	< 6.00	PR	< 100.00	RB	< 40.00
SB	< 8.00	SC	< 1.00	SI	200.00
SM	< 100.00	SN	< 6.00	SR	< 40.00
TA	< 40.00	TB	< 40.00	TI	40.00
TL	< 20.00	TM	< 4.00	V	20.00
W	< 40.00	YB	< 10.00	ZN	< 20.00
ZR	< .50				

LAB. NO. 46244 — REPORT TO: G ENGLE — DATE: 7-11-77
SAMPLE: 6484-140-L76 GRAPHITE — PROJECT NO. 32241460055 — DILUTION: 1.0000 — PLATE NO. 77-050

ELEMENT	CONCENTRATION, PPM	ELEMENT	CONCENTRATION, PPM	ELEMENT	CONCENTRATION, PPM
AG	< .50	AL	20.00	B	4.00
BA	20.00	BE	< .50	BI	< 2.00
CA	100.00	CD	< 10.00	CE	< 80.00
CO	< 4.00	CR	< 10.00	CS	< 100.00
CU	< 1.00	DY	< 20.00	ER	< 6.00
EU	< 10.00	FE	200.00	GD	< 10.00
HF	< 20.00	HO	< 10.00	IN	< 1.00
K	< 10.00	LA	< 10.00	LI	< 1.00
LU	< .50	MG	< .50	MN	< 1.00
MO	< 1.00	NA	< 10.00	NB	< 6.00
ND	< 200.00	NI	< 4.00	P	< 100.00
PB	< 6.00	PR	< 100.00	RB	< 40.00
SB	< 8.00	SC	< 1.00	SI	200.00
SM	< 100.00	SN	< 6.00	SR	< 40.00
TA	< 40.00	TB	< 40.00	TI	40.00
TL	< 20.00	TM	< 4.00	V	20.00
W	< 40.00	YB	< 10.00	ZN	< 20.00
ZR	< .50				

CONCENTRATION BASED ON ORGINAL SAMPLE BEFORE DILUTION WITH DILUENT
> MEANS GREATER THAN
< MEANS LESS THAN THE SENSITIVITYOF THE SPECTROGRAPHIC PROCEDURE USED
RESULTS ARE CORRECT WITHIN A FACTOR OF 40% . (ONE STANDARD DEVIATION)

TABLE 11-23 (Continued)

LAB. NO. 46244 — REPORT TO: G ENGLE — DATE: 7-11-77
SAMPLE: 6484-140-L82 GRAPHITE — PROJECT NO. 32241460055 — DILUTION: 1.0000 — PLATE NO. 77-050

ELEMENT	CONCENTRATION, PPM	ELEMENT	CONCENTRATION, PPM	ELEMENT	CONCENTRATION, PPM
AG	< .50	AL	60.00	B	4.00
BA	20.00	BE	< .50	BI	< 2.00
CA	100.00	CD	< 10.00	CE	< 80.00
CO	< 4.00	CR	< 10.00	CS	< 100.00
CU	< 1.00	DY	< 20.00	ER	< 6.00
EU	< 10.00	FE	200.00	GD	< 10.00
HF	< 20.00	HO	< 10.00	IN	< 1.00
K	< 10.00	LA	< 10.00	LI	< 1.00
LU	< .50	MG	< .50	MN	2.00
MO	< 1.00	NA	< 10.00	NB	< 6.00
ND	< 200.00	NI	< 4.00	P	< 100.00
PB	< 6.00	PR	< 100.00	RB	< 40.00
SB	< 8.00	SC	< 1.00	SI	200.00
SM	< 100.00	SN	< 6.00	SR	< 40.00
TA	< 40.00	TB	< 40.00	TI	40.00
TL	< 20.00	TM	< 4.00	V	20.00
W	< 40.00	YB	< 10.00	ZN	< 20.00
ZR	< .50				

LAB. NO. 46244 — REPORT TO: G ENGLE — DATE: 7-11-77
SAMPLE: 6484-140-L93 GRAPHITE — PROJECT NO. 32241460055 — DILUTION: 1.0000 — PLATE NO. 77-050

ELEMENT	CONCENTRATION, PPM	ELEMENT	CONCENTRATION, PPM	ELEMENT	CONCENTRATION, PPM
AG	< .50	AL	20.00	B	4.00
BA	20.00	BE	< .50	BI	< 2.00
CA	100.00	CD	< 10.00	CE	< 80.00
CO	< 4.00	CR	< 10.00	CS	< 100.00
CU	< 1.00	DY	< 20.00	ER	< 6.00
EU	< 10.00	FE	200.00	GD	< 10.00
HF	< 20.00	HO	< 10.00	IN	< 1.00
K	< 10.00	LA	< 10.00	LI	< 1.00
LU	< .50	MG	< .50	MN	< 1.00
MO	< 1.00	NA	< 10.00	NB	< 6.00
ND	< 200.00	NI	< 4.00	P	< 100.00
PB	< 6.00	PR	< 100.00	RB	< 40.00
SB	< 8.00	SC	< 1.00	SI	200.00
SM	< 100.00	SN	< 6.00	SR	< 40.00
TA	< 40.00	TB	< 40.00	TI	40.00
TL	< 20.00	TM	< 4.00	V	20.00
W	< 40.00	YB	< 10.00	ZN	< 20.00
ZR	< .50				

CONCENTRATION BASED ON ORGINAL SAMPLE BEFORE DILUTION WITH DILUENT
> MEANS GREATER THAN
< MEANS LESS THAN THE SENSITIVITYOF THE SPECTROGRAPHIC PROCEDURE USED
RESULTS ARE CORRECT WITHIN A FACTOR OF 40% , (ONE STANDARD DEVIATION)

TABLE 11-23 (Continued)

LAB. NO. 46244 — REPORT TO: G ENGLE — DATE: 7-11-77
SAMPLE: 6484-140-L111 GRAPHITE — PROJECT NO. 32241460055 — DILUTION: 1.0000 — PLATE NO. 77-050

ELEMENT	CONCENTRATION, PPM	ELEMENT	CONCENTRATION, PPM	ELEMENT	CONCENTRATION, PPM
AG	< .50	AL	40.00	B	6.00
BA	20.00	BE	< .50	BI	< 2.00
CA	100.00	CD	< 10.00	CE	< 80.00
CO	< 4.00	CR	< 10.00	CS	< 100.00
CU	< 1.00	DY	< 20.00	ER	< 6.00
EU	< 10.00	FE	200.00	GD	< 10.00
HF	< 20.00	HO	< 10.00	IN	< 1.00
K	< 10.00	LA	< 10.00	LI	< 1.00
LU	< .50	MG	< .50	MN	60.00
MO	< 1.00	NA	< 10.00	NB	< 6.00
ND	< 200.00	NI	< 4.00	P	< 100.00
PB	< 6.00	PR	< 100.00	RB	< 40.00
SB	< 8.00	SC	< 1.00	SI	200.00
SM	< 100.00	SN	< 6.00	SR	< 40.00
TA	< 40.00	TB	< 40.00	TI	40.00
TL	< 20.00	TM	< 4.00	V	20.00
W	< 40.00	YB	< 10.00	ZN	< 20.00
ZR	< .50				

LAB. NO. 46244 — REPORT TO: G ENGLE — DATE: 7-11-77
SAMPLE: 6484-140-L129 — PROJECT NO. 32241460055 — DILUTION: 1.0000 — PLATE NO. 77-050

ELEMENT	CONCENTRATION, PPM	ELEMENT	CONCENTRATION, PPM	ELEMENT	CONCENTRATION, PPM
AG	< .50	AL	20.00	B	6.00
BA	20.00	BE	< .50	BI	< 2.00
CA	100.00	CD	< 10.00	CE	< 80.00
CO	< 4.00	CR	< 10.00	CS	< 100.00
CU	< 1.00	DY	< 20.00	ER	< 6.00
EU	< 10.00	FE	200.00	GD	< 10.00
HF	< 20.00	HO	< 10.00	IN	< 1.00
K	< 10.00	LA	< 10.00	LI	< 1.00
LU	< .50	MG	< .50	MN	< 1.00
MO	< 1.00	NA	< 10.00	NB	< 6.00
ND	< 200.00	NI	< 4.00	P	< 100.00
PB	< 6.00	PR	< 100.00	RB	< 40.00
SB	< 8.00	SC	< 1.00	SI	200.00
SM	< 100.00	SN	< 6.00	SR	< 40.00
TA	< 40.00	TB	< 40.00	TI	40.00
TL	< 20.00	TM	< 4.00	V	20.00
W	< 40.00	YB	< 10.00	ZN	< 20.00
ZR	< .50				

CONCENTRATION BASED ON ORGINAL SAMPLE BEFORE DILUTION WITH DILUENT
> MEANS GREATER THAN
< MEANS LESS THAN THE SENSITIVITYOF THE SPECTROGRAPHIC PROCEDURE USED
RESULTS ARE CORRECT WITHIN A FACTOR OF 40% , (ONE STANDARD DEVIATION)

TABLE 11-24

FATIGUE TESTS ON H-451 GRAPHITE

IRRADIATED IN CAPSULES OG-1, 2, AND 3

LOT NO: 26A
ORIENTATION: AXIAL
TEMPERATURE: 900-970 C
LOG NO: 5651-2B
LOCATION: MIDLENGTH-CENTER
FLUENCE: 8.5*EXP25 N/M**2

CONTROL TENSILE TESTS

SPECIMEN NO.	DENSITY (MG/M**3)	DIA. (MM)	FRACTURE LOAD (KN)	TENSILE STRENGTH (MPA)
F-01A	.000	5.08	.37	18.4
F-03A	.000	5.06	.44	21.8
F-05A	.000	5.07	.37	18.5
F-07A	.000	5.07	.43	21.3
F-09A	.000	5.08	.46	22.6
F-11A	.000	5.08	.46	22.8
F-13A	.000	5.08	.42	20.8
F-15A	.000	5.08	.35	17.4
F-17A	.000	5.06	.37	18.4
F-19A	.000	5.03	.41	20.4
MEAN:	.000		MEAN:	20.2 MPA (2935.PSI)
STD. DEV:	****		STD. DEV:	1.9 MPA (281.PSI)

TABLE 11-25

FATIGUE TESTS ON H-451 GRAPHITE

IRRADIATED IN CAPSULES OG-1, 2, AND 3

LOT NO: 266 LOG NO: 5651-2A
ORIENTATION: AXIAL LOCATION: MIDLENGTH-CENTER
TEMPERATURE: 900-970 C FLUENCE: 8.5*EXP25 N/M**2

STRESS RATIO, R (MIN. STRESS / MAX. STRESS): -1.0

SPECIMEN NO.	DENSITY (MG/M**3)	MAX. STRESS (MPA)	MIN. STRESS (MPA)	CYCLES TO FAILURE	
F-03A	.000	13.5	-18.4	< 1	(FIRST CYCLE)
F-12A	.000	14.0	-14.4	89	
F-04A	.000	14.1	-14.2	>101100	(RUNOUT)
F-10A	.000	14.1	-14.1	>106200	(RUNOUT)
F-16A	.000	14.1	-14.2	>103100	(RUNOUT)
F-20A	.000	14.1	-13.7	>115200	(RUNOUT)
F-16A	.000	14.4	-14.6	58	
F-09B	.000	15.5	-20.1	< 1	(FIRST CYCLE)
F-06B	.000	16.0	-16.7	>113300	(RUNOUT)
F-04A	.000	16.1	-15.4	>102000	(RUNOUT)
F-02A	.000	16.1	-16.2	>106600	(RUNOUT)
F-13B	.000	16.1	-16.8	36	
F-10A	.000	16.1	-16.2	>113900	(RUNOUT)
F-16A	.000	16.3	-17.2	>123000	(RUNOUT)
F-19A	.000	16.4	-17.2	200	
F-06A	.000	17.9	-17.9	5928	
F-15B	.000	18.1	-18.1	>109500	(RUNOUT)
F-12A	.000	18.1	-18.7	587	
F-18A	.000	18.1	-18.1	24	
F-01B	.000	18.2	-17.9	8	
F-21A	.000	18.4	-17.9	35	
F-02A	.000	18.7	-20.8	< 1	(FIRST CYCLE)
F-08A	.000	19.2	-20.1	< 1	(FIRST CYCLE)
F-11A	.000	19.4	-19.9	5	
F-20A	.000	19.5	-20.1	75	
F-17B	.000	19.5	-19.4	< 1	(FIRST CYCLE)
F-14A	.000	20.1	-19.4	2	
F-21A	.000	20.1	-22.1	257	
F-05A	.000	20.2	-20.2	76	

TABLE 11-26

FATIGUE TESTS ON H-451 GRAPHITE

LOT NO: 408 LOG NO: 5651-90
ORIENTATION: RADIAL LOCATION: QUARTER-LENGTH EDGE

CONTROL TENSILE TESTS

SPECIMEN NO.	DENSITY (MG/M**3)	DIA. (MM)	FRACTURE LOAD (KN)	TENSILE STRENGTH (MPA)
101A	1.742	12.70	1.51	11.9
103A	1.743	12.70	1.88	14.8
105A	1.740	12.70	1.63	12.9
107A	1.749	12.70	1.58	12.5
109A	1.744	12.70	1.56	12.3
111A	1.746	12.70	1.50	11.8
113A	1.746	12.70	1.59	12.6
115A	1.741	12.70	1.55	12.2
117A	1.752	12.70	1.90	15.0
119A	1.744	12.70	1.80	14.2
121A	1.741	12.70	1.71	13.5
123A	1.753	12.71	1.69	13.3
125A	1.744	12.70	1.31	10.3
127A	1.747	12.69	1.47	11.6
129A	1.747	12.70	1.70	13.4
131A	1.736	12.63	1.89	15.1
133A	1.740	12.71	1.86	14.7
135A	1.738	12.70	1.43	11.3
137A	1.736	12.70	1.70	13.4
139A	1.739	12.65	1.82	14.5
141A	1.734	12.71	1.78	14.0
143A	1.738	12.70	1.77	14.0
145A	1.736	12.70	1.85	14.6
147A	1.739	12.70	1.48	11.7
149A	1.732	12.70	1.75	13.8
153A	1.736	12.71	2.46	19.4
155A	1.733	12.71	2.18	17.2
157A	1.789	12.70	2.53	20.0
159A	1.730	12.70	2.28	18.0
MEAN:	1.743		MEAN:	13.9 MPA (2021.PSI)
STD. DEV:	.011		STD. DEV:	2.3 MPA (335.PSI)

TABLE 11-27

FATIGUE TESTS ON H-451 GRAPHITE

LOT NO: 408 LOG NO: 5651-90
ORIENTATION: RADIAL LOCATION: QUARTER-LENGTH EDGE

STRESS RATIO, R (MIN. STRESS / MAX. STRESS): -1.0

SPECIMEN NO.	DENSITY (MG/M**3)	MAX. STRESS (MPA)	MIN. STRESS (MPA)	CYCLES TO FAILURE
105B	1.738	8.6	-9.0	>110700 (RUNOUT)
143B	1.735	8.7	-8.7	>109000 (RUNOUT)
135B	1.736	8.8	-8.8	>107800 (RUNOUT)
120A	1.741	8.8	-8.7	>112100 (RUNOUT)
113B	1.756	8.8	-8.8	>102500 (RUNOUT)
158A	1.732	8.8	-8.8	>150000 (RUNOUT)
150A	1.739	8.8	-8.8	>147700 (RUNOUT)
128A	1.747	8.8	-9.0	>109100 (RUNOUT)
149B	1.739	10.3	-10.3	>100100 (RUNOUT)
141B	1.744	10.3	-10.5	>101900 (RUNOUT)
126A	1.749	10.3	-9.9	21800
119B	1.747	10.3	-10.6	600
156A	1.735	10.3	-10.7	>102400 (RUNOUT)
104A	1.736	10.3	-10.0	>101400 (RUNOUT)
111B	1.754	10.4	-10.5	225
134A	1.725	10.4	-10.4	>141700 (RUNOUT)
136A	1.740	10.7	-13.7	< 1 (FIRST CYCLE)
159B	1.729	11.2	-11.2	87700
152A	1.735	11.2	-11.3	>107300 (RUNOUT)
144A	1.734	11.2	-11.2	>133900 (RUNOUT)
137B	1.733	11.2	-11.2	>109100 (RUNOUT)
102A	1.748	11.2	.0	< 1 (FIRST CYCLE)
123B	1.754	11.8	-14.2	< 1 (FIRST CYCLE)
147B	1.741	11.9	-11.8	43
140A	1.734	11.9	-11.8	1000
117B	1.713	12.0	-11.6	18
125B	1.749	12.0	-12.0	137
110A	1.755	12.0	-12.0	456
155B	1.733	12.0	-12.0	>104400 (RUNOUT)
132A	1.734	12.1	-12.0	>107900 (RUNOUT)
107B	1.740	12.5	-12.9	3
131B	1.725	12.8	-13.9	< 1 (FIRST CYCLE)
129B	1.746	12.9	-12.9	57
122A	1.744	12.9	-12.9	17
114A	1.747	12.9	-12.9	5
101B	1.749	13.3	-13.3	3
116A	1.753	13.5	-13.5	< 1 (FIRST CYCLE)
153B	1.738	13.7	-13.7	3
146A	1.741	13.7	-14.0	1
108A	1.753	14.0	-14.0	7

APPENDIX
TOPICAL REPORTS PUBLISHED DURING THE QUARTER

Wallroth, C. F., C. M. Miller, and J. J. Saurwein, "Residual Stress and Strain Examination in Peach Bottom Fuel Test Elements," General Atomic Report GA-A14324, May 20, 1977.

Engle, G. B., "Properties of Unirradiated HTGR Core Support and Permanent Side Reflector Graphites: PGX, HLM, 2020, and H-440N," ERDA Report GA-A14328, General Atomic Company, May 1977.

Smith, P. D., and R. G. Steinke, "Release of Metallic Fission Products from Multi-Layered Coated Particles," General Atomic Report GA-A14033, June 1977.

Gainey, B. W., "An Evaluation of Carbon Deposition and Possible Consequences in the HTGR: A Review," ERDA Report GA-A13982, General Atomic Company, July 1977.

Smith, C. L., "UC_2 and WAR UC_xO_y Kernal Migration," General Atomic Report GA-A14409, July 1977.

Wallroth, C. F., et al., "Postirradiation Examination of Peach Bottom Fuel Test Element FTE-4," ERDA Report GA-A13452, General Atomic Company, July 1977.

Saurwein, J. J., "STAT, GAPS, STRAIN, DRWDIM. A System of Computer Codes for Analyzing HTGR Fuel Test Element Metrology Data. User's Manual," ERDA Report GA-A14274, General Atomic Company, August 1977.

GENERAL ATOMIC COMPANY
P. O. BOX 81608
SAN DIEGO, CALIFORNIA 92138